Anti-inflammatory drug development focusing on immune mediated diseases

Edited by
José Fernando Oliveira-Costa, Marta Chagas Monteiro, Amit Prasad,
Rajbir Bhatti and Rishi Sharma

Published in
Frontiers in Pharmacology

About Frontiers

Frontiers is more than just an open access publisher of scholarly articles: it is a pioneering approach to the world of academia, radically improving the way scholarly research is managed. The grand vision of Frontiers is a world where all people have an equal opportunity to seek, share and generate knowledge. Frontiers provides immediate and permanent online open access to all its publications, but this alone is not enough to realize our grand goals.

Frontiers journal series

The Frontiers journal series is a multi-tier and interdisciplinary set of open-access, online journals, promising a paradigm shift from the current review, selection and dissemination processes in academic publishing. All Frontiers journals are driven by researchers for researchers; therefore, they constitute a service to the scholarly community. At the same time, the *Frontiers journal series* operates on a revolutionary invention, the tiered publishing system, initially addressing specific communities of scholars, and gradually climbing up to broader public understanding, thus serving the interests of the lay society, too.

Dedication to quality

Each Frontiers article is a landmark of the highest quality, thanks to genuinely collaborative interactions between authors and review editors, who include some of the world's best academicians. Research must be certified by peers before entering a stream of knowledge that may eventually reach the public - and shape society; therefore, Frontiers only applies the most rigorous and unbiased reviews. Frontiers revolutionizes research publishing by freely delivering the most outstanding research, evaluated with no bias from both the academic and social point of view. By applying the most advanced information technologies, Frontiers is catapulting scholarly publishing into a new generation.

What are Frontiers Research Topics?

Frontiers Research Topics are very popular trademarks of the *Frontiers journals series*: they are collections of at least ten articles, all centered on a particular subject. With their unique mix of varied contributions from Original Research to Review Articles, Frontiers Research Topics unify the most influential researchers, the latest key findings and historical advances in a hot research area.

Find out more on how to host your own Frontiers Research Topic or contribute to one as an author by contacting the Frontiers editorial office: frontiersin.org/about/contact

Anti-inflammatory drug development focusing on immune mediated diseases

Topic editors

José Fernando Oliveira-Costa — Secretaria de Saúde do Estado da Bahia, Brazil

Marta Chagas Monteiro — Federal University of Pará, Brazil

Amit Prasad — Indian Institute of Technology Mandi, India

Rajbir Bhatti — Guru Nanak Dev University, India

Rishi Sharma — University of Missouri, United States

Table of
contents

Check for updates

Editorial: Anti-inflammatory drug development focusing on immune mediated diseases

José Fernando Oliveira-Costa[1]* and Amit Prasad[2,3,4]

[1]Center for Infusions and Specialized Medicines of Bahia—CIMEB, Bahia State Health Department,
Salvador, Brazil, [2]School of Biosciences and Bioengineering, Indian Institute of Technology, Mandi, India,
[3]Center for Indian Knowledge System and Mental Health, Indian Institute of Technology, Mand, India,
[4]Center for Human Computer Interaction, Indian Institute of Technology, Mandi, India

KEYWORDS

inflammation, drugs, therapeutics, molecular docking, repurposing

Editorial on the Research Topic
Anti-inflammatory drug development focusing on immune
mediated diseases

Inflammatory diseases are distributed worldwide, affecting approximately 5% of the world population (Bieber et al., 2023). Among these the inflammatory diseases like rheumatoid arthritis, type 1 diabetes mellitus, systemic lupus erythematosus, multiple sclerosis, Crohn's disease, ulcerative colitis, psoriasis, and myasthenia gravis are prominent ones. The ever-increasing number of senior citizens (age >60 years) across the globe and the advent of newer and better diagnostic tools for immune-mediated diseases has produced an increase in the incidence of inflammatory diseases. While the general population grew from one billion in the year 1800 to eight billion at present, and it is estimated that by 2030 one in six people in world will be aged sixty or older (Bolkan et al., 2023; Pereira et al., 2023). In addition to this, studies suggest that there is an increased risk of developing immune-mediated diseases to the individuals who got SARS-CoV-2 infections (Kim et al., 2024). Despite the great advances in the treatment of these medical conditions in recent past, many patients suffer with serious conditions of the disease for a long time. This situation demands constant research, to identify new drugs, with more specific targets and fewer side effects to treat inflammatory diseases (Wang et al., 2015).

In Brazil, despite the guarantee of free access to medicines through the Unified Health System for all citizens as a constitutional right, immune-mediated diseases represent a significant challenge. This is due to its complexity and the lack of adequate resources for early diagnosis and effective treatment. For example, one of the main obstacles to the accurate diagnosis of rheumatological diseases in Brazil is the shortage of specialized professionals. Recent data indicates that 53.3% of the all the rheumatologists in the country live in the capitals of state in the southeast region; 16.8% live in the very populous northeast region, while only 4.1% of medical professionals reside in the north region. This data represents the heterogeneity in the territorial distribution of professionals in Brazil, a developing country. Furthermore, the lack of adequate medical training for those who work in primary care can lead to diagnostic errors or delays in referral to specialists, which ends up worsening the health condition, with irreversible damage to patients (BRAZIL, 2021; Scheffer et al., 2023). The same kind of situation is prevalent in almost all the developing or underdeveloped countries where most of the advance medical facilities are concentrated to

affluent and populous cities and rural areas are devoid of such facilities. Despite the existence of specific clinical protocols for treatment, there is a great difficulty in the diagnosis for immune disease due to complex definition of diagnostic criteria, leading to severe impact on the quality of life of affected individuals (Lin et al., 2023). In this scenario, the discovery of new molecules capable of treating diseases mediated by the immune system remains fundamental.

Identification of new natural products, synthetic molecules, drug repurposing, *in silico* molecular modelling studies associated with chemical synthesis represent important strategies for the development of new drugs (Spitschak et al., 2022; Wainwright et al., 2022). The global demand for new drugs and the associated scientific challenges were motivations for this special edition, with the aim to bring together scientific research works that addressed the development of new immunomodulatory drugs. As a result, we have very interesting articles, coming from different research aspects, which lead us to believe that they will be very useful in discovering new treatments for inflammatory diseases in near future.

The study Li et al. investigated adverse events associated with mepolizumab in the treatment of severe asthma with an eosinophilic phenotype. Reports of expected adverse events were identified, but also unexpected ones, such as coughing, malaise and chest discomfort, recommending continued attention to safety in long-term use and in paediatrics.

Other study, entitled Arjsri et al. examined the potential of exiguaflavanone A and B, present in the root of *Sophora exigua*, in suppressing the proliferation and metastasis of non-small cell lung cancer cells. This kind of lung cancer is induced by inflammation. Through inhibition of the NLRP3 inflammasome pathway, these compounds have demonstrated efficacy in reducing the inflammatory response associated with lung cancer.

The article "Dasatinib suppresses particulate-induced pyroptosis and acute lung inflammation" highlights the efficacy of dasatinib in mitigating inflammatory responses triggered by particulate exposure. Through its action on Src family kinases, dasatinib effectively inhibits pyroptosis induced by particulate materials, such as silica particles, while sparing non-particulate-induced pyroptosis. Furthermore, Dasatinib attenuates acute lung inflammation induced due to exposure to particulate by improving phagolysosomal function and reducing inflammatory mediator release.

Interestingly, the authors of Kim et al., investigated the therapeutic potential of N-benzyl-N-methyldecan-1-amine and its derivative in mitigating 2,4-dinitrobenzenesulfonic acid-induced colitis and collagen-induced rheumatoid arthritis. These compounds were evaluated for their efficacy in ameliorating associated inflammatory symptoms and had shown promising anti-inflammatory properties. This further suggests that they should be considered as potential therapeutic agents for colitis and rheumatoid arthritis.

In the study titled Lu et al., authors describe the abundance of natural flavones found in both edible and medicinal plants, presenting a promising avenue for the treatment of ulcerative colitis, highlighting the importance of concentrated detailed effort in exploring natural remedies for several inflammatory gastrointestinal disorders.

The authors of the research article titled Peng et al. explored the development of a sustained-release phospholipid-based phase separation gel containing berberine for the treatment of rheumatoid arthritis. The formulation aims to enhance drug retention at the site of inflammation, thereby improving therapeutic efficacy while minimizing side effects.

In psoriasis, dysregulated Th17 cell responses contribute to skin inflammation and is a major contributor of immune pathologies to the disease. Authors in Lee et al. investigated the therapeutic potential of aminooxy acetic acid (AOA), a known inhibitor of serine metabolism, in alleviating Th17 mediated psoriasis-like skin inflammation. Through *in vitro* and *in vivo* experiments, it is demonstrated that AOA effectively attenuates Th17 cell differentiation and function, leading to reduced production of pro-inflammatory cytokines such as interleukin-17 and interleukin-22. Their findings highlight AOA as a promising therapeutic candidate for the treatment of psoriasis.

The study Xu et al. explores the structural properties and anti-dermatitis effects of flavonoids-loaded gold nanoparticles (AuNPs), using extracts from *Eupatorium japonicum*. The results demonstrate promising structural attributes of the flavonoids-loaded AuNPs, with significant anti-dermatitis effects by the suppression of the production of inflammatory cytokines (RANTES, TARC, CTACK, IL-6, and IL-8) and intracellular reactive oxygen species.

Neostigmine, a well-known acetylcholinesterase inhibitor, has traditionally been utilized for its ability to enhance skeletal muscle strength, particularly in conditions such as myasthenia gravis and neuromuscular blockade reversal. The authors of the review article Si et al. had reviewed the past 20 years of research and provided new insight about the role of neostigmine use in clinical application.

The study Zhou et al. looked for the impact of dexmedetomidine (DEX), a norepinephrine release inhibitor, on stroke-associated pneumonia (SAP) in mice model. Despite its role in inhibiting norepinephrine release, DEX did not show any improvement in SAP in the mouse model. This suggests that DEX should be used cautiously to alleviate SAP associated symptoms and further studies are required to fully understand the role of DEX in SAP.

Interstitial lung disease (ILD) encompasses a diverse group of chronic lung disorders characterized by inflammation and fibrosis of the interstitial lung tissue, leading to progressive impairment of lung function. Authors in the review article Huo et al. explore the advancements in therapy and treatment options for ILD, which unfortunately remain limited. One promising avenue involves resveratrol, a natural polyphenolic compound renowned for its diverse pharmacological properties. These include antioxidative, anti-inflammatory, and anti-fibrotic effects. Resveratrol achieves this by inhibiting key signalling pathways such as TGF-β/Smad2/3/4, NF-κB, and JAK/STAT, thereby preventing overactivation of immune cells."

Considering the potential activities of resveratrol, the another study "Resveratrol attenuates staphylococcal enterotoxin B-activated immune cell metabolism via upregulation of miR-100 and suppression of mTOR signalling pathway" investigates the effects of resveratrol on immune cell metabolism activated by staphylococcal enterotoxin B (SEB) and explores the underlying molecular mechanisms showing that resveratrol attenuates SEB-induced immune cell metabolism by upregulating miR-100 and suppressing the mTOR signalling pathway.

In the study Sun et al., authors established a HTS model for identifying compounds capable of inhibiting cell adhesion. Thus, using LPS-induced human umbilical vein endothelial cells (HUVECs) and calcein-AM-labelled human monocytic cell THP-1, they established a HTS model for cell adhesion inhibitors, proving to be suitable for screening and validating cell adhesion inhibitors.

In conclusion, the field of anti-inflammatory drug development for immune mediated diseases is evolving rapidly and breath-taking research, supported by innovative techniques is giving transformative breakthroughs and cutting-edge solutions.

However, despite the current research diversity with this edition and optimism for the future, inflammatory diseases are known for their complexity and will remain an intriguing challenge for researchers for future studies too.

Author contributions

JO-C: Conceptualization, Data curation, Formal Analysis, Investigation, Methodology, Project administration, Resources, Supervision, Validation, Visualization, Writing–original draft, Writing–review and editing. AP: Data curation, Formal Analysis, Supervision, Visualization, Writing–review and editing.

Funding

Conflict of interest

The authors declare that the research was conducted in the absence of any commercial or financial relationships that could be construed as a potential conflict of interest.

The author(s) declared that they were an editorial board member of Frontiers, at the time of submission. This had no impact on the peer review process and the final decision.

Publisher's note

All claims expressed in this article are solely those of the authors and do not necessarily represent those of their affiliated organizations, or those of the publisher, the editors and the reviewers. Any product that may be evaluated in this article, or claim that may be made by its manufacturer, is not guaranteed or endorsed by the publisher.

References

Bieber, K., Hundt, J. E., Yu, X., Ehlers, M., Petersen, F., Karsten, C. M., et al. (2023). Autoimmune pre-disease. *Autoimmun. Rev.* 22 (2), 103236. doi:10.1016/j.autrev.2022.103236

Bolkan, C., Teaster, P. B., and Ramsay-Klawsnik, H. (2023). The context of elder maltreatment: an opportunity for prevention science. *Prev. Sci.* 24 (5), 911–925. doi:10.1007/s11121-022-01470-5

BRASIL (2021). Secretaria de Atenção Especializada à Saúde. *Portaria conjunta N.* 16. de 3 de setembro de.

Kim, M. S., Lee, H., Lee, S. W., Kwon, R., Rhee, S. Y., Lee, J. A., et al. (2024). Long-term autoimmune inflammatory rheumatic outcomes of COVID-19: a binational cohort study. *Ann. Intern Med.* 177, 291–302. doi:10.7326/M23-1831

Lin, F. T. D., Mazarroto, E. J., and Gregório, P. C. (2023). Doença de Crohn: aspectos integrativos do diagnóstico ao tratamento. *Res. Soc. Dev.* 12 (2), e29212240368. doi:10.33448/rsd-v12i2.40368

Pereira, W. A. B., Oliveira, I. R., Werner, F., Santos, L. T., Furtado, P. S., Brigagão, R. V., et al. (2023). Aumento da expectativa de vida e crescimento populacional no Brasil e os impactos no número de pessoas vivendo com doenças crônico-degenerativas: desafios para o manejo da Doença de Alzheimer. *Soc. Desenvolv.* 12 (5), e24112531673. doi:10.33448/rsd-v12i5.31673

Scheffer, M., Guilloux, A. G. A., Miotto, B. A., Almeida, C. J., Guerra, A., Cassenote, A., et al. (2023) *Demografia médica no brasil 2023*. São Paulo, SP: FMUSP, AMB, 344.

Spitschak, A., Gupta, S., Singh, K. P., Logotheti, S., and Pützer, B. M. (2022). Drug repurposing at the interface of melanoma immunotherapy and autoimmune disease. *Pharmaceutics* 15 (1), 83. doi:10.3390/pharmaceutics15010083

Wainwright, C. L., Teixeira, M. M., Adelson, D. L., Buenz, E. J., David, B., Glaser, K. B., et al. (2022). Future directions for the discovery of natural product-derived immunomodulating drugs: an IUPHAR positional review. *Pharmacol. Res.* 177, 106076. doi:10.1016/j.phrs.2022.106076

Wang, L., Wang, F. S., and Gershwin, M. E. (2015). Human autoimmune diseases: a comprehensive update. *J. Intern Med.* 278 (4), 369–395. doi:10.1111/joim.12395

Check for updates

Structural properties and anti-dermatitis effects of flavonoids-loaded gold nanoparticles prepared by *Eupatorium japonicum*

Xing Yue Xu[1,2], Sung-Kwon Moon[3], Jin-Kyu Kim[4], Woo Jung Kim[4], Yeon-Ju Kim[1]* and Hoon Kim[3]*

[1]Graduate School of Biotechnology, And College of Life Science, Kyung Hee University, Yongin, South Korea, [2]Beijing Key Laboratory of Traditional Chinese Medicine Basic Research on Prevention and Treatment for Major Diseases, Experimental Research Center, China Academy of Chinese Medical Sciences, Beijing, China, [3]Department of Food and Nutrition, Chung Ang University, Anseong, South Korea, [4]Biocenter, Gyeonggido Business and Science Accelerator, Suwon, South Korea

Recently, green synthesis-based nanoformulations using plants or microorganisms have attracted great interest because of their several advantages. Nanotechnology-based biological macromolecules are emerging materials with potential applications in cosmetics and medications for ameliorating and treating inflammatory skin diseases (ISDs). *Eupatorium japonicum* (EJ), a native Korean medicinal plant belonging to the family Asteraceae, has been traditionally used to prepare prescriptions for the treatment of various inflammatory diseases. EJ-based gold nanoparticles (EJ-AuNPs) were biosynthesized under optimal conditions and characterized their physicochemical properties using various microscopic and spectrometric techniques. Additionally, the effects of EJ-AuNPs on ISDs as well as their underlying mechanisms were investigated in the tumor necrosis factor-α/ interferon-γ (T+I)-induced skin HaCaT keratinocytes. The MTT and live/dead cell staining assays showed that EJ-AuNP treatment was considerably safer than EJ treatment alone in HaCaT cells. Moreover, EJ-AuNP treatment effectively suppressed the production of T+I-stimulated inflammatory cytokines (RANTES, TARC, CTACK, IL-6, and IL-8) and intracellular reactive oxygen species, and such EJ-driven anti-inflammatory effects were shown to be associated with the downregulation of intracellular mitogen-activated protein kinase and nuclear factor-κB signaling pathways. The present study provides preliminary results and a valuable strategy for developing novel anti-skin dermatitis drug candidates using plant extract-based gold nanoparticles.

KEYWORDS

biosynthesized nanomaterial, plant-loaded nanoparticle, inflammatory skin disease, chemokine, HaCaT, secondary metabolites

Introduction

Inflammation is a pivotal biological reaction caused by irritation against harmful stimuli, and is a protective response involving immune cells, blood vessels, and inflammatory mediators (Chen et al., 2017). However, chronic inflammation due to persistent uncontrolled acute inflammation may contribute to multiple chronic diseases, such as allergies, cardiovascular and bowel diseases, diabetes, metabolic syndrome, arthritis, cancer, and autoimmune diseases (Ghasemian et al., 2016; Chen et al., 2017). Skin inflammation, also called dermatitis, is an inflammatory reaction that occurs in the skin tissue and is accompanied by symptoms, such as itchiness, redness, heat, and rash. Persistent pathological inflammatory skin diseases (ISDs) include atopic dermatitis, allergic dermatitis, contact dermatitis, seborrheic dermatitis, stasis dermatitis, etc. (Albanesi and Pastore, 2010; Carretero et al., 2016). Due to the rapid climate change and environmental pollution, an increasing number of people are suffering from chronic dermatitis, which is emerging as a serious social problem (Drakaki et al., 2014).

Recently, nanotechnology-based therapeutics have been considered as emerging materials with potential applications in cosmetics and medications to ameliorate and treat ISDs (Wiesenthal et al., 2011; Puglia and Bonina, 2012; Kakkar et al., 2019). Since the first report on the topical application of nanoparticles in the 1980s, various nanoformulations have been applied to treat ISDs (Kakkar et al., 2019; Campos et al., 2021). Despite the widespread study of nanoformulations, major concerns regarding their cytotoxicity have limited their industrial application (Ahmed et al., 2016; Bahadar et al., 2016). To overcome these limitations, green synthesis-based nanoparticles using plants or microorganisms are of great interest owing to their several advantages over other nanoformulations, such as relatively high biocompatibility and reproducibility, easy and simple preparation procedures, low cost, and eco-friendly nature (Krishnaswamy et al., 2014; Ahmed and Ikram, 2015). Especially, gold nanoparticles (AuNPs) have gained the most attention in various fields because of their several advantages, including synthesis compatibility, biocompatibility, low toxicity, and detection capability (Dykman and Khlebtsov, 2012; Wang et al., 2021). However, as only a few studies have reported their efficacy on the skin, more fundamental research on plant-based gold nanoparticles is required for dermal application as they are known to have various benefits over traditional topical treatments, such as improved skin permeation, regulated drug delivery, and enhanced therapeutic effects (Abdel-Mottaleb et al., 2014).

A native Korean medicinal plant, *Eupatorium japonicum* (EJ), which belongs to the Asteraceae family, is found primarily in Northeast Asia, including Korea, China, and Japan. EJ is traditionally used to prepare prescriptions to treat various digestive diseases, nausea, vomiting, dyspepsia, and diarrhea (Shin et al., 2018). Recently, the therapeutic efficacy of EJ against inflammatory reactions and its underlying mechanisms of action were investigated in RAW 264.7 monocytic, 293T kidney, and rheumatoid arthritis fibroblast-like synovial cells (Gu et al., 2014; Dai et al., 2020; Phan et al., 2021), and it was found that EJ may be useful for controlling and treating ISDs. However, the effects of EJ-mediated nanoparticles on ISDs have not yet been examined.

Therefore, the present study aimed to prepare novel AuNPs using EJ extracts and identify their physicochemical characteristics. In addition, we aimed to explore the efficacy of EJ-based AuNPs in ISDs and their underlying molecular mechanism using an inflammation-induced human keratinocyte model.

Materials and methods

Harvest and extraction of *Eupatorium japonicum* leaf tissue

The leaf tissue of wild EJ plant was harvested from northern Gyeonggi, adjacent to the demilitarized zone in Korea. The plant was identified by Dr. J. K. Kim, a senior researcher at Gyeonggido Business and Science Accelerator, Gyeonggi Biocenter (Suwon, Korea). A voucher specimen was deposited in the same department as described above. Dried leaves were immersed in five volumes (w/v) of 70% ethanol and extracted at 20°C–25°C for 3 days. A polyester filtering cloth (20 μm; Hyundai Micro, Anseong, Korea) was used to filter the extract, which was then concentrated using a rotary evaporator (Buchi Korea Inc., Gwangmyeong, Korea). After drying using a freeze-drier (Ilshin Biobase, Daejeon, Korea), the 70% ethanol extract of EJ leaves was prepared with an extraction yield of 21.1%.

Qualitative determination of major *phytochemicals* by ultra-performance liquid chromatography–tandem mass spectrometry analysis

A UPLC-MS system (LTQ Orbitrap XL, Thermo Electron, Waltham, MA, United States) was used for the qualitative determination of the major phytochemicals in EJ, according to a previously described analytical method (Kim et al., 2021). The detailed analytical conditions are listed in Supplementary Table S1.

Biosynthesis of optimized EJ-AuNPs

To establish the optimal conditions for AuNP biosynthesis from EJ, four parameters were monitored: EJ concentration,

HAuCl$_4$•3H$_2$O concentration, reaction temperature, and time. Briefly, distilled water (1 ml) containing HAuCl$_4$•3H$_2$O (0.5–2.5 mM, 0.5 mM interval) was added to dried EJ (1–6 mg, 1 mg interval), and the mixture was incubated at the designated temperature (30°C–70°C, 10°C interval) for 20–50 min (10 min interval). After the reaction, the color change and absorbance were measured with the eye and using a UV-Vis spectrometer (Agilent Technologies, Inc., Santa Clara, CA, United States), respectively, to ascertain the optimal conditions for the synthesized nanoparticles. To remove the soluble materials, the mixture was centrifuged (12,000 rpm, 20 min), and the precipitated particles were washed with distilled water. This process was repeated four more times to purify the particles. The particles were finally dried using a freeze-drier (Ilshin Biobase, Daejeon, Korea) to obtain AuNPs biosynthesized from EJ (EJ-AuNPs).

Physicochemical analysis of *Eupatorium japonicum*-AuNPs

The thermal stability of the EJ-AuNPs was measured by thermogravimetric analysis (TGA) (TGA/DSC 1; Yeonjin S-Tech Co., Seoul, Korea) at 30°C–600°C. To identify the functional groups on the surface of the EJ-AuNPs, Fourier transform infrared (FT-IR) spectroscopy (PerkinElmer Inc., Waltham, MA, United States) was used in the range 500–4000 cm^{-1}. The particle sizes and size distribution of the EJ-AuNPs were measured using a dynamic light scattering (DLS) particle size analyzer (Otsuka Electronics, Shiga, Japan) at a size range of 1–1000 nm. Field-emission-transmission electron microscopy (FE-TEM; JEM-2100F, JEOL, Ltd., Tokyo, Japan) coupled with selected area electron diffraction (SAED) and energy-dispersive X-ray spectrometry (EDX) was used at a voltage of 200 kV to measure the particle size, microscopic morphology, elemental composition, and crystalline nature of the EJ-AuNPs. A powered X-ray diffractometer (XRD; D8 Advance, Bruker, Karlsruhe, Germany) was used with 1.54 Å CuKα radiation to confirm the purity and crystalline nature of the EJ-AuNPs.

HaCaT cell culture and evaluation of cytotoxic effect

Human epidermal keratinocytes (HaCaT; CLS GmbH, Eppelheim, Germany) were cultured in Dulbecco's modified Eagle's medium (DMEM; GenDEPOT, Katy, TX, United States) containing 10% fetal bovine serum (FBS; GenDEPOT), 100 U penicillin, and 100 μg/ml streptomycin (GenDEPOT). The cells were then incubated in a humidified incubator with 5% carbon dioxide (CO$_2$)/95% air. Cells (1 × 10^4 cells) were plated in a 96-well plate (SPL Life Sciences, Pocheon, Korea) and stabilized for 24 h. The dried EJ-AuNPs or EJ was

diluted with serum-free medium (SFM) at concentrations of 25, 50, and 100 μg/ml. After the cells were washed twice with phosphate-buffered saline (PBS), diluted EJ-AuNPs solution was added to the cells and incubated for a further 24 h. To compare the cytotoxic effect of EJ-AuNPs, only SFM and commercial dexamethasone (20 μg/ml)-containing SFM were added to the cells. The cytotoxic effects of EJ-AuNPs against HaCaT cells were measured using a conventional 3-(4,5-cimethylthiazol-2-yl)-2,5-diphenyl tetrazolium bromide (MTT) solution (Sigma-Aldrich, St. Louis, MO, United States) and a live/dead cell staining kit (Thermo Fisher Scientific, Cambridge, MA, United States), according to the manufacturer's instructions.

Reactive oxygen species staining

HaCaT cells (2 × 10^5 cells) were seeded in a 6-well plate (SPL Life Sciences) and stabilized for 24 h. After the cells were washed twice with PBS, they were treated with fresh SFM containing EJ-AuNPs for 1 h. To compare the levels of ROS in EJ-AuNP-treated cells, only SFM and commercial dexamethasone (20 μg/ml)-containing SFM were added to the cells. Subsequently, the cells were treated with a recombinant protein mixture comprising 10 ng/ml tumor necrosis factor-alpha (TNF-α; 210-TA-100/CF, R&D Systems, Minneapolis, MN, United States) and 10 ng/ml interferon-gamma (IFN-γ; 285-IF-100/CF, R&D Systems) (T+I) for 24 h. After rinsing twice with PBS, the cells were stained using a cellular ROS assay kit (ab113851; Abcam, Cambridge, United Kingdom) according to the manufacturer's instructions. Intracellular ROS levels were visualized using a Leica DM IRB fluorescence microscope (Leica Microsystems, Wetzlar, Germany) and quantified using the GraphPad software (Prism 8; San Diego, CA, United States)

Quantitative reverse transcription-polymerase chain reaction

HaCaT cells (5 × 10^5 cells) were seeded onto a 60 mm dish (SPL Life Sciences) and stabilized for 24 h. After the cells were washed twice with PBS, fresh SFM containing EJ-AuNPs was added to the cells for 1 h. To compare the gene expression levels in EJ-AuNP-treated cells, SFM and commercial dexamethasone (20 μg/ml)-containing SFM were also added to the cells. Subsequently, the cells were treated with T+I mixture for 24 h. After rinsing twice with PBS, total RNA was extracted using the TRIzol reagent (Invitrogen, Carlsbad, CA, United States) and quantified on a nanodrop plate using a microplate spectrophotometer (Epoch, BioTek Instruments, Winooski, VT, United States). Equal amounts of total RNA were reverse-transcribed using the AmfiRivert cDNA synthesis kit (GenDEPOT), and qRT-PCR was performed using the AmfiSure qGreen Q-PCR master mix (GenDEPOT) and

Rotor-gene Q real-time PCR detection system (Qiagen, Hilden, Germany) with SYBR Premix Ex Taq™ II (TaKaRa Bio Inc., Kusatsu, Japan). All primers were designed and provided by Macrogen (Seoul, Korea). The gene-specific primer sequences used in this study are listed in Supplementary Table S2. The level of target gene expression was calculated and normalized against the expression level of the endogenous control gene, glyceraldehyde-3-phosphate dehydrogenase (GAPDH), using formula $2^{-\Delta\Delta Ct}$.

Enzyme-linked immunosorbent assay

HaCaT cells (1×10^4 cells) were seeded in a 96-well plate (SPL Life Sciences) and stabilized for 24 h. After the cells were washed twice with PBS, they were treated with fresh SFM containing EJ-AuNPs for 1 h. To compare the cytokine secretion to EJ-AuNP-treated cells, only SFM and commercial dexamethasone (20 μg/ml)-containing SFM were added to the cells. Subsequently, the cells were treated with the T+I mixture for 24 h. The cell-free culture medium was collected, and pro-inflammatory cytokines, including interleukin (IL)-6 (555220; BD Biosciences, Newark, DE, United States), IL-8 (555,244; BD Biosciences), and thymus and activation-regulated chemokine (TARC) (DY364; R&D Systems), were measured using ELISA, according to the manufacturer's instructions.

Immunoblotting analysis

The HaCaT cell culture method and sample treatment procedures were carried out according to the procedures described in Section 2.6. After rinsing twice with PBS, total protein was isolated from the cells using the Pierce RIPA buffer reagent (Thermo Fisher Scientific) containing protease inhibitors (GenDEPOT) and quantified using a bicinchoninic acid protein assay kit (Thermo Fisher Scientific). Equal amounts of total protein were separated on a 10% sodium dodecyl sulfate-polyacrylamide gel, and the separated proteins were transferred from the gel to a polyvinylidene fluoride membrane (Thermo Fisher Scientific). The membrane was blocked with PBST containing 5% skim milk at 20°C–25°C for 2 h and washed thrice with PBST. The membranes were incubated with primary antibodies against p38 mitogen-activated protein kinase (p38; #8690), c-Jun N-terminal kinase (JNK; #9252), extracellular signal-regulated kinase (ERK1/2; #4695), nuclear factor kappa-light-chain-enhancer of activated B cells p65 (p65; 8242), nuclear factor kappa-light-chain-enhancer of activated B cells inhibitor alpha (IκBα; #4814), β-actin (#3700), p-p38 (#4511), p-JNK (#4668), p-ERK (#4370), p-p65 (#3033), and p-IκBα (#9246) at 4°C overnight. After washing three times with PBST, the membrane was incubated with horseradish peroxidase-conjugated secondary antibody against anti-mouse/

rabbit IgG (#98164) at 20°C–25°C for 1 h. All antibodies were obtained from Cell Signaling Technology (Danvers, MA, United States). The membrane was rinsed five times with PBST, and the protein blots were visualized using the West-Q Pico ECL Solution (GenDEPOT). The expression level of each target protein was quantified using the ImageJ software available in online website (https://imagej.nih.gov/ij/).

Statistical analysis

All experiments were performed in triplicate, and the results are expressed as the mean ± standard deviation. Statistical analyses were performed using PASW Statistics 18 (IBM Co., Armonk, NY, United States). Statistical comparisons between two groups were conducted using the Student's t-test, and $p < 0.05$, $p < 0.01$, and $p < 0.001$ were considered statistically significant at different levels.

Results

Putative identification of major phytochemicals in the EJ extract

First, we aimed to determine the major phytochemicals present in the EJ extract using UPLC-MS/MS analysis. PDA and BPC of the EJ extract are shown in Figures 1A,B, respectively. The molecular weight and ionization pattern of each peak on the BPC were further analyzed by MS (Figure 2A) and MS/MS (Figure 2B) to determine the identity of the putative compounds by retrieving an in-house spectral library and a web-based database. The results showed that an ion peak at 5.85 min in BPC was confirmed as m/z 327.0876 in the positive ionization mode of MS, and MS/MS provided information on the putative identification of melilotoside (CAS No. 618–67-7) by determining its product ion at m/z 310.1402 ($[M+H]^+$). Using the same process, five peaks (6.39, 6.69, 6.88, 7.41, and 9.50 min) on the BPC were putatively identified as rutin (quercetin-3-O-rutinoside), hyperoside (quercetin 3-O-β-galactoside), nictoflorin (kaempferol-3-O-β-rutinoside), cynaroside (luteolin 7-O-β-D-glucoside), and rhamnetin (quercetin 7-methyl ether) by their values of m/z 611.1580 ($[M+H]^+$), 465.1009 ($[M+H]^+$), 595.1637 ($[M+H]^+$), 449.1060 ($[M+H]^+$), and 317.0644 ($[M+H]^+$), respectively. The chemical structures of aforementioned compounds were illustrated in Figure 2C.

Establishment of optimized conditions for EJ-AuNP synthesis

Various conditions to establish optimal conditions for the biosynthesis of EJ-AuNPs were monitored in terms of EJ

FIGURE 1
UPLC-MS chromatogram of the 70% ethanol extract of *E. japonicum* (EJ). **(A)** Photo diode array (PDA) chromatogram, **(B)** Total ion chromatogram (TIC), and putative identification of six major phytochemicals in EJ as listed in Table. EJ (10 mg/ml) was introduced into the UPLC system, and separation and detection conditions were described in Supplementary Table S1.

concentrations (1–6 mg/ml), gold salt concentrations (0.5–2.5 mM), reaction temperatures (30°C–70 °C), and reaction times (20–50 min) using the UV-Vis spectrometric method. Optimal conditions for EJ-AuNP biosynthesis were established by confirming the absorption spectra with the highest peak (solid red line): 5 mg/mL EJ concentration (Figure 3A), 2 mM gold salt (Figure 3B), and reaction at 60°C for 40 min (Figures 3C,D). EJ-AuNPs were synthesized under optimal conditions and used for subsequent experiments.

Characterization of the physiochemical properties of EJ-AuNPs

Figure 4A shows the UV-Vis spectra of EJ-AuNPs and EJ. Although no specific absorbance was observed for EJ, EJ-AuNPs exhibited a robust peak at an absorbance of 547 nm. Given the visible color difference between EJ (transparent yellow) and EJ-AuNPs (dark purple), the absorbance spectral change seemed to be derived from the change in the surface plasmon band of the synthesized EJ-AuNPs. Figure 4B shows

the TGA results which yield the oxidation temperature and residual mass of the sample, indicate the stability of the samples at a temperature range of 0°C–600°C. Following decomposition, the residual mass is considered as the ash contents for carbon-based materials (e.g., EJ), but it could be primarily inorganic nanomaterials, residual metal catalysts from synthesis, or impurities, within the sample, for cases of nanomaterials (Mansfield et al., 2014). During the thermal increase to 600°C, severe weight loss (–68.370%) was observed in EJ, but weak weight loss (–7.642%) occurred in EJ-AuNPs, suggesting that the synthesized EJ-AuNPs have better thermal stability than EJ. Furthermore, physicochemical stability of EJ-AuNPs after 1 month of biosynthesis were evaluated through visible observation, UV-VIS spectrum, and TEM analysis (Supplementary Figure S1), suggesting that EJ-AuNPs could be stable without any physicochemical changes at aforementioned condition (Tran et al., 2022). The size distribution profiles analyzed by DLS revealed that the mean intensity, volume, and number distributions of EJ-AuNPs were 48.4, 174.8, and 69.4 nm, respectively (Figure 4C). In order to identify functional groups which
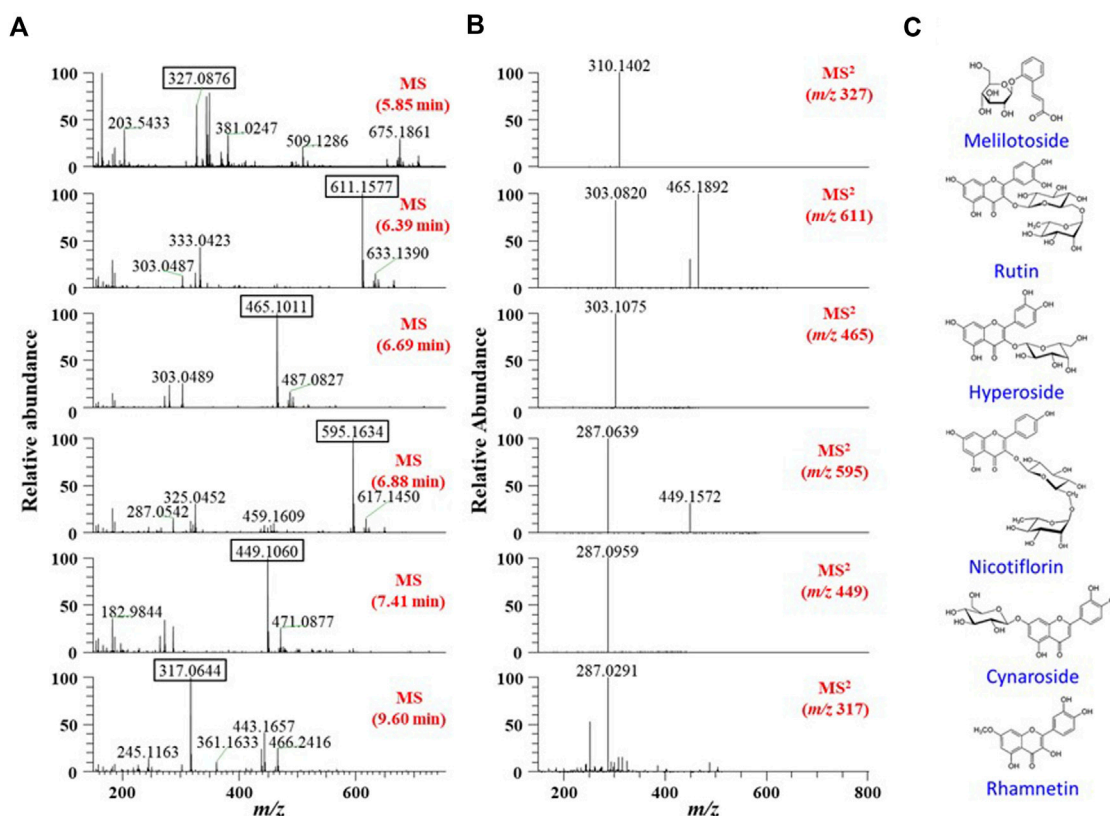
FIGURE 2
(A) MS and (B) MS/MS spectra of six major peaks identified in TIC (Figure 1). Each peak in the spectra was identified using a natural-product database available online and an in-house MS/MS spectral library. (C) Chemical structures of the identified six phytochemicals in EJ.

are responsible for the reduction of Au^{3+} cation and their capping and stabilization, FT-IR spectrum were compared between EJ and EJ-AuNPs (Figures 4D,E, respectively), and possible compound classes were tabulated. The results indicated that EJ and EJ-AuNPs have similar IR spectra each other. According to our in-house spectral library, the broad symmetrical stretching at 3314.7 cm^{-1} in EJ and 3346.6 cm^{-1} in EJ-AuNPs may indicate O–H stretching of the alcohol or N–H stretching of the amine groups. However, given the LC-MS results that flavonoid glycosides were the major components present in the EJ (Figure 1, Figure 2), it is believed that the aforementioned peaks are likely to be the groups of O–H stretching, rather than N–H stretching. The sharp and asymmetrical bands at 2924.4 cm^{-1} and 2855.3 cm^{-1} in EJ and 2921.6 cm^{-1} and 2852.2 cm^{-1} in EJ-AuNPs undoubtedly corresponded to the C–H stretching of alkane, and the peaks at 1731.8 cm^{-1} in EJ and 1728.4 cm^{-1} in EJ-AuNPs probably corresponded to the C=O stretching of the aldehyde (carbonyl) group. The absorption peak at 1642.4 cm^{-1} in EJ-AuNPs and 1598.1 cm^{-1} in EJ correspond to the stretching of alkene, and the peaks at

1371.7 cm^{-1} in EJ and 1452.9 cm^{-1} and 1368.5 cm^{-1} in EJ-AuNPs were associated with to the C–H bending of alkane or aldehyde. The several peaks at 1245–1023 cm^{-1} probably corresponded to the C–O stretching of ester, and the weak characteristic peaks at 879.8 cm-1 in EJ and 980.1 cm^{-1} and 880.6 cm^{-1} in EJ-AuNPs were maybe associated with the C=C bending of alkene.

FE-TEM analysis was performed to identify the predominant shape, size, and crystalline structure of EJ-AuNPs. First, FE-TEM images showed that EJ-AuNPs had a particle size of 31.0–149.1 nm with surface morphologies predominantly of circular, spherical, and polygonal shapes (Figure 5A). To confirm the crystalline nature of the EJ-AuNPs, crystallographic techniques, such as SEAD and XRD, were introduced in this study. The SAED pattern revealed four ring features (111, 200, 220, and 311) observed in the lattice planes, confirming the crystalline structure of the EJ-AuNPs (Figure 5B). This is also verified by the XRD results of EJ-AuNPs, which show diffraction peaks at theta values of 38.27°, 44.31°, 64.65°, and 77.76°, which are calculated for the (111), (200), (220), and (311) planes,
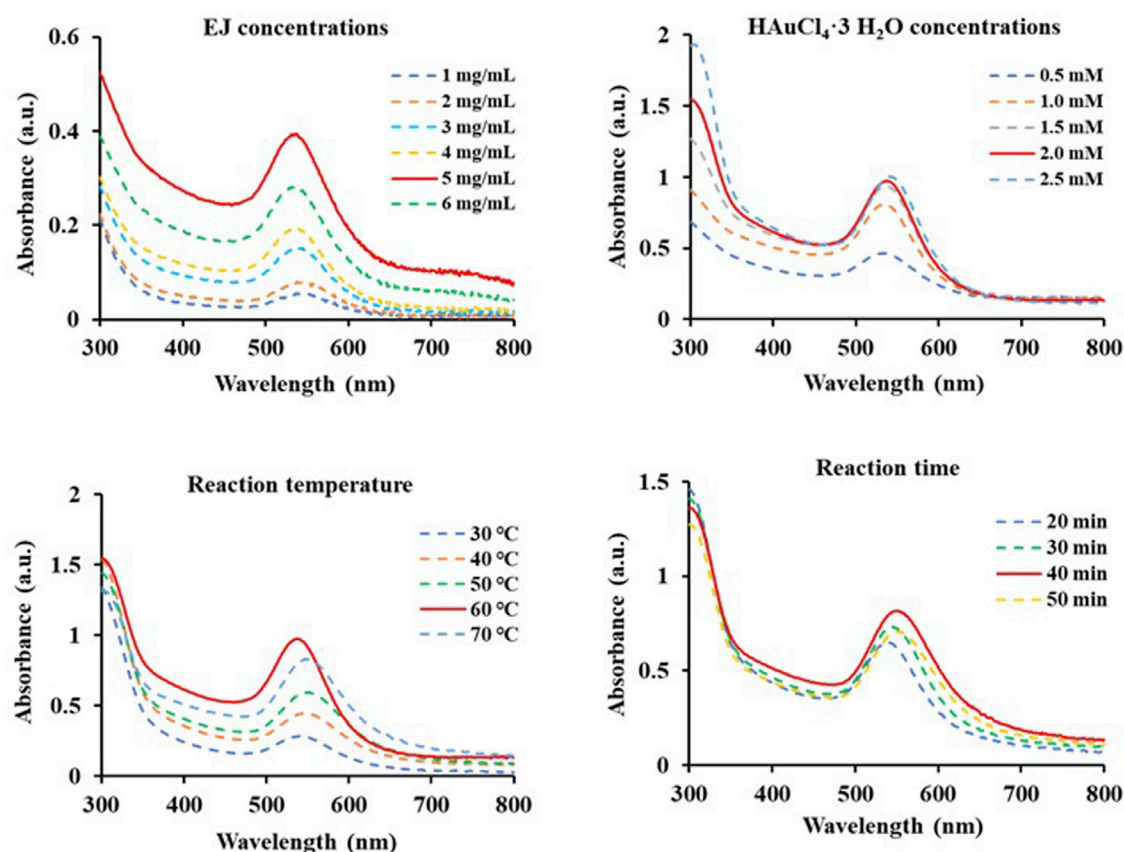
FIGURE 3
Scanning spectra at absorbances of 300−800 nm of diverse EJ-based gold nanoparticles (EJ-AuNPs) synthesized under various conditions depending on EJ concentrations (1−6 mg/ml), HAuCl$_4$●3H$_2$O concentrations (0.5−2.5 mM), reaction temperatures (30°C−70°C), and time (20−50 min). The red solid line in each Figure indicates the optimal condition.

respectively, using Bragg's equation (Figure 5C). Whereas, the XRD spectrum of EJ revealed well-resolved characteristic peaks at theta values of 14.90°, 28.40°, 40.54°, 50.24°, 66.35°, and 73.74°, corresponding to (101), (002), (100), (202), (231), and (251) planes, which are estimated to be amorphous structure with no obvious crystallization (Figure 5C). The purity of the EJ-AuNPs was determined by elemental mapping and EDX spectroscopy. As shown in Figures 5D,E, the distribution of gold elements (red dots) was clearly discernible within the nanoparticles, indicating that EJ-AuNPs were successfully synthesized with high purity. This is also consistent with the result of EDX spectroscopy (Figure 5F), in which only gold element peaks were observed in the synthesized EJ-AuNPs, suggesting that EJ-AuNPs were successfully synthesized without impurities. Excepting the Au peaks, other peaks without symbol observed at 1.9, 8.0, and 8.9 keV were confirmed as copper grids which is used as sample support on the EDX spectrum (Dhandapani et al., 2021).

Effect of EJ and EJ-AuNPs on cytotoxicity in T+I-induced HaCaT cells

The cytotoxic effects of EJ and EJ-AuNPs were evaluated and compared against normal HaCaT cells using a commercial MTT assay and live/dead cell staining. The MTT assay showed that EJ-AuNPs had no cytotoxic effect and even dose-dependently promoted cell proliferation (104.3–119.2%), compared to negative control (NC) cells (Figure 6A). However, significantly reduced viabilities were observed in EJ-treated cells by 12.0–69.4%, compared to NC cells. Figures 6B,C show the representative microscopic images of live/dead staining and their quantified results, respectively. The results showed that EJ-AuNPs did not induce a significant number of dead cells, but a significantly large number of cells were dead (12.1–74.1%) following EJ treatment, similar to the MTT result. These results suggest that EJ-AuNPs were considerably safer than EJ at equivalent concentrations in HaCaT cells.
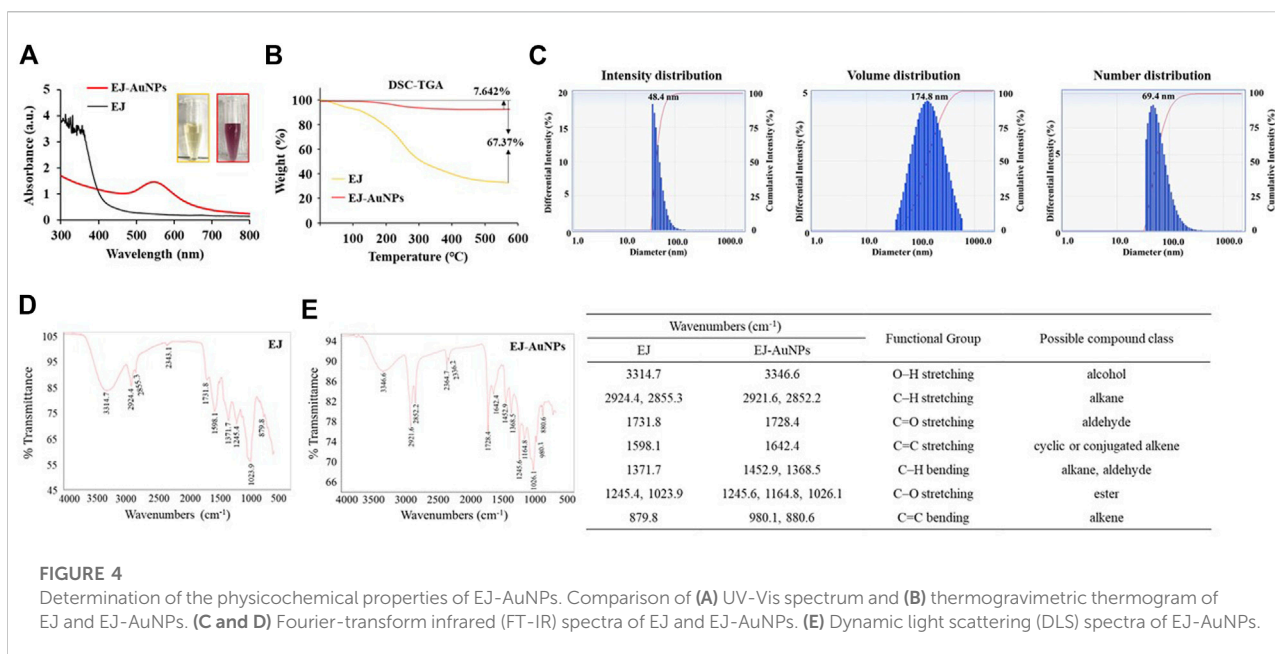
FIGURE 4
Determination of the physicochemical properties of EJ-AuNPs. Comparison of **(A)** UV-Vis spectrum and **(B)** thermogravimetric thermogram of EJ and EJ-AuNPs. **(C and D)** Fourier-transform infrared (FT-IR) spectra of EJ and EJ-AuNPs. **(E)** Dynamic light scattering (DLS) spectra of EJ-AuNPs.
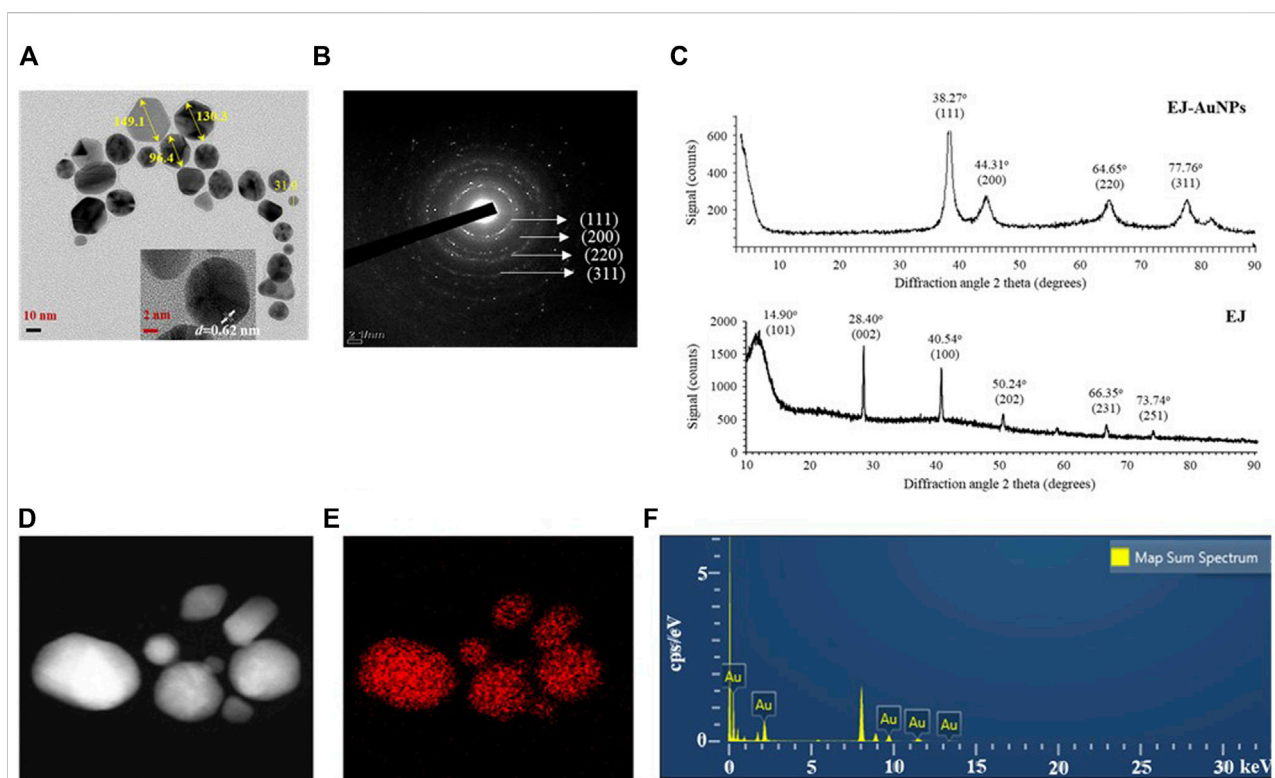
FIGURE 5
Physicochemical characteristics of EJ-AuNPs. **(A)** Transmission electron microscopy (TEM) for determining the surface morphology and particle sizes of EJ-AuNPs. **(B)** Selected area electron diffraction (SAED) pattern and **(C)** X-ray diffraction (XRD) spectrum for determining the crystalline structure of EJ-AuNPs and EJ. **(D)** Electron images of EJ-AuNPs obtained by energy dispersive X-ray (EDX) analysis. **(E)** Gold elemental distribution (red dots) of EJ-AuNPs obtained by EDX analysis. **(F)** EDX spectrum of EJ-AuNPs for identifying elemental distribution.
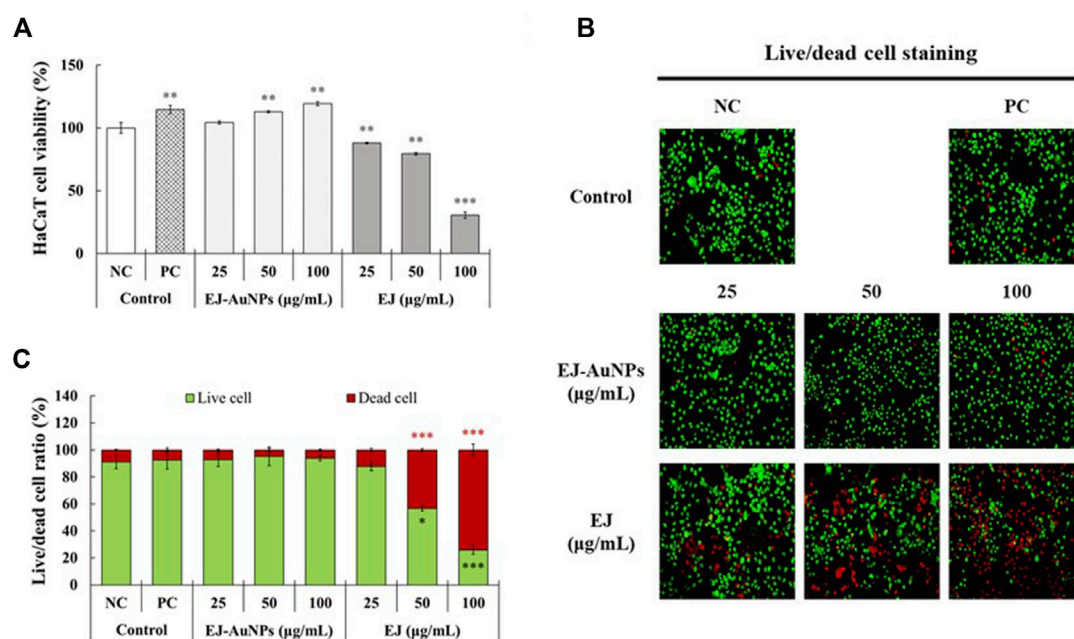
FIGURE 6
Cytotoxic effects of EJ and EJ-AuNPs against HaCaT keratinocytes. **(A)** The MTT assay. **(B)** Microscopic images and their **(C)** quantified results stained by live/dead cell staining dye. Live and dead cells were stained with green and red colors, respectively. NC, negative control treated with medium alone; PC, positive control treated with dexamethasone (20 μg/ml). Asterisks indicate the significant difference between NC and each group. $*p < 0.05$; $**p < 0.01$; $***p < 0.001$.

Effects of EJ-AuNPs on the expression levels of skin dermatitis-associated genes and protein secretion in T+I-induced HaCaT cells

Figure 7 presents the results of skin dermatitis-associated mRNA expression determined by qRT-PCR. Compared to the NC group, excessive expression of pro-inflammatory chemokines, including the regulated on activation, normal T cell expressed and secreted (*RANTES/CCL5*), TARC (*TARC/CCL17*), cutaneous T-cell attracting chemokine (*CTACK/CCL27*), and *IL-8* (*CXCL8*), and interleukin, *IL-6*, were induced in T+I-treated HaCaT cells. Dexamethasone treatment significantly decreased T+I-stimulated gene expression in HaCaT cells. Compared to the T+I group, the expression levels of *RANTES*, *TARC*, *CTACK*, *IL-6*, and *IL-8* genes were significantly downregulated by EJ-AuNP treatment. Next, we evaluated the inhibitory effects of EJ-AuNPs on skin dermatitis-associated cytokine secretion in T+I-induced keratinocytes using ELISA. As expected, T+I-stimulation induced significant secretion of IL-6, IL-8, and TARC in HaCaT keratinocytes, and dexamethasone treatment significantly decreased the level of T+I-stimulated secretion of these pro-inflammatory cytokines (Figures 8A–C). The increased levels of IL-6, IL-8, and TARC after T+I treatment were

significantly decreased in a concentration-dependent manner following EJ-AuNP treatment. These results demonstrate that EJ-AuNPs effectively suppressed the skin dermatitis-associated mediators at the gene expression and protein secretion levels. We further tested the effect of EJ and EJ-AuNPs on the cellular ROS production capacity of T+I-treated HaCaT cells. As shown in Figure 8D, ROS production was significantly increased by T+I stimulation, and significantly decreased by dexamethasone treatment. Compared to T+I-treated cells, ROS production was significantly and concentration-dependently decreased by both EJ and EJ-AuNPs treatments, but higher reduction effects were observed in cells treated with EJ-AuNPs than in those treated with EJ.

Identification of the molecular mechanism underlying skin dermatitis inhibition by EJ-AuNPs

Next, we explored the signaling pathway associated with skin dermatitis inhibition by EJ-AuNPs in T+I-treated HaCaT cells. Figure 9 shows the western blotting images and quantification of phosphorylation associated with the mitogen-activated protein kinase (MAPK) (Figure 9A) and nuclear factor kappa-light-chain-enhancer of activated B cells (NF-κB) (Figure 9B)
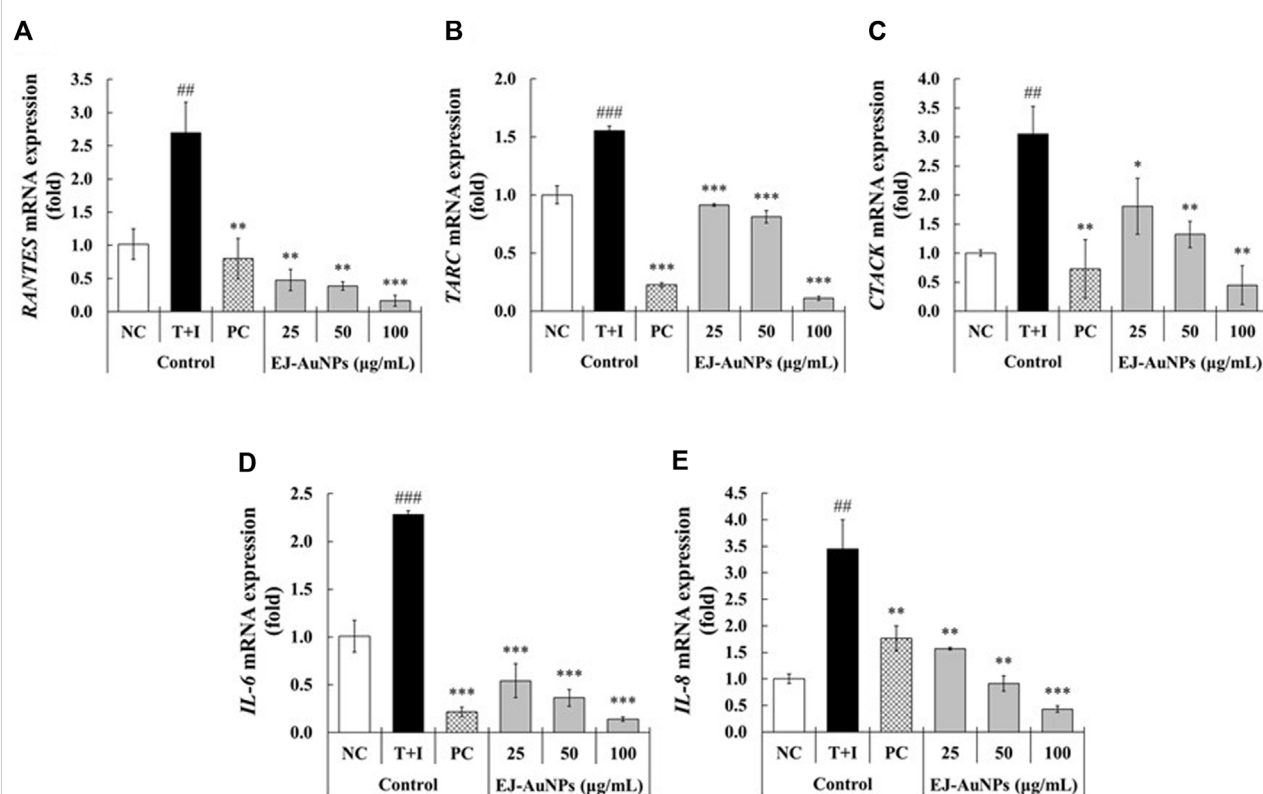
FIGURE 7
Effect of EJ-AuNPs on the expression levels of pro-inflammatory genes, including **(A)** C-C motif chemokine ligand 5 (*CCL5*)/regulated on activation, normal T cell expressed and secreted (*RANTES*), **(B)** thymus and activation-regulated chemokine (*TARC/CCL17*), **(C)** cutaneous T-cell attracting chemokine (*CTACK/CCL27*), **(D)** interleukin *(IL)-6*, and **(E)** *IL-8/CXCL-8*, in the tumor necrosis factor-alpha and interferon-gamma (TNF-α and IFN-γ; T+I)-treated HaCaT keratinocytes. NC, negative control treated with medium alone; T+I, inflammation-induced control treated with T+I alone; PC, positive control treated with dexamethasone (20 μg/ml) followed by T+I stimulation. EJ-AuNPs, sample groups treated with EJ-AuNPs followed by T+I stimulation. The crosshatch marks indicate the significant differences between NC and T+I, and asterisks indicate the significant differences between T+I and each group. *$p < 0.05$; ** and ##, $p < 0.01$; *** and ###, $p < 0.001$.

signaling pathways. T+I treatment significantly elevated the phosphorylation levels of three MAPKs (p38, JNK, and ERK) and NF-κB p65 without changing their corresponding total protein levels in HaCaT cells. Interestingly, T+I treatment significantly increased the phosphorylation levels of nuclear factor of kappa light polypeptide gene enhancer in B-cells inhibitor, alpha (IκBα), but significantly decreased the total protein levels. Following dexamethasone treatment, the levels of phosphorylated p38, JNK, ERK, IκBα, and p65 were significantly reduced, while the expression levels of intact IκBα were significantly upregulated. EJ-AuNP treatment significantly and concentration-dependently reduced the phosphorylation levels of three MAPKs (p38, ERK, and JNK) and two NF-κB-related molecules (IκBα and p65). In addition, the expression levels of intact IκBα were significantly upregulated by EJ-AuNP treatment in a concentration-dependent manner. Based on our finding, mechanism of action of anti-inflammatory activity mediated by EJ-AuNPs in TNF-α/IFN-γ-induced skin inflammatory HaCaT cells were proposed in Figure 10. These

results demonstrate that the inhibitory effect on T+I-stimulated inflammation in HaCaT cells is closely associated with EJ-AuNP-mediated suppression of MAPK and NF-κB signaling.

Discussion

According to recent studies, a number of natural plants have been shown to ameliorate ISDs (Yang et al., 2015; Lim et al., 2016; Yang et al., 2018); however, there are some concerns and limitations to the use of plant extracts and their active compounds in industrial applications due to their low solubility, stability, biocompatibility, and bioavailability (Kyriakoudi et al., 2021). Thus, studies aimed at overcoming these limitations are in high demand. It is well known that AuNPs that have unique physicochemical and multiple surface functionalities have several advantages, such as higher biodegradability, wide flexibility, improved stability, and lower possible adverse effects, facilitating their widespread use in
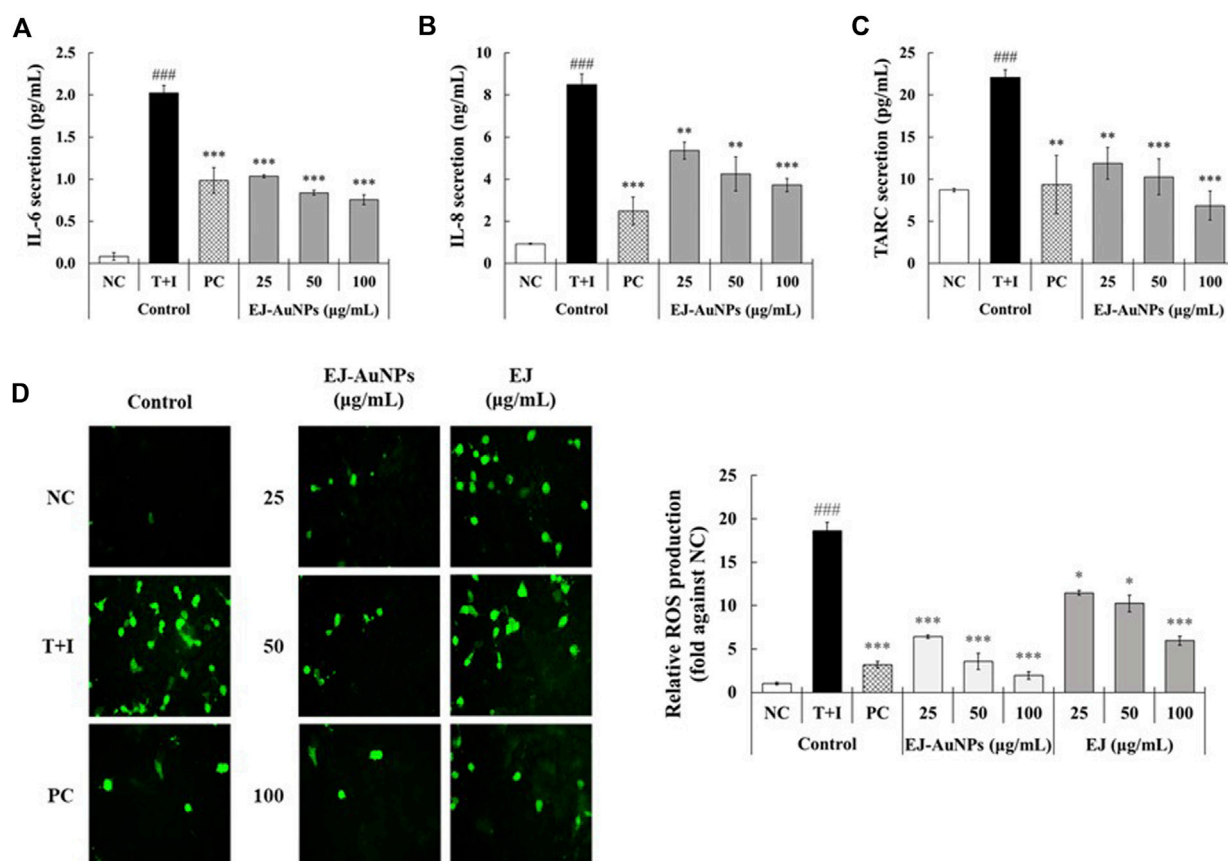
FIGURE 8
Effect of EJ-AuNPs on the secretion of pro-inflammatory cytokines, including **(A)** IL-6, **(B)** IL-8, and **(C)** TARC/CCL17, and production of intracellular **(D)** reactive oxygen species (ROS) in tumor necrosis factor-alpha and interferon-gamma (TNF-α and IFN-γ; T+I)-treated HaCaT keratinocytes. NC, negative control treated with medium alone; T+I, inflammation-induced control treated with T+I alone; PC, positive control treated with dexamethasone (20 μg/ml) followed by T+I stimulation. EJ-AuNPs, sample groups treated with EJ-AuNPs followed by T+I stimulation. The crosshatch marks indicate the significant differences between NC and T+I, and asterisks indicate the significant differences between T+I and each group. *$p < 0.05$; **$p < 0.01$; *** and ###, $p < 0.001$.

biomedical field (Yeh et al., 2012). In the present study, we aimed to synthesize plant-loaded AuNPs by a biological process using the Korean endemic medicinal plant, EJ. First, the major secondary metabolites were confirmed as candidates for bioactive ingredients in the EJ extract using UHPLC equipped with electrospray ionization source (ESI) and MS/MS. As listed in Supplementary Table S1, data-dependent acquisition was accomplished using an ion trap mass spectrometer according to the previous method reported by Kim et al. (2021). Upon MS analysis, flavonoid glycosides, including melilotoside, rutin, hyperoside, nictoflorin, cynaroside, and rhamnetin, were putatively identified as the major phytochemicals in the EJ extract (Figure 1, Figure 2). Until now, only a few studies have been reported on either the physiological activity or active ingredients of EJ. With respect to the major chemical constituents, a previous study identified fatty alcohols, acids, terpenes, phytosterols, phenolic acids, and flavonoids in EJ leaves

(Phan et al., 2021). However, the above-mentioned flavonoid glycosides confirmed in the present study appear to be the first identification of these components in EJ. Nevertheless, as MS analysis generally only facilitates the qualitative identification of putative compounds (Xiao et al., 2012), further studies are necessary for the quantitative identification of the above-mentioned compounds and other bioactive compounds in EJ.

Next, we established an optimal system for EJ-AuNP biosynthesis by monitoring the reaction conditions, such as EJ and gold salt concentrations, reaction pH, and time. Finally, EJ-AuNPs were biosynthesized under the optimized system (Figure 3). In general, the biosynthesis of AuNPs take place in two steps: reduction of Au^{3+} into Au^0 and its agglomeration and stabilization to form the AuNPs (Sheny et al., 2011). Given that various secondary metabolites, such as phenolic acids, flavonoids, terpenoids, and polyphenols in the ethanolic extracts of plants can mainly participate in the AuNPs biosynthesis (Mikhailova,
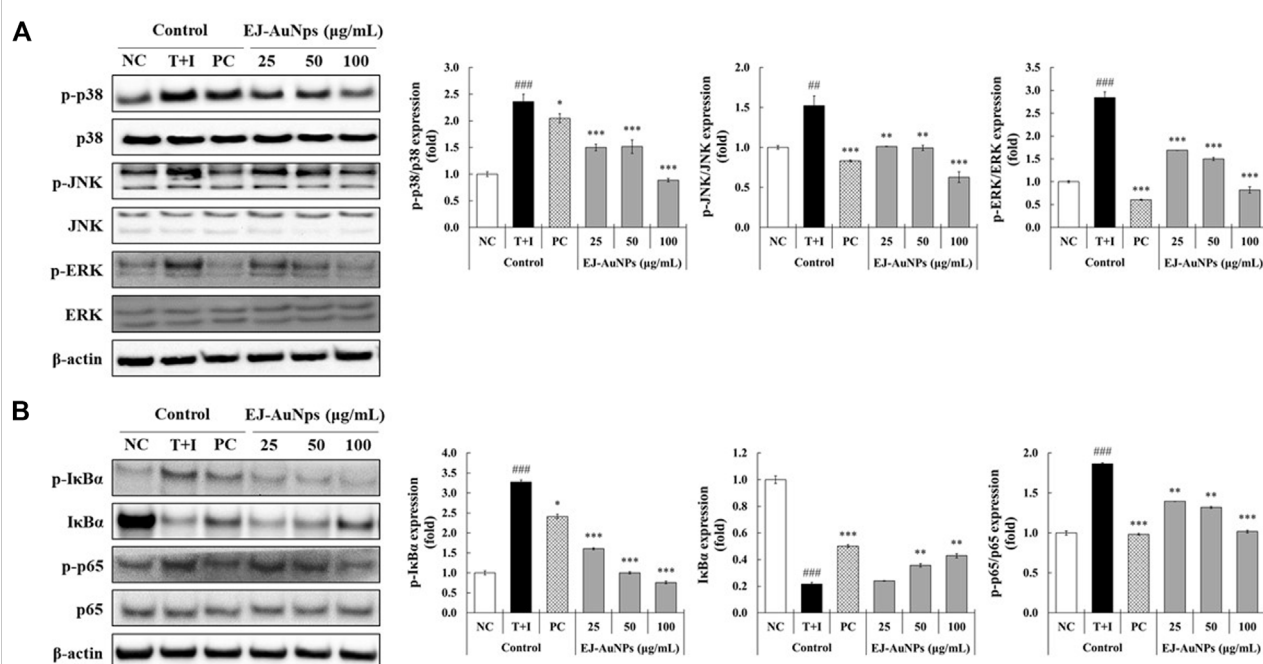
FIGURE 9
Effects of EJ-AuNPs on the **(A)** mitogen-activated protein kinase (MAPK) and **(B)** nuclear factor (NF)-κB signaling pathways in tumor necrosis factor-alpha and interferon-gamma (TNF-α and IFN-γ; T+I)-treated HaCaT keratinocytes. Results are presented as blotting images of expressed respective proteins and their quantification calculated by fold ratio of phosphorylated form/total form, except IκBα. NC, negative control treated with medium alone; T+I, inflammation-induced control treated with T+I alone; PC, positive control treated with dexamethasone (20 μg/ml) followed by T+I stimulation. EJ-AuNPs, sample groups treated with EJ-AuNPs followed by T+I stimulation. The crosshatch marks indicate the significant differences between NC and T+I, and asterisks indicate the significant differences between T+I and each group. *$p < 0.05$; ** and ##, $p < 0.01$; *** and ###, $p < 0.001$.

2021), it can be speculated that aforementioned flavonoids in EJ may be responsible for the reduction in Au ions ($Au^{3+} \rightarrow Au^0$) and corresponding nanoparticles formation. Characterization of nanoparticles can be considered as a collection of analytical results obtained from the physical and chemical characteristics on the nanoparticles' surface to create knowledge on synthesis, properties, and applications of the nanoparticles (Vijayakumar, 2019). Several microscopic and spectrometric technique were used in this study to measure, quantify, and image the surface properties of the synthesized EJ-AuNPs. Using those analyses, the nanoparticles were physicochemically characterized in terms of particle size, shape, and crystalline nature (Figure 4, Figure 5). A helpful information on the characterization techniques for nanoparticles can be available in recently published review article (Mourdikoudis et al., 2018). Consequently, the EJ-AuNPs were synthesized with various surface morphologies, such as circular, spherical, and polygonal shapes, with particle sizes of approximately 50–150 nm and no impurities. TGA result revealed that the synthesized EJ-AuNPs also showed better thermal stability than EJ, suggesting their potential for industrial applications. Furthermore, FT-IR analysis was performed to identify the presence of different functional

groups in EJ and EJ-AuNPs at various positions. Although the biosynthetic mechanism of AuNPs would not been fully elucidated, several studies have reported FT-IR analysis is helpful to explore plant-derived AuNPs grafted on the surface characteristics and to presume the possible interactions of the AuNPs with different functional groups (Lokina et al., 2014; Ajitha et al., 2015; Khandanlou et al., 2020; Mikhailova, 2021). Our IR spectra displayed that EJ-AuNPs contain aromatic, hydroxyl, and carbonyl (aldehyde) groups as the functional groups which would have been derived from flavonoids, such as melilotoside, rutin, hyperoside, nictoflorin, cynaroside, and rhamnetin of EJ. A number of studies have reported that such flavonoids can be strongly involved in the reduction, capping, and stabilization processes in AuNPs biosynthesis (Ajitha et al., 2015; Khandanlou et al., 2020). It can be thus speculated that the functional groups, especially hydroxyl and carbonyl groups, in the aforementioned flavonoids present in EJ play an important role as reducing, capping, and stabilizing agents for EJ-AuNPs formation (Shankar et al., 2004; Sheny et al., 2011; Lokina et al., 2014).

The results of cytotoxic evaluation revealed that EJ-AuNPs induced the promoting effect of normal keratinocyte cell
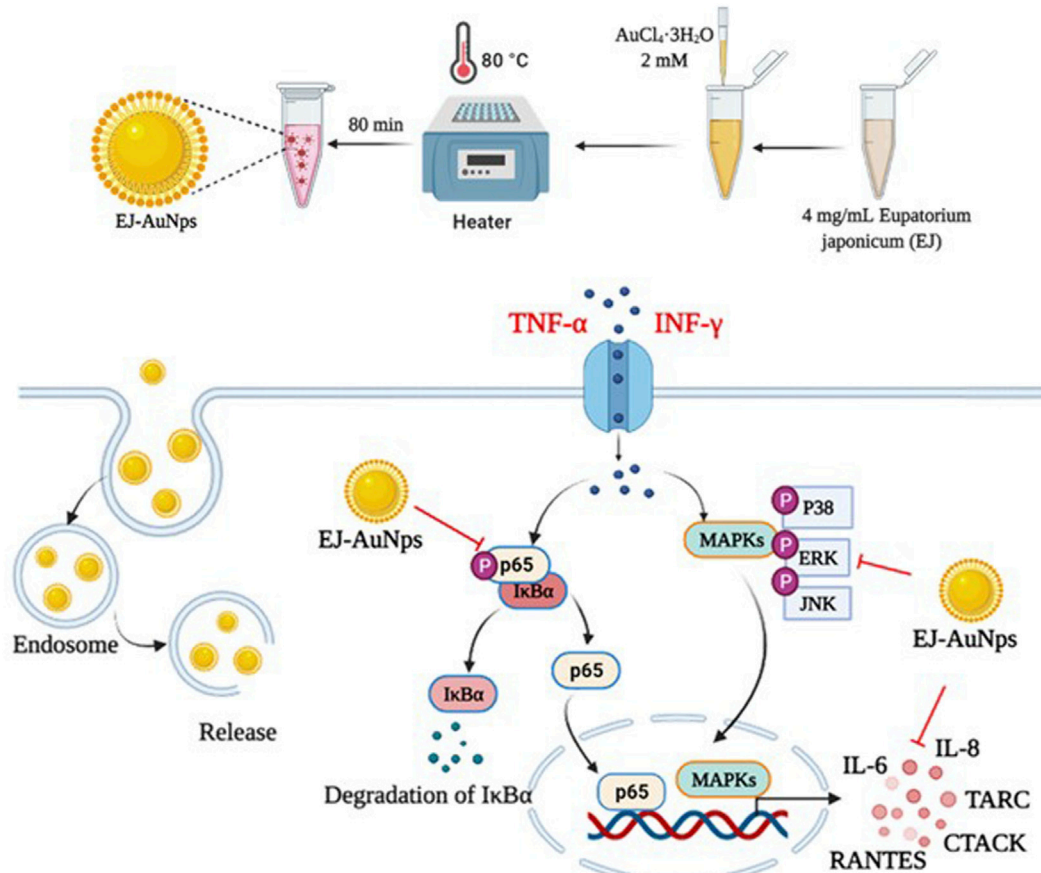
FIGURE 10
Proposed molecular mechanism of anti-inflammatory activity induced by EJ-AuNPs in TNF-α/IFN-γ-induced skin inflammatory HaCaT cells.

proliferation, although EJ showed a significant cytotoxic effect at equivalent concentrations, leading to the favorable safety of EJ-AuNPs when applied to human keratinocytes compared to EJ alone. This seems to be the first study to propose the possibility for lowering cytotoxicity of EJ by forming nanoformulation. From the subsequent experiments, except for EJ where cytotoxic effect was confirmed, only EJ-AuNPs were supposed to evaluate for anti-inflammatory activity.

We further investigated the effects of EJ-AuNPs on ISDs in an inflammatory epidermal keratinocyte model. Actually, during skin inflammatory reaction, epidermal keratinocytes that constitute nearly 90% of epidermal cells play a pivotal role in the progression and pathogenesis of dermatitis-related diseases by communicating with other cells (Lim et al., 2015; Kim et al., 2018). Keratinocytes and their secreted chemokines, primarily CC chemokine ligands (CCLs), including CCL5 (RANTES) (Yang et al., 2018), CCL17 (TARC) (Werfel, 2009), CCL22 (macrophage-derived chemokine, MDC) (Lim et al., 2015), CCL27 (CTACK) (Kakinuma et al., 2003), and CXC chemokine ligand

(CXCLs, such as CXCL8 (IL-8) (Mirandola et al., 2011), are regarded as triggers for the progression of skin inflammatory diseases by mediating the recruitment of immune cells into the inflammatory skin tissue (Homey et al., 2006; Sugaya, 2015). In particular, these inflammatory chemokines can be highly expressed in keratinocytes when stimulated with macrophages or T cell-secreting cytokines, such as TNF-α and IFN-γ (Albanesi et al., 2005; Chieosilapatham et al., 2021). Accordingly, recent studies exploring the potential medications for ISDs have concentrated on the downregulation of these inflammatory chemokines and their underlying mechanisms of action in T+I-induced keratinocytes (Albanesi and Pastore, 2010; Lim et al., 2015; Yang et al., 2015; Juráňová et al., 2017). Our qRT-PCR and ELISA results demonstrated that EJ-AuNPs effectively suppressed the T+I-stimulated inflammatory chemokines (RANTES, TARC, CTACK, and IL-8) in addition to IL-6 in HaCaT keratinocytes (Figure 7, Figure 8). This suggests the possibility of using EJ-AuNPs as anti-inflammatory candidates against ISDs. In addition, the ROS staining

results shown in Figure 8D indicate that these anti-inflammatory effects of EJ-AuNPs are highly associated with the suppression of T+I-stimulated intracellular ROS production in HaCaT cells. Excessive ROS accumulation can cause oxidative stress followed by critical damage of HaCaT cells (Shim et al., 2008; Han et al., 2021). Our results also suggest that EJ-AuNPs can be effective in protecting against this oxidative stress-mediated cell death in ISDs.

Cytokines are important mediators of the immune system, including the inflammatory response. Exposure of keratinocytes to Th cell-secreted cytokines, such as TNF-α and IFN-γ, triggers the undue production of inflammatory cytokines (mainly chemokines, e.g., CCL and CXCL), causing explosive immune responses via migration of leukocytes into inflammatory lesions in the skin (Homey et al., 2006; Nedoszytko et al., 2014). In particular, the MAPK and NF-κB cascades are the best-studied key signaling pathways within the cells involved in various inflammatory responses, such as the keratinocytes (Yang et al., 2015; Yang et al., 2018). MAPK signaling plays important roles in diverse pathological conditions and in the regulation of various cellular functions, including cell differentiation, proliferation, mitosis, survival, and death. Recent studies have reported that mitogenic and proliferative stimuli favorably activate the ERK pathway, whereas inflammatory and environmental stresses preferentially stimulate the activation of p38 and JNK (Khorasanizadeh et al., 2017). Nevertheless, three distinct MAPKs are considered to be key target molecules for the treatment of various diseases, including allergic inflammatory diseases (Khorasanizadeh et al., 2017; Sur et al., 2019). Recent studies have proposed that the nanoparticle-mediated targeting of MAPK is an attractive therapeutic strategy for treating various diseases (Basu et al., 2009; De Araújo Jr et al., 2018). NF-κB is closely involved in the pathogenesis of various inflammatory diseases, such as asthma, bronchitis, colitis, lupus vulgaris, and sclerosis (atherogenic and multiple). NF-κB family of inducible transcription factors are composed of five subfamilies: NF-κB1 (p105/p50), NF-κB2 (p100/p52), RelA (p65), RelB, and c-Rel (Caamaño and Hunter, 2002; Liu et al., 2017). In unstimulated stages, NF-κB proteins are sequestered by a family of their inhibitor proteins, such as IκBα, IκBβ, and IκBγ (Liu et al., 2017). When cells are stimulated by various external stimuli, the inactive form of the NF-κB/IκB complex is activated by IκB phosphorylation and released from the NF-κB protein (Liu et al., 2017). The liberated NF-κB proteins translocate into the nucleus to promote the inflammatory response by inducing the transcription of proinflammatory genes (Shin et al., 2021). To explore the intracellular mechanism underlying EJ-AuNP-driven anti-inflammatory effects, the MAPK and NF-κB signaling pathways were investigated. Figure 9

indicates that the phosphorylation of three MAPKs (ERK, JNK, and p38) and two NF-κB signaling molecules (IκBα and p65) was markedly inhibited by EJ-AuNPs treatment. Taken together, our study demonstrates that the inhibitory effects of EJ-AuNPs on T+I-induced chemokine and cytokine production are significantly associated with the downregulation of the MAPK and NF-κB intracellular signaling pathways. However, the present study has a limitation to be addressed in the further work. That is, the safety and anti-inflammatory efficacy of EJ-AuNPs should be evaluated by *in vivo* system to clearly elucidate their effectiveness and increase their possibility of using as anti-inflammatory agents industrially.

Conclusion

Until now, studies have rarely reported on the application of plant-derived AuNPs for the skin health. To investigate the possibility of using the plant-derived AuNPs as anti-dermatitis candidate, the present study was aimed to prepare novel AuNPs using EJ extracts and evaluate their physicochemical characteristics, anti-inflammatory efficacy, and molecular mechanism. Novel EJ-based gold nanoparticles (EJ-AuNPs) were successfully prepared using a green synthesis method, and the optimized conditions and physicochemical properties of the EJ-AuNPs were characterized using various microscopic and spectrometric analyses. In an *in vitro* skin inflammation model using T+I-induced HaCaT cells, the synthesized EJ-AuNPs inhibited the activation of MAPK and NF-κB signaling, and the inhibition of T+I-stimulated inflammatory mediators (ROS, chemokines, and cytokines) may be associated with the suppression of these pathways. Our study offers preliminary results and a valuable strategy for the development of novel anti-skin dermatitis candidates using plant extract-based AuNPs. The study also suggests a possibility that biological green synthesis of gold nanoparticles from EJ may be useful for exerting anti-inflammatory potential while reducing cytotoxic effect of EJ. However, the present study has a limitation to be addressed in the further work. That is, the safety and anti-inflammatory efficacy of EJ-AuNPs should be evaluated by *in vivo* system to clearly elucidate their effectiveness and increase their possibility of using as anti-inflammatory agents industrially.

Data availability statement

The original contributions presented in the study are included in the article/Supplementary Material, further inquiries can be directed to the corresponding authors.

Author contributions

XYX prepared nanoparticle sample, cultured and maintained the animal cells, and evaluated anti-inflammatory activity of the sample. J-KK and WJK did analytical methods for characterization of the sample. XYX, S-KM, and HK analyzed and validated the raw data and prepared the figures. XYX, S-KM, and HK wrote the original draft of manuscript, and HK and Y-JK reviewed and revised the manuscript. HK supervised overall process of the experiment. All authors read and approved the final manuscript.

Funding

Conflict of interest

The authors declare that the research was conducted in the absence of any commercial or financial relationships that could be construed as a potential conflict of interest.

Publisher's note

All claims expressed in this article are solely those of the authors and do not necessarily represent those of their affiliated organizations, or those of the publisher, the editors and the reviewers. Any product that may be evaluated in this article, or claim that may be made by its manufacturer, is not guaranteed or endorsed by the publisher.

Supplementary material

The Supplementary Material for this article can be found online at: https://www.frontiersin.org/articles/10.3389/fphar.2022.1055378/full#supplementary-material

References

Abdel-Mottaleb, M. M. A., Try, C., Pellequer, Y., and Lamprecht, A. (2014). Nanomedicine strategies for targeting skin inflammation. *Nanomedicine* 9 (11), 1727–1743. doi:10.2217/nnm.14.74

Ahmed, S., Ikram, S., and Yudha, S. S. (2016). Biosynthesis of gold nanoparticles: A green approach. *J. Photochem. Photobiol. B* 161, 141–153. doi:10.1016/j.jphotobiol.2016.04.034

Ahmed, S., and Ikram, S. (2015). Synthesis of gold nanoparticles using plant extract: An overview. *Nano Res. Appl.* 1 (1), 5.

Ajitha, B., Ashok Kumar Reddy, Y., and Sreedhara Reddy, P. (2015). Green synthesis and characterization of silver nanoparticles using Lantana camara leaf extract. *Mat. Sci. Eng. C Mat. Biol. Appl.* 49, 373–381. doi:10.1016/j.msec.2015.01.035

Albanesi, C., and Pastore, S. (2010). Pathobiology of chronic inflammatory skin diseases: Interplay between keratinocytes and immune cells as a target for anti-inflammatory drugs. *Curr. Drug Metab.* 11 (3), 210–227. doi:10.2174/138920010791196328

Albanesi, C., Scarponi, C., Giustizieri, M. L., and Girolomoni, G. (2005). Keratinocytes in inflammatory skin diseases. *Curr. Drug Targets. Inflamm. Allergy* 4 (3), 329–334. doi:10.2174/1568010054022033

Bahadar, H., Maqbool, F., Niaz, K., and Abdollahi, M. (2016). Toxicity of nanoparticles and an overview of current experimental models. *Iran. Biomed. J.* 20 (1), 1–11. doi:10.7508/ibj.2016.01.001

Basu, S., Harfouche, R., Soni, S., Chimote, G., Mashelkar, R. A., and Sengupta, S. (2009). Nanoparticle-mediated targeting of MAPK signaling predisposes tumor to chemotherapy. *Proc. Natl. Acad. Sci. U. S. A.* 106 (19), 7957–7961. doi:10.1073/pnas.0902857106

Caamaño, J., and Hunter, C. A. (2002). NF-kappaB family of transcription factors: Central regulators of innate and adaptive immune functions. *Clin. Microbiol. Rev.* 15 (3), 414–429. doi:10.1128/CMR.15.3.414-429.2002

Campos, E. V. R., Proença, P. L. F., Costa, T. G. d., de Lima, R., Hedtrich, S., Fraceto, L. F., et al. (2021). Hydrogels containing budesonide-loaded nanoparticles to facilitate percutaneous absorption for atopic dermatitis treatment applications. *ACS Appl. Polym. Mat.* 3 (9), 4436–4449. doi:10.1021/acsapm.1c00021

Carretero, M., Guerrero-Aspizua, S., Illera, N., Galvez, V., Navarro, M., García-García, F., et al. (2016). Differential features between chronic skin inflammatory diseases revealed in skin-humanized psoriasis and atopic dermatitis mouse models. *J. Invest. Dermatol.* 136 (1), 136–145. doi:10.1038/JID.2015.362

Chen, L., Deng, H., Cui, H., Fang, J., Zuo, Z., Deng, J., et al. (2017). Inflammatory responses and inflammation-associated diseases in organs. *Oncotarget* 9 (6), 7204–7218. doi:10.18632/oncotarget.23208

Chieosilapatham, P., Kiatsurayanon, C., Umehara, Y., Trujillo-Paez, J. V., Peng, G., Yue, H., et al. (2021). Keratinocytes: Innate immune cells in atopic dermatitis. *Clin. Exp. Immunol.* 204 (3), 296–309. doi:10.1111/cei.13575

Dai, G., Wang, C., Tang, W., Liu, J., and Xue, B. (2020). A 90-day oral toxicity study of the ethanol extract from *Eupatorium japonicum* Thunb and foeniculum vulgare in rats. *Biomed. Res. Int.* 2020, 6859374. doi:10.1155/2020/6859374

De Araújo, R. F., Jr, Pessoa, J. B., Cruz, L. J., Chan, A. B., De Castro Miguel, E., Cavalcante, R. S., et al. (2018). Apoptosis in human liver carcinoma caused by gold nanoparticles in combination with carvedilol is mediated via modulation of MAPK/Akt/mTOR pathway and EGFR/FAAD proteins. *Int. J. Oncol.* 52 (1), 189–200. doi:10.3892/ijo.2017.4179

Dhandapani, S., Xu, X., Wang, R., Puja, A. M., Kim, H., Perumalsamy, H., et al. (2021). Biosynthesis of gold nanoparticles using Nigella sativa and Curtobacterium proimmune K3 and evaluation of their anticancer activity. *Mat. Sci. Eng. C Mat. Biol. Appl.* 127, 112214. doi:10.1016/j.msec.2021.112214

Drakaki, E., Dessinioti, C., and Antoniou, C. V. (2014). Air pollution and the skin. *Front. Environ. Sci.* 2 (11), 1–6. doi:10.3389/fenvs.2014.00011

Dykman, L., and Khlebtsov, N. (2012). Gold nanoparticles in biomedical applications: Recent advances and perspectives. *Chem. Soc. Rev.* 41 (6), 2256–2282. doi:10.1039/c1cs15166e

Ghasemian, M., Owlia, S., and Owlia, M. B. (2016). Review of anti-inflammatory herbal medicines. *Adv. Pharmacol. Sci.* 2016, 9130979. doi:10.1155/2016/9130979

Gu, G.-J., Ahn, S.-I., Lim, S. J., Paek, J. H., Kim, S., Lim, S. S., et al. (2014). *Eupatorium japonicum* extract regulates inflammation through suppression of the TRIF-dependent signaling pathway of toll-like receptors. *Food Sci. Biotechnol.* 23 (2), 587–592. doi:10.1007/s10068-014-0080-x

Han, E. J., Kim, H.-S., Jung, K., Asanka Sanjeewa, K. K., Iresha Nadeeka Madushani Herath, K. H., Lee, W., et al. (2021). *Sargassum horneri* ethanol extract ameliorates TNF-α/IFN-γ-induced inflammation in human keratinocytes and TPA-induced ear edema in mice. *Food Biosci.* 39, 100831. doi:10.1016/j.fbio.2020.100831

Homey, B., Steinhoff, M., Ruzicka, T., and Leung, D. Y. (2006). Cytokines and chemokines orchestrate atopic skin inflammation. *J. Allergy Clin. Immunol.* 118 (1), 178–189. doi:10.1016/j.jaci.2006.03.047

Juráňová, J., Franková, J., and Ulrichová, J. (2017). The role of keratinocytes in inflammation. *J. Appl. Biomed.* 15 (3), 169–179. doi:10.1016/j.jab.2017.05.003

Kakinuma, T., Saeki, H., Tsunemi, Y., Fujita, H., Asano, N., Mitsui, H., et al. (2003). Increased serum cutaneous T cell-attracting chemokine (CCL27) levels in patients with atopic dermatitis and psoriasis vulgaris. *J. Allergy Clin. Immunol.* 111 (3), 592–597. doi:10.1067/mai.2003.114

Kakkar, V., Kumar, M., and Saini, K. (2019). An overview of atopic dermatitis with a focus on nano-interventions. *EMJ Innov.* 3 (1), 44

Khandanlou, R., Murthy, V., and Wang, H. (2020). Gold nanoparticle-assisted enhancement in bioactive properties of Australian native plant extracts, Tasmannia lanceolata and Backhousia citriodora. *Mat. Sci. Eng. C Mat. Biol. Appl.* 112, 110922. doi:10.1016/j.msec.2020.110922

Khorasanizadeh, M., Eskian, M., Gelfand, E. W., and Rezaei, N. (2017). Mitogen-activated protein kinases as therapeutic targets for asthma. *Pharmacol. Ther.* 174, 112–126. doi:10.1016/j.pharmthera.2017.02.024

Kim, T. H., Kim, W. J., Park, S. Y., Kim, H., and Chung, D. K. (2021). *In vitro* anti-wrinkle and skin-moisturizing effects of evening primrose (*Oenothera biennis*) sprout and identification of its active components. *Processes* 9 (1), 145. doi:10.3390/pr9010145

Kim, Y. A., Kim, D. H., Park, C. B., Park, T. S., and Park, B. J. (2018). Anti-inflammatory and skin-moisturizing effects of a flavonoid glycoside extracted from the aquatic plant *Nymphoides indica* in human keratinocytes. *Molecules* 23 (9), 2342. doi:10.3390/molecules23092342

Krishnaswamy, K., Vali, H., and Orsat, V. (2014). Value-adding to grape waste: Green synthesis of gold nanoparticles. *J. Food Eng.* 142, 210–220. doi:10.1016/j.jfoodeng.2014.06.014

Kyriakoudi, A., Spanidi, E., Mourtzinos, I., and Gardikis, K. (2021). Innovative delivery systems loaded with plant bioactive ingredients: Formulation approaches and applications. *Plants* 10 (6), 1238. doi:10.3390/plants10061238

Lim, H. S., Jin, S. E., Kim, O. S., Shin, H. K., and Jeong, S. J. (2015). Alantolactone from *Saussurea lappa* exerts antiinflammatory effects by inhibiting chemokine production and STAT1 phosphorylation in TNF-α and IFN-γ-induced in HaCaT cells. *Phytother. Res.* 29 (7), 1088–1096. doi:10.1002/ptr.5354

Lim, S. J., Kim, M., Randy, A., Nam, E. J., and Nho, C. W. (2016). Effects of *Hovenia dulcis* Thunb. extract and methyl vanillate on atopic dermatitis-like skin lesions and TNF-α/IFN-γ-induced chemokines production in HaCaT cells. *J. Pharm. Pharmacol.* 68 (11), 1465–1479. doi:10.1111/jphp.12640

Liu, T., Zhang, L., Joo, D., and Sun, S.-C. (2017). NF-κB signaling in inflammation. *Signal Transduct. Target. Ther.* 2 (1), 17023. doi:10.1038/sigtrans.2017.23

Lokina, S., Suresh, R., Giribabu, K., Stephen, A., Lakshmi Sundaram, R., and Narayanan, V. (2014). Spectroscopic investigations, antimicrobial, and cytotoxic activity of green synthesized gold nanoparticles. *Spectrochim. Acta. A Mol. Biomol. Spectrosc.* 129, 484–490. doi:10.1016/j.saa.2014.03.100

Mansfield, E., Tyner, K. M., Poling, C. M., and Blacklock, J. L. (2014). Determination of nanoparticle surface coatings and nanoparticle purity using microscale thermogravimetric analysis. *Anal. Chem.* 86 (3), 1478–1484. doi:10.1021/ac402888v

Mikhailova, E. O. (2021). Gold nanoparticles: Biosynthesis and potential of biomedical application. *J. Funct. Biomater.* 12 (4), 70. doi:10.3390/jfb12040070

Mirandola, P., Gobbi, G., Micheloni, C., Vaccarezza, M., Di Marcantonio, D., Ruscitti, F., et al. (2011). Hydrogen sulfide inhibits IL-8 expression in human keratinocytes via MAP kinase signaling. *Lab. Invest.* 91 (8), 1188–1194. doi:10.1038/labinvest.2011.76

Mourdikoudis, S., Pallares, R. M., and Thanh, N. T. K. (2018). Characterization techniques for nanoparticles: Comparison and complementarity upon studying nanoparticle properties. *Nanoscale* 10 (27), 12871–12934. doi:10.1039/C8NR02278J

Nedoszytko, B., Sokołowska-Wojdyło, M., Ruckemann-Dziurdzińska, K., Roszkiewicz, J., and Nowicki, R. (2014). Chemokines and cytokines network in the pathogenesis of the inflammatory skin diseases: Atopic dermatitis, psoriasis and skin mastocytosis. *Postepy Dermatol. Alergol.* 31 (2), 84–91. doi:10.5114/pdia.2014.40920

Phan, M. G., Do, T. T., Nguyen, T. N., Do, T. V. H., Dong, N. P., and Vu, M. T. (2021). Chemical constituents of *Eupatorium japonicum* and anti-Inflammatory, cytotoxic, and apoptotic activities of eupatoriopicrin on cancer stem cells. *Evid. Based. Complement. Altern. Med.* 2021, 6610347. doi:10.1155/2021/6610347

Puglia, C., and Bonina, F. (2012). Lipid nanoparticles as novel delivery systems for cosmetics and dermal pharmaceuticals. *Expert Opin. Drug Deliv.* 9 (4), 429–441. doi:10.1517/17425247.2012.666967

Shankar, S. S., Rai, A., Ahmad, A., and Sastry, M. (2004). Rapid synthesis of Au, Ag, and bimetallic Au core-Ag shell nanoparticles using Neem (Azadirachta indica) leaf broth. *J. Colloid Interface Sci.* 275 (2), 496–502. doi:10.1016/j.jcis.2004.03.003

Sheny, D. S., Mathew, J., and Philip, D. (2011). Phytosynthesis of Au, Ag and Au-Ag bimetallic nanoparticles using aqueous extract and dried leaf of Anacardium occidentale. *Spectrochim. Acta. A Mol. Biomol. Spectrosc.* 79 (1), 254–262. doi:10.1016/j.saa.2011.02.051

Shim, J. H., Kim, K. H., Cho, Y. S., Choi, H. S., Song, E. Y., Myung, P. K., et al. (2008). Protective effect of oxidative stress in HaCaT keratinocytes expressing E7 oncogene. *Amino Acids* 34 (1), 135–141. doi:10.1007/s00726-007-0499-y

Shin, H. Y., Hwang, K. C., Mi, X. J., Moon, S. K., Kim, Y. J., and Kim, H. (2021). Rhamnogalacturonan I-rich polysaccharide isolated from fermented persimmon fruit increases macrophage-stimulatory activity by activating MAPK and NF-κB signaling. *J. Sci. Food Agric.* 102 (7), 2846–2854. doi:10.1002/jsfa.11625

Shin, J.-I., Jeon, Y.-J., Lee, S., Lee, Y. G., Kim, J. B., Kwon, H. C., et al. (2018). Apoptotic and anti-inflammatory effects of *Eupatorium japonicum* Thunb. in rheumatoid arthritis fibroblast-like synoviocytes. *Biomed. Res. Int.* 2018, 1383697. doi:10.1155/2018/1383697

Sugaya, M. (2015). Chemokines and skin diseases. *Arch. Immunol. Ther. Exp.* 63 (2), 109–115. doi:10.1007/s00005-014-0313-y

Sur, B., Kang, S., Kim, M., and Oh, S. (2019). Alleviation of atopic dermatitis lesions by a benzylideneacetophenone derivative via the MAPK signaling pathway. *Inflammation* 42 (3), 1093–1102. doi:10.1007/s10753-019-00971-w

Tran, T. H. M., Puja, A. M., Kim, H., and Kim, Y.-J. (2022). Nanoemulsions prepared from mountain ginseng-mediated gold nanoparticles and silydianin increase the anti-inflammatory effects by regulating NF-κB and MAPK signaling pathways. *Biomater. Adv.* 137, 212814. doi:10.1016/j.bioadv.2022.212814

Vijayakumar, S. (2019). Eco-friendly synthesis of gold nanoparticles using fruit extracts and *in vitro* anticancer studies. *J. Saudi Chem. Soc.* 23 (6), 753–761. doi:10.1016/j.jscs.2018.12.002

Wang, R., Xu, X., Puja, A. M., Perumalsamy, H., Balusamy, S. R., Kim, H., et al. (2021). Gold nanoparticles prepared with Phyllanthus emblica fruit extract and Bifidobacterium animalis subsp. lactis can induce apoptosis via mitochondrial impairment with inhibition of autophagy in the human gastric carcinoma cell line AGS. *Nanomaterials* 11 (5), 1260. doi:10.3390/nano11051260

Werfel, T. (2009). The role of leukocytes, keratinocytes, and allergen-specific IgE in the development of atopic dermatitis. *J. Invest. Dermatol.* 129 (8), 1878–1891. doi:10.1038/jid.2009.71

Wiesenthal, A., Hunter, L., Wang, S., Wickliffe, J., and Wilkerson, M. (2011). Nanoparticles: Small and mighty. *Int. J. Dermatol.* 50 (3), 247–254. doi:10.1111/j.1365-4632.2010.04815.x

Xiao, J. F., Zhou, B., and Ressom, H. W. (2012). Metabolite identification and quantitation in LC-MS/MS-based metabolomics. *Trends Anal. Chem.* 32, 1–14. doi:10.1016/j.trac.2011.08.009

Yang, J.-H., Hwang, Y.-H., Gu, M.-J., Cho, W.-K., and Ma, J. Y. (2015). Ethanol extracts of sanguisorba officinalis l. suppress TNF-α/IFN-γ-induced pro-inflammatory chemokine production in hacat cells. *Phytomedicine* 22 (14), 1262–1268. doi:10.1016/j.phymed.2015.09.006

Yang, J. H., Yoo, J. M., Lee, E., Lee, B., Cho, W. K., Park, K. I., et al. (2018). Anti-inflammatory effects of *Perillae Herba* ethanolic extract against TNF-α/IFN-γ-stimulated human keratinocyte HaCaT cells. *J. Ethnopharmacol.* 211, 217–223. doi:10.1016/j.jep.2017.09.041

Yeh, Y. C., Creran, B., and Rotello, V. M. (2012). Gold nanoparticles: Preparation, properties, and applications in bionanotechnology. *Nanoscale* 4 (6), 1871–1880. doi:10.1039/c1nr11188d

Establishment and application of a high-throughput screening model for cell adhesion inhibitors

Han Sun[1], Xue-Kai Wang[1], Jian-Rui Li[1,2], Mei Tang[1], Hu Li[1,3], Lei Lei[1], Hong-Ying Li[1], Jing Jiang[1], Jia-Yu Li[1], Biao Dong[1,3], Jian-Dong Jiang[1,2,3] and Zong-Gen Peng[1,2,3]*

[1]CAMS Key Laboratory of Antiviral Drug Research, Institute of Medicinal Biotechnology, Chinese Academy of Medical Sciences and Peking Union Medical College, Beijing, China, [2]Beijing Key Laboratory of Antimicrobial Agents, Institute of Medicinal Biotechnology, Chinese Academy of Medical Sciences and Peking Union Medical College, Beijing, China, [3]Key Laboratory of Biotechnology of Antibiotics, The National Health and Family Planning Commission (NHFPC), Institute of Medicinal Biotechnology, Chinese Academy of Medical Sciences and Peking Union Medical College, Beijing, China

The cell adhesion between leukocytes and endothelial cells plays an important balanced role in the pathophysiological function, while excessive adhesion caused by etiological agents is associated with the occurrence and development of many acute and chronic diseases. Cell adhesion inhibitors have been shown to have a potential therapeutic effect on these diseases, therefore, efficient and specific inhibitors against cell adhesion are highly desirable. Here, using lipopolysaccharide-induced human umbilical vein endothelial cells (HUVECs) and calcein-AM-labeled human monocytic cell THP-1, we established a high-throughput screening model for cell adhesion inhibitors with excellent model evaluation parameters. Using the drug repurposing strategy, we screened out lifitegrast, a potent cell adhesion inhibitor, which inhibited cell adhesion between HUVEC and THP-1 cells by directly interrupting the adhesion interaction between HUVEC and THP-1 cells and showed a strong therapeutic effect on the mouse acute liver injury induced by poly (I:C)/D-GalN. Therefore, the screening model is suitable for screening and validating cell adhesion inhibitors, which will promote the research and development of inhibitors for the treatment of diseases caused by excessive cell adhesion.

1 Introduction

The cell adhesion between leukocytes and endothelial cells is a cascade process. Once activated by stimulating factors, such as lipopolysaccharide (LPS), tumor necrosis factor-alpha (TNF-α), and interleukin-1 beta (IL-1β), the endothelial cells upregulate the expression of cell-surface adhesion molecules, including selectins, integrins, immunoglobulin family molecules (vascular cell adhesion molecule-1 (VCAM-1) and intercellular adhesion molecule-1 (ICAM-1)) (Takahashi et al., 1996; Huang et al., 2018), and chemokines such as monocyte chemoattractant protein-1 (MCP-1) (Li et al., 2021), C-X-C motif ligand 10 (CXCL10) (Kawaguchi et al., 2021), and interleukin-8 (IL-8) (Chen et al., 2018). When rolling on the endothelial surface mediated with selectins, the leukocytes slow down and stagnate on the endothelial surface by the chemokines and adhesion molecules, and ultimately undergo migration across the endothelium and basement

membrane through the interaction of integrins and their ligand, immunoglobulin family molecules on the surface of endothelial cells (Ley et al., 2007; Cook-Mills et al., 2011). Normally, cell adhesion plays an important balanced role in the pathophysiological function, while excessive adhesion results in many diseases, such as cardiovascular diseases (atherosclerosis, ischemia-reperfusion injury, thrombosis, and hypercholesterolemia) (Scalia et al., 1998; Blankenberg et al., 2003; Kawamura et al., 2004; McEver, 2015), chronic inflammatory diseases (chronic obstructive pulmonary disease, asthma (Woodside and Vanderslice, 2008), colitis (Sans et al., 1999), keratoconjunctivitis (Perez et al., 2016), and dermatitis (Jung et al., 1996)), autoimmune diseases (Giblin and Lemieux, 2006), and even the migration of tumor cells (Zimmerman and Blanco, 2008; Läubli and Borsig, 2010; Laferrière et al., 2004; O'Hanlon et al., 2002). Some adhesion inhibitors directly or indirectly interrupt the adhesive processes between leukocytes and endothelial cells and thus reduce the excessive cell adhesion, which contributes to the prevention and treatment of these acute and chronic diseases (Ulbrich et al., 2003; Perez et al., 2016). Up to date, only 18 adhesion inhibitors, with 12 monoclonal antibodies and 6 small molecule entities, have been approved by the US FDA for the treatment of related diseases (https://www.fda.gov/, 2022). Because of the low cost, easy oral administration, and good pharmacological effects, small molecule drugs are greatly attractive to research and development (Zimmerman and Blanco, 2008), and efficient and specific small molecule adhesion inhibitors are highly desirable to meet unresolved clinical needs.

To obtain small molecular adhesion inhibitors, a high-throughput screening model for cell adhesion inhibitors is needed to acquire innovative leading compounds. Currently, cell adhesion assays are mainly divided into static adhesion assay and the measurement of adhesion in shear stress (Kucik and Wu, 2005). Static adhesion assays are mainly used to assess the adhesion interaction between cells and extracellular matrix by measuring absorbance or fluorescence intensity (Tolosa and Shaw, 1996; Spessotto et al., 2002; Kucik and Wu, 2005; Humphries, 2009), while the cell adhesion in blood and lymph vessels is measured under shear stress using flow chambers and fluorescence microscopy (Kucik and Wu, 2005). A direct co-culture of two types of cells was established and detected with fluorescence microscopy (Li et al., 2007). For enhancing the adhesion intensity, endothelial cells were stimulated with inducible factors such as IL-1β (Zhong Y. et al., 2020), LPS (Jung et al., 1996; Wang et al., 2019; Zhong M. et al., 2020), TNF-α (Phang et al., 2020; Fallon and Hinds, 2021), or oxidized low-density lipoprotein (ox-LDL) (Gong et al., 2019; Geng et al., 2020). However, in those systems, the fluorescent signal from the labeled THP-1 captured by the activated endothelial cells was detected by fluorescence microscopy. These models are suitable to study the efficacy and mechanism of action of candidates, but not convenient for large-scale drug screening because of their time-consuming and labor-intensive.

In this study, we established a high-throughput screening model for cell adhesion inhibitors using LPS-induced human umbilical vein endothelial cells (HUVECs) and calcein-AM-labeled human monocytic cells THP-1, and lifitegrast, a drug that used for anti-dry eye therapy, was screened out from the FDA-approved drug library and shown to have a good therapeutic effect against mouse acute liver injury induced by poly (I:C)/D-GalN.

2 Materials and methods

2.1 Cell culture and reagents

HUVEC and THP-1 cells were from the Institute of Basic Medicine, Chinese Academy of Medical Sciences and Peking Union Medical College. HUVEC cells were incubated in Dulbecco's modified eagle's medium (DMEM, Gibco, China) supplemented with 10% (v/v) fetal bovine serum (FBS, Gibco, United States), 1% penicillin-streptomycin (Beyotime, Shanghai, China), 1% non-essential amino acids (Sigma-Aldrich, United States), and 0.01 mg/mL insulin (Psaitong, Beijing, China). THP-1 cells were maintained in Roswell Park Memorial Institute 1640 medium (RPMI 1640, Gibco, China) containing 10% (v/v) FBS, 1% penicillin-streptomycin, and 0.05 mM β-Mercaptoethanol (Sigma-Aldrich, United States). The cells were cultured at 37°C in a humidified incubator (Thermo, United States) with 5% CO_2.

2.2 Cytotoxicity assay

The cytotoxicity was analyzed with a staining method. HUVEC cells (1×10^4 cells/well) were seeded in a 96-well plate and treated with various concentrations of LPS for 24 h. Then, the culture supernatants were discarded, and the cells were incubated for 2 h with 10% CCK-8 (TransGen, Beijing, China) solution diluted with the culture medium. The absorbance intensity was measured at 450 nm using an Enspire Multilabel Reader (PerkinElmer, United States).

2.3 Establishment and optimization of the cell adhesion between HUVEC and THP-1 cells

HUVEC cells (1×10^4 cells/well) were seeded in a 96-well plate pre-coated with type I collagen (Corning, United States). After 24 h of incubation, the cells were treated with 1 µg/mL of LPS for 24 h. THP-1 cells were labeled with 5 µM calcein-AM (Invitrogen, United States) for 30 min, then centrifuged at 200 g for 5 min, and resuspended with the culture medium of HUVECs prior to use. The labeled THP-1 cells (4×10^4 cells/ 0.1 mL) were added to the well to co-culture with HUVEC cells for 45 min, then the cells were washed with phosphate buffer solution (PBS, Servicebio, China) using BioTek ELx50 Microplate Strip Washer (BioTek, USA) following the optimized procedure to remove the unadhered THP-1 cells. The fluorescence intensity was measured by Enspire Multilabel Reader (PerkinElmer, USA) with following parameters: top reading mode was used to measure fluorescence intensity at 490 nm excitation wavelength and 510 nm emission wavelength. A 5 × 5 rectangular array with 25 detection points was selected for each well with a distance of 0.72 mm between points to ensure maximum coverage of each well in the 96-well plate. The data for each well was output as the average of the fluorescence intensities of the 25 points.

2.4 The parameters of adhesion model and the screening of adhesion inhibitors

The key screening model parameters, signal-to-noise ratio (S/N), signal background ratio (S/B), coefficient of variation (CV), and Z factor (Z'), were calculated as follows (Zhao et al., 2019): $S/N = (Mean_{signal}—Mean_{background})/SD_{background}$, $S/B = Mean_{signal}/Mean_{background}$, $CV = SD_{control}/Mean_{control} \times 100\%$, and $Z' = 1—(3SD_{signal} + 3SD_{control})/(Mean_{signal}—Mean_{control})$. In screening, 2,791 compounds from the L1000-Approved Drug Library and L6000 Natural Product Library (Topscience Co. Ltd., Shanghai, China) were tested. HUVEC cells were incubated simultaneously with LPS and compound for 24 h, and then the labeled THP-1 cells were added to co-culture for 15 min. After the plate was washed, the fluorescence intensity (FI) was detected. The inhibitory activity of drugs against cell adhesion was calculated as follows: Inhibition rate (%) = $(FI_{drug}—FI_{control})/(FI_{model}—FI_{control}) \times 100\%$.

2.5 Animal experiments

Six to eight-week-old male BALB/c mice (20.0 g ± 1.0 g) with SPF grade were from SPF (Beijing) Biotechnology Co., Ltd. All mice were housed under pathogen-free conditions with a standard 12h- light/dark cycle and fed sterile chow and fluid *ad libitum*. All animal procedures were performed strictly following the national laboratory animal feeding management standards and approved by the Institutional Animal Care and Use Committee of the Institute of Medicinal Biotechnology and Chinese Academy of Medical Sciences (SYXK (Jing)2017-0023).

The mice were randomly divided into 6 groups with 6 mice in each group according to body weight: normal control group, poly (I:C)/D-GalN model group, lifitegrast high-dose group (lifitegrast, 0.5 mg/kg), medium-dose group (lifitegrast, 0.25 mg/kg) and low-dose group (lifitegrast, 0.125 mg/kg), and dexamethasone group (dexamethasone, 1.0 mg/kg). Poly (I:C) (InvivoGen, thrl-picw-250, California) or D-(+)-galactosamine (D-GalN, Sigma-Aldrich, G1639-1G, United States) was diluted in 0.9% sterile saline. Dexamethasone (Dex, Innochem, Beijing, China) or lifitegrast (Aladdin, L171714, Shanghai, China) was diluted in 0.9% sterile saline containing 1% DMSO and 5% tween-80 (vehicle) prior to use.

The mice were administered intraperitoneally 500 mg/kg D-GalN in combination with 5 mg/kg poly (I:C) *via* the tail vein to induce acute liver injury, and the normal control group were treated with the equivalent volume of 0.9% sterile saline. The mice were treated intraperitoneally with the drugs at 2 and 10 h after the poly (I:C)/D-GalN injection, and the normal control group and poly (I:C)/D-GalN model group received the equivalent volume of vehicle. The blood samples were collected for biochemical assays, then the mice were sacrificed, and the liver tissues were collected for the following experiments after 18 h of the poly (I:C)/D-GalN injection.

2.6 Serum alanine aminotransferase measurement

The blood samples were centrifuged at 2,500 g for 10 min, and the sera were isolated. Serum levels of alanine aminotransferase (ALT) were detected with the ALT kits (Nanjing Jiancheng Bioengineering Institute, Nanjing, China) according to the manufacturer's instructions.

2.7 Histopathological analyze

The histopathological changes in the liver were assessed after Hematoxylin and Eosin (H&E) staining. In brief, the liver tissue samples were flushed with PBS, fixed in 4% paraformaldehyde for 2 days, then dehydrated, and paraffin-embedded. The sections were performed H&E staining and scanned panoramically with Pannoramic Scan (3DHISTECH, Hungary).

2.8 Western blot

The liver tissues were homogenized and lysed in ice-cold lysis buffer supplemented with protease and phosphatase inhibitors (Topscience, Shanghai, China) and centrifuged at 12,000 g for 20 min at 4°C, and then the clarified supernatants were collected. Then proteins were quantified with the Pierce BCA Protein Assay Kit (Thermo, United States) assay according to the manufacturer's instructions. The western blot was performed as previously described (Li et al., 2022a; Li et al., 2022b). Briefly, after SDS-PAGE and transmembrane, the target proteins were accordingly probed with first antibodies against GAPDH (10494-1-AP, 1:1,000, Proteintech), phospho-Stat3 (9145, 1:1,000, CST), Stat3 (9139, 1:1,000, CST), phospho-p38 MAPK (4511, 1:1,000, CST), p38 MAPK (8690, 1:1,000, CST), phospho-NF-κB p65 (3033, 1:1,000, CST), NF-κB p65 (6956, 1:1,000, CST), phospho-IκBα (2859, 1:1,000, CST), and IκBα (4814, 1:1,000, CST), respectively. After incubation with the corresponding HRP-conjugated secondary antibody, the signal of the target protein was detected using a ChemiDo XRS gel imager system (Bio-Rad, United States) with Immobilon Western Chemiluminescent HRP Substrate (Millipore, United States) and was scanned by ImageJ software. The ratio of the target protein was normalized to the internal control protein GAPDH, and fold-change was calculated relative to the control group.

2.9 Quantitative real-time reverse transcription polymerase chain reaction (qRT-PCR)

Total RNA was extracted from the liver tissues or HUVEC cells with Magen RNeasy Mini Kit (MGBio, Shanghai, China) according to the manufacturer's instructions. RNA concentration was determined by NanoDrop 2000 (Thermo Scientific, United States). As previously described (Wang et al., 2022), qRT-PCR was performed with the indicated primers (Table 1) and HiScriptII One Step QRT-PCR SYBR Green Kit (Vazyme, Nanjing, China) using the ABI 7500 Fast system (Applied Biosystems, United States). RNA (30–120 ng) was used as a template, and qRT-PCR amplification consisted of 5 min of reverse transcription step at 50°C, then 5 min of an initial denaturation step at 95°C, followed by 40 cycles of PCR at 95°C for 10 s and 60°C for 34 s. Target gene expression levels were

TABLE 1 Primer sequences used in the qRT-PCR.

Gene name	Forward primer (5′-3′)	Reverse primer (5′-3′)
Human *GAPDH*	CGGAGTCAACGGATTTGGTCGTAT	AGCCTTCTCCATGGTGGTGAAGAC
Human *ICAM-1*	TCTTCCTCGGCCTTCCCATA	AGGTACCATGGCCCCAAATG
Human *VCAM-1*	AAGCCGGATCACAGTCAAGTG	TCTTGGTTTCCAGGGACTTC
Human *E-selectin*	CCGAGCGAGGCTACATGAAT	GCCAGAGGAGAAATGGTGCT
Murine *GAPDH*	CTCTGGAAAGCTGTGGCGTGATG	ATGCCAGTGAGCTTCCCGTTCAG
Murine *IL-1β*	TGTCTTGGCCGAGGACTAAGG	TGGGCTGGACTGTTTCTAATGC
Murine *IL-6*	CCATCCAGTTGCCTTCTTGG	TGCAAGTGCATCATCGTTGT
Murine *TNF-α*	AGGGTCTGGGCCATAGAACT	CCACCACGCTCTTCTGTCTAC
Murine *ICAM-1*	GTGGCGGGAAAGTTCCTG	CGTCTGCAGGTCATCTTAGGAG
Murine *MCP-1*	TTAAAAACCTGGATCGGAACCAA	GCATTAGCTTCAGATTTACGGGT
Murine *CXCL10*	GAGCCTATCCTGCCCACG	GGAGCCCTTTTAGACCTT

normalized to the internal control gene *GAPDH* using the $2^{-\Delta\Delta CT}$ method.

2.10 Statistical analyses

All data were presented as mean ± standard error of the mean (SEM). The statistical significance of differences between two-group was analyzed by unpaired *t-tests* and multiple-group comparisons by one-way ANOVA using GraphPad Prism 8. The differences were considered significant at *p*-value <0.05.

3 Results

3.1 The optimization of the cell adhesion condition between endothelial and monocytic cells

To establish the *in vitro* screening model for cell adhesion inhibitors, we used HUVEC endothelial cells and THP-1 monocytes to mimic the cell adhesion interaction (Zhong M. et al., 2020). Firstly, we evaluated whether the detectable fluorescence intensity is linear correlation with the amount of THP-1 cells labeled with calcein-AM. Results showed a good linear relationship between the fluorescence intensity and the amount of labeled THP-1 cells when it ranged from 0 up to 100×10^3 cells/well in a 96-well plate (Figure 1A), indicating that the fluorescence intensity responds to the amount of the captured THP-1 cells. Normally, monocytes less adhere to endothelial cells, while the adhesion interaction was enhanced by LPS-stimulated endothelial cells (Lv et al., 2018). HUVEC cells did not show significant cytotoxicity by the treatment of LPS for 24 h (Figure 1B), while the adhesion of THP-1 cells to the HUVEC cells was enhanced by the LPS stimulation (Figure 1C). Considering the reaction curve and the potential cytotoxicity, we selected 1.0 μg/mL LPS as the stimulation concentration. At the stimulation of 1.0 μg/mL of LPS, THP-1 cells adhered to the

stimulated HUVEC cells in an amount of HUVEC cells manner (Figure 1D). Considering the monolayer state of endothelial cells, HUVEC cells at the density of 4×10^4 cells/well were treated by 1 μg/mL of LPS for different times, and results showed that the most vigorous adhesion appeared at 24 h of treatment (Figure 1E). Then we again verified whether there was a strong linear relationship between fluorescence intensity and the amount of THP-1 cells under 20×10^4 cells/well when HUVEC cells were stimulated by LPS (Figure 1F). At this condition, the adhesion between the stimulated HUVEC cells and THP-1 cells was completed at 15 min without increasing fluorescence intensity by additional co-culture time (Figure 1G). However, the starvation state of THP-1 cells significantly influenced the adhesion, the strongest fluorescence intensity was observed when 0% FBS starved THP-1 cells were added (Figure 1H), while the culture supernatant from LPS induced-HUVEC cells did not influence the adhesion between the stimulated HUVEC cells and THP-1 cells (Figure 1I).

Together, we suggested that HUVEC cells, with a density of 4×10^4 treated by 1 μg/mL of LPS for 24 h, were co-cultured with labeled FBS-free starved THP-1 cells at the density of 4×10^4 cells/well for 15 min presented a good cell adhesion condition to mimic the cell adhesion interaction between HUVEC and THP-1 cells (Figure 1J).

3.2 The parameters of *in vitro* high-throughput screening model for cell adhesion inhibitors and the screening drug candidates

Then, we evaluated whether the cell adhesion model is suitable for screening cell adhesion inhibitors. We analyzed the key evaluation parameters for the quality of high-throughput screening model, such as signal-to-noise ratio (S/N), signal background ratio (S/B), coefficient of variation (CV), and Z factor (Z'), among which Z' is a measure of statistical effect intensity. Results showed that the cell adhesion interaction
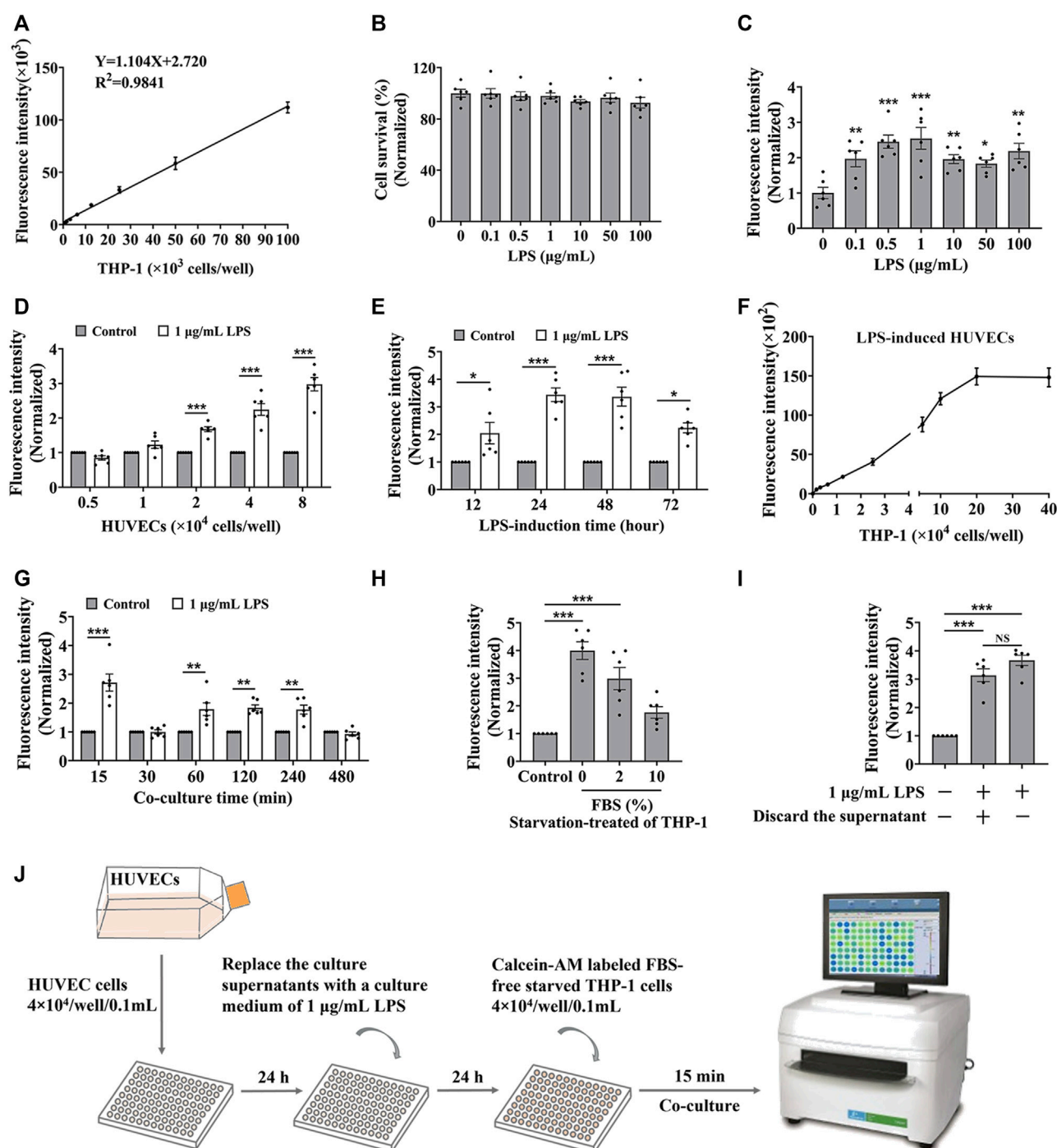
FIGURE 1

The optimization of the cell adhesion condition between endothelial and monocytic cells. **(A)** The linear relationship between fluorescence intensity and the amount of calcein-AM labelled THP-1 cells. **(B)** The cytotoxicity of LPS to HUVEC cells for 24 h. **(C–E)** HUVEC cells (4×10^4 cells/well) were treated by LPS for 24 h **(C)**, or different densities of HUVEC cells were treated by 1 μg/mL LPS for 24 h **(D)**, or HUVEC cells (4×10^4 cells/well) were treated by 1 μg/mL LPS for different time **(E)**, and then co-cultured with labeled THP-1 cells (4×10^4 cells/well) for 45 min; or **(F–H)** HUVEC cells (4×10^4 cells/well) were treated by 1 μg/mL LPS for 24 h, and then co-cultured with different amounts of labeled THP-1 cells for 45 min **(F)** or co-cultured with labeled THP-1 cells (4×10^4 cells/well) for different time **(G)**, or co-cultured with labeled THP-1 cells (4×10^4 cells/well) starved with media containing different concentrations of FBS for 15 min **(H)**, then the fluorescence intensity were detected. **(I)** The fluorescence intensity from the cell adhesion model when the culture supernatants from LPS induced-HUVEC cells were discarded before HUVEC cells (4×10^4 cells/well) co-cultured with labeled THP-1 cells (4×10^4 cells/well) for 15 min. **(J)** The technological diagram of the cell adhesion model between HUVEC and THP-1 cells. Data were presented as mean $\pm$ SEM over three experiments. NS: no significance, $*p < 0.05$, $**p < 0.01$, $***p < 0.001$ vs. Control.

FIGURE 2
The evaluation of *in vitro* high-throughput screening model for cell adhesion inhibitors. **(A)** The reproducibility of the cell adhesion model between the stimulated HUVEC cells and labeled THP-1 cells. **(B)** The adhesion inhibitory activity of BAY-11-7082 and cenicriviroc (CVC) on cell adhesion. HUVEC cells were treated simultaneously by LPS and/or compound (BAY-11-7082 (10 μM) or CVC (1 μM)) for 24 h, and then co-cultured with labeled THP-1 cells for 15 min. Data were presented as mean ± SEM over three experiments. $^{\#\#}p < 0.01$, $^{\#\#\#}p < 0.001$ vs. control, and $^{***}p < 0.001$ vs. model.

TABLE 2 The key evaluation parameters of *in vitro* high-throughput screening model.

Parameters	Value	Good range of values
Signal-to-noise ratio (S/N)	10.3	>3.0
Signal background ratio (S/B)	9.8	>3.0
Coefficient of variation (CV)	8.8%	<20.0%
Z factor (Z')	0.7	$0.5 \leq Z' < 1.0$

between the stimulated HUVEC cells and labeled THP-1 cells was reproducible (Figure 2A), with the S/N value of 10.3, S/B value of 9.8, CV value of 8.8%, and Z' value of 0.7 (Table 2), strongly suggesting the cell adhesion model is suitable for the high-throughput screening of cell adhesion inhibitors. Activated endothelial tissue by LPS upregulate the expression of adhesion molecules and the secretion of chemokines through NF-κB signaling pathway to promote the adhesion interaction with leukocytes (Zhu et al., 2017; Dayang et al., 2019), while BAY-11-7082 as NF-κB inhibitor and cenicriviroc as chemokine receptor (CCR) 2/5 antagonist showed adhesion inhibitory activity *in vivo* and *in vitro* (D'Antoni et al., 2018; Wang et al., 2016). In our optimized model, they were also shown to be strong cell adhesion inhibitors, further suggesting the *in vitro* model is reliable for the screening of cell adhesion inhibitors (Figure 2B).

Drug repurposing strategy is a good strategy for discovering new therapeutic uses of drugs. (Armando et al., 2020). Using this model, 2,791 compounds from the approved drug library and natural product library were tested, and 8 potential adhesion inhibitors were screened out (Table 3), which showed inhibitory activity against the cell adhesion between HUVEC and THP-1 cells at the drug concentration of 1.0 μM. Among which only lifitegrast, a drug for

the treatment of dry eye (Chan and Prokopich, 2019), showed adhesion inhibition rate more than 50% and was comparable to that of cenicriviroc, which has the potential to be developed for the clinical treatment of other adhesion-related diseases.

3.3 Lifitegrast directly interrupts the cell adhesion between HUVEC and THP-1 cells
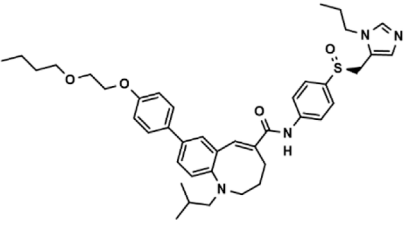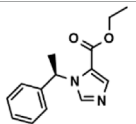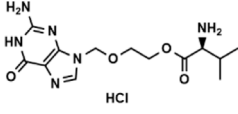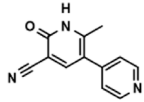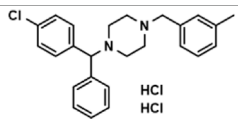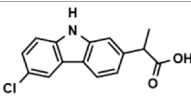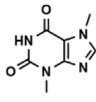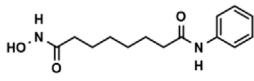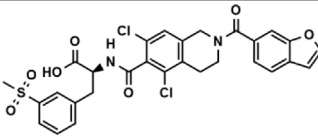
We evaluated the efficacy of lifitegrast against cell adhesion using the standardized screening model. The results showed that lifitegrast inhibited the cell adhesion between HUVEC and THP-1 cells in a dose-dependent manner (Figure 3A) without significant cytotoxicity to HUVEC cells up to 10.0 μM of lifitegrast (Figure 3B). Then lifitegrast at 1.0 μM was used to explore the mechanism against cell adhesion between HUVEC and THP-1 cells.

Firstly, we detected whether lifitegrast influences the expression of adhesion molecules on the surface of HUVEC cells. Results showed that lifitegrast did not decrease the mRNA levels of LPS-induced ICAM-1, VCAM-1, and E-selectin (Figure 3C), which are the main adhesion molecules to promote cell adhesion between leukocytes and endothelial cells (Walzog and Gaehtgens, 2000; Huang et al., 2018; Zhong et al., 2018). Furthermore, additional treated THP-1 cells with lifitegrast for 24 h also did not enhance the inhibitory activity of lifitegrast against cell adhesion (Figure 3D). Those results suggested that the inhibitory activity of lifitegrast against cell adhesion is not through the impact of expressing the adhesion molecules on the cell surface.

Then we explored whether the cell culture supernatants of lifitegrast treatment will influence the cell adhesion between HUVEC and THP-1 cells. HUVEC cells were treated simultaneously by LPS and lifitegrast for 24 h, then the culture supernatants were discarded, and HUVEC cells were co-cultured with labeled THP-1 cells for 15 min. Results showed that the adhesion inhibitory activity of lifitegrast was decreased but not completely disappeared (Figure 3E), suggesting that some substances in the culture supernatants secreted from the treated HUVEC cells have an adhesion inhibitory effect, or lifitegrast directly impacts the cell adhesion.

We next distinguished the potential action of lifitegrast. HUVEC cells were treated by LPS for 24 h, then the culture supernatants were replaced with that of HUVEC cells treated by lifitegrast for 24 h, or with fresh culture medium containing lifitegrast, and the HUVEC cells were co-cultured with labeled THP-1 cells for 15 min. In the two conditions, the adhesion inhibitory activities of lifitegrast were as strong as that of HUVEC cells were treated simultaneously by LPS and lifitegrast for 24 h without replacing culture supernatants (Figure 3E), suggesting that lifitegrast may directly interfere with the cell adhesion interaction. Meanwhile, the adhesion inhibitory activity of lifitegrast increased in a dose-dependent manner with a half maximal inhibitory concentration (IC_{50}) of 25.00 ± 25.28 nM, when the culture supernatants were replaced with fresh culture media containing various concentrations of lifitegrast (Figure 3F), further validating the direct inhibitory activity of lifitegrast against cell adhesion between HUVEC and THP-1 cells. Our results are consistent with previous reports that lifitegrast blocks the interaction of lymphocyte function-associated molecule (LFA-1)

TABLE 3 The effect on cell adhesion of approved drugs.

Drug (1.0 μM)	Chemical structure	Inhibition (%)
Cenicriviroc (CVC)		64.85 ± 3.76
Etomidate		32.17 ± 8.55
Valacyclovir hydrochloride		25.41 ± 1.53
Milrinone		24.45 ± 7.94
Meclizine dihydrochloride		22.87 ± 3.01
Carprofen		46.86 ± 19.4
Theobromine		21.16 ± 12.54
Vorinostat		41.70 ± 5.39
Lifitegrast		67.55 ± 22.99

with its cognate ligand ICAM-1 by binding to LFA-1 (Perez et al., 2016; Chan and Prokopich, 2019).

Collectively, our results suggested that lifitegrast may directly interrupt the interactions between adhesion molecules on the surface of HUVEC and THP-1 cells and thus inhibit cell adhesion (Figure 3G).

3.4 Lifitegrast ameliorates mouse acute liver injury induced by poly (I:C)/D-GalN

To further investigate the effect on cell adhesion of lifitegrast *in vivo*, we used a mouse acute liver injury model induced by poly (I:C)/ D-GalN, which is closely related to the excessive cell adhesion
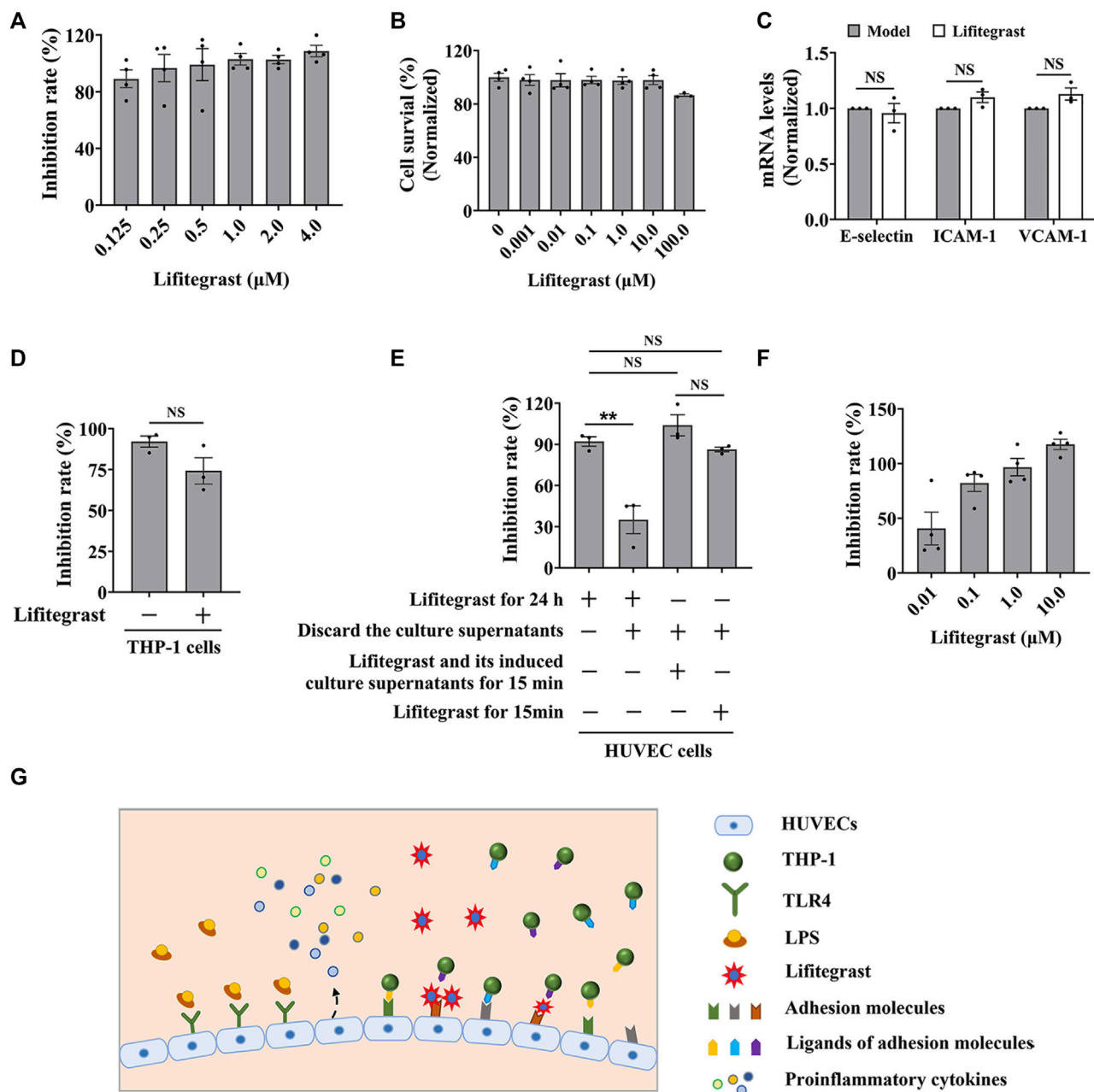
FIGURE 3
Lifitegrast directly interrupts the adhesion interaction between HUVEC and THP-1 cells. **(A)** The inhibitory activity of lifitegrast against cell adhesion in the standardized model. **(B)** The cytotoxicity of lifitegrast to HUVEC cells for 24 h. **(C)** The mRNA levels of adhesion molecules in HUVEC cells treated by LPS and lifitegrast for 24 h. **(D)** In the standardized model, the THP-1 cells were treated additionally with lifitegrast for 24 h. **(E)** HUVEC cells were treated at different stages of cell adhesion, such as adding lifitegrast together with LPS for 24 h, or discarding the culture supernatants of LPS and lifitegrast, or replacing the culture supernatants of LPS with that of lifitegrast, or with fresh culture medium containing lifitegrast, and then co-cultured with labeled THP-1 cells for 15 min. **(F)** HUVEC cells were treated by LPS for 24 h, the culture supernatants were replaced with culture media containing lifitegrast, and then co-cultured with labeled THP-1 cells for 15 min. **(G)** The diagram of lifitegrast against cell adhesion. Data were presented as mean ± SEM over three experiments. NS: no significance, **$p < 0.01$ vs. the group of retained culture supernatants.

condition (An et al., 2017). Here, we used male mice, which are mostly selected in the similar experiments (Gong et al., 2019; Lv et al., 2020; Schneider et al., 2021), to mimic acute liver injury. After the mice were intraperitoneally injected with poly (I:C)/D-GalN, the serum ALT level was significantly increased (Figure 4A), and

H&E staining results showed increased infiltration of inflammatory cells in the liver tissue (Figure 4B). Consequently, inflammatory factors in the liver, such as IL-1β (Figure 4C), IL-6 (Figure 4D), and TNF-α (Figure 4E) were increased in parallel, suggesting that the treatment of poly (I:
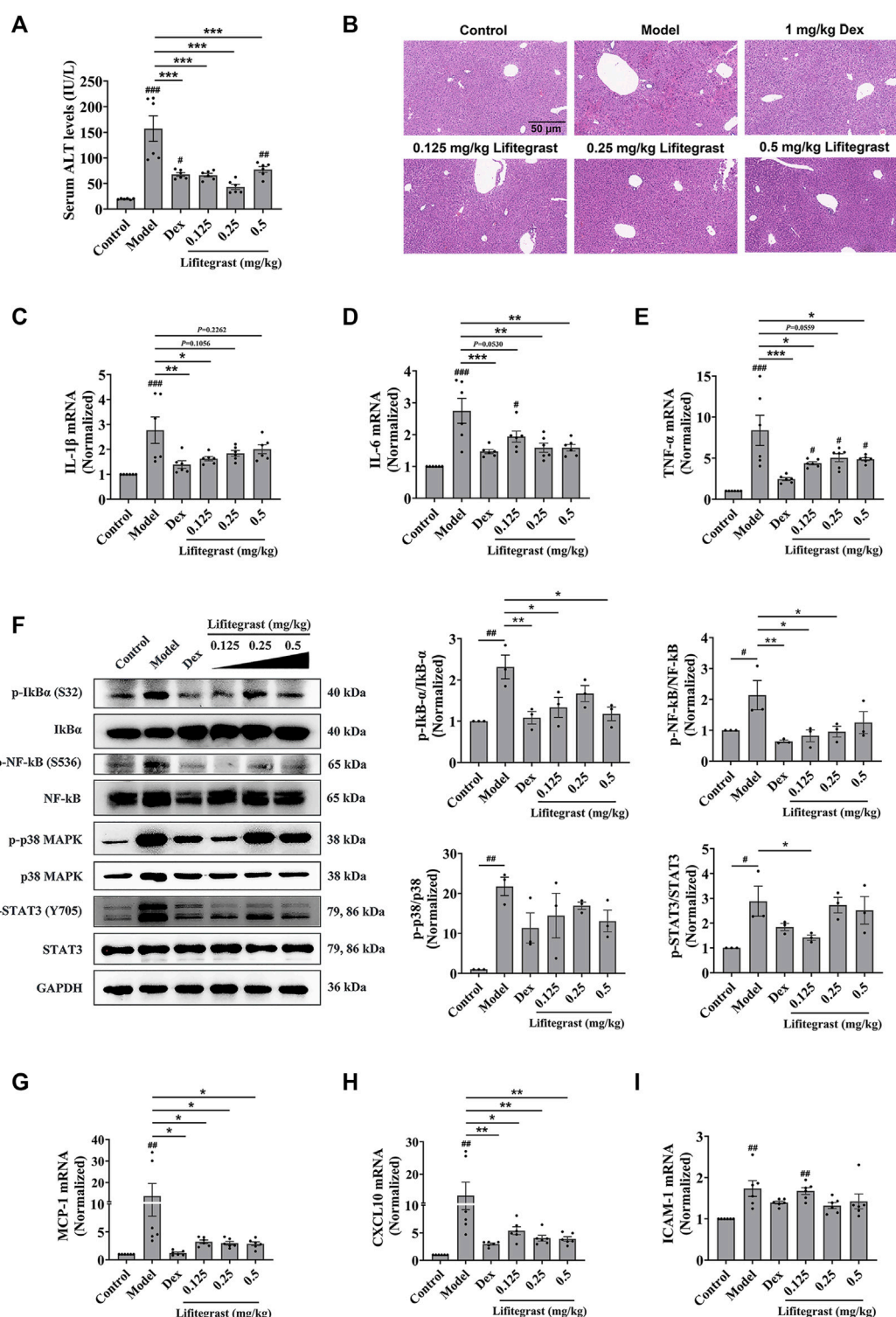
FIGURE 4
Lifitegrast ameliorates mouse acute liver injury induced by Poly(I:C)/D-GalN. **(A)** ALT level in serum, n = 6. **(B)** Liver H&E staining, the scale bar was 50 μm. **(C–E)** The mRNA levels of IL-1β **(C)**, IL-6 **(D)**, and TNF-α **(E)** in the liver, n = 6. **(F)** The phosphorylation levels of inflammatory factors in the liver, n = 3. **(G–I)** The mRNA levels of MCP-1 **(G)**, CXCL10 **(H)**, and ICAM-1 **(I)** in the liver, n = 6. Data were presented as mean ± SEM. #p < 0.05, ##p < 0.01, ###p < 0.001 vs. Control, and *p < 0.05, **p < 0.01, ***p < 0.001 vs. Model.

C)/D-GalN caused mouse acute liver injury. While the intraperitoneal injection treatment of lifitegrast ameliorated the acute liver injury by decreasing the ALT level (Figure 4A)

and reducing the expression of inflammatory factors (Figures 4C–E), and the efficacy of lifitegrast was comparable to that of dexamethasone (Dex) (Figures 4A–E).

Then we validated the potential mechanism of cell adhesion of lifitegrast against the poly (I:C)/D-GalN-induced acute liver injury in mice. After the mice were treated with poly (I:C)/D-GalN, the phosphorylation levels of Stat3, p38 MAPK, IκBα, and NF-κB were increased in the liver (Figure 4F). The chemokines such as MCP-1 (Figure 4G) and CXCL10 (Figure 4H), and adhesion molecule ICAM-1 (Figure 4I) were increased in parallel, suggesting that poly (I:C)/D-GalN induced the excessive cell adhesion and caused acute liver injury. While the intraperitoneal injection treatment of lifitegrast ameliorated the acute liver injury by decreasing the phosphorylation levels of Stat3, p38 MAPK, IκBα and NF-κB (Figure 4F) and reducing the expression of chemokines (Figures 4G, H), but not ICAM-1 (Figure 4I), and the efficacy of lifitegrast was comparable to that of Dex (Figures 4F–I). These results suggested that lifitegrast ameliorates mouse acute liver injury through down-regulating the excessive cell adhesion.

4 Discussion

The occurrence and development of many acute and chronic diseases are closely related to excessive cell adhesion. In response to stimulating factors, vascular endothelial cells release pro-inflammatory cytokines and upregulate the expression of adhesion molecules on the cellular surface, thereby promoting intravascular inflammatory cells to adhere to the endothelium and undergo trans-endothelium migration (Huang et al., 2018). Using LPS-induced HUVEC cells and calcein-AM-labeled THP-1 cells, we established a screening model for cell adhesion inhibitors, achieving rapid, objective and high-throughput screening for cell adhesion inhibitors. HUVEC cells are used as typical endothelial cells for cell adhesion model (Cao et al., 2017). LPS, as an endotoxin, promotes the expression of pro-inflammatory cytokines and adhesion molecules on the cellular surface by acting on toll-like receptor 4 in endothelial cells and activating inflammation-related signaling pathways such as NF-κB signaling pathway (Su et al., 2021). In this study, LPS significantly induced excessive cell adhesion between HUVEC and THP-1 cells, which is consistent with previous reports (Hayden and Ghosh, 2008; Sawa et al., 2008; Lv et al., 2016). However, due to the static mode, this model is not suitable for the screening inhibitors for chemotactic factors which also play important roles in the excessive cell adhesion in vivo (Kim, 2004; Maas et al., 2023).

Drug repurposing strategy is a good strategy for discovering new therapeutic uses of drugs. Using the screening model, we obtained a potential cell adhesion inhibitor lifitegrast. And using the in vitro adhesion model, we verified that lifitegrast directly inhibited the cell adhesion between HUVEC and THP-1 cells, which is consistent with that lifitegrast blocks the interaction of LFA-1 with its cognate ligand ICAM-1 by binding to LFA-1 (Perez et al., 2016; Chan and Prokopich, 2019), further suggesting that the screening model is practicability. Although approved as a novel integrin antagonist, lifitegrast is used only for the treatment of the

dry eye disease. In this study, we demonstrated that lifitegrast also shows a new potential therapeutic usage to treat acute liver injury. The detailed mechanism was associated with not only direct interruption of cell adhesion between leukocytes and endothelial cells but also downregulation of activated inflammatory signaling pathways.

In addition, acute liver failure (ALF) is a rare and serious consequence of acute fulminate liver cell damage, which can develop into a fatal outcome within days or weeks in the clinic (Bernal et al., 2010; Thawley, 2017; Stravitz and Lee, 2019). In terms of etiology, viral hepatitis may account for the majority of ALF cases in developing countries (Dong et al., 2020). In addition, as of May 20, 2022 there have been at least 566 probable cases of acute hepatitis of unknown cause in children under the age of 10 reported from 33 countries (WHO, 2022). Although the cause is unknown, given the epidemiological pattern of cases, it is presumed that these cases are associated with viral infection and may develop to acute liver failure in children (Christie, 2022). Many studies have shown that the infiltration of inflammatory cells in the liver is the key to the mechanism and result of ALF. Under the stimulation of inflammation, the expressions of ICAM-1 and VCAM-1 on the surface of liver sinusoidal endothelial cells (LSECs) are increased and chemokines are secreted, which mediates the adhesion cascade of inflammatory cells and the infiltration in the liver (Lalor and Adams, 2002; Bernal et al., 2010; Sørensen et al., 2015). Then inflammatory cells further cause hepatocyte damage through the direct activation of death receptors or the secretion of cytokines until liver failure (Jaeschke, 2006; Jaeschke and Hasegawa, 2006; Quaglia et al., 2008). Therefore, reasonable intervention for the adhesion process can block liver injury at an early stage to improve ALF. The polyinosine polycytidylic acid (poly (I:C)), a synthetic mimic of double-stranded viral RNA, is commonly used to mimic a moderate acute hepatic injury and a model of viral hepatitis (Takeda and Akira, 2004; Hafner et al., 2013; He et al., 2013; Khan et al., 2021). In this study, the intraperitoneal injection of D-GalN combined with tail vein injection of poly (I:C) caused acute liver injury in mice, and lifitegrast, a drug screened out with the in vitro screening model, ameliorated the acute liver injury, suggesting that lifitegrast might be a candidate for the treatment of acute liver failure though it needs to be validated further.

In summary, using LPS-induced HUVEC cells and calcein-AM-labeled THP-1 cells, we established a high-throughput screening model for cell adhesion inhibitors. Using the drug repurposing strategy, we screened out lifitegrast as a potent cell adhesion inhibitor with directly interrupting cell adhesion interaction between HUVEC and THP-1 cells, and further demonstrated the therapeutic effect on the mouse acute liver injury induced by poly (I:C)/D-GalN. Together, the screening model is suitable for screening cell adhesion inhibitors and validating their mechanism of action, which will promote the research and development of small molecular candidates against cell adhesion.

Data availability statement

The original contributions presented in the study are included in the article/supplementary material, further inquiries can be directed to the corresponding author.

Ethics statement

The animal study was reviewed and approved by Institutional Animal Care and Use Committee of the Institute of Medicinal Biotechnology and Chinese Academy of Medical Sciences.

Author contributions

HS designed and performed the experiments, analyzed the data, and wrote the manuscript. Z-GP oversaw the project, designed the experiments, analyzed the data, and wrote the manuscript. Other authors participated in the experiment performance and data analysis.

Conflict of interest

The authors declare that the research was conducted in the absence of any commercial or financial relationships that could be construed as a potential conflict of interest.

Publisher's note

All claims expressed in this article are solely those of the authors and do not necessarily represent those of their affiliated organizations, or those of the publisher, the editors and the reviewers. Any product that may be evaluated in this article, or claim that may be made by its manufacturer, is not guaranteed or endorsed by the publisher.

References

An, S. Y., Youn, G. S., Kim, H., Choi, S. Y., and Park, J. (2017). Celastrol suppresses expression of adhesion molecules and chemokines by inhibiting JNK-STAT1/NF-κB activation in poly(I:C)-stimulated astrocytes. *BMB Rep.* 50, 25–30. doi:10.5483/bmbrep.2017.50.1.114

Armando, R. G., Mengual Gómez, D. L., and Gomez, D. E. (2020). New drugs are not enough-drug repositioning in oncology: An update. *Int. J. Oncol.* 56, 651–684. doi:10.3892/ijo.2020.4966

Bernal, W., Auzinger, G., Dhawan, A., and Wendon, J. (2010). Acute liver failure. *Lancet* 376, 190–201. doi:10.1016/s0140-6736(10)60274-7

Blankenberg, S., Barbaux, S., and Tiret, L. (2003). Adhesion molecules and atherosclerosis. *Atherosclerosis* 170, 191–203. doi:10.1016/s0021-9150(03)00097-2

Cao, Y., Gong, Y., Liu, L., Zhou, Y., Fang, X., Zhang, C., et al. (2017). The use of human umbilical vein endothelial cells (HUVECs) as an *in vitro* model to assess the toxicity of nanoparticles to endothelium: A review. *J. Appl. Toxicol.* 37, 1359–1369. doi:10.1002/jat.3470

Chan, C. C., and Prokopich, C. L. (2019). Lifitegrast ophthalmic solution 5.0% for treatment of dry eye disease: Overview of clinical trial program. *J. Pharm. Pharm. Sci.* 22, 49–56. doi:10.18433/jpps29895

Chen, L., Liu, X., Pan, Z., Liu, S., Han, H., Zhao, C., et al. (2018). The role of IL-8/CXCR2 signaling in microcystin-LR triggered endothelial cell activation and increased vascular permeability. *Chemosphere* 194, 43–48. doi:10.1016/j.chemosphere.2017.11.120

Christie, B. (2022). Scientists search for cause of hepatitis cases in children. *Bmj* 377, o982. doi:10.1136/bmj.o982

Cook-Mills, J. M., Marchese, M. E., and Abdala-Valencia, H. (2011). Vascular cell adhesion molecule-1 expression and signaling during disease: Regulation by reactive oxygen species and antioxidants. *Antioxid. Redox Signal* 15, 1607–1638. doi:10.1089/ars.2010.3522

D'Antoni, M. L., Mitchell, B. I., McCurdy, S., Byron, M. M., Ogata-Arakaki, D., Chow, D., et al. (2018). Cenicriviroc inhibits trans-endothelial passage of monocytes and is associated with impaired E-selectin expression. *J. Leukoc. Biol.* 104, 1241–1252. doi:10.1002/jlb.5a0817-328rrr

Dayang, E. Z., Plantinga, J., Ter Ellen, B., van Meurs, M., Molema, G., and Moser, J. (2019). Identification of LPS-activated endothelial subpopulations with distinct inflammatory phenotypes and regulatory signaling mechanisms. *Front. Immunol.* 10, 1169. doi:10.3389/fimmu.2019.01169

Dong, V., Nanchal, R., and Karvellas, C. J. (2020). Pathophysiology of acute liver failure. *Nutr. Clin. Pract.* 35, 24–29. doi:10.1002/ncp.10459

Fallon, M. E., and Hinds, M. T. (2021). Single cell morphological metrics and cytoskeletal alignment regulate VCAM-1 protein expression. *Biochem. Biophys. Res. Commun.* 555, 160–167. doi:10.1016/j.bbrc.2021.03.129

Geng, J., Fu, W., Yu, X., Lu, Z., Liu, Y., Sun, M., et al. (2020). Ginsenoside Rg3 alleviates ox-LDL induced endothelial dysfunction and prevents atherosclerosis in ApoE(-/-) mice by regulating PPARγ/FAK signaling pathway. *Front. Pharmacol.* 11, 500. doi:10.3389/fphar.2020.00500

Giblin, P. A., and Lemieux, R. M. (2006). LFA-1 as a key regulator of immune function: Approaches toward the development of LFA-1-based therapeutics. *Curr. Pharm. Des.* 12, 2771–2795. doi:10.2174/138161206777947731

Gong, L., Lei, Y., Liu, Y., Gong, S., Lan, T., Zeng, L., et al. (2019). *Gut microbiota mediates diurnal variation of acetaminophen induced acute liver injury in mice*, 1169, 214051–215459. doi:10.1016/j.jhep.2018.02.024Vaccarin prevents ox-LDL-induced HUVEC EndMT, inflammation and apoptosis by suppressing ROS/p38 MAPK signaling*Am. J. Transl. ResJ Hepatol.*

Hafner, A. M., Corthésy, B., and Merkle, H. P. (2013). Particulate formulations for the delivery of poly(I:C) as vaccine adjuvant. *Adv. Drug Deliv. Rev.* 65, 1386–1399. doi:10.1016/j.addr.2013.05.013

Hayden, M. S., and Ghosh, S. (2008). Shared principles in NF-kappaB signaling. *Cell* 132, 344–362. doi:10.1016/j.cell.2008.01.020

He, J., Lang, G., Ding, S., and Li, L. (2013). Pathological role of interleukin-17 in poly I:C-induced hepatitis. *PLoS One* 8, e73909. doi:10.1371/journal.pone.0073909

Huang, W., Huang, M., Ouyang, H., Peng, J., and Liang, J. (2018). Oridonin inhibits vascular inflammation by blocking NF-κB and MAPK activation. *Eur. J. Pharmacol.* 826, 133–139. doi:10.1016/j.ejphar.2018.02.044

Humphries, M. J. (2009). Cell adhesion assays. *Methods Mol. Biol.* 522, 203–210. doi:10.1007/978-1-59745-413-1_14

Jaeschke, H., and Hasegawa, T. (2006). Role of neutrophils in acute inflammatory liver injury. *Liver Int.* 26, 912–919. doi:10.1111/j.1478-3231.2006.01327.x

Jaeschke, H. (2006). Mechanisms of Liver Injury. II. Mechanisms of neutrophil-induced liver cell injury during hepatic ischemia-reperfusion and other acute inflammatory conditions. *Am. J. Physiol. Gastrointest. Liver Physiol.* 290, G1083–G1088. doi:10.1152/ajpgi.00568.2005

Jung, K., Linse, F., Heller, R., Jung, T. W., Pyun, D. H., Kim, T. J., et al. (1996). Adhesion molecules in atopic dermatitis: VCAM-1 and ICAM-1 expression is increased in healthy-appearing skin. *Allergy,* **51**Meteorin-like protein (METRNL)/IL-41 improves LPS-induced inflammatory responses via AMPK or pparδ-mediated signaling pathways. *Adv. Med. Sci.* 66, 452155–460161. doi:10.1016/j.advms.2021.01.007

Kawaguchi, S., Sakuraba, H., Kikuchi, H., Numao, N., Asari, T., Hiraga, H., et al. (2021). Tryptanthrin suppresses double-stranded RNA-induced CXCL10 expression via inhibiting the phosphorylation of STAT1 in human umbilical vein endothelial cells. *Mol. Immunol.* 129, 32–38. doi:10.1016/j.molimm.2020.11.003

Kawamura, A., Miura, S., Murayama, T., Iwata, A., Zhang, B., Nishikawa, H., et al. (2004). Increased expression of monocyte CD11a and intracellular adhesion molecule-1 in patients with initial atherosclerotic coronary stenosis. *Circ. J.* 68, 6–10. doi:10.1253/circj.68.6

Khan, H. A., Munir, T., Khan, J. A., Shafia Tehseen Gul, A. H., Ahmad, M. Z., Aslam, M. A., et al. (2021). IL-33 ameliorates liver injury and inflammation in Poly I:C and

Concanavalin-A induced acute hepatitis. *Microb. Pathog.* 150, 104716. doi:10.1016/j.micpath.2020.104716

Kim, C. H. (2004). Chemokine-chemokine receptor network in immune cell trafficking. *Curr. Drug Targets Immune Endocr. Metabol. Disord.* 4, 343–361. doi:10.2174/1568008043339712

Kucik, D. F., and Wu, C. (2005). Cell-adhesion assays. *Methods Mol. Biol.* 294, 43–54. doi:10.1385/1-59259-860-9:043

Laferrière, J., Houle, F., and Huot, J. (2004). Adhesion of HT-29 colon carcinoma cells to endothelial cells requires sequential events involving E-selectin and integrin beta4. *Clin. Exp. Metastasis* 21, 257–264. doi:10.1023/b:clin.0000037708.09420.9a

Lalor, P. F., and Adams, D. H. (2002). The liver: A model of organ-specific lymphocyte recruitment. *Expert Rev. Mol. Med.* 4, 1–16. doi:10.1017/s1462399402004155

Läubli, H., and Borsig, L. (2010). Selectins promote tumor metastasis. *Semin. Cancer Biol.* 20, 169–177. doi:10.1016/j.semcancer.2010.04.005

Ley, K., Laudanna, C., Cybulsky, M. I., and Nourshargh, S. (2007). Getting to the site of inflammation: The leukocyte adhesion cascade updated. *Nat. Rev. Immunol.* 7, 678–689. doi:10.1038/nri2156

Li, H., Liu, N. N., Li, J. R., Dong, B., Wang, M. X., Tan, J. L., et al. (2022a). Combined use of bicyclol and berberine alleviates mouse nonalcoholic fatty liver disease. *Front. Pharmacol.* 13, 843872. doi:10.3389/fphar.2022.843872

Li, H., Liu, N. N., Li, J. R., Wang, M. X., Tan, J. L., Dong, B., et al. (2022b). Bicyclol ameliorates advanced liver diseases in murine models via inhibiting the IL-6/STAT3 signaling pathway. *Biomed. Pharmacother.* 150, 113083. doi:10.1016/j.biopha.2022.113083

Li, S., Zhu, W. G., Yan, H., Fan, F. y., Sun, P. y., and Zhu, J. h. (2007). Homocysteine at pathophysiological concentrations enhances binding of dendritic cells to endothelial cells mediated by DC-SIGN. *Int. Immunopharmacol.* 7, 1241–1250. doi:10.1016/j.intimp.2007.05.009

Li, W., Wang, C., Zhang, D., Zeng, K., Xiao, S., Chen, F., et al. (2021). Azilsartan ameliorates ox-LDL-induced endothelial dysfunction via promoting the expression of KLF2. *Aging (Albany NY)* 13, 12996–13005. doi:10.18632/aging.202973

Lv, H., Yu, Z., Zheng, Y., Wang, L., Qin, X., Cheng, G., et al. (2016). Isovitexin exerts anti-inflammatory and anti-oxidant activities on lipopolysaccharide-induced acute lung injury by inhibiting MAPK and NF-κB and activating HO-1/Nrf2 pathways. *Int. J. Biol. Sci.* 12, 72–86. doi:10.7150/ijbs.13188

Lv, H., Zhu, C., Wei, W., Lv, X., Yu, Q., Deng, X., et al. (2020). Enhanced Keap1-Nrf2/Trx-1 axis by daphnetin protects against oxidative stress-driven hepatotoxicity via inhibiting ASK1/JNK and Txnip/NLRP3 inflammasome activation. *Phytomedicine* 71, 153241. doi:10.1016/j.phymed.2020.153241

Lv, Y., Kim, K., Sheng, Y., Cho, J., Qian, Z., Zhao, Y. Y., et al. (2018). YAP controls endothelial activation and vascular inflammation through TRAF6. *Circ. Res.* 123, 43–56. doi:10.1161/circresaha.118.313143

Maas, S. L., Megens, R. T. A., and van der Vorst, E. P. C. (2023). *Ex vivo* perfusion system to analyze chemokine-driven leukocyte adhesion. *Methods Mol. Biol.* 2597, 59–75. doi:10.1007/978-1-0716-2835-5_6

McEver, R. P. (2015). Selectins: Initiators of leucocyte adhesion and signalling at the vascular wall. *Cardiovasc Res.* 107, 331–339. doi:10.1093/cvr/cvv154

O'Hanlon, D. M., Fitzsimons, H., Lynch, J., Tormey, S., Malone, C., and Given, H. F. (2002). Soluble adhesion molecules (E-selectin, ICAM-1 and VCAM-1) in breast carcinoma. *Eur. J. Cancer* 38, 2252–2257. doi:10.1016/s0959-8049(02)00218-6

Perez, V. L., Pflugfelder, S. C., Zhang, S., Shojaei, A., and Haque, R. (2016). Lifitegrast, a novel integrin antagonist for treatment of dry eye disease. *Ocul. Surf.* 14, 207–215. doi:10.1016/j.jtos.2016.01.001

Phang, S. W., Ooi, B. K., Ahemad, N., and Yap, W. H. (2020). Maslinic acid suppresses macrophage foam cells formation: Regulation of monocyte recruitment and macrophage lipids homeostasis. *Vasc. Pharmacol.* 128-129, 106675. doi:10.1016/j.vph.2020.106675

Quaglia, A., Portmann, B. C., Knisely, A. S., Srinivasan, P., Muiesan, P., Wendon, J., et al. (2008). Auxiliary transplantation for acute liver failure: Histopathological study of native liver regeneration. *Liver Transpl.* 14, 1437–1448. doi:10.1002/lt.21568

Sans, M., Panés, J., Ardite, E., Elizalde, J. I., Arce, Y., Elena, M., et al. (1999). VCAM-1 and ICAM-1 mediate leukocyte-endothelial cell adhesion in rat experimental colitis. *Gastroenterology* 116, 874–883. doi:10.1016/s0016-5085(99)70070-3

Sawa, Y., Ueki, T., Hata, M., Iwasawa, K., Tsuruga, E., Kojima, H., et al. (2008). LPS-induced IL-6, IL-8, VCAM-1, and ICAM-1 expression in human lymphatic endothelium. *J. Histochem Cytochem* 56, 97–109. doi:10.1369/jhc.7A7299.2007

Scalia, R., Appel, J. Z., III, and Lefer, A. M. (1998). Leukocyte-endothelium interaction during the early stages of hypercholesterolemia in the rabbit: Role of P-selectin, ICAM-1, and VCAM-1. *Arterioscler. Thromb. Vasc. Biol.* 18, 1093–1100. doi:10.1161/01.atv.18.7.1093

Schneider, K. M., Elfers, C., Ghallab, A., Schneider, C. V., Galvez, E. J. C., Mohs, A., et al. (2021). Intestinal dysbiosis amplifies acetaminophen-induced acute liver injury. *Cell Mol. Gastroenterol. Hepatol.* 11, 909–933. doi:10.1016/j.jcmgh.2020.11.002

Sørensen, K. K., Simon-Santamaria, J., McCuskey, R. S., and Smedsrod, B. (2015). Liver sinusoidal endothelial cells. *Compr. Physiol.* 5, 1751–1774. doi:10.1002/cphy.c140078

Spessotto, P., Giacomello, E., and Perri, R. (2002). Improving fluorescence-based assays for the *in vitro* analysis of cell adhesion and migration. *Mol. Biotechnol.* 20, 285–304. doi:10.1385/mb:20:3:285

Stravitz, R. T., and Lee, W. M. (2019). Acute liver failure. *Lancet* 394, 869–881. doi:10.1016/s0140-6736(19)31894-x

Su, J., Xu, H. T., Yu, J. J., Yan, M. Q., Wang, T., Wu, Y. J., et al. (2021). Luteolin ameliorates lipopolysaccharide-induced microcirculatory disturbance through inhibiting leukocyte adhesion in rat mesenteric venules. *BMC Complement. Med. Ther.* 21, 33. doi:10.1186/s12906-020-03196-9

Takahashi, M., Ikeda, U., Masuyama, J., Funayama, H., Kano, S., and Shimada, K. (1996). Nitric oxide attenuates adhesion molecule expression in human endothelial cells. *Cytokine* 8, 817–821. doi:10.1006/cyto.1996.0109

Takeda, K., and Akira, S. (2004). TLR signaling pathways. *Semin. Immunol.* 16, 3–9. doi:10.1016/j.smim.2003.10.003

Thawley, V. (2017). Acute liver injury and failure. *Vet. Clin. North Am. Small Anim. Pract.* 47, 617–630. doi:10.1016/j.cvsm.2016.11.010

Tolosa, E., and Shaw, S. (1996). A fluorogenic assay of endogenous phosphatase for assessment of cell adhesion. *J. Immunol. Methods* 192, 165–172. doi:10.1016/0022-1759(96)00042-7

Ulbrich, H., Eriksson, E. E., and Lindbom, L. (2003). Leukocyte and endothelial cell adhesion molecules as targets for therapeutic interventions in inflammatory disease. *Trends Pharmacol. Sci.* 24, 640–647. doi:10.1016/j.tips.2003.10.004

Walzog, B., and Gaehtgens, P. (2000). Adhesion molecules: The path to a new understanding of acute inflammation. *News Physiol. Sci.* 15, 107–113. doi:10.1152/physiologyonline.2000.15.3.107

Wang, L., Cao, Y., Gorshkov, B., Zhou, Y., Yang, Q., Xu, J., et al. (2019). Ablation of endothelial Pfkfb3 protects mice from acute lung injury in LPS-induced endotoxemia. *Pharmacol. Res.* 146, 104292. doi:10.1016/j.phrs.2019.104292

Wang, M., Li, J., Li, H., Dong, B., Jiang, J., Liu, N., et al. (2022). Down-regulating the high level of 17-beta-hydroxysteroid dehydrogenase 13 plays a therapeutic role for non-alcoholic fatty liver disease. *Int. J. Mol. Sci.* 23, 5544. doi:10.3390/ijms23105544

Wang, Y., Cao, J., Fan, Y., Xie, Y., Xu, Z., Yin, Z., et al. (2016). Artemisinin inhibits monocyte adhesion to HUVECs through the NF-κB and MAPK pathways *in vitro*. *Int. J. Mol. Med.* 37, 1567–1575. doi:10.3892/ijmm.2016.2579

WHO (2022). WHO. Available: https://www.who.int/news-room/questions-and-answers/item/severe-acute-hepatitis-of-unknown-cause-in-children (Accessed December 1, 2022).

Woodside, D. G., and Vanderslice, P. (2008). Cell adhesion antagonists: Therapeutic potential in asthma and chronic obstructive pulmonary disease. *BioDrugs* 22, 85–100. doi:10.2165/00063030-200822020-00002

Zhao, X., Wang, Y., Cui, Q., Li, P., Wang, L., Chen, Z., et al. (2019). A parallel phenotypic versus target-based screening strategy for RNA-dependent RNA polymerase inhibitors of the influenza A virus. *Viruses* 11, 826. doi:10.3390/v11090826

Zhong, L., Simard, M. J., and Huot, J. (2018). Endothelial microRNAs regulating the NF-κB pathway and cell adhesion molecules during inflammation. *Faseb J.* 32, 4070–4084. doi:10.1096/fj.201701536R

Zhong, M., Zhang, X., Shi, X., and Zheng, C. (2020a). Halofuginone inhibits LPS-induced attachment of monocytes to HUVECs. *Int. Immunopharmacol.* 87, 106753. doi:10.1016/j.intimp.2020.106753

Zhong, Y., He, S., Huang, K., and Liang, M. (2020b). Neferine suppresses vascular endothelial inflammation by inhibiting the NF-κB signaling pathway. *Arch. Biochem. Biophys.* 696, 108595. doi:10.1016/j.abb.2020.108595

Zhu, S., Xu, X., Liu, K., Gu, Q., Wei, F., and Jin, H. (2017). Peptide GC31 inhibits chemokines and ICAM-1 expression in corneal fibroblasts exposed to LPS or poly(I:C) by blocking the NF-κB and MAPK pathways. *Exp. Eye Res.* 164, 109–117. doi:10.1016/j.exer.2017.07.017

Zimmerman, T., and Blanco, F. J. (2008). Inhibitors targeting the LFA-1/ICAM-1 cell-adhesion interaction: Design and mechanism of action. *Curr. Pharm. Des.* 14, 2128–2139. doi:10.2174/138161208785740225

Resveratrol attenuates staphylococcal enterotoxin B-activated immune cell metabolism *via* upregulation of miR-100 and suppression of mTOR signaling pathway

Hasan Alghetaa[1†], Amira Mohammed[1†], Narendra Singh[2], Kiesha Wilson[2], Goushuai Cai[3], Nagireddy Putluri[4], Mitzi Nagarkatti[2] and Prakash Nagarkatti[2]*

[1]Department of Physiology, Biochemistry and Pharmacology, College of Veterinary Medicine, University of Baghdad, Baghdad, Iraq, [2]Department of Pathology, Microbiology and Immunology, School of Medicine, University of South Carolina, Columbia, SC, United States, [3]Department of Environmental Health Sciences, Arnold School of Public Health, University of South Carolina, Columbia, SC, United States, [4]Dan L. Duncan Cancer Center, Advanced Technology Core, Alkek Center for Molecular Discovery, Baylor College of Medicine, Houston, TX, United States

Acute Respiratory Distress Syndrome (ARDS) is triggered by a variety of insults, such as bacterial and viral infections, including SARS-CoV-2, leading to high mortality. In the murine model of ARDS induced by Staphylococcal enterotoxin-B (SEB), our previous studies showed that while SEB triggered 100% mortality, treatment with Resveratrol (RES) completely prevented such mortality by attenuating inflammation in the lungs. In the current study, we investigated the metabolic profile of SEB-activated immune cells in the lungs following treatment with RES. RES-treated mice had higher expression of miR-100 in the lung mononuclear cells (MNCs), which targeted mTOR, leading to its decreased expression. Also, Single-cell RNA-seq (scRNA seq) unveiled the decreased expression of mTOR in a variety of immune cells in the lungs. There was also an increase in glycolytic and mitochondrial respiration in the cells from SEB + VEH group in comparison with SEB + RES group. Together these data suggested that RES alters the metabolic reprogramming of SEB-activated immune cells, through suppression of mTOR activation and its down- and upstream effects on energy metabolism. Also, miR-100 could serve as novel potential therapeutic molecule in the amelioration of ARDS.

KEYWORDS

MiR-100, ARDS (acute respiratory disease syndrome), T-cell metabolism, mTOR, staphylococcal enterotoxin B (SEB), resveratrol, metabolome, ScRNA

Abbreviations: ARDS, acute respiratory distress syndrome; ECAR, extracellular acidic rate; OCR, oxygen consumption rate; PER, proton efflux rate; RES, resveratrol; SEB, *staphylococcus* enterotoxin-B; VEH, vehicle.

Introduction

Acute respiratory distress syndrome (ARDS) is a serious clinical disorder triggered by many etiological agents such as bacterial, fungal and viral infections as well as certain chemical toxicants (de Prost et al., 2017). ARDS is characterized by fluid leaking into the lungs, difficulties in breathing, low blood oxygenation rate and is defined as a life-threatening lung injury. Additionally, ARDS is associated with hyperactivation of the immune response in the lungs, and systemically. This often leads to cytokine secretion, leading to the development of pulmonary edema, alveolar damage, and respiratory as well as multiorgan failure (Nagarkatti et al., 2020). ARDS is extremely challenging to treat because of which almost 40% of people with ARDS die (Dembinski and Mielck, 2018). The pandemic caused by SARS-CoV-2 virus (COVID-19) is also well characterized to trigger ARDS leading to high levels of mortality (Perico et al., 2021). Currently, there are no pharmacological agents approved by the Food and Drug Administration to specifically treat ARDS.

Staphylococcal enterotoxin-B (SEB) is one of many toxins secreted by *Staphylococcus aureus* bacterium and can cause food poisoning outbreak when ingested with contaminated food leading to vomiting, diarrhea and different gastrointestinal symptoms (Ercoli et al., 2017; Guidi et al., 2018). SEB can also cause ARDS when aerosolized because of which it is classified as select agent of biological warfare by CDC (Pohanka, 2019). SEB activates a subfamily of T cells that express Vβ7 and Vβ8 on their T cell receptors thereby activating a significant proportion of T cells to produce cytokines (Sultan et al., 2021). Thus, inhalation of SEB leads to pro-inflammatory cytokine storm systemically (Fries and Varshney, 2013; Popugailo et al., 2019; Mohammed et al., 2020c), which in turn triggers massive proliferation and recruitment of effector T cells, macrophages, and neutrophils from the periphery into the lungs leading lung injury (Savransky et al., 2003; Muralimohan et al., 2008; Rao et al., 2015b; Mohammed et al., 2020c; Ferreira-Duarte et al., 2020). This could also occur due to microRNA dysregulation in immune cells that will lead to hyperactivity of immune cells, especially the T effector cells (Alghetaa et al., 2018; Mohammed et al., 2020a; Mohammed et al., 2020c).

microRNA (miRNA, miR) are small non-coding RNA molecules (~22 nucleotides) that regulate mRNA expression involved in different biological cellular functions such as cell death, cell proliferation and cell metabolism (Ambros, 2004). Recently, several studies have demonstrated aberrant levels of miRNAs associated with ARDS, indicating their complex role in regulating the etiopathology of ARDS (Zhu et al., 2017; Alghetaa et al., 2018; Ferruelo et al., 2018; Wu et al., 2019; Mohammed et al., 2020a). Previous studies from our laboratory found that miRNAs dysregulation mediated by SEB involved multiple pathways that exacerbated the inflammation in the lungs including suppression of T cell apoptosis (Rao et al., 2015a; Elliott et al., 2016; Mohammed et al., 2020a), suppression of TGF-β and T reg signaling (Rao et al., 2015b; Alghetaa et al., 2018), inhibition of SOCS1 (Rao et al., 2014) and increase NF-$_K$B signaling (Rieder et al., 2012). Interestingly, we found that natural products such as cannabinoids and resveratrol reversed the dysregulation caused by SEB, attenuated the ARDS and protected the lungs (Alghetaa et al., 2018; Mohammed et al., 2020a; Mohammed et al., 2020b; Alghetaa et al., 2021).

Previous studies showed that Resveratrol (RES; trans-3,5,4′-trihydroxystilbene), a phytoalexin, was found to prevent SEB-induced ARDS and mortality in mice (Alghetaa et al., 2018; Alghetaa et al., 2021). RES is present in various foods such as grapes, red wine, pistachios, peanuts, blueberries and dark chocolate (Tian and Liu, 2020). Several studies have suggested that resveratrol may be effective in the prevention and treatment of delayed type of hypersensitivity, injured testes, aging and age-related diseases, colitis and colorectal cancers (Alrafas et al., 2019; Khayoon and Al-Rekabi, 2020; Abdulla et al., 2021; Zhou et al., 2021; Abdulla and Al-Okaily, 2022; Al-Salman et al., 2022). While this effect may be mediated through several pathways, one of them may involve mechanistic/mammalian target of rapamycin (mTOR). mTOR is involved in the regulation of aging as well as other functions such as inflammation (Papadopoli et al., 2019). Interestingly, resveratrol has been shown to inhibit mTOR signaling (Liu et al., 2010).

In the current study, we tested the central hypothesis that resveratrol may suppress SEB-mediated hyperactivation of the immune cells through the downregulation of mTOR signaling pathway. We found that while SEB upregulated the expression of mTOR in T cells, resveratrol reversed this action. We also identified miR-100-5p as the key regulator of the mTOR expression induced by resveratrol.

Materials and methods

Experimental animals

Female C3H/HeJ mice 6-8-week-old were purchased from The Jackson Laboratory. All mice were housed in specific pathogen–free conditions at the Association for Assessment and Accreditation of Laboratory Animal Care Internationally Accredited University of South Carolina, School of Medicine, Animal Resource Facility and were kept under 12 light/12 dark cycles at a temperature of ~18°C–23°C and 40%–60% humidity. Food and water were available *ad libitum*. All experiments performed using mice in this study were approved by the Institutional Animal Care and Use Committee, University of South Carolina under animal use protocol (AUP2363).

Chemicals and reagents

Resveratrol (RES) was purchased from Supelco (MO, United States) and prepared freshly in an appropriate vehicle (VEH) consisting of 1% carboxyl methyl cellulose (CMC, Sigma-Aldrich, United States). SEB was obtained from Toxin Technology Inc. (FL, United States) and aliquoted in sterile phosphates buffer saline (PBS) at a stock concentration of 2 μg/μL prior to storage at −20°C until being used.

Experimental design

We used a previously described method to induce ARDS by SEB involving double sensitization with SEB in C3H/HeJ mice which leads to 100% mortality and treatment with RES reverses

this action. Briefly, C3H/HeJ mice pretreated orally with two doses of either 100 mg/kg resveratrol or VEH at 24 h intervals. After the second dose of RES, intranasal administration of 5µg/mouse of SEB was given and then after 90 min from the first SEB dose, a second dose of i. p 2µg/mouse of SEB was given as a fatal model of dual-dose SEB exposure (Rao et al., 2015b; Alghetaa et al., 2018). Endpoint of the experiment was 48 h post first SEB exposure at which time the mice were euthanized and the infiltrating mononuclear cells in the lungs were collected by gradient separation (Elliott et al., 2016).

Mononuclear cell (MNC) isolation from the lungs and cell preparation from the spleens

Mononuclear cells (MNCs) from the lungs were prepared as described previously (Alghetaa et al., 2018; Mohammed et al., 2020b; Alghetaa et al., 2021; Sultan et al., 2021). Briefly, excised lungs were subjected to a mechanical tissue homogenizer (Seward, England). The tissue suspension was filtered and the single-cell mixture was suspended in cold fluorescence-activated cell sorting buffer (FACS) prepared from PBS enriched with 10% fetal bovine serum protein (FBS). RBC-lysis buffer (Sigma-Aldrich, United States) was used to remove the RBC from the mixture before being filtered with a 100 micron-strainer (Fisher Scientific, China). The filtered suspension was layered on Ficoll gradient, Histopaque-1077 (Sigma-Aldrich, United States) to separate MNCs. All MNC preparations were finally suspended in FACS and cell counts were measured by using trypan blue dye *via* auto cell counter 2000 (Bio-Rad, United States). Spleen cell preparations were carried out in a similar fashion except that they were not subjected to Ficoll gradient separation.

Metabolome profiling and measurement of glycolysis and TCA metabolites using LC–MS

Sample preparation for mass spectrometry and metabolomics analysis

Metabolites were extracted from serum using the extraction procedure described previously (Wangler et al., 2017; Kornberg et al., 2018; Amara et al., 2019; Vantaku et al., 2019a; Vantaku et al., 2019b; Vantaku et al., 2019c). Briefly, 50 µl of serum sample was used for the metabolic extraction. The extraction step was started with the addition of 750 µL ice-cold methanol: water (4:1) containing 20 µL spiked internal standards to each cell pellet or tissue sample. Ice-cold chloroform and water were added at a 3:1 ratio for a final proportion of 1:4:3:1 water: methanol:chloroform:water. The organic (methanol and chloroform) and aqueous layers were mixed, dried, and resuspended with 50:50 methanol: water. The extract samples were deproteinized, followed by resuspension, and subjected to LC/MS analysis.

Ten µL of suspended samples were injected and analyzed using a 6,490 triple quadrupole mass spectrometer (Agilent Technologies, Santa Clara, CA) coupled to an HPLC system (Agilent Technologies, Santa Clara, CA) *via* single reaction monitoring (SRM).

Separation of glycolysis, TCA, and pentose pathway metabolites

Tricarboxylic acid cycle and Glycolysis cycle metabolites were identified by using 5 mM ammonium acetate in water as buffer PH 9.9 (A) and 100% acetonitrile as a buffer (B) using Luna 3 µM NH2 100 A^0 Chromatography column (Phenomenex, Torrance, CA). The Gradient used: 0–20 min-80% B (Flow rate 0.2 ml/min); 20–20.10 min- 80% to 2% B; 20.10–25 min-2% B(Flow rate 0.3 ml/min); 25–30 min 80% B (Flowrate 0.35 ml/min); 30–35 min-80%B (Flow rate 0.4 ml/min); 35–38 min 80% B (Flow rate 0.4 ml/min); followed by re-equilibration at the end of the gradient to the initial starting condition 80% B a Flow rate of 0.2 ml/min. All the identified metabolites were normalized by spiked internal standard (Mohammed et al., 2020c).

microRNA (miRNA) array and *in silico* analysis

miRNA analysis was carried out as described previously (Alharris et al., 2018; Neamah et al., 2019). Briefly, total RNA, including miRNA, was isolated from lung mononuclear cells using the miRNeasy kit from QIAGEN and following the protocol of the company. Microarray was performed using Affymetrix miRNA Array (version 4.1). Raw files generated from the miRNA microarray were uploaded to Gene Expression Omnibus (http://www.ncbi.nlm.nih.gov/geo) and deposited under accession number GSE220159. By using Transcriptome Analysis Console (TAC, ThermoFisher, United States), Log2 fold change of more than 3,000 miRNAs was detected from the raw array data, and only those miRNAs that were altered more than 2-fold were considered for further analysis. Filtered miRNAs were analyzed for their role in various biological pathways using Ingenuity Pathway Analysis (IPA) software http://www.ingenuity.com (Qiagen, Germany). Also, microRNA.org database was used to examine the sequence alignment regions between miR-100-5p and its targeted genes.

Activation of spleen cells *in vitro* with SEB

Naïve spleens were excised from C3H/HeJ mice and processed to prepare a single cells suspension. The cells were seeded in U-bottom 96-well plates (Corning, United States) at a concentration of 5×10^5 cells/well in complete DMEM medium (Sigma, United States) supplemented with 10% FBS (Atlanta for Biologicals, United States) 1% penicillin/streptomycin cocktail (Sigma, United States) and 50 µM mercaptoethanol (2-ME, Sigma, United States). Seeded cells were pretreated with either 50 µM RES or VEH for one hour before adding 1 µg/mL SEB to the culture. Activated cultures were incubated for 48 h at 37°C with 5% CO2 and the culture supernatants were collected for further analysis. Collected cultured cells were washed with phosphate buffer saline (PBS) twice before being suspended in FACS buffer. PE-conjugated anti-CD3 antibody (Biolegend, United States) was used to stain all harvested cells and then purified positively by using

EasySep™ PE Positive Selection Kit II magnetic microbeads (STEMCELL, United States).

³H-thymidine incorporation assay

To evaluate the proliferative capacity of activated immune cells, SEB-activated MNCs from lungs or *in vitro* SEB-activated splenocytes were treated with thymidine (methyl-3H; PerkinElmer Health Sciences, United States) isotope at a concentration of 1μCi/well and incubated for 16 h to and then radioactivity was measured using a liquid-scintillation counter (MicroBeta TriLux; PerkinElmer, United States).

RT-PCR assay

To determine the expression of Mtor, Pkm, Prkaa1, Rac1 and Rptor in the lung MNC or PE-selected T cells post-RES or vehicle treatment, RT-PCR was performed. The primer sequence of these genes was determined from the Primer Bank database and then built using Integrated DNA Technologies tools (Table 1). RT-PCR was performed for 40 cycles using the following conditions: 98°C (denaturing temperature) for 30 s, 98°C (annealing temperature) for 10 s, and 60°C (extension temperature) for 30 s. The expression of the above genes was normalized against mouse housekeeping gene Gapdh expression (internal control).

Transfection experiments with miR-100-5p mimic and inhibitor

Transfection of SEB-activated splenocyte cultures with miR-100-5p mimic and inhibitor was performed as previously described (Alharris et al., 2018). Briefly, C3H/HeJ naïve splenocytes were cultured in 24-well plates (2×10^5 cells per well) and activated with 1 μg/mL of SEB for 24 h. Transfections were performed with Qiagen HiPerfect Transfection Reagent and 20 nmol/L of either syn-mmu-miR-100-5p mimic (Qiagen, MSY0000098), anti-mmu-miR-100-5p inhibitor (Qiagen, MIN0000098) or transfection reagent alone (mock, Qiagen). Transfection efficiency was validated with qRT-PCR for miR-100 (Qiagen, MS00031234), and expression of mTOR, Rac1, and Rptor after transfection was determined with RT-PCR (Mohammed et al., 2020a).

Real-time PCR (RT-PCR) for detection of miR-100

Total RNA was isolated from lung mononuclear cells, cultured splenocytes, and miR-100-5p-transfected cells and then converted into cDNA by using miScript RT II kit (Qiagen, Germany) to prepare reverse transcription reaction component. After that, miR-100-5p-specific miScript Primer Assays (Qiagen, MS00031234, forward primer) were mixed with Universal Primer (reverse primer) and QuantiTect SYBR Green PCR Master Mix to quantify the enrichment of miR-100 in these prepared cDNAs. For accurate and reproducible results in miRNA quantification by real-time PCR, the amount of miR-100 was normalized by using an endogenous reference RNA consisting of Snord96A. The cycling conditions for RT-PCR were listed in Table 2.

Flow cytometry analysis of T cell subsets in the lungs

Single cell suspension of mononuclear cells was isolated from the lungs by using the gradient Ficoll layering method and prepared as described previously (Alghetaa et al., 2018). To avoid false positive or false negative immunofluorescence results, all cells were suspended in FACS buffer and incubated with FcγR blocker (Biolegend, United States). Then these cells were permeabilized (Pharmingen BD, United States) and stained with Biolegend anti-CD3, CD4, CD8, T-bet and IFN-γ antibodies conjugated with APC, BV786, PE, BV605 and APC-R700 fluorochromes respectively, which were used according to the manufacturer's protocols.

Immunofluorescence staining of mTOR

To validate the PCR results of upregulated mTOR gene expression, we performed immunofluorescent staining of lung tissue. We calculated the corrected total cell fluorescence (CTCF) for mTOR-stained cells in the lung tissue of naïve, SEB + VEH, and SEB + RES groups using ImageJ software from NIH, we performed immunofluorescent staining as described earlier (Alharris et al., 2018; Sarkar et al., 2019; Alharris et al., 2022). Briefly, the slides with a section of lung tissue were first deparaffinized according to the standard protocol, antigen

TABLE 1 Used primers with their Primer Bank identification number.

mRNA ID	Forward 5′----->3′	Reverse 5′----->3′	Primer bank ID
Gapdh	AGGTCGGTGTGAACGGATTTG	TGTAGACCATGTAGTTGAGGTCA	6679937a1
Mtor	ACCGGCACACATTTGAAGAAG	CTCGTTGAGGATCAGCAAGG	9910228a1
Pkm	GCCGCCTGGACATTGACTC	CCATGAGAGAAATTCAGCCGAG	31981562a1
Prkaa1	GTCAAAGCCGACCCAATGATA	CGTACACGCAAATAATAGGGGTT	26349431a1
Rac1	GAGACGGAGCTGTTGGTAAAA	ATAGGCCCAGATTCACTGGTT	13277918a1
Rptor	CAGTCGCCTCTTATGGGACTC	GGAGCCTTCGATTTTCTCACA	30061325a1

Gapdh, glyceraldehyde-3-phosphate dehydrogenase; Mtor, mechanistic target of rapamycin; Pkm, pyruvate kinase; Prkaa1, protein kinase, AMP-activated, alpha 1 catalytic subunit; Rac1, RAS-related C3 botulinum substrate 1 and Rptor, regulatory associated protein of MTOR.

PCR cycle		Temp	Time	Repeat
Activation step		95C	15 min	N/A
3-step cycle	Denaturation	94C	15 s	40
	Annealing	55C	30 s	
	Extension	70C	30 s	

retrieval was done using an antigen-retrieval solution from Abcam (Cambridge, MA, United States). The slides were then washed with PBS twice, permeabilized with 0.01% Triton X-100 (Sigma) for 15 min, washed three times with PBS for 5 min each, and then incubated overnight at 4°C with primary antibody (mouse-specific mTOR) from Abcam (Cambridge, MA, United States) diluted in 1% FBS in PBS. Next, the slides were washed with PBS three times for 10 min each and incubated with anti-mouse secondary antibody diluted in 1% FBS in PBS for 1 h at 37°C followed by washing the slides three times with PBS. The slides were then stained with DAPI to show the nuclei of the cells and washed three times with PBS and finally mounted with Antifade Mounting Medium from Vector Labs (Burlingame, CA). The tissue was visualized and imaged by usa ing Confocal microscope (Leica, United States).

CellTrace assay of T cell division rate measured by carboxyfluorescein succinimidyl ester (CFSE) nuclear dye

Naïve splenocytes were prepared and suspended in 10 μM CSFE staining protein-free medium for 20 min, followed by staining the cells. The cells were washed twice before grouping them according to the treatment conditions and suspended in complete DMEM medium and seeded them at a concentration of 5×10^5 cell/well in 96-well plates. Treated cells were then incubated for 48 h post 1 μg/mL SEB-activation at 37°C with 5% CO2 and then purified as described above to measure the cell division of T cells.

Real-time metabolism analysis of T cells measured by seahorse XFp

Mitochondrial respiration, glycolytic rate, ATP rate, and fuel substrate dependency were measured based on the quantification of oxygen consumption rates (OCR), extracellular acidification rate, and proton efflux rate (PER). In all of these assessments, initially 2.5×10^5 cells/well of purified T cells were seeded in XFp culture plates (Agilent, United States) by using CellTak cell tissue adhesive (Corning, United States). According to the assay recommendations, the cells were suspended in Agilent Seahorse XF DMEM Medium pH 7.4 (Agilent, United States) supplemented with 10 mM glucose, 1 mM sodium pyruvate, and/or 2 mM glutamine. Mitochondrial stress test, glycolysis stress test, ATP production rate test, glucose dependency test, and fatty acid dependency test were performed according to the manufacturer's protocols. To achieve these measurements, a combination of 1 mM oligomycin, 1 mM fluorocarbonyl-cyanide-phenylhydrazone (FCCP), 0.5 mM rotenone, and antimycin-A and/or 2-deoxy-D-glucose (2-DG) were used according to the assay protocol. Once the assay was finished, all the cells in the run plate were stained with 2 μM final concentration of Hoechst 33,342 dye to quantify the live cell numbers by Cytation5 Imaging Cytometer (BioTek, United States) and to normalize the acquired data accordingly. All acquired data generated by Seahorse XFp were normalized and interpreted kinetically with Seahorse Wave Desktop Software (SWD) (Agilent, United States). Kinetic data of glycolytic and mitochondrial ATP production were generated by using Seahorse XF Real-Time ATP Rate Assay Kit according to the manufacturer's protocol. Briefly, the alterations of concentrations of oxygen and proton in the culture medium due to the mitochondrial and glycolysis processes in living cells was detected *via* the chemical sensors. Oligomycin, an inhibitor of mitochondrial ATP synthase and rotenone/antimycin A chemicals were injected into the microplate to challenge the cellular respiration events by which the sensors calculate the delta of OCR and ECAR. All acquired data were then interpreted by using the SWD into bioenergetic kinetics. For detecting what type of fuel is utilized by mitochondria, Agilent Seahorse XF Mito Fuel Flex Test Kits was used. The assay medium consisting of DMEM for this test was supplemented with 1 mM pyruvate, 2 mM glutamate and 10 mM glucose and the medium pH was adjusted to be 7.4 at the time of analysis. The sensor cartridge was loaded with 30 μM bis-2-(5-phenylacetamido-1,2,4-thiadiazol-2-yl)ethyl sulfide (BPTES), an inhibitor of glutamine oxidation pathway, 40 μM Etomoxir, an inhibitor of long chain fatty acid oxidation, and 20μM UK5099, an inhibitor of glucose oxidation pathway. Afterwards, SWD was used to calculate the dependency, capacity and flexibility of T cells in switching among different sources of energy fuels.

Single-cell RNA-seq (scRNA-seq) and analysis of lung cellular heterogeneity composition

The TC20 Automated Cell Counter (BioRad) was used to measure the cell count and viability of isolated lung cells. The cells were next loaded onto the Chromium Controller (10x Genomics). Following the manufacturer's protocol, the Chromium single cell 5′ reagent kits (10x Genomics) were used to process samples into single-cell RNA-seq (scRNAseq) libraries. Sequencing of those libraries was performed using the NextSeq 550 instrument (Illumina) with a depth of 40k–60k reads per cell. The base call files generated from sequencing the libraries were then processed in the 10x Genomics Cell Ranger pipeline (version 2.0) to create FASTQ files. The FASTQ files were then aligned to the mm10 mouse genome and the read count for each gene in each cell was generated (Mohammed et al., 2020c). Downstream analysis was completed using Seurat suite version 3.0 within R studio (Butler et al., 2018; Stuart et al., 2019). Data were integrated into Seurat using anchor and integration functions. The integrated data were scaled and Principal-component analysis (PCA) was completed for dimensionality reduction. Clusters were made following PCA analysis by adjusting the granularity resolution to 0.25. We determined the number of principal components (PCs) to utilize post-JackStraw

analysis within Seurat to determine PCs with the lowest *p*-value. Differential expressions were determined for each cluster to determine cluster biomarkers, and between the vehicle and resveratrol-treated samples using the default Wilcoxon rank sum test.

Statistical analyses

In this study, we used groups of five mice treated with SEB + VEH or SEB + RES unless stated differently. The metabolome data were log2-transformed and normalized with internal standards on a per-sample, per-method basis. Statistical analyses were performed with a t-test in R Studio (R Studio Inc., Boston, MA). Differential metabolites were identified by adjusting the *p*-values for multiple testing at an FDR (Benjamini Hochberg method) threshold of <0.25. The ANOVA test was applied whenever there were more than two group comparisons with multiple Tukey's corrections. The T-test was applied with the Holm-Sidak correction method to compare two groups. $p < 0.05$ was considered as significant threshold. Significant differences were depicted as $*p < 0.05$, $**p < 0.01$, $***p < 0.001$, $\#p < 0.0001$. Each experiment was performed three independent times unless stated differently.

Results

Resveratrol treatment in SEB-injected mice led to suppression of mTOR pathway via upregulation of miR-100

Previous studies from our laboratory showed that RES is highly effective in preventing SEB-mediated ARDS (Alghetaa et al., 2018; Alghetaa et al., 2021). To investigate the potential role of miRNA in the amelioration effects of RES, we performed microRNA arrays. The majority of miRNAs (miR) in the lung's MNCs showed altered expression when the mice were exposed to SEB and this effect was reversed significantly when RES was used (Figure 1A). When we considered those miRs with a >2-fold change (Figure 1A), we identified 21 miRNAs that were down-regulated and 44 miRs that were upregulated in the SEB + RES group in comparison to the SEB + VEH group (Figure 1B). By using IPA software to predict the target genes of these miRs, we were able to identify pathways that regulated cellular metabolism and proliferation and found that miR-100-5p was of interest because it was down-regulated by SEB exposure and reversed by RES treatment (Figure 1C).
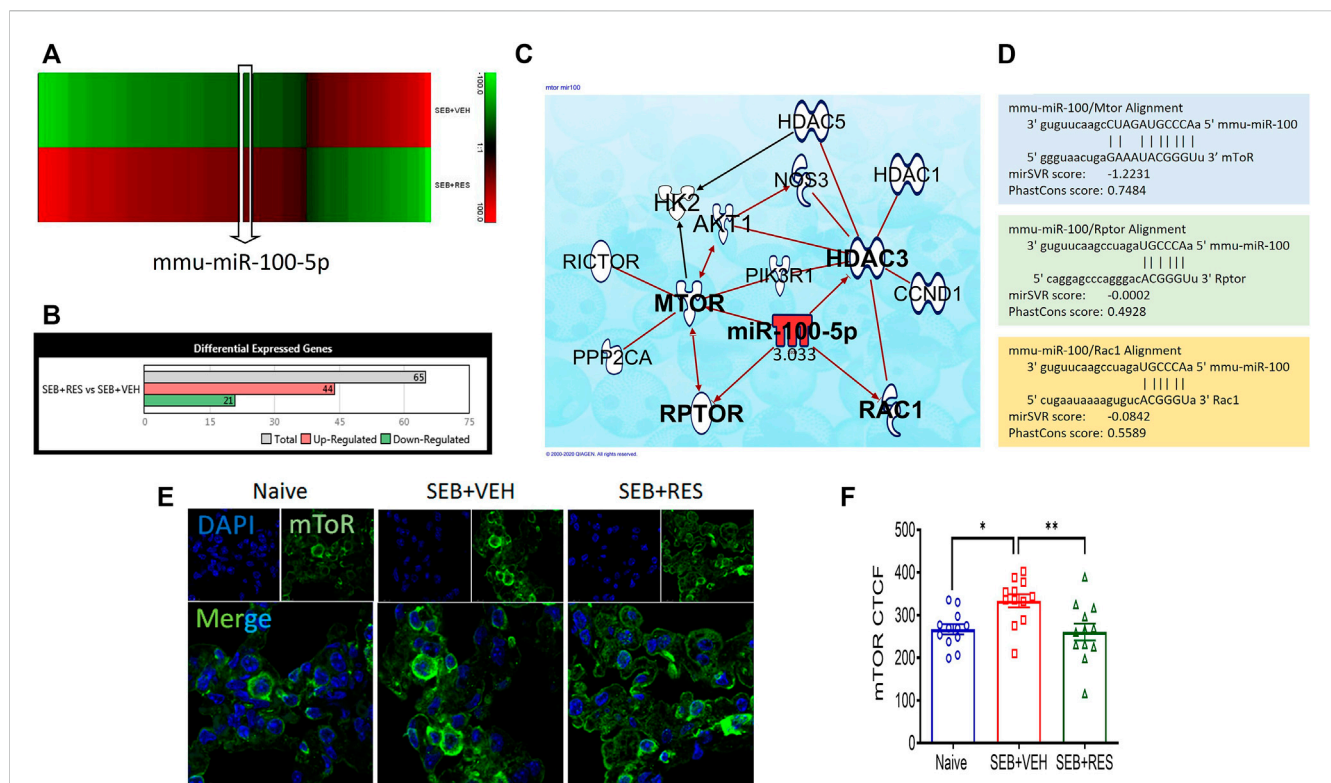
FIGURE 1
Effect of RES on miRNA induction and regulation of mTOR pathway in SEB-activated immune cells. Mice (n = 5) were exposed to SEB and treated with RES as described in Methods. Forty-eight hours later, mice were euthanized and studied as described below: **(A)**. Heat map showing altered expression of miRNAs in the lung mononuclear cells from SEB + VEH vs. SEB + RES groups. Five biological samples were pooled for the *in silico* analyses only, but all validations were performed on individual samples. **(B)**. Bar graph depicting counts of differentially expressed miRNAs with 2-fold change. **(C)**. Ingenuity pathway analysis (IPA) predicted the targeted genes by miR-100. **(D)**. Scheme of alignment regions between miR-100 and its targeted genes (mTOR, Rptor and Rac1). **(E)**. Immunofluorescent staining showing mTOR protein expression in the lung sections imaged by Leica confocal microscope and quantified by ImageJ software. **(F)**. Statistical analysis of mTOR protein expression. Compared values represent mean $\pm$ standard error of means (M$\pm$SE). One-way ANOVA test with multiple Tukey's correction was applied. $p < 0.05$ considered as significant threshold. Significant differences were depicted as $*p < 0.05$, $**p < 0.01$.
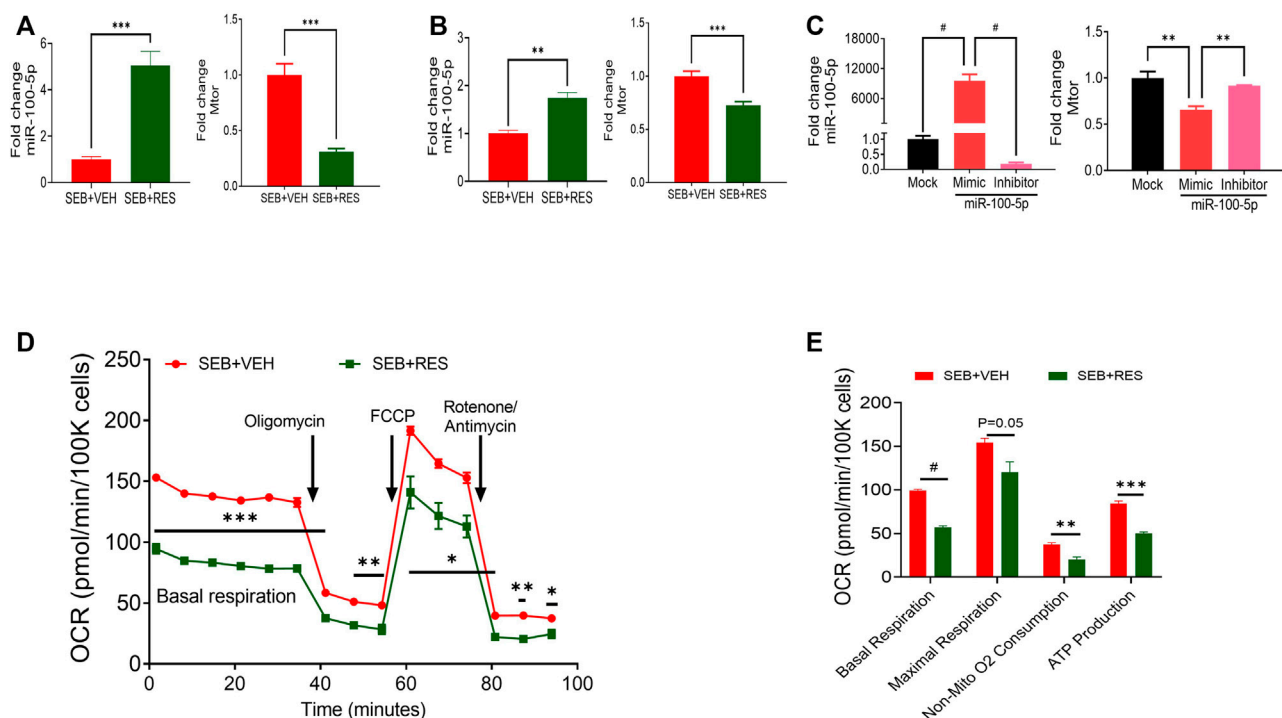
FIGURE 2
In vivo and *in vitro* treatment of RES leads to suppression of mTOR gene expression via upregulation of miR-100 and decreased energy production in SEB-activated T cells. Mice were treated with SEB and RES as described in Figure 1. **(A)** q-RT-PCR showing the levels of expression of miR-100 and mTOR genes in the lung MNCs. **(B)** q-RT-PCR analysis of miR-100 and mTOR gene expression in PE-selected CD3⁺ cells purified from splenocytes activated with SEB and treated with VEH or RES. **(C)** q-RT-PCR analysis of miR-100 and mTOR gene expression in transfected SEB-activated splenocytes with miR-100 mimic siRNA or inhibitor compared to mock-treated group. **(D)**. Real-time analysis of mitochondrial respiration in T cells by using Seahorse system in presence of oligomycin, Carbonyl cyanide-4-phenylhydrazone (FCCP) and combination of rotenone and antimycin. **(E)**. Quantification of selected CD3⁺ T cell respiratory kinetics calculated by report generator software based on changes in oxygen consumption rate (OCR) measured in panel **(D)**. Compared values represent mean ± standard error of means (M±SE). One-way ANOVA test with multiple Tukey's correction was applied to compare more than two groups. T-test was applied with Holm-Sidak correction method to compare two groups. $p < 0.05$ considered as significant threshold. Significant differences were depicted as $*p < 0.05$, $**p < 0.01$, $***p < 0.001$, $\#p < 0.0001$.

Interestingly, the pathway analysis suggested that miR-100-5p may target the mTOR signaling pathway as well as the Regulatory-associated protein of mTOR (RPTOR), and Rac family small GTPase 1 (Rac1). To further confirm the target genes, we used the bioinformatic tool, microrna.org, and found that miR-100-5p did target RPTOR, and Rac1 (Figure 1D). We also studied the mTOR protein expression in the lungs using the immunofluorescence technique and found that mTOR expression was significantly upregulated following SEB treatment when compared to the naïve group and furthermore, RES treatment caused a significant decrease in mTOR expression (Figures 1E,F).

In vivo and *in vitro* treatment with RES leads to suppression of the mTOR gene via upregulation of miR-100-5p and to reduce energy production of SEB-activated T cells

Next, we directly examined the expression of mTOR and miR-100-5p in isolated lung MNCs and found that the SEB + RES group expressed higher levels of miR-100-5p and decreased levels of mTOR when compared to the SEB + VEH group (Figure 2A). Similar observations were made using SEB-activated *in vitro* cultures (Figure 2B). Transfection studies using mimic and inhibitor of miR-100-5p revealed the inverse relationship between the expression of miR-100-5p and mTOR gene expression (Figure 2C). The metabolic kinetics showed that the basal respiration rate, non-mitochondrial oxygen consumption rate, and ATP production rate were significantly higher in T cells of SEB + VEH than in the SEB + RES group (Figures 2D,E).

Single-cell RNA-sequencing (scRNA-seq) reveals downregulation of glucose metabolism-related genes post-RES treatment

scRNA-seq was used to unveil the lung cellular components. We found that the majority of resident and infiltrating immune cells were natural killer T cells (NKT), macrophages (Mac), alveolar macrophages (AM), and myeloid-derived suppressor cells (MDSCs) where each cell phenotype was clustered based on their similarity of transcriptomic profile (Figure 3A). Also, the T-distributed Stochastic Neighbor
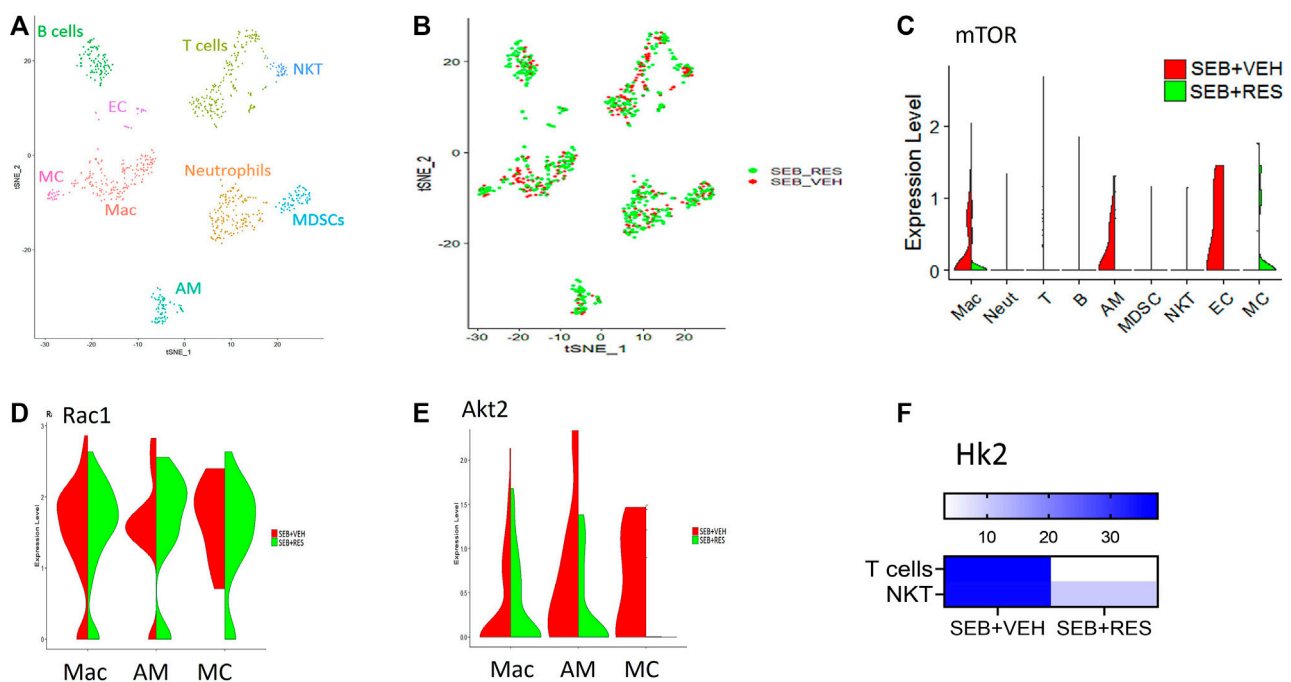
FIGURE 3
Single-cell RNA-sequencing (scRNA-seq) reveals downregulation of glucose metabolism-related genes post-RES treatment. Mice were treated as mentioned in Figure 1 legend. Whole lung tissues were excised and a single cell suspension was prepared. scRNA-seq was performed as described in Methods. The cells studied included: Mac: macrophages, Neut: Neutrophils, T: T cells, **(B)** B cells, AM: Alveolar macrophages, MDSC: Myeloid-derived suppressor cells, EC: Endothelial cells. MC: Monocytes. **(A)** scRNA-seq tSNE colored by cell phenotypes. **(B)** scRNA-seq tSNE colored by group ID consisting of SEB + VEH and SEB + RES. **(C)**. The violin plot depicts the Mtor gene expression levels and enrichments in different lung cellular components. **(D)**. Violin plot depicts Rac1 gene expression levels and enrichment. **(E)**. The violin plot depicts Akt2 gene expression levels and enrichment. **(F)**. Heatmap expression of Hk2 in T cells and NKT cells.
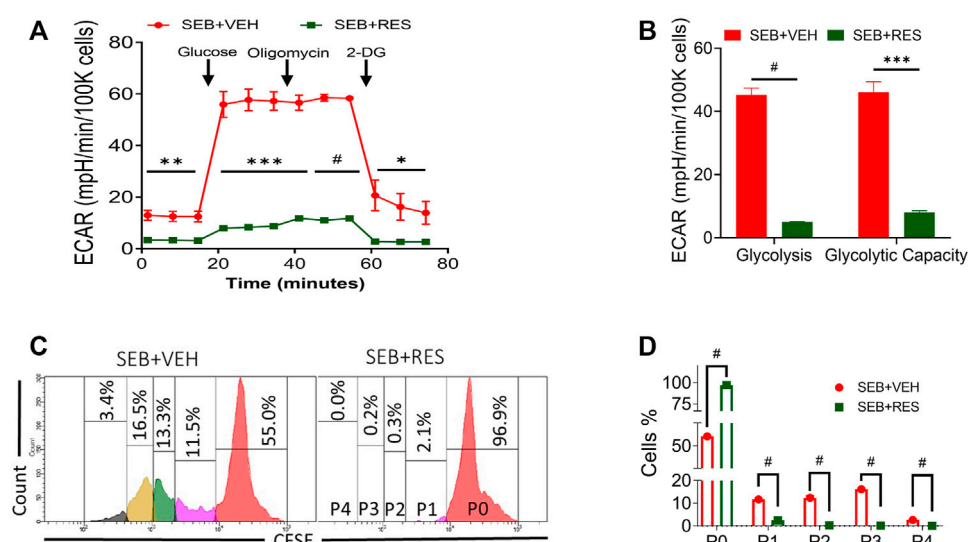
FIGURE 4
Effect of RES on glycolysis and proliferative capacity of SEB-activated T cells. Mice were treated as mentioned in Figure 1 legend. Whole lung tissues were excised and the single cell suspension was prepared for real-time metabolism analysis. **(A)**. Real-time analysis of T cell glycolysis measured by Seahorse system based on the calculation of extracellular acidification rate (ECAR) changes. **(B)**. Glycolysis statistical kinetics of T cells calculated by using Report Generator software. **(C)**. CFSE staining follows T-cell division *in vitro*. Naïve splenocytes were incubated with CFSE dye at a concentration of 10 μM for 20 min at room temperature before being washed and treated with RES or VEH and then activated with 1 μg/ml SEB for 48 h. P, parent cells, 0–4 sequence of cell division. **(D)**. Statistical analysis of T cell divisions depicted as P0-P4. Compared values represent mean ± standard error of means (M ± SE). One-way ANOVA test with multiple Tukey's correction was applied to compare more than two groups. T-test was applied with Holm-Sidak correction method to compare two groups. $p < 0.05$ considered as significant threshold. Significant differences were depicted as $*p < 0.05$, $**p < 0.01$, $***p < 0.001$, $\#p < 0.0001$.

Embedding (tSNE) plot was used to visualize the different cell phenotypes in each study group colored by group ID (Figure 3B). The violin plots showed that the mTOR was highly expressed in macrophages (Mac), alveolar macrophages (AM), and endothelial cells (EC) in the SEB + VEH group and it was significantly decreased in the SEB + RES group (Figure 3C). Furthermore, violin plots also showed other genes related to energy metabolism such as Rac1 (Figure 3D) and Akt2 (Figure 3E), in which Rac1 was increased while Akt2 was decreased in some of the cells examined from the SEB + RES group when compared to the controls. There was also a significant reduction in hexokinase two enzyme (Hk2), a key enzyme of glucose metabolism, in T cells in general and NKT populations of the SEB + RES group in comparison with the SEB + VEH group (Figure 3F).

The findings that Hk2 is inhibited led us to examine the glycolysis rate of glucose in SEB-activated T cells treated with RES or VEH by using the Seahorse system, a real-time metabolism analyzer. Interestingly, we found that RES-treated T cells significantly lowered their glycolysis capacity measured by extracellular acidification rate (ECAR) before and after being challenged with glucose (Figure 4A). According to the kinetic calculation of the metabolic behavior of study groups, the glycolysis rate and glycolytic capacity of SEB-activated T cells treated with VEH were significantly higher than in of SEB + RES group (Figure 4B). All the above changes drove us to examine the cell division of SEB-activated T cells in presence of RES or VEH by using CSFE, a permeable dye. We found that SEB-activated T cells were able to continue in the biological cell divisions and divided for up to four new generations within 48 h into SEB + VEH treated cells (Figures 4C,D), while SEB + RES treatment blocked the cell division (Figures 4C,D).

Effect of RES treatment on reprogramming of SEB-activated T cell mitochondrial function from fatty acid biosynthesis into fatty acid β-oxidation

We also tested the levels of mTOR signaling pathway molecules and found that Rptor and Rac1 were found to be significantly suppressed in lung MNCs in SEB + RES-treated mice when compared to the SEB + VEH group (Figures 5A,B). Because mTOR is the major regulator of energy production in mitochondria and cell proliferation (Morita et al., 2015), we
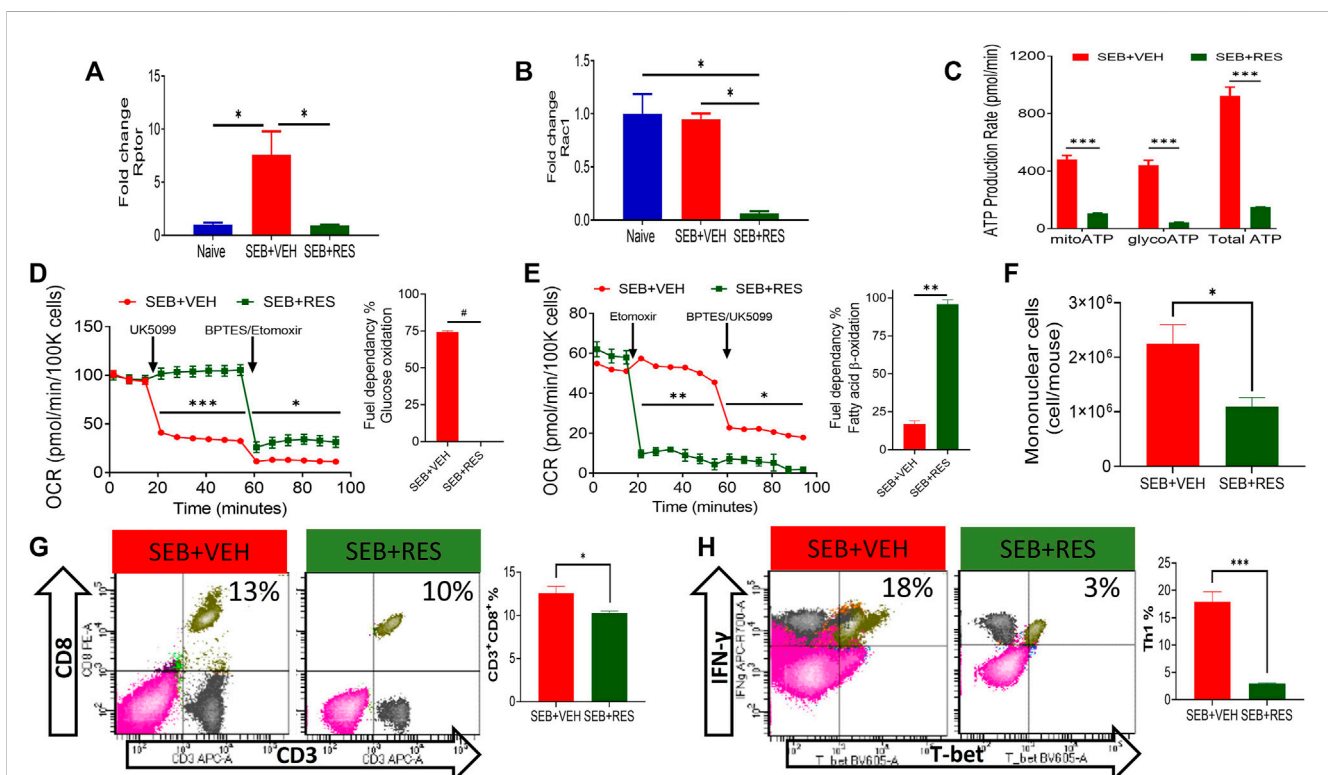
FIGURE 5
Upregulation of miR-100 by RES treatment leads to reprogramming of SEB-activated T cell mitochondrial function from fatty acid biosynthesis into fatty acid β-oxidation. Mice were treated with SEB + VEH or SEB + RES as mentioned in Figure 1 legend. Total RNA isolated from lung MNC was further analyzed. (A,B). Real-time qPCR quantification of Rptor and Rac1 gene expression in the MNCs isolated from the lungs. (C). Real-time kinetic data in live cells showing ATP production by mitochondria (mitoATP), glycolysis (glycoATP) and total ATP in purified T cells. (D,E). Mitochondrial fuel substrate dependency tests detected by Seahorse real-time metabolism analyzer. Glucose (D) and Fatty acid (E) cellular metabolism in purified T cells. (F) Mononuclear cells count per mouse (lung set) isolated from lungs by gradient separation. (G) Flow cytometric analysis of CD3+CD8+ cells gated on singlet population in lung mononuclear cells with a bar graph of statistical analysis. (H) Flow cytometry of T-bet+IFN-γ+ cells gated on CD3+CD4+ cells in lung mononuclear cells with a bar graph of statistical analysis. Compared values represent mean ± standard error of means (M±SE). One-way ANOVA test with multiple Tukey's correction was applied to compare more than two groups. T-test was applied with Holm-Sidak correction method to compare two groups. $p < 0.05$ considered as significant threshold. Significant differences were depicted as *$p < 0.05$, **$p < 0.01$, ***$p < 0.001$, #$p < 0.0001$.

also studied this effect. We noted that there was a significant reduction in the total production of ATP molecules either *via* glycolysis or mitochondrial oxidation (Figure 5C). We found that inhibiting glucose mitochondrial oxidation by using UK5099, a selective mitochondrial pyruvate carrier (MPC) inhibitor, did not change the mitochondrial glucose oxidation rate in T cells from the SEB + RES group, while it caused a significant drop in the mitochondrial oxidative respiration in SEB + VEH, which suggested that these cells were glucose-dependent on their energy production in SEB-activation model (Figure 5D). Furthermore, efforts to detect the alternative fuel substrate utilized by RES-treated SEB-activated T cells led to the finding that fatty acid β-oxidation may be the main pathway of mitochondrial energy production in this group when compared to the SEB + VEH group (Figure 5E). Finally, we found that metabolic reprogramming of infiltrating and resident mononuclear immune cells by RES treatment was associated with a significant reduction in the number of these cells in the lungs of SEB-injected mice (Figure 5F). This reduction in the number of mononuclear cells was accompanied also by a statistical reduction in the effector T cell populations in the lungs of SEB-injected mice treated with RES such as the CD3$^+$CD8$^+$ (Figure 5G) and inflammatory IFN-γ$^+$Th1$^+$ cells (Figure 5H).

Resveratrol-mediated cell-metabolism reprogramming is associated with a reduction in the proliferative activity of SEB-activated immune cells

To further characterize the metabolic pathways, we used LC-MS to determine glucose-derived metabolites in the serum. Interestingly, we found significant upregulation of glucose, α-ketoglutarate, lactate, malate, and pyruvate in the sera of the SEB + VEH group when compared to the SEB + RES group (Figure 6A). The elevated levels of glucose metabolism intermediates were associated with a significant increase in the gene expression of pyruvate kinase enzyme (Pkm) in the lung's infiltrating mononuclear cells (MNC) when compared to naïve or SEB + RES groups (Figure 6B). To detect if this downregulation of glucose metabolism by RES could have an impact on the adenosine triphosphate production, we looked at the expression of AMP-activated protein kinase (Ampk), the gene that regulates cellular energy homeostasis, largely to activate
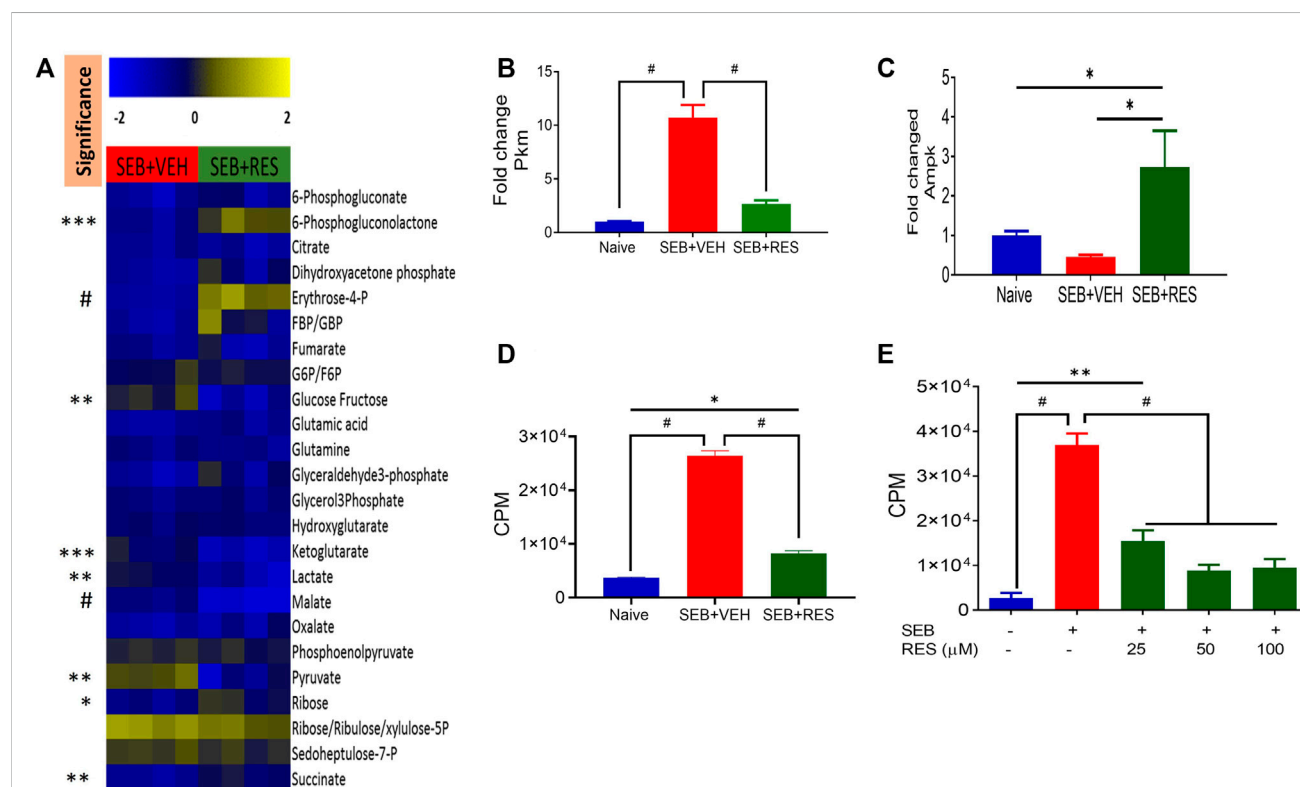
FIGURE 6
Resveratrol-mediated cell metabolism reprogramming leads to a reduction in the proliferative capacity of SEB-activated immune cells. Mice were treated with SEB + VEH or SEB + RES as described in Figure 1. **(A)**. LC-MS results showing serum metabolomic profile (n = 4). **(B)**. Real-time qPCR results of Pkm gene expression in the lung MNC. **(C)**. Real-time qPCR of Ampk gene expression in the lung MNC. **(D)**. Lung mononuclear cells were isolated by gradient separation from different study groups and then seeded in a 96-well plate and incubated with one μCui/well ^{3}H-thymidine for 16 h. CPM: Counts per minute. **(E)**. Naïve splenocytes pretreated with RES one hour prior to 1 μg/mL SEB activation for 48 h, and incubated with ^{3}H-thymidine for 16 h to determine isotope incorporation. Compared values represent mean ± standard error of means (M±SE). One-way ANOVA test with multiple Tukey's correction was applied. $p < 0.05$ considered as significant threshold. Significant differences were depicted as *$p < 0.05$, **$p < 0.01$, ***$p < 0.001$, #$p < 0.0001$.

glucose and fatty acid uptake and oxidation when cellular energy is low. We found that the gene expression of Ampk was significantly higher in the MNC of the SEB + RES group than in naïve or SEB + VEH groups (Figure 6C). It is known that when Ampk is highly expressed this will arrest most of the cellular biological functions in these affected cells. We found that RES treatment *in vitro* caused a significant reduction in the proliferative capacity of SEB-activated MNCs when compared to the SEB + VEH group (Figures 6D,E).

Discussion

Immunometabolism is one of the most exciting areas of translational research that has been studied extensively during the past decade. It refers to the metabolic processes that regulate different immune cell responses in a healthy state as well as during inflammatory responses. Manipulating immunometabolism could pave the way for novel therapies for acute and chronic inflammation as well as autoimmune diseases *via* anabolic and catabolic processes to build or use adenosine tri-phosphate (ATP), respectively (O'Neill et al., 2016).

In the current study, we treated the mice with RES before SEB administration suggesting that RES may be useful as a preventive strategy. This was necessary because SEB being a superantigen, activates a significant proportion of T cells thereby causing a massive cytokine storm within a short period (Mohammed et al., 2020a). Our studies are relevant because SEB is considered a biological warfare agent (Madsen, 2001) and thus, preventive strategies are necessary at the population level. Moreover, with milder forms of ARDS, RES may still be effective when given after the onset lung inflammation. For example, in our previous studies using Ova-induced asthma and lung inflammation, RES was effective when given after the administration of the antigen (Alharris et al., 2022). It is noteworthy that RES is readily available as a dietary supplement in the market and it remains to be established if people who use it are less likely to develop lung inflammation following exposure to external agents.

In the current study, we found that miR-100-5p was upregulated in MNCs isolated from the lungs of mice treated with SEB + RES. Additionally, we found that miR-100-5p regulated the expression of the mTOR signaling pathway. mTOR plays a central role in gene transcription, cell apoptosis, proliferation and differentiation, angiogenesis, tumor formation and development, and cell senescence through PI3K/Akt/mTOR signaling pathway (Hassan et al., 2013), and inhibiting this pathway could have therapeutic promises in leukemia disorders (Bertacchini et al., 2015). The precise role of miR-100-5p in the regulation of inflammation is not clear. Some recent studies suggested that miR-100-5p may play a role in neurodegeneration (Wallach et al., 2021). It was shown that miR-100-5p released from apoptotic cortical neurons, may serve as an endogenous TLR7/8 ligand, leading to neuronal apoptosis (Wallach et al., 2021). The miR-100-5p expression has also been studied in cancer models. In one study, it was shown that miR-100-5p was expressed at lower levels in prostate cancer cells which was associated with increased expression of mTOR thereby affecting the proliferation, migration, and invasion of tumor cells (Ye et al., 2020).

The mTOR has been shown to target a serine/threonine kinase that regulates growth, proliferation, survival, and autophagy based on the nature of the cells involved (Perl, 2016). mTOR forms two interacting complexes, mTORC1, and mTORC2. The latter has been shown to promote the expansion of proinflammatory Th1 and Th17 cells thereby promoting the pathogenesis of autoimmune diseases (Perl, 2016). Thus, the blockade of mTOR signaling is considered to be a potential therapeutic approach to treating inflammatory diseases. It is thus interesting to note that RES which is well characterized for its anti-inflammatory properties may mediate these effects through suppression of the mTOR signaling pathway.

Upon SEB induction of ARDS, we found significantly increased glycolysis and tri-carboxylic acid (TCA) metabolites in the sera of SEB + VEH mice accompanied by an increase in PKM gene in the lung MNCs while suppressing AMPK gene expression. Interestingly, treatment with RES reversed the expression patterns of these genes. Pyruvate kinase (PK) is a key enzyme that catalyzes the dephosphorylation of phosphoenolpyruvate into pyruvate and regulates the production of ATP during glycolysis (Liu et al., 2022). Pyruvate kinase M2 (PKM2) is an important isozyme of PK, which is expressed in immune cells and has been shown to increase the expression of the proinflammatory cytokines (Liu et al., 2022). Thus, RES by decreasing the expression of PK may help suppress inflammatory cytokines induced by SEB. Additionally, PKM2 can also activate mTORC1 by phosphorylating mTORC1 inhibitor AKT1 substrate 1 (AKT1S1) (He et al., 2016).

AMPK and mTOR are two critical kinases that together regulate every aspect of cellular and systemic metabolism, they act as sensors to harmonize the cellular energy and available nutrient levels (Sukumaran et al., 2020). We noted that RES caused an increase in AMPK expression. It is interesting to note that AMPK is also shown to mediate anti-inflammatory effects through activation of SIRT1, PGC-1α, p53, FoxO3a, and p300, and down-regulating the activity of various inflammatory molecules such as NF-κB and AP-1 (Liu et al., 2018). Thus, RES-mediated increase in AMPK may also directly suppress SEB-mediated inflammation through pathways indicated above. Activated AMPK has also been shown to inhibit mTORC1 signaling (Agarwal et al., 2015) as a result of glucose deprivation which leads to a significant reduction in mitochondrial biogenesis (O'Neill et al., 2016; Poznanski et al., 2018; Leprivier and Rotblat, 2020). Because AMPK is activated by metabolic stress and many drugs and xenobiotics, this leads to switching off the anabolic functions of the cells that require ATP consumption and thereby affecting the cell cycle progress (Hardie et al., 2012; Rabinovitch et al., 2017) and limits the ability of the cells to synthesize the required precursors for cell division, consistent with our findings that RES-exposed cells exhibited less proliferation when activated by SEB. Furthermore, RES treatment of SEB-injected mice led to downregulation of the Rac1 gene, a member of the Rho family of GTPases, in the MNCs isolated from the lungs. RAC1 has been shown to regulate cellular glucose uptake through cell membrane glucose transporters (Sylow et al., 2016). Thus, the decrease in Rac1 expression by RES was also associated with the inhibition of HK2, a glycolysis key enzyme, in the lung infiltrating T cells and NKT cells.

One of the limitations of this study was that we used only female mice. It is well-known that the estrogen receptor is a major
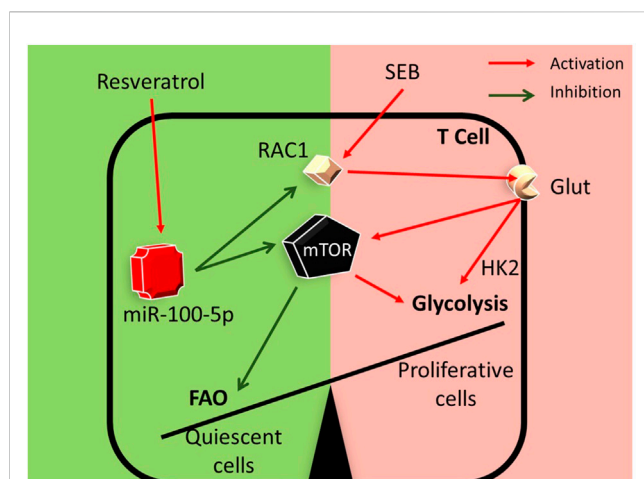
FIGURE 7
Graphical abstract: RES may suppress SEB-mediated hyperimmune response through the following pathway: RES induces miR-100 in activated immune cells which leads to decreased expression of Mtor, Rptor, and Rac1 genes. During T-cell activation, Mtor induces the transcription of many key glycolytic enzymes. mTOR regulates metabolic pathways through the activation of downstream transcriptional factors. Such transcription factors play a key role in the metabolic switch by promoting the expression of enzymes involved in aerobic glycolysis and other anabolic pathways involved in T cell activation and differentiation (Palmer et al., 2015). Thus, RES by suppressing mTOR pathway may alter the metabolic programming in SEB-activated T cells.

modulator of immune response and the superantigen can initiate hyperactive effector cells significantly to a greater level in females versus males (Faulkner et al., 2007). Also, RES is known to act as a phytoestrogen and bind to estrogen receptors (Gehm et al., 1997). Moreover, it acts as an antagonist for the Aryl hydrocarbon receptor (Casper et al., 1999)). Both these receptors and their agonists are known to behave differentially in male vs. female mice (Zuloaga et al., 2014; Lee et al., 2015). It is for these reasons, we included only the female mice, and not a mixture of males and females in the current study, although similar studies need to be undertaken in the male mice as well.

In summary, in the current study, we demonstrate a key mechanism through which RES may suppress SEB-mediated hyperimmune response in the lungs. This pathway involves the induction of miR-100-5p which in turn targets mTOR and decreases its expression. Additionally, while miR-100-5p may also target Rptor and Rac1, key molecules involved in mTOR signaling, based on *in silico* analysis, further studies are necessary to corroborate this. mTOR plays a key role in T cell activation and differentiation through nutrient sensing and antigen-receptor signaling (Salmond, 2018). Thus, RES by suppressing the mTOR pathway may alter the metabolic programming in SEB-activated T cells

thereby suppressing the T cells from dividing and returning to a more quiescent stage (Figure 7).

Data availability statement

The datasets presented in this study can be found in online repositories. The names of the repository/repositories and accession number(s) can be found below: https://www.ncbi.nlm.nih.gov/geo/, GSE220159.

Ethics statement

The animal study was reviewed and approved by Institutional Animal Care and Use Committee, University of South Carolina under animal use protocol (AUP2363).

Author contributions

Conceptualization: HA, MN, and PN; Methodology: HA, MN, and PN, Metabolomics studies: NP and GC; Experimentation and data analysis: HA, AM, NS, and KW, Writing- original draft preparation HA, PN, and MN; writing-review and editing, MN and PN; supervision MN and PN; funding acquisition, MN and PN.

Funding

Conflict of interest

The authors declare that the research was conducted in the absence of any commercial or financial relationships that could be construed as a potential conflict of interest.

Publisher's note

All claims expressed in this article are solely those of the authors and do not necessarily represent those of their affiliated organizations, or those of the publisher, the editors and the reviewers. Any product that may be evaluated in this article, or claim that may be made by its manufacturer, is not guaranteed or endorsed by the publisher.

References

Abdulla, J. M., and Al-Okaily, B. N. (2022). Histomorphometric and histopathological alterations of rat testis following exposure to hydrogen Peroxide: Protective role of resveratrol supplement. *Iraqi J. Vet. Med.* 46 (1), 17–23. doi:10.30539/ijvm.v46i1.1313

Abdulla, O. A., Neamah, W., Sultan, M., Alghetaa, H. K., Singh, N., Busbee, P. B., et al. (2021). The ability of AhR ligands to attenuate delayed type hypersensitivity reaction is associated with alterations in the gut microbiota. *Front. Immunol.* 12, 684727. doi:10.3389/fimmu.2021.684727

Agarwal, S., Bell, C. M., Rothbart, S. B., and Moran, R. G. (2015). AMP-Activated protein kinase (AMPK) control of mTORC1 is p53-and TSC2-independent in pemetrexed-treated carcinoma cells. *J. Biol. Chem.* 290 (46), 27473–27486. doi:10.1074/jbc.M115.665133

Alghetaa, H., Mohammed, A., Sultan, M., Busbee, P., Murphy, A., Chatterjee, S., et al. (2018). Resveratrol protects mice against SEB-induced acute lung injury and mortality by miR-193a modulation that targets TGF-beta signalling. *J. Cell Mol. Med.* 22 (5), 2644–2655. doi:10.1111/jcmm.13542

Alghetaa, H., Mohammed, A., Zhou, J., Singh, N., Nagarkatti, M., and Nagarkatti, P. (2021). Resveratrol-mediated attenuation of superantigen-driven acute respiratory distress syndrome is mediated by microbiota in the lungs and gut. *Pharmacol. Res.* 167, 105548. doi:10.1016/j.phrs.2021.105548

Alharris, E., Alghetaa, H., Seth, R., Chatterjee, S., Singh, N. P., Nagarkatti, M., et al. (2018). Resveratrol attenuates allergic asthma and associated inflammation in the lungs through regulation of miRNA-34a that targets FoxP3 in mice. *Front. Immunol.* 9, 2992. doi:10.3389/fimmu.2018.02992

Alharris, E., Mohammed, A., Alghetaa, H., Zhou, J., Nagarkatti, M., and Nagarkatti, P. (2022). The ability of resveratrol to attenuate ovalbumin-mediated allergic asthma is associated with changes in microbiota involving the gut-lung Axis, enhanced barrier function and decreased inflammation in the lungs. *Front. Immunol.* 13, 805770. doi:10.3389/fimmu.2022.805770

Alrafas, H. R., Busbee, P. B., Nagarkatti, M., and Nagarkatti, P. S. (2019). Resveratrol downregulates miR-31 to promote T regulatory cells during prevention of TNBS-induced colitis. *Mol. Nutr. Food Res.* 64 (1), e1900633. doi:10.1002/mnfr.201900633

Al-Salman, F., Redha, A. A., Aqeel, Z., and Ali, Z. (2022). Phytochemical content, inorganic composition, mineral profile, and evaluation of antioxidant activity of some common medicinal plants. *Iraqi J. Sci.*, 2764–2773. doi:10.24996/ijs.2022.63.7.1

Amara, C. S., Ambati, C. R., Vantaku, V., Badrajee Piyarathna, D. W., Donepudi, S. R., Ravi, S. S., et al. (2019). Serum metabolic profiling identified a distinct metabolic signature in bladder cancer smokers: A key metabolic enzyme associated with patient survival. *Cancer Epidemiol. Biomarkers Prev.* 28 (4), 770–781. doi:10.1158/1055-9965.EPI-18-0936

Ambros, V. (2004). The functions of animal microRNAs. *Nature* 431 (7006), 350–355. doi:10.1038/nature02871

Bertacchini, J., Heidari, N., Mediani, L., Capitani, S., Shahjahani, M., Ahmadzadeh, A., et al. (2015). Targeting PI3K/AKT/mTOR network for treatment of leukemia. *Cell Mol. Life Sci.* 72 (12), 2337–2347. doi:10.1007/s00018-015-1867-5

Butler, A., Hoffman, P., Smibert, P., Papalexi, E., and Satija, R. (2018). Integrating single-cell transcriptomic data across different conditions, technologies, and species. *Nat. Biotechnol.* 36 (5), 411–420. doi:10.1038/nbt.4096

Casper, R. F., Quesne, M., Rogers, I. M., Shirota, T., Jolivet, A., Milgrom, E., et al. (1999). Resveratrol has antagonist activity on the aryl hydrocarbon receptor: Implications for prevention of dioxin toxicity. *Mol. Pharmacol.* 56 (4), 784–790.

de Prost, N., Pham, T., Carteaux, G., Mekontso Dessap, A., Brun-Buisson, C., Fan, E., et al. (2017). Etiologies, diagnostic work-up and outcomes of acute respiratory distress syndrome with no common risk factor: A prospective multicenter study. *Ann. Intensive Care* 7 (1), 69. doi:10.1186/s13613-017-0281-6

Dembinski, R., and Mielck, F. (2018). Ards - an update - Part 1: Epidemiology, pathophysiology and diagnosis. *Anasthesiol Intensivmed. Notfallmed Schmerzther* 53 (2), 102–111. doi:10.1055/s-0043-107166

Elliott, D. M., Nagarkatti, M., and Nagarkatti, P. S. (2016). 3,39-Diindolylmethane ameliorates staphylococcal enterotoxin B-induced acute lung injury through alterations in the expression of MicroRNA that target apoptosis and cell-cycle arrest in activated T cells. *J. Pharmacol. Exp. Ther.* 357 (1), 177–187. doi:10.1124/jpet.115.226563

Ercoli, L., Gallina, S., Nia, Y., Auvray, F., Primavilla, S., Guidi, F., et al. (2017). Investigation of a staphylococcal food poisoning outbreak from a chantilly cream dessert, in umbria (Italy). *Foodborne Pathog. Dis.* 14 (7), 407–413. doi:10.1089/fpd.2016.2267

Faulkner, L., Altmann, D. M., Ellmerich, S., Huhtaniemi, I., Stamp, G., and Sriskandan, S. (2007). Sexual dimorphism in superantigen shock involves elevated TNF-alpha and TNF-alpha induced hepatic apoptosis. *Am. J. Respir. Crit. Care Med.* 176 (5), 473–482. doi:10.1164/rccm.200611-1712OC

Ferreira-Duarte, A. P., Pinheiro-Torres, A. S., Takeshita, W. M., Gushiken, V. O., Roncalho-Buck, I. A., Anhe, G. F., et al. (2020). Airway exposure to Staphylococcal enterotoxin type B (SEB) enhances the number and activity of bone marrow neutrophils via the release of multiple cytokines. *Int. Immunopharmacol.* 78, 106009. doi:10.1016/j.intimp.2019.106009

Ferruelo, A., Penuelas, O., and Lorente, J. A. (2018). MicroRNAs as biomarkers of acute lung injury. *Ann. Transl. Med.* 6 (2), 34. doi:10.21037/atm.2018.01.10

Fries, B. C., and Varshney, A. K. (2013). Bacterial toxins-staphylococcal enterotoxin B. *Microbiol. Spectr.* 1 (2). doi:10.1128/microbiolspec.AID-0002-2012

Gehm, B. D., McAndrews, J. M., Chien, P. Y., and Jameson, J. L. (1997). Resveratrol, a polyphenolic compound found in grapes and wine, is an agonist for the estrogen receptor. *Proc. Natl. Acad. Sci. U. S. A.* 94 (25), 14138–14143. doi:10.1073/pnas.94.25.14138

Guidi, F., Duranti, A., Gallina, S., Nia, Y., Petruzzelli, A., Romano, A., et al. (2018). Characterization of A Staphylococcal food poisoning outbreak in A workplace canteen during the post-earthquake reconstruction of central Italy. *Toxins (Basel)* 10 (12), 523. doi:10.3390/toxins10120523

Hardie, D. G., Ross, F. A., and Hawley, S. A. (2012). AMPK: A nutrient and energy sensor that maintains energy homeostasis. *Nat. Rev. Mol. Cell Biol.* 13 (4), 251–262. doi:10.1038/nrm3311

Hassan, B., Akcakanat, A., Holder, A. M., and Meric-Bernstam, F. (2013). Targeting the PI3-kinase/Akt/mTOR signaling pathway. *Surg. Oncol. Clin. N. Am.* 22 (4), 641–664. doi:10.1016/j.soc.2013.06.008

He, C. L., Bian, Y. Y., Xue, Y., Liu, Z. X., Zhou, K. Q., Yao, C. F., et al. (2016). Pyruvate kinase M2 activates mTORC1 by phosphorylating AKT1S1. *Sci. Rep.* 6, 21524. doi:10.1038/srep21524

Khayoon, H. A., and Al-Rekabi, F. M. K. (2020). Cytotoxic effect of resveratrol on colorectal cancer cell line. *Iraqi J. Veterinary Med.* 44 (1), 68–74. doi:10.30539/ijvm.v44i1.939

Kornberg, M. D., Bhargava, P., Kim, P. M., Putluri, V., Snowman, A. M., Putluri, N., et al. (2018). Dimethyl fumarate targets GAPDH and aerobic glycolysis to modulate immunity. *Science* 360 (6387), 449–453. doi:10.1126/science.aan4665

Lee, J., Prokopec, S. D., Watson, J. D., Sun, R. X., Pohjanvirta, R., and Boutros, P. C. (2015). Male and female mice show significant differences in hepatic transcriptomic response to 2,3,7,8-tetrachlorodibenzo-p-dioxin. *BMC Genomics* 16 (1), 625. doi:10.1186/s12864-015-1840-6

Leprivier, G., and Rotblat, B. (2020). How does mTOR sense glucose starvation? AMPK is the usual suspect. *Cell Death Discov.* 6, 27. doi:10.1038/s41420-020-0260-9

Liu, M., Wilk, S. A., Wang, A., Zhou, L., Wang, R. H., Ogawa, W., et al. (2010). Resveratrol inhibits mTOR signaling by promoting the interaction between mTOR and DEPTOR. *J. Biol. Chem.* 285 (47), 36387–36394. doi:10.1074/jbc.M110.169284

Liu, M. Y., Zhang, M. J., and Xie, M. J. (2018). Molecular mechanisms of anti-inflammatory action of AMPK. *Sheng Li Xue Bao* 70 (3), 329–334.

Liu, C., Liu, C., and Fu, R. (2022). Research progress on the role of PKM2 in the immune response. *Front. Immunol.* 13, 936967. doi:10.3389/fimmu.2022.936967

Madsen, J. M. (2001). Toxins as weapons of mass destruction. A comparison and contrast with biological-warfare and chemical-warfare agents. *Clin. Lab. Med.* 21 (3), 593–606. doi:10.1016/s0272-2712(18)30023-4

Mohammed, A., Alghetaa, H., Sultan, M., Singh, N. P., Nagarkatti, P., and Nagarkatti, M. (2020a). Administration of Δ9-tetrahydrocannabinol (THC) post-staphylococcal enterotoxin B exposure protects mice from acute respiratory distress syndrome and toxicity. *Front. Pharmacol.* 11, 893. doi:10.3389/fphar.2020.00893

Mohammed, A., Alghetaa, H. K., Zhou, J., Chatterjee, S., Nagarkatti, P., and Nagarkatti, M. (2020b). Protective effects of Δ⁹ -tetrahydrocannabinol against enterotoxin-induced acute respiratory distress syndrome are mediated by modulation of microbiota. *Br. J. Pharmacol.* 177 (22), 5078–5095. doi:10.1111/bph.15226

Mohammed, A., H, F. K. A., Miranda, K., Wilson, K., N, P. S., Cai, G., et al. (2020c). Δ9-Tetrahydrocannabinol prevents mortality from acute respiratory distress syndrome through the induction of apoptosis in immune cells, leading to cytokine storm suppression. *Int. J. Mol. Sci.* 21 (17), 6244. doi:10.3390/ijms21176244

Morita, M., Gravel, S. P., Hulea, L., Larsson, O., Pollak, M., St-Pierre, J., et al. (2015). mTOR coordinates protein synthesis, mitochondrial activity and proliferation. *Cell Cycle* 14 (4), 473–480. doi:10.4161/15384101.2014.991572

Muralimohan, G., Rossi, R. J., Guernsey, L. A., Thrall, R. S., and Vella, A. T. (2008). Inhalation of *Staphylococcus aureus* enterotoxin A induces IFN-gamma and CD8 T cell-dependent airway and interstitial lung pathology in mice. *J. Immunol.* 181 (5), 3698–3705. doi:10.4049/jimmunol.181.5.3698

Nagarkatti, P., Miranda, K., and Nagarkatti, M. (2020). Use of cannabinoids to treat acute respiratory distress syndrome and cytokine storm associated with coronavirus disease-2019. *Front. Pharmacol.* 11, 589438. doi:10.3389/fphar.2020.589438

Neamah, W. H., Singh, N. P., Alghetaa, H., Abdulla, O. A., Chatterjee, S., Busbee, P. B., et al. (2019). AhR activation leads to massive mobilization of myeloid-derived suppressor cells with immunosuppressive activity through regulation of CXCR2 and MicroRNA miR-150-5p and miR-543-3p that target anti-inflammatory genes. *J. Immunol.* 203 (7), 1830–1844. doi:10.4049/jimmunol.1900291

O'Neill, L. A., Kishton, R. J., and Rathmell, J. (2016). A guide to immunometabolism for immunologists. *Nat. Rev. Immunol.* 16 (9), 553–565. doi:10.1038/nri.2016.70

Palmer, C. S., Ostrowski, M., Balderson, B., Christian, N., and Crowe, S. M. (2015). Glucose metabolism regulates T cell activation, differentiation, and functions. *Front. Immunol.* 6, 1. doi:10.3389/fimmu.2015.00001

Papadopoli, D., Boulay, K., Kazak, L., Pollak, M., Mallette, F., Topisirovic, I., et al. (2019). mTOR as a central regulator of lifespan and aging. *F1000Res* 8. doi:10.12688/f1000research.17196.1

Perico, L., Benigni, A., Casiraghi, F., Ng, L. F. P., Renia, L., and Remuzzi, G. (2021). Immunity, endothelial injury and complement-induced coagulopathy in COVID-19. *Nat. Rev. Nephrol.* 17 (1), 46–64. doi:10.1038/s41581-020-00357-4

Perl, A. (2016). Activation of mTOR (mechanistic target of rapamycin) in rheumatic diseases. *Nat. Rev. Rheumatol.* 12 (3), 169–182. doi:10.1038/nrrheum.2015.172

Pohanka, M. (2019). Current trends in the biosensors for biological warfare agents assay. *Mater. (Basel)* 12 (14), 2303. doi:10.3390/ma12142303

Popugailo, A., Rotfogel, Z., Supper, E., Hillman, D., and Kaempfer, R. (2019). Staphylococcal and streptococcal superantigens trigger B7/CD28 costimulatory receptor engagement to hyperinduce inflammatory cytokines. *Front. Immunol.* 10, 942. doi:10.3389/fimmu.2019.00942

Poznanski, S. M., Barra, N. G., Ashkar, A. A., and Schertzer, J. D. (2018). Immunometabolism of T cells and NK cells: Metabolic control of effector and regulatory function. *Inflamm. Res.* 67 (10), 813–828. doi:10.1007/s00011-018-1174-3

Rabinovitch, R. C., Samborska, B., Faubert, B., Ma, E. H., Gravel, S. P., Andrzejewski, S., et al. (2017). AMPK maintains cellular metabolic homeostasis through regulation of mitochondrial reactive oxygen species. *Cell Rep.* 21 (1), 1–9. doi:10.1016/j.celrep.2017.09.026

Rao, R., Rieder, S. A., Nagarkatti, P., and Nagarkatti, M. (2014). Staphylococcal enterotoxin B-induced microRNA-155 targets SOCS1 to promote acute inflammatory lung injury. *Infect. Immun.* 82 (7), 2971–2979. doi:10.1128/IAI.01666-14

Rao, R., Nagarkatti, P., and Nagarkatti, M. (2015a). Role of miRNA in the regulation of inflammatory genes in staphylococcal enterotoxin B-induced acute inflammatory lung injury and mortality. *Toxicol. Sci.* 144 (2), 284–297. doi:10.1093/toxsci/kfu315

Rao, R., Nagarkatti, P. S., and Nagarkatti, M. (2015b). Δ(9) Tetrahydrocannabinol attenuates Staphylococcal enterotoxin B-induced inflammatory lung injury and prevents mortality in mice by modulation of miR-17-92 cluster and induction of T-regulatory cells. *Br. J. Pharmacol.* 172 (7), 1792–1806. doi:10.1111/bph.13026

Rieder, S. A., Nagarkatti, P., and Nagarkatti, M. (2012). Multiple anti-inflammatory pathways triggered by resveratrol lead to amelioration of staphylococcal enterotoxin B-induced lung injury. *Br. J. Pharmacol.* 167 (6), 1244–1258. doi:10.1111/j.1476-5381.2012.02063.x

Salmond, R. J. (2018). mTOR regulation of glycolytic metabolism in T cells. *Front. Cell Dev. Biol.* 6, 122. doi:10.3389/fcell.2018.00122

Sarkar, S., Kimono, D., Albadrani, M., Seth, R. K., Busbee, P., Alghetaa, H., et al. (2019). Environmental microcystin targets the microbiome and increases the risk of intestinal inflammatory pathology via NOX2 in underlying murine model of Nonalcoholic Fatty Liver Disease. *Sci. Rep.* 9 (1), 8742. doi:10.1038/s41598-019-45009-1

Savransky, V., Rostapshov, V., Pinelis, D., Polotsky, Y., Korolev, S., Komisar, J., et al. (2003). Murine lethal toxic shock caused by intranasal administration of staphylococcal enterotoxin B. *Toxicol. Pathol.* 31 (4), 373–378. doi:10.1080/01926230390201093

Stuart, T., Butler, A., Hoffman, P., Hafemeister, C., Papalexi, E., Mauck, W. M., 3rd, et al. (2019). Comprehensive integration of single-cell data. *Cell* 177 (7), 1888–1902.e21. doi:10.1016/j.cell.2019.05.031

Sukumaran, A., Choi, K., and Dasgupta, B. (2020). Insight on transcriptional regulation of the energy sensing AMPK and biosynthetic mTOR pathway genes. *Front. Cell Dev. Biol.* 8, 671. doi:10.3389/fcell.2020.00671

Sultan, M., Alghetaa, H., Mohammed, A., Abdulla, O. A., Wisniewski, P. J., Singh, N., et al. (2021). The endocannabinoid anandamide attenuates acute respiratory distress syndrome by downregulating miRNA that target inflammatory pathways. *Front. Pharmacol.* 12, 644281. doi:10.3389/fphar.2021.644281

Sylow, L., Nielsen, I. L., Kleinert, M., Moller, L. L., Ploug, T., Schjerling, P., et al. (2016). Rac1 governs exercise-stimulated glucose uptake in skeletal muscle through regulation of GLUT4 translocation in mice. *J. Physiol.* 594 (17), 4997–5008. doi:10.1113/JP272039

Tian, B., and Liu, J. (2020). Resveratrol: A review of plant sources, synthesis, stability, modification and food application. *J. Sci. Food Agric.* 100 (4), 1392–1404. doi:10.1002/jsfa.10152

Vantaku, V., Donepudi, S. R., Piyarathna, D. W. B., Amara, C. S., Ambati, C. R., Tang, W., et al. (2019a). Large-scale profiling of serum metabolites in African American and European American patients with bladder cancer reveals metabolic pathways associated with patient survival. *Cancer* 125 (6), 921–932. doi:10.1002/cncr.31890

Vantaku, V., Dong, J., Ambati, C. R., Perera, D., Donepudi, S. R., Amara, C. S., et al. (2019b). Multi-omics integration analysis robustly predicts high-grade patient survival and identifies CPT1B effect on fatty acid metabolism in bladder cancer. *Clin. Cancer Res.* 25 (12), 3689–3701. doi:10.1158/1078-0432.CCR-18-1515

Vantaku, V., Putluri, V., Bader, D. A., Maity, S., Ma, J., Arnold, J. M., et al. (2019c). Epigenetic loss of AOX1 expression via EZH2 leads to metabolic deregulations and promotes bladder cancer progression. *Oncogene* 39, 6265–6285. doi:10.1038/s41388-019-0902-7

Wallach, T., Mossmann, Z. J., Szczepek, M., Wetzel, M., Machado, R., Raden, M., et al. (2021). MicroRNA-100-5p and microRNA-298-5p released from apoptotic cortical neurons are endogenous Toll-like receptor 7/8 ligands that contribute to neurodegeneration. *Mol. Neurodegener.* 16 (1), 80. doi:10.1186/s13024-021-00498-5

Wangler, M. F., Chao, Y. H., Bayat, V., Giagtzoglou, N., Shinde, A. B., Putluri, N., et al. (2017). Peroxisomal biogenesis is genetically and biochemically linked to carbohydrate metabolism in Drosophila and mouse. *PLoS Genet.* 13 (6), e1006825. doi:10.1371/journal.pgen.1006825

Wu, X., Wu, C., Gu, W., Ji, H., and Zhu, L. (2019). Serum exosomal MicroRNAs predict acute respiratory distress syndrome events in patients with severe community-acquired pneumonia. *Biomed. Res. Int.* 2019, 3612020. doi:10.1155/2019/3612020

Ye, Y., Li, S. L., and Wang, J. J. (2020). miR-100-5p downregulates mTOR to suppress the proliferation, migration, and invasion of prostate cancer cells. *Front. Oncol.* 10, 578948. doi:10.3389/fonc.2020.578948

Zhou, D. D., Luo, M., Huang, S. Y., Saimaiti, A., Shang, A., Gan, R. Y., et al. (2021). Effects and mechanisms of resveratrol on aging and age-related diseases. *Oxid. Med. Cell Longev.* 2021, 9932218. doi:10.1155/2021/9932218

Zhu, Z., Liang, L., Zhang, R., Wei, Y., Su, L., Tejera, P., et al. (2017). Whole blood microRNA markers are associated with acute respiratory distress syndrome. *Intensive Care Med. Exp.* 5 (1), 38. doi:10.1186/s40635-017-0155-0

Zuloaga, D. G., Zuloaga, K. L., Hinds, L. R., Carbone, D. L., and Handa, R. J. (2014). Estrogen receptor beta expression in the mouse forebrain: Age and sex differences. *J. Comp. Neurol.* 522 (2), 358–371. doi:10.1002/cne.23400

Potential of resveratrol in the treatment of interstitial lung disease

Rongxiu Huo[†], Xinxiang Huang[†], Yanting Yang, Yang Yang and Jinying Lin*

Department of Rheumatology and Immunology, Guangxi Academy of Medical Sciences, The People's Hospital of Guangxi Zhuang Autonomous Region, Nanning, China

Interstitial lung disease (ILD) is a heterogeneous group of diseases characterized by lung injury caused by lung fibroblast proliferation, interstitial inflammation, and fibrosis. Different cell signal transduction pathways are activated in response to various proinflammatory or fibrotic cytokines, such as IL-6, and these cytokines are increased in different ILDs. The overexpressed cytokines and growth factors in ILD can activate TGF-β/Smad2/3/4, NF-κB, and JAK/STAT signal transduction pathways, promote the activation of immune cells, increase the release of pro-inflammatory and pro-fibrotic factors, differentiate fibroblasts into myofibroblasts, and promote the occurrence and development of ILD. This finding suggests the importance of signal transduction pathways in patients with ILD. Recent evidence suggests that resveratrol (RSV) attenuates excessive inflammation and pulmonary fibrosis by inhibiting the TGF-β/Smad2/3/4, NF-κB, and JAK/STAT signal transduction pathways and overactivation of immune cells. In this review, advances in lung protection and the underlying mechanisms of RSV are summarized, and the potential efficacy of RSV as a promising treatment option for ILD is highlighted.

KEYWORDS
interstitial lung disease, resveratrol, signal transduction pathway, immune cells, adverse reaction

Introduction

Interstitial lung disease (ILD) includes a group of heterogeneous diseases, which can be derived from a variety of different etiology, such as infection, drug, radiation-induced lung diseases and autoimmune diseases such as rheumatoid arthritis (RA), etc., leading to damage of alveolar epithelium and lung parenchyma, eventually leading to lung inflammation and fibrosis (Shao et al., 2021). ILD was characterized by inflammation or fibrosis of different degrees in the lung parenchyma. For example, in inflammatory diseases, the histological form is characterized by institutional pneumonia or non-specific interstitial pneumonia, while diseases dominated by fibrosis are characterized by common interstitial pneumonia (Mikolasch et al., 2017) (Figure1).

ILD is one of the most common and serious lung diseases. It was found that the total incidence of ILD was 19.4/100,000, and the most common diagnosis was sarcoidosis (42.6%) (Duchemann et al., 2017). Overactivation of immune cells in ILD patients resulted in the release of pro-inflammatory/pro-fibrotic cytokines and oxidative damage, and abnormal myofibroblast activation was observed with enhanced epithelial-interstitial transformation (EMT) and the secretion of large amounts of collagen for

FIGURE 1

Graphical abstract: Potential targets of RSV in ILD. In immune cells or fibroblasts, RSV exerts anti-inflammatory and antifibrotic effects by inhibiting TGF-β/Smad2/3/4, NF-κB, and JAK/STAT pathways, as well as by regulating heat shock protein 90, inhibiting Akt, ERK1/2 and NF-κB pathways. In addition, RSV can also inhibit SIRT1, reduce α-ASM activation, and play an antifibrotic role. TGF-β, transforming growth factor β; IFN-γ, interferon-γ; TNF-α, tumor necrosis factor; P, phosphate; JAK, janus tyrosine kinase; STAT, signal transducers and activators of transcription; ERK1/2,extracellular signal-regulated protein kinases; AKT, serine-threonine kinase; NF-κB, nuclear factor-kappa B; SIRT1, sirtuin1; α-SMA, α-smooth muscle actin. "ê" indicates activation, and "—ı" indicates inhibition.

post-injury repair (You et al., 2015; Gouda and Bhandary, 2018). This leads to excessive deposition of extracellular matrix (ECM) and the development of interstitial fibrosis (Pardo and Selman, 2002). Eventually, symptoms such as a dry cough, shortness of breath and fatigue. The management and treatment of ILD remains challenging for clinicians. Currently, common therapeutic strategies include glucocorticoids and immunosuppressants (such as cyclophosphamide) (Shao et al., 2021), but sometimes they are resistant to the above-mentioned drugs and have serious adverse reactions (Huo et al., 2022). Therefore, it is urgent to find a drug with significant efficacy and few side effects.

Resveratrol (RSV) is a natural plant antitoxin, which is abundant in a variety of plants such as grapes and peanuts as well as a variety of commercial products, such as grape juice and red wine (Truong et al., 2018). Resveratrol exists in two isomeric forms, cis-trans and trans-trans, but trans is the main form, which has the most effective therapeutic benefits due to its low steric hindrance of the side chain (Cardile et al., 2007; Weiskirchen and Weiskirchen, 2016; Raj et al., 2021). Trans can be reconstituted from yeast extracts and become more biologically active forms with higher stability (Chen et al., 2007; Camont et al., 2009). It has been reported that RSV can slow down the progression of autoimmune diseases, such as RA, systemic lupus erythematosus (SLE), psoriasis (PsO) and inflammatory bowel disease (IBD), etc. (Oliveira et al., 2017). In addition, studies have shown that RSV has inhibitory effects on inflammation and anti-fibrosis, and thus has a therapeutic prospect for pulmonary diseases and fibrosis diseases (Vargas et al., 2016). At present, more and more studies have reported that RSV can play an anti-fibrosis role by inhibiting the

molecules and cells in some signal transduction pathways. In animal model studies, RSV has been shown to improve ILD in mice by inhibiting the expression of Smad and Smad7, inhibiting the over-activation of immune cells, inhibiting inflammation and the proliferation and differentiation of lung fibroblasts, and reducing collagen deposition (Chávez et al., 2008; Liu et al., 2010). Recent studies have found that RSV can also play a beneficial role in the later stage of pulmonary fibrosis by regulating the metabolism of collagen in lung tissue and reducing its deposition in lung interstitium (Wang et al., 2021). In addition, by inhibiting the activation of NF-κB in macrophages and lymphocytes, the expression levels of nitric oxide and tumor necrosis factor-α (TNF-α), interleukin (IL-1β), IL-6, transforming growth factor-β (TGF-β) and TNF in pulmonary fibrosis are reduced to prevent oxidative damage (Yahfoufi et al., 2018; Fu et al., 2020). RSV may inhibit pro-inflammatory factors and down-regulate oxidative stress levels by inhibiting epithel-mesenchymal transformation and down-regulating NF-κB and TGF-β1/smad3 signaling pathways (Wang et al., 2022). At the same time, the autophagy process and the nucleotide-binding domain and leucine-rich repeat protein 3 inflammasome activities are inhibited, and the production of pro-inflammatory factors is reduced, thus improving lung inflammation and fibrosis (Ding et al., 2019). In addition, in the fusion process of autophagosome and lysosome, RSV can relieve their inhibitory state and reverse the destruction of autophagosome—lysosome fusion, thus improving ILD (Bao et al., 2022). These findings suggest that RSV can be used as a potential treatment for ILD (Figure 1).

In this review, we focus on the protective effects and potential mechanisms of RSV against ILD. Meanwhile, this review

TABLE 1 Mechanism of different immune cells in ILD.

Immune cells	Effects in ILD	Mechanisms of different immune cells in ILD
Macrophages	Differentiated into "pro-inflammatory" classic M1 macrophages or "pro-fibrotic" M2a macrophages in ILD Kishore and Petrek (2021). Secreting cytokines and chemokines Kishore and Petrek (2021)	Activating PI3K/AKT, TGF-β/Smad, p38 MAPK, ERK1/2, and JAK/STAT pathways Kishore and Petrek (2021). Produces pro-inflammatory and pro-fibrotic cytokines Wills-Karp and Finkelman (2008); Van Dyken and Locksley (2013). Cytokines:TNF-α, IL-1, IL-4, IL-6, IL-10, IL-12, IL-23, IL-33, IFN-γ, TGF-β, et al. ↑ Kishore and Petrek (2021). Chemokines:CCL2, CCL18, CCL24 MCP-1, MIP-1α, et al. ↑ Kishore and Petrek (2021). Cytokines and chemokines are involved in lung inflammation and pulmonary fibrosis Kishore and Petrek (2021). In addition, inducing the differentiation of fibroblasts into myofibroblasts Wang et al. (2020). Induced epithelia to proliferate Wang et al. (2020)
T cells	Differentiated into Th1, Th2, Th9, and Th22 cells in ILD Deng et al. (2023). Secreting cytokines Deng et al. (2023)	Cytokines: IL-4, IL-5, IL-9, IL-13, IL-17A, IL-22, TGF-β, TNF-α, et al. ↑ Wynn (2008); Desai et al. (2018). Activating PI3K/AKT, TGF-β/Smad, ERK1/2 and JAK/STAT pathways. Activating fibroblasts and myofibroblasts Deng et al. (2023). Extensively promotes ECM production and collagen deposition Deng et al. (2023). Extracellular matrix proteins, types I and III collagen and fibronectin increased in ILD Roberts et al., 2003
B cells	Increased B cell activation and an increased number of memory B cells and plasmablasts in ILD and secreted antibodies and cytokines Heukels et al. (2019); Roman and Chiba (2021)	Cytokines: IL-6, IL-8, BAFF, et al. ↑ Neys et al. (2021), Roman and Chiba (2021). Activating JUK, p38 MAPK, and mTOR pathways Roman and Chiba 2021. Autoantibodies produced are closely associated with ILD Lee et al. (2013), including anti-citcitline protein antibody (ACPA), rheumatoid factor (RF), Sjogren's syndrome-associated antigen A antibody, anti-synthetase antibody or anti-melanoma differentiation-associated protein 5 antibody, anti-topoisomerase I antibody, Anti-U11/U12 ribonucleoprotein antibodies and anti-eukaryotic initiation factor 2B antibodies and so on
NK cells	The number of NK cells and their activity in ILD decreased, and CD56 and CD16 were expressed simultaneously Aquino-Galvez et al. (2009); Cruz et al. (2021). Secreting cytokines. Cruz et al. (2021)	Cytokines: IFN-γ↑, TNF-α↑, TGF-β↓ Cruz et al. (2021). MTOR signaling, JNK, IL-8, and IL-23 signaling were upregulated in ILD Huang et al. (2021). Cytokine imbalance promoted the development of ILD. Expressed higher levels of granzyme B, the most potent NK-cell cytotoxic enzyme Cruz et al. (2021)

Symbols: ↑, up-regulation; ↓, down-regulation.

summarizes the progress of RSV in the treatment of ILD and its related adverse reactions, providing new insights for the treatment of ILD.

Mechanism of ILD formation

Immune cells and ILD

In ILD patients, especially those with autoimmune ILD, immune disorders can activate macrophages, T cells, B cells, and NK cells to damage the alveolar epithelium, and then repeated repair leads to the gradual destruction of functional lung parenchyma, which is replaced by increased deposition of non-functional connective tissue (Chambers and Mercer, 2015), eventually leading to ILD. The mechanism of different types of immune cells in ILD is shown in Table 1.

Macrophages and ILD

Macrophages are immune cells that differentiate from monocytes and play a role in the balance between innate and adaptive immunity. In the process of fibrosis caused by immune imbalance, monocytes in the blood are recruited into the lungs and activated into macrophages under the action of chemokines, and

cytokines are secreted to differentiate fibroblasts into myofibroblasts. In addition, macrophages can be polarised into "pro-inflammatory" classical M1 macrophages that secrete pro-inflammatory and/or pro-fibrotic cytokines, such as interleukin (IL) -1β, or "pro-fibrotic" M2a macrophages that secrete pro-fibrotic cytokines (Kolahian et al., 2016; Bellamri et al., 2019), thus promoting the progression of pulmonary fibrosis. Especially in SSc-ILD. In inflammatory environment, promoting nuclear factor (NF) -κB and Janus kinase (JAK)/signal transductor and transcription activator (STAT) pathways in macrophages to induce the production of pro-inflammatory factors, such as tumor necrosis factor (TNF) -α, IL-1, IL-6, etc. (Balachandran and Adams, 2013), can promote the occurrence of ILD.

T cells and ILD

At present, preclinical studies have determined that some T cell subtypes are associated with fibrosis, such as Th2 and Th17, which promote fibrosis. Up-regulation of Pd-1 on CD4+ T cells increases type 1 collagen synthesis and promotes pulmonary fibrosis through STAT 3-mediated IL-17A and TGF-β production (Celada et al., 2018). At present, the most studied ILD are IPF and SSc-ILD. The two diseases share similar common features, such as T cell profiles (Th2, Th17, increased ratio of CD4 to CD8 T cells), T cell cytokine profiles (IL-4, IL-5, IL-10, and IL-17 of IPF, and IL-4, IL-5, IL-6, IL-

10, IL-13, and IL-22 in SSc-ILD (Bagnato and Harari, 2015). In RA-ILD, like IPF and SSc-ILD, the expression of IL-17 receptor was up-regulated, indicating that Th17 cell-mediated immunity was involved in the pathogenesis of ILD (Wang et al., 2019; Zhang et al., 2019). Furthermore, the number of CD4+ T cells in lung tissues of RA-ILD patients was significantly higher than that of idiopathic UIP patients, suggesting that immune dysregulation may be more prevalent in RA-ILD patients than in idiopathic UIP patients (Turesson et al., 2005). These results indicated that the imbalance of T cell subsets might be involved in ILD formation.

B cells and ILD

As a result of immune disorders in patients with autoimmune diseases, autoantigens are presented to CD4+ helper T cells by antigen-presenting cells and then further presented to B cells, so that B cells differentiate into plasma cells and produce and secrete autoantibodies. Recently, several studies have pointed to a possible role of B cells in IPF, RA, or ILD associated with connective tissue disease. Some studies have found that, compared with healthy people, the phenotype distribution of B cells in the peripheral blood of IPF patients is abnormal, and the percentage of plasmabytes in IPF patients is negatively correlated with forced vital capacity (Xue et al., 2013). The authors detected focal aggregates of CD20-positive B cells in all IPF lung tissues using immunohistochemistry (Xue et al., 2013). Atkins et al. (2006) compared the lung biopsy specimens of patients with RA-ILD and control subjects and observed obvious follicular B cell hyperplasia in patients with RA-ILD. Recent studies have also found that the total peripheral blood B cell count is higher in patients with RA-ILD, but the frequency of memory B cells is lower. The mechanism may be that some of them selectively migrate to the lung tissue (Shimizu et al., 2021). In some ILDs, B cell production of antibodies may play a key role. For example, there is an association between antibodies, including anti-citrullinated protein antibodies (ACPA) and rheumatoid factor (RF), and the risk of RA-ILD (Katsumata et al., 2019). The presence of Sjogren's syndrome-related antigen A antibody is a predisposing factor for ILD in patients with Sjogren's syndrome (Flament et al., 2016). Anti-synthetase antibody or anti-melanoma differentiation-associated protein 5 (MDA5) antibodies are associated with myositis-related ILD, while anti-topoisomerase I (anti-scl70), anti-U11/U12, and anti-eukaryotic initiation factor 2B antibodies are associated with SSc-ILD (Kuwana et al., 2021). These results suggest that B cell-formed autoantibodies may be involved in the formation of ILD.

Natural killer (NK) cells and ILD

Previous studies have shown that NK cells play a key role in the pathogenesis of acute lung injury (Liu et al., 2016). There are two different NK environments in human pulmonary fibrosis: one in the lung and the other in the peripheral blood. In pulmonary fibrosis, NK cells are thought to counteract the fibrotic activity of TGF-β by producing the anti-fibrotic mediator interferon-γ (IFN-γ), thereby inducing anti-fibrotic signals in the lung (Culley, 2009). As for NK

cells in the peripheral blood, studies have found that the percentage and absolute number of NK cells in the peripheral blood of 11 IPF patients are both high (Esposito et al., 2005). In addition, a retrospective study found that the absolute and relative counts of CD3−CD56+ NK cells in the peripheral blood of patients with RA-ILD were higher than those of patients with RA, whereas the percentages of T cells and CD4+ T cells were lower, suggesting that the occurrence of RA-ILD may be unbalanced with the lymphocyte subsets of patients. In particular, CD3−CD56+ NK cells are associated with T cell imbalances (Lai et al., 2019). The increase in the percentage and absolute number of CD3−CD56+ NK cells clearly suggests a possible involvement in the pathogenesis of human ILD and suggests a novel approach for studying ILD. These results suggest that NK cells may be involved in the formation of profibrotic, antifibrotic, and ILD conditions; however, further studies are needed.

Cytokine and growth factor-related signal transduction pathways and ILD

Multiple molecular pathways are activated by pro-inflammatory/pro-fibrotic cytokines (e.g., IL-6, IL-17, and TNF-α) and growth factors (e.g., TGF-β), which are increased in different ILD. The above overexpressed cytokines and growth factors in ILD were activated in the corresponding intracellular signal transduction pathways, such as the Smad-dependent and Smad-independent signaling pathways, NF-κB and JAK/STAT signaling pathways, which were closely related to the occurrence and development of ILD (Figure 2).

① Activation of a Smad-dependent signaling pathway: after TGF-β induction, the downstream transduction molecule Smad2 binds to Smad3, which is subsequently phosphorylated and activated to form trimers with Smad4 and transmit signals from the cell membrane to the nucleus (Feng and Derynck, 2005).

② Activation of the Smad independent signaling pathway and the NF-κB pathway: TGF-β receptor complex or TNF-α interacts with tumor necrosis factor receptor-associated protein 6 (TRAF6) to promote its own ubiquitination (Tzavlaki and Moustakas, 2020). TRAF6 activates TGF-β-activated kinase 1 (TAK1) through Lys63-linked polyubiquitination, which in turn is activated by phosphorylating MAP kinase kinases (MKK) MKK4, MKK3, and MKK6. MKKS further activate their downstream kinases JNK and p38, which can then phosphorylate their target transcription factors (TF) and regulate transcription (Tzavlaki and Moustakas, 2020). In addition, TGF-β-induced ShcA tyrosine phosphorylation promotes Ras protein activation. This leads to the sequential activation of Raf, mitogen activated protein kinase, and extracellular signal-regulated protein kinase (ERK1/2). Activated ERK1/2 phosphorylates TF. TGF-β also promotes the activation of rapamycin C2 through phosphatidylinositol 3-kinase (PI3K), which further recruits and phosphorylates serine/threonine kinase (AKT) (Tzavlaki and Moustakas, 2020), thereby activating the NF-kB pathway. Studies have shown that TGF-β can also induce Sirtuin 1 activation and activate α-smooth muscle actin (α-SMA) (Ma and Li, 2020). In addition, IL-17 forms heterodimer complexes with its receptors IL-17RA and IL-17RC to recruit NF-κB activator 1(Act1) through SEFIR domain interactions. Subsequently, Act1 binds to TRAF6 *via*
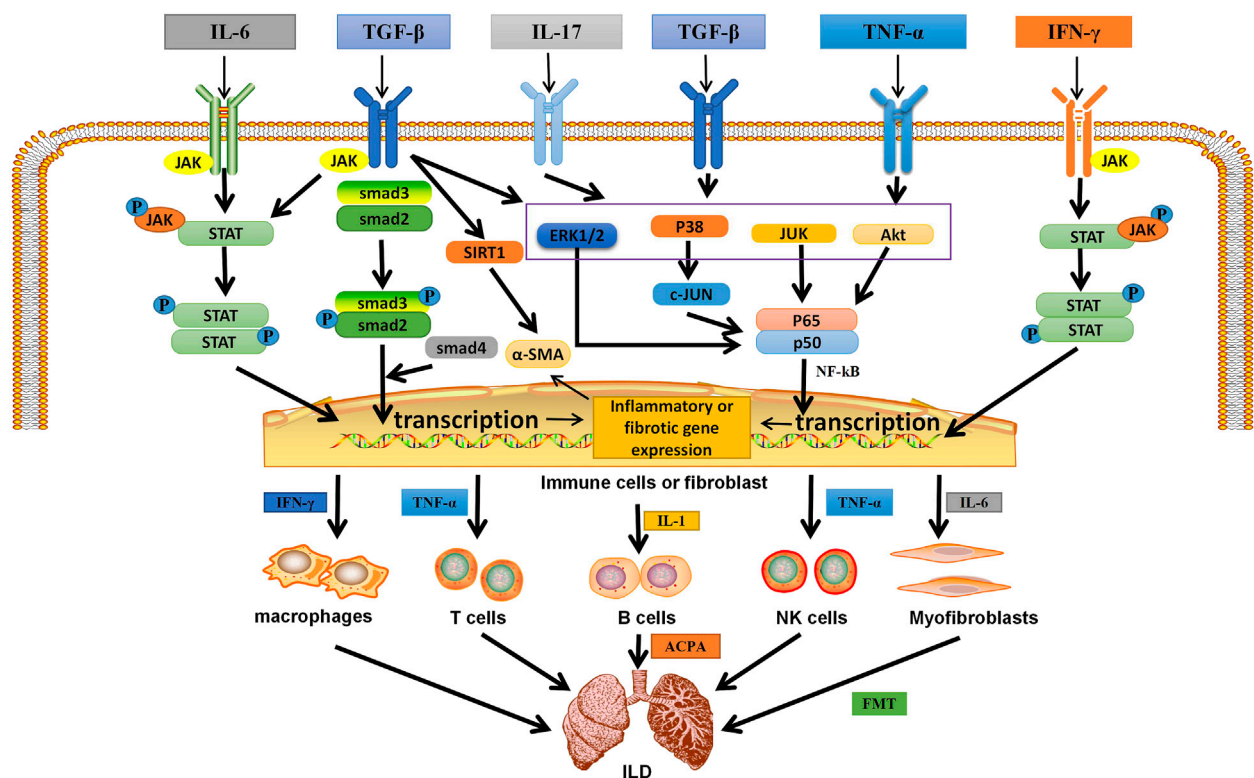
FIGURE 2
The related mechanism of ILD occurrence. Cytokines and growth factors, after binding to their corresponding receptors in immune cells or myofibroblasts, can be activated through different signal transduction pathways. Activated immune cells can secrete a variety of cytokines. They further activate macrophages; T, B, and NK cells; and myofibroblasts. They are over-activated and can secrete pro-inflammatory and pro-fibrotic cytokines, which is the environment for the formation of inflammation and fibrosis in the lung. Meanwhile, in different autoimmune diseases, B cells secrete corresponding antibodies, which are related to pulmonary fibrosis. In addition, IL-6 can activate myofibroblasts, causing them to undergo EMT and form ECM, which is deposited in the lung. Eventually ILD is formed. IL, interleukin; TGF-β, transforming growth factor β; IFN-γ, interferon-γ; TNF-α, tumor necrosis factor; P, phosphate; JAK, janus tyrosine kinase; STAT, signal transducers and activators of transcription; ERK1/2,extracellular signal-regulated protein kinases; AKT, serine-threonine kinase; NF-κB, nuclear factor-kappa B; SIRT1, sirtuin1; α-SMA, α-smooth muscle actin; ACPA, anticitrullinated peptide antibodie; ECM,extracellular matrix; EMT, epithelial-mesenchymal transition; ILD,Interstitial lung disease.

its TRAF6 binding site, recruiting TRAF6 into the IL-17R complex) (Zhu and Qian, 2012). Act1 acts as E3 ubiquitin ligase to polymerize TRAF6. TRAF6 also acts as an E3 ubiquitin ligase, which may ubiquitinate TAK1 complex and activate PI3K/AKT leading to NF-κB activation (Zhu and Qian, 2012). In addition, heat shock protein (HSP) is also involved in ILD formation. HSP90 has been shown to directly regulate ERK through dissociation of the ERk-HSP90-CDC37 complex (Erazo et al., 2013), thereby activating the ERK pathway. HSP90 also regulates AKT, and activation of AKT pathway has been reported in different cells with different pathological functions for pulmonary fibrosis (Colunga Biancatelli et al., 2020).

③JAK/STAT signaling pathway: Activation of the JAK/STAT pathway begins with the binding of ligands (usually cytokines, growth factors, such as IL-6, TGF-β, and IFN-γ) to their receptors, inducing JAK dimerization. The receptor-associated JAK is then activated and phosphorylates the tyrosine residue in the tail of its receptor cell to form p-JAK. These phosphorylations act as docking sites for STAT and bind to them *via* its SH2 domain, which phosphorylates STAT and is activated by tyrosine phosphorylation to form p-STAT, which subsequently becomes a dimer and translocations from the cytoplasm to the nucleus, where

they act as transcription factors (Montero et al., 2021). Thus, STATs are activated by JAKs and transferred from cytoplasm to nucleus, and then bind to specific DNA sequences to direct gene transcription, resulting in increased expression of pro-inflammatory cytokines TNF-α and IL-1β and pro-fibrotic cytokine IL-6 in the lung (Yang et al., 2019).

In the lung, the above cytokines and growth factors are activated in immune cells through the above signal transduction pathways, resulting in the expression of pro-inflammatory, pro-fibrosis genes and α-SMA (Ma and Li, 2020), thus activating more immune cells (including macrophages, T cells, B cells, and NK cells) and lung fibroblasts (Figure 2). The above pathway can up-regulate the expression of macrophage related polarization markers (such as CD86 and CD206), and cause macrophages to differentiate into "pro-inflammatory" M1 macrophages and release inflammatory factors (such as IFN-γ), and "pro-fibrotic" M2a macrophages and release pro-fibrotic cytokines (IL-6) (Lescoat et al., 2020). T cells and NK cells release pro-inflammatory cytokines (such as IFN-γ, TNF-α, IL-1, and IL-17) and pro-fibrotic cytokines (IL-6) (Figure 2) (Alesci et al., 2022). In addition to releasing cytokines, B cells can also differentiate into plasma cells and secrete ACPA, anti-SCL70 antibodies (Bellamri et al., 2019). Moreover, positive feedback

TABLE 2 Effects of RSV on immune cells.

Immune cells	Effects of RSV on immune cells
Macrophages	Decrease COX-2 expression; Modulate NF-κB activation; Eexert antioxidant properties; Inhibit cytokine secretion, such as TNF-α and IL-6, etc. Yang et al. (2017); Chen and Musa (2021)
T cells	Inhibit T cell activation; Reduce Th17 cells; Reduce IL-17,IFN-γ and TGF-β,etc; Modulate T cell regulation Poles et al. (2021)
B cells	Inhibit TGF-β expression; Induced SIRT1; Inactivates STAT3 Lai et al. (2019)
NK cells	Effect on NK cells killing activity; Decrease cytokine expression, such as IFN-γ,TNF-α and IL-13, etc. Krzewski and Strominger (2008); Lai et al. (2019)

amplifies the above signaling pathways and promotes the occurrence of pulmonary inflammation and fibrosis (Lescoat et al., 2020). Lung fibroblasts can induce self-proliferation or mesenchymal transformation through the pathway, resulting in abnormal expression of α-SMA and EMC components, thus causing fibroblasts to lose differentiation and obtain mesenchymal phenotype of myofibroblasts, ultimately leading to ILD formation (Duchemann et al., 2017) (Figure 2).

Effects of RSV on immune cells

RSV can enter cells by a variety of means (e.g. passive diffusion, endocytosis, or *via* transporters) and bind to specific receptors, such as the integrin receptor alphavβ3 (Delmas and Lin, 2011; Ho et al., 2020). It helps regulate innate and adaptive immunity, such as macrophages, B cells, T cells, and NK cells, thereby inhibiting overactivation of cells, reducing the production of pro-inflammatory or pro-fibrotic factors, and controlling the progression of ILD. Effects of RSV on immune cells (Table 2).

RSV and autoimmune diseases

The development of autoimmune diseases may result in damage to one or more body tissues or organs. Autoimmune diseases disorders of immune cells in the body, which cause immune cells to overactivate and produce a large number of inflammatory factors, such as TNF-α, IFN-γ, and IL-1β. Overstrong immune response can simultaneously attack different organs or tissues, leading to local or systemic immune response, such as RA, amyotrophic lateral sclerosis (ALS), PsO, SLE, IBD, etc. (Oliveira et al., 2017). RSV is a well-studied substance known for its effects on a large number of chronic diseases and its numerous therapeutic benefits, including anti-regulatory immunity, anti-inflammatory, etc. In autoimmune diseases, RSV can inhibit synovial macrophages, reduce angiogenesis, leukocyte and lymphocyte recruitment, fibroblast proliferation and protease secretion, especially in RA, and thus inhibit cartilage and bone destruction at pus formation sites (Oliveira et al., 2017). It can also inhibit the differentiation of T lymphocytes into Th2 and Th17, and reduce the activation of B cells and the production of autoantibodies (Oliveira et al., 2017). Cytokines are also closely related to autoimmune diseases. For example, macrophages increase the recruitment of neutrophils at the site of inflammation through the activation of NF-κB, and produce related cytokines (IFN-γ, TNF-α, IL-17, IL-21, and

IL-23, etc.). In experimental animals, When IL-6, TNF-α and other disorders occur, they are sufficient to cause destructive arthritis (Oliveira et al., 2017). RSV not only inhibited TNF-α and IL-1β-induced NF-κB activation, but also activated SIRT1 and inhibited RelA acetylation in mice with arthritis. In addition, the expression of NF-κB-induced inflammatory factors such as TNF-α, IL-1β, IL-6, metalloproteinase (MMP)-1 and MMP3 is decreased (Yamamoto and Gaynor, 2001). It can also reduce the mRNA expression levels of IL17 and IL19, reduce the thickness of animal skin and improve the damage caused by psoriasis (Malaguarnera, 2019). In addition, RSV reduced mRNA expression levels of IL-6, TNF-α, IFN-γ, JAK, and STAT when treating inflammatory mice (Yang et al., 2019). It is suggested that RSV can inhibit the anti-inflammatory effect of JAK/STAT signaling pathway. Therefore, RSV may have some efficacy in the treatment of autoimmune diseases by regulating the immune system and interfering with multiple cellular and molecular processes (see Table 3). Epithelial interstitial transformation (EMT) is an important factor in the development of pulmonary fibrosis (Tian et al., 2017). Some studies have found that the activation of NF-κB is an effective inducer of EMT activation, suggesting a close relationship between pulmonary fibrosis, inflammation and EMT (Chua et al., 2007; Chen et al., 2018a). In autoimmune diseases, some cytokines, such as IFN-γ, TNF-α, IL-17, and IL-6, are associated with ILD (Montero et al., 2021). In addition, it has been found that JAK-STAT pathway plays an important role in early alveolitis and the development of ILD (Banerjee et al., 2017). In RA-ILD mouse models, intraperitoneal injection of a JAK inhibitor (tofacitinib) improved symptoms and inhibited the progression of ILD (Sendo et al., 2019). RSV can not only reduce the levels of NF-κB and JAK-STAT, but also reduce the levels of IFN-γ, TNF-α, IL-17, and other cytokines, so RSV may have the potential to treat ILD, especially auto-immune-related ILD.

RSV and ILD

ILD is associated with decreased lung function, and complications can lead to rapid deterioration of the clinical course of ILD patients. In the past few years, two anti-fibrosis drugs pirfenidone and Nidanib have been approved for the treatment of ILD patients, but there are associated adverse reactions, including gastrointestinal adverse reactions, fatigue, weight loss, etc. (Morrow et al., 2022). More and more studies confirm that RSV is an ideal treatment for ILD. Fagone et al. (2011) studied the effect of RSV on TGF-β-induced myoblast activation of human lung fibroblasts. They found that RSV inhibited collagen

TABLE 3 Study on RSV in autoimmune diseases.

Diseases	The role of RSV in autoimmune diseases	Study on the correlation of resveratrol in autoimmune diseases
RA	RSV is able to act by reducing the production of autoantibodies, Th17 population, oxidative stress and NF-κB activation. Resveratrol also reduces COX2 and PGE2 expression and activates SIRT1 Yamamoto and Gaynor (2001); Tsai et al. (2017); Malaguarnera (2019)	Chen et al. (2014) reported that oral administration of resveratrol (10 or 50 mg/kg body weight) for 2 weeks reversed arthritis dysfunction in adjuvant arthritis rats. Riveiro-Naveira et al. (2016) used an acute model of antigen-induced arthritis in rats treated with resveratrol (12.5 mg/kg) daily for 2 months by oral gavage. They observed significantly reduced knee swelling, which suggests that oral administration of resveratrol can reduce severity in this model
SLE	RSV acts as an SIRT1 activator, inhibiting proliferation of B and T cells and antibody production Cardile et al. (2007)	Wang et al. (2014) used alupus BALB/c mouse model, in which the mice received an 0.5 mL injection of pristane and were treated with RSV (50 mg/kg/day and 75 mg/kg/day) over 7 months and the serum levels of autoantibodies and kidney damage were assessed. They found that resveratrol was able to attenuate proteinuria, decrease IgM and IgG kidney deposition, and reduce kidney histological lesions
PsO	Inhibiting the production of IL-17 (produced by Th17), IFN (produced by Th1) and directly inhibiting the proliferation of keratinocytesl Lynde et al. (2014)	Kjær et al. (2015) used a mouse model of imiquimod-induced psoriasis, a study demonstrated that RSV could ameliorate the damage caused by psoriasis, reducing the thickness of the animals' skins
ALS	RSV acts by activating SIRT1 and regulates its substrate expression, increases the SOD1 useful life, reduces ROS, and acts in mitochondrial biogenesis as an antioxidant and antiapoptoticl Yamamoto and Gaynor (2001)	ALS mouse model was intraperitoneally injected with RSV at the dose of 25 mg/kg body weight/day. RSV can significantly attenuate the motor neuron loss and reduce the muscle atrophy and dysfunction in the ALS micel Malaguarnera (2019)
IBD	RSV is capable of acting on the inhibition of inflammatory cells (Th1 and Th17 profiles) inflammatory cytokines (TNF-α,IL-1β) and neutralizing ROSl Cardile et al. (2007)	Martín et al. (2004) used RSV (5–10 mg/kg) gavage treatment, performed at 48, 24, and 1 h prior to the induction of colitis, resulted in improved acute experimental colitis, demonstrating a chemopreventive role of RSV in animal models 24 h later. Likewise, clinical signs of the disease-diarrhea, weight loss, and bleeding-were attenuated in the animals that received this dietl Sánchez-Fidalgo et al. (2010)

production, lung fibroblast proliferation, and α-SMA protein levels by inhibiting the phosphorylation of ERK1/2 and Akt, and down-regulated TGF-β1 levels by inhibiting TGF-β1/Smad2/3/4 signaling pathways, improving pulmonary fibrosis in mouse models (Fagone et al., 2011). In addition, RSV also down-regulates TGF-β-induced Smad2/3 phosphorylation by reducing the phosphorylation levels of c-Jun, α-SMA, p-Smad2, Smad7, and p38, significantly reducing TGF-β-induced collagen deposition and alleviating symptoms in rats (Wang et al., 2018). Recent results showed that RSV (40 mg/kg) could not only inhibit the expression of TGF-β1 in IPF rats, but also inhibit the phosphorylation of Smad2/3 and ERK1/2, significantly reduce the elevated levels of TNF-α, IL-6, and IL-13 excitability in ILD rats, and inhibit the damage of alveolar wall. Inflammatory cell infiltration, congestion and edema are reduced (Liu et al., 2020). These results indicate that RSV can inhibit TGF-β/Smad2/3/4 and NF-κB signaling pathways to play anti-inflammatory and antifibrotic roles.

In addition, Li et al. found that RSV targeted TAK1, significantly inhibited TAK1 activation, inhibited alveolar macrophages in alveoli, and reduced lung inflammation and pulmonary fibrosis in mice (Li et al., 2017). In bleomycin-induced EMT-related pulmonary fibrosis, SIRT1 expression is decreased, and the expression of type I collagen and α-SMA is increased (Rong et al., 2016). After RSV treatment, SIRT1 expression is increased, which reduces alveolar epithelial cell damage, fibroblast proliferation, collagen deposition and pulmonary fibrosis, and is related to lung protection (Ma and Li, 2020).

A recent study evaluated the effect of RSV on RA-ILD. We treated RA-ILD rats with RSV (10 mg/kg/day) orally for 4 weeks,

and found that RSV inhibited the JAK/STAT signaling pathway (i.e. the expression of JAK and STAT were significantly reduced in lung tissue) and decreased the levels of pro-inflammatory cytokines TNF-α, IL-6, and IL-1β. Meanwhile, it can promote the production of anti-inflammatory factor IL-10 and reduce lung inflammation (Colunga Biancatelli et al., 2020). In addition, the authors found that RSV improved pulmonary pathology (reduced inflammatory cell infiltration, reduced collagen deposition, significantly thinner alveolar wall thickness) and reduced fibrosis degree (Colunga Biancatelli et al., 2020). Therefore, RSV plays an anti-inflammatory and antifibrotic role by regulating the JAK/STAT signaling pathway, thereby improving RA-ILD.

In ILD, HSP90 expression was increased, and HSP90 ATPase activity was increased in fibroblasts isolated from fibrotic lung injury (Sontake et al., 2017). HSP90 may also contribute to the development of pulmonary fibrosis through IL-6, as HSP90 mediates activation of the nuclear factor kappa light chain enhancer in the B cell (NF-κB) dependent inflammatory pathway, promoting IL-6 production (Bohonowych et al., 2014; Bellaye et al., 2018). In IPF, alveolar epithelial type II cells promote pulmonary fibrosis through HSP90-AKT signaling (Chen et al., 2021). In SSc-ILD patients, HSP90 was overexpressed, and HSP90 could promote the persistence of myoblasts in pulmonary fibrosis by enhancing TGF-β signal transduction pathway (Štorkánová et al., 2021). In RA-ILD, IFN-γ produced by T cells stimulated by anti-citrullinated HSP90 indicated a TH1 immune response, and thus participated in the development of ILD (Chen et al., 2018b). In addition, inhibition of HSP90 has an effective antifibrotic effect *in vitro* and in mouse pulmonary fibrosis models

(Koh et al., 2015). The use of HSP90 inhibitors showed that inhibition of HSP90 can down-regulate the expression of AKT, ERK, and NF-κB, regulate the stability of TGF-β receptor, and interfere with the Smad and non-Smad (P-ERK) TGF-β signaling cascade. Thus, EMT is reduced and cell proliferation, formation of fibrotic mediators and ECM are reduced (Schumacher et al., 2007). Studies have shown that RSV can inhibit HSP90 (Liu et al., 2014). RSV inhibition of HSP90 can not only down-regulate MEK1/2 and ERK phosphorylation and NF-κB expression, but also reduce IL-2, IFN-γ, and TNF-α levels (Huang et al., 2020). Therefore, RSV may have similar effects as an inhibitor of HSP90. HSP90 may be the target of RSV, which can inhibit signal transduction pathways, reduce cytokine levels and play the role of anti-fibrosis, so as to achieve the purpose of treating ILD. However, there is still a lack of relevant research, and more studies are expected to further confirm. In conclusion, RSV inhibits different signaling pathways and immune cells, and therefore has therapeutic potential for treating ILD.

Potential adverse reactions to RSV

In general, RSV ingestion is generally well tolerated. In animal models, RSV has been shown to be non-irritating and genotoxic to the skin and eyes. After 90 days of subchronic toxicity test, RSV was found to have no adverse effects on the body and no reproductive toxicity at the maximum dose of 700 mg/(kgd) (Williams et al., 2009). This preliminarily proves that RSV is non-toxic and safe. However, some studies have found that RSV has certain side effects. When rats were treated with 1.0 and 3.0 g/(kgd) RSV, different degrees of dehydration, dyspnea, nephrotoxicity and elevated serum liver enzymes were observed in female and male rats (Shaito et al., 2020). This indicates that high dose RSV has certain toxicity (Hebbar et al., 2005). When administered continuously for 4 weeks at doses of 0, 300, 1,000, and 3,000 mg/kg/day, no adverse reactions occurred at doses up to 300 mg/kg/day, whereas 1,000 and 3,000 mg/kg/day caused renal toxicity (Crowell et al., 2004). When RSV was administered simultaneously to rats at (0.3, 1.0, or 3.0 g/kg/day), abnormal expression of liver genes was noted, possibly indicating liver injury (Hebbar et al., 2005). A significant increase in bilirubin levels was observed at 1,000 (mg/kg)/day RSV in rats, but no adverse effects were observed at 200 mg/(kgd) in rats and 600 mg/(kgd) in dogs (Johnson et al., 2011). The toxicity of RSV to target organs remains to be further studied.

In human subjects, a daily RSV dose of 450 mg has been reported to be safe for a 60 kg person (Moon et al., 2004). However, some adverse effects have been reported, and high dose RSV intake appears to have negative effects on metabolic status, endothelial health, inflammation, and cardiovascular markers in human patients (Ramírez-Garza et al., 2018). For example, higher doses of RSV (1,000 mg/day) have recently been shown to increase biomarkers of cardiovascular risk (e.g., oxidized LDL, soluble intercellular adhesion molecule-1, etc.), while lower doses have no effect on the same biomarkers (Mankowski et al., 2020). In a recent meta-analysis of 18 studies included, adverse reactions occurred in two studies (Zhang et al., 2021), one of which initially administered 500 mg,

qd, followed by an increase of 500 mg daily every 3 days, with a maximum dose of 3,000 mg daily (1,000 mg, tid). Adverse events occurred in three of the five patients. In the RSV group, one patient with a history of fatty liver disease developed asymptomatic and mild elevated alanine aminotransferase, another patient developed diarrhea and mild hypoglycemia, and one patient developed mild cellulitis at the biopsy site (Goh et al., 2014). In another study, which administered RSV 500 mg once daily plus losartan 12.5 mg, only two patients (one RSV and one placebo) complained of side effects of gastritis, such as mild dyspepsia, throughout the study of 30 patients in the RSV and placebo groups (Sattarinezhad et al., 2019). Therefore, more *in vivo* studies involving animal models are necessary, and more clinical trials of RSV in humans are needed to verify its efficacy and safety, especially before it can be considered for therapeutic or prophylactic use in humans.

Conclusion

ILD is one of the most important factors that directly affect the quality of life of patients. Long-term use of immunosuppressant and antifibrotic drugs can lead to many inevitable side effects. In addition, current drug treatments are still insufficient to reduce ILD progression and mortality worldwide. Bioactive natural ingredients derived from natural herbs may provide additional benefits in the prevention and treatment of ILD and represent an important source of new drug screening and development.

RSV inhibits TGF-β/Smad, NF-κB, and JAK/STAT pathways and immune cells, reduces the levels of pro-inflammatory and pro-fibrotic cytokines, and has powerful anti-inflammatory and anti-fibrotic effects. Therefore, TGF-β/Smad, NF-κB, and JAK/STAT pathways are potential targets of RSV in the treatment of ILD. It is also a potential and beneficial candidate for combination with other clinical antifibrosis agents. In addition, Piceatannol (PIC), a derivative of RSV, promotes autophagy by inhibiting the TGF-β1-Smad3/ERK/P38 signaling pathway, resulting in a decrease in the number of activated myoblasts, significantly reducing BLM-induced collagen deposition and myoblast accumulation (Sheng et al., 2022; Tieyuan et al., 2022). It also indicated that the related derivatives of RSV and the extracted compounds may also be able to treat ILD. However, the oral bioavailability of RSV is very low, with a maximum oral bioavailability of only 20%, although the total absorption rate in the gut is as high as 70% (Walle et al., 2004). Oral and intravenous radioisotope labeling of 14C RSVS suggests that the stage of biotransformation is a rate-limiting factor in RSV bioavailability. Therefore, targeted delivery of RSV to desired tissues or increased stability of RSV *in vivo* through the development of slow release systems are critical for improving bioavailability (Santos et al., 2019; Thipe et al., 2019). In addition, RSVS have been reported to have synergistic therapeutic effects when combined with other bioactive ingredients and micronutrients, giving RSVS a more stable chemical structure, higher solubility, and easier absorption in the small intestine (Williamson and Manach, 2005).

The drug dosage of RSV in the treatment of ILD is still unclear, as the dosage used in different studies varies. If clinical studies of RSV dose gradient Settings exist, deeper mechanisms of therapeutic effect may be clearly understood. Future studies should further explore the effects of

different drug doses of RSV on treatment and the deeper mechanism, and open a new window for the treatment of ILD. Although the results of most studies on polyphenols have proved promising, further research on animals and humans is warranted. By extensively evaluating the biological activity, efficacy, safety and appropriate dose of RSV, and determining specific molecular targets and structure-activity relationships, it provides a new way for clinicians to treat ILD.

Author contributions

RH and XH wrote the manuscript. YTY and YY collected the references. JL reviewed and revised the manuscript. All authors read and approved the final manuscript.

Conflict of interest

The authors declare that the research was conducted in the absence of any commercial or financial relationships that could be construed as a potential conflict of interest.

Publisher's note

All claims expressed in this article are solely those of the authors and do not necessarily represent those of their affiliated organizations, or those of the publisher, the editors and the reviewers. Any product that may be evaluated in this article, or claim that may be made by its manufacturer, is not guaranteed or endorsed by the publisher.

References

Alesci, A., Nicosia, N., Fumia, A., Giorgianni, F., Santini, A., and Cicero, N. (2022). Resveratrol and immune cells: A link to improve human health. *Molecules* 27 (2), 424. doi:10.3390/molecules27020424

Aquino-Galvez, A., Pérez-Rodríguez, M., Camarena, A., Falfan-Valencia, R., Ruiz, V., Montaño, M., et al. (2009). MICA polymorphisms and decreased expression of the MICA receptor NKG2D contribute to idiopathic pulmonary fibrosis susceptibility. *Hum. Genet.* 125 (5-6), 639–648. doi:10.1007/s00439-009-0666-1

Atkins, S. R., Turesson, C., Myers, J. L., Tazelaar, H. D., Ryu, J. H., Matteson, E. L., et al. (2006). Morphologic and quantitative assessment of CD20+ B cell infiltrates in rheumatoid arthritis-associated nonspecific interstitial pneumonia and usual interstitial pneumonia. *Arthritis Rheum.* 54 (2), 635–641. doi:10.1002/art.21758

Bagnato, G., and Harari, S. (2015). Cellular interactions in the pathogenesis of interstitial lung diseases. *Eur. Respir. Rev.* 24 (135), 102–114. doi:10.1183/09059180.00003214

Balachandran, S., and Adams, G. P. (2013). Interferon-γ-induced necrosis: An antitumor biotherapeutic perspective. *J. Interferon Cytokine Res.* 33 (4), 171–180. doi:10.1089/jir.2012.0087

Banerjee, S., Biehl, A., Gadina, M., Hasni, S., and Schwartz, D. M. (2017). JAK-STAT signaling as a target for inflammatory and autoimmune diseases: Current and future prospects. *Drugs* 77 (5), 521–546. doi:10.1007/s40265-017-0701-9

Bao, L., Ye, J., Liu, N., Shao, Y., Li, W., Fan, X., et al. (2022). Resveratrol ameliorates fibrosis in rheumatoid arthritis-associated interstitial lung disease via the autophagy-lysosome pathway. *Molecules* 27 (23), 8475. doi:10.3390/molecules27238475

Bellamri, N., Morzadec, C., Joannes, A., Lecureur, V., Wollin, L., Jouneau, S., et al. (2019). Alteration of human macrophage phenotypes by the anti-fibrotic drug nintedanib. *Int. Immunopharmacol.* 72, 112–123. doi:10.1016/j.intimp.2019.03.061

Bellaye, P. S., Shimbori, C., Yanagihara, T., Carlson, D. A., Hughes, P., Upagupta, C., et al. (2018). Synergistic role of HSP90α and HSP90β to promote myofibroblast persistence in lung fibrosis. *Eur. Respir. J.* 51 (2), 1700386. doi:10.1183/13993003.00386-2017

Bohonowych, J. E., Hance, M. W., Nolan, K. D., Defee, M., Parsons, C. H., and Isaacs, J. S. (2014). Extracellular Hsp90 mediates an NF-κB dependent inflammatory stromal program: Implications for the prostate tumor microenvironment. *Prostate* 74 (4), 395–407. doi:10.1002/pros.22761

Camont, L., Cottart, C. H., Rhayem, Y., Nivet-Antoine, V., Djelidi, R., Collin, F., et al. (2009). Simple spectrophotometric assessment of the trans-/cis-resveratrol ratio in aqueous solutions. *Anal. Chim. Acta* 634 (1), 121–128. doi:10.1016/j.aca.2008.12.003

Cardile, V., Chillemi, R., Lombardo, L., Sciuto, S., Spatafora, C., and Tringali, C. (2007). Antiproliferative activity of methylated analogues of E- and Z-resveratrol. *Z Naturforsch C J. Biosci.* 62 (3-4), 189–195. doi:10.1515/znc-2007-3-406

Celada, L. J., Kropski, J. A., Herazo-Maya, J. D., Luo, W., Creecy, A., Abad, A. T., et al. (2018). PD-1 up-regulation on CD4+ T cells promotes pulmonary fibrosis through STAT3-mediated IL-17A and TGF-β1 production. *Sci. Transl. Med.* 10 (460), eaar8356. doi:10.1126/scitranslmed.aar8356

Chambers, R. C., and Mercer, P. F. (2015). Mechanisms of alveolar epithelial injury, repair, and fibrosis. *Ann. Am. Thorac. Soc.* 12 (1), S16–S20. doi:10.1513/AnnalsATS.201410-448MG

Chávez, E., Reyes-Gordillo, K., Segovia, J., Shibayama, M., Tsutsumi, V., Vergara, P., et al. (2008). Resveratrol prevents fibrosis, NF-kappaB activation and TGF-beta increases induced by chronic CCl4 treatment in rats. *J. Appl. Toxicol.* 28 (1), 35–43. doi:10.1002/jat.1249

Chen, H., Chen, Q., Jiang, C. M., Shi, G. Y., Sui, B. W., Zhang, W., et al. (2018). Triptolide suppresses paraquat induced idiopathic pulmonary fibrosis by inhibiting TGFB1-dependent epithelial mesenchymal transition. *Toxicol. Lett.* 284, 1–9. doi:10.1016/j.toxlet.2017.11.030

Chen, H., He, A., Li, H., Chen, H., Xie, H., Luo, L., et al. (2021). TSSK4 upregulation in alveolar epithelial type-II cells facilitates pulmonary fibrosis through HSP90-AKT signaling restriction and AT-II apoptosis. *Cell Death Dis.* 12 (10), 938. doi:10.1038/s41419-021-04232-3

Chen, J., Song, S., Liu, Y., Liu, D., Lin, Y., Ge, S., et al. (2018). Autoreactive T cells to citrullinated HSP90 are associated with interstitial lung disease in rheumatoid arthritis. *Int. J. Rheum. Dis.* 21 (7), 1398–1405. doi:10.1111/1756-185X.13316

Chen, L., and Musa, A. E. (2021). Boosting immune system against cancer by resveratrol. *Phytother. Res.* 35 (10), 5514–5526. doi:10.1002/ptr.7189

Chen, X., He, H., Wang, G., Yang, B., and Ren, W. (2007). Stereospecific determination of cis- and trans-resveratrol in rat plasma by HPLC: Application to pharmacokinetic studies. *Biomed. Chromatogr.* 21 (3), 257–265. doi:10.1002/bmc.747

Chen, X., Lu, J., An, M., Ma, Z., Zong, H., and Yang, J. (2014). Anti-inflammatory effect of resveratrol on adjuvant arthritis rats with abnormal immunological function via the reduction of cyclooxygenase-2 and prostaglandin E2. *Mol. Med. Rep.* 9 (6), 2592–2598. doi:10.3892/mmr.2014.2070

Chua, H. L., Bhat-Nakshatri, P., Clare, S. E., MorimiyA, A., Badve, S., and NaksHatri, H. (2007). NF-kappaB represses E-cadherin expression and enhances epithelial to mesenchymal transition of mammary epithelial cells: Potential involvement of ZEB-1 and ZEB-2. *Oncogene* 26 (5), 711–724. doi:10.1038/sj.onc.1209808

Colunga Biancatelli, R. M. L., Solopov, P., Gregory, B., and Catravas, J. D. (2020). HSP90 inhibition and modulation of the proteome: Therapeutical implications for idiopathic pulmonary fibrosis (IPF). *Int. J. Mol. Sci.* 21 (15), 5286. doi:10.3390/ijms21155286

Crowell, J. A., Korytko, P. J., Morrissey, R. L., Booth, T. D., and Levine, B. S. (2004). Resveratrol-associated renal toxicity. *Toxicol. Sci.* 82 (2), 614–619. doi:10.1093/toxsci/kfh263

Cruz, T., Jia, M., Sembrat, J., Tabib, T., Agostino, N., Bruno, T. C., et al. (2021). Reduced proportion and activity of natural killer cells in the lung of patients with idiopathic pulmonary fibrosis. *Am. J. Respir. Crit. Care Med.* 204 (5), 608–610. doi:10.1164/rccm.202012-4418LE

Culley, F. J. (2009). Natural killer cells in infection and inflammation of the lung. *Immunology* 128 (2), 151–163. doi:10.1111/j.1365-2567.2009.03167.x

Delmas, D., and Lin, H. Y. (2011). Role of membrane dynamics processes and exogenous molecules in cellular resveratrol uptake: Consequences in bioavailability and activities. *Mol. Nutr. Food Res.* 55 (8), 1142–1153. doi:10.1002/mnfr.201100065

Deng, L., Huang, T., and Zhang, L. (2023). T cells in idiopathic pulmonary fibrosis: Crucial but controversial. *Cell Death Discov.* 9 (1), 62. doi:10.1038/s41420-023-01344-x

Desai, O., Winkler, J., Minasyan, M., and Herzog, E. L. (2018). The role of immune and inflammatory cells in idiopathic pulmonary fibrosis. *Front. Med. (Lausanne)* 5, 43. doi:10.3389/fmed.2018.00043

Ding, S., Wang, H., Wang, M., Bai, L., Yu, P., and Wu, W. (2019). Resveratrol alleviates chronic "real-world" ambient particulate matter-induced lung inflammation and fibrosis by inhibiting NLRP3 inflammasome activation in mice. *Ecotoxicol. Environ. Saf.* 182, 109425. doi:10.1016/j.ecoenv.2019.109425

Duchemann, B., Annesi-Maesano, I., Jacobe de Naurois, C., Sanyal, S., Brillet, P. Y., Brauner, M., et al. (2017). Prevalence and incidence of interstitial lung diseases in a multi-ethnic county of Greater Paris. *Eur. Respir. J.* 50(2), 1602419. doi:10.1183/13993003.02419-2016

Erazo, T., Moreno, A., Ruiz-Babot, G., Rodríguez-Asiain, A., Morrice, N. A., Espadamala, J., et al. (2013). Canonical and kinase activity-independent mechanisms for extracellular signal-regulated kinase 5 (ERK5) nuclear translocation require dissociation of Hsp90 from the ERK5-Cdc37 complex. *Mol. Cell Biol.* 33 (8), 1671–1686. doi:10.1128/MCB.01246-12

Esposito, I., Perna, F., Ponticiello, A., Gilli, M., and Sanduzzi, A. (2005). Natural killer cells in Bal and peripheral blood of patients with idiopathic pulmonary fibrosis (IPF). *Int. J. Immunopathol. Pharmacol.* 18 (3), 541–545. doi:10.1177/039463200501800314

Fagone, E., Conte, E., Gili, E., Fruciano, M., Pistorio, M. P., Lo Furno, D., et al. (2011). Resveratrol inhibits transforming growth factor-β-induced proliferation and differentiation of *ex vivo* human lung fibroblasts into myofibroblasts through ERK/Akt inhibition and PTEN restoration. *Exp. Lung Res.* 37 (3), 162–174. doi:10.3109/01902148.2010.524722

Feng, X. H., and Derynck, R. (2005). Specificity and versatility in tgf-beta signaling through Smads. *Annu. Rev. Cell Dev. Biol.* 21, 659–693. doi:10.1146/annurev.cellbio.21.022404.142018

Flament, T., Bigot, A., Chaigne, B., Henique, H., Diot, E., and Marchand-Adam, S. (2016). Pulmonary manifestations of Sjögren's syndrome. *Eur. Respir. Rev.* 25 (140), 110–123. doi:10.1183/16000617.0011-2016

Fu, Y., Yan, M., Xie, C., Hu, J., Zeng, X., and Hu, Q. (2020). Polydatin relieves paraquat-induced human MRC-5 fibroblast injury through inhibiting the activation of the NLRP3 inflammasome. *Ann. Transl. Med.* 8 (12), 765. doi:10.21037/atm-20-4570

Goh, K. P., Lee, H. Y., Lau, D. P., Supaat, W., Chan, Y. H., and Koh, A. F. Y. (2014). Effects of resveratrol in patients with type 2 diabetes mellitus on skeletal muscle SIRT1 expression and energy expenditure. *Int. J. Sport Nutr. Exerc Metab.* 24 (1), 2–13. doi:10.1123/ijsnem.2013-0045

Gouda, M. M., and Bhandary, Y. P. (2018). Curcumin down-regulates IL-17A mediated p53-fibrinolytic system in bleomycin induced acute lung injury *in vivo*. *J. Cell Biochem.* 119 (9), 7285–7299. doi:10.1002/jcb.27026

Hebbar, V., Shen, G., Hu, R., Kim, B. R., Chen, C., Korytko, P. J., et al. (2005). Toxicogenomics of resveratrol in rat liver. *Life Sci.* 76 (20), 2299–2314. doi:10.1016/j.lfs.2004.10.039

Heukels, P., van Hulst, J. A. C., van Nimwegen, M., Boorsma, C. E., Melgert, B. N., von der Thusen, J. H., et al. (2019). Enhanced Bruton's tyrosine kinase in B-cells and autoreactive IgA in patients with idiopathic pulmonary fibrosis. *Respir. Res.* 20 (1), 232. doi:10.1186/s12931-019-1195-7

Ho, Y., Li, Z. L., Shih, Y. J., Chen, Y. R., Wang, K., Whang-Peng, J., et al. (2020). Integrin αvβ3 in the mediating effects of dihydrotestosterone and resveratrol on breast cancer cell proliferation. *Int. J. Mol. Sci.* 21 (8), 2906. doi:10.3390/ijms21082906

Huang, H., Liao, D., Zhou, G., Zhu, Z., Cui, Y., and Pu, R. (2020). Antiviral activities of resveratrol against rotavirus *in vitro* and *in vivo*. *Phytomedicine* 77, 153230. doi:10.1016/j.phymed.2020.153230

Huang, Y., Oldham, J. M., Ma, S. F., Unterman, A., Liao, S. Y., Barros, A. J., et al. (2021). Blood transcriptomics predicts progression of pulmonary fibrosis and associated natural killer cells. *Am. J. Respir. Crit. Care Med.* 204 (2), 197–208. doi:10.1164/rccm.202008-3093OC

Huo, R., Guo, Q., Hu, J., Li, N., Gao, R., Mi, L., et al. (2022). Therapeutic potential of janus kinase inhibitors for the management of interstitial lung disease. *Drug Des. Devel Ther.* 16, 991–998. doi:10.2147/DDDT.S353494

Johnson, W. D., Morrissey, R. L., Usborne, A. L., KapetanovIc, I., Crowell, J. A., Muzzio, M., et al. (2011). Subchronic oral toxicity and cardiovascular safety pharmacology studies of resveratrol, a naturally occurring polyphenol with cancer preventive activity. *Food Chem. Toxicol.* 49 (12), 3319–3327. doi:10.1016/j.fct.2011.08.023

Katsumata, M., Hozumi, H., Yasui, H., Suzuki, Y., Kono, M., Karayama, M., et al. (2019). Frequency and clinical relevance of anti-cyclic citrullinated peptide antibody in idiopathic interstitial pneumonias. *Respir. Med.* 154, 102–108. doi:10.1016/j.rmed.2019.06.016

Kishore, A., and Petrek, M. (2021). Roles of macrophage polarization and macrophage-derived miRNAs in pulmonary fibrosis. *Front. Immunol.* 12, 678457. doi:10.3389/fimmu.2021.678457

Kjær, T. N., Thorsen, K., Jessen, N., Stenderup, K., and Pedersen, S. B. (2015). Resveratrol ameliorates imiquimod-induced psoriasis-like skin inflammation in mice. *PLoS One* 10 (5), e0126599. doi:10.1371/journal.pone.0126599

Koh, R. Y., Lim, C. L., Uhal, B. D., Abdullah, M., Vidyadaran, S., Ho, C. C., et al. (2015). Inhibition of transforming growth factor-β via the activin receptor-like kinase-5 inhibitor attenuates pulmonary fibrosis. *Mol. Med. Rep.* 11 (5), 3808–3813. doi:10.3892/mmr.2015.3193

Kolahian, S., Fernandez, I. E., Eickelberg, O., and Hartl, D. (2016). Immune mechanisms in pulmonary fibrosis. *Am. J. Respir. Cell Mol. Biol.* 55 (3), 309–322. doi:10.1165/rcmb.2016-0121TR

Krzewski, K., and Strominger, J. L. (2008). The killer's kiss: The many functions of NK cell immunological synapses. *Curr. Opin. Cell Biol.* 20 (5), 597–605. doi:10.1016/j.ceb.2008.05.006

Kuwana, M., Gil-Vila, A., and Selva-O'Callaghan, A. (2021). Role of autoantibodies in the diagnosis and prognosis of interstitial lung disease in autoimmune rheumatic disorders. *Ther. Adv. Musculoskelet. Dis.* 13, 1759720X211032457. doi:10.1177/1759720X211032457

Lai, N. L., Jia, W., Wang, X., Luo, J., Liu, G. Y., Gao, C., et al. (2019). Risk factors and changes of peripheral NK and T cells in pulmonary interstitial fibrosis of patients with rheumatoid arthritis. *Can. Respir. J.* 2019, 7262065. doi:10.1155/2019/7262065

Lee, J. S., Kim, E. J., Lynch, K. L., Elicker, B., Ryerson, C. J., Katsumoto, T. R., et al. (2013). Prevalence and clinical significance of circulating autoantibodies in idiopathic pulmonary fibrosis. *Respir. Med.* 107 (2), 249–255. doi:10.1016/j.rmed.2012.10.018

Lescoat, A., Lelong, M., Jeljeli, M., Piquet-Pellorce, C., Morzadec, C., Ballerie, A., et al. (2020). Combined anti-fibrotic and anti-inflammatory properties of JAK-inhibitors on macrophages *in vitro* and *in vivo*: Perspectives for scleroderma-associated interstitial lung disease. *Biochem. Pharmacol.* 178, 114103. doi:10.1016/j.bcp.2020.114103

Li, J., Liang, C., Zhang, Z. K., Pan, X., Peng, S., Lee, W. S., et al. (2017). TAK1 inhibition attenuates both inflammation and fibrosis in experimental pneumoconiosis. *Cell Discov.* 3, 17023. doi:10.1038/celldisc.2017.23

Liu, G., Friggeri, A., Yang, Y., Milosevic, J., Ding, Q., Thannickal, V. J., et al. (2010). miR-21 mediates fibrogenic activation of pulmonary fibroblasts and lung fibrosis. *J. Exp. Med.* 207 (8), 1589–1597. doi:10.1084/jem.20100035

Liu, L. L., He, J. H., Xie, H. B., Yang, Y. S., Li, J. C., and Zou, Y. (2014). Resveratrol induces antioxidant and heat shock protein mRNA expression in response to heat stress in black-boned chickens. *Poult. Sci.* 93 (1), 54–62. doi:10.3382/ps.2013-03423

Liu, M., Zeng, X., Wang, J., Fu, Z., and Liu, M. (2016). Immunomodulation by mesenchymal stem cells in treating human autoimmune disease-associated lung fibrosis. *Stem Cell Res. Ther.* 7 (1), 63. doi:10.1186/s13287-016-0319-y

Liu, Y. L., Chen, B. Y., Nie, J., Zhao, G. H., Zhuo, J. Y., Yuan, J., et al. (2020). Polydatin prevents bleomycin-induced pulmonary fibrosis by inhibiting the TGF-β/Smad/ERK signaling pathway. *Exp. Ther. Med.* 20 (5), 62. doi:10.3892/etm.2020.9190

Lynde, C. W., Poulin, Y., Vender, R., Bourcier, M., and Khalil, S. (2014). Interleukin 17A: Toward a new understanding of psoriasis pathogenesis. *J. Am. Acad. Dermatol* 71 (1), 141–150. doi:10.1016/j.jaad.2013.12.036

Ma, B. N., and Li, X. J. (2020). Resveratrol extracted from Chinese herbal medicines: A novel therapeutic strategy for lung diseases. *Chin. Herb. Med.* 12 (4), 349–358. doi:10.1016/j.chmed.2020.07.003

Malaguarnera, L. (2019). Influence of resveratrol on the immune response. *Nutrients* 11 (5), 946. doi:10.3390/nu11050946

Mankowski, R. T., You, L., Buford, T. W., Leeuwenburgh, C., Manini, T. M., Schneider, S., et al. (2020). Higher dose of resveratrol elevated cardiovascular disease risk biomarker levels in overweight older adults - a pilot study. *Exp. Gerontol.* 131, 110821. doi:10.1016/j.exger.2019.110821

Martín, A. R., Villegas, I., La Casa, C., and de la Lastra, C. A. (2004). Resveratrol, a polyphenol found in grapes, suppresses oxidative damage and stimulates apoptosis during early colonic inflammation in rats. *Biochem. Pharmacol.* 67 (7), 1399–1410. doi:10.1016/j.bcp.2003.12.024

Mikolasch, T. A., Garthwaite, H. S., and Porter, J. C. (2017). Update in diagnosis and management of interstitial lung disease. *Clin. Med. (Lond).* 17 (2), 146–153. doi:10.7861/clinmedicine.17-2-146

Montero, P., Milara, J., Roger, I., and Cortijo, J. (2021). Role of JAK/STAT in interstitial lung diseases; molecular and cellular mechanisms. *Int. J. Mol. Sci.* 22 (12), 6211. doi:10.3390/ijms22126211

Moon, R. T., Kohn, A. D., De Ferrari, G. V., and Kaykas, A. (2004). WNT and beta-catenin signalling: Diseases and therapies. *Nat. Rev. Genet.* 5 (9), 691–701. doi:10.1038/nrg1427

Morrow, L. E., Hilleman, D., and Malesker, M. A. (2022). Management of patients with fibrosing interstitial lung diseases. *Am. J. Health Syst. Pharm.* 79 (3), 129–139. doi:10.1093/ajhp/zxab375

Neys, S. F. H., Heukels, P., van Hulst, J. A. C., Rip, J., Wijsenbeek, M. S., Hendriks, R. W., et al. (2021). Aberrant B cell receptor signaling in naïve B cells from patients with idiopathic pulmonary fibrosis. *Cells* 10 (6), 1321. doi:10.3390/cells10061321

Oliveira, A. L. B., Monteiro, V. V. S., Navegantes-Lima, K. C., Reis, J. F., Gomes, R. d. S., Rodrigues, D. V. S., et al. (2017). Resveratrol role in autoimmune disease-A mini-review. *Nutrients* 9 (12), 1306. doi:10.3390/nu9121306

Pardo, A., and Selman, M. (2002). Idiopathic pulmonary fibrosis: New insights in its pathogenesis. *Int. J. Biochem. Cell Biol.* 34 (12), 1534–1538. doi:10.1016/s1357-2725(02)00091-2

Poles, J., Karhu, E., McGill, M., McDaniel, H. R., and Lewis, J. E. (2021). The effects of twenty-four nutrients and phytonutrients on immune system function and inflammation: A narrative review. *J. Clin. Transl. Res.* 7 (3), 333–376.

Raj, P., Thandapilly, S. J., Wigle, J., Zieroth, S., and Netticadan, T. (2021). A comprehensive analysis of the efficacy of resveratrol in atherosclerotic cardiovascular disease, myocardial infarction and heart failure. *Molecules* 26 (21), 6600. doi:10.3390/molecules26216600

Ramírez-Garza, S. L., Laveriano-Santos, E. P., Marhuenda-Muñoz, M., Storniolo, C. E., Tresserra-Rimbau, A., Vallverdu-Queralt, A., et al. (2018). Health effects of resveratrol: Results from human intervention trials. *Nutrients* 10 (12), 1892. doi:10.3390/nu10121892

Riveiro-Naveira, R. R., Valcárcel-Ares, M. N., Almonte-Becerril, M., Vaamonde-Garcia, C., Loureiro, J., Hermida-Carballo, L., et al. (2016). Resveratrol lowers synovial

hyperplasia, inflammatory markers and oxidative damage in an acute antigen-induced arthritis model. *Rheumatol. Oxf.* 55 (10), 1889–1900. doi:10.1093/rheumatology/kew255

Roberts, A. B., Russo, A., Felici, A., and Flanders, K. C. (2003). Smad3: A key player in pathogenetic mechanisms dependent on TGF-beta. *Ann. N. Y. Acad. Sci.* 995, 1–10. doi:10.1111/j.1749-6632.2003.tb03205.x

Roman, J., and Chiba, H. (2021). B cells in idiopathic pulmonary fibrosis: Targeting immune cells with antifibrotic agents. *Am. J. Respir. Cell Mol. Biol.* 64 (6), 652–654. doi:10.1165/rcmb.2021-0101ED

Rong, L., Wu, J., Wang, W., Zhao, R. P., Xu, X. W., and Hu, D. (2016). Sirt 1 activator attenuates the bleomycin-induced lung fibrosis in mice via inhibiting epithelial-to-mesenchymal transition (EMT). *Eur. Rev. Med. Pharmacol. Sci.* 20 (10), 2144–2150.

Sánchez-Fidalgo, S., Cárdeno, A., Villegas, I., Talero, E., and de la Lastra, C. A. (2010). Dietary supplementation of resveratrol attenuates chronic colonic inflammation in mice. *Eur. J. Pharmacol.* 633 (1-3), 78–84. doi:10.1016/j.ejphar.2010.01.025

Santos, A. C., Pereira, I., Magalhães, M., Pereira-Silva, M., Caldas, M., Ferreira, L., et al. (2019). Targeting cancer via resveratrol-loaded nanoparticles administration: Focusing on *in vivo* evidence. *AAPS J.* 21 (4), 57. doi:10.1208/s12248-019-0325-y

Sattarinezhad, A., Roozbeh, J., Shirazi Yeganeh, B., and ShaMs, M. (2019). Resveratrol reduces albuminuria in diabetic nephropathy: A randomized double-blind placebo-controlled clinical trial. *Diabetes Metab.* 45 (1), 53–59. doi:10.1016/j.diabet.2018.05.010

Schumacher, J. A., Crockett, D. K., Elenitoba-Johnson, K. S., and Lim, M. S. (2007). Proteome-wide changes induced by the Hsp90 inhibitor, geldanamycin in anaplastic large cell lymphoma cells. *Proteomics* 7 (15), 2603–2616. doi:10.1002/pmic.200700108

Sendo, S., Saegusa, J., Yamada, H., Nishimura, K., and Morinobu, A. (2019). Tofacitinib facilitates the expansion of myeloid-derived suppressor cells and ameliorates interstitial lung disease in SKG mice. *Arthritis Res. Ther.* 21 (1), 184. doi:10.1186/s13075-019-1963-2

Shaito, A., Posadino, A. M., Younes, N., Hasan, H., Halabi, S., Alhababi, D., et al. (2020). Potential adverse effects of resveratrol: A literature review. *Int. J. Mol. Sci.* 21 (6), 2084. doi:10.3390/ijms21062084

Shao, T., Shi, X., Yang, S., Zhang, W., Li, X., Shu, J., et al. (2021). Interstitial lung disease in connective tissue disease: A common lesion with heterogeneous mechanisms and treatment considerations. *Front. Immunol.* 12, 684699. doi:10.3389/fimmu.2021.684699

Sheng, H., Lin, G., Zhao, S., Li, W., Zhang, Z., Zhang, W., et al. (2022). Antifibrotic mechanism of Piceatannol in bleomycin-induced pulmonary fibrosis in mice. *Front. Pharmacol.* 13, 771031. doi:10.3389/fphar.2022.771031

Shimizu, T., Nagafuchi, Y., Harada, H., Tsuchida, Y., Tsuchiya, H., Hanata, N., et al. (2021). Decreased peripheral blood memory B cells are associated with the presence of interstitial lung disease in rheumatoid arthritis: A case-control study. *Mod. Rheumatol.* 31 (1), 127–132. doi:10.1080/14397595.2020.1719596

Sontake, V., Wang, Y., Kasam, R. K., Sinner, D., Reddy, G. B., Naren, A. P., et al. (2017). Hsp90 regulation of fibroblast activation in pulmonary fibrosis. *JCI Insight* 2 (4), e91454. doi:10.1172/jci.insight.91454

Štorkánová, H., Oreská, S., Špiritović, M., Heřmánková, B., Bubová, K., Komarc, M., et al. (2021). Plasma Hsp90 levels in patients with systemic sclerosis and relation to lung and skin involvement: A cross-sectional and longitudinal study. *Sci. Rep.* 11 (1), 1. doi:10.1038/s41598-020-79139-8

Thipe, V. C., Panjtan Amiri, K., Bloebaum, P., Raphael Karikachery, A., Khoobchandani, M., Katti, K. K., et al. (2019). Development of resveratrol-conjugated gold nanoparticles: Interrelationship of increased resveratrol corona on anti-tumor efficacy against breast, pancreatic and prostate cancers. *Int. J. Nanomedicine* 14, 4413–4428. doi:10.2147/IJN.S204443

Tian, R., Zhu, Y., Yao, J., Meng, X., Wang, J., Xie, H., et al. (2017). NLRP3 participates in the regulation of EMT in bleomycin-induced pulmonary fibrosis. *Exp. Cell Res.* 357 (2), 328–334. doi:10.1016/j.yexcr.2017.05.028

Tieyuan, Z., Ying, Z., Xinghua, Z., Huimin, W., and Huagang, L. (2022). Piceatannol-mediated JAK2/STAT3 signaling pathway inhibition contributes to the alleviation of oxidative injury and collagen synthesis during pulmonary fibrosis. *Int. Immunopharmacol.* 111, 109107. doi:10.1016/j.intimp.2022.109107

Truong, V. L., Jun, M., and Jeong, W. S. (2018). Role of resveratrol in regulation of cellular defense systems against oxidative stress. *Biofactors* 44 (1), 36–49. doi:10.1002/biof.1399

Tsai, M. H., Hsu, L. F., Lee, C. W., Chiang, Y. C., Lee, M. H., How, J. M., et al. (2017). Resveratrol inhibits urban particulate matter-induced COX-2/PGE2 release in human fibroblast-like synoviocytes via the inhibition of activation of NADPH oxidase/ROS/NF-κB. *Int. J. Biochem. Cell Biol.* 88, 113–123. doi:10.1016/j.biocel.2017.05.015

Turesson, C., Matteson, E. L., Colby, T. V., Vuk-Pavlovic, Z., Vassallo, R., Weyand, C. M., et al. (2005). Increased CD4+ T cell infiltrates in rheumatoid arthritis-associated interstitial pneumonitis compared with idiopathic interstitial pneumonitis. *Arthritis Rheum.* 52 (1), 73–79. doi:10.1002/art.20765

Tzavlaki, K., and Moustakas, A. (2020). TGF-B signaling. *Biomolecules* 10 (3), 487. doi:10.3390/biom10030487

Van Dyken, S. J., and Locksley, R. M. (2013). Interleukin-4- and interleukin-13-mediated alternatively activated macrophages: Roles in homeostasis and disease. *Annu. Rev. Immunol.* 31, 317–343. doi:10.1146/annurev-immunol-032712-095906

Vargas, J. E., Souto, A. A., Pitrez, P. M., Stein, R. T., and Porto, B. N. (2016). Modulatory potential of resveratrol during lung inflammatory disease. *Med. Hypotheses* 96, 61–65. doi:10.1016/j.mehy.2016.09.023

Walle, T., Hsieh, F., DeLegge, M. H., Oatis, J. E., Jr, and Walle, U. K. (2004). High absorption but very low bioavailability of oral resveratrol in humans. *Drug Metab. Dispos.* 32 (12), 1377–1382. doi:10.1124/dmd.104.000885

Wang, D., Zhang, J., Lau, J., Wang, S., Taneja, V., Matteson, E. L., et al. (2019). Mechanisms of lung disease development in rheumatoid arthritis. *Nat. Rev. Rheumatol.* 15 (10), 581–596. doi:10.1038/s41584-019-0275-x

Wang, J., He, F., Chen, L., Li, Q., Jin, S., Zheng, H., et al. (2018). Resveratrol inhibits pulmonary fibrosis by regulating miR-21 through MAPK/AP-1 pathways. *Biomed. Pharmacother.* 105, 37–44. doi:10.1016/j.biopha.2018.05.104

Wang, J., Xu, L., Xiang, Z., Ren, Y., Zheng, X., Zhao, Q., et al. (2020). Macrophages promote epithelial proliferation following infectious and non-infectious lung injury through a Trefoil factor 2-dependent mechanism. *Cell Death Dis.* 11 (2), 136. doi:10.1038/s41419-020-2329-z

Wang, L., Shao, M., Jiang, W., and Huang, Y. (2022). Resveratrol alleviates bleomycin-induced pulmonary fibrosis by inhibiting epithelial-mesenchymal transition and down-regulating TLR4/NF-κB and TGF-β1/smad3 signalling pathways in rats. *Tissue Cell* 79, 101953. doi:10.1016/j.tice.2022.101953

Wang, Z., Li, X., Chen, H., Han, L., Ji, X., Wang, Q., et al. (2021). Resveratrol alleviates bleomycin-induced pulmonary fibrosis via suppressing HIF-1α and NF-κB expression. *Aging (Albany NY)* 13 (3), 4605–4616. doi:10.18632/aging.202420

Wang, Z. L., Luo, X. F., Li, M. T., Xu, D., Zhou, S., Chen, H. Z., et al. (2014). Resveratrol possesses protective effects in a pristane-induced lupus mouse model. *PLoS One* 9 (12), e114792. doi:10.1371/journal.pone.0114792

Weiskirchen, S., and Weiskirchen, R. (2016). Resveratrol: How much wine do you have to drink to stay healthy? *Adv. Nutr.* 7 (4), 706–718. doi:10.3945/an.115.011627

Williams, L. D., Burdock, G. A., and Edwards, J. A. (2009). Safety studies conducted on high-purity trans-resveratrol in experimental animals. *Food Chem. Toxicol.* 47 (9), 2170–2182. doi:10.1016/j.fct.2009.06.002

Williamson, G., and Manach, C. (2005). Bioavailability and bioefficacy of polyphenols in humans. II. Review of 93 intervention studies. *Am. J. Clin. Nutr.* 81, 243S–255S. doi:10.1093/ajcn/81.1.243S

Wills-Karp, M., and Finkelman, F. D. (2008). Untangling the complex web of IL-4- and IL-13-mediated signaling pathways. *Sci. Signal* 1 (51), pe55. doi:10.1126/scisignal.1.51.pe55

Wynn, T. A. (2008). Cellular and molecular mechanisms of fibrosis. *J. Pathol.* 214 (2), 199–210. doi:10.1002/path.2277

Xue, J., Kass, D. J., Bon, J., Vuga, L., Tan, J., Csizmadia, E., et al. (2013). Plasma B lymphocyte stimulator and B cell differentiation in idiopathic pulmonary fibrosis patients. *J. Immunol.* 191 (5), 2089–2095. doi:10.4049/jimmunol.1203476

Yahfoufi, N., Alsadi, N., Jambi, M., and Matar, C. (2018). The immunomodulatory and anti-inflammatory role of polyphenols. *Nutrients* 10 (11), 1618. doi:10.3390/nu10111618

Yamamoto, Y., and Gaynor, R. B. (2001). Therapeutic potential of inhibition of the NF-kappaB pathway in the treatment of inflammation and cancer. *J. Clin. Invest.* 107 (2), 135–142. doi:10.1172/JCI11914

Yang, C. M., Chen, Y. W., Chi, P. L., Lin, C. C., and Hsiao, L. D. (2017). Resveratrol inhibits BK-induced COX-2 transcription by suppressing acetylation of AP-1 and NF-κB in human rheumatoid arthritis synovial fibroblasts. *Biochem. Pharmacol.* 132, 77–91. doi:10.1016/j.bcp.2017.03.003

Yang, G., Lyu, L., Wang, X., Bao, L., Lyu, B., and Lin, Z. (2019). Systemic treatment with resveratrol alleviates adjuvant arthritis-interstitial lung disease in rats via modulation of JAK/STAT/RANKL signaling pathway. *Pulm. Pharmacol. Ther.* 56, 69–74. doi:10.1016/j.pupt.2019.03.011

You, X. Y., Xue, Q., Fang, Y., Liu, Q., Zhang, C. F., Zhao, C., et al. (2015). Preventive effects of Ecliptae Herba extract and its component, ecliptasaponin A, on bleomycin-induced pulmonary fibrosis in mice. *J. Ethnopharmacol.* 175, 172–180. doi:10.1016/j.jep.2015.08.034

Zhang, J., Wang, D., Wang, L., Wang, S., Roden, A. C., Zhao, H., et al. (2019). Profibrotic effect of IL-17A and elevated IL-17RA in idiopathic pulmonary fibrosis and rheumatoid arthritis-associated lung disease support a direct role for IL-17A/IL-17RA in human fibrotic interstitial lung disease. *Am. J. Physiol. Lung Cell Mol. Physiol.* 316 (3), L487–L497. doi:10.1152/ajplung.00301.2018

Zhang, T., He, Q., Liu, Y., Chen, Z., and Hu, H. (2021). Efficacy and safety of resveratrol supplements on blood lipid and blood glucose control in patients with type 2 diabetes: A systematic review and meta-analysis of randomized controlled trials. *Evid. Based Complement. Altern. Med.* 2021, 5644171. doi:10.1155/2021/5644171

Zhu, S., and Qian, Y. (2012). IL-17/IL-17 receptor system in autoimmune disease: Mechanisms and therapeutic potential. *Clin. Sci. (Lond).* 122 (11), 487–511. doi:10.1042/CS20110496

N-benzyl-N-methyldecan-1-amine and its derivative mitigate 2,4- dinitrobenzenesulfonic acid-induced colitis and collagen-induced rheumatoid arthritis

Ji Eun Kim[1†], Changyu Kang[2†], Phatcharaporn Budluang[3†], Natpaphan Yawut[3], Il-Rae Cho[4], Yun Ju Choi[1], Jaejeong Kim[2], Sanghyun Ju[2], Beomgu Lee[5], Dong Hyun Sohn[5], Hyung-Soon Yim[6], Kyeong Won Lee[6], Jinsol Han[7], Youngmi Jung[7], Ho Young Kang[8], Jin Kyoon Park[9], Yunjin Jung[2]*, Dae Youn Hwang[1]* and Young-Hwa Chung[3,4]*

[1]Department of Biomaterials Science (BK21 FOUR Program), College of Natural Resources and Life Science, Pusan National University, Miryang, Republic of Korea, [2]College of Pharmacy, Pusan National University, Busan, Republic of Korea, [3]Department of Cogno-Mechatronics Engineering, Optomechatronics Research Institute, Pusan National University, Busan, Republic of Korea, [4]Hayoung Meditech Inc., Busan, Republic of Korea, [5]Department of Microbiology and Immunology, College of Medicine, Pusan National University, Yangsan, Republic of Korea, [6]Korea Institute of Ocean Science and Technology, Marine Biotechnology Research Center, Busan, Republic of Korea, [7]Department of Biological Science, Department of Integrated Biological Science, Pusan National University, Busan, Republic of Korea, [8]Department of Microbiology, Pusan National University, Busan, Republic of Korea, [9]Department of Chemistry and Chemistry Institute of Functional Materials, Pusan National University, Busan, Republic of Korea

As our previous study revealed that *N*-benzyl-*N*-methyldecan-1-amine (BMDA), a new molecule originated from *Allium sativum*, exhibits anti-neoplastic activities, we herein explored other functions of the compound and its derivative [decyl-(4-methoxy-benzyl)-methyl-amine; DMMA] including anti-inflammatory and anti-oxidative activities. Pretreatment of THP-1 cells with BMDA or DMMA inhibited tumor necrosis factor (TNF)-α and interleukin (IL)-1β production, and blocked c-jun terminal kinase (JNK), p38 mitogen-activated protein kinase (MAPK), MAPKAP kinase (MK)2 and NF-κB inflammatory signaling during LPS stimulation. Rectal treatment with BMDA or DMMA reduced the severity of colitis in 2,4-dinitrobenzenesulfonic acid (DNBS)-treated rat. Consistently, administration of the compounds decreased myeloperoxidase (MPO) activity (representing neutrophil infiltration in colonic mucosa), production of inflammatory mediators such as cytokine-induced neutrophil chemoattractant (CINC)-3 and TNF-α, and activation of JNK and p38 MAPK in the colon tissues. In addition, oral administration of these compounds ameliorated collagen-induced

rheumatoid arthritis (RA) in mice. The treatment diminished the levels of inflammatory cytokine transcripts, and protected connective tissues through the expression of anti-oxidation proteins such as nuclear factor erythroid-related factor (Nrf)2 and heme oxygenase (HO)1. Additionally, aspartate aminotransferase (AST) and alanine aminotransferase (ALT) levels did not differ between the BMDA- or DMMA-treated and control animals, indicating that the compounds do not possess liver toxicity. Taken together, these findings propose that BMDA and DMMA could be used as new drugs for curing inflammatory bowel disease (IBD) and RA.

Introduction

Garlic (*Allium sativum*) possesses not only anticancer activity but also anti-inflammatory properties. The bioactive components of garlic have been largely classified in two groups: water-soluble and oil-soluble organosulfur composites. The water-soluble organosulfur compounds include *S*-allylmercaptocysteine, *S*-allyl cysteine, and allicin while lipid-soluble organosulfur compounds comprise ajoene, diallyl trisulfide diallyl disulfide, and diallyl sulfide (Kim et al., 2016; Zhang et al., 2020). For example, allicin, a mjor ingredient of garlic, downregulates HIF-1α leading to the enhanced sensitization to cisplatin in non-small cell lung cancer (Pandey et al., 2020) and activates Nrf2 signaling, resulting in decrease of LPS-mediated inflammation in human umbilical vein endothelial cells (Zhang et al., 2017). As a lipid-soluble organosulfur compound, diallyl trisulfide inhibits cancer stem cell phenotypes by hindering the action of Forkhead box Q1 and also suppresses LPS-induced inflammation through the NF-κB pathway (Lee et al., 2018).

N-Benzyl-*N*-methyldecan-1-amine (BMDA), recently separated from garlic extracts, arrests cells at G2/M phase in U937 human leukemia cells (Jeong et al., 2014). The result is attributed to the reduced levels of cyclin-dependent kinase(Cdk) 1 and 2, and conversely the enhanced expression of p21 Cdk inhibitor in the absence of p53 (Jeong et al., 2014). In addition, our previous study showed that BMDA, which is synthesized by an organic chemical method rather than extraction from raw garlic, inhibits a novel oncogene-induced TGF-β signaling through Akt-ERK1/2 and β-catenin pathways, leading to the prevention of cancer stem cell-like phenotypes (Kaowinn et al., 2018).

Inflammatory bowel disease (IBD) including Crohn's disease and ulcerative colitis displays severe inflammatory lesions in the gastrointestinal tract (Abraham and Cho, 2009). It has been reported that the mucosal inflammation is caused by the dysregulated immune response to gut microflora besides environmental and genetic factors, although the etiology of IBD remains undetermined (Abraham and Cho, 2009; Uhlig and Powrie, 2018). Pharmacotherapies using chemical drugs, such as aminosalicylates, glucocorticoids, the peroxisome proliferator-activated receptor ligands, and biological drugs including anti-integrin and anti-tumor necrosis factor antibodies, have been applied for the treatment of IBD (Triantafillidis et al., 2011; Rath et al., 2018). However, we face great challenges to cure IBD due to low efficacy, resistance to the chemical drugs, and adverse side effects (Pithadia and Jain, 2011).

Rheumatoid arthritis (RA), a systematic chronic inflammatory disease, exhibits destruction of cartilage and bone in the hand and foot in which infiltration of inflammatory immune cells, synovial hyperplasia, and pannus formation were manifested although the etiology and pathogenesis remains to be thoroughly investigated (Noss and Brenner, 2008; Huang et al., 2021). Treatment paradigms have shifted from non-steroid anti-inflammatory drugs for an initial stage of RA to the administration of anti-TNF-α antibodies or JNK inhibitors for a late stage of RA (Demoruelle and Deane, 2012; Smolen et al., 2017). However, these treatments for the progressed RA also exhibit adverse side effects, including vulnerable infection of *Mycobacterium tuberculosis*, cytomegalovirus, heart failure, and malignancy (Hyrich et al., 2004).

In this study, we explore whether BMDA, a novel small compound derived from garlic, and its derivative DMMA, possess anti-inflammatory and anti-oxidative effects that can alleviate the pathological progression of colitis and RA. We first document that rectal treatment of colitis with BMDA or DMMA in DNBS-treated rat, an acute inflammatory disease model, and oral treatment with these small molecules in collagen-induced RA, a chronic inflammatory disease model, relieve the inflammatory process of the diseases.

Materials and methods

Antibodies and reagents

Antibodies against JNK (Cat. No; 9252s), p38 MAPK (Cat. No; 8690s), MK2 (Cat. No; 3042s), NF-κB (Cat. No; 4764) and their phospho-specific antibodies (Cat. No; 9255s, 9216s, 3316s, and 3033s, respectively) were acquired from Cell Signaling Technology (Danvers, MA, United States). Anti-HO1(Cat. No; sc-390991), - Nrf2 (Cat. No; sc-365949), -TNF-α (Cat. No; sc-52746), and -β-actin (Cat. No; sc-8432) antibodies purchased from Santa Cruz Biotechnology (Santa Cruz, CA, United States) were used to detect expression of the corresponding proteins. Lipopolysaccharide (LPS) and 2,4-dinitrobenzenesulfonic acid were acquired from Merck (St. Louis, MO, United States). Complete Freund's adjuvant (CFA), incomplete Freund's adjuvant (IFA), and bovine collagen type 2 obtained from Chondrex (Redmond, WA, United States) were utilized for induction of RA.

Cell culture

Human monocytic THP-1 cells obtained from Korean Cell Bank (Seoul, Korea) were maintained in RPMI-1640 including 10% fetal bovine serum, 100 units/mL penicillin, and 100 μg/mL streptomycin at 37°C in a 5% CO_2 atmosphere.

Animal

For the care and use laboratory animals, animal experiments were carried out in consonance with the Laboratory Animal Resources Guide. The Pusan National University Animal Care and Use Committee approved protocols of the animal study related to rat colitis and RA (PNU-2021-3068 for rat colitis and PNU-2021-3014 for RA). Sprague Dawley (SD) rats (250–260 g, 7 weeks old, 20 male) and DBA/1 mice (22–25 g, 6 weeks old, 24 male) acquired from Samtako Biokorea (Ohsan, Korea) and Orient Bio Inc. (Seongnam, Korea) were used, respectively. They were kept under specific pathogen-free conditions (a 12-h interval cycle for lighting at 23 ± 2°C temperature and 50%–55% humidity) and free accessed to tap water and food.

Synthesis of BMDA and DMMA

As previously described (Kaowinn et al., 2018), BMDA was synthesized with N-benzylmethylamine and decanal as starting materials using the reductive amination method (Molecules and Materials, Daejeon, Korea). DMMA was also synthesized with 1-(4-methoxyphenyl)-N-methylmethanamine and decanal using the same method (Molecules and Materials). The structures and molecular weights of the synthesized molecules were confirmed using H^1-NMR and liquid chromatography-mass spectrometry (LCMS). ^{1}H NMR (500 MHz, $CDCl_3$) of BMDA was as follows: δ_H 7.41–7.19 (m, 5H), 3.50 (s, 2H), 2.37 (dd, J = 18.0, 10.4 Hz, 2H), 2.21 (s, 3H), 1.53 (dd, J = 14.3, 7.1 Hz, 2H), 1.39–1.20 (m, 14H), 0.91 (t, J = 6.9 Hz, 3H) ppm, and its molecular weight was also confirmed by LCMS (ESI+): m/z = 262.4 [M + H]$^+$. ^{1}H NMR (500 MHz, $CDCl_3$) of DMMA was as follows: δ_H 7.24 (d, J = 8.6 Hz, 2H), 6.88 (d, J = 8.7 Hz, 2H), 3.83 (s, 3H), 3.45 (s, 2H), 2.40–2.33 (m, 2H), 2.19 (s, 3H), 1.52 (d, J = 7.2 Hz, 2H), 1.28 (s, 14H), 0.91 (t, J = 6.9 Hz, 3H) ppm; LCMS (ESI+): m/z = 292.5 [M + H]$^+$.

Induction of colitis in rats

As previously described (Kim et al., 2019), experimental colitis was generated in rats. Shortly, SD rats (male, 250–260 g) were starved for 24 h, except for tap water before the induction of colitis. Isoflurane was used for a light anesthesia of the rats. The rats were rectally inserted into the colon with a rubber cannula (2 mm OD). DNBS dissolved in 50% aqueous ethanol (48 mg, 0.4 mL^{-1}) was interfused into the colon with the rubber cannula for 3 consecutive days. According to previously reported criteria, colonic damage score (CDS) was analyzed (Hong et al., 2012). The CDS assessment was performed by four independent observers blinded to the treatment conditions.

Type II bovine collagen-induced rheumatoid arthritis (RA) in mice

Experimental RA was employed in mice as previously described (Kang et al., 2018). Bovine type II collagen (100 μg) mingled with an equal volume of CFA was introduced to DBA/1 mice (male, 7-8 weeks old) at the tail base of the animal. Day 0 indicates the day of the first immunization. On day 18 after the first immunization, the mice were augmented for immunity with an equal amount of the same collagen emulsified with 1:1 (v.v^{-1}) IFA at the subcutaneous tail base and maintained for additional 2 weeks. Thickness of the paw at the widest point of the ankle joint was assessed using an electric caliper. All mice of subset groups were sacrificed in a CO_2 gas chamber at 45 days after the first immunization.

Hematoxylin and eosin staining analysis

The rear paws of DBA/1 mice were decalcified with EDTA for 2 weeks after fixation of the tissues with 10% formalin for 48 h. They were subsequently implanted in paraffin wax and sliced with 4 μm thickness on glass slides. Using hematoxylin and eosin (H&E, Merck), the sliced tissues were stained and observed by an optical microscopy equipped with the Leica Application Suite (Leica Microsystems, Glattbrugg, Switzerland). To grade inflammation and cartilage and bone destruction, histopathological alterations of the rear paws were scored by a 5-point grading system that was previously described (Kang et al., 2020). Synovitis was analyzed on the basis of the criteria which were mentioned previously (Kang et al., 2020).

Quantitative real time–polymerase chain reaction (qRT-PCR) analysis

Using RNA isolation solution (RNA Bee, Tet-Test Inc., Friendswood, TX, USA), total RNAs were purified from paw connective tissues and followed by synthesis of cDNA with Superscript II reverse transcriptase (Thermo-Fisher Scientific Inc., Cambridge, MA, United States). qRT-PCR was carried out to measure the relative quantities of IL-1β, IL-6 and TNF-α mRNAs using 2× Power SYBR Green (Toyobo Co., Osaka, Japan). The PCR reaction conditions were in this manner: denaturation step (1 min at 95°C), amplifying step (40 cycles of 15 s at 95°C, 15 s at 57°C, and 45 s at 72°C), and melt curve step (15 s at 95°C and 60 s at 60°C). The primer sequences of the cytokines were as follows: IL-1β, sense primer: 5′-GCACA TCAAC AAGAG CTTCA GGCAG-3′ and anti-sense primer: 5′-GCTGC TTGTGAGGTG CTGAT GTAC-3'; IL-6, sense 5′-TTG GGA CTG ATG TTG TTG ACA-3′ and anti-sense 5′-TCA TCG CTG TTG ATA CAA TCA GA-3'; TNF-α, sense 5′-CCT GTA GCC CAC GTC GTA GC-3′ and anti-sense 5′-TTG ACC TCA GCG CTG ACT TG-3′. Additional analyses such as the fluorescence intensity, threshold cycle (Ct), threshold values, and housekeeping genes were performed as previously described (Livak and Schmittgen, 2001).

Western blotting

As previously described (Kaowinn et al., 2019), proteins from cell lysates were separated using 10% SDS-polyacrylamide gel, and

FIGURE 1
Structure and identification of BMDA and DMMA **(A)** Structure and ^{1}H-NMR result after the synthesis of BMDA. **(B)** Structure and ^{1}H-NMR result after the synthesis of DMMA.
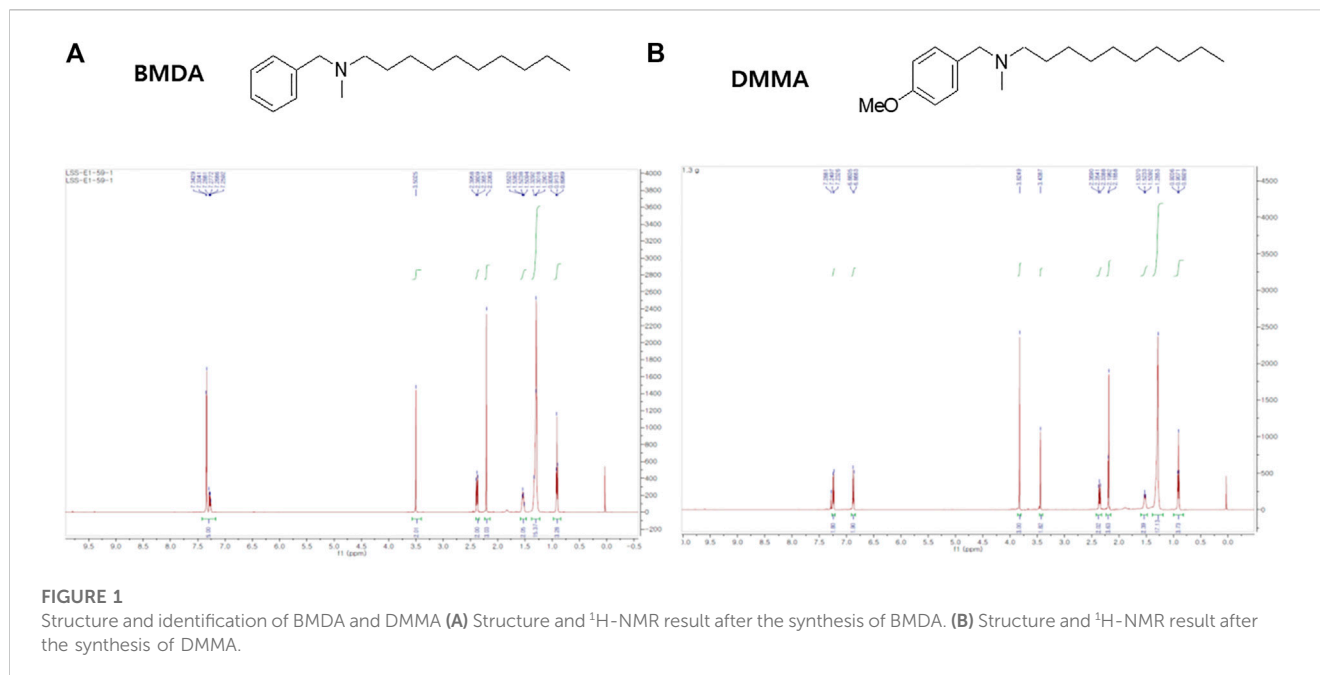
followed by transfer of the proteins onto nitrocellulose membranes. Primary antibodies (1:500–1,000 dilution) and subsequently a horseradish peroxidase conjugated-secondary antibody (1: 1,000 dilution) were added to the membrane. Images were visualized with an ImageQuant LAS 4000 Mini (GE Healthcare, Piscataway, NJ, United States) after adding an ECL solution (Thermo Fisher Scientific).

ELISA

The cytokine concentrations of TNF-α and IL-1β in the culture supernatants from THP-1 cells stimulated with LPS alone, LPS + BMDA, or LPS + DMMA were analyzed with ELISA kits provided by R&D Systems (Minneapolis, MN, United States) in accordance with the manufacturer's protocols. The level of cytokine-induced neutrophil chemoattractant (CINC)-3 in the agitated distal colon was also quantified with an ELISA kit (R&D Systems) as previously mentioned (Yang et al., 2019).

Measurement of myeloperoxidase (MPO) activity

The distal colon segments stored at −80°C were minutely chopped up in 1 mL of 0.5% HTAB (pH 6.0) and disrupted using a Polytron homogenizer on ice. The colon tissues were thereafter sonicated for 10 s, freeze-thawed three times, and followed by centrifugation at 14,000 rpm at 4°C. The supernatant (0.1 mL) was then mixed with 2.9 mL of 50 μM PBS enclosing 0.0005% hydrogen peroxide and 0.167 mg/mL odianishidine hydrochloride. The color change of the sample was detected in absorbance at 460 nm using a spectrophotometer (Shimadzu, Kyoto, Japan) for 5 min. The enzyme (MPO) one unit was defined as the decaying 1 μmol of peroxide per minute at 25°C.

Measurement of AST/ALT

For measurement of serum aspartate aminotransferase (AST) and alanine aminotransferase (ALT) levels, GOT (glutamate-oxaloacetate transaminase for AST) and GPT (glutamate pyruvate transaminase for ALT) reagents (Asan Pharmaceutical, Asan, Korea) were used based on the manufacturer's protocol. Shortly, after GOT or GPT buffer (100 μL)was added to mouse serum (20 μL), the mixtures were incubated for 30 min or for 60 min at 37°C, respectively. Thereafter, 2,4-dinitrophenylhydrazine colorimetric solution (100 μL, 0.0198%) was added to the mixtures, and followed by the incubation at 25°C for 20 min. The reaction was terminated with 0.4 N NaOH (1 mL) and the absorbance of the reaction color was measured at 505 nm.

Statistical analysis

All data were described as mean ± standard deviation. Error bars indicate standard deviation. Student's unpaired t-test was utilized for comparing the two groups as a statistical analysis. The significance of the result was set at p-value <0.05.

Results

BMDA and its derivative DMMA inhibit LPS-induced inflammation *in vitro*

The chemical structures of BMDA and its derivative DMMA were synthesized by the reductive amination method (Afanasyev et al., 2019) and were confirmed by H^1-NMR, as presented in Figures 1A, B. Before inquiring that BMDA and DMMA possess anti-inflammation features, we first examined whether these compounds, themselves harbor toxicity to human monocyte THP-1 cells. While LPS (1 μg mL^{-1})
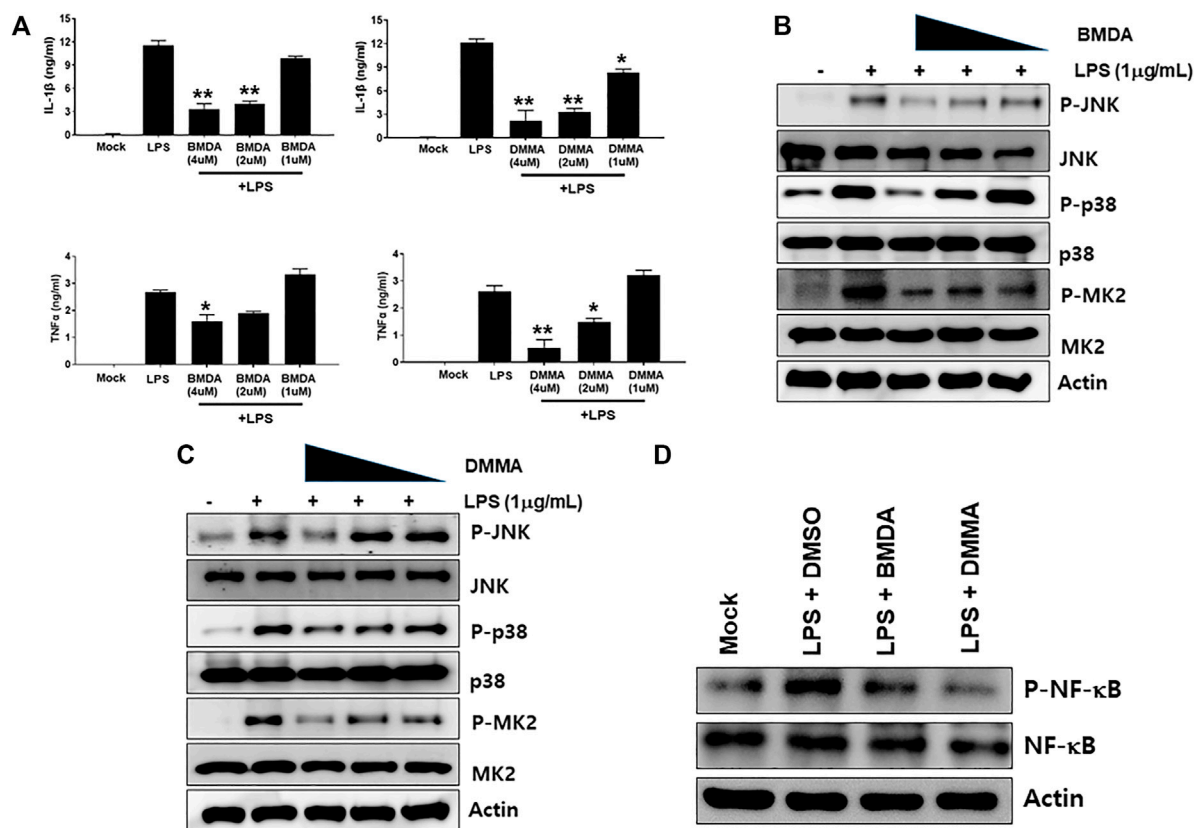
FIGURE 2
BMDA or DMMA inhibits LPS-induced inflammation through downregulation of JNK/P38 MAPK-MK2 and NF-κB signaling **(A)** After THP-1 cells were pretreated with BMDA (1, 2, and 4 μM), DMMA (1, 2, and 4 μM), or DMSO as a control for 3 h, they were stimulated with LPS (1 μg mL^{-1}). The cells were harvested 4 h post-stimulation and subsequently TNF-α and IL-1β cytokines were measured by ELISA. [For IL-1β ELISA, **; $p < 0.01$, LPS vs. BMDA (2 or 4 μM)+LPS, LPS vs. DMMA(2 or 4 μM)+LPS. *; $p < 0.05$, LPS vs. DMMA (1 μM)+LPS. For TNF-α ELISA, **; $p < 0.01$, LPS vs. DMMA (4 μM)+LPS. *; $p < 0.05$, LPS vs. BMDA (4 μM)+LPS, LPS vs. DMMA (2 μM)+LPS]. **(B, C)** THP-1 cells were pretreated with BMDA or DMMA for 3 h and subsequently stimulated with LPS for 1 h. Then, phosphorylation levels of JNK, p38 MAPK, and MK2 in the cells were examined by immunoblotting. **(D)** The cells were pretreated with BMDA (4 μM) or DMMA (4 μM) for 3 h, followed by stimulation of the cells with LPS (1 μg mL^{-1}) for 1 h. Then, the cells were harvested and phosphorylation levels of NF-κB p65 protein were detected by immunoblotting.

induced a slight cell death of THP-1 cells, BMDA and DMMA rather protected the cells from cell death caused by LPS stimulation (Supplementary Figure S1). To examine whether TNF-α and IL-1β cytokine production from THP-1 cells during LPS stimulation are inhibited by pretreatment with BMDA or DMMA, the inflammatory cytokine production was measured in the culture supernatant of the cells by ELISA. BMDA and DMMA clearly diminished TNF-α and IL-1β cytokine production from LPS-stimulated THP-1 cells in a dose-dependent manner (1, 2, and 4 μM) (Figure 2A). To illustrate signaling pathways mediated by inflammatory cytokines such as TNF-α and IL-1β are inactivated by BMDA or DMMA administration, THP-1 cells pretreated with BMDA or DMMA at different concentrations for 3 h were triggered with LPS as a stimulant for 1 h. BMDA and DMMA treatment reduced the phosphorylation levels of JNK and p38MAPK, which are involved in inflammatory cytokines, oxidation, and cellular stress (Figures 2B, C, Supplementary Figures S2A, B). Phosphorylation levels of MK2, a downstream molecule of p38MAPK, also decreased in a similar manner (Figures 2B, C, Supplementary Figure S2C). In addition, as NF-κB p65 protein is known to be involved in inflammatory cytokine production and signaling, phosphorylation

levels of NF-κB p65, which is indicating that activated NF-kB protein moves into the nucleus, were examined under the same conditions. During LPS stimulation, pretreatment with BMDA or DMMA inhibited phosphorylation of NF-κB p65 protein (Figure 2D, Supplementary Figure S2D). These results indicate that both BMDA and DMMA possess anti-inflammatory properties *in vitro* through inactivation of JNK/p38MAPK-MK2 and the downregulation of NF-κB.

Rectal treatment with BMDA or DMMA alleviates DNBS-induced rat colitis

To explore the anti-inflammatory properties of BMDA and DMMA *in vivo*, a DNBS-induced rat colitis model that mimics IBD was employed. As reported in a previous study (Hong et al., 2012), the DNBS-induced IBD rat model is highly reproducible and an acute inflammatory disease model. In particular, to investigate the direct anti-inflammatory effects of BMDA and DMMA on the cell surface of tissues, we attempted enema treatment of male Sprague
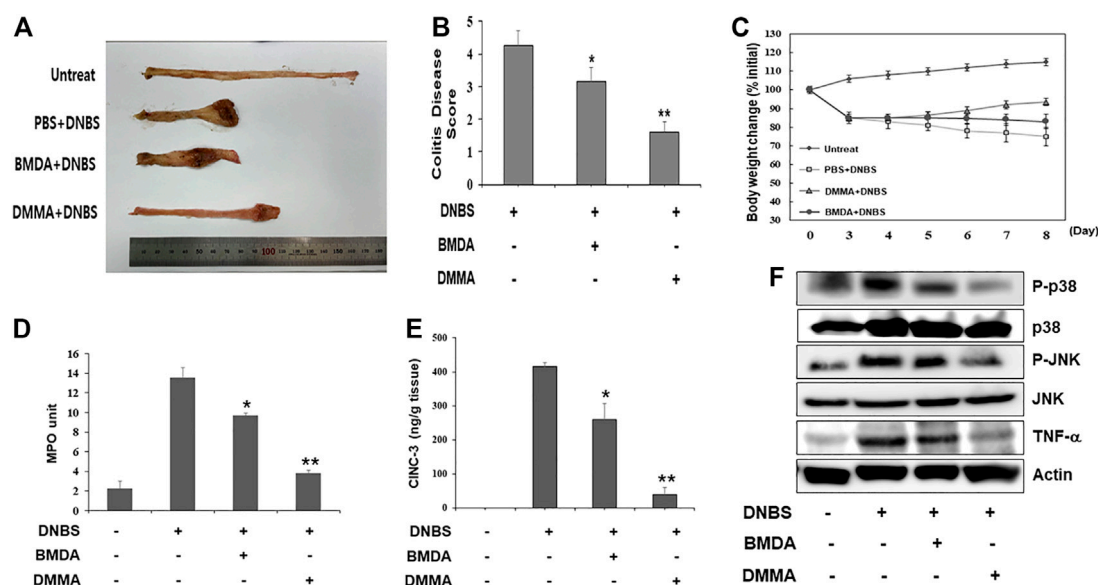
FIGURE 3
Rectal treatment with BMDA or DMMA relieves DNBS-induced colitis by decreasing inflammatory mediators **(A)** Distal colons of DNBS-induced colitis from rats (n = 5 rats per group) treated with BMDA (100 µg, 0.5 mL^{-1} PBS per rat), DMMA (100 µg.0.5 mL^{-1} PBS per rat), or PBS (0.5 mL) as a control for 5 days were photographed. Representative images are shown. **(B)** DNBS-induced colitis in rats treated with BMDA, DMMA, or PBS was evaluated by colon damage score described in Materials and Methods. (**$p < 0.01$, PBS + DNBS vs. DMMA + DNBS. *$p < 0.05$, PBS + DNBS vs. BMDA + DNBS) **(C)** Body weight of rats treated with DNBS for three consecutive days was measured from starting day for rectal administration of BMDA, DMMA or PBS, and the measurement was thereafter kept for 5 days. **(D)** Myeloperoxidase (MPO) activity from inflamed distal colons of rats treated with BMDA, DMMA, or PBS was measured. (**$p < 0.01$, PBS + DNBS vs. DMMA + DNBS. * $p < 0.05$, PBS + DNBS vs. BMDA + DNBS) **(E)** Concentration of CINC-3 from inflamed distal colons of rats treated with BMDA, DMMA, or PBS were measured by ELISA. (**; $p < 0.01$, PBS + DNBS vs. DMMA + DNBS. * $p < 0.05$, PBS + DNBS vs. BMDA + DNBS) **(F)** The distal colons of DNBS-induced colitis from the rats treated with BMDA, DMMA, or PBS were minced and prepared for immunoblotting. Phosphorylation levels of JNK and p38 MAPK, and expression levels of TNF-α in the colons were examined with their specific antibodies.

Dawley rats with BMDA or DMMA. After rectal administration with DNBS was performed during three consecutive days to induce IBD, BMDA (0.4 mg kg^{-1} body weight) or DMMA (0.4 mg kg^{-1} body weight) diluted with PBS was rectally administered for 5 days. Rats treated with PBS showed very severe colitis inflammation accompanied by hemorrhagic lesions and shorter colon length than untreated rats (Figures 3A, B). BMDA treatment reduced colitis severity but failed to restore colon length (Figures 3A, B). However, the rats treated with DMMA showed reduced colitis inflammation and longer colon length than rats treated with PBS (Figures 3A,B). Interestingly, DMMA treatment resulted in improved colitis inflammation and longer colon length than BMDA treatment (Figures 3A, B). However, BMDA or DMMA administration did not fully recover body weight as seen in untreatment group (Figure 3C) Consistent with the colitis score results, DMMA treatment resulted in lower activity and concentration of inflammatory mediators, such as MPO activity and CINC-3 in the colonic tissues than those from BMDA or PBS treatment (Figures 3D, E). In addition, when signaling molecules involved in inflammation were examined in the colonic tissues, phosphorylation levels of JNK and p38MAPK and expression levels of TNF-α were decreased during BMDA or DMMA administration (Figure 3F). Based on these results, both BMDA and DMMA treatment exhibited anti-inflammatory effects on DNBS-induced acute colitis, and furthermore, DMMA showed greater therapeutic efficacy than BMDA for the treatment of DNBS-induced rat colitis.

Oral administration with BMDA or DMMA alleviates collagen-induced RA

As we demonstrated that both BMDA and DMMA have anti-inflammatory effects in an acute inflammatory disease model, such as DNBS-induced rat colitis (Figures 3A–F), we wondered whether these small molecules could alleviate chronic inflammatory diseases, such as collagen-induced RA. We were also curious whether oral administration of BMDA or DMMA could exert anti-inflammatory effects in collagen-induced RA. DBA/1 mice were consecutively treated with a mixture of CFA and type 2 bovine collagen (1:1), followed by IFA and the collagen (1:1) 18 days later. Three days after the second co-administration, the mice were separated into three groups: vehicle, BMDA, and DMMA. BMDA or DMMA diluted with corn oil was orally administered to the animals every day for 21 days after grouping. The vehicle group treated with corn oil showed a gradual increase in paw thickness (from ~2.1 to ~3.4 mm) until 30 days after the first immunization and maintained paw thickness (from ~3.4 to ~3.6 mm) thereafter (Figures 4A, B). BMDA or DMMA treatment reduced the progression of inflammation in the paw compared to vehicle treatment, but inflammation in the paw reached its maximum around 35 days after the first immunization and then drastically decreased until 42 days (BMDA; ~2.5 mm, DMMA; ~2.8 mm) (Figures 4A, B). Interestingly, BMDA exerted slightly greater anti-inflammatory efficacy than DMMA, which was the opposite in the DNBS-induced rat colitis model (Figures 4A, B).
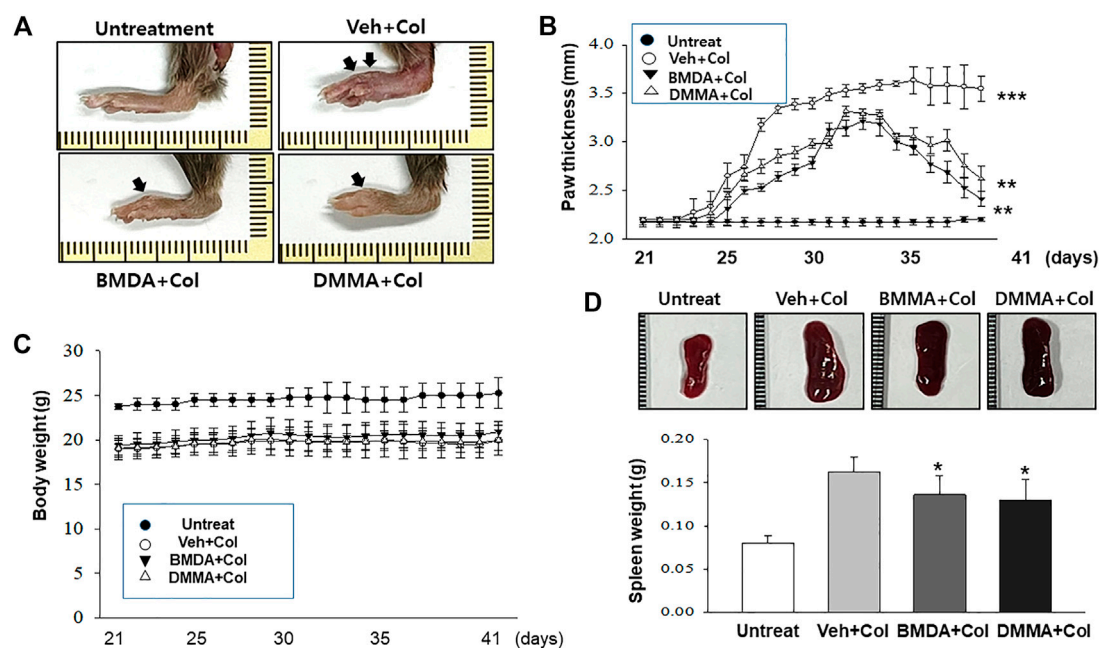
FIGURE 4
Oral administration of BMDA or DMMA reduces collagen-induced RA **(A)** RA was induced in DBA mice by collagen. Hind paw tissues from the mice ($n = 6$ mice per group) orally treated with BMDA (0.5 mg0.2 mL^{-1} corn oil per mouse), DMMA (0.5 mg0.2 mL^{-1}corn oil per mouse), or corn oil (0.2 mL) as a control were photographed. Representative images are shown. **(B)** Thickness of hind paw from the animals were measured from the first day to 21 days after sensitization of collagen and IFA every other day using a caliper. Vehicle (Veh) indicates corn-oil. (***; $p < 0.001$, untreatment vs. Veh + Collagen (Col), **; $p < 0.01$, Veh + Collagen(Col) vs. BMDA + Col, Veh + Col vs. DMMA + Col) **(C)** Body weight of the animal was also measured when hind paw thickness was measured. **(D)** Spleen size and weight of the animals were measured 21 days post-sensitization of collagen and IFA. (**; $p < 0.01$, untreatment vs. Veh + Collagen (Col), *; $p < 0.05$, Veh + Collagen(Col) vs. BMDA + Col, Veh + Col vs. DMMA + Col).

BMDA and DMMA treatment failed to completely recover the collagen-induced loss of body weight (Figure 4C). The protocol for collagen-induced RA increased the spleen size and weight in the DBA/1 mice, but BMDA or DMMA treatment inhibited the increase in the spleen size and weight (Figure 4D). Furthermore, staining of the hind paw tissues in the vehicle-treated mice with hematoxylin-eosin showed severe synovitis, but synovitis was clearly reduced in the hind paw tissues of BMDA- or DMMA-treated mice (Figures 5A, B). When mRNA levels of inflammatory cytokines were examined in the hind paw tissues of the animals, BMDA or DMMA treatment diminished transcript levels of IL-1β, IL-6, and TNF-α in the tissues compared with those in the tissues from vehicle-treated animals (Figure 5C). Interestingly, when the expression levels of anti-oxidation proteins such as HO1 and Nrf2 were examined, BMDA or DMMA treatment inhibited collagen-induced decrease of HO1 and Nrf2 protein levels in the tissues of vehicle-treated animals (Figure 5D). Moreover, as we were curious about the toxicity of BMDA and DMMA, the levels of AST and ALT, an indicator of liver toxicity, were measured in the sera of animals treated with vehicle, BMDA, or DMMA. We found that the levels of AST and ALT in the mice treated with BMDA or DMMA were similar to those in the animals treated with vehicle (Figure 6), indicating that neither BMDA nor DMMA induced toxicity in the liver of animals orally treated with BMDA or DMMA for 3 weeks. Based on these results, oral administration of BMDA and DMMA exhibited anti-inflammatory and anti-oxidative effects in collagen-induced RA, a chronic inflammatory disease model.

Discussion

This study was initiated to explore whether BMDA and DMMA possess therapeutic effects on both acute and chronic inflammatory diseases. In addition, we wondered whether these small molecules exert the anti-inflammatory activity irrespective of a route administration. To answer these questions, we thus employed DNBS-induced colitis representing an acute inflammatory disease model and collagen-induced RA displaying a relatively chronic inflammatory disease model. Moreover, we implemented the direct delivery of BMDA and DMMA to epithelial cells of colorectal colon in the rats bearing colitis and oral administration of them to mice suffering RA in order to remedy the inflammatory diseases irrespective of a route administration.

We report for the first time that BMDA and its derivative, DMMA, exert anti-inflammatory effects on DNBS-induced colitis and collagen-induced RA disease, which could be attributed to the downregulation of p38MAPK-MK2 inflammation and suppression of the NF-κB signaling pathway. As a consequence, BMDA or DMMA administration reduced expression levels of inflammatory cytokines such as IL-1β and TNF-α in LPS-stimulated THP-1 cells *in vitro* and in tissues from DNBS-induced colitis and collagen-induced arthritis *in vivo*. However, a careful examination revealed BMDA showing a slightly better therapeutic effect than DMMA on collagen-induced RA, but the opposite result was observed in DNBS-induced colitis. To explain these findings, we propose that the structure of DMMA itself is more effective in suppressing inflammatory progression in DNBS-induced colitis. However, orally administered DMMA might be converted to another
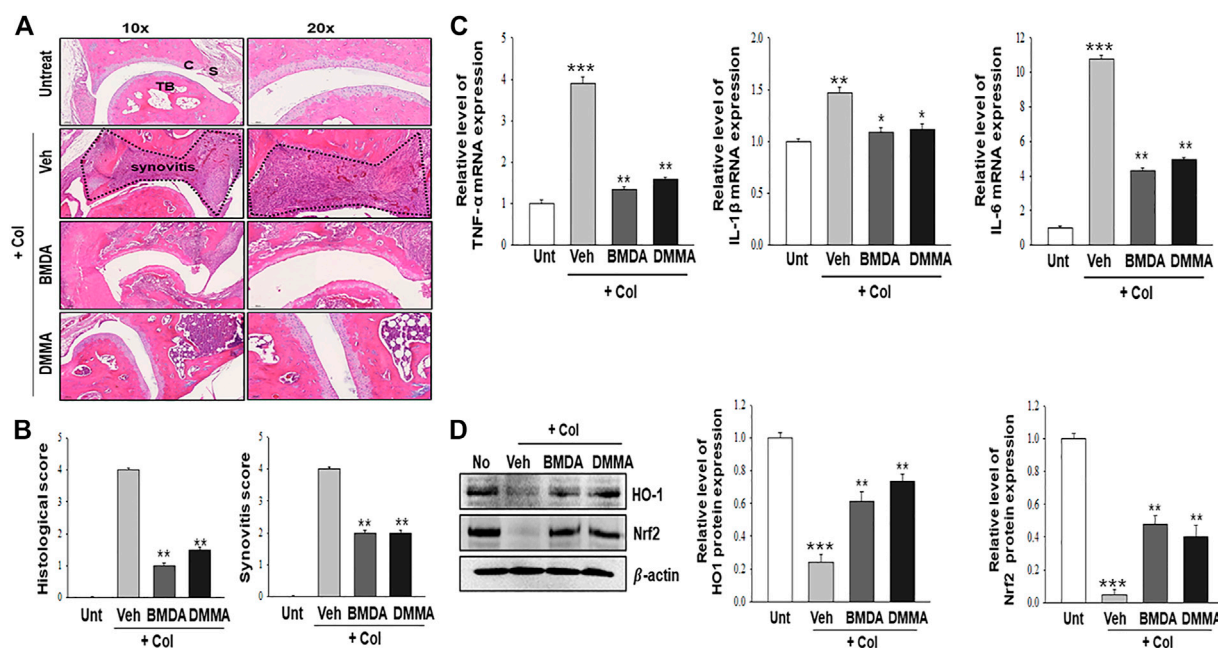
FIGURE 5
BMDA or DMMA-mediated reduction of severity is attributed to decrease of inflammatory cytokine transcripts and enhancement of anti-oxidation protein expression **(A, B)** Histopathological analysis on hind paw tissues of the animals orally treated with BMDA, DMMA, or corn oil as a control was performed with hematoxylin and eosin staining 21 days post-sensitization of collagen and IFA. Synovitis score was evaluated as described previously (Kang et al., 2020). **(C)** cartilage, S: synovium, TB: trabecular bone. (**; $p < 0.01$, Veh + Col vs. BMDA + Col, Veh + Col vs. DMMA + Col) **(C)** Transcript levels of inflammatory cytokines such as TNF-α, IL-1β, and IL-6 were measured by qRT-PCR from the paw tissues of the animals. (For TNF-α and IL-6 qRT-PCR, ***; $p < 0.001$, untreatment vs. Veh + Col, **; $p < 0.01$, Veh + Col vs. BMDA + Col, Veh + Col vs. DMMA + Col. For IL-1β qRT-PCR, **; $p < 0.01$, untreatment vs. Veh + Col, *; $p < 0.05$, Veh + Col vs. BMDA + Col, Veh + Col vs. DMMA + Col) **(D)** Expression of anti-oxidation proteins such as HO1 and Nrf2 was examined by immunoblotting and the relative expression of the proteins was analyzed after scanning using AlphaView, version 3.2.2 (Cell Biosciences Inc., Santa Clara, CA, United States). (For HO1 protein, ***; $p < 0.001$, untreatment vs. Veh + Col, **; $p < 0.01$, Veh + Col vs. BMDA + Col, Veh + Col vs. DMMA + Col. For Nrf2 protein, ***; $p < 0.001$, untreatment vs. Veh + Col, **; $p < 0.01$, Veh + Col vs. BMDA + Col, Veh + Col vs. DMMA + Col).
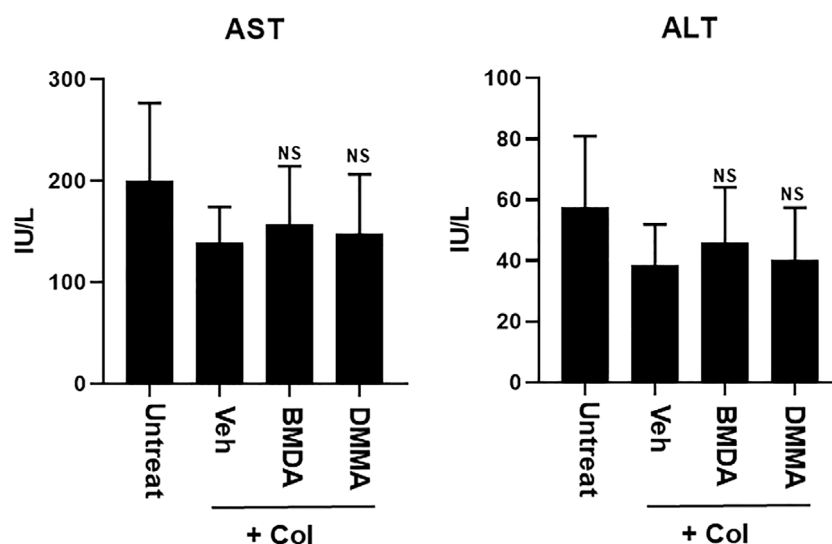
FIGURE 6
Oral treatment with BMDA or DMMA does not affect liver toxicity in the RA-carrying mice. AST and ALT levels were measured in the sera of RA-carrying mice that were orally treated with BMDA, DMMA, or corn oil 21 days post-sensitization of collagen and IFA. NS indicates not significant (ns; Veh + Col vs. BMDA + Col, Veh + Col vs. DMMA + Col).

form or be metabolized during delivery from the mouth to the small intestine and then to the blood circulation, which could be a cause for the low effectiveness on the pathological progression of collagen-induced RA. In a future study, we would explore whether the structure of BMDA or DMMA should be examined in the sera after oral treatment.

Allicin, a key constituent of garlic, decreases LPS-induced oxidative stress and NF-κB activity through the Nrf2 anti-oxidative signaling pathway, leading to the prevention of endothelial cell apoptosis (Pandey et al., 2020). A recent study also reported that allicin treatment increased regulatory T cell populations but decreased the number of Th17 cells in collagen-induced arthritis through the upregulation of MEKK2 expression (Zhang and Gong, 2021). Diallyl trisulfide also reduced arthritis induced by collagen through inhibition of the Wnt and NF-κB signaling pathways (Liang et al., 2019). Similar to allicin and diallyl trisulfide, both BMDA and DMMA diminished NF-κB expression and translocation into the nucleus. Because spleen weight and size were reduced after oral treatment with BMDA or DMMA in collagen-induced DBA/1 mice compared to those in vehicle-treated mice, we might set up the hypothesis that BMDA or DMMA administration suppresses the proliferation of T and B cell populations reacting with RA-relevant autoantigens. A study to determine whether BMDA or DMMA treatment inhibits proliferation and activation of the T17 population, which is known to play a critical role in RA pathogenesis, remains to be undertaken as future work.

Interestingly, allicin and diallyl trisulfide have also shown anticancer activity (Pandey et al., 2020) (Kim et al., 2016). Further investigation has demonstrated that these compounds reduce antioxidant protein levels, such as Nrf2 and HO1, leading to the upregulation of ROS, which eventually results in the induction of apoptosis or autophagy (Zhang and Yang, 2019). These results indicate that the same compounds could induce the upregulation or downregulation of antioxidant protein levels, depending on the experimental setup. Thus, we carefully interpret these results from the viewpoint of garlic compound concentration, treatment time, and cell line type. Additionally, our previous study reported that treatment with a high concentration of BMDA (40 mg kg^{-1} body weight) inhibited the development of tumors in vivo (Kaowinn et al., 2018) compared to the concentration of BMDA (0.4 mg kg^{-1} body weight) in DNBS-induced rat colitis and its concentration (20 mg kg^{-1} body weight) in a collagen-induced RA model. Therefore, further studies are needed to optimize the concentrations of BMDA and DMMA for clinical application in IBD and RA.

Conclusion

Both BMDA and DMMA possess anti-inflammatory properties by downregulating the JNK/p38MAPK-MK2 and NF-κB inflammatory signaling pathways in vitro. In addition, treatment with these compounds reduce severity of inflammation in DNBS-induced rat colitis and collagen-induced RA mouse model. These discoveries propose that BMDA and DMMA could be developed as novel remedial drugs for curing IBD and RA.

Data availability statement

The original contributions presented in the study are included in the article/Supplementary Material, further inquiries can be directed to the corresponding authors.

Ethics statement

The animal study was reviewed and approved by the Pusan National University Animal Care and Use Committee (PNU 2021 3068 for rat colitis and PNU-2021-3014 for RA).

Author contributions

JK, CK, and PB established conditions in vivo, conducted animal experiments, acquired the data, and wrote manuscript. NY, I-RC YC, JK, SJ, BL, H-SY, KL, and JH, conducted and in vitro experiments, acquired and analyzed the data. DS, YoJ, HK, and JP supervised in vitro experiments, interpreted the results, and contributed to the discussion. YuJ, and DH supervised animal experiments, interpreted the results, contributed the discussion, and revised the manuscript. Y-HC organized all experiments, wrote, and revised the manuscripts, with comments from all authors, and provided funding for the study.

Conflict of interest

Author I-RC was employed by Hayoung Meditech Inc.

The remaining authors declare that the research was conducted in the absence of any commercial or financial relationships that could be construed as a potential conflict of interest.

Publisher's note

All claims expressed in this article are solely those of the authors and do not necessarily represent those of their affiliated organizations, or those of the publisher, the editors and the reviewers. Any product that may be evaluated in this article, or claim that may be made by its manufacturer, is not guaranteed or endorsed by the publisher.

Supplementary material

The Supplementary Material for this article can be found online at: https://www.frontiersin.org/articles/10.3389/fphar.2023.1095955/full#supplementary-material

References

Abraham, C., and Cho, J. H. (2009). Inflammatory bowel disease. *N. Engl. J. Med.* 361, 2066–2078. doi:10.1056/NEJMra0804647

Afanasyev, O. I., Kuchuk, E., Usanov, D. L., and Chusov, D. (2019). Reductive amination in the synthesis of pharmaceuticals. *Chem. Rev.* 119, 11857–11911. doi:10.1021/acs.chemrev.9b00383

Demoruelle, M. K., and Deane, K. D. (2012). Treatment strategies in early rheumatoid arthritis and prevention of rheumatoid arthritis. *Curr. Rheumatol. Rep.* 14, 472–480. doi:10.1007/s11926-012-0275-1

Hong, S., Yum, S., Yoo, H. J., Kang, S., Yoon, J. H., Min, D., et al. (2012). Colon-targeted cell-permeable NFκB inhibitory peptide is orally active against experimental colitis. *Mol. Pharm.* 9, 1310–1319. doi:10.1021/mp200591q

Huang, J., Fu, X., Chen, X., Li, Z., Huang, Y., and Liang, C. (2021). Promising therapeutic targets for treatment of rheumatoid arthritis. *Front. Immunol.* 12, 686155. doi:10.3389/fimmu.2021.686155

Hyrich, K. L., Silman, A. J., Watson, K. D., and Symmons, D. P. (2004). Anti-tumour necrosis factor alpha therapy in rheumatoid arthritis: An update on safety. *Ann. Rheum. Dis.* 63, 1538–1543. doi:10.1136/ard.2004.024737

Jeong, J. W., Park, S., Park, C., Chang, Y. C., Moon, D. O., Kim, S. O., et al. (2014). N-benzyl-N-methyldecan-1-amine, a phenylamine derivative isolated from garlic cloves, induces G2/M phase arrest and apoptosis in U937 human leukemia cells. *Oncol. Rep.* 32, 373–381. doi:10.3892/or.2014.3215

Kang, E. J., Kim, H. J., Choi, J. H., Noh, J. R., Kim, J. H., Lee, I. B., et al. (2020). Humulus japonicus extract ameliorates collagen-induced arthritis in mice through regulation of overall articular inflammation. *Int. J. Mol. Med.* 45, 417–428. doi:10.3892/ijmm.2019.4417

Kang, L. J., Kwon, E. S., Lee, K. M., Cho, C., Lee, J. I., Ryu, Y. B., et al. (2018). 3'-Sialyllactose as an inhibitor of p65 phosphorylation ameliorates the progression of experimental rheumatoid arthritis. *Br. J. Pharmacol.* 175, 4295–4309. doi:10.1111/bph.14486

Kaowinn, S., Kaewpiboon, C., Kim, J. E., Lee, M. R., Hwang, D. Y., Choi, Y. W., et al. (2018). N-Benzyl-N-methyl-dodecan-1-amine, a novel compound from garlic, exerts anti-cancer effects on human A549 lung cancer cells overexpressing cancer upregulated gene (CUG)2. *Eur. J. Pharmacol.* 841, 19–27. doi:10.1016/j.ejphar.2018.09.035

Kaowinn, S., Oh, S., Moon, J., Yoo, A. Y., Kang, H. Y., Lee, M. R., et al. (2019). CGK062, a small chemical molecule, inhibits cancer upregulated gene 2-induced oncogenesis through NEK2 and β-catenin. *Int. J. Oncol.* 54, 1295–1305. doi:10.3892/ijo.2019.4724

Kim, S. H., Kaschula, C. H., Priedigkeit, N., Lee, A. V., and Singh, S. V. (2016). Forkhead box Q1 is a novel target of breast cancer stem cell inhibition by diallyl trisulfide. *J. Biol. Chem.* 291, 13495–13508. doi:10.1074/jbc.M116.715219

Kim, W., Kim, S., Ju, S., Lee, H., Jeong, S., Yoo, J. W., et al. (2019). Colon-Targeted delivery facilitates the therapeutic switching of sofalcone, a gastroprotective agent, to an anticolitic drug via Nrf2 activation. *Mol. Pharm.* 16, 4007–4016. doi:10.1021/acs.molpharmaceut.9b00664

Lee, H. H., Jeong, J. W., Hong, S. H., Park, C., Kim, B. W., and Choi, Y. H. (2018). Diallyl trisulfide suppresses the production of lipopolysaccharide-induced inflammatory mediators in BV2 microglia by decreasing the NF-κB pathway activity associated with toll-like receptor 4 and CXCL12/CXCR4 pathway blockade. *J. Cancer Prev.* 23, 134–140. doi:10.15430/JCP.2018.23.3.134

Liang, J. J., Li, H. R., Chen, Y., Zhang, C., Chen, D. G., Liang, Z. C., et al. (2019). Diallyl Trisulfide can induce fibroblast-like synovial apoptosis and has a therapeutic effect on collagen-induced arthritis in mice via blocking NF-κB and Wnt pathways. *Int. Immunopharmacol.* 71, 132–138. doi:10.1016/j.intimp.2019.03.024

Livak, K. J., and Schmittgen, T. D. (2001). Analysis of relative gene expression data using real-time quantitative PCR and the 2(-Delta Delta C(T)) Method. *Methods* 25, 402–408. doi:10.1006/meth.2001.1262

Noss, E. H., and Brenner, M. B. (2008). The role and therapeutic implications of fibroblast-like synoviocytes in inflammation and cartilage erosion in rheumatoid arthritis. *Immunol. Rev.* 223, 252–270. doi:10.1111/j.1600-065X.2008.00648.x

Pandey, N., Tyagi, G., Kaur, P., Pradhan, S., Rajam, M. V., and Srivastava, T. (2020). Allicin overcomes hypoxia mediated cisplatin resistance in lung cancer cells through ROS mediated cell death pathway and by suppressing hypoxia inducible factors. *Cell Physiol. Biochem.* 54, 748–766. doi:10.33594/000000253

Pithadia, A. B., and Jain, S. (2011). Treatment of inflammatory bowel disease (IBD). *Pharmacol. Rep.* 63, 629–642. doi:10.1016/s1734-1140(11)70575-8

Rath, T., Billmeier, U., Ferrazzi, F., Vieth, M., Ekici, A., Neurath, M. F., et al. (2018). Effects of anti-integrin treatment with vedolizumab on immune pathways and cytokines in inflammatory bowel diseases. *Front. Immunol.* 9, 1700. doi:10.3389/fimmu.2018.01700

Smolen, J. S., Landewé, R., Bijlsma, J., Burmester, G., Chatzidionysiou, K., Dougados, M., et al. (2017). EULAR recommendations for the management of rheumatoid arthritis with synthetic and biological disease-modifying antirheumatic drugs: 2016 update. *Ann. Rheum. Dis.* 76, 960–977. doi:10.1136/annrheumdis-2016-210715

Triantafillidis, J. K., Merikas, E., and Georgopoulos, F. (2011). Current and emerging drugs for the treatment of inflammatory bowel disease. *Drug Des. Devel. Ther.* 5, 185–210. doi:10.2147/DDDT.S11290

Uhlig, H. H., and Powrie, F. (2018). Translating Immunology into therapeutic concepts for inflammatory bowel disease. *Annu. Rev. Immunol.* 36, 755–781. doi:10.1146/annurev-immunol-042617-053055

Yang, Y., Kim, W., Kim, D., Jeong, S., Yoo, J. W., and Jung, Y. (2019). A colon-specific prodrug of metoclopramide ameliorates colitis in an experimental rat model. *Drug Des. Devel. Ther.* 13, 231–242. doi:10.2147/dddt.s185257

Zhang, M., Pan, H., Xu, Y., Wang, X., Qiu, Z., and Jiang, L. (2017). Allicin decreases lipopolysaccharide-induced oxidative stress and inflammation in human umbilical vein endothelial cells through suppression of mitochondrial dysfunction and activation of Nrf2. *Cell Physiol. Biochem.* 41, 2255–2267. doi:10.1159/000475640

Zhang, Q., and Yang, D. (2019). Allicin suppresses the migration and invasion in cervical cancer cells mainly by inhibiting NRF2. *Exp. Ther. Med.* 17, 1523–1528. doi:10.3892/etm.2018.7104

Zhang, Y., and Gong, Y. (2021). Allicin regulates Treg/Th17 balance in mice with collagen-induced arthritis by increasing the expression of MEKK2 protein. *Food Sci. Nutr.* 9, 2364–2371. doi:10.1002/fsn3.2034

Zhang, Y., Liu, X., Ruan, J., Zhuang, X., Zhang, X., and Li, Z. (2020). Phytochemicals of garlic: Promising candidates for cancer therapy. *Biomed. Pharmacother.* 123, 109730. doi:10.1016/j.biopha.2019.109730

Natural flavones from edible and medicinal plants exhibit enormous potential to treat ulcerative colitis

Qiang Lu[1], Yuhong Xie[2], Jingbin Luo[3], Qihai Gong[4,5] and Cailan Li[2,4,5]*

[1]Department of Pharmaceutical Sciences, Zhuhai Campus, Zunyi Medical University, Zhuhai, China,
[2]Department of Pharmacology, Zhuhai Campus, Zunyi Medical University, Zhuhai, China, [3]China
Traditional Chinese Medicine Holdings Company Limited, Foshan, China, [4]Key Laboratory of Basic
Pharmacology of Ministry of Education and Joint International Research Laboratory of Ethnomedicine of
Ministry of Education, Zunyi Medical University, Zunyi, China, [5]Key Laboratory of Basic Pharmacology of
Guizhou Province and School of Pharmacy, Zunyi Medical University, Zunyi, China

Ulcerative colitis (UC) is a chronic aspecific gut inflammatory disorder that primarily involves the recta and colons. It mostly presents as a long course of repeated attacks. This disease, characterized by intermittent diarrhoea, fecal blood, stomachache, and tenesmus, severely decreases the living quality of sick persons. UC is difficult to heal, has a high recurrence rate, and is tightly related to the incidence of colon cancer. Although there are a number of drugs available for the suppression of colitis, the conventional therapy possesses certain limitations and severe adverse reactions. Thus, it is extremely required for safe and effective medicines for colitis, and naturally derived flavones exhibited huge prospects. This study focused on the advancement of naturally derived flavones from edible and pharmaceutical plants for treating colitis. The underlying mechanisms of natural-derived flavones in treating UC were closely linked to the regulation of enteric barrier function, immune-inflammatory responses, oxidative stress, gut microflora, and SCFAs production. The prominent effects and safety of natural-derived flavones make them promising candidate drugs for colitis treatment.

Introduction

Ulcerative colitis (UC) is a major type of inflammatory bowel disease, which has been widely prevalent all over the world (Alsoud et al., 2021). Traditionally, UC is considered to be a common Western disorder (Ge et al., 2021). It was announced that the yearly morbidity of colitis in European countries is as high as 0.0243%, and that in Northern America is up to 0.0192% (Du and Ha, 2020). By comparison, the annual morbidity of UC in Asian nationalities is fairly lower, at less than 0.01% (Wei et al., 2021). Whereas, in recent years, due to the changes in life and environment, the annual incidence rate of UC among Asian nationalities has been rising steadily over time (Hirten and Sands, 2021; Zeng et al., 2022). Consequently, this disease brought great pressure to the financial and medical services of all countries.

UC is a chronic nonspecific inflammatory disorder of the colon and rectum with uncertain aetiology (Sinopoulou et al., 2021). The lesion is confined to the mucosal and

submucosal layers of intestinum crassum. Furthermore, the majority of lesions are found in the rectum and sigmoid colon, but they can also extend to the descending colon or the whole colon (Li et al., 2022). UC has a long course and often occurs repeatedly. Moreover, this disease occurs at any age, although it most frequently strikes people between the ages of 20 and 40 (Li C. L. et al., 2021). Although the aetiology of UC is uncertain, it is generally accepted that genes are an important cause of colitis. Psychological factors play an important role in the deterioration of UC. Following colectomy, the original morbid spirit, such as depression or social isolation, is obviously improved. In addition, it is also recognized that colitis is an autoimmune disease (Fiorino et al., 2021).

To date, there are still no satisfactory clinical drugs for colitis in terms of efficacy and safety. Nowadays, the drugs for colitis primarily consist of 5-amino salicylic acids, glucocorticoids and immunosuppressors, which lack specificity and are difficult to cure UC, accompanied by some adverse reactions, such as high recurrence, elevated resistance, etc. In this case, natural flavones raised extensive concerns as their no/low toxicity and excellent anti-inflammatory, antioxidative, antineoplastic, antibacterial, and immune-regulative activities in the prophylaxis and therapy of gastrointestinal diseases, tumors, and cardiovascular problems (Juca et al., 2020; Jeong et al., 2022). Numerous studies have testified that many kinds of flavones (Figure 1) from edible and medicinal plants possessed excellent therapeutic effects and safety in UC by multiple mechanisms involving ameliorating oxidative damage, reducing the inflammatory responses, preserving enteric barrier function, and adjusting gut flora structure, indicating that natural-derived flavones have the potentiality to suppress the progression of UC and put off the clinical course of this disease. Therefore, in this review, our team summarized the acting mechanisms of natural-derived flavones inhibiting colitis, such as apigenin, baicalein, diosmetin, sinensetin, wogonin, etc. These would provide new perspectives to develop effective medications for the management of colitis.

Methods

For the sake of identifying the research connected with the therapeutic role and acting mechanism of natural flavones treating UC, our team conducted an extensive search of relevant articles in several databases, including Web of Science, PubMed, Elsevier, Google Scholar, and CNKI, covering the period from their inception until May 2023. We employed a combination of the following keywords during the literature retrieval: ("flavone" OR "flavonoid") AND ("colitis" OR "colonitis" OR "UC"). All papers providing abstract will be considered.

After the search, the retrieved studies underwent a rigorous screened. Initially, studies on the therapeutic role and mechanisms of natural flavones treating UC were screened on the basis of titles and abstracts. For studies that were not able to be conclusively identified during the initial screening, their full-text versions were further evaluated. At last, all relevant studies including cell experiments, animal experiments and clinical trials were gathered and imported into EndNote software as support resources for the present review.

Natural flavones against ulcerative colitis

The amount of identified flavonoids has risen to four thousand since the discovery of the first type of flavonoid vitamin P (namely, rutin), the amount of identified flavonoids has been up to four thousand. Of which, some possess powerful pharmacologic action and exhibit great potential in the exploitation of new medicines and their clinic practice. Based on the fundamental structure, currently known flavonoids are separated into seventeen classes, and flavones are the most important class and have received extensive attention. Therefore, the present review focused on natural-derived
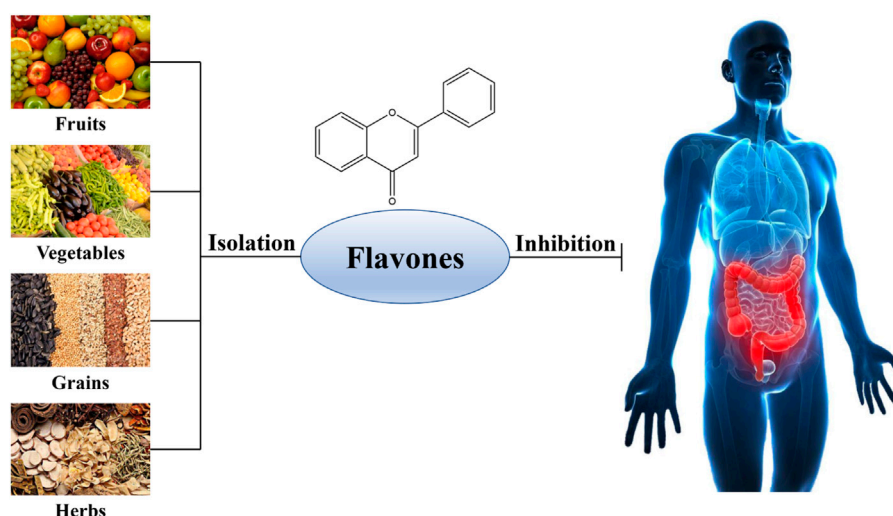
FIGURE 1
Natural sources of flavones against ulcerative colitis.

TABLE 1 Natural flavones separated from edible and medicinal plants.

No.	Flavones	Molecular formula	Molecular weight (g/mol)	Potential side effects	Main sources	References
1	Acacetin	$C_{16}H_{12}O_5$	284.26	Cytochrome P450 inhibition	*Acacia farnesiana; Robinia pseudoacacia; Saussurea involucrata; Turnera diffusa*	Ren et al. (2021); Zhou et al. (2020)
2	Apigenin	$C_{15}H_{10}O_5$	270.24	No	*Apium graveolens; Matiricaria recutita; Melissa axillaris*	Marquez-Flores et al. (2016)
3	Baicalein	$C_{15}H_{10}O_5$	270.24	No	*Scutellaria baicalensis; Oroxylum indicum; Plantago major*	Li et al. (2021g); Liu et al. (2020a); Luo et al. (2017); Yao et al. (2020); Zhong et al. (2019)
4	Baicalin	$C_{21}H_{18}O_{11}$	446.36	No	*Scutellaria baicalensis; Oroxylum indicum; Plantago major*	Shen et al. (2019); Zhang et al. (2017); Zhu et al. (2020a); Zhu et al. (2020b)
5	Chrysin	$C_{15}H_{10}O_4$	254.24	No	*Oroxylum indicum; Passiflora caerulea*	Dou et al. (2013); Garg and Chaturvedi (2022)
6	Diosmetin	$C_{16}H_{12}O_6$	300.26	No	*Citrus limon; Citrus medica; Mentha spicata; Mentha canadensis*	Li et al. (2021d); Yu and Liu (2021)
7	Diosmin	$C_{28}H_{32}O_{15}$	608.54	Mild nervous disorder	*Citrus limon; Citrus medica; Mentha spicata; Mentha canadensis*	Gerges et al. (2022); Shalkami et al. (2018)
8	Eupatilin	$C_{18}H_{16}O_7$	344.32	No	*Artemisia argyi; Artemisia asiatica; Artemisia princeps*	Sapkota et al. (2017); Zhou et al. (2018)
9	Fortunellin	$C_{28}H_{32}O_{14}$	592.55	Not clear	*Citrus japonica*	Xiong et al. (2018)
10	Licoflavone B	$C_{25}H_{26}O_4$	390.47	Not clear	*Glycyrrhiza uralensis; Glycyrrhiza inflata; Glycyrrhiza glabra*	Zhang et al. (2022)
11	Linarin	$C_{28}H_{32}O_{14}$	592.55	No	*Buddleja officinalis; Mentha arvensis; Mentha haplocalyx; Chrysanthemum indicum*	Jin et al. (2022); Mottaghipisheh et al. (2021)
12	Lonicerin	$C_{27}H_{30}O_{15}$	594.52	Not clear	*Lonicera japonica*	Lv et al. (2021)
13	Luteolin	$C_{15}H_{10}O_6$	286.24	No	*Lonicera japonica; Chrysanthemum indicum; Perilla frutescens*	Li et al. (2016); Li et al. (2021a); Li et al. (2021b); Suga et al. (2021); Vukelic et al. (2020); Zuo et al. (2021)
14	Nobiletin	$C_{21}H_{22}O_8$	402.39	No	*Citrus sinensis; Citrus paradise; Citrus aurantum*	Hagenlocher et al. (2019); Xiong et al. (2015)
15	Oroxylin A	$C_{16}H_{12}O_5$	284.26	No	*Oroxylum indicum; Scutellaria baicalensis; Scutellaria rehderiana*	Sajeev et al. (2022a); Zhou et al. (2017)
16	Pectolinarigenin	$C_{17}H_{14}O_6$	314.29	No	*Cirsium chanroenicum; Cirsium setidens; Cirsium japonicum*	Cheriet et al. (2020); Feng et al. (2022)
17	Sinensetin	$C_{20}H_{20}O_7$	372.37	No	*Citrus sinensis; Citrus reticulata; Citrus aurantium*	Jie et al. (2021); Xiong et al. (2019)
18	Tangeretin	$C_{20}H_{20}O_7$	372.37	No	*Citrus unshiu; Citrus reticulata; Citrus depressa*	Chen et al. (2021a); Eun et al. (2017)
19	Tricin	$C_{17}H_{14}O_7$	330.29	No	*Medicago sativa; Triticum aestivum; Hordeum vulgare*	Li et al. (2021f); Shalini et al. (2016)
20	Wogonin	$C_{16}H_{12}O_5$	284.26	Weak developmental toxicities and genotoxicities	*Scutellaria baicalensis*	Zhao et al. (2011); Zhou et al. (2022)
21	Wogonoside	$C_{22}H_{20}O_{11}$	460.4	No	*Scutellaria baicalensis*	Huang et al. (2020); Liu et al. (2020b); Sun et al. (2015)

flavones for the treatment of UC. The general information of the included flavones is given in Table 1, while the chemical structures are presented in Figure 2. Additionally, Table 2 provides the pharmacological information of these flavones.
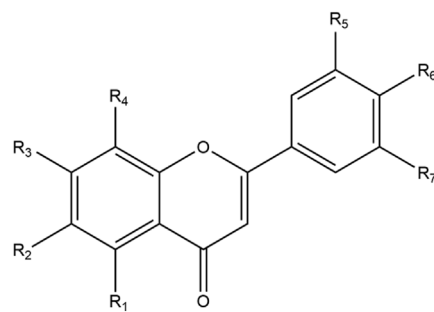
	R1	R2	R3	R4	R5	R6	R7
1	OH	H	OH	H	H	OCH₃	H
2	OH	H	OH	H	H	OH	H
3	OH	OH	OH	H	H	H	H
4	OH	OH	OGlcA	H	H	H	H
5	OH	H	OH	H	H	H	H
6	OH	H	OH	H	H	OCH₃	OH
7	OH	H	OGlc(6→1)Rha	H	H	OCH₃	OH
8	OH	OCH₃	OH	H	H	OCH₃	OCH₃
9	OH	H	OGlc(2→1)Rha	H	H	OCH₃	H
10	H	CH₂CH = C(CH₃)₂	OH	H	H	OH	CH₂CH = C(CH₃)₂
11	OH	H	ORha(1→6)Glc	H	H	OCH₃	H
12	OH	H	OGlc(2→1)Rha	H	OH	OH	H
13	OH	H	OH	H	H	OH	OH
14	OCH₃	OCH₃	OCH₃	OCH₃	H	OCH₃	OCH₃
15	OH	OCH₃	OH	H	H	H	H
16	OH	OCH₃	OH	H	H	OCH₃	H
17	OCH₃	OCH₃	OCH₃	H	H	OCH₃	OCH₃
18	OCH₃	OCH₃	OCH₃	OCH₃	H	OCH₃	H
19	OH	H	OH	H	OCH₃	OH	OCH₃
20	OH	H	OH	OCH₃	H	H	H
21	OH	H	OGlcA	OCH₃	H	H	H

FIGURE 2
Chemical structures of naturally derived flavones for the treatment of ulcerative colitis.

Acacetin is a natural product discovered in many plants, including *Acacia farnesiana*, *Saussurea involucrata*, and *Turnera diffusa* (Wu et al., 2018). Researchers reported that acacetin possesses multiple pharmacologic functions covering anti-cancer, anti-inflammation, anti-obesity, cardioprotection, and neuroprotection (Singh et al., 2020). Ren et al. (2021) probed whether acacetin could improve UC in mice induced by DSS. Results showed that acacetin alleviated the clinic signs of DSS-treated UC, as determined by weight reduction, diarrhoea, colonic shortening, inflammatory infiltration, and histologic damage. Acacetin was found to suppress the *in vitro* inflammatory response of macrophages as well as the production of inflammation mediators in UC murine models. Moreover, a few characters of the intestinal microflora were disordered in DSS-treated UC mice, as manifested by a prominent decrease in microflora richness and a remarkable

TABLE 2 Molecular mechanisms of naturally derived flavones against ulcerative colitis.

Name	Model	Effective dosage	Route of administration	Mechanism of action	References
Acacetin	DSS elicited UC in C57BL/6 mice	50, 150 mg/kg	Oral gavage	Up: *Firmicutes*; *Turicibacter* Down: TNF-α; IL-6; IL-1β; COX-2; iNOS; *Bacteroidaceae*; *Deferribacteres*; *Deferribacteraceae*; *Enterobacteriaceae*; *Escherichia-Shigella*; *Faecalibaculum*; *Proteobacteria*	Ren et al. (2021)
Apigenin	TNBS or DSS induced UC in Wistar rats or C57BL/6 mice	1, 3 and 10 mg/kg	Dietary administration	Down: MMP-3; TNF-α; IL-6; IL-1β; IL-18; COX-2; mPGES; iNOS; NALP3; Cl-caspase-1; pro-caspase-11; Cl-caspase-11	Marquez-Flores et al. (2016)
Baicalein	TNBS or DSS evoked UC in Balb/c mice or ICR mice or C57BL/6 mice LPS stimulated THP-1 cells and RAW264.7 cells	10, 20, 40 mg/kg *in vivo* 10, 25, 50 μM *in vitro*	Oral administration (*in vivo*)	Up: ZO-1; occludin; IκBα; CYP1A1; CD4$^+$ CD25$^+$ Foxp3$^+$ T cells; IL-10; IL-22; TGF-β; AhR (nuclear); RORγt$^+$ IL-22 ILC3 Down: MPO; NO; iNOS; COX-2; ICAM-1; MCP-1; TNF-α; IL-1α; IL-1β; IL-6; IL-17; IL-17A; TLR4; MyD88; p-IκBα; p65; p-p65; p-p38; p-IRAK-1; p-JNK; p-ERK; NLRP3; ASC; caspase-1; MD-2/TLR4; Cyclin D1; STAT3; p-STAT3; IKKβ; CD11b$^+$ cells; NOD2; SphK1; S1PR1; CD4$^+$ IL-17$^+$ T cells; AhR (cytosol)	Li et al. (2021g); Liu et al. (2020a); Luo et al. (2017); Yao et al. (2020); Zhong et al. (2019)
Baicalin	TNBS or DSS induced UC in SD rats or C57BL/6 mice LPS stimulated RAW264.7 cells or HT-29 cells	25, 50, 100, 120, 150 mg/kg *in vivo* 5, 10, 20, 40 μM, 100 ng/mL *in vitro*	Oral gavage (*in vivo*)	Up: ZO-1; occludin; SOD; CAT; GSH; GSH-Px; IκB-α; IL-10; Bcl-2; FOXP3; β-catenin; CD4$^+$CD25$^+$ Foxp3$^+$ cells; *Firmicutes*; *Bacteroidaceae*; *Christensenellaceae*; *Peptosreptococcaceae*; *Ruminococcaceae*; *Clostridiales*; acitric acid; butyric acid; propionic acid; *Butyricimonas* spp.; *Roseburia* spp., *Subdoligranulum* spp.; *Eubacteriu* spp. Down: MPO; NO; TNF-α; IL-1β; IL-6; IL-17; IL-33; p65; p-p65; p-IκBα; MDA; PGE$_2$; caspase-3; caspase-9; Bax; Bcl-2/Bax; Cyt-c; p-IKKβ/IKKβ; p-IKBα/IKBα; RORγt; CD4$^+$ IL17$^+$ cells; Th17/Treg; p-PI3K/PI3K; p-AKT/AKT; Fas; FasL; *Proteobacteria*; *Actinobacteria*	Shen et al. (2019); Zhang et al. (2017); Zhu et al. (2020a); Zhu et al. (2020b)
Chrysin	DSS evoked UC in C57BL/6 mice	25 mg/kg	Oral gavage	Up: IκBα; Cyp3a11; MDR1 Down: p-p65; p-IκBα; iNOS; COX-2; ICAM-1; TNF-α; MCP-1; IL-6; MPO	Dou et al. (2013)
Diosmetin	TNBS evoked UC in Wistar rats DSS evoked UC in C57BL/6 mice LPS stimulated Caco-2 and IEC-6 cells	25, 50, 100, and 200 mg/kg *in vivo* 25, 50, and 100 μM *in vitro*	Oral gavage (*in vivo*)	Up: ZO-1; occludin; claudin-1; TEER; SOD; CAT; GSH-Px; GSH; circ-Sirt1; Sirt1; total Nrf2; nuclear Nrf2; HO-1; *Bacteroidetes*; *Cyanobacteria*; *Odoribacteraceae*; *Prevotella*; *Rikenellaceae*; *Ruminococcus*; *Coprococcus*; *Roseburia*; *Oscillospira*, *Anaeroplasma*; *Synergistales* Down: MDA; TNF-α; IL-1β; IL-6; IFN-γ; NF-κB; acetyl-NF-κB; apoptotic index; COX-2; *Firmicutes*; *Eggerthella*; *Flavobacterium*; *Clostridium*	Li et al. (2021d); Yu and Liu (2021)
Diosmin	TNBS induced UC in Wistar rats AA induced UC in Swiss albino rats	5, 10, 25, and 50 mg/kg	Oral administration	Up: GSH Down: TNF-α; COX-2; MPO; MDA; caspase-3	Shalkami et al. (2018)
Eupatilin	DSS evoked UC in C57BL/6 mice	10, 20 mg/kg *in vivo*	Oral administration (*in vivo*)	Up: ZO-1; occludin; IκB; p-AMPK/AMPK	Zhou et al. (2018)

(Continued on following page)

TABLE 2 (*Continued*) Molecular mechanisms of naturally derived flavones against ulcerative colitis.

Name	Model	Effective dosage	Route of administration	Mechanism of action	References
	LPS induced THP-M macrophage TNF-α damaged NCM460 cells	5 and 10 μM *in vitro*		Down: TNF-α; IL-1β; MPO; ROS; NOX4; p-ERK/ERK; p-pJNK/pJNK; p-p38/p38; p-p65/p65	
Fortunellin	TNBS elicited UC in SD rats	20 and 80 mg/kg	Gavage administration	Up: SOD; GSH; Bcl-2; p-Akt; miR-374a; TEER	Xiong et al. (2018)
				Down: IL-6; TNF-α; IL-1β; MPO; MDA; ROS; PTEN; Cl-caspase-3; Bax; p-GSK-3β	
Licoflavone B	DSS elicited UC in C57BL/6 mice	40, 80 and 120 mg/kg	Oral administration	Up: ZO-1; occludin; claudin-1; IL-10; *Bacteroidetes*; *Lactobacillus*; *Ileibacterium*; *Enterobacter*; *Vibrionaceae*; *Faecalibacterium*; *Tannerellaceae*; *Adlercreutzia*; *Ahniella*; *WX65*; *Faecalibaculum*; *Rhodanobacteraceae*; *Streptococcus*; *Micromonospora*; *Bacteroides*; *Eubacterium_coprostanoligenes*; *Parabacteroides*	Zhang et al. (2022)
				Down: IL-4; IL-6; TNF-α; IL-1β; p-ERK; p-p38; p-JNK; p-ERK/ERK; *Firmicutes*; *Firmicutes/Bacteroidetes*; *Enterococcus*; *Alloprevotella*; *Eubacterium_ruminantium_group*	
Linarin	DSS evoked UC in C57BL/6J mice	25 and 50 mg/kg	Oral gavage	Up: mucin 2; ZO-1; occludin; claudin-1; IL-10; acetic acid; butyric acid; propionic acid; isobutyric acid; isovaleric acid; valeric acid	Jin et al. (2022)
				Down: MPO; IL-6; IFN-γ; TNF-α; IL-1β	
Lonicerin	DSS evoked UC in C57BL/6 mice	3, 10, and 30 mg/kg *in vivo*	Oral administration (*in vivo*)	Up: ATG5; NF-κB p65 (cytosol); LC3B-I/II	Lv et al. (2021)
	LPS stimulated THP-1 or BMDMs cells	1, 3, 10, and 30 μM *in vitro*		Down: MPO; F4/80+ macrophages; Cl-caspase-1; IL-1β; IL-18; IL-6; TNF; IL-1; NLRP3; EZH2; NF-κB p65 (nuclear); p-p65; p62	
Luteolin	DSS elicited UC in C57BL/6 mice or Wistar rat	5, 10, 20, 50 and 100 mg/kg *in vivo*	Oral administration (*in vivo*)	Up: ZO-1; occludin; claudin 1; TEER; SOD; CAT; Nrf2; HO-1; NQO1; p-ERK1/2; proliferating cells/crypt; SHP-1; PPAR-γ; *Bacteroidetes*; *Bacteroidaceae*; *Lactobacillus*; *Lachnospiraceae_NK4A136_group*; *Roseburia*; *Bacteroides*; *Butyricicoccus*; arginine metabolism; proline metabolism; starch metabolism; sucrose metabolism	Li et al. (2016); Li et al. (2021a); Li et al. (2021b); Suga et al. (2021); Vukelic et al. (2020); Zuo et al. (2021)
	TNF-α, and IFN-γ stimulated Caco-2 cells 5-HT stimulated RBL-2H3 cells	25, 50, 100, and 150 μM *in vitro*		Down: MDA; TNF-α; IL-1β; IL-6; p-JNK1/2; p-p38; p-Akt; p-STAT3; NF-κB p65; TNF-α; COX-2; Cl-caspase-3; caspase-9; Cl-caspase-9; cleaved PARP; p21; LC3B-II; Atg5; HMGB1; TLR4; MyD88; p-p65/p65; TPH-1; 5-HT; CLDN2; p-STAT3; STAT3; IL-17; IL-23; *Firmicutes*; *Proteobacteria*; *Prevotella_9*; the ability of DNA repair; ribosome metabolism; purine metabolism	
Nobiletin	TNBS elicited UC in SD rats	20, 40 and 50 mg/kg *in vivo* 10, 20, 40 and 80 μM *in vitro*	Oral administration (*in vivo*)	Down: TEER; MPO; mast cells; TNF-α; IL-1β; IL-6; NO; PGE₂; iNOS; COX-2; MLCK; p65; PI3K; p-Akt; CCL2; COL13A1	Hagenlocher et al. (2019); Xiong et al. (2015)
	IL-10−/− BALB/c mice				
	LPS stimulated Caco-2 cells				
	LPS stimulated human intestinal fibroblasts				

(Continued on following page)

TABLE 2 (*Continued*) Molecular mechanisms of naturally derived flavones against ulcerative colitis.

Name	Model	Effective dosage	Route of administration	Mechanism of action	References
Oroxylin A	DSS evoked UC in C57BL/6 mice LPS combined ATP stimulated THP-Ms or BMDMs cells	100 and 200 mg/kg *in vivo* 25, 50 and 100 μM *in vitro*	Dietary administration (*in vivo*)	Up: p65 (cytoplasm), IκBα Down: MPO; iNOS; TNF-α; IL-6; IL-1β; NLRP3; F4/80; p65; p-IκBα; Cl-IL-1β; Cl-caspase-1; ASC speck formation	Zhou et al. (2017)
Pectolinarigenin	DSS elicited UC in C57BL/6J mice LPS stimulated RAW 264.7 and THP1 cell lines	2.5, 5 and 10 mg/kg *in vivo* 10 and 20 μM *in vitro*	Oral administration (*in vivo*)	Up: Nrf2; IκBα; SOD; CAT; GSH; mucin 2 Down: NF-κB p-p65; p-IκBα; COX-2; iNOS; IL-6; IL-1β; TNF-α; MPO; MDA	Feng et al. (2022)
Sinensetin	TNBS evoked UC in SD rats TNF-α stimulated Caco-2 cells	20 and 80 mg/kg *in vivo* 20 and 40 μM *in vitro*	Oral gavage (*in vivo*)	Up: TEER; LC3ll/l; p-ULK1; AMPK; p-AMPK Down: IL-1β; IL-6; IFN-γ; MPO; p62; claudin-2; Cl-capsase-3; Cl-capsase-9	Xiong et al. (2019)
Tangeretin	TNBS evoked UC in C57BL/6 mice LPS stimulated DCs	10 or 20 mg/kg *in vivo* 5, 10, and 20 μM *in vitro*	Oral administration (*in vivo*)	Up: ZO-1; occludin; claudin-1; IL-10; Foxp3; Tregs differentiation; *Firmicutes*; *Lachnospiraceae*; *Lactobacillaceae*; valeric; acetic acids; butyric acids Down: TNF-α; IL-1β; IL-12; IL-17; IL-23; IL-12/IL-10; TNF-α/IL-10; IFN-γ; iNOS; COX-2; MPO; differentiation of Th1 and Th17 cells; MHC ll; CD40; CD80; CD86; p-p65; T-bet; RORγt; p-TAK1; p-IκBα; p-IRAK1; p-IKK-α/β; p-p38; p-ERK; p-JNK; *Bacteroidetes*; *Rikenellaceae*; *Marinifilaceae*; *Enterobacteriaceae*; *Rikenellaceae_RC9_gut_group*; *Alistipes*	Chen et al. (2021a); Eun et al. (2017)
Tricin	DSS evoked UC in BALB/c mice LPS stimulated RAW264.7 cells	75, 100 and 150 mg/kg *in vivo* 12.5, 25 and 50, μM *in vitro*	Oral gavage (*in vivo*)	Up: *Bacteroidetes* Down: Nitrite; TNF-α; IL-1β; IL-6; MIP-2; MPO; MDSC; Treg cells; p-p65; *Firmicutes*; *Proteobacteria*; *Deferribacteres*; *Helicobacter*; *Ruminiclostridium_5*; *Streptococcus*; *Veillonella*; *Mucispirillum*; *Klebsiella*; *Haemophilus*	Li et al. (2021f)
Wogonin	DSS induced UC in BALB/c mice	30 mg/kg	Oral gavage	Up: SOD; GST; GSH; IL-10; Bax; caspas-3; caspas-9; Nrf2; HO-1 Down: MPO; NO; TBARS; TNF-α; IL-6; PGE_2; Bcl-2; COX-2; iNOS; TLR4; p-p65	Zhou et al. (2022)
Wogonoside	DSS evoked UC in Balb/C or C57BL/6 mice LPS stimulated THP-1 cells TNF-α stimulated Caco-2 cells	12.5, 25 and 50 mg/kg *in vivo* 12.5, 25 and 50 μM *in vitro*	Oral gavage (*in vivo*)	Up: ZO-1; occludin; claudin1; TEER; NF-κB (cytoplasm); TXNIP Down: MPO; iNOS; TNF-α; IL-1β; IL-6; IL-13; IL-18; IFN-γ; MIP-1α; NF-κB (nucleus); p-IκBα; p-p65; Cl-caspase-1; pro-caspase-1; Cl-caspase-1/pro-caspase-1; Cl-IL-1β; NLRP3; ASC; CD11b⁺F4/80⁺ monocyte/macrophages; CD11b⁺Gr-1⁺ neutrophils; F4/80⁺ cells; pMLC2/MLC2; MLCK	Huang et al. (2020); Liu et al. (2020b); Sun et al. (2015)

alteration in bacteria profiles. Whereas, acacetin administration inhibited this unbalance and recovered intestine microflora to levels consistent with normal group. Collectively, the results manifested that acacetin could mitigate DSS-treated UC in mice, at least in part, by suppressing inflammation and modulating the gut microflora.

Apigenin is a usual dietary flavone which is broadly existent in some fruits, vegetables and pharmaceutical plants. It has various bioactivities involving anti-cancer, anti-oxidation, anti-inflammation, anti-bacteria, and anti-virus (Ginwala et al., 2019; Salehi et al., 2019). Marquez-Flores et al. (2016) elucidated the protective effect and mechanism of dietary apigenin enrichment in DSS-evoked colitis murine models. Apigenin supplementation reduced the macroscopic symptoms and histopathological injury of UC, according to the findings. Moreover, it reduced the expression of mPGES, COX-2 and iNOS in colon tissues and

decreased the serum MMP-3 level. Likewise, apigenin diet decreased TNF-α and IL-1β secretion in LPS-activated splenocytes. In addition, apigenin's anti-inflammatory effect was linked to the suppression of both canonical and non-canonical NLRP3 inflammasome paths via modulating cleaved caspase-1 and caspase-11 enzymes to reduce IL-1β and IL-18 expressions. In conclusion, an apigenin supplement may offer a basis for formulating a novel dietary method for preventing and treating UC.

Baicalein, a main active constituent in the roots of *Scutellaria baicalensis*, was testified to possess multifarious effects involving anti-cancer, anti-inflammation, anti-oxidation, anti-hepatotoxicity, as well as neuroprotection (Dinda et al., 2017; Song et al., 2021). Luo et al. (2017) probed the function and mechanism of baicalein against UC in TNBS-evoked UC model. Experimental results revealed that baicalein relieved the seriousness of TNBS-treated UC in mice through reducing MPO activity and pro-infammatory factors expression. The downregulation of NF-κB and p38 MAPK was related to the reduced expression of TLR4 and its adaptor MyD88 in mucosa. *In vitro*, baicalein suppressed the TLR4/MyD88 signal cascades (NF-κB and MAPKs) in LPS-activated macrophages. Besides, baicalein could bind to the hydrophobic domain of the MD-2 pocket and restrain the formation of LPS-evoked MD-2/TLR4 complex. Moreover, baicalein decreased NLRP3 infammasome excitation and downriver IL-1β expression in a dosage-dependent mode. Therefore, these results indicated that baicalein might ameliorate TNBS-treated UC by the suppression of TLR4/MyD88 signal cascade and desactivation of NLRP3 infammasome. Zhong et al. (2019) found that the protection of baicalein on UC was correlated with inhibiting NF-κB and STAT3 signal pathways. Yao et al. (2020) discovered that baicalein administration alleviated UC in mice via suppressing S1P-STAT3 signal pathway. In the experiment of Liu C. et al. (2020), they proved that baicalein could prevent DSS-evoked UC, and the therapeutical mechanism may be relevant with the modulation of Th17/Treg differentiation by AhR excitation. In another research, Li Y. Y. et al. (2021) demonstrated that baicalein ameliorated UC through improving the enteric epithelia barrier by AhR/IL-22 pathway in ILC3s. Taken together, baicalein may be beneficial in the therapy of UC.

Baicalin is a biologically active flavone glycoside separated from the dry roots of *S. baicalensis* and possesses diversified effects covering anti-virus, anti-inflammation, anti-bacteria, hepatoprotection, and cardioprotection (Guo et al., 2019; Jin et al., 2019). The role and mechanism of baicalin in the treatment of colitis was investigated by Zhu et al. (2020a). Experimental data showed that baicalin observably alleviated TNBS-elicited UC through decreasing the levels of pro-inflammatory factor (TNF-α, IL-6 and IL-1β), elevating the content of anti-inflammatory mediator IL-10, and enhancing the expression of TJ proteins ZO-1 and β-catenin, which may be attained by blocking the PI3K/AKT signal path. Furthermore, baicalin obviously restrained the disequilibrium between pro- and anti-inflammatory cytokines and markedly reduced apoptosis through blocking the PI3K/AKT signal path in LPS-treated HT-29 cells, which was consistently in line with the *in vivo* finding. Therefore, these results illustrated that baicalin could treat colitis by the inhibition of PI3K/AKT signal pathway. Zhu et al. (2020b) further found that baicalin probably protected mice against UC via

maintaining Th17/Treg balance and modulating both gut microflora and SCFAs. Among the research from Zhang et al. (2017), they proved that baicalin could attenuate DSS-evoked UC via restraining IL-33 expression and NF-κB excitation. Shen et al. (2019) also discovered that baicalin exerted a regulatory role on the IKK/IKB/NF-κB signal cascade and apoptosis-associated proteins in murine models of colitis. Collectively, baicalin might be a perspective therapy candidate for colitis.

Chrysin, a natural flavone in many plants, including *Oroxylum indicum* and *Passiflora caerulea*. Studies proved that chrysin has anticancerous, antidiabetic, antidepressive, immunoregulatory, and neuroprotective activities (Kasala et al., 2015; Garg and Chaturvedi, 2022). Dou et al. (2013) evaluated the efficacy of chrysin as a putative murine PXR activator in suppressing UC. Chrysin administration alleviated inflammatory signs in DSS or TNBS induced murine models and caused a decrease in NF-κB target genes (e.g., iNOS, COX-2, ICAM-1, and MCP-1) in the colonic tissues. Chrysin restrained the phosphorylation/degradation of IκBα, resulting in lower colonic of MPO, TNF-α and IL-6 levels. Consistent with the *in vivo* findings, chrysin prevented LPS-activated migration of NF-κB p65 into the nucleus of RAW264.7 cells. Moreover, chrysin dosage-dependently stimulated human/murinse PXR in reporter gene experiments and up-modulated xenobiotic detoxification genes in the colonic mucosa, but not in the liver. RNA interference-mediated silencing of PXR demonstrated the crucial role that PXR plays in chrysin's induction of xenobiotic detoxification genes and excitation of NF-κB. *In vitro* PXR transduction experiments confirmed that chrysin suppresses NF-κB transcriptional activity. The results suggested that chrysin's role in UC inhibition is primarily mediated by the PXR/NF-κB pathway. In conclusion, chrysin has the potential to be developed as gut-specific PXR agonists.

Diosmetin, a flavone commonly found in citrus plants, exhibits a wide range of effects covering anti-inflammation, anti-tumor, anti-apoptosis, and anti-bacteria (Zhang et al., 2012; Patel et al., 2013). A study conducted by Yu and Liu (2021) investigated the mechanism and efficacy of diosmetin in treating UC using TNBS-induced colitis rats as a model. Experimental results exhibited that diosmetin notably reduced colon anabrosis and inflammatory symptoms in the colon mucosa. TNBS-induced decrease of SOD and CAT was observably inhibited, but MDA content in the colon tissues was reduced. After diosmetin administration, the concentrations of TNF-α, IL-6 and NF-κB and the quantity of apoptotic cells were markedly decreased. In another research, Li H. L. et al. (2021) investigated the function and mechanism of diosmetin against UC in DSS-evoked UC mice. Results demonstrated that diosmetin exerted therapeutical roles in DSS-treated UC by several paths, involving the decrease of proinflammatory cytokines and oxidant stress, the elevated expression of TJ proteins (ZO-1, claudin-1 and occludin), and the regulation of intestinal microflora. The circ-Sirt1/Sirt1 axis partially mediates the therapeutic effects of diosmetin on UC. However, further studies are needed to determine whether diosmetin modulates the composition of intestinal microflora through the Sirt1 pathway. Therefore, diosmetin could be effectively adopted to prevent and treat UC.

Diosmin is a dietary flavone glycoside abundantly existed in citrus plants. Numerous studies have proven that diosmin possesses anti-inflammatory, antioxidative, anticancerous, hepatoprotective, neuroprotective, and renoprotective effects (Zheng et al., 2020;

Gerges et al., 2022). Shalkami et al. (2018) investigated the efficacy of diosmin on colitis. Evidences manifested that acetic acid led to a rise of DAI and colonic injury index scores. The indexes of inflammation (MPO, TNF-α and COX-2) and oxidant stress (MDA and decreased GSH) were notably increased. These variations were related to raise in colonic caspase-3 expression. Diosmin treatment dosage-dependently decreased the DAI and colonic injury index scores. Moreover, diosmin caused a prominent decline of inflammatory and oxidant stress markers in addition to decreasing caspase-3 level. Collectively, diosmin treatment reduced colitis progression, deciding by its capacity to suppress inflammation, oxidant stress, and apoptosis in the colons of rats.

Eupatilin is a natural flavone mainly existed in Artemisia plants, such as *Artemisia argyi*, *Artemisia asiatica* and *Artemisia princeps* (Nageen et al., 2020). Numerous studies indicated that eupatilin possesses multiple bioactivities ranging from anti-ulcer, anti-inflammation, and anti-cancer (Cho et al., 2011; Sapkota et al., 2017). Zhou et al. (2018) investigated the activity of eupatilin against UC and illustrated the mechanism. Experimental results elucidated that eupatilin significantly mitigated inflammatory reactions in LPS-provoked macrophages. Eupatilin notably safeguarded colon epithelia through reducing over expression of TJs and NOX4, and improving AMPK excitation in TNF-α excited NCM460 cells. Moreover, *in vivo* research proved that eupatilin therapy markedly alleviated the symptoms and pathological variations of UC murines. Administration of an AMPK pharmacologic suppressant in mice resulted in a decrease in the therapeutic effects of eupatilin. In brief, eupatilin could ameliorate DSS-treated murine colitis via restraining the inflammatory response and keeping the integrity of the intestine epithelia barrier by AMPK excitation.

Fortunellin, a natural dietary flavone mainly existed in *Citrus japonica*, has multifarious bioactivities covering anti-tumor, anti-oxidation, and anti-inflammation (Zhao et al., 2017; Panagiotopoulos et al., 2021). Xiong et al. (2018) explored the function and mechanism of fortunellin in treating UC using TNBS-induced colitis rats as a model. Fortunellin alleviated the clinical signs of UC, involving excessive inflammatory symptoms and oxidative stress. Fortunellin reduced the apoptosis of epithelial cells in UC by suppressing PTEN expression. Fortunellin-caused decrease of PTEN could be neutralized by miR-374a decline. Furthermore, miR-374a knockdown *in vivo* partially restrained the effect of fortunellin on UC model. Together, PTEN suppression facilitates the reinforced effect of fortunellin on UC. Fortunellin targeting miR-374a is a negative modulator of PTEN. This research offers new ideas into the pathologic mechanism and therapy alternatives of UC.

Licoflavone B is a minor flavone in licorice, which is a kind of medicinal and edible Chinese herbal medicine (de Carvalho et al., 2015; Liu et al., 2022). Zhang et al. (2022) examined the efficacy and mechanism of licoflavone B against UC in DSS-exposed C57BL/6 murines. Experimental result showed that licoflavone B notably restrained DSS induced weight reduction, DAI rise, histologic injury, and colon inflammation, manifesting that licoflavone B possesses a beneficial effect on UC. It was discovered that licoflavone B maintained the integrity of the colon barrier through suppressing the apoptosis of colon cells and increasing the levels of ZO-1, occludin, and claudin-1. Furthermore, licoflavone B

remodeled the microbiota composition via restraining detrimental bacterium and promoting beneficial microbes. Besides, licoflavone B exhibited an anti-colitis effect via the blockage of the MAPK path. In conclusion, the results provided worthy information for the exploration of new anti-colitis drugs.

Linarin, a natural flavone existed in the plants of Buddleja, Mentha, and Cirsium, possesses various activities covering anti-inflammation, anti-allergen, as well as hepatoprotection (Han et al., 2018; Mottaghipisheh et al., 2021). Jin et al. (2022) evaluated the protection of linarin against DSS-evoked colitis in C57BL/6J murines and explored the possible mechanisms. Experimental results displayed that linarin administration relieved the DSS-evoked histopathologic injury, and strengthened the mucosa layer and enteric barrier function. Significantly, linarin markedly lowered MPO vitality and the levels of pro-inflammatory factors, whereas increased the mRNA expression of anti-inflammatory factor in colonal tissues. Furthermore, linarin recovered the intestinal flora injured by DSS. Linarin also partially enhanced the relative amounts of SCFAs-generating bacterium and the levels of SCFAs. The findings of the study suggest that linarin may be a promising nutritional intervention for the treatment of UC.

Lonicerin is a flavone glycoside extracted from *Lonicera japonica*, the flower buds of which are often employed for treating inflammatory and infectious disorders (Xu et al., 2019). Lv et al. (2021) reported the therapeutical role of lonicerin on intestine inflammation via binding directly to EZH2 histone methyltransferase. The modification of H3K27me3 by EZH2 was found to promote ATG5 expression, which in turn results in elevatory autophagy and expedites autolysosome-mediated degradation of NLRP3. The dynamic simulation study shows that the mutation of EZH2 residues (His1 and Arg685) greatly reduces the protective role of lonicerin. Moreover, *in vivo* researches verified that lonicerin treatment disturbs the assembly of NLRP3-ASC-pro-caspase-1 complex and relieves UC in a dose-dependent manner, an effect that is attenuated via administering an EZH2-overexpressing plasmid. Therefore, the results suggest that lonicerin may be a potential anti-inflammatory epigenetic agent, and the EZH2/ATG5/NLRP3 axis could be a novel therapeutic target for the treatment of UC and other inflammatory ailments.

Luteolin is a common dietary flavone in some edible plants, including *Chrysanthemum indicum*, *L. japonica*, and *Perilla frutescens* (Ganai et al., 2021). Previous studies have demonstrated that possess numerous beneficial effects, including anti-carcinogenic, anti-oxidative, anti-inflammatory, anti-allergic, and antimicrobial effects (Nabavi et al., 2015; Aziz et al., 2018). Li et al. (2016) probed the function and mechanism of luteolin against UC in DSS-evoked colitis murines. The results displayed that luteolin prominently decreased DAI scores, and restrained colonal shortening and histologic injury. Furthermore, luteolin effectually lowered the levels of inflammatory factors, covering iNOS, TNF-α and IL-6. Administration of luteolin was found to increase the levels of colon contents of SOD and CAT, as well as the expression of Nrf2 and its downstream targets, such as HO-1 and NQO1. These findings suggested that luteolin may restrain UC by activation of the Nrf2 signal path. Among the study from Vukelic et al. (2020), the researchers discovered that luteolin has the potential to attenuate experimental UC by exerting anti-inflammatory, anti-apoptotic, and anti-autophagic effects. These effects are mediated by the inhibition

of JNK1/2, p38, PI3K/Akt, NF-κB, and STAT3 signal paths, along with the induction of ERK1/2. In the research of Suga et al. (2021), they discovered that luteolin may possess the potential to relieve inflammation responses through reducing excessive 5-HT by inhibition of TPH-1 in RBL-2H3 cells. Zuo et al. (2021) proved that luteolin notably mitigated DSS-elicited UC, and the mechanism was associated with the modulation of enteric HMGB1-TLR-NF-κB signal path. In two other studies, Li et al. (2021a), Li et al. (2021b) indicated that luteolin could maintain intestine epithelia barrier function by suppressing STAT3 signaling and alleviate inflammatory reactions by regulating intestinal microflora in the treatment of colitis. Altogether, luteolin may be a prospective therapeutic drug for UC.

Nobiletin is a natural dietary flavone prevailingly found in a few citrus plants composed of *citrus sinensis*, *citrus paradise*, and *citrus aurantum* (Ashrafizadeh et al., 2020). Modern studies proved that nobiletin possesses multiple pharmacological actions, including anti-cancer, anti-inflammation, anti-oxidation, anti-dementia, and neuroprotection (Braidy et al., 2017). Hagenlocher et al. (2019) explored the function of nobiletin on inflammation and fibrosis in IL-10$^{-/-}$ colitis. The results showed that nobiletin administration caused a decline of clinic signs and a longer life expectancy. Moreover, histologic scores of UC were decreased in comparison with normal groups. Administration of nobiletin in IL-10$^{-/-}$ mice was found to decrease the number of mast cells and reduce their degranulation, which was positively correlated with the DAI. Besides, nobiletin administration also led to a decrease in fibrotic marker collagen deposition. In LPS stimulated human intestinal fibroblasts, the levels of collagen and pro-inflammatory factors COL13A1, IL-6, TNF, and CCL2 was down-modulated after nobiletin administration. Therefore, nobiletin administration was found to reduce signs and markers of inflammation, as well as the deposition and expression of fibrotic collagen in UC murines. Among another test, Xiong et al. (2015) investigated the effects of nobiletin on the exaggerated inflammatory reaction and weakened barrier function in UC rats. Experimental data manifested that nobiletin played anti-inflammatory roles in TNBS-treated UC by reducing iNOS and COX-2 levels. Nobiletin recovered the barrier function destroyed following TNBS treatment via the control of the Akt-NF-κB-MLCK signalling. In conclusion, nobiletin might be a prospective candidate for the treatment of colitis.

Oroxylin A, a main ingredient in the roots of *O. indicum* and *S. baicalensis*, possessed a wide range of beneficial bioactivities, including anti-inflammatory, antineoplastic, anticoagulative, cytoprotective, and neuroprotective bioactivities (Sajeev et al., 2022a; Sajeev et al., 2022b). Zhou et al. (2017) investigated the role of oroxylin A on DSS-treated mice UC by targeting NLRP3 inflammasome. The results displayed that oroxylin A alleviated UC, characterized by inhibiting weight reduction, colonic length shortening and inflammatory infiltration. The levels of TNF-α, IL-1β, and IL-6 in colons were also notably lowered by oroxylin A. Moreover, oroxylin A prominently inhibited the NLRP3 level in gut mucosa tissues. Besides, NLRP3 gene knockout mice had an obvious protective effect on UC treated by DSS, and oroxylin A administration exhibited no roles on relieving inflammatory symptoms in NLRP3$^{-/-}$ murine. Further research discovered that oroxylin A dosage-dependently suppressed the excitation of NLRP3 inflammasome in BMDMs and THP-Ms,

leading to a decrease in cleaved caspase-1 and cleaved IL-1β. Moreover, luteolin A mitigated the expression of NLRP3 protein depending on the suppression of p65 and nuclear transsituation. In addition, oroxylin A specifically inhibited the formation of ASC specks and the assembly of inflammasomes, both of which contributed to the blockade of the NLRP3 inflammasome. The above evidences indicated that oroxylin A suppressed NLRP3 inflammasome excitation and might be potentially employed to treat colitis.

Pectolinarigenin, a natural flavone existed in Cirsium and Citrus species, possesses different bioactivities including anti-inflammatory, antidiabetic, as well as anticancer properties (Lee et al., 2018; Cheriet et al., 2020). Feng et al. (2022) probed the possible protective effects of pectolinarigenin on LPS-treated macrophage cells and DSS-evoked UC mice. The results displayed that pectolinarigenin suppressed the LPS-evoked NF-κB excitation through disturbing IκB-α degradation. Subsequently, elevated Nrf2 protein expression was found on pectolinarigenin administrated RAW 264.7 and THP1 cells. Besides, they uncovered that pectolinarigenin mediated the NF-κB/Nrf2 path modulation, subsequently restrained the levels of iNOS, COX-2, IL-6, IL-1β, and TNF-α in RAW 264.7 and THP1 cells. Moreover, pectolinarigenin dosage-dependently mitigated colonic inflammation through adjusting NF-κB/Nrf2 signal path and improving MPO vitality and redox modulators in DSS-evoked UC mice. Likewise, we found the minimal pathologic injuries in the pectolinarigenin-treated mice colons, and the rise of goblet cell population and mucin-2 generation. Collectively, the results manifested that pectolinarigenin alleviated the DSS-evoked UC in murine through modulating the NF-κB/Nrf2 path. Therefore, pectolinarigenin may hold potential as a therapeutic agent for the treatment of UC.

Sinensetin, a dietary flavone mainly existed in citrus plants such as *Citrus sinensis*, was discovered to possess anticancerous, antioxidative, anti-inflammatory as well as antibacterial effects (Kim et al., 2020; Jie et al., 2021). Xiong et al. (2019) probed the therapeutic potential and underlying mechanism of sinensetin against UC in TNBS and DSS evoked UC rats. Sinensetin reversed colitis-related rise in intestine penetrability, notably facilitated epithelia cells autophagy, reduced epithelia cells apoptosis, and lowered mucosa claudin-2. Sinenstetin relieved the clinical signs in UC rats and mice. Knockdown of AMPK changed the encouragement of epithelia autophagy by sinensetin. Collectively, sinensetin markedly relieved intestine barrier dysfunction in UC through boosting epithelia cells autophagy, and further suppressing apoptosis and claudin-2 expression. Thus, these findings indicated the new promising benefit of sinensetin in UC.

Tangeretin is a polymethoxylated dietary flavone existed broadly in citrus plants, involving *Citrus unshiu*, *Citrus reticulata*, and *Citrus depressa*. Studies have proved that tangeretin possesses diversified biological activities, such as anti-inflammation, anti-cancer, and neuroprotection (Alhamad et al., 2021; Arafa et al., 2021). Eun et al. (2017) studied the therapeutic potential and underlying mechanism of tangeretin in treating UC. The results showed that tangeretin restrained TNF-α, IL-12, and IL-23 levels and NF-κB excitation in LPS-activated dendritic cells, but not affected IL-10 level. Moreover, tangeretin restrained the excitation and translocation of p65 into the nucleus *in vitro* through suppressing LPS binding to dendritic cells. Tangeretin treatment

inhibited the inflammatory reactions, involving NF-κB and MAPK excitation and MPO vitality, in the colons of murine with TNBS evoked UC. Tangeretin elevated TNBS induced low expression of TJs including occludin, claudin-1, and ZO-1. Tangeretin also suppressed TNBS-evoked differentiation of Th1 and Th17 cells and the levels of T-bet, RORγt, interferon-γ, IL-12, IL-17, and TNF-α. Whereas, tangeretin elevated TNBS-restrained differentiation of regulatory T cells and the levels of Foxp3 and IL-10. The results suggested that tangeretin might ameliorate UC through repressing IL-12 and TNF-α productions and NF-κB excitation via the suppression of LPS bond on immunocytes. In another research of Chen B. et al. (2021), they also probed the therapeutic potential and underlying mechanism of tangeretin against UC in DSS-evoked colitis mice. Experimental results indicated that dietary tangeretin could relieve UC through restraining inflammatory reactions, recovering intestine barrier function, and regulating intestine microflora.

Tricin is a dietary flavone monomer broadly distributed in grains, and has antineoplastic, anti-inflammatory, and antiangiogenic properties (Shalini et al., 2016; Jiang et al., 2020). Li X. X. et al. (2021) studied the potential protective mechanism of tricin on LPS-stimulated RAW264.7 cells and probed the effect of tricin on UC mice treated by 4.5% DSS for 7 days. The result displayed that tricin observably decreased NO level in LPS stimulated RAW264.7 cells and the anti-inflammation role of tricin was proved to inhibit the NF-κB pathway. Moreover, tricin administration (150 mg/kg) markedly mitigated colonic length decline, decreased MPO vitality and DAI scores, and recovered the elevatory myeloid-derived suppressor cells in acute UC mice. The effect of DSS on intestinal flora, including the incremental population of *Proteobacteria* and *Ruminococcaceae*, was indicated to be alleviated by tricin therapy. Therefore, tricin could improve acute colitis through relieving colon inflammation and regulating intestinal microflora profile.

Wogonin, a natural flavone in *S. baicalensis*, has multifold functions, including anti-oxidation, anti-inflammation, anti-cancer, anti-virus, and neuroprotection (Wu et al., 2016; Huynh et al., 2020). Zhou et al. (2022) investigated the role and mechanism of wogonin against UC in DSS-treated colitis mice. Results exhibited that DSS strikingly reduced weight and colonic length, and elevated inflammatory symptoms in the colon. Wogonin effectively restrained colon ulcer, neutrophil infiltration and histologic variations elicited by DSS. The increase of pro-inflammatory factors (e.g., TNF-α, IL-6, COX-2, iNOS) and decreased activities of antioxidative enzymes (e.g., SOD, GST and GSH) were also notably regulated after wogonin treatment. In addition, wogonin activated apoptosis by suppressing Bcl-2 and elevating the contents of Bax, caspase-3, and -9. Further investigation revealed that wogonin's protective role against DSS-induced UC was closely linked to the modulation of the Nrf2/TLR4/NF-B signaling.

Wogonoside, one of the main flavones from *S. baicalensis*, was discovered to possess multifarious pharmacologic actions including anti-inflammation, anti-cancer, and anti-oxidation (Chen et al., 2013; Liu Q. et al., 2020). Sun et al. (2015) assessed the action and mechanism of wogonoside against UC in DSS-elicited murine colitis. Experimental data certified that wogonoside dosage-dependently alleviated DSS-evoked weight reduction and colonic

length shortening. Furthermore, wogonoside reversed DSS-evoked colon pathologic injury, notably restrained inflammation cell infiltration and reduced MPO and iNOS vitalities. The contents of pro-inflammatory mediators in serums and colons were also markedly suppressed by wogonoside. Besides, wogonoside significantly reduced the generation of IL-1β, TNF-α and IL-6 and restrained mRNA levels of pro-IL-1β and NLRP3 in PMA-differentiated monocytic THP-1 cells by preventing the activizaion of NF-κB and NLRP3 inflammasome. Therefore, these evidences verified that wogonoside exhibited an anti-inflammatory function via control of NF-κB and NLRP3 inflammasome. Among the experiment of Huang et al. (2020), the researchers explored whether wogonoside regulates intestine barrier function. The results manifested that wogonoside mitigated gut inflammation in UC and exerted a protective action on gut epithelia barrier function both *in vivo* and *in vitro*. Meanwhile, it was proven that wogonoside regulated gut epithelia TJs primarily via suppressing the MLCK/pMLC2 signal pathway. Additionally, Liu Q. et al. (2020) also explored the tissular distribution of wogonoside and its therapeutical effect on UC and the probable mechanism. Results testified that wogonoside could be absorbed by the colon and relieve inflammation reactions by suppressing NLRP3 inflammasome formation and excitation, which was associated with an inhibiting role on the TXNIP-dependent NF-κB signal pathway. In summary, wogonoside shows promise as a new medication for treating UC.

Discussion

UC is a multifactorial persistent inflammatory bowel disorder. The destruction of the gut barrier is associated with UC and can result in pathogenetic antigen intrusion (Lee et al., 2020). Therefore, novel means of restoring the epithelial and mucus barrier, facilitating mucosa healing, and decreasing mucosa penetrability are regarded as promising methods for treating UC (Li J. J. et al., 2021). TJ forms a paracellular osmotic barrier to limit the traverse of ions, small solutes, and water (Han et al., 2023). Among various proteins that make up the TJ, ZO are the main tightly linked cytoskeletal proteins related to epithelia integrity, occludin is a crucial protein in maintaining barrier function and TJ stabilization, while claudin-1 is a membrane-spanning protein that forms part of the TJ strands (Atsugi et al., 2020; Kuo et al., 2021). The formation and disruption of the multiprotein complex made up of ZO-1, occludin and claudin-1 in intestinal epithelia cells could observably influence the intestine epithelia barrier function (Lan et al., 2021; Liu and Zhu, 2022). In the present review, natural flavones involving diosmetin, licoflavone B, luteolin, tangeretin, and wogonoside were found to notably reduce paracellular permeability and increase TEER value which was concomitant with increased levels of TJ proteins (ZO-1, occludin, and claudin-1). These evidences indicated that flavones could suppress the breakdown of intestinal barrier in UC models evoked by DSS, TNBS and LPS *in vivo* and *in vitro*.

Oxidant stress exerts a crucial action in pathophysiology of UC (Wojcik-Grzybek et al., 2022). Studies have revealed that increased production of ROS destroys the cellular macromolecules (DNA, lipids and proteins) and breaks epithelia cell integrity (Juan et al., 2021). Superoxide anion, continuously produced through

endogenous processes and exogenous sources, is the main free radical to induce oxidative injury, which can be restrained by the first-line defense enzyme systems like SOD and CAT (Qiu et al., 2021). SOD converts the superoxide anion into H_2O_2, a metabolite that is easy to diffuse and stable, and then CAT further neutralizes H_2O_2 into water (Yu et al., 2023). CAT could enhance the oxidative resistibility and preserve the low steady state level of ROS. GSH, as a capital hydrophilic and intracellular nonenzymatic antioxidant, exerts an important effect in relieving tissue injury through eliminating reactive oxygen and nitrogen species (Ighodaro and Akinloye, 2018; Wu et al., 2021). Early studies showed that GSH concentration was found to be evidently decreased in colonic tissues when antioxidants were neutralized by released oxygen derived free radicals (Hu et al., 2021). The reduction of GSH can further cause a rise in MDA level, a final product of lipid peroxidation that finally brings about oxidative injury. As demonstrated in the present review, baicalin, diosmetin, fortunellin, luteolin, and wogonin could notably elevate the levels of the antioxidative enzymes SOD, GSH, GST, and CAT and suppress ROS and MDA activity induced by AA, DSS or TNBS treatment in the colitis tissue. These data indicated that natural flavones can effectively alleviate colitis by reducing oxidative stress.

Hyperactive inflammation cells, particularly neutrophils and macrophages, generate some pro-inflammatory factors, ROS, MPO and nitrogen metabolites, which are related to the pathogenic mechanism of colitis (Saraiva et al., 2022). Moreover, COX-2 and iNOS are pro-inflammatory enzymes that can be induced in inflamed tissues, leading to the generation of NO and PGE_2 (Zhao et al., 2022). Elevated production of inflammatory cytokines, such as TNF-α, IL-1β, and IL-6, could injure gut epithelia cells and exacerbate colitis (Ahmad et al., 2021). IL-10 takes part in a Th2-mediated immunological response, and suppresses TNF-α, IL-1β, and IL-6 levels, exerting an anti-inflammatory action in the intestine mucosa immunity system. Thus, modulating the balance between pro- and anti-inflammatory factors is regarded as a necessary therapy approach for colitis (Yin et al., 2020; Zhuang et al., 2021). In this review, we firstly revealed that all natural-derived anti-colitis flavones could remarkably modulate the balance of pro- and anti-inflammatory cytokines in colonic tissues of colitis murine via attenuating pro-inflammatory agents and elevating anti-inflammatory factors.

The intrinsic immunity system identifies the existence of specific bacteria antigens through a broad family of pattern-recognition receptor (PRR). TLR4 belongs to the PRR that can recognize LPS (endotoxin), a main ingredient of gram-negative bacteria's outer membrane, and stimulate the generation of pro-inflammatory factors, causing an inflammatory reaction (Dai et al., 2022). Moreover, TLR4 level was elevated in colon tissues and gut epithelia cells of UC animals and patients (Fajstova et al., 2020). Convincing proofs proves the therapeutic role of restraining TLR4/MyD88 signal molecules, subsequently resulting in the devitalization of NF-κB and MAPKs, and the suppression of pro-inflammatory factors (Ma et al., 2020). In this review, we found that natural-derived flavones, including baicalein, luteolin and wogonin observably restrained the enhancement of TLR4 and MyD88 in TNBS or DSS-treated UC murine and in LPS-treated macrophages or intestinal epithelial cells. Subsequently, the TNBS or LPS-treated excitation of NF-κB and MAPKs pathways and their downstream

regulatory genes, including pro-inflammatory mediators (e.g., TNF-α, IL-6, and IL-1β), adhesion molecules (e.g., ICAM-1), NO and PGE_2 were suppressed. These results showed that downregulation of TLR4/MyD88 signal cascades was associated with the anti-inflammatory roles of the above natural-derived anti-colitis flavones in UC models in vivo and in vitro.

Besides, the generation of pro-inflammatory factors is also modulated by a multiprotein complex known as inflammasome, which mainly consists of 3 ingredients including NLR, ASC and caspase-1. Among a variety of inflammasome, NLRP3 inflammasome composed of NLRP3, ASC and pro-caspase-1 is the most widely investigated (Mangan et al., 2018). The NLRP3 inflammasome plays a vital role in regulating the inflammatory response in the intestines and maintaining homeostasis by mediating multiple pro-inflammatory signals (Busch et al., 2022; Martinez-Lopez et al., 2022). After stimulation, NLRP3 recruits ASC adaptor to accelerate the recruitment of pro-caspase-1. Pro-caspase-1 then aggregates and automatically splits to produce active caspase-1. Activating caspase-1 is needed to transform pro-IL-1β and pro-IL-18 into their mature active forms IL-1β and IL-18 (Paik et al., 2021). Subsequently, IL-1β and IL-18 are secreted outside of the cell, trigger the "waterfall" cascade of downstream signaling, and participate in the development of numerous inflammatory illnesses, including UC (Chen C. et al., 2021). Chen et al. discovered that the serum levels of NLRP3, caspase-1, HMGB1 and IL-1β were significantly increased in UC patients (Chen et al., 2020). In congruence with previous investigations, in this review, we discovered that natural-derived anti-colitis flavones, such as baicalein, oroxylin A, lonicerin and wogonoside notably preserved IL-1β and IL-18 production, which was linked to the suppression of NLRP3, ASC and caspase-1 in a dosage-dependent mode both in TNBS- or DSS-induced UC murine and LPS-treated THP-1 or RAW264.7 cells.

Furthermore, research personnel obtained crucial insight into gut microflora constitution during gut inflammation and have uncovered novel directions for colitis therapy (Li et al., 2020). Some studies have emphasized that the prominent variations in intestinal microflora constitution in colitis sufferers can bring about intestine inflammation (Wang et al., 2022). Serious imbalance is primarily presented in the intestine of colitis sufferers, where there is a decrease in Firmicutes and Bacteroidetes, and an increase in Proteobacteria. The elevated endotoxin generated by Proteobacteria may cause damage to the gut's penetrability, resulting in adhesion and invasion of gut epithelia cells, destruction of the host's defenses, excitation of the inflammatory reaction, alterations in the composition of intestinal microflora, and eventually facilitating the occurrence of colitis (Jang et al., 2019). Moreover, Enterobacteriaceae, facultative anaerobic bacteria, are associated with the pathogenesis of colitis through aggravating intestinal inflammation and barrier injury (Kim et al., 2021; Qin et al., 2021). Escherichia-Shigella, gram-negative bacteria with an outer LPS membrane, can intrude into the colon epithelia and cause intestinal inflammation (Dai et al., 2021). Roseburia and Lactobacillus are probiotic strains with vital roles in maintaining intestinal homeostasis, inducing host's colonic goblet cells, modulating immune system and promoting SCFAs productions (Zhang et al., 2020; Wang et al., 2021). In this review, the levels of Proteobacteria, Enterobacteriaceae and Escherichia-Shigella were reduced, while those of Bacteroidetes, Roseburia and Lactobacillus were elevated after acacetin, baicalin, diosmetin, luteolin, licoflavone B, and
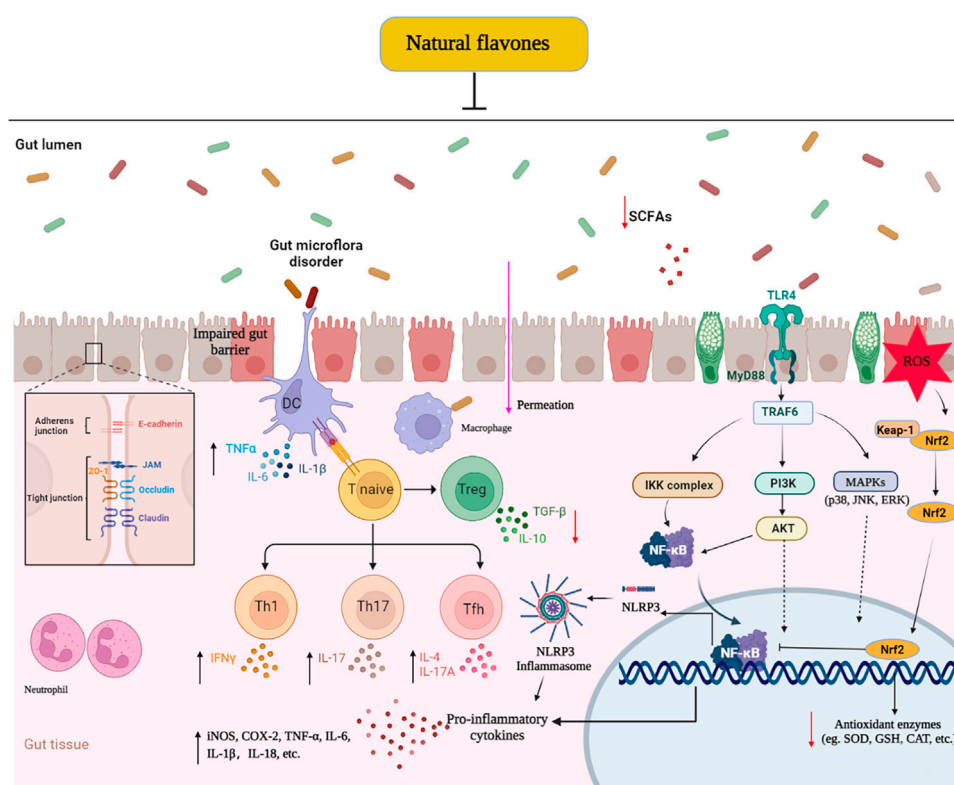
FIGURE 3
Molecular mechanisms of naturally derived flavones in the remedy of ulcerative colitis. ↓: Decrease, ↑: Increase: Inhibit.

tangeretin administration in DSS treated murine UC. Surprisingly, some of them significantly increased overall richness and diversity while also regulating the composition of gut microbiota in a manner similar to the control group.

SCFAs, such as acetate, butyrate and propionate, are important energy sources and metabolites of intestinal microorganisms and colon epithelia cells, which exert remarkable action in preserving intestine homeostasis and strengthening gut barrier function (Feng et al., 2018; Venegas et al., 2019). Consistent with former researches, this research indicated that enteric SCFAs were reduced after DSS exposure, and baicalin and tangeretin administration could reverse these alterations through elevating the acetate, propionate, valeric and butyrate contents. Moreover, baicalin enriched certain specific bacteria populations that could motivate the generation of SCFAs, such as *Butyricimonas* spp., and *Lactobacillus* spp., manifesting that their protective action against DSS-evoked UC was mechanistically connected with elevating SCFAs generation mediated by their remodeling roles on the intestinal flora.

Conclusion

This paper first generalizes the effective protection and potential mechanisms of natural flavones against UC *in vivo* and *in vitro* models. Their therapeutic roles manifested as the alleviation of clinical symptoms, relief of colonic mucosal injury, and inhibition of inflammatory responses. The potential mechanism of these effects mainly involves the blockage of various signalling pathways, including TLR4/MyD88/NF-κB, MAPKs, PI3K/AKT, and NLRP3 inflammasome, which regulate the intestinal microflora and Treg/Th17 balance, decreasing inflammatory responses and oxidative stress, and increasing TJ expression (Figure 3). The present review highlights the effects of flavones derived from natural sources in the treatment of UC by promoting gut homeostasis, improving intestinal barrier function, reducing oxidative stress, and regulating the immuno-inflammatory response. These findings revealed that these naturally derived flavones are effective and prospective drug candidates for UC and other inflammatory diseases. Whereas, the latent mechanism or toxicology of most natural flavones remains in-depth research, and their actual effect on colitis sufferers has not been verified in clinical experiments. Thus, more efforts should be focused to illuminating the molecular mechanisms and long-range effect and security in clinically relevant experiments to accelerate the perspective utilization of these flavones as colitis remedies in the near future.

Author contributions

CL proceeded the design of this study. QL, CL, and YX conducted the literature search. QL, CL, and JL constructed the figures and tables. QL wrote the manuscript. CL and QG made revisions to the manuscript. All authors contributed to the article and approved the submitted version.

Funding

Conflict of interest

Author JL was employed by the company China Traditional Chinese Medicine Holdings Company Limited.

The remaining authors declare that the research was conducted in the absence of any commercial or financial relationships that could be construed as a potential conflict of interest..

Publisher's note

References

Ahmad, A., Ansari, M. M., Mishra, R. K., Kumar, A., Vyawahare, A., Verma, R. K., et al. (2021). Enteric-coated gelatin nanoparticles mediated oral delivery of 5-aminosalicylic acid alleviates severity of DSS-induced ulcerative colitis. *Mat. Sci. Eng. C Mat. Biol. Appl.* 119, 111582. doi:10.1016/j.msec.2020.111582

Alhamad, D. W., Elgendy, S. M., Al-Tel, T. H., and Omar, H. A. (2021). Tangeretin as an adjuvant and chemotherapeutic sensitizer against various types of cancers: A comparative overview. *J. Pharm. Pharmacol.* 73 (5), 601–610. doi:10.1093/jpp/rgab013

Alsoud, D., Verstockt, B., Fiocchi, C., and Vermeire, S. (2021). Breaking the therapeutic ceiling in drug development in ulcerative colitis. *Lancet Gastroenterol. Hepatol.* 6 (7), 589–595. doi:10.1016/S2468-1253(21)00065-0

Arafa, E. A., Shurrab, N. T., and Buabeid, M. A. (2021). Therapeutic implications of a polymethoxylated flavone, tangeretin, in the management of cancer via modulation of different molecular pathways. *Adv. Pharmacol. Pharm. Sci.* 2021, 4709818. doi:10.1155/2021/4709818

Ashrafizadeh, M., Zarrabi, A., Saberifar, S., Hashemi, F., Hushmandi, K., Hashemi, F., et al. (2020). Nobiletin in cancer therapy: How this plant derived-natural compound targets various oncogene and onco-suppressor pathways. *Biomedicines* 8 (5), 110. doi:10.3390/biomedicines8050110

Atsugi, T., Yokouchi, M., Hirano, T., Hirabayashi, A., Nagai, T., Ohyama, M., et al. (2020). Holocrine secretion occurs outside the tight junction barrier in multicellular glands: Lessons from Claudin-1-deficient mice. *J. Invest. Dermatol.* 140 (2), 298–308. doi:10.1016/j.jid.2019.06.150

Aziz, N., Kim, M. Y., and Cho, J. Y. (2018). Anti-inflammatory effects of luteolin: A review of *in vitro, in vivo*, and *in silico* studies. *J. Ethnopharmacol.* 225, 342–358. doi:10.1016/j.jep.2018.05.019

Braidy, N., Behzad, S., Habtemariam, S., Ahmed, T., Daglia, M., Nabavi, S. M., et al. (2017). Neuroprotective effects of citrus fruit-derived flavonoids, nobiletin and tangeretin in alzheimer's and Parkinson's disease. *CNS Neurol. Disord. Drug Targets* 16 (4), 387–397. doi:10.2174/1871527316666170328113309

Busch, M., Ramachandran, H., Wahle, T., Rossi, A., and Schins, R. P. F. (2022). Investigating the role of the NLRP3 inflammasome pathway in acute intestinal inflammation: Use of THP-1 knockout cell lines in an advanced triple culture model. *Front. Immunol.* 13, 898039. doi:10.3389/fimmu.2022.898039

Chen, B., Luo, J. K., Han, Y. H., Du, H. J., Liu, J., He, W., et al. (2021a). Dietary tangeretin alleviated dextran sulfate sodium-induced colitis in mice via inhibiting inflammatory response, restoring intestinal barrier function, and modulating gut microbiota. *J. Agric. Food Chem.* 69 (27), 7663–7674. doi:10.1021/acs.jafc.1c03046

Chen, C., Liu, X. Q., Gong, L. J., Zhu, T. Y., Zhou, W. X., Kong, L. Y., et al. (2021b). Identification of Tubocapsanolide A as a novel NLRP3 inhibitor for potential treatment of colitis. *Biochem. Pharmacol.* 190, 114645. doi:10.1016/j.bcp.2021.114645

Chen, Y., Hui, H., Yang, H., Zhao, K., Qin, Y. S., Gu, C., et al. (2013). Wogonoside induces cell cycle arrest and differentiation by affecting expression and subcellular localization of PLSCR1 in AML cells. *Blood* 121 (18), 3682–3691. doi:10.1182/blood-2012-11-466219

Chen, Y. M., Wu, D., and Sun, L. J. (2020). Clinical significance of high-mobility group box 1 protein (HMGB1) and nod-like receptor protein 3 (NLRP3) in patients with ulcerative colitis. *Med. Sci. Monit.* 26, e919530. doi:10.12659/MSM.919530

Cheriet, T., Ben-Bachir, B., Thamri, O., Seghiri, R., and Mancini, I. (2020). Isolation and biological properties of the natural flavonoids pectolinarin and pectolinarigenin-A Review. *Antibiot. Basel* 9 (7), 417. doi:10.3390/antibiotics9070417

Cho, J. H., Lee, J. G., Yang, Y. I., Kim, J. H., Ahn, J. H., Baek, N. I., et al. (2011). Eupatilin, a dietary flavonoid, induces G2/M cell cycle arrest in human endometrial cancer cells. *Food Chem. Toxicol.* 49 (8), 1737–1744. doi:10.1016/j.fct.2011.04.019

Dai, W. B., Long, L. H., Wang, X. Q., Li, S., and Xu, H. P. (2022). Phytochemicals targeting Toll-like receptors 4 (TLR4) in inflammatory bowel disease. *Chin. Med.* 17 (1), 53. doi:10.1186/s13020-022-00611-w

Dai, Z. F., Ma, X. Y., Yang, R. L., Wang, H. C., Xu, D. D., Yang, J. N., et al. (2021). Intestinal flora alterations in patients with ulcerative colitis and their association with inflammation. *Exp. Ther. Med.* 22 (5), 1322. doi:10.3892/etm.2021.10757

de Carvalho, L. S. A., Geraldo, R. B., de Moraes, J., Pinto, P. L. S., Pinto, P. D., Pereira, O. D., et al. (2015). Schistosomicidal activity and docking of *Schistosoma mansoni* ATPDase 1 with licoflavone B isolated from *Glycyrrhiza inflata* (Fabaceae). *Exp. Parasitol.* 159, 207–214. doi:10.1016/j.exppara.2015.09.015

Dinda, B., Dinda, S., DasSharma, S., Banik, R., Chakraborty, A., and Dinda, M. (2017). Therapeutic potentials of baicalin and its aglycone, baicalein against inflammatory disorders. *Eur. J. Med. Chem.* 131, 68–80. doi:10.1016/j.ejmech.2017.03.004

Dou, W., Zhang, J. J., Zhang, E. Y., Sun, A. N., Ding, L. L., Chou, G. X., et al. (2013). Chrysin ameliorates chemically induced colitis in the mouse through modulation of a PXR/NF-kappa B signaling pathway. *J. Pharmacol. Exp. Ther.* 345 (3), 473–482. doi:10.1124/jpet.112.201863

Du, L. L., and Ha, C. (2020). Epidemiology and pathogenesis of ulcerative colitis. *Gastroenterol. Clin. North Am.* 49 (4), 643–654. doi:10.1016/j.gtc.2020.07.005

Eun, S. H., Woo, J. T., and Kim, D. H. (2017). Tangeretin inhibits IL-12 expression and NF-kappa B activation in dendritic cells and attenuates colitis in mice. *Planta Med.* 83 (6), 527–533. doi:10.1055/s-0042-119074

Fajstova, A., Galanova, N., Coufal, S., Malkova, J., Kostovcik, M., Cermakova, M., et al. (2020). Diet rich in simple sugars promotes pro-inflammatory response via gut microbiota alteration and TLR4 signaling. *Cells* 9 (12), 2701. doi:10.3390/cells9122701

Feng, Y. H., Wang, Y., Wang, P., Huang, Y. L., and Wang, F. J. (2018). Short-chain fatty acids manifest stimulative and protective effects on intestinal barrier function through the inhibition of NLRP3 inflammasome and autophagy. *Cell Physiol. biochem.* 49 (1), 190–205. doi:10.1159/000492853

Feng, Y. L., Bhandari, R., Li, C. M., Shu, P. F., and Shaikh, I. I. (2022). Pectolinarigenin suppresses LPS-induced inflammatory response in macrophages and attenuates DSS-induced colitis by modulating the NF-kappa B/Nrf2 signaling pathway. *Inflammation* 45 (6), 2529–2543. doi:10.1007/s10753-022-01710-4

Fiorino, G., Danese, S., Giacobazzi, G., and Spinelli, A. (2021). Medical therapy versus surgery in moderate-to-severe ulcerative colitis. *Dig. Liver Dis.* 53 (4), 403–408. doi:10.1016/j.dld.2020.09.022

Ganai, S. A., Sheikh, F. A., Baba, Z. A., Mir, M. A., Mantoo, M. A., and Yatoo, M. A. (2021). Anticancer activity of the plant flavonoid luteolin against preclinical models of various cancers and insights on different signalling mechanisms modulated. *Phytother. Res.* 35 (7), 3509–3532. doi:10.1002/ptr.7044

Garg, A., and Chaturvedi, S. (2022). A comprehensive review on chrysin: Emphasis on molecular targets, pharmacological actions and bio-pharmaceutical aspects. *Curr. Drug Targets* 23 (4), 420–436. doi:10.2174/1389450122666210824141044

Ge, H. F., Cai, Z. A. Z., Chai, J. L., Liu, J. Y., Liu, B. Q., Yu, Y. D., et al. (2021). Egg white peptides ameliorate dextran sulfate sodium-induced acute colitis symptoms by inhibiting the production of pro-inflammatory cytokines and modulation of gut microbiota composition. *Food Chem.* 360, 129981. doi:10.1016/j.foodchem.2021.129981

Gerges, S. H., Wahdan, S. A., Elsherbiny, D. A., and El-Demerdash, E. (2022). Pharmacology of diosmin, a citrus flavone glycoside: An updated review. *Eur. J. Drug Metab. Pharmacokinet.* 47 (1), 1–18. doi:10.1007/s13318-021-00731-y

Ginwala, R., Bhavsar, R., Chigbu, D. I., Jain, P., and Khan, Z. K. (2019). Potential role of flavonoids in treating chronic inflammatory diseases with a special focus on the anti-inflammatory activity of apigenin. *Antioxidants* 8 (2), 35. doi:10.3390/antiox8020035

Guo, L. T., Wang, S. Q., Su, J., Xu, L. X., Ji, Z. Y., Zhang, R. Y., et al. (2019). Baicalin ameliorates neuroinflammation-induced depressive-like behavior through inhibition of toll-like receptor 4 expression via the PI3K/AKT/FoxO1 pathway. *J. Neuroinflamm.* 16, 95. doi:10.1186/s12974-019-1474-8

Hagenlocher, Y., Gommeringer, S., Held, A., Feilhauer, K., Koninger, J., Bischoff, S. C., et al. (2019). Nobiletin acts anti-inflammatory on murine IL-10$^{-/-}$ colitis and human intestinal fibroblasts. *Eur. J. Nutr.* 58 (4), 1391–1401. doi:10.1007/s00394-018-1661-x

Han, H., You, Y., Cha, S., Kim, T. R., Sohn, M., and Park, J. (2023). Multi-species probiotic strain mixture enhances intestinal barrier function by regulating inflammation and tight junctions in lipopolysaccharides stimulated caco-2 cells. *Microorganisms* 11 (3), 656. doi:10.3390/microorganisms11030656

Han, X., Wu, Y. C., Meng, M., Sun, Q. S., Gao, S. M., and Sun, H. (2018). Linarin prevents LPS-induced acute lung injury by suppressing oxidative stress and inflammation via inhibition of TXNIP/NLRP3 and NF-kappa B pathways. *Int. J. Mol. Med.* 42 (3), 1460–1472. doi:10.3892/ijmm.2018.3710

Hirten, R. P., and Sands, B. E. (2021). New therapeutics for ulcerative colitis. *Annu. Rev. Med.* 72, 199–213. doi:10.1146/annurev-med-052919-120048

Hu, T. T., Fan, Y., Long, X. Y., Pan, Y. N., Mu, J. F., Tan, F., et al. (2021). Protective effect of *Lactobacillus plantarum* YS3 on dextran sulfate sodium-induced colitis in C57BL/6J mice. *J. Food Biochem.* 45 (2), e13632. doi:10.1111/jfbc.13632

Huang, S. W., Fu, Y. J., Xu, B., Liu, C., Wang, Q., Luo, S., et al. (2020). Wogonoside alleviates colitis by improving intestinal epithelial barrier function via the MLCK/pMLC2 pathway. *Phytomedicine* 68, 153179. doi:10.1016/j.phymed.2020.153179

Huynh, D. L., Ngau, T. H., Nguyen, N. H., Tran, G. B., and Nguyen, C. T. (2020). Potential therapeutic and pharmacological effects of wogonin: An updated review. *Mol. Biol. Rep.* 47 (12), 9779–9789. doi:10.1007/s11033-020-05972-9

Ighodaro, O. M., and Akinloye, O. A. (2018). First line defence antioxidants-superoxide dismutase (SOD), catalase (CAT) and glutathione peroxidase (GPX): Their fundamental role in the entire antioxidant defence grid. *Alex. J. Med.* 54 (4), 287–293. doi:10.1016/j.ajme.2017.09.001

Jang, H. M., Park, K. T., Noh, H. D., Lee, S. H., and Kim, D. H. (2019). Kakkalide and irisolidone alleviate 2,4,6-trinitrobenzenesulfonic acid-induced colitis in mice by inhibiting lipopolysaccharide binding to toll-like receptor-4 and proteobacteria population. *Int. Immunopharmacol.* 73, 246–253. doi:10.1016/j.intimp.2019.05.008

Jeong, S. H., Kim, H. H., Ha, S. E., Park, M. Y., Bhosale, P. B., Abusaliya, A., et al. (2022). Flavones: Six selected flavones and their related signaling pathways that induce apoptosis in cancer. *Int. J. Mol. Sci.* 23 (18), 10965. doi:10.3390/ijms231810965

Jiang, B., Song, J., and Jin, Y. (2020). A flavonoid monomer tricin in gramineous plants: Metabolism, bio/chemosynthesis, biological properties, and toxicology. *Food Chem.* 320, 126617. doi:10.1016/j.foodchem.2020.126617

Jie, L. H., Jantan, I., Yusoff, S. D., Jalil, J., and Husain, K. (2021). Sinensetin: An insight on its pharmacological activities, mechanisms of action and toxicity. *Front. Pharmacol.* 11, 553404. doi:10.3389/fphar.2020.553404

Jin, C. N., Liu, J. Y., Jin, R. Y., Yao, Y. P., He, S. L., Lei, M., et al. (2022). Linarin ameliorates dextran sulfate sodium-induced colitis in C57BL/6J mice via the improvement of intestinal barrier, suppression of inflammatory responses and modulation of gut microbiota. *Food Funct.* 13 (20), 10574–10586. doi:10.1039/d2fo02128e

Jin, X., Liu, M. Y., Zhang, D. F., Zhong, X., Du, K., Qian, P., et al. (2019). Baicalin mitigates cognitive impairment and protects neurons from microglia-mediated neuroinflammation via suppressing NLRP3 inflammasomes and TLR4/NF-kappa B signaling pathway. *CNS Neurosci. Ther.* 25 (5), 575–590. doi:10.1111/cns.13086

Juan, C. A., de la Lastra, J. M. P., Plou, F. J., and Perez-Lebena, E. (2021). The chemistry of reactive oxygen species (ROS) revisited: Outlining their role in biological macromolecules (DNA, lipids and proteins) and induced pathologies. *Int. J. Mol. Sci.* 22 (9), 4642. doi:10.3390/ijms22094642

Juca, M. M., Cysne, F. M. S., de Almeida, J. C., Mesquita, D. D., Barriga, J. R. D., Ferreira, K. C. D., et al. (2020). Flavonoids: Biological activities and therapeutic potential. *Nat. Prod. Res.* 34 (5), 692–705. doi:10.1080/14786419.2018.1493588

Kasala, E. R., Bodduluru, L. N., Madana, R. M., Athira, K. V., Gogoi, R., and Barua, C. C. (2015). Chemopreventive and therapeutic potential of chrysin in cancer: Mechanistic perspectives. *Toxicol. Lett.* 233 (2), 214–225. doi:10.1016/j.toxlet.2015.01.008

Kim, J. W., Kim, C. Y., Kim, J. H., Jeong, J. S., Lim, J. O., Ko, J. W., et al. (2021). Prophylactic catechin-rich green tea extract treatment ameliorates pathogenic enterotoxic escherichia coli-induced colitis. *Pathogens* 10 (12), 1573. doi:10.3390/pathogens10121573

Kim, S. M., Ha, S. E., Lee, H. J., Rampogu, S., Vetrivel, P., Kim, H. H., et al. (2020). Sinensetin induces autophagic cell death through p53-related AMPK/mTOR signaling in hepatocellular carcinoma HepG2 cells. *Nutrients* 12 (8), 2462. doi:10.3390/nu12082462

Kuo, W. T., Zuo, L., Odenwald, M. A., Madha, S., Singh, G., Gurniak, C. B., et al. (2021). The tight junction protein ZO-1 is dispensable for barrier function but critical for effective mucosal repair. *Gastroenterology* 161 (6), 1924–1939. doi:10.1053/j.gastro.2021.08.047

Lan, H., Zhang, L. Y., He, W., Li, W. Y., Zeng, Z., Qian, B., et al. (2021). Sinapic acid alleviated inflammation-induced intestinal epithelial barrier dysfunction in lipopolysaccharide- (LPS-) treated caco-2 cells. *Mediat. Inflamm.* 2021, 5514075. doi:10.1155/2021/5514075

Lee, H. J., Saralamma, V. V. G., Kim, S. M., Ha, S. E., Raha, S., Lee, W. S., et al. (2018). Pectolinarigenin induced cell cycle arrest, autophagy, and apoptosis in gastric cancer cell via PI3K/AKT/mTOR signaling pathway. *Nutrients* 10 (8), 1043. doi:10.3390/nu10081043

Lee, Y., Sugihara, K., Gillilland, M. G., Jon, S., Kamada, N., and Moon, J. J. (2020). Hyaluronic acid-bilirubin nanomedicine for targeted modulation of dysregulated intestinal barrier, microbiome and immune responses in colitis. *Nat. Mat.* 19 (1), 118–126. doi:10.1038/s41563-019-0462-9

Li, B. L., Du, P. L., Du, Y., Zhao, D. Y., Cai, Y. R., Yang, Q., et al. (2021a). Luteolin alleviates inflammation and modulates gut microbiota in ulcerative colitis rats. *Life Sci.* 269, 119008. doi:10.1016/j.lfs.2020.119008

Li, B. L., Zhao, D. Y., Du, P. L., Wang, X. T., Yang, Q., and Cai, Y. R. (2021b). Luteolin alleviates ulcerative colitis through SHP-1/STAT3 pathway. *Inflamm. Res.* 70 (6), 705–717. doi:10.1007/s00011-021-01468-9

Li, C. L., Ai, G. X., Wang, Y. F., Lu, Q., Luo, C. D., Tan, L. H., et al. (2020). Oxyberberine, a novel gut microbiota-mediated metabolite of berberine, possesses superior anti-colitis effect: Impact on intestinal epithelial barrier, gut microbiota profile and TLR4-MyD88-NF-kappa B pathway. *Pharmacol. Res.* 152, 104603. doi:10.1016/j.phrs.2019.104603

Li, C. L., Dong, N., Wu, B. W., Mo, Z. M., Xie, J. H., and Lu, Q. (2021c). Dihydroberberine, an isoquinoline alkaloid, exhibits protective effect against dextran sulfate sodium-induced ulcerative colitis in mice. *Phytomedicine* 90, 153631. doi:10.1016/j.phymed.2021.153631

Li, C. L., Wang, J. H., Ma, R. F., Li, L. H., Wu, W. F., Cai, D. K., et al. (2022). Natural-derived alkaloids exhibit great potential in the treatment of ulcerative colitis. *Pharmacol. Res.* 175, 105972. doi:10.1016/j.phrs.2021.105972

Li, H. L., Wei, Y. Y., Li, X. H., Zhang, S. S., Zhang, R. T., Li, J. H., et al. (2021d). Diosmetin has therapeutic efficacy in colitis regulating gut microbiota, inflammation, and oxidative stress via the circ-sirt1/sirt1 axis. *Acta Pharmacol. Sin.* 43 (4), 919–932. doi:10.1038/s41401-021-00726-0

Li, J. J., Zhang, L., Wu, T., Li, Y. F., Zhou, X. J., and Ruan, Z. (2021e). Indole-3-propionic acid improved the intestinal barrier by enhancing epithelial barrier and mucus barrier. *J. Agr. Food Chem.* 69 (5), 1487–1495. doi:10.1021/acs.jafc.0c05205

Li, X. X., Chen, S. G., Yue, G. L., Kwok, H. F., Lau, B. S., Zhneg, T., et al. (2021f). Natural flavone tricin exerted anti-inflammatory activity in macrophage via NF-κB pathway and ameliorated acute colitis in mice. *Phytomedicine* 90, 153625. doi:10.1016/j.phymed.2021.153625

Li, Y., Shen, L., and Luo, H. S. (2016). Luteolin ameliorates dextran sulfate sodium-induced colitis in mice possibly through activation of the Nrf2 signaling pathway. *Int. Immunopharmacol.* 40, 24–31. doi:10.1016/j.intimp.2016.08.020

Li, Y. Y., Wang, X. J., Su, Y. L., Wang, Q., Huang, S. W., Pan, Z. F., et al. (2021g). Baicalein ameliorates ulcerative colitis by improving intestinal epithelial barrier via AhR/IL-22 pathway in ILC3s. *Acta Pharmacol. Sin.* 43 (6), 1495–1507. doi:10.1038/s41401-021-00781-7

Liu, C., Li, Y. Y., Chen, Y. P., Huang, S. W., Wang, X. J., Luo, S., et al. (2020a). Baicalein restores the balance of Th17/Treg cells via aryl hydrocarbon receptor to attenuate colitis. *Mediat. Inflamm.* 2020, 5918587. doi:10.1155/2020/5918587

Liu, L. L., Geng, X. J., Zhang, J. Y., Li, S. H., and Gao, J. (2022). Structure-based discovery of Licoflavone B and Ginkgetin targeting c-Myc G-quadruplex to suppress c-Myc transcription and myeloma growth. *Chem. Biol. Drug Des.* 100 (4), 525–533. doi:10.1111/cbdd.14064

Liu, Q., Zuo, R., Wang, K., Nong, F. F., Fu, Y. J., Huang, S. W., et al. (2020b). Oroxindin inhibits macrophage NLRP3 inflammasome activation in DSS-induced ulcerative colitis in mice via suppressing TXNIP-dependent NF-kappa B pathway. *Acta Pharmacol. Sin.* 41 (6), 771–781. doi:10.1038/s41401-019-0335-4

Liu, X. F., and Zhu, H. Q. (2022). Curcumin improved intestinal epithelial barrier integrity by up-regulating ZO-1/Occludin/Claudin-1 in septic rats. *Evid. Based Compl. Alt. Med.* 2022, 2884522. doi:10.1155/2022/2884522

Luo, X. P., Yu, Z. L., Deng, C., Zhang, J. J., Ren, G. Y., Sun, A. N., et al. (2017). Baicalein ameliorates TNBS-induced colitis by suppressing TLR4/MyD88 signaling cascade and NLRP3 inflammasome activation in mice. *Sci. Rep.* 7, 16374. doi:10.1038/s41598-017-12562-6

Lv, Q., Xing, Y., Liu, J., Dong, D., Liu, Y., Qiao, H. Z., et al. (2021). Lonicerin targets EZH2 to alleviate ulcerative colitis by autophagy-mediated NLRP3 inflammasome inactivation. *Acta Pharm. Sin. B* 11 (9), 2880–2899. doi:10.1016/j.apsb.2021.03.011

Ma, H. M., Zhou, M. J., Duan, W. B., Chen, L. Y., Wang, L. L., and Liu, P. (2020). Anemoside B4 prevents acute ulcerative colitis through inhibiting of TLR4/NF-kappa

B/MAPK signaling pathway. *Int. Immunopharmacol.* 87, 106794. doi:10.1016/j.intimp.2020.106794

Mangan, M. S. J., Olhava, E. J., Roush, W. R., Seidel, H. M., Glick, G. D., and Latz, E. (2018). Targeting the NLRP3 inflammasome in inflammatory diseases. *Nat. Rev. Drug Discov.* 17 (8), 588–606. doi:10.1038/nrd.2018.97

Marquez-Flores, Y. K., Villegas, I., Cardeno, A., Rosillo, M. A., and Alarcon-de-la-Lastra, C. (2016). Apigenin supplementation protects the development of dextran sulfate sodium induced murine experimental colitis by inhibiting canonical and non-canonical inflammasome signaling pathways. *J. Nutr. Biochem.* 30, 143–152. doi:10.1016/j.jnutbio.2015.12.002

Martinez-Lopez, A., Rivero-Pino, F., Villanueva, A., Toscano, R., Grao-Cruces, E., Marquez-Paradas, E., et al. (2022). Kiwicha (*Amaranthus caudatus* L) protein hydrolysates reduce intestinal inflammation by modulating the NLRP3 inflammasome pathway. *Food Funct.* 13 (22), 11604–11614. doi:10.1039/d2fo02177c

Mottaghipisheh, J., Taghrir, H., Dehsheikh, A. B., Zomorodian, K., Irajie, C., Sourestani, M. M., et al. (2021). Linarin, a glycosylated flavonoid, with potential therapeutic attributes: A comprehensive review. *Pharmaceuticals* 14 (11), 1104. doi:10.3390/ph14111104

Nabavi, S. F., Braidy, N., Gortzi, O., Sobarzo-Sanchez, E., Daglia, M., Skalicka-Wozniak, K., et al. (2015). Luteolin as an anti-inflammatory and neuroprotective agent: A brief review. *Brain Res. Bull.* 119 (1-11), 1–11. doi:10.1016/j.brainresbull.2015.09.002

Nageen, B., Sarfraz, I., Rasul, A., Hussain, G., Rukhsar, F., Irshad, S., et al. (2020). Eupatilin: A natural pharmacologically active flavone compound with its wide range applications. *J. Asian. Nat. Prod. Res.* 22 (1), 1–16. doi:10.1080/10286020.2018.1492565

Paik, S., Kim, J. K., Silwal, P., Sasakawa, C., and Jo, E. K. (2021). An update on the regulatory mechanisms of NLRP3 inflammasome activation. *Cell. Mol. Immunol.* 18 (5), 1141–1160. doi:10.1038/s41423-021-00670-3

Panagiotopoulos, A. A., Karakasiliotis, I., Kotzampasi, D. M., Dimitriou, M., Sourvinos, G., Kampa, M., et al. (2021). Natural polyphenols inhibit the dimerization of the SARS-CoV-2 main protease: The case of fortunellin and its structural analogs. *Molecules* 26 (19), 6068. doi:10.3390/molecules26196068

Patel, K., Gadewar, M., Tahilyani, V., and Patel, D. K. (2013). A review on pharmacological and analytical aspects of diosmetin: A concise report. *Chin. J. Integr. Med.* 19 (10), 792–800. doi:10.1007/s11655-013-1595-3

Qin, Y. T., Zhao, R. F., Qin, H., Chen, L., Chen, H. Q., Zhao, Y. L., et al. (2021). Colonic mucus-accumulating tungsten oxide nanoparticles improve the colitis therapy by targeting Enterobacteriaceae. *Nano Today* 39, 101234. doi:10.1016/j.nantod.2021.101234

Qiu, J. M., Qin, C. F., Wu, S. G., Ji, T. Y., Tang, G. T., Lei, X. Y., et al. (2021). A novel salvianolic acid A analog with resveratrol structure and its antioxidant activities *in vitro* and *in vivo*. *Drug Dev. Res.* 82 (1), 108–114. doi:10.1002/ddr.21734

Ren, J., Yue, B., Wang, H., Zhang, B., Dou, W., Yu, Z., et al. (2021). Acacetin ameliorates experimental colitis in mice via inhibiting macrophage inflammatory response and regulating the composition of gut microbiota. *Front. Physiol.* 11, 577237. doi:10.3389/fphys.2020.577237

Sajeev, A., Hegde, M., Daimary, U. D., Kumar, A., Girisa, S., Sethi, G., et al. (2022a). Modulation of diverse oncogenic signaling pathways by oroxylin A: An important strategy for both cancer prevention and treatment. *Phytomedicine* 105, 154369. doi:10.1016/j.phymed.2022.154369

Sajeev, A., Hegde, M., Girisa, S., Devanarayanan, T. N., Alqahtani, M. S., Abbas, M., et al. (2022b). Oroxylin A: A promising flavonoid for prevention and treatment of chronic diseases. *Biomolecules* 12 (9), 1185. doi:10.3390/biom12091185

Salehi, B., Venditti, A., Sharifi-Rad, M., Kregiel, D., Sharifi-Rad, J., Durazzo, A., et al. (2019). The therapeutic potential of apigenin. *Int. J. Mol. Sci.* 20 (6), 1305. doi:10.3390/ijms20061305

Sapkota, A., Gaire, B. P., Cho, K. S., Jeon, S. J., Kwon, O. W., Jang, D. S., et al. (2017). Eupatilin exerts neuroprotective effects in mice with transient focal cerebral ischemia by reducing microglial activation. *PloS One* 12 (2), e0171479. doi:10.1371/journal.pone.0171479

Saraiva, A. L., Vieira, T. N., Notario, A. F. O., Luiz, J. P. M., Silva, C. R., Goulart, L. R., et al. (2022). CdSe magic-sized quantum dots attenuate reactive oxygen species generated by neutrophils and macrophages with implications in experimental arthritis. *Nanomed. Nanotechnol. Biol. Med.* 42, 102539. doi:10.1016/j.nano.2022.102539

Shalini, V., Pushpan, C. K., Sindhu, G., Jayalekshmy, A., and Helen, A. (2016). Tricin, flavonoid from Njavara reduces inflammatory responses in hPBMCs by modulating the p38MAPK and PI3K/Akt pathways and prevents inflammation associated endothelial dysfunction in HUVECs. *Immunobiology* 221 (2), 137–144. doi:10.1016/j.imbio.2015.09.016

Shalkami, A. S., Hassan, M., and Bakr, A. G. (2018). Anti-inflammatory, antioxidant and anti-apoptotic activity of diosmin in acetic acid-induced ulcerative colitis. *Hum. Exp. Toxicol.* 37 (1), 78–86. doi:10.1177/0960327117694075

Shen, J., Cheng, J. Z., Zhu, S. G., Zhao, J., Ye, Q. Y., Xu, Y. Y., et al. (2019). Regulating effect of baicalin on IKK/IKB/NF-kB signaling pathway and apoptosis-related proteins

in rats with ulcerative colitis. *Int. Immunopharmacol.* 73, 193–200. doi:10.1016/j.intimp.2019.04.052

Singh, S., Gupta, P., Meena, A., and Luqman, S. (2020). Acacetin, a flavone with diverse therapeutic potential in cancer, inflammation, infections and other metabolic disorders. *Food Chem. Toxicol.* 145, 111708. doi:10.1016/j.fct.2020.111708

Sinopoulou, V., Gordon, M., Dovey, T. M., and Akobeng, A. K. (2021). Interventions for the management of abdominal pain in ulcerative colitis. *Cochrane Database Syst. Rev.* 7, CD013589. doi:10.1002/14651858.CD013589.pub2

Song, J. K., Zhang, L., Xu, Y. F., Yang, D. Z., Zhang, L., Yang, S. Y., et al. (2021). The comprehensive study on the therapeutic effects of baicalein for the treatment of COVID-19 *in vivo* and *in vitro*. *Biochem. Pharmacol.* 183, 114302. doi:10.1016/j.bcp.2020.114302

Suga, N., Murakami, A., Arimitsu, H., Nakamura, T., Nakamura, Y., and Kato, Y. (2021). Luteolin suppresses 5-hydroxytryptamine elevation in stimulated RBL-2H3 cells and experimental colitis mice. *J. Clin. Biochem. Nutr.* 69 (1), 20–27. doi:10.3164/jcbn.20-192

Sun, Y., Zhao, Y., Yao, J., Zhao, L., Wu, Z. Q., Wang, Y., et al. (2015). Wogonoside protects against dextran sulfate sodium-induced experimental colitis in mice by inhibiting NF-kappa B and NLRP3 inflammasome activation. *Biochem. Pharmacol.* 94 (2), 142–154. doi:10.1016/j.bcp.2015.02.002

Venegas, D. P., De la Fuente, M. K., Landskron, G., Gonzalez, M. J., Quera, R., Dijkstra, G., et al. (2019). Short chain fatty acids (SCFAs)-mediated gut epithelial and immune regulation and its relevance for inflammatory bowel diseases. *Front. Immunol.* 10, 277. doi:10.3389/fimmu.2019.00277

Vukelic, I., Detel, D., Baticic, L., Potocnjak, I., and Domitrovic, R. (2020). Luteolin ameliorates experimental colitis in mice through ERK-mediated suppression of inflammation, apoptosis and autophagy. *Food Chem. Toxicol.* 145, 111680. doi:10.1016/j.fct.2020.111680

Wang, C., Wei, S. Y., Liu, B. J., Wang, F. Q., Lu, Z. Q., Jin, M. L., et al. (2022). Maternal consumption of a fermented diet protects offspring against intestinal inflammation by regulating the gut microbiota. *Gut Microbes* 14 (1), 2057779. doi:10.1080/19490976.2022.2057779

Wang, T., Wang, P. P., Ge, W. P., Shi, C., Xiao, G. N., Wang, X., et al. (2021). Protective effect of a multi-strain probiotics mixture on azoxymethane/dextran sulfate sodium-induced colon carcinogenesis. *Food Biosci.* 44, 101346. doi:10.1016/j.fbio.2021.101346

Wei, S. C., Sollano, J., Hui, Y. T., Yu, W., Estrella, P. V. S., Llamado, L. J. Q., et al. (2021). Epidemiology, burden of disease, and unmet needs in the treatment of ulcerative colitis in Asia. *Expert Rev. Gastroenterol. Hepatol.* 15 (3), 275–289. doi:10.1080/17474124.2021.1840976

Wojcik-Grzybek, D., Hubalewska-Mazgaj, M., Surmiak, M., Sliwowski, Z., Dobrut, A., Mlodzinska, A., et al. (2022). The combination of intestinal alkaline phosphatase treatment with moderate physical activity alleviates the severity of experimental colitis in obese mice via modulation of gut microbiota, attenuation of proinflammatory cytokines, oxidative stress biomarkers and DNA oxidative damage in colonic mucosa. *Int. J. Mol. Sci.* 23 (6), 2964. doi:10.3390/ijms23062964

Wu, S. M., Wang, P., Qin, J. W., Pei, Y. B., and Wang, Y. L. (2021). GSH-depleted nanozymes with dual-radicals enzyme activities for tumor synergic therapy. *Adv. Funct. Mat.* 31 (31), 2102160. doi:10.1002/adfm.202102160

Wu, W. Y., Li, Y. D., Cui, Y. K., Wu, C., Hong, Y. X., Li, G., et al. (2018). The natural flavone acacetin confers cardiomyocyte protection against hypoxia/reoxygenation injury via AMPK-mediated activation of Nrf2 signaling pathway. *Front. Pharmacol.* 9, 497. doi:10.3389/fphar.2018.00497

Wu, X., Zhang, H. J., Salmani, J. M. M., Fu, R., and Chen, B. A. (2016). Advances of wogonin, an extract from *Scutellaria baicalensis*, for the treatment of multiple tumors. *OncoTargets Ther.* 9, 2935–2943. doi:10.2147/OTT.S105586

Xiong, Y. J., Chen, D. P., Yu, C. C., Lv, B. C., Peng, J. Y., Wang, J. Y., et al. (2015). Citrus nobiletin ameliorates experimental colitis by reducing inflammation and restoring impaired intestinal barrier function. *Mol. Nutr. Food Res.* 59 (5), 829–842. doi:10.1002/mnfr.201400614

Xiong, Y. J., Deng, Z. B., Liu, J. N., Qiu, J. J., Guo, L., Feng, P. P., et al. (2019). Enhancement of epithelial cell autophagy induced by sinensetin alleviates epithelial barrier dysfunction in colitis. *Pharmacol. Res.* 148, 104461. doi:10.1016/j.phrs.2019.104461

Xiong, Y. J., Qiu, J. J., Li, C. Y., Qiu, Y., Guo, L., Liu, Y. J., et al. (2018). Fortunellin-induced modulation of phosphatase and tensin homolog by microRNA-374a decreases inflammation and maintains intestinal barrier function in colitis. *Front. Immunol.* 9, 83. doi:10.3389/fimmu.2018.00083

Xu, Z. R., Li, K., Pan, T. W., Liu, J., Li, B., Li, C. X., et al. (2019). Lonicerin, an anti-algE flavonoid against *Pseudomonas aeruginosa* virulence screened from Shuanghuanglian formula by molecule docking based strategy. *J. Ethnopharmacol.* 239, 111909. doi:10.1016/j.jep.2019.111909

Yao, J., Liu, T., Chen, R. J., Liang, J., Li, J., and Wang, C. G. (2020). Sphingosine-1-phosphate signal transducer and activator of transcription 3 signaling pathway contributes to baicalein-mediated inhibition of dextran sulfate sodium-induced experimental colitis in mice. *Chin. Med. J.* 133 (3), 292–300. doi:10.1097/CM9.0000000000000627

Yin, S. J., Yang, H. F., Tao, Y., Wei, S. M., Li, L. H., Liu, M. J., et al. (2020). Artesunate ameliorates DSS-induced ulcerative colitis by protecting intestinal barrier and inhibiting inflammatory response. *Inflammation* 43 (2), 765–776. doi:10.1007/s10753-019-01164-1

Yu, C. G., Lv, Y. J., Li, X. D., Bao, H. Y., Cao, X. L., Huang, J., et al. (2023). SOD-Functionalized gold nanoparticles as ROS scavenger and CT contrast agent for protection and imaging tracking of mesenchymal stem cells in Idiopathic pulmonary fibrosis treatment. *Chem. Eng. J.* 459, 141603. doi:10.1016/j.cej.2023.141603

Yu, X. Y., and Liu, Y. (2021). Diosmetin attenuate experimental ulcerative colitis in rats via suppression of NF-kappa B, TNF-alpha and IL-6 signalling pathways correlated with down-regulation of apoptotic events. *Eur. J. Inflamm.* 19, 205873922110672. doi:10.1177/20587392211067292

Zeng, J., Wang, Z., and Yang, X. J. (2022). Factors predicting clinical and endoscopic remission with placebo therapy in east asian patients with ulcerative colitis: A systematic review and meta-analysis. *Eur. J. Clin. Pharmacol.* 78 (7), 1069–1077. doi:10.1007/s00228-022-03312-3

Zhang, C. L., Zhang, S., He, W. X., Lu, J. L., Xu, Y. J., Yang, J. Y., et al. (2017). Baicalin may alleviate inflammatory infiltration in dextran sodium sulfate-induced chronic ulcerative colitis via inhibiting IL-33 expression. *Life Sci.* 186, 125–132. doi:10.1016/j.lfs.2017.08.010

Zhang, G. W., Wang, L., and Pan, J. H. (2012). Probing the binding of the flavonoid diosmetin to human serum albumin by multispectroscopic techniques. *J. Agr. Food Chem.* 60 (10), 2721–2729. doi:10.1021/jf205260g

Zhang, J., Xu, X. Q., Li, N., Cao, L., Sun, Y., Wang, J. C., et al. (2022). Licoflavone B, an isoprene flavonoid derived from licorice residue, relieves dextran sodium sulfate-induced ulcerative colitis by rebuilding the gut barrier and regulating intestinal microflora. *Eur. J. Pharmacol.* 916, 174730. doi:10.1016/j.ejphar.2021.174730

Zhang, M., Hao, X. N., Aziz, T., Zhang, J., and Yang, Z. N. (2020). Exopolysaccharides from *Lactobacillus plantarum* YW11 improve immune response and ameliorate inflammatory bowel disease symptoms. *Acta Biochim. Pol.* 67 (4), 485–493. doi:10.18388/abp.2020_5171

Zhao, C. H., Zhang, Y., Liu, H. Y., Li, P., Zhang, H., and Cheng, G. C. (2017). Fortunellin protects against high fructose-induced diabetic heart injury in mice by suppressing inflammation and oxidative stress via AMPK/Nrf-2 pathway regulation. *Biochem. Biophys. Res. Commun.* 490 (2), 552–559. doi:10.1016/j.bbrc.2017.06.076

Zhao, J. M., Xu, J. X., Zhang, Z. Q., Shao, Z. T., and Meng, D. L. (2022). Barrigenol-like triterpenoid saponins from the husks of Xanthoceras sorbifolia bunge and their anti-inflammatory activity by inhibiting COX-2 and iNOS expression. *Phytochemistry* 204, 113430. doi:10.1016/j.phytochem.2022.113430

Zhao, L., Chen, Z., Zhao, Q., Wang, D. D., Guo, Q. L., You, Q., et al. (2011). Developmental toxicity and genotoxicity studies of wogonin. *Regul. Toxicol. Pharmacol.* 60 (2), 212–217. doi:10.1016/j.yrtph.2011.03.008

Zheng, Y., Zhang, R., Shi, W., Li, L., Wu, L., Chen, Z., et al. (2020). Metabolism and pharmacological activities of the natural health-benefiting compound diosmin. *Food Funct.* 11 (10), 8472–8492. doi:10.1039/d0fo01598a

Zhong, X. C., Surh, Y. J., Do, S. G., Shin, E., Shim, K. S., Lee, C. K., et al. (2019). Baicalein inhibits dextran sulfate sodium-induced mouse colitis. *J. Cancer Prev.* 24 (2), 129–138. doi:10.15430/JCP.2019.24.2.129

Zhou, K., Cheng, R., Liu, B., Wang, L., Xie, H. F., and Zhang, C. F. (2018). Eupatilin ameliorates dextran sulphate sodium-induced colitis in mice partly through promoting AMPK activation. *Phytomedicine* 46, 46–56. doi:10.1016/j.phymed.2018.04.033

Zhou, W., Liu, X. T., Zhang, X., Tang, J. J., Li, Z. Y., Wang, Q., et al. (2017). Oroxylin A inhibits colitis by inactivating NLRP3 inflammasome. *Oncotarget* 8 (35), 58903–58917. doi:10.18632/oncotarget.19440

Zhou, Y. D., Dou, F. F., Song, H. W., and Liu, T. (2022). Anti-ulcerative effects of wogonin on ulcerative colitis induced by dextran sulfate sodium via Nrf2/TLR4/NF-kappa B signaling pathway in BALB/c mice. *Environ. Toxicol.* 37 (4), 954–963. doi:10.1002/tox.23457

Zhou, Y. F., Tu, Y. Y., Zhou, Q., Hua, A. L., Geng, P. W., Chen, F. F., et al. (2020). Evaluation of acacetin inhibition potential against cytochrome P450 *in vitro* and *in vivo*. *Chem. Biol. Interact.* 329, 109147. doi:10.1016/j.cbi.2020.109147

Zhu, L., Shen, H., Gu, P. Q., Liu, Y. J., Zhang, L., and Cheng, J. F. (2020a). Baicalin alleviates TNBS-induced colitis by inhibiting PI3K/AKT pathway activation. *Exp. Ther. Med.* 20 (1), 581–590. doi:10.3892/etm.2020.8718

Zhu, L., Xu, L. Z., Zhao, S., Shen, Z. F., Shen, H., and Zhan, L. B. (2020b). Protective effect of baicalin on the regulation of Treg/Th17 balance, gut microbiota and short-chain fatty acids in rats with ulcerative colitis. *Appl. Microbiol. Biotechnol.* 104 (12), 5449–5460. doi:10.1007/s00253-020-10527-w

Zhuang, H. D., Lv, Q., Zhong, C., Cui, Y. R., He, L. L., Zhang, C., et al. (2021). Tiliroside ameliorates ulcerative colitis by restoring the M1/M2 macrophage balance via the HIF-1α/glycolysis pathway. *Front. Immunol.* 12, 649463. doi:10.3389/fimmu.2021.649463

Zuo, T., Yue, Y. Z., Wang, X. H., Li, H., and Yan, S. A. (2021). Luteolin relieved DSS-induced colitis in mice via HMGB1-TLR-NF-kappa B signaling pathway. *Inflammation* 44 (2), 570–579. doi:10.1007/s10753-020-01354-2

Glossary

AA	acetic acid
Akt	protein kinase B
AMPK	AMP-activated protein kinase
Bcl-2	B-cell lymphoma 2
BMDMs	bone marrow-derived macrophages
CAT	catalase
Cl	cleaved
COX-2	cyclooxygenase 2
DAI	disease activity index
DCs	dendritic cells
DSS	dextran sodium sulfate
ERK	extracellular signal-regulated protein kinase
EZH2	enhancer of zeste homolog 2
Foxp3	forkhead box P3
GSH	glutathione
GSK-3β	glycogen synthase kinase-3β
GST	glutathione S-transferase
HMGB1	high mobility group box protein 1
HO-1	heme oxygenase-1
ICAM-1	intercellular adhesion molecule-1
IκBα	inhibitor kappa B alpha
IL	interleukin
iNOS	inducible nitric oxide synthase
IRAK1	interleukin 1 receptor associated kinase 1
LPS	lipopolysaccharide
MAPK	Mitogen activated protein kinases
MCP-1	monocyte chemotactic protein-1
MD-2	myeloid diferentiation protein-2
MDR1	multidrug resistance 1
MIP	macrophage inflammatory protein
MLCK	myosin light chain kinase
MMP	matrix metalloproteinases
MPO	myeloperoxidase

NF-κB	nuclear transcription factor κB
NLRP3	NOD-like receptor 3
NO	nitric oxide
NOD2	nucleotidebinding oligomerization domain 2
NOX4	NADPH oxidases 4
NQO-1	NADP(H):quinone oxidoreductase 1
Nrf2	nuclear factor-erythroid 2-related factor 2
PGE2	prostaglandin E2
PPAR-γ	peroxisome proliferator-activated receptor γ
p-STAT3	phosphorylated signal transducer and activator of transcription 3
PTEN	phosphatase and tensin homolog
PXR	pregnane x receptor
ROS	reactive oxygen species
RORγt	tretinoic-acid-receptor-related orphan nuclear receptor gamma t
SCFAs	short-chain fatty acids
SHP-1	SH2-containing protein tyrosine phosphatase-1
SOD	superoxide dismutase
SphK1	sphingosine kinase 1
S1PR1	sphingosine 1-phosphate receptor 1
TAK1	transforming growth factor beta activated kinase 1
TBARS	thiobarbituric acid reactive substances
TEER	transepithelial electrical resistance
TGF	transforming growth factor
TJ	tight junction
TJP1	tight junction protein 1
TLR4	toll-like receptor 4
TNBS	24,6-trinitrobenzene sulfonic acid
TNF	tumor necrosis factor
Treg	regulatory T cell
TXNIP	thioredoxin-interacting protein
UC	ulcerative colitis
ULK1	UNC-51 like autophagy activating kinase 1
JNK	c-Jun N-terminal kinases

Check for updates

A sustained-release phospholipid-based phase separation gel loaded with berberine for treating rheumatoid arthritis

Xiong Peng[1], Yuping Yang[1], Chenqi Guo[1], Qin He[1], Yan Li[2], Tao Gong[1] and Jia Li[3]*

[1]Key Laboratory of Drug-Targeting and Drug Delivery System of the Education Ministry and Sichuan Province, Sichuan Engineering Laboratory for Plant-Sourced Drug and Sichuan Research Center for Drug Precision Industrial Technology, West China School of Pharmacy, Sichuan University, Chengdu, China, [2]Sichuan Institute for Drug Control, NMPA Key Laboratory for Quality Control and Evaluation of Vaccines and Biological Products, Chengdu, China, [3]National Clinical Research Center for Oral Diseases, West China Hospital of Stomatology, Sichuan University, Chengdu, China

Berberine (BBR) has a long history of use in the treatment of Rheumatoid arthritis (RA) and is considered one of the most promising natural product for the treatment of RA. However, oral administration of berberine has low bioavailability and requires frequent administration, resulting in poor patient compliance. In this study, we developed a BBR-loaded phospholipid-based phase separation gel (BBR-PPSG) to achieve sustained drug release and long-term therapeutic effect. The stability of BBR-PPSG was verified and it was found that it can be stored for a long time. The pharmacokinetic study on rats and rabbits showed that BBR-PPSG not only achieved 1-month of sustained release, but also significantly increased the area under the curve (AUC) by nearly 9-fold and prolonged the half-life ($t_{1/2}$) by 10-fold. By constructing rat and rabbit models of RA, we also proved that BBR-PPSG administration once a month effectively alleviated joint swelling, and significantly reduce TNF-α levels in AIA rats and OIA rabbits. Histopathological analysis of rabbit joint sections revealed that after intra-articular injection of BBR-PPSG, the synovial cell layer remained intact, while in the model group, the synovial cells were significantly reduced and exhibited necrosis. MicroCT data analysis showed that the values of Tb.N and Tb. Sp in the BBR-PPSG group were significantly better than those in the model group ($p < 0.05$). This study addressed the limitations of frequent administration of BBR by developing a phospholipid-based phase separation gel system for berberine delivery, achieving long-term sustained release. The BBR-PPSG demonstrated good biocompatibility, simple preparation and excellent stability, thus holding potential as a novel pharmaceutical formulation for RA treatment.

1 Introduction

Rheumatoid arthritis (RA) is a systemic immune disease characterized by chronic inflammation of joint tissues, and its primary target is synovial tissues and articular cartilage. It can affect people of all races, regions, and ages worldwide, with a global overall prevalence of approximately 1%, being more common in the age range of 40–50 years (van der Horst-Bruinsma et al., 2009; Smolen et al., 2016; Wang K. et al., 2017). The main clinical symptoms were arthrocele, dysarthrose, pain and poor flexion and extension. As the disease progresses, it can lead to synovitis with cartilage and bone destruction. In severe cases, patients can suffer joint functional disability, organ failure and even death. It not only seriously affects the quality of life, but also causes some patients to lose their ability to work for 10 years, becoming the biggest killer of physical disability (Gwinnutt et al., 2022). Unfortunately, the pathogenesis of rheumatoid arthritis is still unclear. Presumably, it may be related to such factors as immunity, gene, environment, and infection (Yu et al., 2013). Rheumatoid factor (RF) is one of the important serum criteria for the diagnosis of rheumatoid arthritis, and its positive rate in rheumatoid arthritis is about 80% (Wu et al., 2021). In RA inflammatory state, various pathophysiological changes of RA are mediated by secretion of various pro-inflammatory cytokines (TNF-α, IL-1β, IL-17 and IL-23) and chemokines (RANKL, GM-CSF and MMPs). TNF-α and IL-1β are the major cytokines in RA synovium (Rockel and Kapoor, 2016; Asif et al., 2017). In addition, erythrocyte sedimentation rate increased significantly during the active phase of rheumatoid arthritis (Wasserman, 2011). RA cannot be cured completely so far. Clinical treatment mainly aims to relieve inflammation and control the development of the disease. Long-term oral or intra-articular injection is usually used.

Berberine (BBR), an isoquinoline alkaloid extracted from Ranunculaceae plants such as Coptis chinensis, is widely sourced, easily extracted and broadly used in clinical treatment (Huang D. N. et al., 2021). Studies have showed that berberine has anti-inflammatory, antibacterial, hypoglycemia, antiarrhythmic and immunomodulatory effects, and with further research, more pharmacological effects have been discovered (Qiu et al., 2014; Zhang T. et al., 2015; Pozsgay et al., 2017). Berberine has been used in clinical treatment of RA for many years and is considered one of the most promising natural product derivative drugs for treating RA (Huang S. M. et al., 2021). In clinical practice, berberine is often used in combination with other anti-RA drugs to enhance efficacy and reduce adverse reactions. Clinical trials have shown that combined treatment with berberine and other anti-RA drugs increases the effective rate by about 15% and reduces adverse reactions by 7% compared with the non-berberine group (Wang et al., 2013). In recent years, many studies have been conducted to explore the mechanism of berberine's anti-RA effects. Berberine exerts therapeutic effects from multiple pathways and targets, including regulating immune response, inhibiting synovial hyperplasia, inhibiting angiogenesis, reducing bone erosion, and regulating gut microbiota (Huang D. N. et al., 2021).

Although increasing evidence suggests that BBR can combat RA both *in vivo* and *in vitro*, there are still some drawbacks to its clinical use. Berberine is usually formulated as regular tablets or capsules, which need to be taken three times a day for a long time (Liu et al., 2016). Frequent administration not only constrains patient compliance, but also presents limitations such as low bioavailability and gastrointestinal discomfort (Liu et al., 2010; Wang X. et al., 2017). Sustained-release formulations with fewer doses, good compliance, local administration, and reliable quality and safety are expected to become a long-term medication option for RA patients.

The phospholipid-based phase separation gel (PPSG) is a sustained-release drug delivery system developed by our research group. PPSG consists of ethanol, medium chain triglyceride and 70% (w/w) phospholipid (Zhang et al., 2019a; Zhang et al., 2020; Wang et al., 2016). *In vitro*, PPSG is a flowing liquid and the viscosity is affected by the proportion of prescription, which is about 165 to 500 cP (Zhang et al., 2019b; Han et al., 2016). After injection into the body, PPSG gradually semi-solidifies with the exchange of ethanol and body fluids and transforms into a gel that adheres to the tissue to become a "drug reservoir", slowly degrades in the body, and releases the drug into the injection area. In addition, PPSG can be degraded completely in about 1 month, avoiding the need for a second invasive surgery. PPSG is absorbable, and all raw materials are commonly used non-toxic reagents, so its side effects are also minimal (Zhang et al., 2019b).

Combined with previous studies, we intend to prepare berberine phospholipid-based phase separation gel (BBR-PPSG). It is expected that inject BBR-PPSG into the articular cavity can reduce the frequency of administration and systemic toxicity, improve bioavailability. Furthermore, the pharmacokinetic parameters and the comprehensive therapeutic effects of BBR-PPSG in different animal models of RA will be verified.

2 Materials and methods

2.1 Materials

Berberine Chloride Hydrate was purchased from Shanghai Aladdin Bio-Chem Technology Co., LTD. (Shanghai, China); Soyabean lecithin S100 was purchased from Lipoid Co. LTD. (Ludwigshafen, Germany); Injection-grade medium-chain triglyceride (MCT) was obtained from Beiya Medical Oil Co. Ltd. (Tieling, China); HPLC-grade Ethanol was purchased from Tianjin Kemiou Chemical Reagent Co., LTD. (Tianjin, China).

Enzyme-linked immunosorbent assay (ELISA) kits for detecting rat TNF-α and IL-1β levels were purchased from Ruixin Biotech Chengdu, China. ELISA kits to determine rabbits' TNF-α levels and RF were purchased from Signalway Antibody (MD, United States). Complete Freund's adjuvant (CFA, 1 mg/ml of heat-killed mycobacteria) was purchased from Sigma-Aldrich Chemical Co (Shang Hai, China). CFA (10 mg/ml) was purchased from Chondrex (Washington DC, United States). Ovalbumin (OVA) was procured from Sigma-Aldrich Chemical Co.

2.2 Experimental Animals

Male Sprague-Dawley rats (160–180 g) were raised in specific pathogen-free condition with a relative humidity of 55% (45%–70%), a 12-h light/dark cycle, and a standard temperature-controlled

environment (22°C ± 2°C). New Zealand rabbits (4-week-old, 1.8–2.0 kg) were raised in specific pathogen-free condition with a relative humidity of 65% (55%–70%), a 12-h light/dark cycle, and a standard temperature-controlled environment (20°C ± 5°C). All rabbits were allowed free access to standard food and water. All animals were obtained from Chengdu DaShuo Experimental Animal Co., Ltd. (Chengdu, China).

All animal protocols and experiments were carried out in accordance with the requirements of the National Act on the Use of Experimental Animals (China) and were approved by the Animal Ethics Committee of Sichuan University (SYXK-Chuan-2018–113).

2.3 Preparation of PPSG

Blank PPSG was prepared by simple magnetic stirring with S100, MCT and 85% ethanol at the ratio of 70:15:15 for 2 h. Then, berberine powder was added into the gel system, sealed, ultrasonic at 50°C for 10 min, and stirred for 5 min to form berberine phospholipid-based phase separation gel.

Preparation of berberine injection: Berberine hydrochloride was dissolved by DMSO, and then diluted with water to obtain berberine injection (BBR-I).

2.4 Stability of BBR-PPSG

The prepared BBR-PPSG was filled with nitrogen, sealed with gland and stored for 1 year at 4°C and 37°C respectively. BBR content was measured at the 1st, 3rd, 5th, 10th, 15th, 20th, 25th, 30th, 60th, 90th, 120th, 240th, and 360th days. The content of BBR was determined by HPLC on KromasilC18 column (4.6 × 250 mm, 5 μm) using 50 mL acetonitrile and 0.02 mol/L potassium dihydrogen phosphate solution (25:75) as mobile phase. The flow rate was 1.0 mL/min, column temperature was 25°C and detection wavelength was 424 nm.

2.5 Pharmacokinetics of BBR-PPSG

Healthy male SD rats were randomly divided into three groups (n = 6): BBR-I-O group (oral berberine injection), BBR-I-S group (subcutaneous injection of berberine injection), BBR-PPSG-S group (subcutaneous injection of berberine phospholipid-based phase separation gel). The concentration of BBR in both BBR-I and BBR-PPSG was 1 mg/ml, and each group was given a single dose of 1 ml. Each group was administered only once. 500μL of blood was collected by blood collection vessel at 0.5, 1, 2, 4, 8, 12 h, 1, 2, 3, 4, 8, 10, 15, 20, 25, 27, and 30 days after medication, then centrifuged immediately at 6000 rpm for 5 min. Plasma samples (100 μL) were collected and stored at −40°C. The plasma BBR concentration was determined by liquid chromatography mass spectrometry (LC-MS). The conditions for liquid chromatography were as follows: C18 column; methanol-water (containing 0.1% formic acid) (v/v) was mobile phase with gradient elution; the flow rate was 0.2 mL/min; the sample size was 10 μ; the column temperature was 25°C. The mass spectrum conditions were as follows: electrospray ion source (ESI); ion polarity; positive ion mode; multi-response

monitoring (MRM); Berberine [M + H] + m/z 337.2→291.1 was the target ion pair.

Healthy rabbits were randomly divided into two groups (n = 6): BBR-I-A group (intra-articular injection of BBR injection), BBR-PPSG-A (intra-articular injection of berberine phospholipid-based phase separation gel). The concentrations of BBR in BBR-I and BBR-PPSG were both 1 mg/ml. Each knee joint of the hind legs was administered once, 0.5 ml/joint. Plasma BBR concentration was measured at 0.25, 0.5, 1, 2, 4, 8, 12 h, 1, 2, 3, 5, 8, 10, 15, 21, and 25 days after medication. The collection and detection methods were consistent with those of rats.

2.6 Therapeutic effects of BBR-PPSG in rats

2.6.1 AIA rat model

As one of the most common animal models, adjuvant induced arthritis (AIA) rat models were widely used in the evaluation of anti-rheumatoid drugs and rheumatoid arthritis. Its clinical and histological features were similar to those of human rheumatoid arthritis (Whitehouse, 2007). The AIA rat model was established according to Gong's research (Gong et al., 2020). The model was induced by intradermal injection of CFA containing 10 mg/mL heat-killed mycobacteria into the two hind paws of rats respectively.

2.6.2 Groups

The AIA rats were randomly divided into 4 groups (n = 7): model group (subcutaneously injected normal saline, 1 ml/d, for 30 days), BBR-I-O group (oral BBR injection, 180 mg kg^{-1}·d^{-1}, 1 ml/d for 30 days), BBR-I-S group (subcutaneous injection of BBR injection, 4.896 mg kg^{-1}·d^{-1}, 1 ml/d for 30 days), and BBR-PPSG-S group (subcutaneous injection of BBR-PPSG solution, 146.88 mg/rat, 1 ml, only once). The BBR-PPSG-S group was injected only once on the back. 7 healthy rats were selected as controls. All 5 groups of rats were weighed at day 1, 4, 7, 10, 13, 16, 20, 25 and 30, and the thickness of their paws was measured with vernier calipers.

2.6.3 TNF-α and IL-1β level in serum

Blood Samples were collected by orbit on day 25. Serum samples were obtained by centrifuging at 5000 rpm for 8 min and stored at −80°C for use. Serum TNF- α and IL-1 β levels were measured by ELISA.

2.7 Therapeutic effects of BBR-PPSG in rabbits

2.7.1 OIA rabbit model

According to Dumonde's research, OVA was added to the rabbit RA model in order to improve RA symptoms in rabbits. The local joint inflammatory response was induced and maintained after multiple injections of OVA to ensure that the rabbit RA model was eligible for long-term sustained-release treatment of PPSG (Dumonde and Glynn, 1962). Oil induced arthritis (OIA) rabbit modeling involved two steps: OVA and CFA mixed emulsion was injected into the back of rabbits once a week for 2 weeks; Then the mixed emulsion was injected into the knee cavity once a week for 2 weeks. Blood

samples of rabbits were collected from auricular veins before and at 4 and 6 weeks after modeling to detect rheumatoid factor concentration.

2.7.2 Groups

After the establishment of OIA model, the rabbits were randomly divided into 3 groups (n = 6): model group (posterior knee joint cavities were injected with saline, 0.5 ml/joint, for 28 days), BBR-I-A group (posterior knee joint cavities were injected with BBR-I, 4.59 mg $kg^{-1} \cdot d^{-1}$, 0.5 ml/joint, for 28 days), and BBR-PPSG-A group (posterior knee joint cavities were injected with BBR-PPSG, 137.7 mg/joint, 0.5 ml/joint, only once). Seven healthy rabbits were included as control. The thickness of the knee joint was measured with a vernier caliper on the 1st, 3rd, 6th, 9th, 12th, 15th, 21st, and 28th days after administration.

2.7.3 Histopathological examination

Two days after the last administration of BBR injection to the knee joint, all rabbits were killed by air injection through the ear vein, and the muscle tissue around the knee joint and other tissues were taken for histological analysis. The tibia and femur about 3 cm above and below the patella were removed to obtain a complete knee joint cavity. The hind leg knee joints of each rabbit were fixed in 4% paraformaldehyde, decalcified in 15% (w ≤ v) ethylenediaminetetraacetic acid solution for 2 months, embedded in paraffin, and sliced to a thickness of about 5 μm. Finally, hematoxylin-eosin (HE) staining was used to prepare pathological tissues. The histopathological morphology of the knee joint was observed under an optical microscope (Olympus BX53, Tokyo, Japan).

2.7.4 TNF- α level and erythrocyte sedimentation rate

Rabbits' blood sample were collected from the auricular veins on day 28, centrifuged at 5000rpm for 8min to obtain serum, and then stored at −80°C for use. Serum TNF- α level was measured by ELISA kits, and erythrocyte sedimentation rate was determined by sedimentation tube.

2.7.5 Micro-CT analysis

Micro-CT (VivaCT 80, SCANCO Medical AG, Switzerland) was used to scan the knee joints of each group at 70 kV, 114 μA, 8 W, and 35 μm resolution. The dataset was reconstructed to obtain 3D images of the distal femur joints and trabeculae. Osseous function parameters included bone mineral density (BMD), bone volume to total volume ratio (BV/TV), bone surface area to bone volume ratio (BS/BV), trabecular number (Tb. N), trabecular thickness (Tb. Th), and trabecular separation (Tb. Sp). Three rabbits were randomly selected from each group, and the micro-CT analysis was performed on one hind leg knee joint of each rabbit.

2.8 Statistical analysis

Results were presented as mean ± standard deviation (SD). Pharmacokinetic parameters were calculated using nonlinear regression in Drug and Statistics software 2.0 (Mathematical Pharmacology Professional Committee of China, Shanghai,

China). All other statistical analyses were performed using GraphPad Prism 6.0 (GraphPad Software, CA, United States). Differences between two groups were assessed using Student's t-test; differences between multiple groups were assessed using one-way analysis of variance (ANOVA). Difference was considered statistically significant when p is less than 0.05.

3 Results

3.1 Preparation and characterization of BBR-PPSG

The preparation of BBR-PPSG is shown in Figure 1A. Briefly, BBR-PPSG was prepared by magnetic stirring. BBR was uniformly suspended in the gel system. Before the phase transition, the blank PPSG appeared as a transparent yellow solution with good fluidity (Figure 1B). It changed liquidity after losing ethanol. Due to the insolubility of BBR in ethanol, BBR-PPSG appeared as a yellow suspended solution. BBR-PPSG also lost fluidity during the evaporation of ethanol.

The stability experiment of BBR-PPSG (10 mg/ml) stored at 4°C and 37°C was observed. As shown in the Figure 1C, there was little change in concentration in both groups after 3 months, with a decrease in concentration of about 0.6%. One year later, the decrease was 2.9% at 4°C and only 5.0% at 37°C. Moreover, there was no sedimentation or stratification. The results show that BBR loading in phospholipid gel has good stability. The preservation of BBR-PPSG is not affected by temperature, and can be stored at room temperature and low temperature for a long time.

3.2 Pharmacokinetics

We have studied the release of BBR-PPSG as a long-term sustained release drug in rats and rabbits (Figures 2A, B). Among the three groups of rats, the blood drug concentration in BBR-I-S group was highest 30 min after administration, which subsequently decreased and was undetectable on the second day (Figure 2C). The BBR-I-O group had the lowest concentration among the three groups and failed to detect BBR after 48 h. The BBR-PPSG-S group had higher blood concentration than the other two groups after 24 h. BBR-PPSG was released continuously for 30 days, and the plasma BBR concentration at 20th days was close to that at 10th day and over 40 ng/ml at 30th days. Compared with the other two groups, the AUC and $t_{1/2}$ of BBR-PPSG-S group were significantly higher, while the T_{max} value was reduced (Table 1).

The pharmacokinetics results of rabbits were shown in Figure 2D. During the first 2 days, the plasma concentration curves of the two groups were very similar. However, after 2 days, the BBR concentration in BBR-PPSG-A group was significantly higher than that in BBR-I-A group. Moreover, BBR was still detectable in plasma up to 25 days in the BBR-PPSG-A group. Compared with BBR-I-A group, the BBR-PPSG-A group showed a markedly higher AUC and $t_{1/2}$ values (Table 2).

Poor bioavailability of berberine was seen in rats, consistent with previous studies. Berberine has extremely low water solubility, and oral administration is the main factor limiting
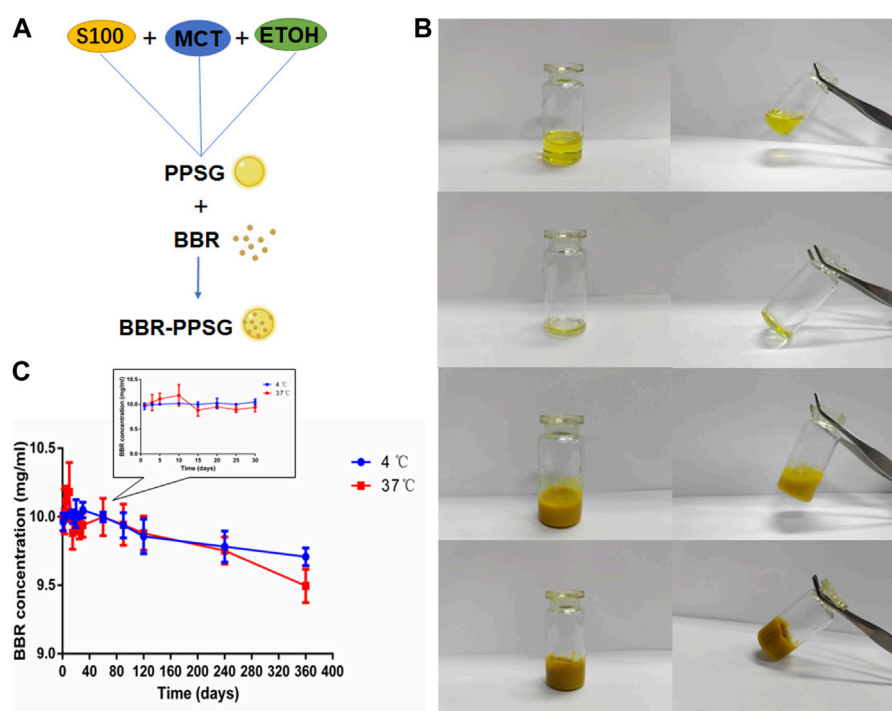
FIGURE 1
Preparation and characterization of BBR-PPSG. **(A)** Preparation of BBR-PPSG. **(B)** Photographs of PPSG and BBR-PPSG. **(C)** Stability of BBR-PPSG.
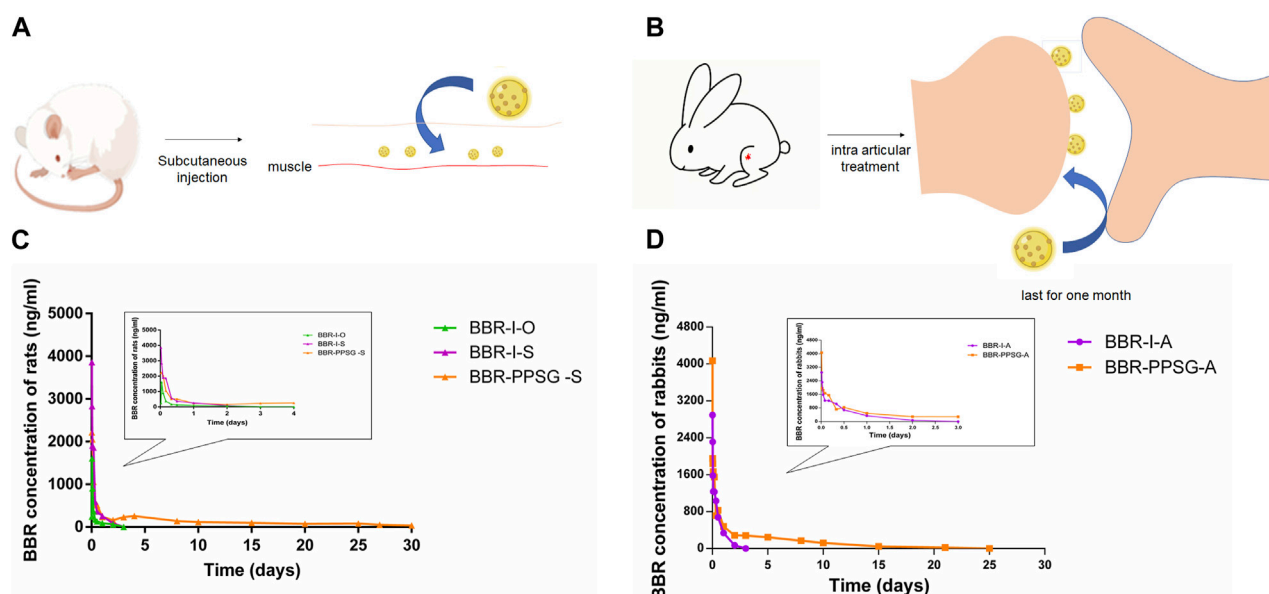
FIGURE 2
Pharmacokinetic results of BBR-PPSG in rats and rabbits. **(A)** Schematic diagram of subcutaneous injection in rats. **(B)** Schematic diagram of joint injection in rabbits. **(C)** Pharmacokinetic curve in rats (n = 6). **(D)** Pharmacokinetic curve in rabbits (n = 6).

its application (Feng et al., 2021). Berberine injection can improve the bioavailability to a certain extent, but the rapid metabolism after injection requires frequent administration. Preparing berberine as a sustained-release gel not only achieved 1-month sustained release but also greatly improved its bioavailability.

3.3 Therapeutic efficacy in rats

3.3.1 Model verification

Figure 3A shows the establishment of AIA rat model. The weight growth of rats in each group after administration was shown in Figure 3B. The weight of AIA rats increased slowly compared with

TABLE 1 Pharmacokinetic data of rats.

Parameter	BBR-I-O	BBR-I-S	BBR-PPSG-S
AUC $_{(0-t)}$ ng/L*h	7654.13 ± 638.47	23,451.97 ± 7387.07	94,679.83 ± 7280.92
$t_{1/2}$ h	19.4 ± 6.96	14.45 ± 0.52	215.87 ± 138.91
T_{max} h	1.00	1.40 ± 1.48	0.70 ± 0.27
C_{max} ng/L	1607.04 ± 221.91	5001.54 ± 1274.02	2425.81 ± 220.12

TABLE 2 Pharmacokinetic data of rabbits.

Parameter	BBR-I-A	BBR-PPSG-A
AUC $_{(0-t)}$ ng/L*h	24,810.21 ± 1990.16	87,734.04 ± 6819.04
$t_{1/2}$ h	11.15 ± 1.91	98.44 ± 14.71
T_{max} h	0.30 ± 0.11	0.25
C_{max} ng/L	3177.57 ± 943.79	4078.12 ± 1660.84

the health group, and there was no significant difference among the AIA groups. The thickness of paw is also more swollen in AIA rats, as shown in Figure 3C. Figure 3D showed the paw photos of rats in each group on the 25th days. AIA rats were more swollen than the healthy rats. On the 25th days, the TNF-α and IL-1β values of rats in AIA groups were significantly higher than those of healthy rats (Table 3). In terms of body weight, paw thickness and cytokine level, there were statistical differences between the model groups and the healthy group, indicating that the AIA rats' model was established successfully.

3.3.2 Efficacy evaluation

In terms of weight gain in rats, the body weight of the three medication groups was higher than that of the model group. There was no significant difference in body weight at day 25 among the three groups. Compared with the model group, the swelling degree of the paw in the three medication groups was lighter, and the comparison of data also had statistical differences, but there was no statistical difference among the three medication groups. In addition, compared with the model group, the cytokine levels in the three medication groups were also improved, and the values of TNF-α and IL-1β were statistically different between the BBR-PPSG-S group and the model group. There were statistical differences in TNF-α level between the BBR-PPSG-S group and the other two groups, while IL-1β values had no statistical difference.

In general, the treatment groups improved the RA status of rats, verifying the therapeutic effect of BBR on RA. Among the three medication groups, BBR-PPSG-S group had the heaviest body weight, the thinnest paw thickness, and the lowest TNF-α and IL-1β values. Except for TNF-α, there was no significant difference among the three groups. These results indicated that compared with daily continuous administration, BBR-PPSG not only achieved the goal of sustained release for nearly 1 month, but also had similar therapeutic effect to daily administration.

3.4 Therapeutic efficacy in rabbits

3.4.1 Validation of the OIA rabbit model

Figure 4A shows the histopathological results of rabbits in the model group. Joint surface defects, synovial hyperplasia, cellulose exudation, and bone tissue destruction were observed in OIA knee section of rabbit model. There was obvious inflammatory cell infiltration in lung tissue and individual inflammatory cell infiltration in liver tissue. The kidney sections showed flattened, detached, loose, and edematous renal tubular epithelial cells, with evident inflammatory cell infiltration. In addition to the obvious histopathological features, the concentration of rheumatoid factor (RF) also increased with the degree of arthritis (Figure 5B; 0 week: 0.97 ± 0.02 μg/ml, 4 weeks: 1.41 ± 0.10 μg/ml, 6 weeks: 1.91 ± 0.03 μg/ml). The above results indicate that the OIA rabbit model was successfully established.

3.4.2 Inflammation relief effect

The effect of berberine in each group was shown in Figure 5. At the end of treatment, the thickness of the knee joint in three groups were as follows: BBR-PPSG-A group < BBR-I-A group < model group (Figure 5A). Compared with the two treatment groups, the BCR-PPSG-A group had the lowest thickness during the study period, and there was no statistical difference between the two groups.

The increase of TNF-α level in the rheumatoid inflammatory microenvironment leads to the gradual increase of synovial hyperplasia fluid, resulting in synovial hyperplasia and articular cartilage destruction. TNF-α, as one of the criteria for the treatment of RA, is also considered one of the key indicators for the treatment of arthritis in advanced AIA rats and OIA rabbits. The TNF-α level of rabbits in each group was detected, and compared with the model group, the TNF-α level of rabbits in the two groups were significantly lower, with statistical differences. Although the lowest value was found in the BBR-PPSG-A group, there was no statistical difference between the two groups (Figure 5B). In comparison with the erythrocyte sedimentation rate of the model group, the two medication groups were lower, and only BBR-PPSG-A group and the model group had statistical differences. However, there was also a statistical difference between the two treatment groups, indicating that the effect of the BBR-PPSG-A group was superior to that of the BBR-I-A group (Figure 5C). The values of TNF-α and ESR in all treatment groups were lower than those in model group, indicating that inflammation was effectively controlled during treatment.

In order to further prove that BBR-PPSG can control inflammation and reduce cartilage destruction, rabbit knee joint sections were taken for HE staining at the end of the study to observe histopathological changes and inflammatory status. HE stained sections of the model group showed severe synovial hyperplasia, inflammatory synovial cell infiltration with bone and cartilage destruction, complete disappearance of some articular cartilage and bone tissue, and tendon fibrosis (Figures 5D, E). As marked with the triangle, few chondrocytes were found in the cartilage layer, where 6-8 layers of fibrocytes appeared instead, indicating fiber repair hyperplasia after chondrocyte necrosis. Trabecular collapse was pointed with arrows. The images showed that synovial inflammation and cartilage loss were significantly reduced in the
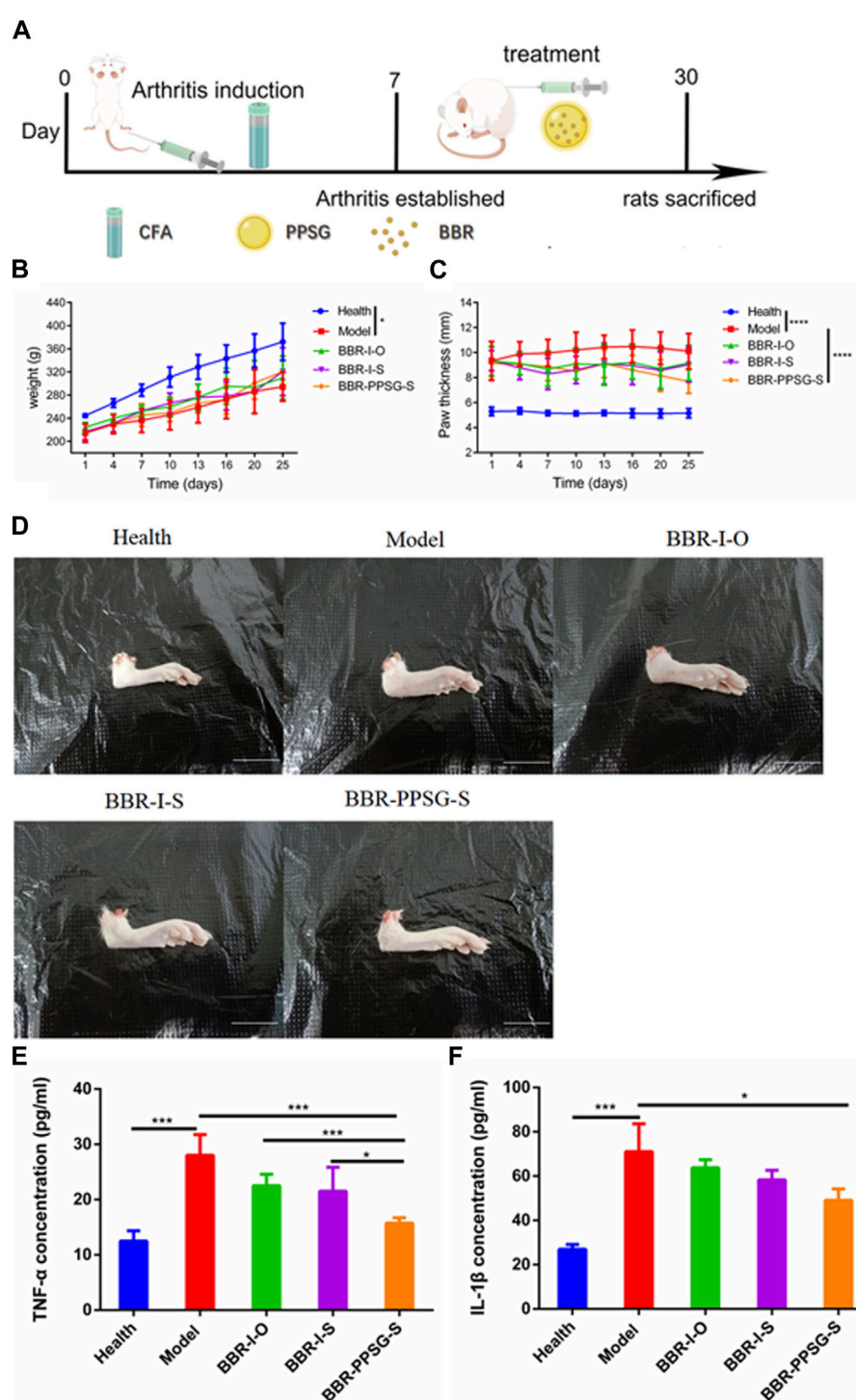
FIGURE 3
Evaluation of therapeutic effect on AIA rats' model. **(A)** Schematic diagram of arthritis induction and subcutaneous injection in rats. **(B)** Bodyweights of rats. **(C)** Paw thicknesses of rats. **(D)** Representative pictures of hind paw (Scale bar = 20 mm). **(E)** Serum levels of TNF-α. **(F)** Serum levels of IL-1β. Data represent mean ± SD (n = 7). *$p < 0.05$, **$p < 0.01$, ***$p < 0.001$, ****$p < 0.0001$.

treatment group compared to the model group, and the therapeutic effect was better in the BBR-PPSG-A group than in the BBR-I-A group (Figure 5E). Combined with Elisa results, it was not difficult to find that the inflammatory synovial microenvironment was gradually restored after BBR-PPSG-A treatment, and the cartilage injury was effectively reversed, with only mild synovial hyperplasia (Table 4). These results indicate that BBR-PPSG not only achieves the purpose of sustained release, but also has better therapeutic effect than BBR-I, effectively alleviating arthritic synovial inflammation and cartilage destruction in OIA rabbits.

TABLE 3 TNF-α and IL-1β values of rats in different groups.

	Health	Model	BBR-I-O	BBR-I-S	BBR-PPSG-S
TNF-α (pg/ml)	12.63 ± 2.00	28.22 ± 3.56	22.68 ± 2.00	21.95 ± 3.98	16.08 ± 1.25
IL-1β (pg/ml)	27.34 ± 1.96	71.69 ± 12.43	64.23 ± 3.67	59.01 ± 4.54	49.46 ± 5.15
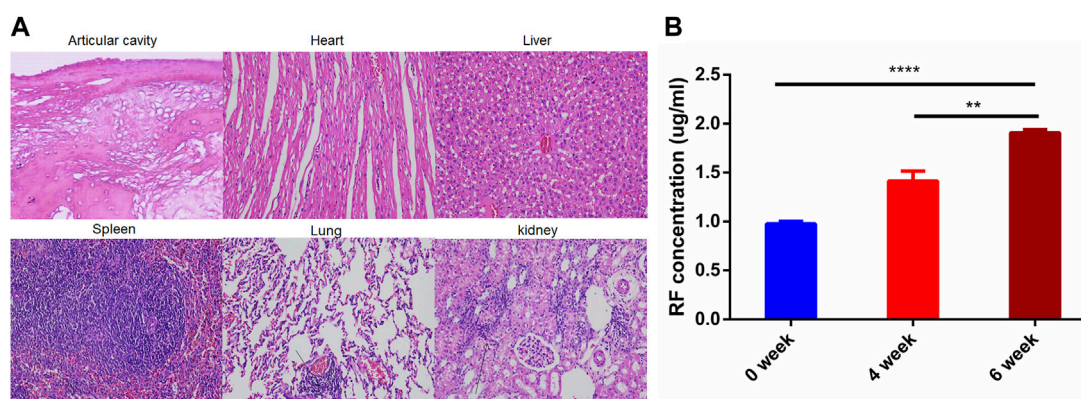
FIGURE 4
OIA Rabbit Model. **(A)** HE staining images of joint cavity, heart, liver, spleen, and kidney in OIA rabbits **(B)** RF concentration OIA rabbits. ****$p <$ 0.0001.

3.4.3 Bone preservation

Osteoporosis is widespread in RA patients because RA severely destroys osteoblasts and enhances bone resorption (Auréal et al., 2020; Berardi et al., 2021). BMD, BV/TV, BS/BV, Tb. N and Tb. SP are important indicators for evaluating bone function. To further demonstrate the protective effect of BH against RA, we used Micro CT as a supplementary test. Micro-CT imaging can accurately display lesion location and indicate the functional status of bone (Deng et al., 2021).

OIA rabbits showed significant bone erosion and significant decrease in bone density (Figure 6A). Micro CT analysis showed that knee inflammation in the model group on day 30 was characterized by rough bone surface and severe bone erosion. Bone tissue image reconstruction in the BBR-I-A and BBR-PPSG-A groups was superior to that in the model group, and the surface was smooth, indicating that the degree of bone erosion was reduced to a certain extent (Figure 6A). Among all the parameters of bone function, there were statistical differences between the model group and the healthy group, indicating the success of modeling. In terms of efficacy, the data in each group of BBR-PPSG-A were close to the healthy group, and were improved compared with the model group. The three groups had statistical differences, indicating that BBR-PPSG-A can alleviate the loss of bone function in late-stage inflammation. Compared with BBR-I-A, four parameters of BBR-PPSG-A were better than those of BBR-I-A, with a statistically significant difference in 1 group. Combined with the above-mentioned cytokine detection results, compared with continuous injection of berberine solution for 28 days, the gel group injected only once has a better overall effect in controlling rheumatoid joints and achieves long-term sustained release effect.

4 Discussion

Berberine possesses various pharmacological effects; however, it has limitations in terms of solubility, absorption and biological distribution. Studies have shown that the low bioavailability of BBR is mainly attributed to two factors: poor water solubility, which hinders gastrointestinal absorption, and extensive (Liu et al., 2010). Many studies have focused on improving the bioavailability of BBR by improving formulation or delivery systems. Some studies have prepared nano-scale BBR by reducing the size of BBR particles, thereby improving the solubility of BBR, enhancing the efficacy and reducing the adverse reactions (Wang et al., 2015; Xie et al., 2017; Sahibzada et al., 2018). Other studies have loaded BBR onto drug delivery systems. Yu loaded BBR onto polymer–lipid hybrid nanoparticles (PEG–lipid–PLGA NPs) to improve the efficiency of oral BBR administration. This compound enhanced the liposolubility of BBR, and increased its relative oral bioavailability by 343% compared to BBR alone (Yu et al., 2017). Zhang et al. (2014) prepared berberine-phospholipid complex using TPGS 1000 and SiO2 as carriers. The berberine-phospholipid complex exhibited higher solubility and dissolution rate. Significant improvements in C_{max} and $AUC_{0\rightarrow t}$ were obtained and the relative oral bioavailability was increased by 322.66% compared to BBR. Additionally, some studies have prepared
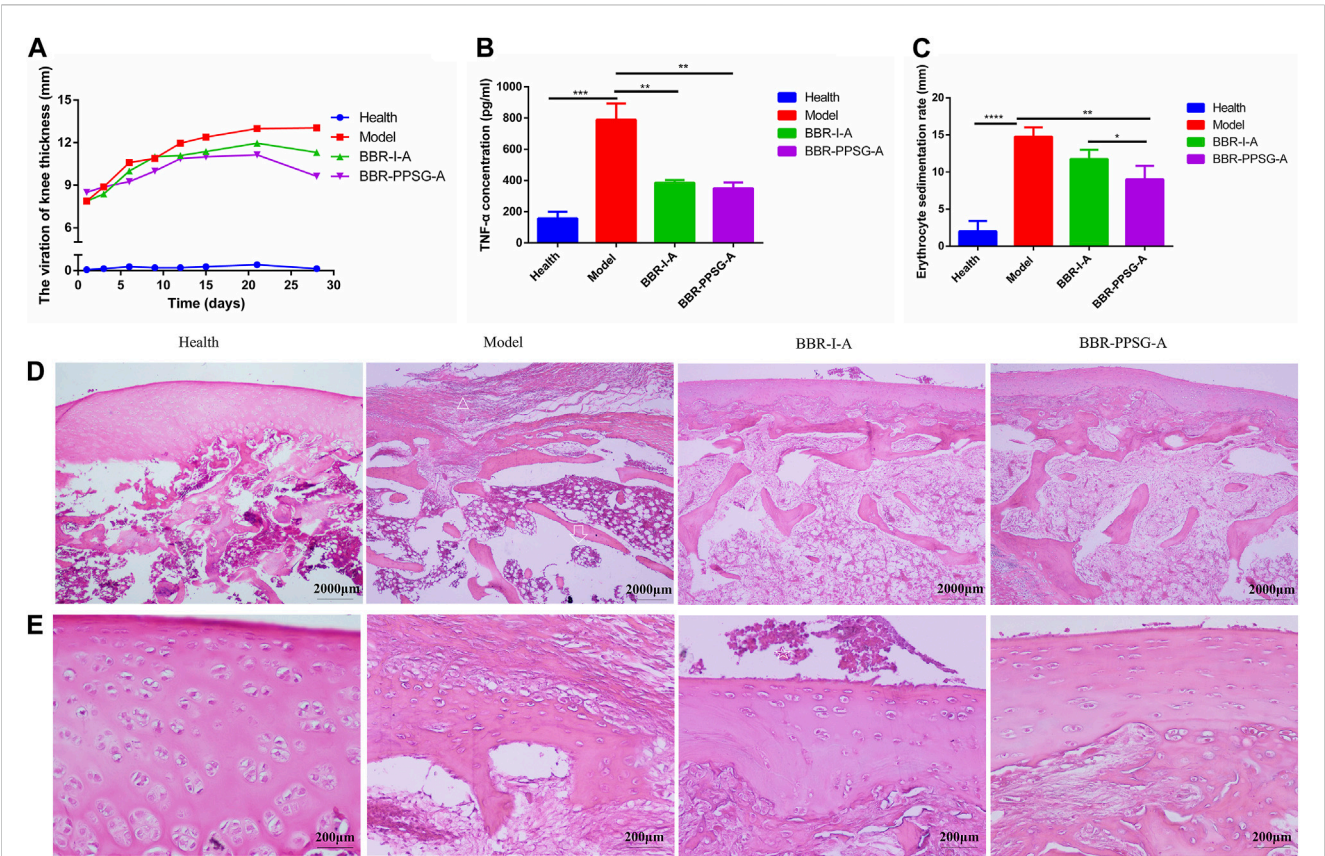
FIGURE 5
Evaluation of therapeutic effect on OIA rabbits. **(A)** Thickness of rabbit's knee joint. **(B)** TNF-α level in rabbit serum. **(C)** Erythrocyte sedimentation rate. **(D)** HE-stained pictures of knee joints (Scale bar = 50 μm) **(E)** HE-stained pictures of knee joints (Scale bar = 200 μm). Results are presented as mean ± SD (n = 6).

TABLE 4 TNF-α and ESR values of rabbits in different groups.

	Health	Model	BBR-I-A	BBR-PPSG-A
TNF-α (pg/ml)	156.37 ± 42.31	789.51 ± 105.07	385.24 ± 17.55	349.47 ± 36.86
ESR (mm)	1.76 ± 1.15	14.76 ± 1.08	11.80 ± 1.22	9.04 ± 1.59

berberine as liposomes to enhance absorption. Lin developed polyethylene glycol (PEG) berberine liposomes, which effectively reduced the clearance rate of berberine in both plasma and tissues (Lin et al., 2013). Nguyen et al. (2014) prepared chitosan-coated BBR nano-liposomes, which exhibited better stability and slower BBR release kinetics. The aforementioned studies have all demonstrated effective enhancement of bioavailability by reducing the size of BBR particles, delivering BBR with carriers, or preparing BBR liposomes. The BBR-loaded phospholipid-based phase separation gel developed in this study not only increased the AUC and prolonged the half-life, but also exhibited sustained release properties.

An appropriate animal models is the basis for research on rheumatoid arthritis, which is a serious autoimmune disease that mainly leads to the destruction and inflammation of local joint tissues (Allen et al., 2018; Schneider and Krüger, 2013). Animal

models of RA are usually induced by genetics, immunity, and environmental factors. In the process of induction, common methods include injecting substances such as anti-collagen, anti-DNA antibodies, lipopolysaccharides, bacteria and viruses to trigger abnormal response in the animal immune system, which could mimic the clinical symptoms and histopathology changes of human rheumatoid arthritis (Zhao et al., 2022). In animal research, mice, rats, rabbits, sheep, and other animals are often used (Yamashita et al., 2002; Abdalmula et al., 2014) In this study, rat and rabbit RA models were established respectively, in order to provide a more accurate theoretical and experimental basis for the prevention and treatment of rheumatoid arthritis.

The AIA rat model is widely used in the evaluation of antirheumatic drugs and rheumatoid arthritis, and its clinical and histological characteristics are similar to those of human rheumatoid arthritis, making it one of the most common animal models
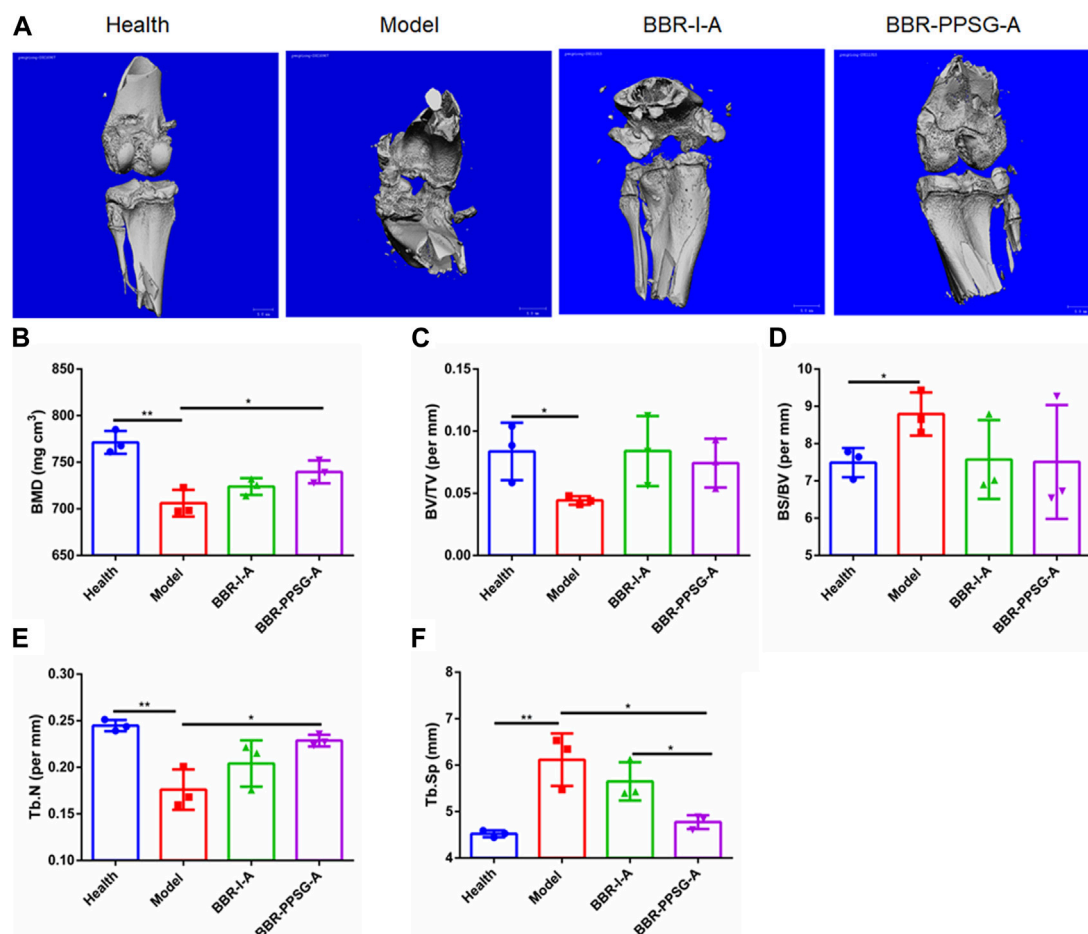
FIGURE 6
Bone function protection. **(A)** Micro-CT images of knee joints. **(B–F)** Quantitative micro-CT analysis of BMD, BV/TV, BS/BV, Tb. N, and Tb. Sp of the joints at the endpoint of the experiment. Data represent mean $\pm$ SD (n = 3).

(Bevaart, et al., 2010). Therefore, the AIA rat model was first established in this study. Compared with healthy rats, the rats in the model group showed joint swelling and increased serum inflammatory cytokines IL-1β and TNF-α, which indicated that the AIA rat model was successfully established. Although the success rate of AIA model building is high, the maintenance time is relatively short (Huang S. M. et al., 2021; Zhao et al., 2022). Moreover, considering the differences in pathophysiology among various animal models of Freund's adjuvant, including different morbidity, onset time and symptoms of arthritis, the rabbit RA model was included in our study, which was induced by OVA referring to Dumonde in 1962 (Dumonde and Glynn, 1962). Multiple subcutaneous injections of exogenous antigens promote the production of a large number of antibodies in the body, so that the antigens and antibodies are deposited in the synovium of the joint, activate the immune cells and complement system of the body, and eventually produce the antigen-antibody-complement immune complex, thus inducing local joint inflammation and joint swelling (Nandakumar, 2010).

This study first investigated the therapeutic effect of BBR-PPSG on RA rats. After confirming its favorable therapeutic effect on rheumatoid arthritis, BBR-PPSG was injected into the lesion site of

RA rabbits to visually investigate the pathological and physiological changes of the lesion site. The pharmacokinetic and pharmacodynamic results of the two animal models both showed that BBR-PPSG could significantly reduce the level of inflammatory factors and improve the joint pathological status, and the curative effect lasted for about 1 month. Among RA rats, the results of the BBR-PPSG group were the closest to the health group, and both were better than the oral and injection groups. Compared with daily medication, BBR-PPSG not only significantly reduces the frequency of administration, but also ensures the therapeutic effect.

Cartilage and bone destruction are the main clinical features of RA, and protecting bone and cartilage from erosion is currently the main goal of treating rheumatoid arthritis. In the rabbit model, despite directly observing the therapeutic effect through joint cavity injection, the bone protection function of the preparation was also verified through CT imaging and CT data. The results of cytokines, histopathology and CT further confirmed the therapeutic effect of BBR-PPSG on RA. In the CT images, it is obvious that the joint bone morphology of the BBR-PPSG group was better than that of the injection group, which was greatly improved compared to the model group and was also reflected in specific bone functional parameters.

Except confirmed therapeutic effect, the advantages of this product preparation should be also highlighted. Phospholipid based phase separation gel, a solvent-induced *in situ* formation gel, is a novel sustained drug delivery system developed by our team in recent years (Zhang T. et al., 2015). The gel is simple, safe and consists of only phospholipid, ethanol, and injection grade oil. Convenient preparation with a lower cost, makes it suitable for industrial production preparation. Previous studies showed that PPSG has no significant cytotoxicity when co-cultured with L929 and HUVEC cell lines. Compared the PPSG content of each component, and ethanol at 70:15:15 has the slowest and least release rate, which contributes to control sudden release and effectively reduce adverse stimuli at the injection site. Besides, this proportion has high biocompatibility and can be biodegradable (Zhang X. et al., 2015; Zhang et al., 2019a). Therefore, we did not conduct the study of each proportion, and directly used the optimal proportion.

The sol-gel transformation process of PPSG is from outside to inside, which is completed in 12 min in 37°C PBS buffer. About 4 h after subcutaneous injection in rats, the gel turns to a coagulated state completely (Zhang et al., 2019b). Under atomic microscopy, the liquid PPSG was uniform, indicating that the phospholipids in the PPSG were completely dissolved. Images of solidified PPS clearly displayed phospholipid precipitate particles, which can act as repositories for the sustained release of drugs after phase transformation when PPSGS exposed to water (Zhang et al., 2019b). Compared with berberine solution by oral or subcutaneous injection, the gel shows a slower release rate *in vivo*, which can prolong action time and reduce toxicity. Moreover, BBR-PPSG also provides good stability and can be stored for a long time within a certain temperature range.

5 Conclusion

In this study, we developed and validated a BBR-PPSG system for the treatment of RA. A single dose of BCR-PPSG could be released smoothly and continuously in animals for 1 month. By establishing adjuvant induced arthritis model in rats and ovalbumin induced arthritis model in rabbits, we showed BBR-PPSG could effectively relieve joint swelling, inflammatory cell infiltration, reduce the levels of TNF-α and IL-1β, and maintain the stability of synovial chondrocytes. Furthermore, Micro-CT analysis of bone erosion in OIA rabbits with inflammatory joints reveals that bone functional parameters in BBR-PPSG group were repaired and reversed. These results suggest that BBR-PPSG has the potential for long-term inflammatory relief and bone recovery against RA.

Data availability statement

The original contributions presented in the study are included in the article/supplementary material, further inquiries can be directed to the corresponding author.

Ethics statement

The animal study was reviewed and approved by the National Act on the Use of Experimental Animals (China).

Author contributions

JL contributed to quality control and write the manuscript. XP and CG contributed to perform the experiments and draft the manuscript. XP and YY contributed to acquisition and the accuracy of the data. TG revised the manuscript. All authors contributed to the article and approved the submitted version.

Funding

Acknowledgments

Conflict of interest

The authors declare that the research was conducted in the absence of any commercial or financial relationships that could be construed as a potential conflict of interest.

Publisher's note

All claims expressed in this article are solely those of the authors and do not necessarily represent those of their affiliated organizations, or those of the publisher, the editors and the reviewers. Any product that may be evaluated in this article, or claim that may be made by its manufacturer, is not guaranteed or endorsed by the publisher.

References

Abdalmula, A., Washington, E. A., House, J. V., Dooley, L. M., Blacklaws, B. A., Ghosh, P., et al. (2014). Clinical and histopathological characterization of a large animal (ovine) model of collagen-induced arthritis. *Vet. Immunol. Immunop.* 159 (1-2), 83–90. doi:10.1016/j.vetimm.2014.03.007

Allen, A., Carville, S., McKenna, F., and Guideline, D. G. (2018). Diagnosis and management of rheumatoid arthritis in adults: Summary of updated NICE guidance. *BMJ* 362, k3015. doi:10.1136/bmj.k3015

Asif, A. M., Fox, D. A., and Ruth, J. H. (2017). Synovial cellular and molecular markers in rheumatoid arthritis. *Semin. Immunol.* 39 (4), 385–393. doi:10.1007/s00281-017-0631-3

Auréal, M., Machuca-Gayet, I., and Coury, F. (2020). Rheumatoid arthritis in the view of osteoimmunology. *Biomolecules* 11 (1), 48. doi:10.3390/biom11010048

Berardi, S., Corrado, A., Maruotti, N., Cici, D., and Cantatore, F. P. (2021). Osteoblast role in the pathogenesis of rheumatoid arthritis. *Mol. Biol. Rep.* 48 (3), 2843–2852. doi:10.1007/s11033-021-06288-y

Bevaart, L., Vervoordeldonk, M. J., and Tak, P. P. (2010). Evaluation of therapeutic targets in animal models of arthritis: How does it relate to rheumatoid arthritis? *Arthritis Rheum.* 62 (8), 2192–2205. doi:10.1002/art.27503

Deng, C., Zhang, Q., He, P., Zhou, B., He, K., Sun, X., et al. (2021). Targeted apoptosis of macrophages and osteoclasts in arthritic joints is effective against advanced inflammatory arthritis. *Nat. Commun.* 12 (1), 2174. doi:10.1038/s41467-021-22454-z

Dumonde, Dc, and Glynn, Le (1962). The production of arthritis in rabbits by an immunological reaction to fibrin. *Br. J. Exp. Pathol.* 43 (4), 373–383.

Feng, X., Wang, K., Cao, S., Ding, L., and Qiu, F. (2021). Pharmacokinetics and excretion of berberine and its nine metabolites in rats. *Front. Pharmacol.* 11, 594852. doi:10.3389/fphar.2020.594852

Gong, T., Tan, T., Zhang, P., Li, H., Deng, C., Huang, Y., et al. (2020). Palmitic acid-modified bovine serum albumin nanoparticles target scavenger receptor-A on activated macrophages to treat rheumatoid arthritis. *Biomaterials* 258, 120296. doi:10.1016/j.biomaterials.2020.120296

Gwinnutt, J. M., Norton, S., Hyrich, K. L., Lunt, M., Combe, B., Rincheval, N., et al. (2022). Exploring the disparity between inflammation and disability in the 10-year outcomes of people with rheumatoid arthritis. *Rheumatol. Oxf.* 61 (12), 4687–4701. doi:10.1093/rheumatology/keac137

Han, L., Xue, J., Wang, L., Peng, K., Zhang, Z., Gong, T., et al. (2016). An injectable, low-toxicity phospholipid-based phase separation gel that induces strong and persistent immune responses in mice. *Biomaterials* 105, 185–194. doi:10.1016/j.biomaterials.2016.08.007

Huang, D. N., Wu, F. F., Zhang, A. H., Sun, H., and Wang, X. J. (2021). Efficacy of berberine in treatment of rheumatoid arthritis: From multiple targets to therapeutic potential. *Pharmacol. Res.* 169, 105667. doi:10.1016/j.phrs.2021.105667

Huang, S. M., Zhong, S. J., Liao, X. Q., Hu, S. Y., and Hu, Z. X. (2021). Animal model analysis of rheumatoid arthritis based on clinical characteristics of Chinese and Western medicine. *Zhongguo Zhong Yao Za Zhi* 46 (19), 5152–5158. Chinese. doi:10.19540/j.cnki.cjcmm.20210617.701

Lin, Y. C., Kuo, J. Y., Hsu, C. C., Tsai, W. C., Li, W. C., Yu, M. C., et al. (2013). Optimizing manufacture of liposomal berberine with evaluation of its antihepatoma effects in a murine xenograft model. *Int. J. Pharm.* 441 (1-2), 381–388. doi:10.1016/j.ijpharm.2012.11.017

Liu, C. S., Zheng, Y. R., Zhang, Y. F., and Long, X. Y. (2016). Research progress on berberine with a special focus on its oral bioavailability. *Fitoterapia* 109, 274–282. doi:10.1016/j.fitote.2016.02.001

Liu, Y. T., Hao, H. P., Xie, H. G., Lai, L., Wang, Q., Liu, C. X., et al. (2010). Extensive intestinal first-pass elimination and predominant hepatic distribution of berberine explain its low plasma levels in rats. *Drug Metab. Dispos.* 38 (10), 1779–1784. doi:10.1124/dmd.110.033936

Nandakumar, K. S. (2010). Pathogenic antibody recognition of cartilage. *Cell. Tissue Res.* 339 (1), 213–220. doi:10.1007/s00441-009-0816-8

Nguyen, T. X., Huang, L., Liu, L., Elamin, A., Gauthier, M., and Yang, G. (2014). Chitosan-coated nano-liposomes for the oral delivery of berberine hydrochloride. *J. Mater Chem. B* 2 (41), 7149–7159. doi:10.1039/c4tb00876f

Pozsgay, J., Szekanecz, Z., and Sármay, G. (2017). Antigen-specific immunotherapies in rheumatic diseases. *Nat. Rev. Rheumatol.* 13 (9), 525–537. doi:10.1038/nrrheum.2017.107

Qiu, S., Sun, H., Zhang, A. H., Xu, H. Y., Yan, G. L., Han, Y., et al. (2014). Natural alkaloids: Basic aspects, biological roles, and future perspectives. *Chin. J. Nat. Med.* 12 (6), 401–406. doi:10.1016/S1875-5364(14)60063-7

Rockel, J. S., and Kapoor, M. (2016). Autophagy: Controlling cell fate in rheumatic diseases. *Nat. Rev. Rheumatol.* 12 (9), 517–531. doi:10.1038/nrrheum.2016.92

Sahibzada, M., Sadiq A, Faidah H., Khurram, M., Amin, M., Haseeb, A., Kakar, M., et al. (2018). Berberine nanoparticles with enhanced *in vitro* bioavailability: Characterization and antimicrobial activity. *Drug Des. Devel Ther.* 14 (12), 303–312. doi:10.2147/DDDT.S156123

Schneider, M., and Krüger, K. (2013). Rheumatoid arthritis--early diagnosis and disease management. *Dtsch. Arztebl. Int.* 110 (27-28), 477–484. doi:10.3238/arztebl.2013.0477

Smolen, J. S., Aletaha, D., and McInnes, I. B. (2016). Rheumatoid arthritis. *Lancet* 388 (10055), 2023–2038. doi:10.1016/S0140-6736(16)30173-8

van der Horst-Bruinsma, I. E., Lems, W. F., and Dijkmans, B. A. (2009). A systematic comparison of rheumatoid arthritis and ankylosing spondylitis. *Clin. Exp. Rheumatol.* 27 (55), S43–S49. doi:10.1007/978-3-7091-0520-7_8

Wang, H. W., Wang, J., and Gao, Z. X. (2013). Berberine combined with methotrexate in the treatment of 29 cases of rheumatoid arthritis. *Fujian J. TCM Oct.* 44 (5), 39–40. Chinese. doi:10.13260/j.cnki.jfjtcm.011399

Wang, K., Feng, X., Chai, L., Cao, S., and Qiu, F. (2017). The metabolism of berberine and its contribution to the pharmacological effects. *Drug Metab. Rev.* 49 (2), 139–157. doi:10.1080/03602532.2017.1306544

Wang, M., Shan, F., Zou, Y., Sun, X., Zhang, Z. R., Fu, Y., et al. (2016). Pharmacokinetic and pharmacodynamic study of a phospholipid-based phase separation gel for once a month administration of octreotide. *J. Control Release* 230, 45–56. doi:10.1016/j.jconrel.2016.03.036

Wang, X., He, X., Zhang, C. F., Guo, C. R., Wang, C. Z., and Yuan, C. S. (2017). Anti-arthritic effect of berberine on adjuvant-induced rheumatoid arthritis in rats. *Biomed. Pharmacother.* 89, 887–893. doi:10.1016/j.biopha.2017.02.099

Wang, Z., Wu, J., Zhou, Q., Wang, Y., and Chen, T. (2015). Berberine nanosuspension enhances hypoglycemic efficacy on streptozotocin induced diabetic C57BL/6 mice. *Evid. Based Complement. Altern. Med.* 2015, 239749. doi:10.1155/2015/239749

Wasserman, A. M. (2011). Diagnosis and management of rheumatoid arthritis. *Am. Fam. Physician* 84 (11), 1245–1252. doi:10.1001/jama.2018.13103

Whitehouse, M. W. (2007). Adjuvant arthritis 50 years on: The impact of the 1956 article by C. M. Pearson, 'Development of arthritis, periarthritis and periostitis in rats given adjuvants. *Inflamm. Res.* 56 (4), 133–138. doi:10.1007/s00011-006-6117-8

Wu, C. Y., Yang, H. Y., Luo, S. F., and Lai, J. H. (2021). From rheumatoid factor to anti-citrullinated protein antibodies and anti-carbamylated protein antibodies for diagnosis and prognosis prediction in patients with rheumatoid arthritis. *Int. J. Mol. Sci.* 22 (2), 686. doi:10.3390/ijms22020686

Xie, D., Xu, Y., Jing, W., Juxiang, Z., Hailun, L., Yu, H., et al. (2017). Berberine nanoparticles protects tubular epithelial cells from renal ischemia-reperfusion injury. *Oncotarget* 8 (15), 24154–24162. doi:10.18632/oncotarget.16530

Yamashita, A., Yonemitsu, Y., Okano, S., Nakagawa, K., Nakashima, Y., Irisa, T., et al. (2002). Fibroblast growth factor-2 determines severity of joint disease in adjuvant-induced arthritis in rats. *J. Immunol.* 168 (1), 450–457. doi:10.4049/jimmunol.168.1.450

Yu, F., Ao, M., Zheng, X., Li, N., Xia, J., Li, Y., et al. (2017). PEG-lipid-PLGA hybrid nanoparticles loaded with berberine-phospholipid complex to facilitate the oral delivery efficiency. *Drug Deliv.* 24 (1), 825–833. doi:10.1080/10717544.2017.1321062

Yu, H., Lu, C., Tan, M. T., and Moudgil, K. D. (2013). Comparative antigen-induced gene expression profiles unveil novel aspects of susceptibility/resistance to adjuvant arthritis in rats. *Mol. Immunol.* 56 (4), 119707–119709. doi:10.1016/j.molimm.2013.05.230

Zhang, P., Chen, D., Tian, Y., Li, H., Gong, T., Luo, J., et al. (2020). Comparison of three *in-situ* gels composed of different oil types. *Int. J. Pharm.* 587, 119707. doi:10.1016/j.ijpharm.2020.119707

Zhang, T., Luo, J., Peng, Q., Dong, J., Wang, Y., Gong, T., et al. (2019a). Injectable and biodegradable phospholipid-based phase separation gel for sustained delivery of insulin. *Colloids Surf. B Biointerfaces* 176, 194–201. doi:10.1016/j.colsurfb.2019.01.003

Zhang, T., Peng, Q., San, F. Y., Luo, J. W., Wang, M. X., Wu, W. Q., et al. (2015). A high-efficiency, low-toxicity, phospholipids-based phase separation gel for long-term delivery of peptides. *Biomaterials* 45, 1–9. doi:10.1016/j.biomaterials.2014.12.042

Zhang, T., Qin, X. Y., Cao, X., Li, W. H., Gong, T., and Zhang, Z. R. (2019b). Thymopentin-loaded phospholipid-based phase separation gel with long-lasting immunomodulatory effects: *In vitro* and *in vivo* studies. *Acta Pharmacol. Sin.* 40 (4), 514–521. doi:10.1038/s41401-018-0085-8

Zhang, X., Zhao, Y., Xu, J., Xue, Z., Zhang, M., Pang, X., et al. (2015). Modulation of gut microbiota by berberine and metformin during the treatment of high-fat diet-induced obesity in rats. *Sci. Rep.* 5, 14405. doi:10.1038/srep14405

Zhang, Z., Chen, Y., Deng, J., Jia, X., Zhou, J., and Lv, H. (2014). Solid dispersion of berberine-phospholipid complex/TPGS 1000/SiO$_2$: Preparation, characterization and *in vivo* studies. *Int. J. Pharm.* 465 (1-2), 306–316. doi:10.1016/j.ijpharm.2014.01.023

Zhao, T., Xie, Z., Xi, Y., Liu, L., Li, Z., and Qin, D. (2022). How to model rheumatoid arthritis in animals: From rodents to non-human primates. *Front. Immunol.* 13, 887460. doi:10.3389/fimmu.2022.887460

As an inhibitor of norepinephrine release, dexmedetomidine provides no improvement on stroke-associated pneumonia in mice

Miaomiao Zhou[1†], Qiong Luo[1†] and Younian Xu[2,3]*

[1]Anesthesiology Department, Zhongnan Hospital of Wuhan University, Wuhan, China, [2]Anesthesiology Department, Union Hospital, Tongji Medical College, Huazhong University of Science and Technology, Wuhan, China, [3]Institute of Anesthesia and Critical Care Medicine, Union Hospital, Tongji Medical College, Huazhong University of Science and Technology, Wuhan, China

Background: Dexmedetomidine (DEX) is commonly employed as a sedative agent to attenuate sympathetic tone and reduce norepinephrine (NE) levels. In the context of stroke-associated pneumonia (SAP), which is believed to arise from heightened sympathetic nervous system activity and elevated NE release, the precise influence of DEX remains uncertain.

Methods: In this study, we generated an SAP model using middle cerebral artery occlusion (MCAO) and examined NE levels, immunological statuses in the brain and periphery, pneumonia symptoms, and extent of infarction. We aimed to determine the effects of DEX on SAP and explore the underlying. Despite its potential to reduce NE levels, DEX did not alleviate SAP symptoms or decrease the infarct area. Interestingly, DEX led to an increase in spleen size and spleen index. Furthermore, we observed a decrease in the CD3+ T cell population in both the blood and brain, but an increase in the spleen following DEX administration. The precise mechanism linking decreased CD3$^+$ T cells and DEX's role in SAP requires further investigation.

Conclusion: The clinical use of DEX in stroke patients should be approached with caution, considering its inability to alleviate SAP symptoms and reduce the infarct area. Further research is necessary to fully understand the relationship between decreased CD3$^+$ T cells and DEX's influence on SAP.

KEYWORDS

ischemic stroke, stroke-associated pneumonia, dexmedetomidine, norepinephrine, immunity

Introduction

Stroke is a leading cause of death worldwide, whose outcome depends on the occurrence of complications (Langhore et al., 2000; Weimar et al., 2002). Stroke-induced immunodepression (SID) can increase susceptibility to infections (Bellinger et al., 2008), among which SAP is the most frequent infectious complication, reportedly occurring in 6.7%–36.98% of stroke patients (Badve et al., 2019). SAP may lead to lengthy hospitalization, poor functional outcomes, and high mortality (Saposnik et al., 2008; Finlayson et al., 2011; Koennecke et al., 2011).

Following a large ischemic stroke, the sympathetic nervous system (SNS) is activated, causing the release of norepinephrine (NE), which subsequently leads to the activation of β2-

adrenergic receptors (β2-ARs) (Prass et al., 2006). The β2-ARs, densely expressed on all significant immune cell subtypes, then communicated the signaling pathway and managed the peripheral immune system to be suppressive, by lowering the synthesis and release of inflammatory mediators (Bosmann et al., 2012; Martín-Cordero et al., 2013) and triggering the release of anti-inflammatory cytokines (Hervé et al., 2017; Aaç et al., 2018) from activated macrophages and lymphocytes. Such anti-inflammatory responses are regarded as a compensatory mechanism to prevent the post-ischemic brain from severe and harmful inflammatory responses (Chamorro et al., 2007; Iadecola and Anrather, 2011). However, anti-inflammatory reactions increase susceptibility to systemic infections after stroke, especially pneumonia. A bystander autoimmune factor directed against antigens of the central nervous system can be released as a result of the inflammation caused by pneumonia, which can worsen the prognosis for stroke patients. Therefore, it is critical to prevent stroke-associated pneumonia (Winklewski et al., 2014).

Dexmedetomidine (DEX) is an efficient and highly selective agonist of α2 adrenergic receptors (α2-ARs). By activating presynaptic α2-ARs, DEX reduces sympathetic nerve activity by preventing NE release from the locus coeruleus nucleus (Jorm and Stamford, 1993). Due to its ability to prevent NE release, DEX possesses immune-protective qualities (Wang et al., 2019). DEX protects the brain by preventing microglia from activating, lowering the neuroinflammatory response, and minimizing neuron necrosis and apoptosis, according to both *in vivo* and *in vitro* studies (Kim et al., 2017; Gao et al., 2019). Regarding lung inflammation, researchers have found that DEX reduces inflammatory responses in the lung tissues through a variety of anti-inflammatory channels, including the cholinergic anti-inflammatory system and the TLR4/NF-κB pathway (Wu et al., 2013; Liu et al., 2016).

The present study was undertaken to determine the effects of DEX on cerebral and peripheral immune states in stroke mice and to explore whether DEX would improve symptoms of SAP as well as benefit neuronal outcomes.

Methods

Mice/animals

In all experiments, male C57BL/6 mice weighing 22–27 g at 8–10 weeks old were used. Treatment and surgery outcomes were distributed to animals across cages in a random sequence. The Institutional Animal Care and Use Committee of Tongji Medical College, Huazhong University of Science and Technology, gave its approval to all procedures (IACUC Number: 2,419). The National Institutes of Health Guidelines for the Care and Use of Laboratory Animals were followed in all investigations. We attempted to use as few animals as possible.

SAP model and drug treatment

In our earlier article (Xu et al., 2022), we have shown that the MCAO model in C57/bl6 mice is the ideal model for studying

SAP, and the success rate in creating the SAP model was 100%. The exclusion criteria should be: 1. No obvious cerebral infarction was seen by TTC; 2. Mice that dead after the MCAO procedure. The middle cerebral artery occlusion (MCAO) was primarily conducted (Chiang et al., 2011). The agonist of the α2-ARs, dexmedetomidine (DEX) (Hengrui, China), was diluted in 0.9% sodium chloride at 15 mM (25 µg/kg) and then delivered intraperitoneally at P1 (three times daily, every 2 h since 24 h after reperfusion) and P2 (once daily) hours following MCAO (Groups designated as either M-DEX or M-saline, respectively).

Blood and tissue sample collection

72 h after MCAO, mice were quickly put to death by cervical dislocation. Eyeball removal was used to extract blood, and brain, lung, and spleen tissues were also harvested. The spleen index was calculated as the weight of the spleen (mg)/body weight g)×10.

Evaluation of sympathetic activity

NE concentrations could be used as a proximate indicator of sympathetic activity (Myers et al., 1981; Gendron et al., 2002; Bieber et al., 2017). To determine the baseline NE level, we treated mice with pentobarbital 50 mg/kg, i.p., to obtain sedation. To prevent NE spillover, we only collected the first two drops of blood after immediately removing the eyeball. Homogenized tissues must first be used for the spleen NE level assessment. Then, centrifuging tissue and blood samples and measuring the NE concentrations under the manufacturer's instructions. The microplate reader was used to find the OD value at 450 nm (AMR-100, Aosheng, China).

Histopathological examination of spleen and lung tissues

The lung and spleen tissues were taken out, fixed with 10% formalin, and prepared for histological analysis. The spleen and lung tissues were microtome dissected into 6-m thick sections after being translucent, dehydrated, soaked, and fixed in paraffin wax. The sections were then stained with hematoxylin/eosin (HE) to assess them. A histopathological scoring system (ranging from 0–26) was utilized to assess the pathology of pulmonary infection. We obtained averaging scores from each lung by evaluating the quantity and quality of peri-bronchiolar and peri-bronchial infiltrates, luminal exudates, peri-vascular infiltrates, and parenchyma (Cimolai et al., 1992).

Assessment of infarct volume

As previously described, the infarct volume was assessed by TTC staining (Liang et al., 2014). Using Image-Pro Plus 6.0 software, the infarct regions and total area on each slice were calculated, and the result was expressed as the percentage of infarction in the entire area.

Isolation of immune cells from blood, spleen, and brain

Red blood cells (RBCs) were lysed with ACK buffer before being rinsed with PBS. The cells were then maintained on ice until staining. The spleens were minced, and the cell suspension passed through a 40 μm cell strainer, and then cells were treated with ACK buffer to lyse red cells. The homogenates of the brain were centrifuged at 30% Percoll after digestion for half an hour at 37°C in 3 ml of 0.08% trypsin diluted with DMEM, then the cells were gathered as pellets and washed in PBS.

Flow cytometry

Isolated leukocytes were centrifuged using a 37%–70% Percoll density gradient. After three rounds of washing with buffer (PBS with 0.5% bovine serum albumin and 0.02% sodium azide), cells were stained for 20 min at 4°C with the antibodies listed below. CD3 is a T cell receptor complex that is expressed in T cells. B cells have a cell surface protein called B220 that helps with antigen-based B cell activation. According to CD45 and CD11b expression patterns, we identified three distinct cell populations in the brain: CD11b+CD45low (microglia), CD11bhighCD45high (granulocytes and macrophages), and CD11b−CD45high (lymphoid cells). In the CD11bhighCD45high population, two subpopulations were identified: F4/80 + Gr1+ (activated macrophages) and F4/80−Gr1+(granulocytes). To identify the leukocyte phenotypes, we used FlowJO software for single-cell flow cytometry analysis.

Quantification of cytokines in cerebral and lung tissues

By using widely available immuno-enzymatic commercial assays specific to equine species, we identified pro and anti-inflammatory cytokines (TNF-α, IL-1β, and INF-γ) (Cloud-Clone Corp, Wuhan, China). Plasma was created by centrifuging whole blood at 1,500 g for 10 min to analyze all cytokines. Following the manufacturer's instructions, samples were frozen and filtered before being used for analysis using mouse-specific ELISAs (Bioswamp, China).

Immunofluorescence detection of spleen

For immunofluorescence detection, serial frozen spleen sections were washed in 0.05% BSA in PBS and blocked using species-specific normal serum according to the secondary antibody. Primary antibodies were incubated for 1 h at room temperature. B cells were detected using a monoclonal antibody (mAb) B220 (2.5 μg ml−1) to detect CD45R (BD Pharmingen, United States). T cells were detected using an anti-CD3 antibody (5 μg ml−1) to detect CD3 (2.5 μg ml−1, BD Pharmingen, United States). After adding the primary antibody, sections were washed in TBST buffer (Sigma, United States). And 1 μL Goat Anti-Rat IgG (HRP) secondary antibody (Abbkine, United States) was coupled to Alexa Fluor™ 488, Alexa Fluor™ 555 dyes, or Alexa Fluor™ 647 fluorochromes (Thermo Fisher Scientific, United States) were incubated for 45 min

FIGURE 1
NE concentrations in the mice of the SHAM, M-saline, and M-DEX groups. **(A)** Spleens from the aforementioned three groups were displayed (SHAM n = 3, M-saline n = 6, M-DEX n = 4), and **(B)** spleen index, assessed 72 h after MCAO in the saline and DEX-treated MCAO mice as an index of immunological response (SHAM n = 3, M-saline n = 6, M-DEX n = 4). **(C)** Plasma and **(D)** spleen NE levels in the saline, DEX-treated MCAO mice were assessed 1 h after a stroke (n = 4 per group). ** indicates $p < 0.01$, ** indicates $p < 0.001$, and **** indicates $p < 0.0001$ by one-way ANOVA with Holm−Sidak correction.

at 37°C. Sections were washed in PBS–BSA and mounted in a fluorescent mounting medium, and images were captured using a Leica Stellaris five confocal microscope (Leica, Wetzlar, German).

Digital images were analyzed using ImageJ software. Three spleens from each experimental group were analyzed. From each spleen, one section, 100 μm apart, was studied, and on each section, we collected data from eight individual areas of white pulp. Fluorescent intensity thresholds were applied, and the number of pixels of each color (green and red) was automatically counted and used to determine the area of immunolabelling for each cell type.

Statistical analysis

Data are presented as the mean ± s.d. For statistical analysis, GraphPad Prism software (version 8.0) was employed. The outliers

FIGURE 2
The influence of α2-ARs agonist DEX on stroke-associated pneumonia and infarction area. **(A)** Representative TTC-stained coronal serial sections of cortical infarcts in the saline, and DEX-treated MCAO mice 3 days after stroke. **(B)** Infarct volumes of MCAO in the saline, and DEX-treated MCAO mice 3 days following the stroke (n = 3 per group). **(C)** representative 12-μm section of HE-stained lungs from the SHAM, M-saline, and M-DEX groups, lung sections from saline, and DEX-treated MCAO mice revealed signs of pneumonia (thickening of alveolar walls and neutrophilic infiltrates) ×40. **(D)** Quantitative analysis of histopathological lung injury scores (n = 4 animals per group). Effects of DEX on the expression of pro-inflammatory cytokines in the lung, in the groups of SHAM, saline, and DEX-treated MCAO mice 72 h after occlusion (n = 5 per group), the levels of pro-inflammatory cytokines **(E)** TNF-α, **(F)** IL-1β, and **(G)** IFN-γ were measured. Mann-Whitney test was used to analyze HPS scores, and one-way ANOVA with Holm−Sidak correction was used for the analysis of cytokines. *, p < 0.05, ** indicated p < 0.01, and *** indicated p < 0.001.

were recognized by the ROUT approach and eliminated from the analysis (Q = 1.000%). A two-tailed Student's t-test was used to compare two groups, a one-way ANOVA with Holm-Sidak correction was used to compare pairs of data from three different groups, and a Mann-Whitney test was used to compare the histopathological score between two groups after verifying that these datasets' normal distributions are accurate (Kolmogorov-Smirnov test). A p-value of less than 0.05 was considered significant, whereas values of less than 0.01, 0.001, and 0.0001 were highly significant.

Results

DEX's effects on NE release

NE only has anti-inflammatory effects in micromolar quantities (Sander et al., 2001). The spleen's NE nerve terminals, which produce a significant amount of NE in the vicinity of antigen-activated immune cells, were hypothesized to be primarily responsible for the immune-modulatory impact (Bergquist et al., 1998). We then tested the hypothesis that providing mice with DEX decreases NE levels and shields them from SAP. At first, NE levels in plasma and spleen 72 h after stroke were both assayed, and we observed no reduction in the M-DEX group when compared to the M-saline group (Figures 1A,B). We ascribed the unchanged level of NE at that point to the loss of efficacy caused by the diminished or eliminated concentration of DEX. Hence, we examined the levels of NE in the plasma and spleen 1 h after the three-dose of DEX applications the first day after MCAO. Not surprisingly, NE levels were lower than in the M-saline group, from 352.4 ± 29.1% to 221.7 ± 22.4% in plasma and 176.5 ± 9.8% to 94.1 ± 6.6% in the spleen (Figures 1C,D). The decreasing amplitude reached 37% in plasma and 46.7% in the spleen.

DEX failed to improve SAP or diminish infarction area 3ds after MCAO

Figure 2A depicts the sites of ischemic lesions 3 days after a stroke. The average size of the ischemic lesions in the stroke mice spanned 33.3% of the entire brain, and there were no changes between the M-DEX group's infarct volume and that of the MCAO group, which was 29.5 ± 3.5% (Figure 2B).

Images of the HE-stained lung sections from the three groups, including the SHAM, M-saline, and M-DEX groups, are shown in Figure 2C. Inflammatory pathological changes including thickened alveolar septa, intra-alveolar inflammatory infiltration, and interstitial congestion were seen in the sections of the M-saline and M-DEX groups. Figure 2D displays the histopathological results for the three groups (the Sham, M-saline, and M-DEX groups). The findings demonstrated that all the mice developed pneumonia 72 h after an MCAO stroke, and the HPS in the M-saline group were all below ten, while two in four of the HPS in the M-DEX group were above ten. When TNF-α, IL-1β, and IFN-γ were analyzed as pro-
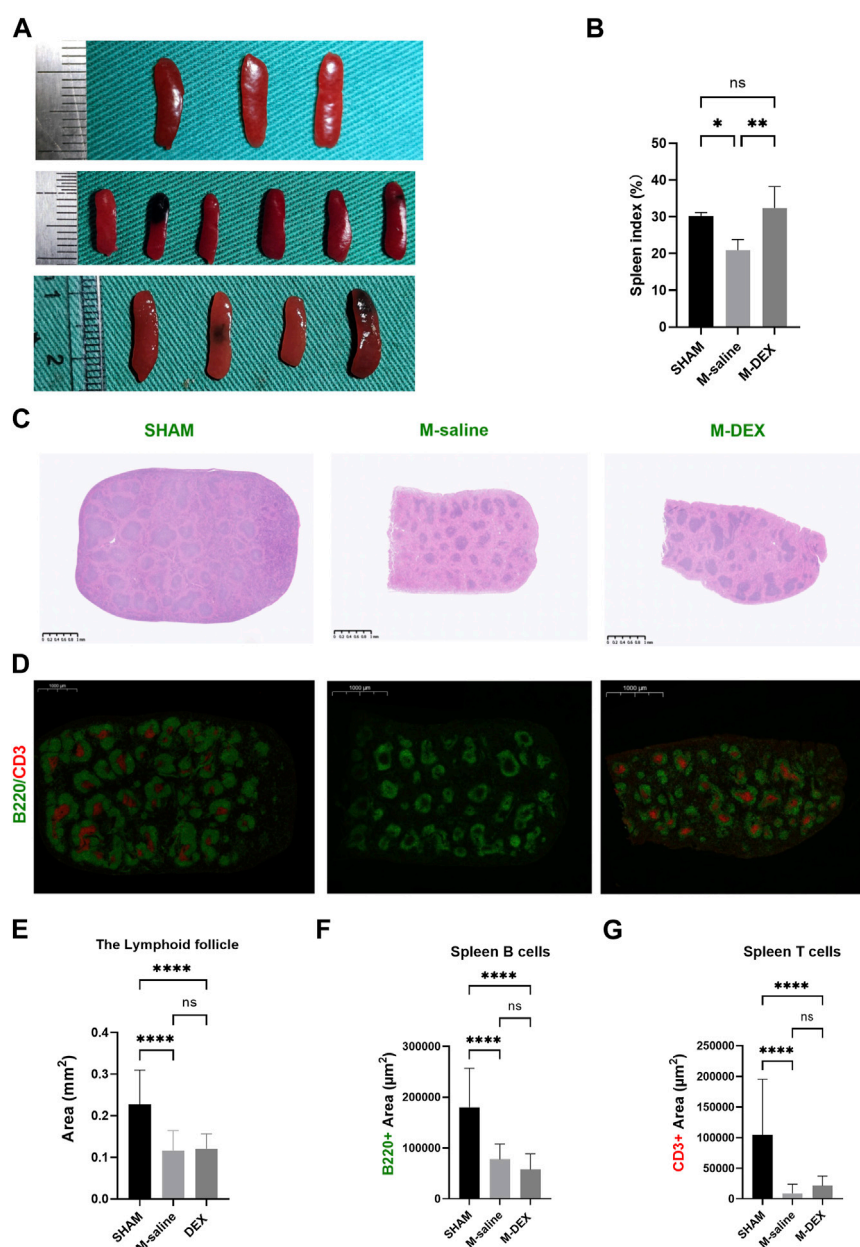
FIGURE 3
Effects of DEX on the spleen, including spleen index, and alterations to its morphology and immunology. **(A)** Histological sections of spleens in the SHAM, M-saline, and M-DEX groups. **(B)** Spleen index in the SHAM, M-saline, and M-DEX groups (SHAM $n = 3$, M-saline $n = 6$, M-DEX $n = 4$) **(C)** showed histological sections of spleens in the SHAM, M-saline, and M-DEX groups, and multiple B cell follicles can be seen. **(D)** displays fluorescent histological sections of spleens in the SHAM, M-saline, and M-DEX groups, B cells were immunolabelled with B220 antibody (green), and T cells with CD3 antibody (red). **(E)** Quantification of the areas of lymphoid follicles in the three groups 3 days after MCAO ($n = 3$ per group). **(F)** The absolute measurement of B220 fluorescence, and **(G)** CD3$^+$ fluorescence areas, as a measure of B cells and T cells respectively ($n = 3$ per group). Data were shown as mean $\pm$ s.d. $*p < 0.05$, $**p < 0.01$; $***p < 0.001$; $****p < 0.0001$, one-way ANOVA with Holm−Sidak correction was used to compare each column to every other column among the three groups.

inflammatory cytokines, we found that DEX therapy did not affect their expression in the lung (Figures 2E–G). Combing these two findings, we concluded that DEX treatment provided no reduction or alleviation of pneumonia, DEX-treated MCAO mice may even have a higher susceptibility to pneumonia or more severe inflammatory sign of pneumonia than the saline-treated MCAO mice.

Effects of DEX administration on the spleen, including spleen index, and its morphological and immunological alterations

As shown in Figure 3A, we noticed that the spleen dramatically shrank at 3ds after MCAO, and DEX
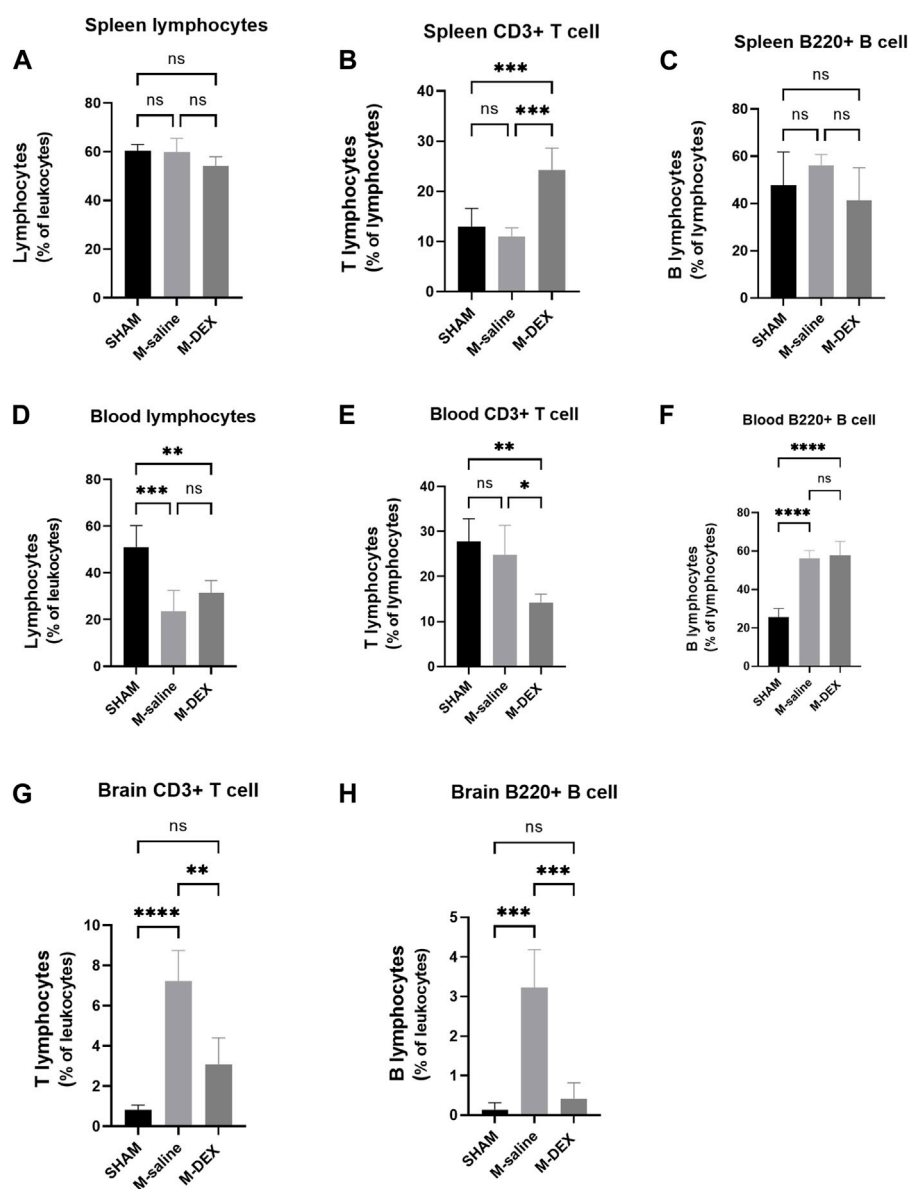
FIGURE 4
Effects of DEX on the ratios of total lymphocytes, as well as the two main subsets of lymphocytes T-cells and B-cells, in the spleen, blood, and brain. Cell subpopulation percentages in the SHAM, M-saline, and M-DEX groups 72 h after stroke, including **(A)** total lymphocytes, **(B)** total CD3+ T cells, and **(C)** B cells (B220+) in the spleen (n = 5 per group); **(D)** total lymphocytes, **(E)** total CD3+ T cells, and **(F)** B cells (B220+) in the blood (n = 5 per group); **(G)** total CD3+ T cells and **(H)** B cells (B220+) in the brain (n = 5 per group). * signifies $p < 0.05$, **$p < 0.01$, ***$p < 0.001$, and ****$p < 0.0001$.

administration significantly increased the spleen size that MCAO induced. The administration of DEX also countered the reduction of the spleen weight in MCAO mice (data was not shown). The results showed that the spleen index in the M-DEX group was significantly higher than in the M-saline group, indicating that DEX could restore the peripheral immunity that had been weakened by MCAO (Figure 3B).

The morphological features in the spleen were also disrupted by MCAO, mainly manifested as the shrank size of the B-cell follicle after MCAO, accompanied by a decrease in the areas of B220 fluorescence, suggesting a reduction in the B-cell

population in the spleen (Figures 3C,E,F). In our results, the CD3+ fluorescence vanished in two of the three spleens in the MCAO group, while all the CD3+ fluorescence in the M-DEX group though diminished remarkably, remained, indicating that there was a sharp drop in the T cell population after the MCAO procedure (Figure 3D). The mean CD3+ fluorescence measures in the M-DEX group were higher than those of the M-saline group, suggesting that CD3+ T cells in the spleen had partially recovered following DEX treatment (Figure 3G). However, the B220 fluorescence region had no differences between the two groups (Figure 3F).
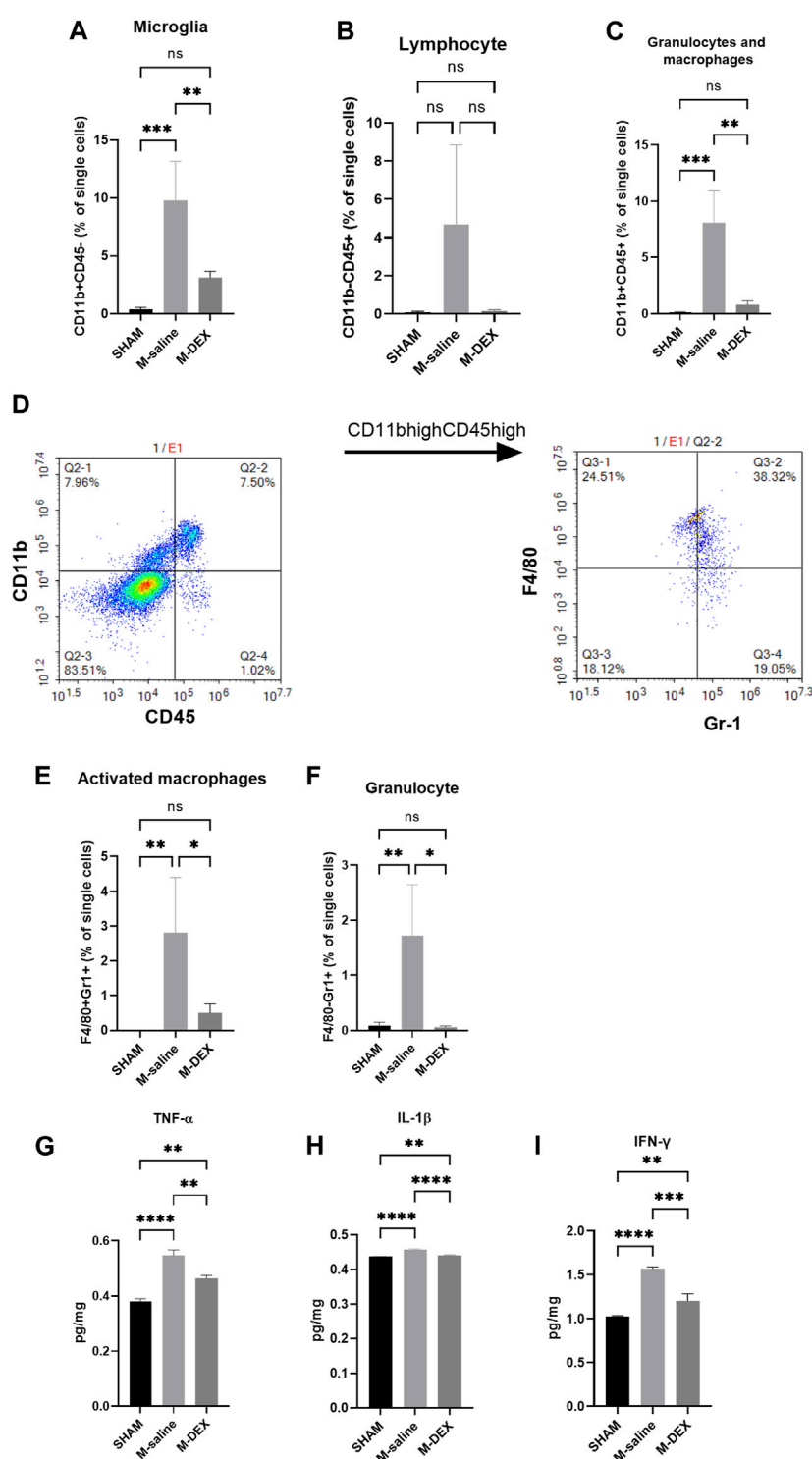
FIGURE 5
Effects of DEX on central immunity. Percentages of immune cell subpopulations including **(A)** microglia, **(B)** lymphocytes, **(C)** granulocytes, and macrophages in the cerebral 72 h after stroke in the SHAM, M-saline, and M-DEX groups (SHAM n = 4, M-saline n = 4, M-DEX n = 3) were assessed. Then, granulocytes and macrophages were sorted further with CD11b and CD45 **(D)**. **(E, F)** show granulocytes and macrophages, respectively. We also analyzed the effects of stroke and DEX application on the expression of pro-inflammatory cytokines in the cerebral brain in MCAO models. Pro-inflammatory cytokines including **(G)** TNF-α, **(H)** IFN-γ, and **(I)** IL-1β levels in sham-operated and saline, DEX-treated MCAO mice 72 h after occlusion. (One-way ANOVA with Holm-Sidak correction, n = 3 per group in all the analyses of cytokines) *, $p < 0.05$, **, $p < 0.01$, ***, $p < 0.001$, and ****, $p < 0.0001$.

Effects of DEX therapy on the ratio of lymphocyte, and the two major lymphocyte subtypes, T and B cells, in the spleen, blood, and brain

We questioned whether there was a connection in the populational alteration of the T and B cell population among the spleen, blood, and brain since DEX influenced the splenic T and B cell populations and the lymphocyte population in the ischemia brain. The proportion of lymphocytes, T, and B cells in the spleen was additionally examined by flow cytometry at first. The findings indicated that there was a general decrease in the total cell population in the spleen after MCAO stroke because none of the three types of proportions altered between the SHAM and M-saline groups (Figures 4A–C). The proportion of CD3+ T cells significantly increased after DEX treatment, and this result was consistent with the immunofluorescence of the spleen results, which showed a reserved red fluorescence in all the MCAO spleen, indicating that DEX helped to maintain more T cells in the spleen after MCAO.

Next, the peripheral blood was analyzed to determine the percentage of T, B, and total lymphocytes. The M-saline group in our study had a much-decreased blood lymphocyte population, as seen in other studies, which suggested that the MCAO mice experienced immunological suppression (Figure 4D). However, compared to the SHAM group, our research showed a greater B cell population in the M-saline and M-DEX groups (Figure 4F), the elevation of the B cell population in the two groups may result from the abundant expulsion of B cells from the spleen. Both of the above changes in the stroke mice were not affected by DEX treatment. No variation of the T cell population in the MCAO groups compared to the SHAM group may be due to less expulsion of T cells from the spleen, but higher composition of T cell population in the blood. Our research revealed that the T cell population in the blood reduced after DEX treatment, which contrasted with the finding that more T cells were retained in the spleen after DEX treatment (Figure 4E).

Since the ischemic brain is the primary site that induces immune changes in the whole body, we examined its effects on the ratio of T cells to B cells in the ischemic brain and discovered that both ratios were enhanced, with 7.23% of T cell populations and 3.23% of B cell populations. The amplitude of rise in the T cell population was noticeably greater than that in the B cell population. Following DEX therapy, both of the two populations drastically decreased (Figures 4G, H).

DEX's effects on the primary cerebral immune state in the stroke mice

We then tested the main immune cell populations, identified with CD11b and CD45 in the ischemic brain. We found that all the immune cell populations, including microglial cells, lymphocytes, granulocytes, and macrophages, increased after MCAO. The magnitudes of change in lymphocyte, granulocyte, and macrophage populations were more obvious than in the microglial population (Figures 5A–C). DEX treatment largely reversed the impact of ischemia on the immune cell populations (Figures 5A–C). The population of granulocyte and macrophage was

further analyzed with Gr1 and F4/80 markers to identify each separately. In the CD11bhighCD45high population, two subpopulations were identified (Figure 5D): F4/80 + Gr1+ (activated macrophages) and F4/80–Gr1+ (granulocytes). There were more activated macrophages and significantly higher numbers of granulocytes in the M-saline group than in the SHAM group, and DEX inhibited the increase (Figures 5E,F).

The impact of DEX on the immuno-state of the stroked cerebral ischemic brain was unclear. First, we looked at cytokine generation in the ischemic brain. In the MCAO mice, levels of the pro-inflammatory cytokines TNF-α, IL-1β, and IFN-γ were all increased (Figures 5G–I). When DEX was administered to MCAO mice, the production of pro-inflammatory cytokines was largely reversed.

DEX delivery caused enlarged spleen as well as pneumonia in the normal mice

Spleen images from the sham mice treated with PBS and DEX are individually shown in Supplement Figure A. It was obvious to see that the spleens in the DEX-treated sham mice were digested with blood, and larger than the PBS-treated ones, and the spleen index rose from 21.7% to 42.7% in the DEX-treated sham mice (Supplement Figure B). We discovered that 72 h after the MCAO procedure, all sham mice treated with DEX developed pneumonia, with substantial infiltration of inflammatory cells. These findings demonstrated that DEX treatment after MCAO stroke will not prevent mice from developing pneumonia, but would rather make their lungs worse.

Discussion

This study assessed the impact of DEX, a selective α2-AR agonist, on the central and peripheral immune system, as well as its effects on cerebral and lung tissues, given the fact that α2-ARs play a crucial role in down-regulating the SNS activity (Yuan et al., 2020), the enhancement of which is regarded as the underlying cause of SAP. In contrast to the untreated MCAO animals, DEX resulted in a lower blood T cell population but a higher retained T cell population in the spleen. However, SAP was not improved.

Stroke mice displayed a stronger sympathetic tone than sham mice, as shown by higher NE levels (Xu et al., 2022). It is well-recognized that the depressed immune state that was brought about by increased sympathetic tone was the main cause of SAP (Faura, et al., 2021). Massive sympathetic discharge triggers lung inflammation (Avlonitis et al., 2005). In addition, providing animals with NE can also result in pulmonary edema and inflammation (Rassler et al., 2003). Thus, we hypothesized that lowering NE levels in MCAO mice might alleviate lung inflammation. It is common knowledge that DEX would reduce NE levels (Nelson et al., 2003; Kang et al., 2020). We first analyzed the plasma and the spleen NE levels, when samples were collected 24 h after the last dose of DEX, that is, 72 h after stroke, and no variation was observed between M-saline and M-DEX group. We then analyzed the NE levels again with samples collected 1 h after the three doses of first-day DEX application and verified that both the

plasma and spleen NE levels were decreased as supposed. Moreover, we noticed that DEX treatment enlarged MCAO mice's shrunk spleen, a characteristic associated with severe stroke (Seifert et al., 2012). Since NE has been demonstrated to cause significant splenic atrophy (Mignini et al., 2003), the increase in spleen size may be explained by the decreased NE levels brought by DEX.

Given that the spleen is a reliable indicator of immune function, and the sizes varied between the three groups, we measured the morphological and immunological alteration of the spleen in the MCAO mice to ascertain whether DEX administration would reverse the intrinsic effects that were caused by MCAO. As the largest secondary lymphoid organ, the spleen serves as the reservoir mainly for two subsets of lymphocytes, B- and T-lymphocytes, and plays a crucial role in initiating the immune response. The B220+ B-cell follicles in the MCAO spleen showed a shrinkage, which was consistent with the change of the follicles presented by HE images. Inconsistent with the changes in the spleen size, DEX did not increase the size of the B-cell follicles. As to the CD3+ T-cells, their aggregation disappeared in the MCAO spleen, while DEX treatment partially restored the aggregation of the CD3+ T-cells. The flow cytometry analysis showed that the ratio of total lymphocytes, and the two subsets, B- and T-lymphocytes were not altered in the MCAO spleen when compared to the Sham group, indicating that there was an overall decline of cells in the spleen. In line with immunofluorescence's findings, DEX treatment raised the ratio of CD3+ T-cells in the spleen while maintaining the ratio of total lymphocytes to B-lymphocytes.

Emerging research indicates that ischemic stroke evokes spleen contraction and disrupts the peripheral immune system. As a result, we looked at the proportions of total lymphocytes and the two major subgroups, B- and T-lymphocytes, in the peripheral blood. As demonstrated in prior research, we also established that MCAO stroke caused a significant decline in the percentage of total lymphocytes. However, the ratio of the B- and T-lymphocytes to the total lymphocytes were not altered, indicating that there was a total loss of B- and T-lymphocytes in the blood after the MCAO stroke. DEX application made no change in the proportion of the total lymphocytes but decreased the ratio of the CD3+ T-cells to the total lymphocytes. We postulated that DEX may depress immunity by preventing the recruitment of CD3+ T-cells from the spleen to the blood because the proportions of the blood CD3+ T-cells were decreased and the spleen CD3+ T-cells were increased after DEX administration.

As the origin of the immune responses, the immuno-state of the ischemic brain was further examined. First, the ratios of the total lymphocytes and the two subsets, B- and T-lymphocytes, were studied. The results demonstrated that overall lymphocyte ratios, as well as ratios of B- and T-lymphocytes, increased after MCAO stroke, with the rise in CD3+ T-cells being more prominent. Treatment with DEX could inhibit all ratio increases mentioned above. Then, we looked at the changes in the proportion of other immune cells and the expression of pro-inflammatory cytokines. We discovered that the number of residual microglia was unaffected by MCAO, even though that activated microglia were reported to be the predominant phagocytic cells in the ischemic brain (Schilling et al., 2005). We hypothesized that this was because microglial cells were more activated than proliferated. However, 3 days after MCAO, the blood-born population of activated macrophage and granulocyte

cells all showed dramatic increases, and DEX therapy led to a widespread, significant decrease of immune cell populations in the ischemic brain. Accordingly, cytokine analysis showed that pro-inflammatory cytokines, including TNF-α, IL-1β, and IFN-γ, were up-regulated in the MCAO brain, and DEX treatment inhibited the expression of these pro-inflammatory cytokines. The suppression of DEX on immunological responses in the brain suggested that fewer peripheral immune cells would be recruited by the ischemic brain.

As shown by our study, DEX's anti-inflammatory effects on the ischemic brain did not aid to diminish the infarction area. It had been established that inhibition of the neuroinflammatory response following ischemic stroke would even increase stroke size (Lechtenberg et al., 2019). Considering DEX's ability to lower peripheral sympathetic tone, we reasoned that its administration would boost peripheral immunological response and lessen the MCAO mice's susceptibility to pneumonia. However, all mice developed pneumonia after DEX treatment, and HPS scores were equal to or higher than those of the mice in the M-saline group. The immune suppression induced by stroke is mainly characterized by a reduced lymphocyte population. DEX's application to the MCAO mice didn't help to improve the lymphocyte ratio, even worse, caused a decrease in the CD3+ T-cell population.

The decrease in total T-cells denotes an inhibited immunological performance. Previous studies implied that immunodepression, characterized by total T-cell reduction was the cause of SAP (Faura et al., 2021). Plentiful studies have shown that elevations in NE or activation of β2-ARs can induce CD3+ T cell lymphopenia (Huang et al., 2010; Oros-Pantoja et al., 2011; Zieziulewicz et al., 2013). Even though DEX decreased NE levels, it also caused a decline in the blood CD3+ T cells. Furthermore, it is commonly recognized that NE production and subsequent activation of the β2-ARs are the causes of SAP and that blocking β-ARs with propranolol can help avoid SAP while DEX administration has no therapeutic effects on SAP. In conclusion, we considered that DEX's impact on the immune cell distribution was irrelevant to the decline of NE concentration. As stated above, DEX had been proved to reduce sepsis induced lung inflammation through a variety of anti-inflammatory pathways. Different theories of pneumonia, in our opinion, account for the variations in DEX's effects. For instance, peripheral inflammation characterizes pneumonia brought on by LPS, and DEX's anti-inflammatory effect is helpful in reducing the inflammatory response. However, peripheral immunosuppression characterizes pneumonia brought on by MCAO mice, and DEX's anti-inflammatory effect worsens the condition, which is not helpful for SAP prognosis.

We also looked at how DEX might affect the pulmonary tissues of normal mice and how the size of their spleens changed after being treated with DEX. We administered DEX to the normal mice with the same dose and procedure as we did to the MCAO mice, and found that after exposure to DEX, all mice developed pneumonia. Additionally, larger spleens were observed in the DEX-treated group than in the PBS-treated group, suggesting an alteration of immunity occurred after DEX application. DEX is widely accepted as an anti-inflammatory drug, which has been shown to suppress

inflammatory responses in multiple organs (Bao and Tang, 2020). Although the decrease in spleen size matched that of the MCAO mice, it was unclear what specifically had happened to the distribution of immune cells in the normal mice treated with DEX. Hence, it remains to be determined whether the decrease in CD3^{+} T cells was the cause of DEX's involvement in the lung in both MCAO and normal mice.

Limits

There are still some limitations in our study. First, it is necessary to clarify the specific immunological changes in DEX-treated normal mice and compare them to those in DEX-treated MCAO mice, which may shed light on whether SAP is caused by a decrease in the blood CD3^{+} T cells; Second, the mechanism by which DEX caused the decline in the blood CD3^{+} T cells has not been figured out. Hence, further research is required.

Conclusion

This work emphasizes the impact of DEX on post-stroke central and peripheral immunological responses and outcomes, particularly the implications of SAP. According to our research, we believe DEX may not be appropriate for stroke patients. The reasons are outlined below. First, DEX produced a fall in the blood CD3^{+} T cells, which may exacerbate immunological depression in SAP mice; Second, combining the effects of DEX on the histology of the lungs in SAP mice or normal mice, DEX medication may induce lung injury.

Data availability statement

The original contributions presented in the study are included in the article/supplementary material, further inquiries can be directed to the corresponding authors.

Ethics statement

The animal study was reviewed and approved by The Institutional Animal Care and Use Committee of Tongji Medical College, Huazhong University of Science and Technology.

Author contributions

MZ and QL contributed to the conception and design of the study. MZ, QL collected the samples and organized the database, and performed the statistical analysis. MZ, QL, and YX wrote the first draft of the manuscript. All authors contributed to the article and approved the submitted version.

Funding

Conflict of interest

The authors declare that the research was conducted in the absence of any commercial or financial relationships that could be construed as a potential conflict of interest.

Publisher's note

All claims expressed in this article are solely those of the authors and do not necessarily represent those of their affiliated organizations, or those of the publisher, the editors and the reviewers. Any product that may be evaluated in this article, or claim that may be made by its manufacturer, is not guaranteed or endorsed by the publisher.

References

Avlonitis, V. S., Wigfield, C. H., Kirby, J. A., and Dark, J. H. (2005). The hemodynamic mechanisms of lung injury and systemic inflammatory response following brain death in the transplant donor. *Am. J. Transpl.* 5 (4 Pt 1), 684–693. doi:10.1111/j.1600-6143. 2005.00755.x

Badve, M. S., Zhou, Z., van de Beek, D., Anderson, C. S., and Hackett, M. L. (2019). Frequency of post-stroke pneumonia: Systematic review and meta-analysis of observational studies. *Int. J. Stroke* 14 (2), 125–136. doi:10.1177/1747493018806196

Bao, N., and Tang, B. (2020). Organ-protective effects and the underlying mechanism of dexmedetomidine. *Mediat. Inflamm.* 2020, 6136105. doi:10.1155/2020/6136105

Bellinger, D. L., Millar, B. A., Perez, S., Carter, J., Wood, C., ThyagaRajan, S., et al. (2008). Sympathetic modulation of immunity: Relevance to disease. *Cell Immunol.* 252 (1-2), 27–56. doi:10.1016/j.cellimm.2007.09.005

Bergquist, J., Tarkowski, A., Ewing, A., and Ekman, R. (1998). Catecholaminergic suppression of immunocompetent cells. *Immunol. Today* 19 (12), 562–567. doi:10. 1016/s0167-5699(98)01367-x

Bieber, M., Werner, R. A., Tanai, E., Hofmann, U., Higuchi, T., Schuh, K., et al. (2017). Stroke-induced chronic systolic dysfunction driven by sympathetic overactivity. *Ann. Neurol.* 82 (5), 729–743. doi:10.1002/ana.25073

Bosmann, M., Grailer, J. J., Zhu, K., Matthay, M. A., Sarma, J. V., Zetoune, F. S., et al. (2012). Anti-inflammatory effects of β2 adrenergic receptor agonists in experimental acute lung injury. *FASEB J.* 26 (5), 2137–2144. doi:10.1096/fj.11-201640

Chamorro, A., Urra, X., and Planas, A. M. (2007). Infection after acute ischemic stroke: A manifestation of brain-induced immunodepression. *Stroke* 38 (3), 1097–1103. doi:10.1161/01.STR.0000258346.68966.9d

Chiang, T., Messing, R. O., and Chou, W. H. (2011). Mouse model of middle cerebral artery occlusion. *J. Vis. Exp.* 48, 2761. doi:10.3791/2761

Cimolai, N., Taylor, G. P., Mah, D., and Morrison, B. J. (1992). Definition and application of a histopathological scoring scheme for an animal model of acute Mycoplasma pneumoniae pulmonary infection. *Microbiol. Immunol.* 36 (5), 465–478. doi:10.1111/j.1348-0421.1992.tb02045.x

Faura, J., Bustamante, A., Miró-Mur, F., and Montaner, J. (2021). Stroke-induced immunosuppression: Implications for the prevention and prediction of post-stroke infections. *J. Neuroinflammation* 18 (1), 127. doi:10.1186/s12974-021-02177-0

Finlayson, O., Kapral, M., Hall, R., Asllani, E., Selchen, D., Saposnik, G., et al. (2011). Risk factors, inpatient care, and outcomes of pneumonia after ischemic stroke. *Neurology* 77 (14), 1338–1345. doi:10.1212/WNL.0b013e31823152b1

Gao, J., Sun, Z., Xiao, Z., Du, Q., Niu, X., Wang, G., et al. (2019). Dexmedetomidine modulates neuroinflammation and improves outcome via alpha2-adrenergic receptor signaling after rat spinal cord injury. *Br. J. Anaesth.* 123 (6), 827–838. doi:10.1016/j.bja. 2019.08.026

Gendron, A., Teitelbaum, J., Cossette, C., Nuara, S., Dumont, M., Geadah, D., et al. (2002). Temporal effects of left versus right middle cerebral artery occlusion on spleen

lymphocyte subsets and mitogenic response in Wistar rats. *Brain Res.* 955 (1-2), 85–97. doi:10.1016/s0006-8993(02)03368-1

Hervé, J., Haurogné, K., Bacou, E., Pogu, S., Allard, M., Mignot, G., et al. (2017). β2-adrenergic stimulation of dendritic cells favors IL-10 secretion by CD4+ T cells. *Immunol. Res.* 65 (6), 1156–1163. doi:10.1007/s12026-017-8966-3

Huang, C. J., Webb, H. E., Garten, R. S., Kamimori, G. H., and Acevedo, E. O. (2010). Psychological stress during exercise: Lymphocyte subset redistribution in firefighters. *Physiol. Behav.* 101 (3), 320–326. doi:10.1016/j.physbeh.2010.05.018

Iadecola, C., and Anrather, J. (2011). The immunology of stroke: From mechanisms to translation. *Nat. Med.* 17 (7), 796–808. doi:10.1038/nm.2399

Jorm, C. M., and Stamford, J. A. (1993). Actions of the hypnotic anaesthetic, dexmedetomidine, on noradrenaline release and cell firing in rat locus coeruleus slices. *Br. J. Anaesth.* 71 (3), 447–449. doi:10.1093/bja/71.3.447

Kang, R., Jeong, J. S., Ko, J. S., Lee, S. Y., Lee, J. H., Choi, S. J., et al. (2020). Intraoperative dexmedetomidine attenuates norepinephrine levels in patients undergoing transsphenoidal surgery: A randomized, placebo-controlled trial. *BMC Anesthesiol.* 20 (1), 100. doi:10.1186/s12871-020-01025-7

Kim, E., Kim, H. C., Lee, S., Ryu, H. G., Park, Y. H., Kim, J. H., et al. (2017). Dexmedetomidine confers neuroprotection against transient global cerebral ischemia/reperfusion injury in rats by inhibiting inflammation through inactivation of the TLR-4/NF-κB pathway. *Neurosci. Lett.* 649, 20–27. doi:10.1016/j.neulet.2017.04.011

Koennecke, H. C., Belz, W., Berfelde, D., Endres, M., Fitzek, S., Hamilton, F., et al. (2011). Factors influencing in-hospital mortality and morbidity in patients treated on a stroke unit. *Neurology* 77 (10), 965–972. doi:10.1212/WNL.0b013e31822dc795

Langhorne, P., Stott, D. J., Robertson, L., MacDonald, J., Jones, L., McAlpine, C., et al. (2000). Medical complications after stroke: A multicenter study. *Stroke* 31 (6), 1223–1229. doi:10.1161/01.str.31.6.1223

Lechtenberg, K. J., Meyer, S. T., Doyle, J. B., Peterson, T. C., and Buckwalter, M. S. (2019). Augmented β2-adrenergic signaling dampens the neuroinflammatory response following ischemic stroke and increases stroke size. *J. Neuroinflammation* 16 (1), 112. doi:10.1186/s12974-019-1506-4

Liang, X., Hu, Q., Li, B., McBride, D., Bian, H., Spagnoli, P., et al. (2014). Follistatin-like 1 attenuates apoptosis via disco-interacting protein 2 homolog A/Akt pathway after middle cerebral artery occlusion in rats. *Stroke* 45 (10), 3048–3054. doi:10.1161/STROKEAHA.114.006092

Liu, Z., Wang, Y., Wang, Y., Ning, Q., Zhang, Y., Gong, C., et al. (2016). Dexmedetomidine attenuates inflammatory reaction in the lung tissues of septic mice by activating cholinergic anti-inflammatory pathway. *Int. Immunopharmacol.* 35, 210–216. doi:10.1016/j.intimp.2016.04.003

Martín-Cordero, L., García, J. J., Hinchado, M. D., Bote, E., and Ortega, E. (2013). Influence of exercise on NA- and Hsp72-induced release of IFN γ by the peritoneal suspension of macrophages and lymphocytes from genetically obese Zucker rats. *J. Physiol. Biochem.* 69 (1), 125–131. doi:10.1007/s13105-012-0196-5

Mignini, F., Streccioni, V., and Amenta, F. (2003). Autonomic innervation of immune organs and neuroimmune modulation. *Auton. Autacoid Pharmacol.* 23 (1), 1–25. doi:10.1046/j.1474-8673.2003.00280.x

Myers, M. G., Norris, J. W., Hachinski, V. C., and Sole, M. J. (1981). Plasma norepinephrine in stroke. *Stroke* 12 (2), 200–204. doi:10.1161/01.str.12.2.200

Nelson, L. E., Lu, J., Guo, T., Saper, C. B., Franks, N. P., and Maze, M. (2003). The alpha2-adrenoceptor agonist dexmedetomidine converges on an endogenous sleep-promoting pathway to exert its sedative effects. *Anesthesiology* 98 (2), 428–436. doi:10.1097/00000542-200302000-00024

Oros-Pantoja, R., Jarillo-Luna, A., Rivera-Aguilar, V., Sánchez-Torres, L. E., Godinez-Victoria, M., and Campos-Rodríguez, R. (2011). Effects of restraint stress on NALT structure and nasal IgA levels. *Immunol. Lett.* 135 (1-2), 78–87. doi:10.1016/j.imlet.2010.10.001

Prass, K., Braun, J. S., Dirnagl, U., Meisel, C., and Meisel, A. (2006). Stroke propagates bacterial aspiration to pneumonia in a model of cerebral ischemia. *Stroke* 37 (10), 2607–2612. doi:10.1161/01.STR.0000240409.68739.2b

Rassler, B., Reissig, C., Briest, W., Tannapfel, A., and Zimmer, H. G. (2003). Pulmonary edema and pleural effusion in norepinephrine-stimulated rats-hemodynamic or inflammatory effect? *Mol. Cell Biochem.* 250 (1-2), 55–63. doi:10.1023/a:1024942132705

Sander, D., Winbeck, K., Klingelhöfer, J., Etgen, T., and Conrad, B. (2001). Prognostic relevance of pathological sympathetic activation after acute thromboembolic stroke. *Neurology* 57 (5), 833–838. doi:10.1212/wnl.57.5.833

Saposnik, G., Hill, M. D., O'Donnell, M., Fang, J., Hachinski, V., Kapral, M. K., et al. (2008). Variables associated with 7-day, 30-day, and 1-year fatality after ischemic stroke. *Stroke* 39 (8), 2318–2324. doi:10.1161/STROKEAHA.107.510362

Schilling, M., Besselmann, M., Müller, M., Strecker, J. K., Ringelstein, E. B., and Kiefer, R. (2005). Predominant phagocytic activity of resident microglia over hematogenous macrophages following transient focal cerebral ischemia: An investigation using green fluorescent protein transgenic bone marrow chimeric mice. *Exp. Neurol.* 196 (2), 290–297. doi:10.1016/j.expneurol.2005.08.004

Seifert, H. A., Hall, A. A., Chapman, C. B., Collier, L. A., Willing, A. E., and Pennypacker, K. R. (2012). A transient decrease in spleen size following stroke corresponds to splenocyte release into systemic circulation. *J. Neuroimmune Pharmacol.* 7 (4), 1017–1024. doi:10.1007/s11481-012-9406-8

Wang, K., Wu, M., Xu, J., Wu, C., Zhang, B., Wang, G., et al. (2019). Effects of dexmedetomidine on perioperative stress, inflammation, and immune function: Systematic review and meta-analysis. *Br. J. Anaesth.* 123 (6), 777–794. doi:10.1016/j.bja.2019.07.027

Weimar, C., Roth, M. P., Zillessen, G., Glahn, J., Wimmer, M. L. J., Busse, O., et al. (2002). Complications following acute ischemic stroke. *Eur. Neurol.* 48 (3), 133–140. doi:10.1159/000065512

Winklewski, P. J., Radkowski, M., and Demkow, U. (2014). Cross-talk between the inflammatory response, sympathetic activation and pulmonary infection in the ischemic stroke. *J. Neuroinflammation* 11, 213. doi:10.1186/s12974-014-0213-4

Wu, Y., Liu, Y., Huang, H., Zhu, Y., Zhang, Y., Lu, F., et al. (2013). Dexmedetomidine inhibits inflammatory reaction in lung tissues of septic rats by suppressing TLR4/NF-κB pathway. *Mediat. Inflamm.* 2013, 562154. doi:10.1155/2013/562154

Xu, Y., Ge, Y., Zhou, M., and Zhang, Z. (2022). Clenbuterol, a selective β2-adrenergic receptor agonist, inhibits or limits post-stroke pneumonia, but increases infarct volume in MCAO mice. *J. Inflamm. Res.* 15, 295–309. doi:10.2147/JIR.S344521

Yuan, D., Liu, Z., Kaindl, J., Maeda, S., Zhao, J., Sun, X., et al. (2020). Activation of the α 2B adrenoceptor by the sedative sympatholytic dexmedetomidine. *Nat. Chem. Biol.* 16 (5), 507–512. doi:10.1038/s41589-020-0492-2

Zieziulewicz, T. J., Mondal, T. K., Gao, D., and Lawrence, D. A. (2013). Stress-induced effects, which inhibit host defenses, alter leukocyte trafficking. *Cell Stress Chaperones* 18 (3), 279–291. doi:10.1007/s12192-012-0380-0

New advances in clinical application of neostigmine: no longer focusing solely on increasing skeletal muscle strength

Shangkun Si[1†], Xiaohu Zhao[1†], Fan Su[2]*, Hongxiu Lu[2]*, Dongbin Zhang[2]*, Li Sun[2], Fulei Wang[1] and Li Xu[1]

[1]Shandong University of Traditional Chinese Medicine, Jinan, China, [2]Department of Anesthesiology, Affiliated Hospital of Shandong University of Traditional Chinese Medicine, Jinan, China

Neostigmine is a clinical cholinesterase inhibitor, that is, commonly used to enhance the function of the cholinergic neuromuscular junction. Recent studies have shown that neostigmine regulates the immune-inflammatory response through the cholinergic anti-inflammatory pathway, affecting perioperative neurocognitive function. This article reviews the relevant research evidence over the past 20 years, intending to provide new perspectives and strategies for the clinical application of neostigmine.

1 Introduction

Neostigmine has become a classic anticholinesterase drug since it was introduced in the 1930s. It inhibits acetylcholinesterase (AChE) activity, produces cholinergic effects, and enhances the transmission function of the neuromuscular junction, helping increase skeletal muscle strength. It is commonly used clinically to antagonize the residual muscle relaxation effect of non-depolarizing muscle relaxants following anesthesia surgery, and is also used to treat myasthenia gravis, postoperative functional flatulence, and urinary retention, etc., (Pohanka, 2012). In recent years, applications to modulate immune-inflammatory response through the cholinergic anti-inflammatory pathway (CAP) and affect neurocognitive function have been reported in turn, marking new progress in the clinical applications of this drug. This paper conducts a review in order to provide new evidence for the clinical application of neostigmine (The methodology of this mini-review is shown in Supplementary Material).

2 Pharmacological overview: cholinergic effect

Neostigmine is a carbamate derivative, belonging to the quaternary ammonium group, and is clinically used as a parasympathetic agent and cholinesterase inhibitor (ChE-Is). Its chemical structure (Kim et al., 2013) is shown in Supplementary Material. The positively charged nitrogen in the neostigmine molecule electrostatically binds to the peripheral

anionic site of AChE, whereas the carbamate group in the molecule covalently binds to the serine residue in the catalytic site of the enzyme. Through serine carbamylation, the activity of AChE is reversibly inhibited. As a result, the half-life of ACh in cholinergic synapses is prolonged and the activation of nicotinic/muscarinic cholinergic receptors (nAChRs/mAChRs) is increased, ultimately producing cholinergic effects (Eldufani and Blaise, 2019). In addition, neostigmine-induced inhibition of voltage-gated potassium channels can prolong action potentials in motor neurons and thereby increase ACh release at the neuromuscular junction to increase muscle fiber contraction. Neostigmine can also directly activate postsynaptic nAChRs at the motor endplate (Liu et al., 2022a). The commonly used routes of administration are intravenous and intramuscular injection; neostigmine is difficult to be absorbed orally by the gastrointestinal tract. Due to its structural properties (quaternary amine), the drug has difficulty crossing the blood-brain barrier (BBB) and entering the central nervous system (CNS) (Luo et al., 2018).

3 Conventional application: classical theater

3.1 Muscle strength: increasing

Increasing skeletal muscle strength is the classic application of neostigmine. Neostigmine reduces the activity of AChE, thereby prolonging the half-life of ACh at the neuromuscular junction. As a result, the increased ACh-induced activation of muscle AChRs increases muscle strength. These effects make it an important alternative drug for post-anesthesia residual muscle relaxation (non-depolarizing muscle relaxation) (Fuchs-Buder et al., 2023), myasthenia gravis (Feibel, 2021), acute colonic pseudo-obstruction (Adiamah et al., 2017), constipation (Kapoor, 2008), urinary retention (Cao et al., 2022), neurotoxic snake bites (Anil et al., 2010) and other conditions or diseases that cause muscular weakness due to dysfunction of the cholinergic muscle junction.

However, since the cholinergic effect of neostigmine is limited by the amount of synaptic ACh release, it has a ceiling effect on the enhancement of muscle strength (Blobner et al., 2020). If neostigmine is administered when the neuromuscular function is normal or has fully recovered, abnormal muscle weakness may be observed due to desensitization of nAChRs caused by excessive ACh accumulation at synapses (Naguib and Kopman, 2018). Therefore, neuromuscular function monitoring is important in order to confirm the proper timing of administration (Kopman and Naguib, 2015; Phillips and Stewart, 2018). Neostigmine activates both nAChRs and mAChRs at the same time, thus it must be combined with anticholinergic drugs (such as atropine, etc.) to avoid its muscarinic side effects (arrhythmia, increased secretion, nausea, or vomiting, etc.) under different application purposes (Tajaate et al., 2018).

3.2 Analgesia: adjuvants

Ach is one of multiple neurotransmitters involved in regulating the production and transmission of nociceptive signals in the spinal cord. Physiological (trauma, pain, etc.) or pharmacological stimulation (activation of α2-adrenergic receptors in the spinal cord or opioid receptors in the brain stem) contribute to release of ACh. Cholinergic receptors are present in the superficial and deep dorsal horn of the spinal cord, and are involved in transmission and modulation of nociceptive signals (Eldufani and Blaise, 2019). Clinical application of neostigmine has been widely reported for perioperative adjunctive analgesia (Swain et al., 2017; Prabhakar et al., 2019). It helps to enhance the analgesic effect, prolong the analgesic time, and reduce the consumption of analgesics such as morphine, ketamine and clonidine. The drug is typically injected intrathecally or epidurally (Habib and Gan, 2006), with less use of peripheral blockade. It inhibits the activity of AChE, increasing the concentration of endogenous ACh in spinal cord synapses. Then, through mAChRs, the transmission of nociceptive signals in the spinal dorsal horn are inhibited (Duttaroy et al., 2002; Lauretti, 2015), and nociceptive signaling of various afferent fibers (such as Aβ, C and Aδ fibers) (Buerkle et al., 1998) are modulated, thus inhibiting central sensitization, and increasing the pain threshold (Naguib and Yaksh, 1994). In addition, the release of NO in the spinal cord is promoted, producing analgesic effects (Prabhakar et al., 2019).

However, neostigmine has dose-related side effects when used for adjuvant analgesia, such as nausea and vomiting, which to some extent limit its application (Prabhakar et al., 2019). Further research is needed to optimize the medication regimen.

4 New applications: new arena for label-off usage

4.1 Immune and inflammatory regulation

For a long time, immune and inflammation regulation have not been considered to be the main effects of acetylcholinesterase inhibitors such as neostigmine. However, recent evidence has shed new light on this issue.

The cholinergic anti-inflammatory pathway (CAP) is an important endogenous immunomodulatory mechanism in the body (Borovikova et al., 2000; Hoover, 2017). The local immune-inflammatory signal transmitted to the CNS nucleus tractus solitarius via the vagal afferent nerve is the driving factor of CAP. ACh released from vagal efferent nerve fibers in the inflammatory reflex pathway activates α7nAChRs expressed on immune cells (such as macrophages). Subsequently, the synthesis and release of pro-inflammatory cytokines/mediators such as tumor necrosis factor-α (TNF-α), interleukin-1β (IL-1β), interleukin-6 (IL-6), and high mobility group protein box 1 (HMGB1) are inhibited through PI3K/Akt, JAK2/STAT3, NF-κB, Nrf2/HO-1 and other pathways. Finally, the tissue damage caused by inflammation and oxidative stress is improved (Fodale and Santamaria, 2008). CAP is mainly activated by central cholinergic transmission, electrical stimulation of the vagus nerve, or cholinergic agonists. AChE-Is inhibits AChE to increase the level and duration of ACh, activate α7nAChR and amplify the activity of the CAP system to exert anti-inflammatory effects, thus improving inflammatory response damage (Nizri et al., 2006). Therefore, in terms of
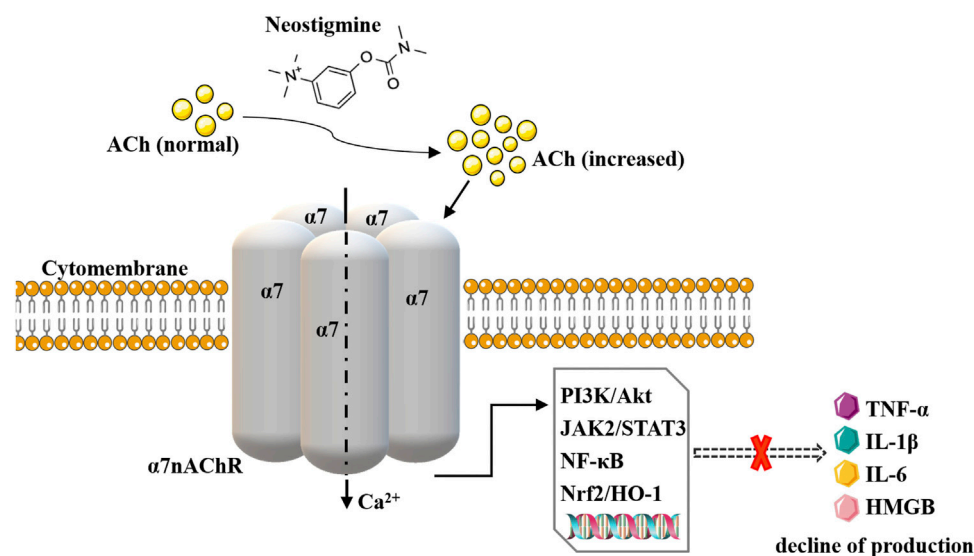
FIGURE 1
Schematic representation of neostigmine acting on CAP. Neostigmine increases the effect of ACh on α7nAChRs and amplifies CAP activity, reducing the levels of pro-inflammatory cytokines such as TNF-α, IL-1β, IL-6, and HMGB1 through PI3K/Akt, NF-kappaB, JAK2/STAT3 and other pathways.

pharmacological mechanism, it has the potential to become an immune-inflammatory regulatory drug (Pohanka, 2014). See Figure 1.

A series of studies over the last 20 years has reported the immune-inflammatory regulatory effects of neostigmine (Miceli and Jacobson, 2003; Akinci et al., 2005; Pollak et al., 2005; Freeling et al., 2008; Hofer et al., 2008; Liu et al., 2012; Sun et al., 2012; Kalb et al., 2013; Li et al., 2014; Schneider et al., 2014; Steinebrunner et al., 2014; Zhou et al., 2014; Qian et al., 2015; Kanashiro et al., 2016; Xu et al., 2016; Abdel-Salam et al., 2018; Herman et al., 2018; Bitzinger et al., 2019; Antunes et al., 2020a; Antunes et al., 2020b; Lyu et al., 2021; El-Tamalawy et al., 2022). Its peripheral administration increases the effect of ACh on α7nAChRs and amplifies CAP activity. Through PI3K/Akt (Antunes et al., 2020a), NF-kappaB (Hofer et al., 2008; Antunes et al., 2020a), JAK2/STAT3 (Xu et al., 2016) and other pathways, it reduces the levels of pro-inflammatory cytokines such as TNF-α, IL-1β, IL-6, and HMGB1 and upregulates activity of anti-inflammatory factors such as IL-10 (Paparini et al., 2015). It can regulate the migration, recruitment, and infiltration of immune cells, inhibiting inflammatory response, oxidative stress injury and apoptosis (Liu et al., 2012). As detailed in Table 1, management with neostigmine (either prophylactic or delayed administration) triggers immunomodulatory effects in a variety of animal models (including arthritis, pancreatitis, colitis, sepsis and organ injury or failure, etc.). Some studies (Liu et al., 2012; Sun et al., 2012; Li et al., 2014; Zhou et al., 2014; Qian et al., 2015; Xu et al., 2016; Lyu et al., 2021) have found that the combination of anisodamine and neostigmine produces good anti-inflammatory effects (better than that of neostigmine alone). The mechanisms are as follows: anisodamine blocks mAChRs to prevent its non-specific parasympathetic side effects (Li et al., 2014), and indirectly enables more endogenous ACh to bind to α7nAChRs (Poupko et al., 2007; Liu et al., 2009; Zhao et al., 2011), ultimately enhancing the effect of CAP (Liu et al., 2009; Xu et al., 2011; Zhao et al., 2011; Zhang et al., 2023).

Contrary to the findings above, however, some studies report that neostigmine does not modulate immune and inflammatory responses (Tyagi et al., 2010; Kox et al., 2011; Leib et al., 2011; Zhang et al., 2016). However, the reasons for the ineffectiveness have not been fully elucidated. Meanwhile, studies have reported that while neostigmine plays an immune-inflammatory regulatory role through CAP (activation of α7nAChRs), parasympathetic side effects may be observed (due to activation of mAChRs) (Akinci et al., 2005), requiring combination with anticholinergic drugs (e.g., anisodamine, the collaborator mentioned above) or dosage control, thus its application is somewhat limited. In addition, the above anti-inflammatory data on neostigmine are mostly nonclinical studies, and only one study reported its clinical anti-inflammatory effect in septic shock patients. Clinical evidence that neostigmine affects other inflammatory diseases is scarce, which limits the external validity and clinical anti-inflammatory application promotion. More large-sample and multi-center clinical studies are required to provide evidence for the regulatory effect of neostigmine on inflammation.

4.2 Perioperative neurocognitive protection

Perioperative neurocognitive disorders (PND) refer to the decline and deterioration of abilities in multiple cognitive domains during the perioperative period, including preoperative cognitive dysfunction, postoperative delirium (POD), and postoperative cognitive dysfunction (POCD). (Evered et al., 2018). The pathological role of CNS inflammatory response caused by anesthesia and surgery in PND has been widely reported (Liu et al., 2022b). Anesthesia and surgery (tissue damage or pathogenic attack) induce activation of the body's

TABLE 1 Neostigmine regulation of immune and inflammatory responses.

Author/Year	Model	Mode/dose	Mechanism/pathway	Inflammation-related index
Miceli and Jacobson (2003)	Acute dinitrobenzene sulfonic acid colitis Rats	s.c. 50 µg/kg	-	MPO (proximal to the anus) and combined macroscopic colonic damage score↓
Akinci et al. (2005)	Septic shock Mice	i.p. 0.1 or 0.3 mg/kg every 6 h for 3 days	-	Interstitial inflammation in the lungs↓; Vacuolar degeneration in the liver↓; Total liver injury↓
Pollak et al. (2005)	LPS-induced inflammation Mice	i.p. 0.15 mg/kg	AChE	IL-1β (hippocampus and blood)↓
Hofer et al. (2008)	Sepsis induced by cecal ligation and puncture Mice	i.p. 80 µg/kg three times daily for 3 days	NF-κB	Pulmonary neutrophil invasion↓; MPO activity (lung)↓; Survival↑
Freeling et al. (2008)	Heart with pressure overload Rats	i.p. 3 or 6 µg/kg per day for 14 days	-	Heart tissue: TNF-α↓, IL-10↑; Cardiac hypertrophy↓; Ventricular function↑
Sun et al. (2012)	Endotoxic shock Mice/Hemorrhagic shock Dogs	Mice: i.p. 12.5 or 25 or 50 µg/kg at 0, 3, and 6 h after LPS exposure; Dogs: i.v. 5.25 µg/kg	α7nAChR	Serum: TNF-α and IL-1β↓; Survival rate↑; Liver: damage, infiltration by inflammatory cells and putrescence of hepatic cells↓
Liu et al. (2012)	Ischemic stroke Rats	unknow 40 or 80 µg/kg	α7nAChR	Serum: TNF-α and IL-6↓; Neurological deficit score↓; Infarct size↓; Ischemic penumbra: cleaved caspase 8, Bad, and Bax↓, Bcl-2 and Bcl-xl↑
Kalb et al. (2013)	Laparotomy combined with LPS Rats	i.p. 100 µg/kg before the LPS-application, and s.c. 100 µg/kg for 3 times	-	IL-1β (cortex and hippocampus)↓; IL-1β and TNF-α (spleen and plasma)↓
Schneider et al. (2014)	Necrotizing pancreatitis Rats	i.p. loading dose of 0.05 mg/kg and then 0.0124 mg/kg per hour for 9 h	-	MPO (pancreatic tissue) and HMGB1 (serum)↓; Pancreatic morphological damage↓
Li et al. (2014)	Biliary drainage and partial hepatectomy Rats	i.p. 50 µg/kg twice per day for 2 days	-	Remnant livers: TNF-α, IL-1β, IL-6, MCP-1 and MIP-1α↓; Serum: TNF-α and IL-1β↓; Migration and infiltration of neutrophils and the hepatocyte injury↓
Zhou et al. (2014)	Collagen-induced arthritis Mice	i.p. 50 µg/kg per day for 10 days	-	Serum: TNF-α, IL-6 and IL-1β↓; Anti-type II collagen specific antibodies IgG and IgG$_{2a}$↓; Arthritis index and joint swelling↓
Steinebrunner et al. (2014)	Acute liver failure induced by acetaminophen Mice	i.p. 80 µg/kg either 1 h before or 1, 7, 12, 24 h after application of APAP	-	Serum: TNF-α and IL-1β↓; Hepatocellular damage↓(LDH, ALT↓); Histopathological liver damage and apoptosis↓; Survival↑
Qian et al. (2015)	Ischemic stroke Rats/Mice	i.v. 40 µg/kg	α7nAChR	Serum: TNF-α, IL-6 and IL-1α↓; Infarct size and neurological deficit score↓; Ischemic penumbra: Bad and Bax↓, Bcl-2 and Bcl-xl↑
Xu et al. (2016)	Acute lethal crush syndrome Rats/Rabbits	Rats: i.p. 40 µg/kg; Rabbits: i.p. 20 µg/kg	α7nAChR; JAK2-STAT3	24 h survival rate↑; Compressed muscle: TNF-α, IL-6 and IL-10↓; Serum and compressed muscle: H$_2$O$_2$, MPO and NO↓
Kanashiro et al. (2016)	Antigen-Induced Arthritis Mice	s.c. 12.5, 25 and 50 µg/kg twice a day for 7 days	-	Neutrophil recruitment in the knee joint↓
Herman et al. (2018)	Immune stress Ewes	i.v. 0.5 mg	α7nAChR	IL-1β (serum)↓; Hypothalamus: IL-1β, IL-6, and TNF-α↓
Abdel-Salam et al. (2018)	Acute malathion exposure Rats	i.p. 200 or 400 µg/kg	AChE; BChE	GSH (brain)↑; Neuronal degeneration (cortex and hippocampus)↓ GFAP(hippocampus)↓; Liver damage↓
Bitzinger et al. (2019)	CLP-induced sepsis Rats	i.p. 75 µg/kg four times over 24 h	-	ROS production and CD11b upregulation↓
Antunes et al. (2020a)	Allergic asthma Mice	i.p. 80 µg/kg per day for 3 days	AChE; α7nAChR; NF-κB; PI3K/Akt	Lung tissue: IL-4, IL-5, IL-13, IL-1β, TNF-α and ROS↓, CAT↑; EPO activity in BAL↓; Peribronchial and perivascular inflammatory infiltrates↓
Antunes et al. (2020b)	Allergic asthma Mice	i.p. 80 µg/kg per day for 3 days	AChE	Leukocyte recruitment (BAL)↓; Leukocyte infiltrate (lung)↓; ROS and CAT (cerebral cortex)↓; SOD/CAT ratio↑
Lyu et al. (2021)	Biliary obstruction Rats	i.p. 50 µg/kg per day for 7 days	-	Serum: CRP, TNF-α and IL-1β↓; Liver function↑(ALT, AST, TB, DB, and GGT↓)

TABLE 1 (*Continued*) Neostigmine regulation of immune and inflammatory responses.

Author/Year	Model	Mode/dose	Mechanism/ pathway	Inflammation-related index
El-Tamalawy et al. (2022)	Sepsis or septic shock Patients	i.v. 0.2 mg/h for 120 h	-	SOFA and Progression from sepsis to septic shock↓; Incidence of shock reversal↑

Tip: MPO, myeloperoxidase; Bad and Bax are pro-apoptosis protein; MCP-1, monocyte chemotactic protein 1, a protein secreted by astrocytes that promotes inflammation; MIP-1α is a macrophage inflammatory protein; Bcl-2, and Bcl-xl are anti-apoptosis protein; GSH, glutathione; GFAP, glial fibrillary acidic protein; BAL, bronchoalveolar lavage; CAT, catalase; EPO, eosinophil peroxidase; SOFA, sequential organ failure assessment.

immune-inflammatory system, resulting in a rapid increase in levels of pro-inflammatory cytokines (e.g., IL-1β, TNF-α, and IL-6) in a short period of time, causing peripheral local inflammation. Anesthesia and surgery can also increase the permeability of the BBB (Glumac et al., 2019). Inflammatory factors enter the CNS from the periphery through the BBB (Banks et al., 1995), and at the same time, peripheral inflammatory signals are transmitted to the brain through the afferent nerve. Then immune-related cells (such as astrocytes and microglia) in the hippocampus and other regions of the brain are activated, and pro-inflammatory cytokines such as IL-1β are released, thus causing a central immune-inflammatory response (Needham et al., 2017). The whole process interferes with the activity of neurons and synaptic transmission in the cerebral cortex or hippocampal region of the brain, ultimately affecting perioperative cognitive function (Cibelli et al., 2010; Fidalgo et al., 2011; Liu and Yin, 2018; Liu et al., 2022b). Neostigmine, as the most typical cholinesterase inhibitor in used general anesthesia, is often used to antagonize postoperative residual neuromuscular blockade and is occasionally used as an adjunct to perioperative analgesia. At the same time, cholinergic system activity and CAP activity can be increased through the cholinergic effect of neostigmine. Therefore, whether neostigmine could improve CNS immune-inflammation impairment by increasing cholinergic system activity and through mechanisms such as CAP, and thus be an exposure factor for improving perioperative cognitive function, is a clinical question worth investigating.

4.2.1 Neostigmine on central anti-inflammation and neuro-protection: nonclinical studies

Animal experiments have shown that neostigmine inhibits AChE, increases cholinergic system activity and neurotransmission (Pollak et al., 2005), and then activates CAP, regulates the activation level of CNS immune cells such as microglia and astrocytes, and reduces the expression of pro-inflammatory cytokines such as IL-1β (Kalb et al., 2013), thereby attenuating or delaying the inflammatory response, oxidative stress and neuronal degeneration in the cerebral cortex and hippocampus of the surgical stress model rats (Abdel-Salam et al., 2018), maintaining synaptic plasticity (Tozzi et al., 2015), and finally exerting central immune-inflammatory response regulation and neuroprotective effects (Antunes et al., 2020b). However, the data above only reported the central anti-inflammatory and neuroprotective effects of neostigmine, without quantitative evaluation of neurocognitive function changes in animals.

4.2.2 Neostigmine on perioperative neurocognitive function: clinical studies

An earlier study by Prohovnik et al. (1997) found that intravenous administration of neostigmine (11 μg/kg) exhibited a reversal effect on scopolamine-induced memory deficits in healthy subjects (no difference from the effect of 22 μg/kg of physostigmine, which can be transferred into the CNS). One case report showed that intravenous neostigmine improved patients' delirium symptoms while treating postoperative acute colonic pseudo-obstruction (Lankarani-Fard and Castle, 2006). Zhu et al. found that the incidence of early postoperative cognitive decline in elderly patients undergoing radical resection of gastrointestinal cancer following intravenous injection of 0.04 mg/kg neostigmine in PACU was significantly lower than in the control group (Zhu et al., 2020). Cozanitis et al. showed that the postoperative Wechsler Memory Scale scores of elderly cataract surgery patients in the neostigmine group were similar to those in the galantamine group (a type of AChE-Is, acting on the CNS, commonly used in neurodegenerative diseases such as Alzheimer's disease and Parkinson's disease) (Cozanitis et al., 2012). However, Batistaki et al. came to the opposite conclusion: no significant difference in POCD incidence in middle-aged and elderly surgical patients in the neostigmine group compared with sugammadex (Batistaki et al., 2017); and Liu et al. indicated that application of neostigmine in patients undergoing colon cancer surgery did not reduce the incidence of POD (Liu et al., 2022a). The reasons are speculated as follows: i) Neostigmine is mainly used postoperatively, with rapid half-life elimination and short duration of action (Carron et al., 2016), thus making it difficult to account for the influence of anesthetic surgical factors on the CNS in a short period of time; ii) Neostigmine is often combined with anticholinergic drugs such as atropine to avoid its non-specific parasympathetic adverse reactions, while anticholinergic effects antagonize the cholinergic and CAP effects of neostigmine (Zwart and Vijverberg, 1997; Gonzalez-Rubio et al., 2006). The clinical data above show the potential of neostigmine to improve perioperative neurocognitive function. However, there was heterogeneity in the type of surgery involved in these studies, and the quantitative assessment tools of cognitive function were not consistent. At the same time, some studies did not provide sample size estimation basis. This limited heterogeneity control may therefore introduce bias, and the results need to be viewed with caution.

Many issues need to be explored before the effects of neostigmine on central anti-inflammatory and neuroprotective effects are confirmed. It is generally accepted that drugs need to be present in the central compartment to have CNS effects (Pavlov et al., 2009; Noori et al., 2012; Herman et al., 2019). As a quaternary ammonium compound, however, neostigmine does not readily cross the BBB and stays in the peripheral compartment when delivered via non-central routes of administration. Thus, it is difficult to understand how peripheral administration of neostigmine

modulates inflammation in the CNS. Through literature review and collation, the mechanisms are speculated as follows. i) Increased BBB permeability: Anesthesia and surgery, inflammatory response, stress, and other factors increase BBB permeability (Friedman et al., 1996; Beck et al., 2003; Danielski et al., 2018; Glumac et al., 2019). Peripheral neostigmine may enter the CNS through the damaged BBB to function (Zhu et al., 2020). However, the results of current studies on the effect of peripheral administration of neostigmine on central AChE activity under certain specific conditions are controversial (Pollak et al., 2005; Kalb et al., 2013; Zhang et al., 2016; Abdel-Salam et al., 2018; Dubrovskii et al., 2018; Antunes et al., 2020b). Therefore, the available evidence is still inconclusive about whether neostigmine can directly play a corresponding role through the BBB into the CNS in some special cases. ii) Improving peripheral inflammation: Peripheral inflammatory signals are transmitted to the CNS via vagal afferent nerves, while peripheral pro-inflammatory cytokines reach the brain parenchyma through the BBB (due to increased BBB permeability or active transport mechanisms). Both the nervous signals and humoral factors to some extent directly or indirectly cause CNS immune-inflammatory responses (Banks et al., 1995; Needham et al., 2017; Noll et al., 2017). Neostigmine reduces the peripheral inflammatory response level and expression of pro-inflammatory cytokines. Then, the transmission of peripheral inflammatory signals to the central system is attenuated (Herman et al., 2017; Herman et al., 2018), and the CNS is less affected by peripheral pro-inflammatory cytokines passing through the BBB (peripheral pro-inflammatory cytokines need to be enriched to a critical level in order to affect the CNS (Antunes et al., 2020b)), thus reducing the central immune-inflammatory response (Pollak et al., 2005; Steinman, 2010; Kalb et al., 2013) (The relationship between neostigmine and neuroprotective effects is shown in Supplementary Material). iii) Other potentially significant factors: neostigmine may be involved in changes in cognitive function by modulating the peripheral cholinergic cerebrovascular circulation (Kocsis et al., 2014). This view is based on the functional basis of high energy and oxygen consumption in the brain. Contrary to most people's perception, carbamate compounds such as neostigmine may exert CNS effects in certain circumstances - an important point that should not be ignored in the evaluation of the effects of neostigmine!

5 Conclusion and perspective

Recent studies have shown that the classic cholinergic effect of neostigmine may play a new role in immune-inflammatory regulation and perioperative neurocognitive protection through CAP. However, the function, downstream regulatory targets and transduction pathways of CAP are still not completely clear. Current studies on neostigmine in immune-inflammation regulation and perioperative neurocognitive protection are mostly animal experiments, and more clinical studies are needed for verification. Considering the non-specific

parasympathetic side effects of neostigmine under different application purposes, further research on the reasonable medication regimen is required. It is believed that with deep follow-up research, new and comprehensive neostigmine usage strategies will be observed.

Author contributions

SS conceived, designed, and conducted the study, analyzed the data, and wrote the manuscript. XZ, LX, and FW helped design the study and review the manuscript. DZ, LS, and HL helped conceive, design, and conduct the study and analyze the data. FS helped conceive, design, and conduct the study, analyze the data, and write the manuscript. All authors contributed to the article and approved the submitted version.

Conflict of interest

The authors declare that the research was conducted in the absence of any commercial or financial relationships that could be construed as a potential conflict of interest.

Publisher's note

All claims expressed in this article are solely those of the authors and do not necessarily represent those of their affiliated organizations, or those of the publisher, the editors and the reviewers. Any product that may be evaluated in this article, or claim that may be made by its manufacturer, is not guaranteed or endorsed by the publisher.

Supplementary material

The Supplementary Material for this article can be found online at: https://www.frontiersin.org/articles/10.3389/fphar.2023.1227496/full#supplementary-material

References

Abdel-Salam, O., Youness, E. R., Esmail, R., Mohammed, N. A., Khadrawy, Y. A., Sleem, A. A., et al. (2018). Protection by neostigmine and atropine against brain and liver injury induced by acute malathion exposure. *J. Nanosci. Nanotechnol.* 18, 510–521. doi:10.1166/jnn.2018.13933

Adiamah, A., Johnson, S., Ho, A., and Orbell, J. (2017). Neostigmine and glycopyrronium: A potential safe alternative for patients with pseudo-obstruction without access to conventional methods of decompression. *Bmj Case Rep.* 2017, bcr2017221249. doi:10.1136/bcr-2017-221249

Akinci, S. B., Ulu, N., Yondem, O. Z., Firat, P., Guc, M. O., Kanbak, M., et al. (2005). Effect of neostigmine on organ injury in murine endotoxemia: Missing facts about the cholinergic antiinflammatory pathway. *World J. Surg.* 29, 1483–1489. doi:10.1007/s00268-005-0073-2

Anil, A., Singh, S., Bhalla, A., Sharma, N., Agarwal, R., and Simpson, I. D. (2010). Role of neostigmine and polyvalent antivenom in Indian common krait (Bungarus caeruleus) bite. *J. Infect. Public Health* 3, 83–87. doi:10.1016/j.jiph.2010.01.002

Antunes, G. L., Silveira, J. S., Kaiber, D. B., Luft, C., Da, C. M., Marques, E. P., et al. (2020a). Cholinergic anti-inflammatory pathway confers airway protection against oxidative damage and attenuates inflammation in an allergic asthma model. *J. Cell. Physiol.* 235, 1838–1849. doi:10.1002/jcp.29101

Antunes, G. L., Silveira, J. S., Kaiber, D. B., Luft, C., Dos, S. T., Marques, E. P., et al. (2020b). Neostigmine treatment induces neuroprotection against oxidative stress in cerebral cortex of asthmatic mice. *Metab. Brain Dis.* 35, 765–774. doi:10.1007/s11011-020-00558-7

Banks, W. A., Kastin, A. J., and Broadwell, R. D. (1995). Passage of cytokines across the blood-brain barrier. *Neuroimmunomodulation* 2, 241–248. doi:10.1159/000097202

Batistaki, C., Riga, M., Zafeiropoulou, F., Lyrakos, G., Kostopanagiotou, G., and Matsota, P. (2017). Effect of sugammadex versus neostigmine/atropine combination on postoperative cognitive dysfunction after elective surgery. *Anaesth. Intensive Care* 45, 581–588. doi:10.1177/0310057X1704500508

Beck, K. D., Brennan, F. X., Moldow, R. L., Ottenweller, J. E., Zhu, G., and Servatius, R. J. (2003). Stress interacts with peripheral cholinesterase inhibitors to cause central nervous system effects. *Life Sci.* 73, 41–51. doi:10.1016/s0024-3205(03)00255-8

Bitzinger, D. I., Gruber, M., Tummler, S., Malsy, M., Seyfried, T., Weber, F., et al. (2019). *In vivo* effects of neostigmine and physostigmine on neutrophil functions and evaluation of acetylcholinesterase and butyrylcholinesterase as inflammatory markers during experimental sepsis in rats. *Mediat. Inflamm.* 2019, 8274903. doi:10.1155/2019/8274903

Blobner, M., Hunter, J. M., Meistelman, C., Hoeft, A., Hollmann, M. W., Kirmeier, E., et al. (2020). Use of a train-of-four ratio of 0.95 versus 0.9 for tracheal extubation: An exploratory analysis of POPULAR data. *Br. J. Anaesth.* 124, 63–72. doi:10.1016/j.bja.2019.08.023

Borovikova, L. V., Ivanova, S., Zhang, M., Yang, H., Botchkina, G. I., Watkins, L. R., et al. (2000). Vagus nerve stimulation attenuates the systemic inflammatory response to endotoxin. *Nature* 405, 458–462. doi:10.1038/35013070

Buerkle, H., Boschin, M., Marcus, M. A., Brodner, G., Wusten, R., and Van Aken, H. (1998). Central and peripheral analgesia mediated by the acetylcholinesterase-inhibitor neostigmine in the rat inflamed knee joint model. *Anesth. Analg.* 86, 1027–1032. doi:10.1097/00000539-199805000-00023

Cao, M., Wu, X., and Xu, J. (2022). A systematic review and meta-analysis of neostigmine for urinary retention after surgeries. *Transl. Androl. Urol.* 11, 190–201. doi:10.21037/tau-22-16

Carron, M., Toniolo, A., and Ori, C. (2016). Prolonged cholinergic effects after the reversal of neuromuscular blockade with neostigmine. *J. Clin. Anesth.* 28, 85. doi:10.1016/j.jclinane.2015.06.017

Cibelli, M., Fidalgo, A. R., Terrando, N., Ma, D., Monaco, C., Feldmann, M., et al. (2010). Role of interleukin-1beta in postoperative cognitive dysfunction. *Ann. Neurol.* 68, 360–368. doi:10.1002/ana.22082

Cozanitis, D., Keinonen, M., and Maunuksela, E. L. (2012). Effect on cognition of galanthamine administered for neuromuscular block reversal in octogenarians undergoing cataract surgery. *Anaesthesiol. Intensive Ther.* 44, 76–80.

Danielski, L. G., Giustina, A. D., Badawy, M., Barichello, T., Quevedo, J., Dal-Pizzol, F., et al. (2018). Brain barrier breakdown as a cause and consequence of neuroinflammation in sepsis. *Mol. Neurobiol.* 55, 1045–1053. doi:10.1007/s12035-016-0356-7

Dubrovskii, V. N., Shalabodov, A. D., and Belkin, A. V. (2018). Effects of neostigmine and physostigmine on activity of Na(+),K(+)-ATPase in various subdivisions of rat brain. *Bull. Exp. Biol. Med.* 166, 50–53. doi:10.1007/s10517-018-4287-3

Duttaroy, A., Gomeza, J., Gan, J. W., Siddiqui, N., Basile, A. S., Harman, W. D., et al. (2002). Evaluation of muscarinic agonist-induced analgesia in muscarinic acetylcholine receptor knockout mice. *Mol. Pharmacol.* 62, 1084–1093. doi:10.1124/mol.62.5.1084

El-Tamalawy, M. M., Soliman, M. M., Omara, A. F., Rashad, A., Ibrahim, O. M., and El-Shishtawy, M. M. (2022). Efficacy and safety of neostigmine adjunctive therapy in patients with sepsis or septic shock: A randomized controlled trial. *Front. Pharmacol.* 13, 855764. doi:10.3389/fphar.2022.855764

Eldufani, J., and Blaise, G. (2019). The role of acetylcholinesterase inhibitors such as neostigmine and rivastigmine on chronic pain and cognitive function in aging: A review of recent clinical applications. *Alzheimers Dement. (N Y)* 5, 175–183. doi:10.1016/j.trci.2019.03.004

Evered, L., Silbert, B., Knopman, D. S., Scott, D. A., DeKosky, S. T., Rasmussen, L. S., et al. (2018). Recommendations for the nomenclature of cognitive change associated with anaesthesia and surgery-2018. *Br. J. Anaesth.* 121, 1005–1012. doi:10.1016/j.bja.2017.11.087

Feibel, R. M. (2021). Henry R. Viets, MD, and the history of myasthenia gravis. *Neurology* 96, 322–326. doi:10.1212/WNL.0000000000011239

Fidalgo, A. R., Cibelli, M., White, J. P., Nagy, I., Maze, M., and Ma, D. (2011). Systemic inflammation enhances surgery-induced cognitive dysfunction in mice. *Neurosci. Lett.* 498, 63–66. doi:10.1016/j.neulet.2011.04.063

Fodale, V., and Santamaria, L. B. (2008). Cholinesterase inhibitors improve survival in experimental sepsis: A new way to activate the cholinergic anti-inflammatory pathway. *Crit. Care Med.* 36, 622–623. doi:10.1097/CCM.0B013E31816297CE

Freeling, J., Wattier, K., LaCroix, C., and Li, Y. F. (2008). Neostigmine and pilocarpine attenuated tumour necrosis factor alpha expression and cardiac hypertrophy in the heart with pressure overload. *Exp. Physiol.* 93, 75–82. doi:10.1113/expphysiol.2007.039784

Friedman, A., Kaufer, D., Shemer, J., Hendler, I., Soreq, H., and Tur-Kaspa, I. (1996). Pyridostigmine brain penetration under stress enhances neuronal excitability and induces early immediate transcriptional response. *Nat. Med.* 2, 1382–1385. doi:10.1038/nm1296-1382

Fuchs-Buder, T., Romero, C. S., Lewald, H., Lamperti, M., Afshari, A., Hristovska, A. M., et al. (2023). Peri-operative management of neuromuscular blockade: A guideline from the European society of anaesthesiology and intensive care. *Eur. J. Anaesthesiol.* 40, 82–94. doi:10.1097/EJA.0000000000001769

Glumac, S., Kardum, G., and Karanovic, N. (2019). Postoperative cognitive decline after cardiac surgery: A narrative review of current knowledge in 2019. *Med. Sci. Monit.* 25, 3262–3270. doi:10.12659/MSM.914435

Gonzalez-Rubio, J. M., Garcia, D. D. A., Egea, J., Olivares, R., Rojo, J., Gandia, L., et al. (2006). Blockade of nicotinic receptors of bovine adrenal chromaffin cells by nanomolar concentrations of atropine. *Eur. J. Pharmacol.* 535, 13–24. doi:10.1016/j.ejphar.2006.01.057

Habib, A. S., and Gan, T. J. (2006). Use of neostigmine in the management of acute postoperative pain and labour pain: A review. *Cns Drugs* 20, 821–839. doi:10.2165/00023210-200620100-00004

Herman, A. P., Skipor, J., Krawczynska, A., Bochenek, J., Wojtulewicz, K., Antushevich, H., et al. (2017). Peripheral inhibitor of AChE, neostigmine, prevents the inflammatory dependent suppression of GnRH/LH secretion during the follicular phase of the estrous cycle. *Biomed. Res. Int.* 2017, 6823209. doi:10.1155/2017/6823209

Herman, A. P., Skipor, J., Krawczynska, A., Bochenek, J., Wojtulewicz, K., Pawlina, B., et al. (2019). Effect of central injection of neostigmine on the bacterial endotoxin induced suppression of GnRH/LH secretion in ewes during the follicular phase of the estrous cycle. *Int. J. Mol. Sci.* 20, 4598. doi:10.3390/ijms20184598

Herman, A. P., Tomaszewska-Zaremba, D., Kowalewska, M., Szczepkowska, A., Oleszkiewicz, M., Krawczynska, A., et al. (2018). Neostigmine attenuates proinflammatory cytokine expression in preoptic area but not choroid plexus during lipopolysaccharide-induced systemic inflammation. *Mediat. Inflamm.* 2018, 9150207. doi:10.1155/2018/9150207

Hofer, S., Eisenbach, C., Lukic, I. K., Schneider, L., Bode, K., Brueckmann, M., et al. (2008). Pharmacologic cholinesterase inhibition improves survival in experimental sepsis. *Crit. Care Med.* 36, 404–408. doi:10.1097/01.CCM.0B013E31816208B3

Hoover, D. B. (2017). Cholinergic modulation of the immune system presents new approaches for treating inflammation. *Pharmacol. Ther.* 179, 1–16. doi:10.1016/j.pharmthera.2017.05.002

Kalb, A., von Haefen, C., Sifringer, M., Tegethoff, A., Paeschke, N., Kostova, M., et al. (2013). Acetylcholinesterase inhibitors reduce neuroinflammation and -degeneration in the cortex and hippocampus of a surgery stress rat model. *Plos One* 8, e62679. doi:10.1371/journal.pone.0062679

Kanashiro, A., Talbot, J., Peres, R. S., Pinto, L. G., Bassi, G. S., Cunha, T. M., et al. (2016). Neutrophil recruitment and articular hyperalgesia in antigen-induced arthritis are modulated by the cholinergic anti-inflammatory pathway. *Basic Clin. Pharmacol. Toxicol.* 119, 453–457. doi:10.1111/bcpt.12611

Kapoor, S. (2008). Management of constipation in the elderly: Emerging therapeutic strategies. *World J. Gastroenterol.* 14, 5226–5227. doi:10.3748/wjg.14.5226

Kim, S., Bolton, E. E., and Bryant, S. H. (2013). PubChem3D: Conformer ensemble accuracy. *J. Cheminform* 5, 1. doi:10.1186/1758-2946-5-1

Kocsis, P., Gyertyan, I., Eles, J., Laszy, J., Hegedus, N., Gajari, D., et al. (2014). Vascular action as the primary mechanism of cognitive effects of cholinergic, CNS-acting drugs, a

rat phMRI BOLD study. *J. Cereb. Blood Flow. Metab.* 34, 995–1000. doi:10.1038/jcbfm.2014.47

Kopman, A. F., and Naguib, M. (2015). Neostigmine: You can't have it both ways. *Anesthesiology* 123, 231–233. doi:10.1097/ALN.0000000000000678

Kox, M., Pompe, J. C., Peters, E., Vaneker, M., van der Laak, J. W., van der Hoeven, J. G., et al. (2011). α7 nicotinic acetylcholine receptor agonist GTS-21 attenuates ventilator-induced tumour necrosis factor-α production and lung injury. *Br. J. Anaesth.* 107, 559–566. doi:10.1093/bja/aer202

Lankarani-Fard, A., and Castle, S. C. (2006). Postoperative delirium and Ogilvie's syndrome resolving with neostigmine. *J. Am. Geriatr. Soc.* 54, 1016–1017. doi:10.1111/j.1532-5415.2006.00759.x

Lauretti, G. R. (2015). The evolution of spinal/epidural neostigmine in clinical application: Thoughts after two decades. *Saudi J. Anaesth.* 9, 71–81. doi:10.4103/1658-354X.146319

Leib, C., Goser, S., Luthje, D., Ottl, R., Tretter, T., Lasitschka, F., et al. (2011). Role of the cholinergic antiinflammatory pathway in murine autoimmune myocarditis. *Circ. Res.* 109, 130–140. doi:10.1161/CIRCRESAHA.111.245563

Li, C. H., Zhang, X., Ge, X. L., Huang, X., Zhang, A. Q., and Gu, W. Q. (2014). Effects of combined anisodamine and neostigmine treatment on the inflammatory response and liver regeneration of obstructive jaundice rats after hepatectomy. *Biomed. Res. Int.* 2014, 362024. doi:10.1155/2014/362024

Liu, A. J., Zang, P., Guo, J. M., Wang, W., Dong, W. Z., Guo, W., et al. (2012). Involvement of acetylcholine-α7nAChR in the protective effects of arterial baroreflex against ischemic stroke. *Cns Neurosci. Ther.* 18, 918–926. doi:10.1111/cns.12011

Liu, C., Shen, F. M., Le, Y. Y., Kong, Y., Liu, X., Cai, G. J., et al. (2009). Antishock effect of anisodamine involves a novel pathway for activating alpha7 nicotinic acetylcholine receptor. *Crit. Care Med.* 37, 634–641. doi:10.1097/CCM.0b013e31819598f5

Liu, F., Lin, X., Lin, Y., Deng, X., Guo, Y., Wang, B., et al. (2022a). The effect of neostigmine on postoperative delirium after colon carcinoma surgery: A randomized, double-blind, controlled trial. *Bmc Anesthesiol.* 22, 267. doi:10.1186/s12871-022-01804-4

Liu, Y., Fu, H., and Wang, T. (2022b). Neuroinflammation in perioperative neurocognitive disorders: From bench to the bedside. *Cns Neurosci. Ther.* 28, 484–496. doi:10.1111/cns.13794

Liu, Y., and Yin, Y. (2018). Emerging roles of immune cells in postoperative cognitive dysfunction. *Mediat. Inflamm.* 2018, 6215350. doi:10.1155/2018/6215350

Luo, J., Chen, S., Min, S., and Peng, L. (2018). Reevaluation and update on efficacy and safety of neostigmine for reversal of neuromuscular blockade. *Ther. Clin. Risk Manag.* 14, 2397–2406. doi:10.2147/TCRM.S179420

Lyu, S. C., Wang, J., Xu, W. L., Wang, H. X., Pan, F., Jiang, T., et al. (2021). Therapeutic effect of combining anisodamine with neostigmine on local scar formation following roux-en-Y choledochojejunostomy in a novel rat model. *Front. Pharmacol.* 12, 700050. doi:10.3389/fphar.2021.700050

Miceli, P. C., and Jacobson, K. (2003). Cholinergic pathways modulate experimental dinitrobenzene sulfonic acid colitis in rats. *Auton. Neurosci.* 105, 16–24. doi:10.1016/S1566-0702(03)00023-7

Naguib, M., and Kopman, A. F. (2018). Neostigmine-induced weakness: What are the facts? *Anaesthesia* 73, 1055–1057. doi:10.1111/anae.14322

Naguib, M., and Yaksh, T. L. (1994). Antinociceptive effects of spinal cholinesterase inhibition and isobolographic analysis of the interaction with mu and alpha 2 receptor systems. *Anesthesiology* 80, 1338–1348. doi:10.1097/00000542-199406000-00022

Needham, M. J., Webb, C. E., and Bryden, D. C. (2017). Postoperative cognitive dysfunction and dementia: What we need to know and do. *Br. J. Anaesth.* 119, i115–i125. doi:10.1093/bja/aex354

Nizri, E., Hamra-Amitay, Y., Sicsic, C., Lavon, I., and Brenner, T. (2006). Anti-inflammatory properties of cholinergic up-regulation: A new role for acetylcholinesterase inhibitors. *Neuropharmacology* 50, 540–547. doi:10.1016/j.neuropharm.2005.10.013

Noll, F., Behnke, J., Leiting, S., Troidl, K., Alves, G. T., Muller-Redetzky, H., et al. (2017). Self-extracellular RNA acts in synergy with exogenous danger signals to promote inflammation. *Plos One* 12, e0190002. doi:10.1371/journal.pone.0190002

Noori, H. R., Fliegel, S., Brand, I., and Spanagel, R. (2012). The impact of acetylcholinesterase inhibitors on the extracellular acetylcholine concentrations in the adult rat brain: A meta-analysis. *Synapse* 66, 893–901. doi:10.1002/syn.21581

Paparini, D., Gori, S., Grasso, E., Scordo, W., Calo, G., Perez, L. C., et al. (2015). Acetylcholine contributes to control the physiological inflammatory response during the peri-implantation period. *Acta Physiol. (Oxf)* 214, 237–247. doi:10.1111/apha.12494

Pavlov, V. A., Parrish, W. R., Rosas-Ballina, M., Ochani, M., Puerta, M., Ochani, K., et al. (2009). Brain acetylcholinesterase activity controls systemic cytokine levels through the cholinergic anti-inflammatory pathway. *Brain Behav. Immun.* 23, 41–45. doi:10.1016/j.bbi.2008.06.011

Phillips, S., and Stewart, P. A. (2018). Catching a unicorn: Neostigmine and muscle weakness-not neostigmine for all, but quantitative monitoring for everyone. *Anesthesiology* 129, 381–382. doi:10.1097/ALN.0000000000002295

Pohanka, M. (2012). Acetylcholinesterase inhibitors: A patent review (2008 - present). *Expert Opin. Ther. Pat.* 22, 871–886. doi:10.1517/13543776.2012.701620

Pohanka, M. (2014). Inhibitors of acetylcholinesterase and butyrylcholinesterase meet immunity. *Int. J. Mol. Sci.* 15, 9809–9825. doi:10.3390/ijms15069809

Pollak, Y., Gilboa, A., Ben-Menachem, O., Ben-Hur, T., Soreq, H., and Yirmiya, R. (2005). Acetylcholinesterase inhibitors reduce brain and blood interleukin-1beta production. *Ann. Neurol.* 57, 741–745. doi:10.1002/ana.20454

Poupko, J. M., Baskin, S. I., and Moore, E. (2007). The pharmacological properties of anisodamine. *J. Appl. Toxicol.* 27, 116–121. doi:10.1002/jat.1154

Prabhakar, A., Lambert, T., Kaye, R. J., Gaignard, S. M., Ragusa, J., Wheat, S., et al. (2019). Adjuvants in clinical regional anesthesia practice: A comprehensive review. *Best. Pract. Res. Clin. Anaesthesiol.* 33, 415–423. doi:10.1016/j.bpa.2019.06.001

Prohovnik, I., Arnold, S. E., Smith, G., and Lucas, L. R. (1997). Physostigmine reversal of scopolamine-induced hypofrontality. *J. Cereb. Blood Flow. Metab.* 17, 220–228. doi:10.1097/00004647-199702000-00012

Qian, J., Zhang, J. M., Lin, L. L., Dong, W. Z., Cheng, Y. Q., Su, D. F., et al. (2015). A combination of neostigmine and anisodamine protects against ischemic stroke by activating α7nAChR. *Int. J. Stroke* 10, 737–744. doi:10.1111/ijs.12458

Schneider, L., Jabrailova, B., Soliman, H., Hofer, S., Strobel, O., Hackert, T., et al. (2014). Pharmacological cholinergic stimulation as a therapeutic tool in experimental necrotizing pancreatitis. *Pancreas* 43, 41–46. doi:10.1097/MPA.0b013e3182a85c21

Steinebrunner, N., Mogler, C., Vittas, S., Hoyler, B., Sandig, C., Stremmel, W., et al. (2014). Pharmacologic cholinesterase inhibition improves survival in acetaminophen-induced acute liver failure in the mouse. *Bmc Gastroenterol.* 14, 148. doi:10.1186/1471-230X-14-148

Steinman, L. (2010). Modulation of postoperative cognitive decline via blockade of inflammatory cytokines outside the brain. *Proc. Natl. Acad. Sci. U. S. A.* 107, 20595–20596. doi:10.1073/pnas.1015282107

Sun, L., Zhang, G. F., Zhang, X., Liu, Q., Liu, J. G., Su, D. F., et al. (2012). Combined administration of anisodamine and neostigmine produces anti-shock effects: Involvement of α7 nicotinic acetylcholine receptors. *Acta Pharmacol. Sin.* 33, 761–766. doi:10.1038/aps.2012.26

Swain, A., Nag, D. S., Sahu, S., and Samaddar, D. P. (2017). Adjuvants to local anesthetics: Current understanding and future trends. *World J. Clin. Cases* 5, 307–323. doi:10.12998/wjcc.v5.i8.307

Tajaate, N., Schreiber, J. U., Fuchs-Buder, T., Jelting, Y., and Kranke, P. (2018). Neostigmine-based reversal of intermediate acting neuromuscular blocking agents to prevent postoperative residual paralysis: A systematic review. *Eur. J. Anaesthesiol.* 35, 184–192. doi:10.1097/EJA.0000000000000741

Tozzi, A., Sclip, A., Tantucci, M., de Iure, A., Ghiglieri, V., Costa, C., et al. (2015). Region- and age-dependent reductions of hippocampal long-term potentiation and NMDA to AMPA ratio in a genetic model of Alzheimer's disease. *Neurobiol. Aging* 36, 123–133. doi:10.1016/j.neurobiolaging.2014.07.002

Tyagi, E., Agrawal, R., Nath, C., and Shukla, R. (2010). Cholinergic protection via alpha7 nicotinic acetylcholine receptors and PI3K-Akt pathway in LPS-induced neuroinflammation. *Neurochem. Int.* 56, 135–142. doi:10.1016/j.neuint.2009.09.011

Xu, Z. P., Wang, H., Hou, L. N., Xia, Z., Zhu, L., Chen, H. Z., et al. (2011). Modulatory effect of anisodamine on airway hyper-reactivity and eosinophilic inflammation in a murine model of allergic asthma. *Int. Immunopharmacol.* 11, 260–265. doi:10.1016/j.intimp.2010.12.001

Xu, Z. Q., Shao, B. Z., Ke, P., Liu, J. G., Liu, G. K., Chen, X. W., et al. (2016). Combined administration of anisodamine and neostigmine rescued acute lethal crush syndrome through α7nAChR-dependent JAK2-STAT3 signaling. *Sci. Rep.* 6, 37709. doi:10.1038/srep37709

Zhang, J., Zhang, L., Sun, X., Yang, Y., Kong, L., Lu, C., et al. (2016). Acetylcholinesterase inhibitors for alzheimer's disease treatment ameliorate acetaminophen-induced liver injury in mice via central cholinergic system regulation. *J. Pharmacol. Exp. Ther.* 359, 374–382. doi:10.1124/jpet.116.233841

Zhang, Y., Zou, J., Wan, F., Peng, F., and Peng, C. (2023). Update on the sources, pharmacokinetics, pharmacological action, and clinical application of anisodamine. *Biomed. Pharmacother.* 161, 114522. doi:10.1016/j.biopha.2023.114522

Zhao, T., Li, D. J., Liu, C., Su, D. F., and Shen, F. M. (2011). Beneficial effects of anisodamine in shock involved cholinergic anti-inflammatory pathway. *Front. Pharmacol.* 2, 23. doi:10.3389/fphar.2011.00023

Zhou, J. X., Ke, P., Huan, G., Shao, B. Z., and Liu, C. (2014). Combined treatment with anisodamine and neostigmine inhibits joint inflammation in collagen-induced arthritis mice. *Cns Neurosci. Ther.* 20, 186–187. doi:10.1111/cns.12213

Zhu, B., Sun, D., Yang, L., Sun, Z., Feng, Y., and Deng, C. (2020). The effects of neostigmine on postoperative cognitive function and inflammatory factors in elderly patients - a randomized trial. *Bmc Geriatr.* 20, 387. doi:10.1186/s12877-020-01793-4

Zwart, R., and Vijverberg, H. P. (1997). Potentiation and inhibition of neuronal nicotinic receptors by atropine: Competitive and noncompetitive effects. *Mol. Pharmacol.* 52, 886–895. doi:10.1124/mol.52.5.886

Check for updates

Aminooxy acetic acid suppresses Th17-mediated psoriasis-like skin inflammation by inhibiting serine metabolism

Jong Yeong Lee[1†], Ji-Hyun Lee[1†], Hyo Jung Lim[1], Eonho Kim[2], Dae-Ki Kim[1]* and Jin Kyeong Choi[1]*

[1]Department of Immunology, Jeonbuk National University Medical School, Jeonju-si, Republic of Korea,
[2]Department of Physical Education, Dongguk University, Seoul, Republic of Korea

Background: Psoriasis is a common chronic inflammatory skin disease characterized by an external red rash that is caused by abnormal proliferation and differentiation of keratinocytes and immune T cells. This study aimed to elucidate the role of aminooxy acetic acid (AOA) in alleviating psoriasis from the perspective of immunology and metabolomics. Therefore, contributing to the development of new drugs as candidates for psoriasis treatment.

Methods: To investigate the symptom-alleviating effects and the related mechanisms of AOA on the treatment of psoriasis, we used a 12-O-tetradecanoylphorbol-13-acetate-induced psoriasis-like skin mouse model and interleukin (IL)-17-stimulated human keratinocytes.

Results: The results showed that AOA ameliorated psoriasis-related symptoms and decreased inflammation-associated antimicrobial peptides and T-helper 17 (Th17)-associated cytokines in a mouse model of psoriasis. Furthermore, AOA inhibited the activation of mechanistic target of rapamycin (mTOR) by suppressing serine metabolism-related genes. Importantly, mTOR inhibition ameliorated psoriatic disease by affecting the differentiation of various T cells and normalizing the Th17/regulatory T (Treg) cell balance. In addition, IL-17-stimulated human keratinocytes showed the same results as in the *in vivo* experiments.

Conclusion: Taken together, these results suggest that targeting the serine metabolism pathway in the treatment of psoriasis is a novel strategy, and that AOA could be utilized as a novel biologic to treat psoriasis.

1 Introduction

Psoriasis has an estimated global prevalence of 3%–4% and is a chronic recurrent inflammatory immune-mediated skin disease (Michalek et al., 2017). Psoriasis is characterized by clinical symptoms such as distinct red and scaly plaques, and histological symptoms such as hyperproliferation of keratinocytes, dermal inflammatory

---

Abbreviations: AOA, aminooxy acetic acid; IL-17, interleukin-17; Th17, T-helper 17; mTOR, mammalian target of rapamycin; Treg, regulatory T cell.

cell infiltration, and angiogenesis (Pasparakis et al., 2014). In psoriasis, the eruptions appear mainly on the elbows and knees initially, and small eruptions on the skin gradually spread, covering the skin of the whole body with the eruption. In addition to skin eruptions, psoriasis is associated with psoriatic arthritis, autoimmune disease, cardiovascular disease, and metabolic disease. Moreover, the risk of cancer is higher in patients with psoriasis (Furue et al., 2020). The pathogenesis of psoriasis remains unclear; however, it is mainly associated with an abnormal immune response caused by the stimulation of genetic and environmental factors (Kamiya et al., 2019).

Because of the complex cellular and related molecular pathogenesis of psoriasis, no satisfactory strategies have been developed to treat this disease. Currently used drugs for psoriasis include methotrexate, cyclosporine, the phosphodiesterase 4 inhibitor apremilast, ixekizumab, dithranol, guselkumab, brodalumab, and secukinumab (de Carvalho et al., 2017). However, the use of these drugs has many adverse effects that limit their clinical application. These include drug resistance, hormonal imbalance, high recurrence rate, and poor prognosis (Jiang et al., 2020). In addition, treatments such as mild topical therapy, phototherapy, steroids, and vitamin D3 analogs suppress psoriasis inflammation, but these have less coverage and are less effective (Mason et al., 2002). Therefore, the development of novel safe and effective anti-psoriatic drugs is urgently required.

Aminooxy acetic acid (AOA) suppresses pyridoxal-5'-phosphate-dependent transaminases, which regulate the interconversion of alpha (α)-amino and α-keto acids. The redox balance of this reaction is maintained by converting the nitrogen donor, glutamate, to α-ketoglutaric acid (Son et al., 2013). According to a previous study, AOA attenuated autoimmune encephalomyelitis and suppressed the severity of autoimmune uveitis by modulating the fate of T cells (Wang et al., 2016; Mei et al., 2020). Thus, AOA affects T cell differentiation by regulating amino acid metabolic pathway-related genes.

Psoriasis is caused by hyper immunity, which causes abnormalities in immune function. In psoriasis, T-cell activity increases causing excessive secretion of immune substances that induce keratinocyte proliferation and inflammation (Hu et al., 2021). Both T helper type 17 (Th17) and regulatory T (Treg) cells are increased in psoriasis skin lesions. Th17 and Treg cells play critical roles in the immune response and antagonize each other in immune disorders. Therefore, the Th17/Treg balance is important for maintaining immune homeostasis in the body (Zhang et al., 2021). However, the proportion of Treg cells in psoriatic skin tissue is relatively low, which leads to a hyperimmune response. As such, psoriasis is caused by an imbalance of Th17 and Treg cells. Therefore, the solution to this is to increase the number of Treg cells to rescue the balance between them.

Skin immune cells can engage in metabolic pathways of certain nutrients to maintain homeostasis, and high levels of amino acids and metabolites can promote or control the recurrence of skin diseases (Cibrian et al., 2020). Serine is a non-essential amino acid that can be taken directly into cells or synthesized via the serine biosynthetic pathway by 3-phosphoglycerate (3-PG), an intermediate in the glycolysis pathway (Zeng et al., 2019). Serine has recently been reported as an essential metabolite for T cell and keratinocyte proliferation (Ma et al., 2017; Cappello et al., 2022). In

addition, T cell, keratinocyte proliferation and other inflammatory cell expansion were reduced without exogenous serine/glycine (Ma et al., 2017; Cappello et al., 2022). Based on these reports, limiting serine metabolism may have substantial therapeutic implication for immunotherapy and inflammatory immune cell regulation in diseases. Therefore, we investigate the regulate the pathogenesis of Th17-mediated psoriasis-like skin by inhibiting the serine metabolism using AOA.

2 Material and methods

2.1 Animals

Nine-week-old female C57BL/6J mice ($n = 20$) were purchased from NARA Biotech (Pyeongtaek, Korea) and housed in a laminar cabinet. Throughout this study, mice were maintained at $22 \pm 2°C$, $55\% \pm 5\%$ humidity, and in a 12 h light/dark cycle. The research protocol was approved by the Institute Animal Protection and Utilization Committee of Jeonbuk National University (approval number JBNU 2021-0169).

2.2 TPA induced psoriasis model

TPA was diluted in acetone and dimethyl sulfoxide (DMSO) (7:1) (Hiraganahalli Bhaskarmurthy and Evan Prince, 2021). Both ear surfaces were treated from day zero to seven (2.5 μg/mouse). The mice used in this experiment was assigned to four groups ($n = 5$ per group) as follows: control, TPA, TPA plus AOA (125 and 250 μg/mouse). AOA was administered seven times to the abdominal cavity. During the same period, non-immune control mice and TPA-induced psoriasis mice were administered phosphate-buffered saline (PBS) to the abdominal cavity. During the 7 days of the experimental period, ear thickness was evaluated with a dial thickness measuring device (Mitutoyo Co., Tokyo, Japan) as an inflammatory indicator, and the weight of the mouse was measured. After the final treatment, the mice were euthanized using CO_2 and ear samples were acquired and used for further analysis. Part of the ear tissue was stored in a $-80°C$ freezer for subsequent RNA and protein analysis, while another ear tissue was fixed in 4% formaldehyde for pathological analysis. Furthermore, to isolate single cells from the ear skin, the skin tissue was placed in a fresh enzyme medium (RPMI-1640 medium containing 0.4 mg/ml Liberase from Roche and penicillin/streptavidin) at $37°C$ for 1.5 h. Subsequently, the cells were disrupted and filtered using a 70 μm cell strainer. The filtered single cells were then analyzed by flow cytometry.

2.3 Flow cytometry

On day seven, the ears of TPA-induced psoriasis mice were collected and finely ground. The cells were then soaked in media containing Liberase (Roche) and incubated for 1 h and 30 min. The cells were filtered using a 70 μm Nylon cell filter, centrifuged at $400 \times$ g for 8 min, and red blood cells were removed with ammonium-Chloride-Potassium (ACK) lysing buffer and washed with PBS

(Lorenz and von Stebut, 2014). The separated cells were stimulated for 4 h using phorbol-12-myristate-acetate (PMA), ionomycin, and a Golgi plug kit (BD Pharmingen). A viability staining kit (Invitrogen) was used to distinguish dead cells. Tregs and cytokines were expressed as anti-mouse CD4 (clone RM4-5, Biolegend), anti-mouse IFN-γ (clone XMG1.2, BD Pharmagen), anti-mouse Foxp3 (clone FJK-16s, eBioscience), anti-mouse IL-10 (clone JES5-16E3, BD Pharmagen), anti-mouse IL-17A (clone TC11-18H10, BD Pharmagen). In the FACS analysis, cells were stained with fluorescent dyes and monoclonal antibodies, and dead cells were excluded. Each cell was classified according to the fluorophore of the antibody, and the gate in the analysis was set using less than 0.5% isotype control. The FACS analysis was performed using a software from the manufacturer Attune NxT Flow Cytometer (Invitrogen).

2.4 Histological analysis

The ears ($n = 20$) were fixed with 4% formaldehyde and placed in paraffin. The sections were cut at 5 μm and stained with hematoxylin and eosin (H&E). Skin thickness was measured by H&E staining in five randomly selected fields at ×200 magnification for each sample.

2.5 Cell culture and cell viability analysis

The HaCaT human keratinocyte cell line was purchased from CLS Cell Lines Service (Eppelheim, Germany). Cells were cultured in 10% fetal bovine serum (FBS), Dulbecco's Modified Eagle Medium (DMEM) containing antibiotics (100 U/mL penicillin G, 100 μg/mL streptomycin), 5% CO_2, and 37°C.

IL-17A (100 ng/ml; PeproTech) Serine (400 μM; Sigma), glycine (400 μM; Sigma), and SHMT1/2 inhibitor RZ-2994 (2 μM; Cayman Chemical) were added to cell culture media as indicated. Cell viability was measured by 3-(4,5-dimethylthiazol-2-yl)-2,5-diphenyltetrazolium bromide (MTT) analysis. AOA was added at different concentrations for 24 h. Subsequently, MTT (5 mg/mL) was added to each well, and the plate was incubated for 2 h. Formazan crystals were dissolved by treatment with DMSO, and the absorbance of each sample was expressed as a percentage of the control group.

2.6 ELISA

HaCaT cells were activated *in vitro* for 48 h by stimulation with IL-17A (100 ng/ml) in presence or absence of AOA or RZ2994. Supernatants were collected after a 48 h in culture. Serine levels were quantified using kits from Serine ELISA kit (Abcam).

2.7 Quantitative real time polymerase chain reaction (qPCR)

qPCR was performed to confirm the mRNA expression in the ears of HaCaT cells and mice, and RNA was isolated using RNAiso

Plus (Takara Bio). Reversal transfer was performed at 45°C (60 min) and 95°C (5 min). cDNA (100 ng) were mixed with 1 μL (0.4 μM) of forward and reverse primer solutions. The final mixture (10 μL) was obtained using 5 μL of SYBR premix (Nanohelix, Daejeon, Korea) and dH₂O (1 μL). The primers used are listed in Supplementary Table S1. Normalization and quantification of mRNA expression were performed using the StepOnePlus Real-Time PCR (Applied Biosystems) software.

2.8 Western blot

On day seven of the experiment, the ears and cells of TPA-induced psoriasis mice were homogenized and dissolved, and western blotting was performed. After mixing Tissue Protein Extraction Reagent (T-PER), Phosphor stop, and ethylenediaminetetraacetic acid (EDTA)-free, 200 μL was added to each ear for homogenization, pulverization, and centrifugation at $10,000 \times g$ for 5 min to use only the supernatant. In the case of cells, IL-17A (100 ng/mL) stimulated (1×10^6 cells/well in a six-well plate) the cells for 48 h to induce the production of signaling molecules. Cells were washed with cold PBS, 100 μL of lysate buffer was added, and cells were sonicated for 30 s. Subsequently, centrifugation was performed for 10 min to collect the supernatant. The protein extract (20 μg/lane) was fractionated by 6%–10% gradient sodium dodecyl sulfate-polyacrylamide gel electrophoresis (SDS-PAGE) and then transferred to a polyvinylidene fluoride (PVDF) membrane (Bio-Rad). A tris-buffered saline Tween 20 (TBS-T) buffer containing 5% bovine serum albumin (BSA) was lightly stirred at room temperature for 1 h and then treated with a specific antibody solution at 4°C overnight. The antibodies used were to detect phosphoglycerate dehydrogenase (PHGDH) (Abcam), phosphohydroxythreonine aminotransferase (PSAT)1, phosphoserine phosphatase (PSPH) (Invitrogen), phosphorylated (p)-AMP-activated protein kinase (AMPK)α, AMPKα, p-mTOR, mTOR, serine hydroxy methyltransferase (SHMT)1, SHMT2, and β-actin (Cell Signaling Technology). The PVDF membrane was washed with TBST buffer to remove redundant antibody structures, and the secondary antibody was stirred gently at room temperature for 1 h. Immunodetection was performed using Super Signal™ West Pico PLUS Thermo Scientific.

2.9 Th17 cell polarization

Naïve CD4⁺ T cells were isolated from the total splenocytes of 6-weeks-old C57BL6/J mice using the CD4⁺CD62L⁺ T cell isolation kit (Miltenyi Biotec) according to manufacturer's protocol. The isolated naïve CD4⁺ T cells were then polarized into Th17 cells by adding 25 ng/ml IL-6 (R&D systems), 3 ng/ml TGF-β (PeproTech), 10 μg/ml anti-IL-4 (R&D systems), and 10 μg/ml anti-IFN-γ (R&D systems) in presence of plate bound anti-CD3 (5 μg/ml, BioXcell) and anti-CD28 (5 μg/ml, BioXcell) for 5 days. The cells were cultured in TexMACS Medium (Miltenyi Biotec) with 10% FBS, 1% penicillin/streptomycin and 1% glutamate (Sigma-Aldrich). The treatment of AOA on Th17 cells was conducted on day 3 and analyzed on day 5.
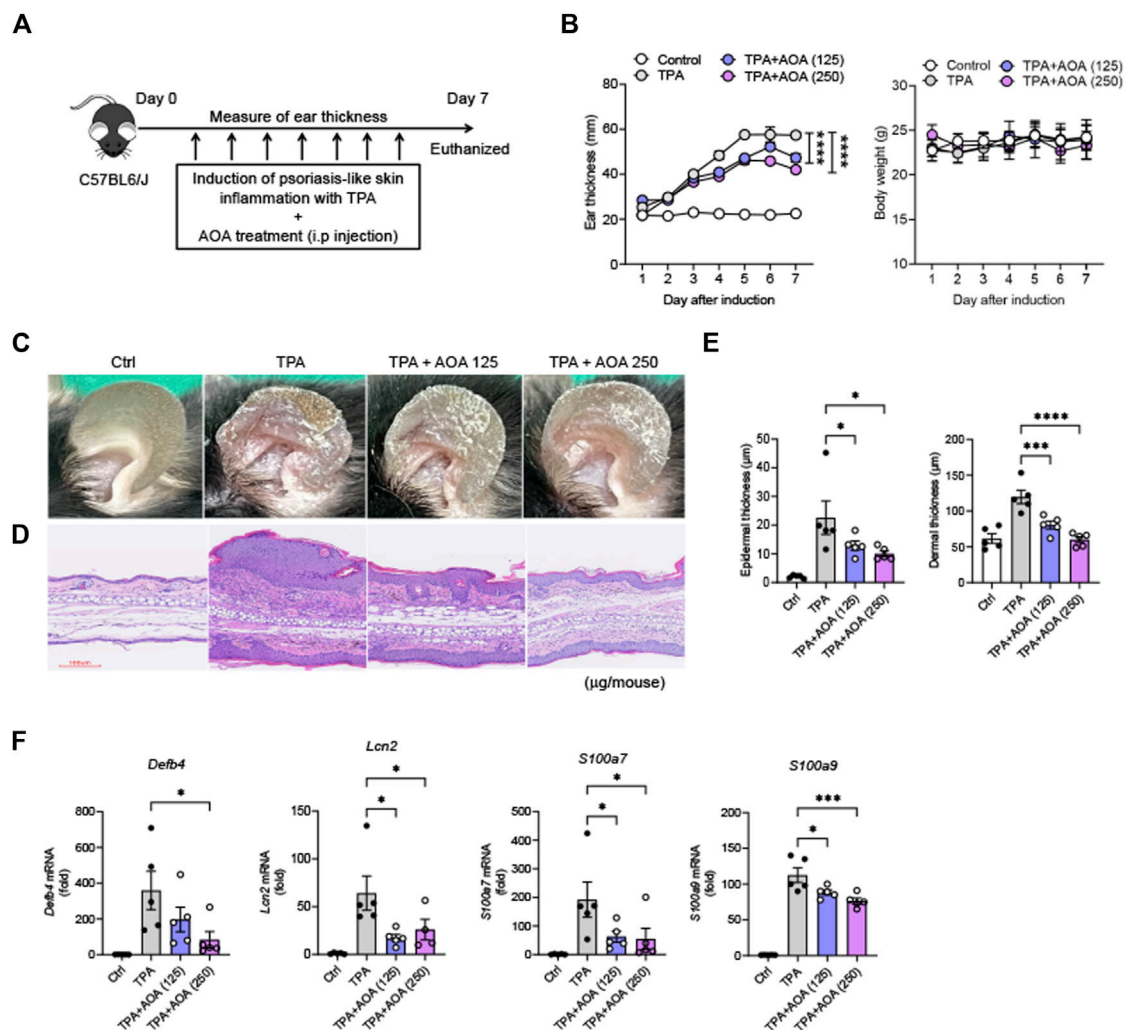
FIGURE 1
AOA confers protection against TPA-induced psoriasis mouse model. **(A)** Schematics showing the experiment schedule for the animal model of TPA-induced psoriasis and treatment strategy. **(B)** Ear thickness (mm) and body weight change (g). **(C)** Representative photographs of mouse ear skin in each group. **(D)** Representative images of H&E staining (×200 magnification; scale bar = 100 μm) in each group. **(E)** Epidermal and dermal thickness (μm). **(F)** The mRNA expression of psoriasis-associated antimicrobial peptides (*Defb4*, *Lcn2*, *S100a7*, and *S100a9*). All data are showed as the mean ± SEM of three independent experiments. Values were analyzed by Holm-Šídák *post hoc* test. *$p < 0.05$, **$p < 0.01$, ***$p < 0.001$, and ****$p < 0.0001$ vs TPA-induced only group. AOA, aminooxy acetic acid; TPA, 12-O-tetradecanoylphorbol-13-acetate; H&E, hematoxylin and eosin; SEM, standard error of the mean; Defb4, defensin β 4; Lcn2, lipocalin 2.

2.10 Statistical analysis

GraphPad Prism 9 was used for data analysis, and one-way analysis of variance (ANOVA) or *t*-test was used, as well as the Holm-Šídák *post hoc* test. Statistical significance was set at $p < 0.05$, and the data are expressed as mean ± standard error of the mean (SEM).

3 Results

3.1 AOA ameliorates skin pathology and inhibits amplified psoriasis-associated genes in mouse model

We derived an experimental animal model of psoriasis to investigate the alleviating effects of AOA and related mechanisms

of psoriasis symptoms. AOA was injected daily intraperitoneally (i.p.) (125 μg/mouse or 250 μg/mouse; i.p.) for 7 days (Figure 1A). In this study, mice in the group in which psoriasis-like skin was induced by TPA showed significant thickening of the ear skin compared to mice in the normal group. However, AOA attenuated ear skin thickening during psoriasis progression in mice. Compared to the normal group, no significant difference in body weight was observed between the TPA and AOA treatment groups (Figure 1B). In addition, we visually confirmed that the administration of AOA caused a significant recovery of psoriasis-like symptoms in the ear skin of the TPA-induced psoriasis model (Figure 1C). H&E staining was performed to analyze histopathological changes such as epidermal hyperkeratosis and hypertrophy in the ear tissues of each group. The epidermal and dermal thicknesses were significantly greater in the TPA group than in the normal group. However, AOA treatment alleviated the TPA-
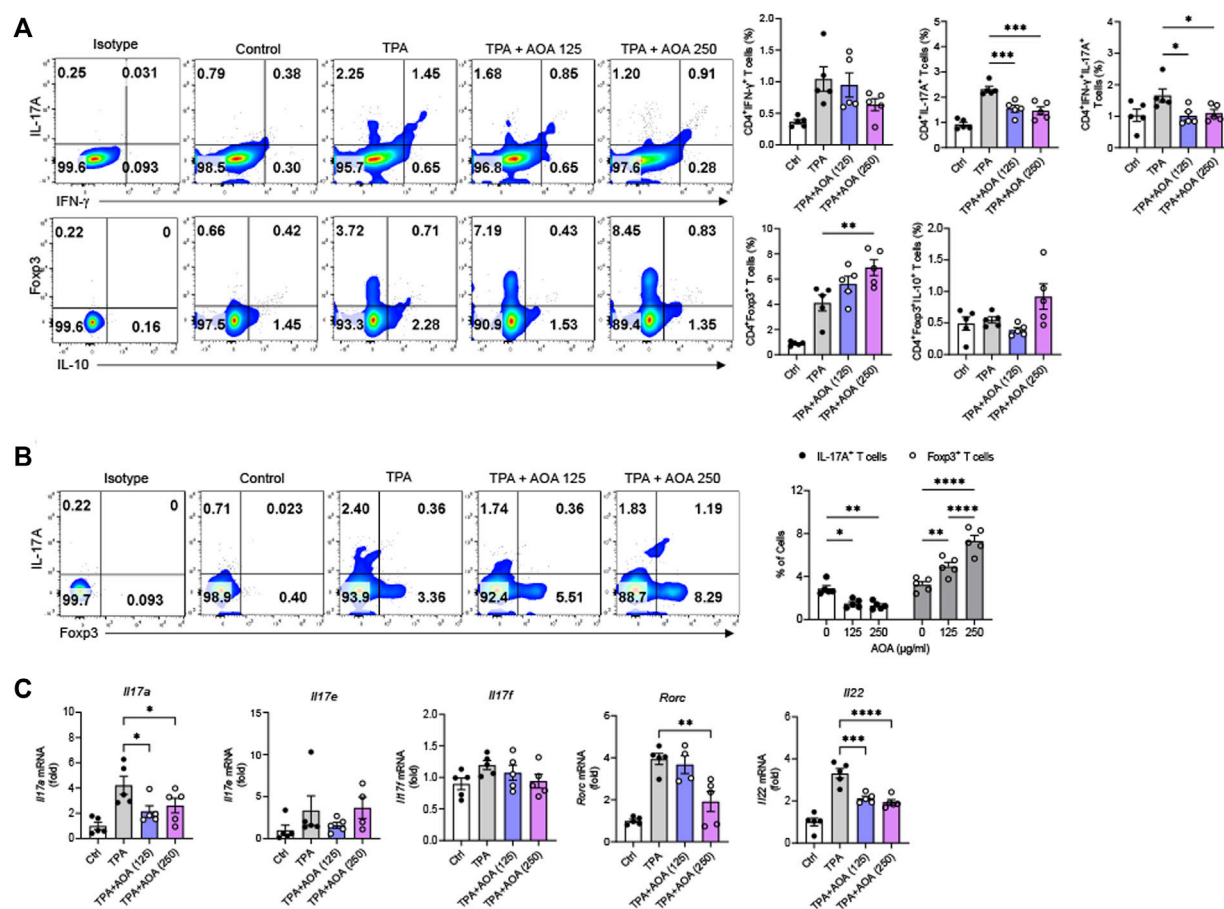
FIGURE 2
AOA reprograms Th17 cell expansion into Treg cells in the TPA-induced psoriatic skin. Cells of the ear skin were collected from each mouse and analyzed by FACS. **(A)** Analysis of changes in IFN-γ-, -IL-17A-, Foxp3-, or IL-10-expressing CD4$^+$ T cells in mouse ear skin cells by AOA treatment in TPA-induced psoriasis mice. **(B)** AOA reprograms Th17 cell differentiation into Treg cells. **(C)** The mRNA expression of psoriasis-associated Th17 cytokines (*IL17A, IL17E, IL17F, RORC, and IL22*). All data are showed as the mean ± SEM of three independent experiments. Values were analyzed by Holm–Šídák *post hoc* test. *$p < 0.05$, **$p < 0.01$, ***$p < 0.001$, and ****$p < 0.0001$ vs TPA-induced only group. AOA, aminooxy acetic acid; TPA, 12-O-tetradecanoylphorbol-13-acetate; H&E, hematoxylin and eosin; SEM, standard error of the mean; Th17, T helper type 17; IL, interleukin; FACS, fluorescent activated cell sorting; RORC, RAR related orphan receptor C.

induced epidermal and dermal thickening of ear tissues (Figures 1D, E). To examine the anti-inflammatory effect of AOA on psoriasis, we observed changes in the expression of antimicrobial peptides, such as defensin β 4 (*Defb4*), lipocalin 2 (*Lcn2*), *S100a7*, and *S100a9*, which are known to amplify local inflammatory processes. As shown in Figure 1F, the mRNA expression levels of antimicrobial peptides increased by TPA were significantly decreased after treatment with AOA.

3.2 AOA inhibits Th17 and induces Treg cells during psoriasis-like skin inflammation

During the inflammatory process of psoriasis, naïve CD4$^+$ T cells differentiate into Th1 or Th17 cells upon stimulation with various cytokines, promoting the activity of the adaptive immune system (Hiraganahalli Bhaskarmurthy and Evan Prince, 2021). In addition, immune dysfunction occurs due to an imbalance of T cells, in which the proportion of Treg cells that

regulate immune excess is relatively low compared to Th17 cells in psoriasis (Zhang et al., 2021). Therefore, to investigate how AOA affects the regulation of T cells in skin inflammatory lesions in a TPA-induced psoriasis-like mouse model, we isolated cells from the ear and identified them using FACS. As expected, the number of Th17 cells in the ear of the AOA-treated mice was significantly reduced compared to that in the untreated group, and the number of Treg cells increased. The number of Th1 cells was decreased by AOA treatment compared with that in the TPA group, but the difference was not significant. In addition, there was no increase in the number of Foxp3$^+$IL-10$^+$ IL-10-expressing Tregs (Figure 2A). AOA significantly reduced the expansion of IL-17A-producing Th17 cells and significantly induced the expansion of Foxp3$^+$ Treg cells in psoriasis-like skin (Figure 2B). This suggests that AOA has a reprogramming function that inhibits Th17 cell differentiation and promotes Treg cell differentiation in a dose-dependent manner. In addition, AOA treatment significantly decreased the expression levels of *Il17a*, RAR related orphan receptor C (*Rorc*), and *IL22* in ear skin of the psoriasis-like mouse model. *Il17e* and
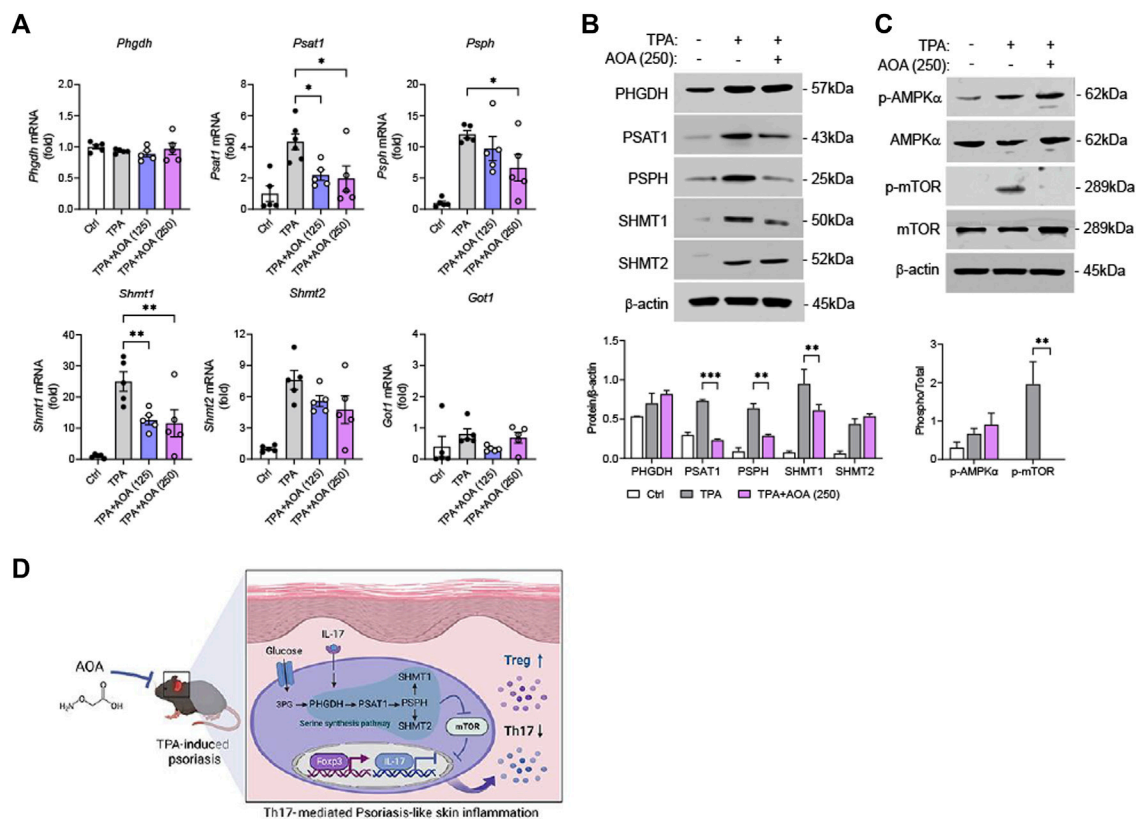
FIGURE 3
AOA inhibits serine metabolism and mTOR pathway in the TPA-induced psoriatic skin. **(A)** The mRNA expression of serine metabolism related genes of mouse ear tissues analyzed by qPCR. **(B)** The protein expression of serine metabolism related genes of mice ear tissues as analyzed by western blot, and bar graph of the relative intensities. **(C)** The protein expression of AMPK/mTOR of mice ear tissues as analyzed by western blot, and bar graph of the relative intensities. All data are showed as the mean $\pm$ SEM of three independent experiments. **(D)** A schematic diagram of the effects of AOA in the TPA-induced psoriasis-like model. AOA inhibits the serine metabolism-mTOR axis pathway activated in mouse skin tissue and subsequently reduces Th17-mediated inflammatory cytokines. Values were analyzed by Holm–Šídák *post hoc* test. *$p < 0.05$, **$p < 0.01$, ***$p < 0.001$, and ****$p < 0.0001$ vs TPA-induced only group. AOA, aminooxy acetic acid; TPA, 12-O-tetradecanoylphorbol-13-acetate; H&E, hematoxylin and eosin; SEM, standard error of the mean; qPCR, quantitative real time polymerase chain reaction; mTOR; mechanistic target of rapamycin; AMPK, AMP-activated protein kinase.

Il17f also decreased compared to the TPA group, but the difference was not significant (Figure 2C).

3.3 AOA inhibits mTOR via serine metabolism in psoriasis-like skin inflammation

We investigated the underlying mechanisms to determine through which pathway AOA reprograms T-cell differentiation and alleviates the symptoms of psoriasis. Previous studies have shown that AOA is a pan-transaminase inhibitor that inhibits the synthesis of several amino acids (aspartate, glycine, alanine, and serine) (Xu et al., 2017). Therefore, we investigated the effect of AOA on the expression of serine metabolic components in TPA-induced psoriasis-like skin lesions. First, we verified the expression levels of the serine biosynthesis pathway (*Phgdh*, *Psat1* and *Psph*) and serine entry into the one-carbon metabolism pathway (*Shmt1* and *Shmt2*) using qPCR. As shown in Figure 3A, AOA significantly inhibited the expression of *Psat1* and *Psph* without affecting the

expression of *Phgdh* in the serine biosynthesis pathway. In addition, the expression of *Shmt1* in serine entry into the one-carbon metabolism pathway was significantly suppressed by AOA. The expression of *Shmt2* was also decreased by AOA, but the difference was not statistically significant. Notably, AOA did not significantly affect the expression of glutamic-oxaloacetic transaminase 1 (Got1), indicating that treatment with AOA did not affect aspartic biosynthesis in the psoriatic skin environment. Furthermore, protein expression was confirmed by western blotting. The expression of *Psat1*, *Psph*, and *Shmt1* was significantly reduced by AOA in TPA-induced psoriatic skin, consistent with the qPCR results (Figure 3B). We next investigated the protein expression changes in AMPK activation and mTOR phosphorylation by AOA in TPA-induced psoriatic skin. The results showed that AOA treatment attenuated the phosphorylation of mTOR without significantly affecting AMPK activity (Figure 3C). Taken together, AOA can reduce the production of Th17-mediated inflammatory factors and increase Foxp3^{+} Tregs by inhibiting both activated serine metabolism and mTOR in the skin of a TPA-induced psoriasis mouse model (Figure 3D).
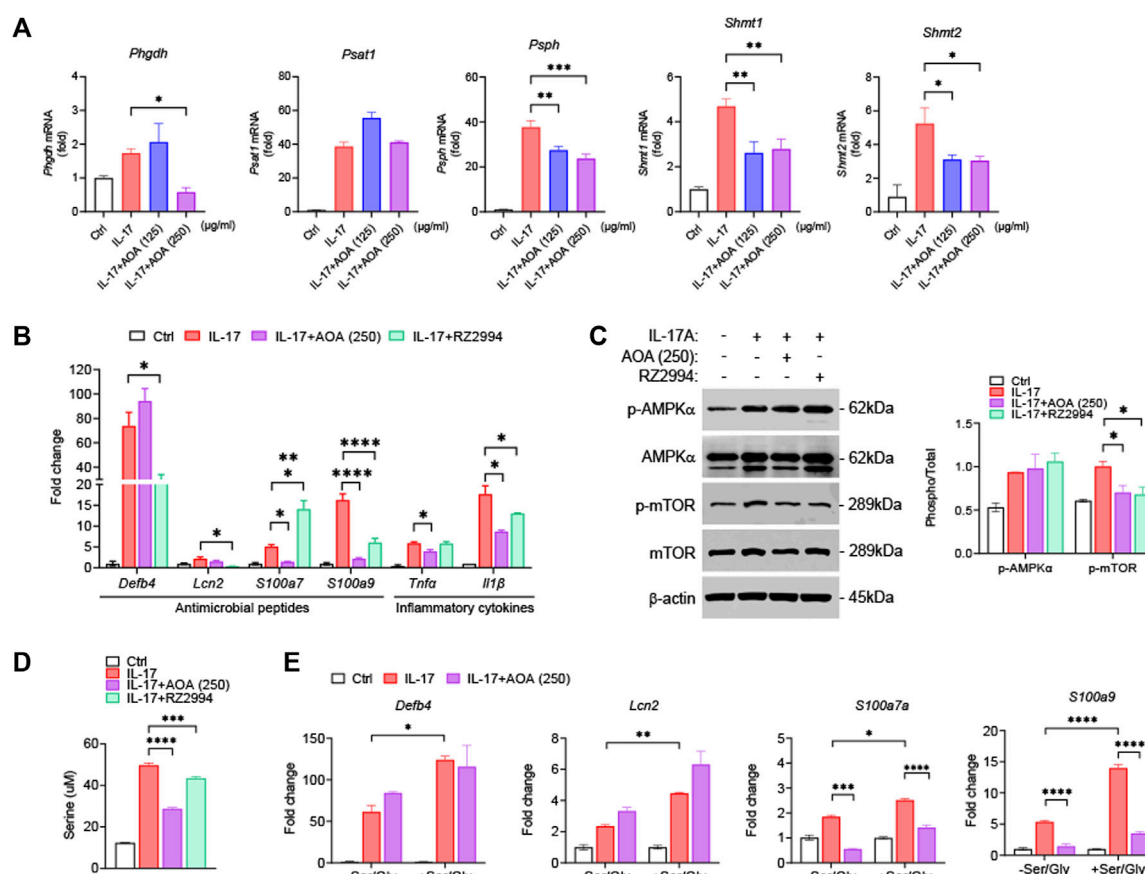
FIGURE 4
AOA ameliorates IL-17-mediated keratinocyte inflammation by inhibiting mTOR through the restriction of serine metabolism. **(A)** The mRNA expression of serine metabolism related genes of human keratinocytes analyzed by qPCR. **(B)** The mRNA expression of psoriasis-associated antimicrobial peptides (*Defb4, Lcn2, S100a7,* and *S100a9*) by human keratinocytes analyzed by qPCR. **(C)** The protein expression of AMPK/mTOR by human keratinocytes analyzed by western blot, and bar graph of the relative intensities. **(D)** Analysis of serine levels from the supernatants were analyzed by ELISA. **(E)** Gene expression of IL-17A-stimulated human keratinocytes cultured in serine/glycine-free medium, or serine/glycine-free medium containing serine (400 μM) and glycine (400 μM) in the presence or absence of AOA. All data are showed as the mean $\pm$ SEM of three independent experiments. Values were analyzed by Holm-Šídák *post hoc* test. *$p < 0.05$, **$p < 0.01$, ***$p < 0.001$, and ****$p < 0.0001$ vs IL-17-stimulated only group. AOA, aminooxy acetic acid; SEM, standard error of the mean; qPCR, quantitative real time polymerase chain reaction; mTOR; mechanistic target of rapamycin; AMPK, AMP-activated protein kinase; Defb4, defensin β 4; Lcn2, lipocalin 2.

3.4 Immuno-suppressive effects of AOA require serine metabolism in IL-17-mediated psoriatic keratinocytes

To examine whether the effect of AOA on the inhibition of psoriasis-related mechanisms *in vitro* was similar to those *in vivo*, we used IL-17-stimulated HaCaT cells. First, we investigated the effect of AOA on the viability of HaCaT cells. We confirmed that AOA treatment at concentrations of 0–250 μg/mL did not induce cytotoxicity in HaCaT cells (Supplementary Figure S1). Certain metabolic pathways control cell activation/proliferation/differentiation and modulate the shift towards inflammatory or anti-inflammatory responses. In psoriasis, immune-metabolic interactions may orchestrate IL-17-induced pathogenicity, which can induce skin plaques as well as systemic inflammatory responses and psoriasis-related comorbidities (Krueger and Brunner, 2018). Further, IL-17-mediated keratinocyte psoriasis is associated with increased levels of various inflammatory cytokines in the skin. Recent findings have highlighted serine/glycine control as a

metabolic hub that can regulate the proliferation and expansion of inflammatory cells (Cappello et al., 2022). Therefore, we examined the whether the effects of AOA on the expression of serine metabolism-related genes in IL-17-stimulated HaCaT cells. As shown in Figure 4A, all genes involved in serine metabolism were significantly increased in IL-17-stimulated cells compared to those in non-stimulated control cells. The expression of *Phgdh* was significantly decreased by treatment with a high concentration of AOA, and no significant change in *Psat1* was observed after AOA treatment. AOA showed a significant inhibitory effect on the expression of *Psph, Shmt1*, and *Shmt2* at all the tested concentrations. To compare and observe the anti-inflammatory effect of AOA and RZ2994, a known SHMT1/SHMT2 inhibitor, in IL-17-stimulated HaCaT cells, we examined the changes in the expression of antimicrobial peptides (*Defb4, Lcn2, S100a7,* and *S100a9*) and inflammatory cytokines (*Tnfα* and *Il1β*). As a result, the expression levels of *Lcn2, S100a7, S100a9, Tnfα,* and *Il1β*, which were increased by IL-17 stimulation, were found to be decreased upon AOA treatment. Additionally, the expression of *Defb4, Lcn2,*

S100a9, and *Il1β*, which elevated after stimulation with IL-17 were reduced by RZ2994 (Figure 4B).

We next investigated whether AOA or RZ2994 could inhibit mTOR phosphorylation by activating AMPK in IL-17-stimulated HaCaT cells. Both AOA and RZ2994 significantly inhibited mTOR phosphorylation. However, neither AOA nor RZ2994 increased AMPK activation (Figure 4C). These results, consistent with *in vivo* experiments, suggest that AOA can inhibit inflammatory mediators by directly regulating mTOR phosphorylation without requiring AMPK activation by inhibiting serine metabolism.

Next, to clarify the anti-inflammatory effect of AOA through the serine metabolic pathway in psoriasis-like skin inflammation, we investigated whether AOA regulates the extracellular released serine levels by inhibiting intracellular serine synthesis. AOA inhibited expression of intracellular serine synthesis enzymes and demonstrated a significant downregulation of extracellular released serine levels, as estimated by ELISA (Figure 4D). Additionally, to understand the role of extracellular serine utilization in keratinocytes, we added serine/glycine (glycine was added because serine can be reversibly converted to glycine by SHMT) to IL-17A-stimulated keratinocytes. We observed a more significant increase in expression of IL-17-mediated inflammatory genes in keratinocytes supplemented with serine/glycine than in those lacking serine/glycine (Figure 4E). Taken together, these results indicated that the inflammatory response of keratinocytes mediated by IL-17 depends on the supply of serine, and AOA reduces the inflammatory response of keratinocytes through the restriction of serine metabolism.

3.5 AOA suppresses serine metabolism in Th17 cells

It has been reported that effector T cells, which proliferate rapidly *in vitro* and *in vivo*, require a sufficient supply of serine, and serine restriction can inhibit T cell expansion (Ma et al., 2017). After demonstrating that AOA reduces inflammation by inhibiting serine metabolism in Th17-mediated psoriasis, we investigated whether this drug could also reduce the inhibition of serine metabolism and IL-17A production in mouse primary Th17 cells. Consistent with the *in vivo* results, AOA inhibited IL-17A production in Th17 cells (Supplementary Figure S2). Furthermore, both RNA and protein levels of serine metabolic enzymes (PHGDH, PSAT1, PSPH, and SHMT1/2) were considerably reduced in AOA-treated Th17 cells (Figures 5A, B). These results suggest that AOA may impact the function of Th17 cells by inhibiting serine metabolism.

4 Discussion

Psoriasis is a chronic inflammatory, immune-mediated skin disease characterized by erythematous plaques covered with silvery-white scales (Lowes et al., 2014). Drugs available to treat psoriasis cause serious adverse effects. Therefore, novel effective drugs that cause fewer adverse effects are urgently needed to treat psoriasis. Through this study, we demonstrate that AOA is a potential novel treatment strategy for psoriasis.

Recent studies have revealed that keratinocytes and T cell-mediated immune responses contribute to the onset of psoriasis and its progression to chronic disease (Schlaak et al., 1994; Yuan et al., 2020). Dysfunction of T cells, including Th1, Th17, and Treg cells, and the resulting abnormal release of related cytokines that activate keratinocytes, play an important role in the onset and progression of psoriasis (Hu et al., 2021). Although psoriasis was considered a Th1-mediated skin disease in earlier studies, Th17 cells have recently been shown to play a key role in psoriatic disease (Szabo et al., 2000; Quaglino et al., 2011). In psoriasis, Th17 cells are highly activated and infiltrate the psoriatic skin lesions. The secretion of Th17-related cytokines such as IL-17A, IL-17E and IL-17F is upregulated in infiltrated Th17 cells and keratinocytes in psoriatic lesions (Martin et al., 2013). Among them, the expression of IL17A is predominant in psoriasis skin lesions, and IL-17 increases the secretion of antimicrobial peptides (*Defb4*, *Lcn2*, *S100a7*, and *S100a9*) by keratinocytes. This promotes the response of inflammatory cells and enhances the proliferation of keratinocytes (Lai et al., 2012). *Defb4* and *Lcn2* are psoriasis-specific antimicrobial peptides highly expressed in psoriatic plaques, and *Defb4* can attract Th17 cells (Kolbinger et al., 2017). *S100a7* is involved in wound healing and keratinocyte differentiation, and *S100A9* increases the production of various cytokines and chemokines in keratinocytes and is involved in keratinocyte proliferation (Hegyi et al., 2012).

According to our results, AOA reduced ear thickness and ameliorated pathological damage in mice with TPA-induced psoriasis-like skin. In addition, by confirming that AOA significantly reduced the expression of psoriasis-associated antimicrobial peptides (*Defb4*, *Lcn2*, *S100a7*, and *S100a9*), we revealed that AOA ameliorated psoriasis-related symptoms and had anti-inflammatory effects in a mouse model of psoriasis.

The exact role of Treg cells in the pathogenesis of psoriasis is largely unknown, although studies have suggested that Treg cells may ameliorate psoriasis *in vivo* (Kanda et al., 2021). Treg cells expressing FOXP3 suppress immune responses and maintain immune homeostasis. Therefore, in the treatment of psoriasis, controlling the balance between Th17 and Treg cells is key (Nussbaum et al., 2021). We have provided evidence that in a potential novel psoriasis treatment strategy, AOA can improve psoriasis by inhibiting differentiation into Th17 cells and inducing differentiation into Treg cells, thereby regulating the Th17/Treg balance. Moreover, AOA decreased IL-17A, RORC, and IL-22 secretion by Th17 cells, confirming that AOA is effective in the immune regulation of psoriasis.

To date, most research on psoriasis has focused on dysfunction of the immune response, although metabolite imbalance is also involved in the progression of psoriasis (Gisondi et al., 2018). Kamleh et al. found that the levels of free circulating amino acids such as arginine, alanine, glycine, serine, and threonine were altered in the plasma of patients with psoriasis (Kamleh et al., 2015). In addition, Aigar et al. demonstrated that patients with psoriasis have impaired amino acid and lipid metabolism (Ottas et al., 2017). When the immune response is activated, T cells increase the enzymes involved in serine, glycine, and 1-carbon metabolism and elevate the processing of serine into one-carbon metabolism. Therefore, serine is a highly important amino acid in the regulation of T cell activity, and reprogramming serine metabolism is key in regulating immune diseases (Ma et al., 2017).
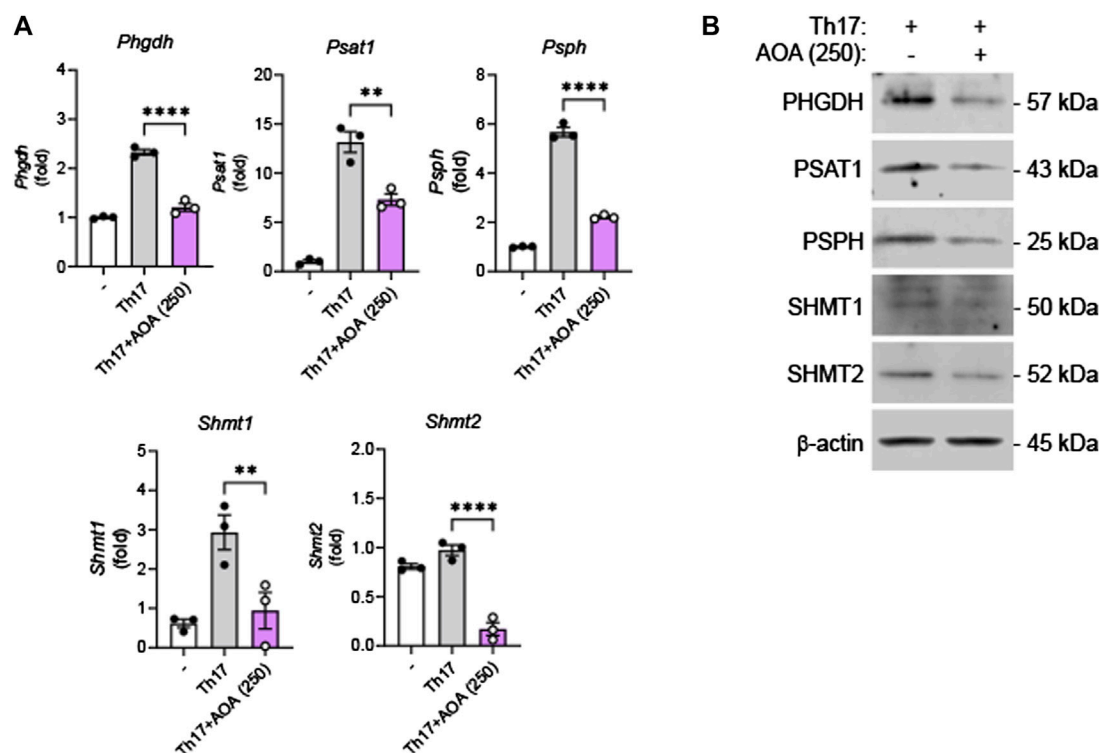
FIGURE 5
Inhibition of serine metabolism in Th17 cells by AOA. Splenic CD4$^+$CD62L$^+$ naïve T cells from C57BL6/J mice were isolated and polarized under Th17 conditions with anti-CD3/28 antibodies for 5 days. **(A)** The mRNA expression of serine metabolism related genes of mouse primary Th17 cells analyzed by qPCR. **(B)** The protein expression of serine metabolic pathways by mouse primary Th17 cells analyzed by western blot, and bar graph of the relative intensities. All data are showed as the mean ± SEM of three independent experiments. Values were analyzed by Holm-Šídák *post hoc* test. *$p < 0.05$, **$p < 0.01$, and ****$p < 0.0001$.

In this study, we examined serine as an important metabolite that modulates the immune response in psoriasis, and aimed to investigate the effect of AOA on the molecular mechanisms related to serine metabolism in psoriasis. In addition, control of amino acids or inhibition of mTOR can prevent the activation of immune cells and the differentiation of keratinocytes in psoriasis (Cibrian et al., 2020). Considering these data, we sought to determine whether AMPK/mTOR is the signaling pathway involved in serine metabolism regulated by AOA regulates in psoriasis.

AMPK is an enzyme involved in cellular homeostasis and metabolic stress regulation, and phosphorylation of AMPK acts as a regulator of pathways such as AMPK/mTOR (Xiang et al., 2019). mTOR is a Ser/Thr kinase, activated mTOR is regulated by amino acid levels and controls the biosynthetic steps required for cell survival, proliferation, and cytokine release (Saxton and Sabatini, 2017). The activation of mTOR is important for the activation of Th1, Th2, and Th17 cells, whereas inhibition of mTOR induces differentiation into FOXP3$^+$ Treg cells (Delgoffe et al., 2009). In keratinocytes of psoriatic skin, mTOR is upregulated by stimulation with IL-17 and IL-22, and upregulated mTOR plays an important role in the proliferation and differentiation of defective keratinocytes (Cibrian et al., 2020). The described studies can help elucidate the diagnosis and pathogenesis of psoriasis, and their use will help discover beneficial therapeutic agents for the treatment of this disease.

To elucidate the role of AOA in the treatment of psoriasis from an immunological and metabolomic standpoint, we identified a relevant mechanism in TPA-induced psoriasis mice and IL-17-stimulated human keratinocytes. AOA inhibited *Psat1, Psph*, and *Shmt1 in vivo* and significantly decreased *Phgdh, Psph, Shmt1*, and *Shmt2 in vitro*. This suggests that AOA alleviates the symptoms of psoriasis by suppressing pathway-related genes involved in serine metabolism. In addition, by confirming that AOA inhibits increased mTOR phosphorylation both *in vitro* and *in vivo*, we concluded that decreased serine by AOA is involved in the regulation of mTOR activation and suppression of mTOR phosphorylation. HaCaT cells have mainly been used for mechanistic studies, i.e., those investigating the effects of AOA on serine metabolizing enzymes and the inhibition of psoriasis-related inflammation mediated by regulating the expression of these enzymes. However, although HaCaT is a keratinocyte cell line, the results obtained with HaCaT cells may not be fully reproduced *in vivo*. Considering that we have further demonstrated, as shown in Figure 5, that AOA inhibits cytokine production and serine metabolism in Th17 cells, AOA may hold potential as a therapeutic agent in other immune diseases characterized by Th17 cell development. However, it is essential to conduct further investigations to assess its safety and efficacy.

5 Conclusion

AOA improved psoriasis-related symptoms by suppressing Th17-mediated cytokines, such as IL-17 and IL-22, and by reducing antimicrobial peptides in a psoriasis treatment model. In addition, AOA regulates serine by targeting and inhibiting serine metabolism-related genes and downregulating the activation of mTOR through serine metabolism control. This decreased activation of mTOR by AOA suggests that psoriasis can be alleviated by normalizing the imbalance of Th17/Treg cells. Therefore, we propose that AOA is a potential alternative treatment for relieving psoriasis.

Data availability statement

The original contributions presented in the study are included in the article/Supplementary Material, further inquiries can be directed to the corresponding authors.

Ethics statement

The animal study was approved by Animal Experiment Ethics Committee of Jeonbuk National University, and the approved number is JBNU 2021-0169. The study was conducted in accordance with the local legislation and institutional requirements.

Author contributions

JL performed most of the experiments, prepared figures, and edited the manuscript; J-HL wrote the manuscript and data analysis; HL assisted with the animal experiments; EK designed serine experiments; D-KK critically reviewed, and edited the manuscript; JC conceived, designed, and supervised the project, and revised the manuscript. All authors contributed to the article and approved the submitted version.

Acknowledgments

Conflict of interest

The authors declare that the research was conducted in the absence of any commercial or financial relationships that could be construed as a potential conflict of interest.

Publisher's note

All claims expressed in this article are solely those of the authors and do not necessarily represent those of their affiliated organizations, or those of the publisher, the editors and the reviewers. Any product that may be evaluated in this article, or claim that may be made by its manufacturer, is not guaranteed or endorsed by the publisher.

Supplementary material

The Supplementary Material for this article can be found online at: https://www.frontiersin.org/articles/10.3389/fphar.2023.1215861/full#supplementary-material

References

Cappello, A., Mancini, M., Madonna, S., Rinaldo, S., Paone, A., Scarponi, C., et al. (2022). Extracellular serine empowers epidermal proliferation and psoriasis-like symptoms. *Sci. Adv.* 8, eabm7902. doi:10.1126/sciadv.abm7902

Cibrian, D., De La Fuente, H., and Sanchez-Madrid, F. (2020). Metabolic pathways that control skin homeostasis and inflammation. *Trends Mol. Med.* 26, 975–986. doi:10.1016/j.molmed.2020.04.004

De Carvalho, A. V., Duquia, R. P., Horta, B. L., and Bonamigo, R. R. (2017). Efficacy of immunobiologic and small molecule inhibitor drugs for psoriasis: a systematic review and meta-analysis of randomized clinical trials. *Drugs R. D.* 17, 29–51. doi:10.1007/s40268-016-0152-x

Delgoffe, G. M., Kole, T. P., Zheng, Y., Zarek, P. E., Matthews, K. L., Xiao, B., et al. (2009). The mTOR kinase differentially regulates effector and regulatory T cell lineage commitment. *Immunity* 30, 832–844. doi:10.1016/j.immuni.2009.04.014

Furue, M., Furue, K., Tsuji, G., and Nakahara, T. (2020). Regulation of filaggrin, loricrin, and involucrin by IL-4, IL-13, IL-17a, IL-22, AHR, and NRF2: pathogenic implications in atopic dermatitis. *Int. J. Mol. Sci.* 21, 5382. doi:10.3390/ijms21155382

Gisondi, P., Fostini, A. C., Fossa, I., Girolomoni, G., and Targher, G. (2018). Psoriasis and the metabolic syndrome. *Clin. Dermatol* 36, 21–28. doi:10.1016/j.clindermatol.2017.09.005

Hegyi, Z., Zwicker, S., Bureik, D., Peric, M., Koglin, S., Batycka-Baran, A., et al. (2012). Vitamin D analog calcipotriol suppresses the Th17 cytokine-induced proinflammatory S100 "alarmins" psoriasin (S100A7) and koebnerisin (S100A15) in psoriasis. *J. Invest. Dermatol* 132, 1416–1424. doi:10.1038/jid.2011.486

Hiraganahalli Bhaskarmurthy, D., and Evan Prince, S. (2021). Effect of Baricitinib on TPA-induced psoriasis like skin inflammation. *Life Sci.* 279, 119655. doi:10.1016/j.lfs.2021.119655

Hu, P., Wang, M., Gao, H., Zheng, A., Li, J., Mu, D., et al. (2021). The role of helper T cells in psoriasis. *Front. Immunol.* 12, 788940. doi:10.3389/fimmu.2021.788940

Jiang, B. W., Zhang, W. J., Wang, Y., Tan, L. P., Bao, Y. L., Song, Z. B., et al. (2020). Convallatoxin induces HaCaT cell necroptosis and ameliorates skin lesions in psoriasis-like mouse models. *Biomed. Pharmacother.* 121, 109615. doi:10.1016/j.biopha.2019.109615

Kamiya, K., Kishimoto, M., Sugai, J., Komine, M., and Ohtsuki, M. (2019). Risk factors for the development of psoriasis. *Int. J. Mol. Sci.* 20, 4347. doi:10.3390/ijms20184347

Kamleh, M. A., Snowden, S. G., Grapov, D., Blackburn, G. J., Watson, D. G., Xu, N., et al. (2015). LC-MS metabolomics of psoriasis patients reveals disease severity-dependent increases in circulating amino acids that are ameliorated by anti-TNFα treatment. *J. Proteome Res.* 14, 557–566. doi:10.1021/pr500782g

Kanda, N., Hoashi, T., and Saeki, H. (2021). The defect in regulatory T cells in psoriasis and therapeutic approaches. *J. Clin. Med.* 10, 3880. doi:10.3390/jcm10173880

Kolbinger, F., Loesche, C., Valentin, M. A., Jiang, X., Cheng, Y., Jarvis, P., et al. (2017). β-Defensin 2 is a responsive biomarker of IL-17A-driven skin pathology in patients with psoriasis. *J. Allergy Clin. Immunol.* 139, 923–932.e8. doi:10.1016/j.jaci.2016.06.038

Krueger, J. G., and Brunner, P. M. (2018). Interleukin-17 alters the biology of many cell types involved in the genesis of psoriasis, systemic inflammation and associated comorbidities. *Exp. Dermatol* 27, 115–123. doi:10.1111/exd.13467

Lai, Y., Li, D., Li, C., Muehleisen, B., Radek, K. A., Park, H. J., et al. (2012). The antimicrobial protein REG3A regulates keratinocyte proliferation and differentiation after skin injury. *Immunity* 37, 74–84. doi:10.1016/j.immuni.2012.04.010

Lorenz, B., and Von Stebut, E. (2014). Isolation of T cells from the skin. *Methods Mol. Biol.* 1193, 3–13. doi:10.1007/978-1-4939-1212-4_1

Lowes, M. A., Suarez-Farinas, M., and Krueger, J. G. (2014). Immunology of psoriasis. *Annu. Rev. Immunol.* 32, 227–255. doi:10.1146/annurev-immunol-032713-120225

Ma, E. H., Bantug, G., Griss, T., Condotta, S., Johnson, R. M., Samborska, B., et al. (2017). Serine is an essential metabolite for effector T cell expansion. *Cell Metab.* 25, 482. doi:10.1016/j.cmet.2017.01.014

Martin, D. A., Towne, J. E., Kricorian, G., Klekotka, P., Gudjonsson, J. E., Krueger, J. G., et al. (2013). The emerging role of IL-17 in the pathogenesis of psoriasis: preclinical and clinical findings. *J. Invest. Dermatol* 133, 17–26. doi:10.1038/jid.2012.194

Mason, J., Mason, A. R., and Cork, M. J. (2002). Topical preparations for the treatment of psoriasis: a systematic review. *Br. J. Dermatol* 146, 351–364. doi:10.1046/j.1365-2133.2000.04713.x

Mei, S., Huang, Y., Li, N., Xu, Z., Xu, J., Dai, Q., et al. (2020). Aminooxy-acetic acid inhibits experimental autoimmune uveitis by modulating the balance between effector and regulatory lymphocyte subsets. *Curr. Mol. Med.* 20, 624–632. doi:10.2174/1566524020666200211112219

Michalek, I. M., Loring, B., and John, S. M. (2017). A systematic review of worldwide epidemiology of psoriasis. *J. Eur. Acad. Dermatol Venereol.* 31, 205–212. doi:10.1111/jdv.13854

Nussbaum, L., Chen, Y. L., and Ogg, G. S. (2021). Role of regulatory T cells in psoriasis pathogenesis and treatment. *Br. J. Dermatol* 184, 14–24. doi:10.1111/bjd.19380

Ottas, A., Fishman, D., Okas, T. L., Kingo, K., and Soomets, U. (2017). The metabolic analysis of psoriasis identifies the associated metabolites while providing computational models for the monitoring of the disease. *Arch. Dermatol Res.* 309, 519–528. doi:10.1007/s00403-017-1760-1

Pasparakis, M., Haase, I., and Nestle, F. O. (2014). Mechanisms regulating skin immunity and inflammation. *Nat. Rev. Immunol.* 14, 289–301. doi:10.1038/nri3646

Quaglino, P., Bergallo, M., Ponti, R., Barberio, E., Cicchelli, S., Buffa, E., et al. (2011). Th1, Th2, Th17 and regulatory T cell pattern in psoriatic patients: modulation of cytokines and gene targets induced by etanercept treatment and correlation with clinical response. *Dermatology* 223, 57–67. doi:10.1159/000330330

Saxton, R. A., and Sabatini, D. M. (2017). mTOR signaling in growth, metabolism, and disease. *Cell* 168, 361–371. doi:10.1016/j.cell.2017.03.035

Schlaak, J. F., Buslau, M., Jochum, W., Hermann, E., Girndt, M., Gallati, H., et al. (1994). T cells involved in psoriasis vulgaris belong to the Th1 subset. *J. Invest. Dermatol* 102, 145–149. doi:10.1111/1523-1747.ep12371752

Son, J., Lyssiotis, C. A., Ying, H., Wang, X., Hua, S., Ligorio, M., et al. (2013). Glutamine supports pancreatic cancer growth through a KRAS-regulated metabolic pathway. *Nature* 496, 101–105. doi:10.1038/nature12040

Szabo, S. J., Kim, S. T., Costa, G. L., Zhang, X., Fathman, C. G., and Glimcher, L. H. (2000). A novel transcription factor, T-bet, directs Th1 lineage commitment. *Cell* 100, 655–669. doi:10.1016/s0092-8674(00)80702-3

Wang, C., Chen, H., Zhang, M., Zhang, J., Wei, X., and Ying, W. (2016). Malate-aspartate shuttle inhibitor aminooxyacetic acid leads to decreased intracellular ATP levels and altered cell cycle of C6 glioma cells by inhibiting glycolysis. *Cancer Lett.* 378, 1–7. doi:10.1016/j.canlet.2016.05.001

Xiang, H. C., Lin, L. X., Hu, X. F., Zhu, H., Li, H. P., Zhang, R. Y., et al. (2019). AMPK activation attenuates inflammatory pain through inhibiting NF-κB activation and IL-1β expression. *J. Neuroinflammation* 16, 34. doi:10.1186/s12974-019-1411-x

Xu, T., Stewart, K. M., Wang, X., Liu, K., Xie, M., Ryu, J. K., et al. (2017). Metabolic control of T(H)17 and induced T(reg) cell balance by an epigenetic mechanism. *Nature* 548, 228–233. doi:10.1038/nature23475

Yuan, X., Li, N., Zhang, M., Lu, C., Du, Z., Zhu, W., et al. (2020). Taxifolin attenuates IMQ-induced murine psoriasis-like dermatitis by regulating T helper cell responses via Notch1 and JAK2/STAT3 signal pathways. *Biomed. Pharmacother.* 123, 109747. doi:10.1016/j.biopha.2019.109747

Zeng, J. D., Wu, W. K. K., Wang, H. Y., and Li, X. X. (2019). Serine and one-carbon metabolism, a bridge that links mTOR signaling and DNA methylation in cancer. *Pharmacol. Res.* 149, 104352. doi:10.1016/j.phrs.2019.104352

Zhang, W., Liu, X., Zhu, Y., Liu, X., Gu, Y., Dai, X., et al. (2021). Transcriptional and posttranslational regulation of Th17/Treg balance in health and disease. *Eur. J. Immunol.* 51, 2137–2150. doi:10.1002/eji.202048794

Check for updates

*CORRESPONDENCE
Naoki Takemura,
✉ takemura-na@phs.osaka-u.ac.jp
Tatsuya Saitoh,
✉ saitohtatsuya@phs.osaka-u.ac.jp

†These authors have contributed equally
to this work and share last authorship

Dasatinib suppresses particulate-induced pyroptosis and acute lung inflammation

Yixi Pan[1], Kenta Ikoma[1], Risa Matsui[1], Akiyoshi Nakayama[2], Naoki Takemura[1]*[†] and Tatsuya Saitoh[1,3,4]*[†]

[1]Laboratory of Bioresponse Regulation, Graduate School of Pharmaceutical Sciences, Osaka University, Osaka, Japan, [2]Department of Integrative Physiology and Bio-Nano Medicine, National Defense Medical College, Saitama, Japan, [3]Global Center for Medical Engineering and Informatics, Osaka University, Osaka, Japan, [4]Center for Infectious Diseases for Education and Research (CiDER), Osaka University, Osaka, Japan

Background: Humans are constantly exposed to various industrial, environmental, and endogenous particulates that result in inflammatory diseases. After being engulfed by immune cells, viz. Macrophages, such particulates lead to phagolysosomal dysfunction, eventually inducing pyroptosis, a form of cell death accompanied by the release of inflammatory mediators, including members of the interleukin (IL)-1 family. Phagolysosomal dysfunction results in the activation of the nod-like receptor family pyrin domain containing 3 (NLRP3) inflammasome, an immune complex that induces pyroptosis upon exposure to various external stimuli. However, several particulates induce pyroptosis even if the NLRP3 inflammasome is inhibited; this indicates that such inhibition is not always effective in treating diseases induced by particulates. Therefore, discovery of drugs suppressing particulate-induced NLRP3-independent pyroptosis is warranted.

Methods: We screened compounds that inhibit silica particle (SP)-induced cell death and release of IL-1α using RAW264.7 cells, which are incapable of NLRP3 inflammasome formation. The candidates were tested for their ability to suppress particulate-induced pyroptosis and phagolysosomal dysfunction using mouse primary macrophages and alleviate SP-induced NLRP3-independent lung inflammation.

Results: Several Src family kinase inhibitors, including dasatinib, effectively suppressed SP-induced cell death and IL-1α release. Furthermore, dasatinib suppressed pyroptosis induced by other particulates but did not suppress that induced by non-particulates, such as adenosine triphosphate. Dasatinib reduced SP-induced phagolysosomal dysfunction without affecting phagocytosis of SPs. Moreover, dasatinib treatment strongly suppressed the increase in IL-1α levels and neutrophil counts in the lungs after intratracheal SP administration.

Abbreviations: ASM, acid sphingomyelinase; ATP, adenosine triphosphate; BAL, bronchoalveolar lavage; BMDMs, bone marrow-derived macrophages; CXCL, chemokine (C-X-C motif) ligand; Cyto D, cytochalasin D; ELISA, enzyme-linked immunosorbent assay; FCS, fetal calf serum; FDA, Food and Drug Administration; HRP, horseradish peroxidase; IL, interleukin; LAMP-1, lysosome-associated membrane protein-1; LDH, lactate dehydrogenase; LLoMe, L-leucyl-L-leucine methyl ester; LPS, lipopolysaccharide; MSU, monosodium urate; NLRP3, Nod-like receptor family pyrin domain containing 3; PIP2, phosphatidylinositol 4,5-bisphosphate; p-SFK, phosphorylated Src family kinase; SFK, Src family kinase; SP, silica particle.

Conclusion: Dasatinib suppresses particulate-induced pyroptosis and can be used to treat relevant inflammatory diseases.

Introduction

The prevalence of inflammatory diseases caused by environmental pollution, overnutrition, and aging is increasing in, both, developed and developing countries (Barquera et al., 2015; Lopez and Kuller, 2019; von Schneidemesser et al., 2020; Kimura et al., 2021). Therefore, there is an urgent need to address these global health problems. Particulate irritants that result in aberrant inflammation by stimulating immune cells are involved in the pathogenesis of modern diseases. For example, the inhalation of particulates comprising crystalline silica, such as yellow dust and $PM_{2.5}$, results in pneumoconiosis and allergies (Dostert et al., 2008; Kuroda et al., 2016). Amorphous silica can also lead to pneumoconiosis (Cho et al., 2007). Moreover, the ingestion of microplastics, a recent cause of serious marine pollution, induces liver injury (Mu et al., 2022). Industrial materials such as asbestos and carbon nanotubes lead to pneumoconiosis and mesothelioma, whereas titanium dioxide causes dermatitis and enteritis (Dostert et al., 2008; Yazdi et al., 2010; Palomaki et al., 2011). In addition, metabolic crystalline particles, including monosodium urate (MSU), cholesterol, and calcium oxalate crystals, generated in the body owing to overnutrition, cause gout, arteriosclerosis, and nephritis, respectively (Martinon et al., 2006; Duewell et al., 2010; Mulay et al., 2012). Harmful particulates also include protein aggregates, such as amyloid-β deposits, which lead to Alzheimer's disease with aging (Halle et al., 2008). Therefore, there is an urgent need to develop effective therapeutic strategies by elucidating particulate-induced inflammatory responses.

The immune system is the host's defense mechanism against infection. It induces the production of inflammatory mediators by sensing pathogens using pattern recognition receptors thereby triggering inflammation for their clearance (Takeuchi and Akira, 2010). In contrast, the immune system also induces inflammation in response to particulate irritants, leading to tissue injury and dysfunction. Particulates induce immune cell pyroptosis, a form of cell death accompanied by the release of inflammatory mediators, particularly members of the interleukin (IL)-1 family (Hornung et al., 2008; Yang et al., 2019). Drugs that prevent pyroptosis can potentially treat inflammatory diseases induced by particulate irritants.

Invading or intrinsic particulates are engulfed by immune cells such as macrophages. Phagosomes containing foreign substances undergo maturation by sequentially recruiting various proteins, including Rab guanosine triphosphatase, and eventually fusing with lysosomes to form phagolysosomes, which digest the engulfed substances (Kinchen and Ravichandran, 2008). However, particulates with sharp crystal structures and/or particular surface properties destabilize the phagolysosomal membrane, resulting in the leakage of its contents (Hornung et al., 2008). Phagolysosomal dysfunction activates the nod-like receptor family pyrin domain containing 3 (NLRP3), an intracellular pattern recognition receptor, which senses microbial invasion (Yang et al., 2019). Upon activation, NLRP3 forms a protein complex (termed inflammasome) with the adaptor molecule apoptosis-associated speck-like protein containing a caspase recruitment domain and caspase-1 (Yang et al., 2019). Caspase-1 induces the maturation of cytokines of the IL-1 family, such as IL-1β and IL-18, and gasdermin D, which form pores in the plasma membrane and induce cytokine release and subsequent cell death (Yang et al., 2019). To date, drugs targeting the NLRP3 inflammasome and its downstream cytokines have been developed to treat pyroptosis-induced inflammatory diseases (Yang et al., 2019). However, recent studies suggest that targeting NLRP3 inflammasome-associated responses are insufficient in treating inflammatory diseases induced by particulates, such as silica particles (SPs) and MSU, because these particulates continue to induce cell death and inflammatory mediator release in the absence of NLRP3 or gasdermin D (Yazdi et al., 2010; Groß et al., 2012; Rabolli et al., 2014; Kuroda et al., 2016; Rashidi et al., 2019; Ikoma et al., 2022). IL-1α is an important molecule among those released during NLRP3-independent cell death owing to its proinflammatory effects by binding to the same receptor as IL-1β. Several animal studies have reported that IL-1α plays critical roles in the development of particulate-induced inflammatory diseases (Yazdi et al., 2010; Groß et al., 2012; Rabolli et al., 2014; Kuroda et al., 2016; Ikoma et al., 2022). However, preventing NLRP3-independent cell death and the resultant release of inflammatory mediators remains a key challenge during the development of efficient treatment strategies for inflammatory diseases induced by particulate irritants.

In a previous study, we proposed the natural compound oridonin as an effective drug candidate for treating particulate-induced inflammatory diseases (Ikoma et al., 2022). Oridonin suppressed particulate-induced NLRP3-independent cell death and IL-1α release and attenuated NLRP3-independent lung inflammation in a mouse model of silicosis. However, oridonin and its derivatives are still not clinically approved. In the present study, we performed a library screening via drug repositioning to identify compounds that can suppress particulate-induced cell death and IL-1α release. Consequently, we identified dasatinib, a clinically approved drug, as a potential therapeutic agent for particulate-induced inflammatory diseases.

Materials and methods

Reagents and cell lines

Pfizer and Food and Drug Administration (FDA)-approved drug libraries were kindly provided by the Center for Supporting Drug Discovery and Life Science Research, Graduate School of Pharmaceutical Sciences, Osaka University. Lipopolysaccharide

(LPS) from *Escherichia coli* O111:B4 was purchased from Invivogen (San Diego, CA, United States). Plain and fluorescent amorphous SPs (Sicastar; 500, 1,500, and 3,000 nm in diameter) were purchased from MicroMod (Rostock, Germany). Chemi-Lumi One Super and MSU were purchased from Nacalai Tesque (Kyoto, Japan). Gobi Kosa dust (yellow dust) was purchased from the National Institute for Environmental Studies (Ibaraki, Japan). Adenosine triphosphate (ATP) was purchased from Enzo Life Sciences (Farmingdale, NY, United States). DRAQ7 was purchased from Biostatus (Loughborough, United Kingdom). Bosutinib, cytochalasin D (Cyto D), dasatinib, L-leucyl-L-leucine methyl ester (LLoMe), PD-161570, and iFluor-488-conjugated phalloidin were purchased from Cayman Chemical Company (Ann Arbor, Michigan, United States). PD-166285 dihydrochloride was purchased from Tocris Biosciences (Abingdon, United Kingdom). Dasatinib hydrochloride for *in vivo* experiments was purchased from MedChem Express (Monmouth Junction, NJ, United States). Hoechst 33342, LysoTracker Deep Red, and ProLong Gold antifade Mountant were purchased from Thermo Fisher Scientific (Waltham, MA, United States). DRAQ5 and the enzyme-linked immunosorbent assay (ELISA) kits for mouse IL-1β were purchased from BioLegend (San Diego, CA, United States). Can Get Signal Immunoreaction Enhancer Solution was purchased from Toyobo (Osaka, Japan). Immobilon Forte Western horseradish peroxidase (HRP) substrate was purchased from Merck Millipore (Burlington, MA, United States). Collagenase (crude type) was purchased from FUJIFILM Wako Pure Chemical Corporation (Osaka, Japan) and DNase I was purchased from Sigma-Aldrich (St. Louis, MO, United States). The ELISA kits for mouse chemokine (C-X-C motif) ligand (CXCL) 1 and mouse and human IL-1α and IL-1β were purchased from R&D Systems (Minneapolis, MN, United States). The cytotoxicity lactate dehydrogenase (LDH) assay kit (WST) was purchased from Dojindo Laboratories (Kumamoto, Japan).

RAW264.7, a mouse macrophage cell line, and THP-1, a human monocytic cell line, were purchased from Riken (Ibaraki, Japan).

Antibodies

Anti-phospho-Src family (D49G4), anti-RAB5A, member RAS oncogene family (RAB5A) (E6N8S), HRP-conjugated anti-mouse IgG, and HRP-conjugated anti-rabbit IgG antibodies were purchased from Cell Signaling Technology (Danvers, MA, United States). Anti-lysosome-associated membrane protein-1 (LAMP-1) (1D4B) and anti-phosphatidylinositol 4,5-bisphosphate (PIP2) (2C11) antibodies were purchased from Abcam (Cambridge, United Kingdom). Anti-actin antibody (C-11) was purchased from Santa Cruz Biotechnology (Dallas, TX, United States). Alexa Fluor-labeled secondary antibodies and HRP-conjugated anti-goat IgG (H + L) antibodies were purchased from Thermo Fisher Scientific. The Alexa Fluor 488-conjugated anti-mouse CD11b (M1/70), Pacific Blue-conjugated anti-mouse CD45 (30-F11), allophycocyanin-conjugated anti-mouse CD68 (FA-11), fluorescein isothiocyanate-conjugated anti-mouse CD80 (16-10A1), phycoerythrin-cyanine7-conjugated anti-mouse CD86 (GL-1), Alexa Fluor 647-conjugated anti-mouse Ly-6G (1A8), phycoerythrin-cyanine7-conjugated anti-

mouse Ly-6C (HK1.4), and phycoerythrin-conjugated anti-mouse major histocompatibility complex class II (M5/114.15.2) antibodies were purchased from BioLegend.

MSU crystal formation

MSU crystals were prepared using a previously described method (Ikoma et al., 2022).

Mice

C57BL/6J mice (5-week-old females) were purchased from Japan SLC, Inc. (Shizuoka, Japan). During the experimental period, all mice were housed in standard cages in a temperature-controlled room under a 12-h light/dark cycle at the animal care facility of the Graduate School of Pharmaceutical Sciences, Osaka University. Mice were provided *ad libitum* access to standard laboratory mouse chow and drinking water.

Screening of compounds that can inhibit particulate-induced cell death and IL-1α release

RAW264.7 cells were seeded at a density of 3.5×10^4 cells/well into glass-bottom 96-well plates and primed with LPS (100 ng/mL) for 16 h in Eagle's minimal essential medium supplemented with 10% fetal calf serum (FCS), penicillin (100 U/mL), streptomycin (100 μg/mL), and non-essential amino acids (Nacalai Tesque, 100x). Cells were pretreated with each compound (5 μM) from the Pfizer- and FDA-approved drug libraries for 30 min and then stimulated with SPs (500 nm in diameter, 500 μg/mL) in the presence of DRAQ7 (2 μM) and Hoechst 33342 (1 μg/mL) for 2 h. After the supernatants were collected, the cells were fixed with 4% paraformaldehyde for 15 min and then rinsed with ice-cold phosphate buffered saline. Images were acquired from four fields per well using the Cell Voyager CV8000 High Content Screening System (Yokogawa Electric Corp., Tokyo, Japan). Hoechst 33342-positive and DRAQ7-negative cells and Hoechst 33342 and DRAQ7 double-positive cells were considered viable and dead cells, respectively. The cell death rate was calculated by dividing the number of dead cells by the total number of cells using CellPathfinder software (Yokogawa Electric Corp.). IL-1α levels in the cell culture supernatants were measured using ELISA, as described below. A test compound was defined as a hit if the mean percentage inhibition of cell death and IL-1α release was >50%.

Macrophage preparation and stimulation

To prepare bone marrow-derived macrophages (BMDMs), mouse bone marrow cells were cultured with macrophage colony-stimulating factor (10 ng/mL) in Roswell Park Memorial Institute (RPMI) 1,640 supplemented with 10% FCS, penicillin, and streptomycin. 5 days after culture initiation, cells were collected and used as BMDMs. The BMDMs were seeded at a density of 4×10^5

cells/well in 48-well plates and primed with LPS (200 ng/mL) in RPMI1640 supplemented with 10% FCS for 6 h. The primed cells were pretreated with bosutinib (20 μM), Cyto D (20 μM), dasatinib (20 μM), PD-161570 (20 μM), or PD-166285 (20 μM) for 30 min and then stimulated with SPs (500, 1,500 or 3,000 nm in diameter, 300 μg/mL), MSU (300 μg/mL), yellow dust (500 μg/mL), or ATP (3 mM) for 2 h or with LLoMe (0.5 mM) for 3 h.

THP-1 cells were seeded at a density of 4×10^5 cells/well in 48-well plates and induced for macrophage differentiation by culturing them with phorbol 12-myristate 13-acetate (10 ng/mL) in RPMI1640 supplemented with 10% FCS for 1 day, followed by an additional 2 days of culture in phorbol 12-myristate 13-acetate-free medium. THP-1 cells were primed with LPS (50 ng/mL) in RPMI1640 supplemented with 10% FCS for 16 h. The primed cells were pretreated with dasatinib (20 μM) for 30 min and then stimulated with SPs (1,500 nm in diameter, 500 μg/mL) for 4 h.

The supernatants from each culture condition were collected after centrifuging the samples at 440 ×*g* and 4°C for 5 min. The supernatants and cell samples were analyzed.

Cell viability measurement

Cell viability was determined by measuring LDH activity in the culture supernatants using the cytotoxicity LDH assay kit (WST) according to the manufacturer's instructions.

Immunoblotting

Cell samples were washed and lysed with 30 μL of the lysis buffer containing 62.5 mM Tris–HCl (pH 6.8 at 25°C), 2% (w/v) sodium dodecyl sulfate, 10% (v/v) glycerol, 0.01% (w/v) bromophenol blue, and 42 mM dithiothreitol. Samples were then processed for immunoblotting using a previously described method (Matsui et al., 2022). Each protein was probed with the appropriate antibodies listed in the subsection "Antibodies," and the blots were visualized using Immobilon Forte Western HRP Substrate (Merck Millipore) or Chemi-Lumi One Super (Nacalai Tesque). Immunoreactive bands were detected using FUSION Solo S (Vilber Lourmat, Collégien, France) and quantified using the ImageJ software bundled with 64-bit Java 8. (Version 1.53t) (National Institutes of Health, MD, United States).

Observation of particulate uptake by BMDMs

BMDMs were cultured on coverslips and primed with LPS (200 ng/mL) for 6 h. Further, they were pretreated with Cyto D (20 μM) or dasatinib (20 μM) for 30 min and stimulated with fluorescent SPs (1,500 nm in diameter, 20 μg/mL) for 2 h. The stimulated cells were fixed with 4% paraformaldehyde for 15 min and permeabilized with digitonin (50 μg/mL) for 15 min. The membrane-permeabilized cells were stained with iFluor-488-conjugate phalloidin (1000-fold dilution) and DRAQ5 (200 μM) for 30 min. Images were obtained using the Cell Voyager

CV8000 High Content Screening system, and the number of phagocytosed SPs per cell was counted using the CellPathfinder software.

Immunocytochemistry

BMDMs were cultured on coverslips and fixed with 3% paraformaldehyde. Immunocytochemistry was performed as described previously (Ikoma et al., 2022). Samples were visualized under an inverted fluorescence microscope (DMI6000B; Leica Microsystems, Wetzlar, Germany) and photographed using the Application Suite X software imaging system (Leica Microsystems).

Induction of lung inflammation

Mice were randomly divided into four groups and anesthetized via isoflurane inhalation. The groups received different treatments as follows: 1) intratracheal administration of phosphate buffered saline; 2) intratracheal SP administration (100 mg/kg); 3) intratracheal SP administration (100 mg/kg) in combination with intragastric dasatinib administration (30 mg/kg); and 4) intratracheal administration of SP (100 mg/kg) in combination with dasatinib (10 mg/kg). Bronchoalveolar lavage (BAL) fluid was collected 12 h after the intratracheal administration of SPs. Subsequently, 1 mL of phosphate buffered saline was flushed into the lungs, with a recovery of approximately 700 μL of BAL fluid. The remaining lung tissues were used for isolating lung leukocytes as described below. In separate experiments, the lungs were collected 12 h after the intratracheal administration of SPs for histological analysis.

Isolation of lung leukocytes

Lung tissues were minced using a pair of scissors and subsequently digested with collagenase (2 mg/mL) and DNase I (100 μg/mL) in RPMI1640 medium supplemented with 10% FCS with continuous stirring at 37°C for 60 min. The suspended cells were centrifuged at a density-gradient of 40%–80% (v/v) Percoll. Cells (lung leukocytes) were collected from the interface, washed, and then used in further experiments.

Flow cytometric analysis

BMDMs were stained with LysoTracker Deep Red according to the manufacturer's instructions. Lung leukocytes were stained with antibodies against mouse CD11b, CD45, CD68, CD80, CD86, Ly-6C, Ly-6G, and major histocompatibility complex class II, according to the manufacturer's instructions. CD45^{+} CD11b^{+} Ly-6C[med] Ly-6G^{high} cells were identified as neutrophils (Ikoma et al., 2022). CD45^{+} CD80^{+} CD86^{+} major histocompatibility complex class II^{high} CD68^{+} cells were identified as M1 macrophages (Supplementary Figure S1) (Haloul et al., 2019; Nascimento Da Conceicao et al., 2021). The data were acquired using a flow cytometer (CytoFLEX; Beckman Coulter, Brea, CA, United States) and analyzed using the FlowJo software (TreeStar, Ashland, OR, United States).

TABLE 1 List of candidate drugs that inhibit particulate-induced cell death accompanied by interleukin (IL)-1α release.

Stimulation	Candidate drugs	Cell death (%)	IL-1α (pg/mL)	Reference
None	—	4 ± 0.2	201.5 ± 0.7	—
Silica particles	—	54.1 ± 3	3192.7 ± 36.2	—
	Bosutinib	3.3 ± 0.9	125.7 ± 35.4	Golas et al. (2003)
	Dasatinib	26.6 ± 4	1262.7 ± 766.7	Lombardo et al. (2004)
	PD-161570	7.9 ± 3.5	229.8 ± 0.1	Hamby et al. (1997)
	PD-166285	4.5 ± 1.4	143 ± 4.2	Panek et al. (1997)
	PD-173952	2.7 ± 1.3	718.4 ± 44.1	Dorsey et al. (2002)
	PD-407824	4.4 ± 0.6	1524.5 ± 261.7	Palmer et al. (2006)

Histological analysis

The mouse lungs were fixed for 24 h with 10% formalin and embedded in paraffin. Five-micrometer sections of the mouse lungs were stained with hematoxylin and eosin and observed under the BZ-X800 automated high-resolution microscope (Keyence, Osaka, Japan) with an analysis application.

ELISA

Mouse CXCL1, mouse and human IL-1α and IL-1β levels in the culture supernatant and BAL fluid were measured using ELISA kits, according to the manufacturer's instructions.

Statistical analyses

All data was calculated using GraphPad Prism 8.0 software (Boston, MA, United States). One-way analysis of variance and the Tukey–Kramer *post hoc* test were performed for multiple group comparisons. Statistical significance was set at a *p*-value of <0.05.

Results

Dasatinib suppresses particulate-induced pyroptosis in macrophages

RAW264.7 cells are a macrophage cell line with impaired apoptosis-associated speck-like protein containing a caspase recruitment domain expression and negligible effects on the NLRP3 inflammasome (Pelegrin et al., 2008). These cells were used to identify inhibitors against particulate-induced NLRP3 inflammasome-independent pyroptosis. Candidate inhibitors were screened by elucidating whether the treatment of LPS-primed RAW264.7 cells with the test compounds before SP stimulation suppressed cell death and IL-1α release. SP-induced cell death was determined using CellVoyager CV8000, which allows high-throughput imaging-based screening. Two nuclear staining

dyes, Hoechst 33342 and DRAQ7, were used to determine cell viability. Hoechst 33342 was used to stain the cell nuclei, whereas DRAQ7, a membrane-impermeable dye, was used to stain the nuclei of dead cells. Accordingly, Hoechst 33342-positive and DRAQ7-negative cells and Hoechst 33342 and DRAQ7 double-positive cells were considered viable and dead cells, respectively (Supplementary Figure S2A). Simultaneously, IL-1α levels in the culture supernatants were also measured. Screening of 1,240 compounds present in the Pfizer- and FDA-approved libraries identified two anticancer drugs, bosutinib and dasatinib, which suppressed SP-induced cell death and IL-1α release (Table 1; Supplementary Figures S2B, C). Similar results were obtained for PD-161570, PD-166285, PD-173952, and PD-407824. Interestingly, all the drug candidates targeted Src family kinases (SFKs), well-known signaling factors involved in various cellular functions, including the induction of inflammatory responses, cell proliferation, cell differentiation, and metabolism (Parsons and Parsons, 2004; Byeon et al., 2012).

Further, mouse primary macrophages were used to validate the effects of bosutinib, dasatinib, PD-161570, and PD-166285 (PD-173952 and PD-407824 were excluded because they are not approved yet and exhibit relatively weak suppressive effects against SP-induced pyroptosis). To assess whether these drugs inhibit SP-induced macrophage pyroptosis, we measured IL-1β and LDH release as indicators of pyroptosis, in addition to IL-1α release. LDH is released when the plasma membrane ruptures and is often used to measure the incidence of lytic cell death, including pyroptosis (Kayagaki et al., 2021). All the drug candidates significantly suppressed SP-induced cell death accompanied by IL-1α and IL-1β release in BMDMs (Figures 1A–C). Since dasatinib is clinically well-studied (Araujo and Logothetis, 2010), it was used as a representative of these candidates in subsequent experiments. We investigated whether dasatinib effectively suppresses SP-induced pyroptosis in human cells. Dasatinib was found to successfully suppress SP-induced cell death accompanied by IL-1α and IL-1β release in phorbol 12-myristate 13-acetate-treated macrophage-like THP-1 cells (Figures 1D–F). Furthermore, dasatinib did not affect the viability of BMDMs during the 12 h treatment at concentrations required to inhibit SP-induced pyroptosis (Figure 1G). Therefore, dasatinib and other SFK inhibitors effectively suppressed particulate-induced pyroptosis.
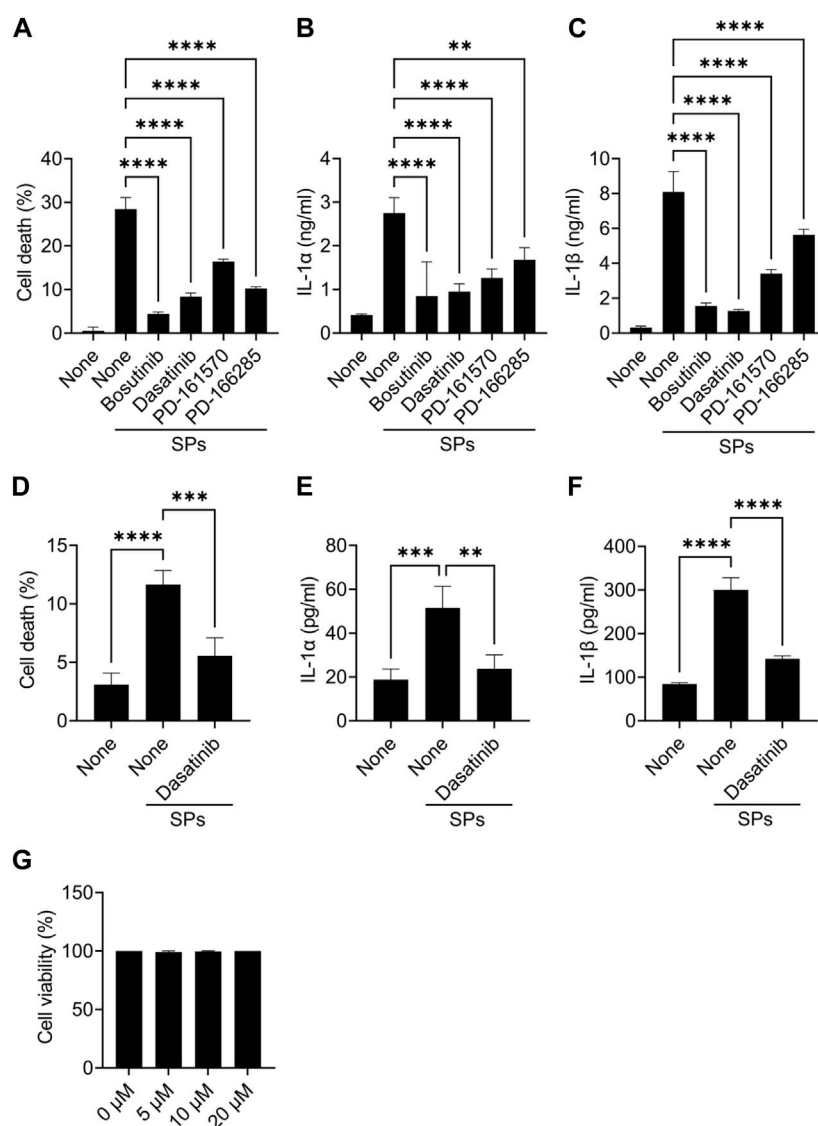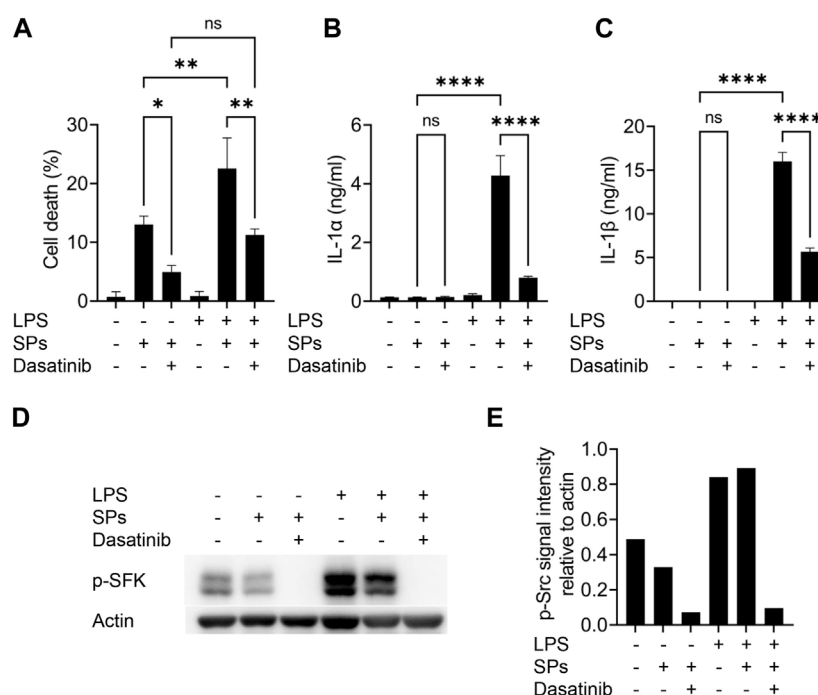
FIGURE 1
Dasatinib suppresses silica particle (SP)-induced cell death accompanied by interleukin-1 (IL-1) α release. **(A−C)** Bone marrow-derived macrophages (BMDMs) were primed with lipopolysaccharide (LPS) (200 ng/mL) for 6 h. The cells were then treated with 20 μM of bosutinib, dasatinib, PD-161570, or PD-166285 and were stimulated or not stimulated with SPs (1,500 nm in diameter, 300 μg/mL) for 2 h. **(A)** The cell death rate was determined by measuring lactate dehydrogenase (LDH) activity in the culture supernatant. **(B,C)** IL-1α and IL-1 beta (β) levels in the culture supernatants were measured using enzyme-linked immunosorbent assay (ELISA). **(D−F)** Phorbol 12-myristate 13-acetate-differentiated THP-1 cells were primed with LPS (50 ng/mL) for 16 h. The cells were then treated with dasatinib (20 μM) and were stimulated or not stimulated with SPs (1,500 nm in diameter, 500 μg/mL) for 4 h. **(D)** Cell death rate was determined by measuring LDH activity in the culture supernatant. **(D,E)** IL-1α and IL-1β levels in the culture supernatants were measured using ELISA. **(G)** BMDMs were treated with increasing doses of dasatinib (0−20 μM) for 12 h; thereafter, the cell death rate was determined by measuring LDH activity in the culture supernatant. The results are presented as the mean ± standard deviations (SD) of values from triplicate wells. **, $p < 0.01$; ***, $p < 0.001$; and ****, $p < 0.0001$.

Increase in active SFK levels enhance particulate-induced cell death

Macrophages were initially primed with LPS to induce intracellular IL-1α and IL-1β expression by activating toll-like receptor 4. However, toll-like receptor 4 increases the levels of active SFKs by enhancing their transcription and phosphorylation at Tyr416 (Boggon and Eck, 2004; Maa and Leu, 2016). Thus, we determined whether SFKs mediate particulate-induced cell death without priming. As a result, dasatinib significantly suppressed SP-induced cell death in BMDMs even without LPS priming, although the unprimed cells did not release IL-1α and IL-1β upon SP stimulation (Figures 2A–C). Immunoblotting revealed the phosphorylation of SFKs at Tyr416 (phosphorylated SFKs; p-SFKs) in unprimed BMDMs (Figures 2D, E). Furthermore, LPS priming significantly enhanced SP-induced cell death of BMDMs and increased p-SFK levels. Interestingly, dasatinib decreased SP-induced cell death rates and p-SFK levels in LPS-primed BMDMs to levels comparable to those observed in dasatinib-treated unprimed BMDMs. SP stimulation tended to

FIGURE 2
Lipopolysaccharide (LPS)-priming increases the levels of phosphorylated Src family kinases (p-SFKs) and enhances silica particle (SP)-induced pyroptosis. **(A–E)** Unprimed and LPS-primed bone marrow-derived macrophages (BMDMs) were treated with dasatinib (20 μM) and stimulated or not stimulated with SPs (1,500 nm in diameter, 300 μg/mL) for 2 h. **(A)** The cell death rate was determined by measuring lactate dehydrogenase (LDH) activity in the culture supernatants. **(B,C)** Interleukin-1 alpha (IL-1α) and IL-1 beta (β) levels in the culture supernatants were measured using enzyme-linked immunosorbent assay (ELISA). **(D)** Immunoblotting of p-SFKs in the cell extracts of BMDMs. **(E)** Quantification of p-SFK levels compared to actin control under conditions indicated in **(D)**. The results are presented as the mean ± SD of values from triplicate wells. *, $p < 0.05$; **, $p < 0.01$; and ****, $p < 0.0001$; ns, not significant.

slightly decrease p-SFKs levels in unprimed BMDMs, but did not affect those in LPS-primed cells. To summarize, these results suggest that basal p-SFK levels can mediate particulate-induced cell death, and an increase in p-SFK levels via priming is associated with particulate-induced cell death.

Dasatinib suppresses particulate-induced pyroptosis of various sizes or materials
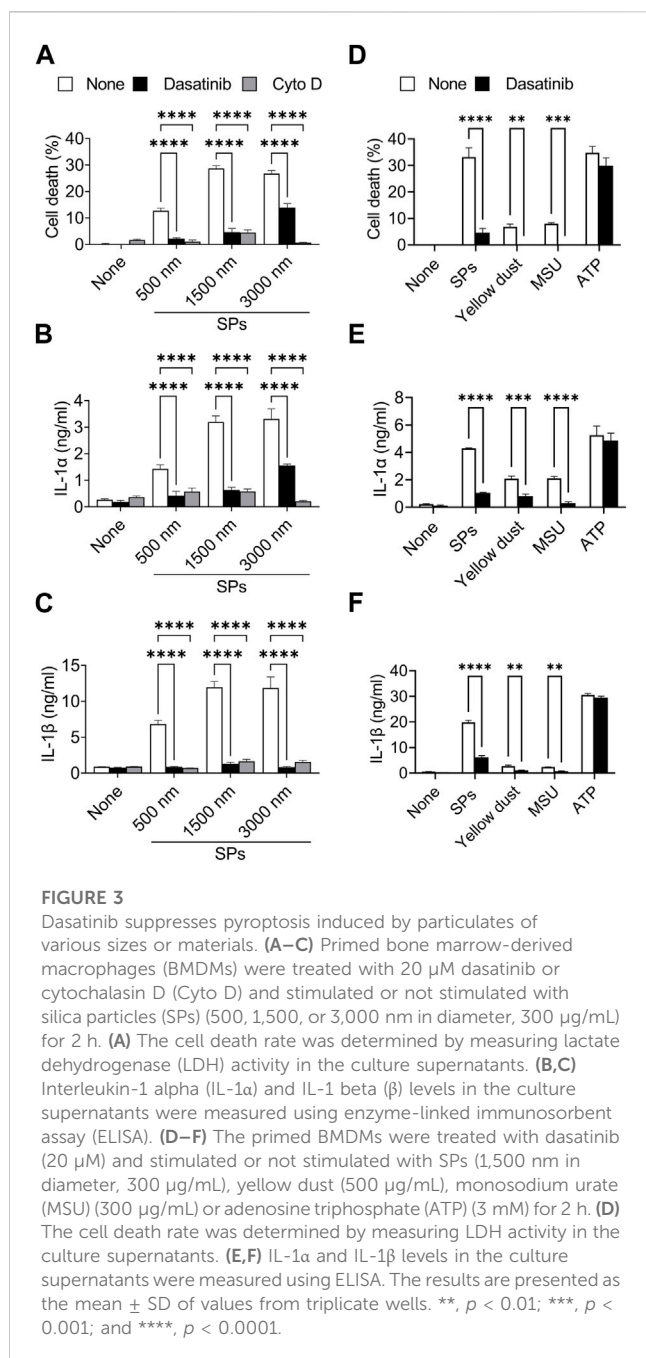
Particulates exhibit size-dependent variations in inflammatory properties and cytotoxicities (Kusaka et al., 2014; Nishijima et al., 2017; Chen et al., 2022). We evaluated the suppressive effects of dasatinib on pyroptosis induced by SPs of different sizes. An actin-polymerization inhibitor, Cyto D, almost completely suppressed cell death accompanied by IL-1α and IL-1β release in BMDMs induced by SPs with diameters of 500, 1,500, and 3,000 nm (Figures 3A–C), indicating these SPs were incorporated via phagocytosis. Thus, dasatinib significantly suppressed the cell death of BMDMs accompanied by IL-1α and IL-1β release induced by SPs, the efficacy of which varied with SP size.

Furthermore, dasatinib suppressed cell death and IL-1α and IL-1β release induced by yellow dust, which contains crystalline silica, and MSU crystals (Figures 3D–F), indicating that it suppresses pyroptosis induced by particulates of various materials.

In addition, we determined whether dasatinib suppresses pyroptosis induced by external stimuli other than particulates. ATP activates the NLRP3 inflammasome by inducing mitochondrial dysfunction, resulting in pyroptosis (Yang et al., 2019). However, dasatinib did not suppress ATP-induced cell death and IL-1α and IL-1β release (Figures 3D–F). Therefore, the suppressive effects of dasatinib on pyroptosis are selective and are strongly exhibited during particulate-induced pyroptosis.

Dasatinib suppresses particulate-induced phagolysosomal dysfunction without affecting phagocytosis

We further attempted to elucidate the mechanism underlying the effect of dasatinib on particulate-induced cellular responses. SFKs regulate Fcγ receptor-mediated phagocytosis (Suzuki et al., 2000). Therefore, we investigated whether dasatinib inhibits the phagocytosis of SPs by BMDMs. BMDMs were visualized by staining the nuclei and filamentous actin with fluorescent dyes after stimulation with fluorescent SPs and counting the number of SPs incorporated into the cytoplasm under a microscope (Figure 4A). Cyto D markedly decreased the number of incorporated SPs; whereas, dasatinib had no effects on SP phagocytosis (Figure 4B). Therefore, the suppression of

FIGURE 3
Dasatinib suppresses pyroptosis induced by particulates of various sizes or materials. **(A–C)** Primed bone marrow-derived macrophages (BMDMs) were treated with 20 µM dasatinib or cytochalasin D (Cyto D) and stimulated or not stimulated with silica particles (SPs) (500, 1,500, or 3,000 nm in diameter, 300 µg/mL) for 2 h. **(A)** The cell death rate was determined by measuring lactate dehydrogenase (LDH) activity in the culture supernatants. **(B,C)** Interleukin-1 alpha (IL-1α) and IL-1 beta (β) levels in the culture supernatants were measured using enzyme-linked immunosorbent assay (ELISA). **(D–F)** The primed BMDMs were treated with dasatinib (20 µM) and stimulated or not stimulated with SPs (1,500 nm in diameter, 300 µg/mL), yellow dust (500 µg/mL), monosodium urate (MSU) (300 µg/mL) or adenosine triphosphate (ATP) (3 mM) for 2 h. **(D)** The cell death rate was determined by measuring LDH activity in the culture supernatants. **(E,F)** IL-1α and IL-1β levels in the culture supernatants were measured using ELISA. The results are presented as the mean $\pm$ SD of values from triplicate wells. **, $p < 0.01$; ***, $p < 0.001$; and ****, $p < 0.0001$.

particulate-induced pyroptosis by dasatinib is unlikely to be caused by the inhibition of phagocytic activity against particulates.

Flow cytometric analysis of BMDMs stained with LysoTracker Deep Red, an acidotropic fluorescent dye which labels acidic organelles, including phagolysosomes, was performed to elucidate whether dasatinib suppresses SP-induced phagolysosomal dysfunction (Ikoma et al., 2022). The stimulation of BMDMs with SPs decreased the fluorescence intensity of LysoTracker Deep Red, indicating loss of the interior acidity of the phagolysosomes owing to leakage of their contents (Figures 4C, D). Dasatinib significantly decreased the population of LysoTracker Deep Red-negative cells among SP-stimulated cells. Thus, dasatinib was found to suppress particulate-induced phagolysosomal dysfunction.

Furthermore, we elucidated whether dasatinib reduced lysosomal dysfunction and subsequent pyroptosis induced by the lysosomotropic compound LLoMe. LLoMe accumulates in the lysosomes and is processed by the lysosomal thiol protease dipeptidyl peptidase I (Uchimoto et al., 1999). This process results in lysosomal dysfunction. Dasatinib decreased the population of LysoTracker Deep Red-negative cells among LLoMe-stimulated cells (Figures 4E, F). Furthermore, it significantly suppressed LLoMe-induced cell death and IL-1α and IL-1β release (Supplementary Figures S3A–C). Therefore, these results indicating that dasatinib suppressed pyroptosis by preventing phagolysosomal and lysosomal dysfunction.

Phosphorylated SFKs accumulate around particulate-engulfed phagosomes

Based on the findings of the present study, SFKs potentially mediate the dysfunction of SP-containing phagolysosomes. SFKs, including Src, Fyn, Lyn, and Yes, are recruited to actin-rich phagocytic cups during Fcγ receptor-mediated phagocytosis (Majeed et al., 2001). Therefore, we performed immunofluorescence analysis of BMDMs to investigate the spatio-temporal activity of SFK after the cells phagocytose particulates. In the initial stages of phagocytosis, PIP2 accumulates and initiates actin polymerization to extend the pseudopod and engulf the target (e.g., particulates) (Scott et al., 2005). Without SP stimulation, both PIP2 and p-SFKs were distributed throughout the cytoplasm of LPS-primed BMDMs (Figure 5). SPs were surrounded by PIP2 in BMDMs 15 min after SP stimulation. Furthermore, p-SFK accumulated around some PIP2-surrounded SPs. Dasatinib abolished p-SFK signals but did not affect the intensity or distribution of the PIP2 signals. These observations suggest that p-SFKs accumulate around the phagosomes engulfing particulates during the initial stages of phagocytosis.

Next, we stained p-SFKs with an early phagosome marker, RAB5A, 30 min after SP stimulation. We observed RAB5A-positive vesicles in the cytoplasm of BMDMs without SP stimulation (Figure 6). Most of the engulfed SPs were surrounded by RAB5A, and some of the RAB5A-surrounded SPs were also surrounded by p-SFK. Dasatinib did not influence the intensity or distribution of RAB5A signals. Furthermore, we performed immunostaining for LAMP-1, a lysosomal membrane protein used as a marker for late phagosomes and phagolysosomes (Kinchen and Ravichandran, 2008). We detected LAMP-1-positive vesicles in the cytoplasm of BMDMs without SP stimulation (Figure 7). Thirty minutes after stimulation, SPs were surrounded by LAMP-1, indicating that SP-engulfed phagosomes matured on fusing with lysosomes. However, LAMP-1 was not detected around p-SFK-surrounded SPs. Dasatinib did not affect LAMP-1 distribution after SP stimulation. In summary, p-SFKs may act on particulate-engulfed phagosomes mainly during the early stages of maturation.

Dasatinib treatment alleviates particulate-induced lung inflammation

Finally, we evaluated the anti-inflammatory effects of dasatinib on SP-induced lung inflammation in mice. In this model, intratracheally
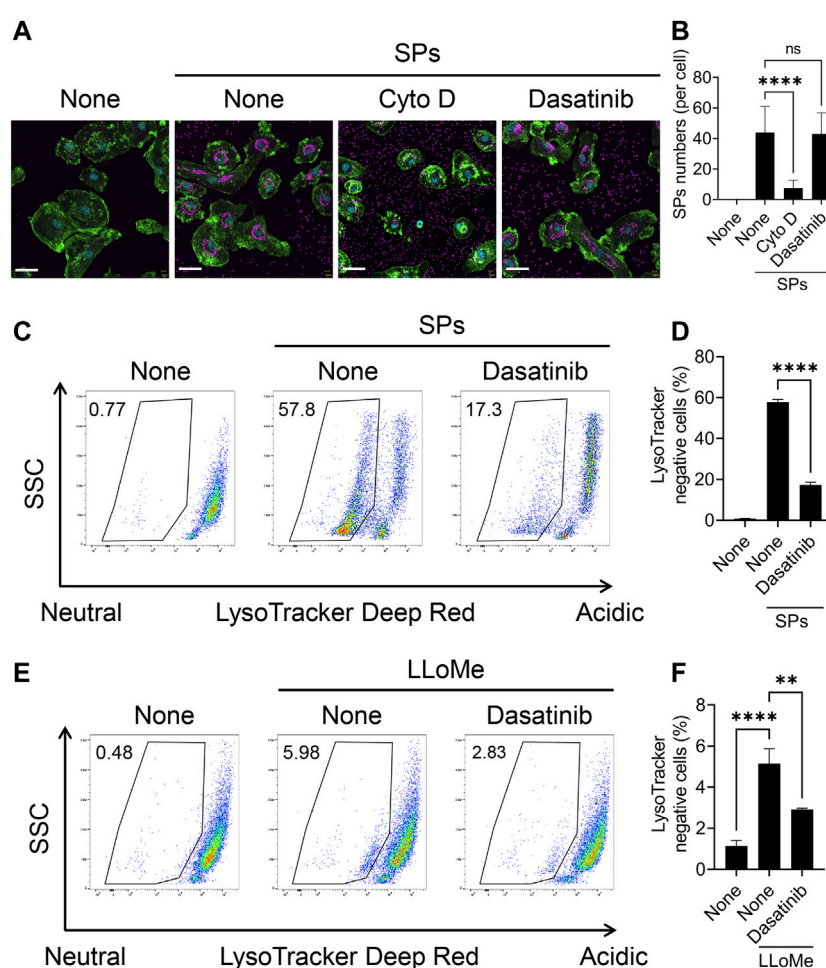
FIGURE 4
Dasatinib suppresses phagolysosomal and lysosomal dysfunction induced by silica particle (SP) and L-leucyl-L-leucine methyl ester (LLoMe) stimulation. **(A)** Primed bone marrow–derived macrophages (BMDMs) were treated with 20 μM cytochalasin D (Cyto D) or dasatinib and stimulated or not stimulated with fluorescent SPs (1,500 nm in diameter, 20 μg/mL; magenta) for 2 h. Actin (green) and nuclei (cyan) were stained with phalloidin and DRAQ5, respectively. Scale bar; 30 μm. **(B)** Numbers of SPs in BMDMs. The results are presented as the mean ± SD of values from 74 cells. **(C)** Flow cytometric analysis of the primed BMDMs treated with dasatinib (20 μM) and stimulated or not stimulated with SPs (1,500 nm in diameter, 300 μg/mL) for 2 h. The cells were stained with the fluorescent dye LysoTracker Deep Red. The data are representative of three independent experiments. **(D)** Percentages of the LysoTracker Deep Red–negative population were calculated. The results are presented as the mean ± SD of values from triplicate wells. **(E)** Flow cytometric analysis of primed BMDMs treated with dasatinib (20 μM) and stimulated or not stimulated with LLoMe (0.5 μM) for 3 h. The cells were stained with the fluorescent dye LysoTracker Deep Red. The data are representative of three independent experiments. **(F)** Percentages of the LysoTracker Deep Red–negative population were calculated. The results are presented as the mean ± SD of values from triplicate wells. $**$, $p < 0.01$, and $****$, $p < 0.0001$; ns, not significant.

administered SPs induce IL-1α release from pulmonary macrophages in an NLRP3-independent manner, resulting in neutrophil recruitment and inflammation (Ikoma et al., 2022). Dasatinib is an orally administered drug. We also tested topical treatment of the lung with dasatinib by its intratracheal administration. Both, intragastric and intratracheal administrations of dasatinib suppressed SP-induced lung inflammation. Dasatinib administrations via these routes significantly decreased IL-1α and IL-1β levels in the BAL fluid of mice after the intratracheal administration of SPs (Figures 8A, B). Furthermore, dasatinib administration through both the routes suppressed the levels of a neutrophil chemoattractant, CXCL1, and decreased the number of neutrophils in the mouse lungs after SP administration, although the inhibitory effect was stronger with intratracheal administration than that with intragastric

administration (Figures 8C–E). These routes also suppressed the increase in pro-inflammatory M1 macrophages in the mouse lungs after SP administration (Figures 8F, G). Consistent with these findings, histological analysis revealed that both dasatinib treatment routes suppressed immune cell infiltration into the lungs after SP administration (Figure 8H). In summary, dasatinib effectively suppressed particulate-induced NLRP3-independent lung inflammation.

Discussion

To our knowledge, this study is the first to demonstrate that the FDA-approved drug, dasatinib, suppresses particulate-induced cell
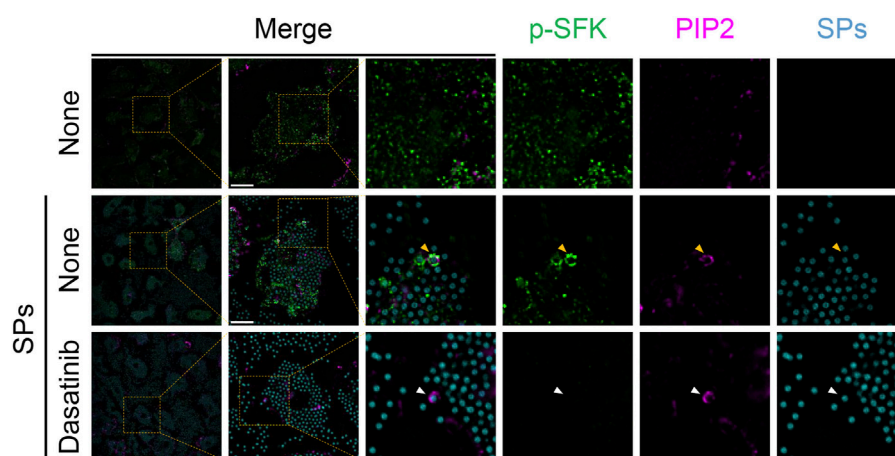
FIGURE 5
Phosphorylated Src family kinases (p-SFKs) accumulate around silica particle (SP)-containing phagocytic cups shortly after the phagocytosis of SPs. Primed bone marrow-derived macrophages (BMDMs) were treated with dasatinib (20 μM) and stimulated or not stimulated with fluorescent SPs (1,500 nm in diameter, 300 μg/mL; cyan). 15 min after stimulation with fluorescent SPs, p-SFKs (green) and phosphatidylinositol 4,5-bisphosphate (PIP2) (magenta) were stained with specific antibodies. The white arrowhead indicates SP surrounded by PIP2. Yellow arrowheads indicate SPs surrounded by both p-SFKs and PIP2. Scale bar; 10 μm.
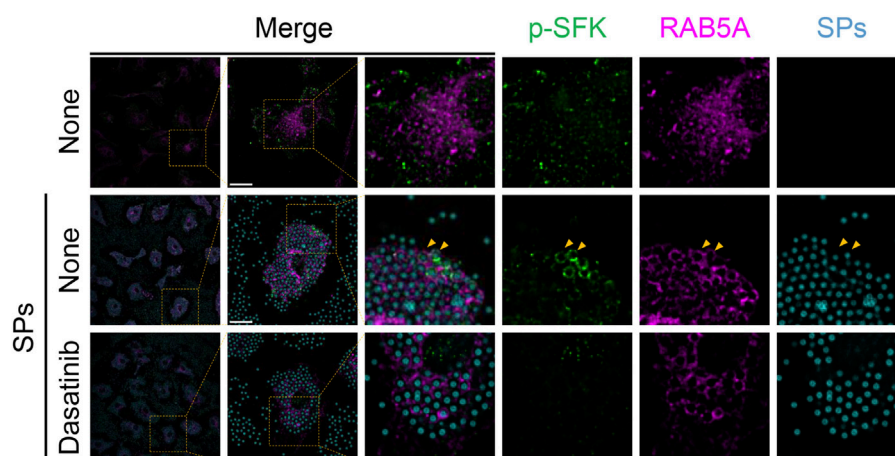

FIGURE 6
Phosphorylated Src family kinases (p-SFKs) accumulate around silica particle (SP)-containing early phagosomes. Primed bone marrow-derived macrophages (BMDMs) were treated with dasatinib (20 μM) and stimulated or not stimulated with fluorescent SPs (1,500 nm in diameter, 300 μg/mL; cyan). Thirty minutes after stimulation with fluorescent SPs, p-SFKs (green) and RAB5A (magenta) were stained with specific antibodies. Yellow arrowheads indicate SPs surrounded by both p-SFKs and RAB5A. Scale bar; 10 μm.

death and IL-1α release, both of which occur even in the absence of the NLRP3 inflammasome (Ikoma et al., 2022). The results suggest that dasatinib decreased particulate-induced phagolysosomal dysfunction, thereby preventing pyroptosis. A previous study reported that c-Src^{Y527F} (a constitutively active form of c-Src)-transduced murine embryonic fibroblasts become increasingly sensitive to drug-induced cell death, triggering permeabilization of the lysosomal membrane (Fehrenbacher et al., 2008). In addition, c-Src inhibition decreases *Mycobacterium tuberculosis*-induced lysosomal destabilization (Amaral et al., 2018). Therefore, dasatinib-targeted SFKs may promote particulate-

induced phagolysosomal membrane destabilization. Interestingly, p-SFKs accumulated around the phagocytic cups formed immediately after the phagocytosis of particulates and persisted even after becoming early phagosomes. SFKs activate acid sphingomyelinase (ASM), a lysosomal ceramide-producing enzyme (Kumazoe et al., 2020), which is present in early phagosomes (Wähe et al., 2010). When activated, ASM converts membrane sphingomyelin to ceramide, which is then converted to sphingosine by ceramidase (Gault et al., 2010). The accumulation of sphingosine enhances membrane permeabilization in a detergent-like manner (Boya and Kroemer, 2008). Interestingly, ASM
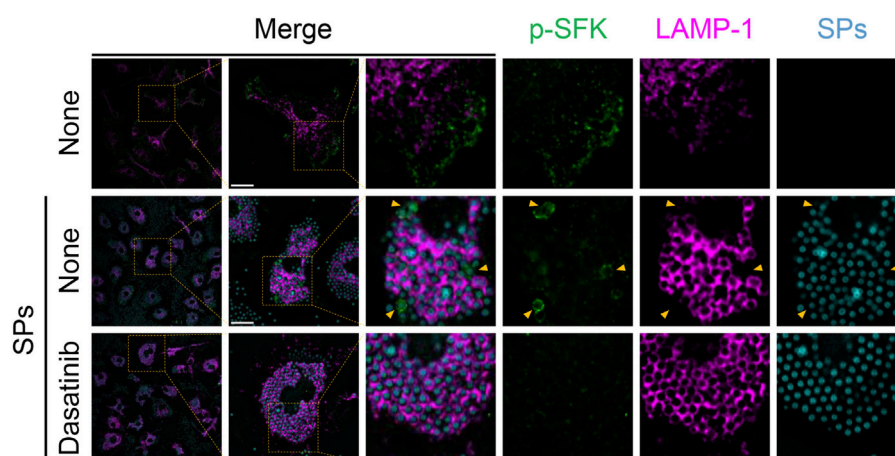
FIGURE 7
Silica particle (SP)-containing phagosomes are surrounded by phosphorylated Src family kinases (p-SFKs) but not lysosome-associated membrane protein-1 (LAMP-1). Primed bone marrow-derived macrophages (BMDMs) were treated with dasatinib (20 μM) and stimulated or not stimulated with fluorescent SPs (1,500 nm in diameter, 300 μg/mL; cyan). Thirty minutes after stimulation with fluorescent SPs, p-SFKs (green), and LAMP-1 (magenta) were stained with specific antibodies. Yellow arrowheads indicate p-SFK-surrounded SPs. Scale bar; 10 μm.

inhibitors inhibit SP-induced cell death (Thibodeau et al., 2004; Biswas et al., 2017). Therefore, ASM may function as a downstream factor of dasatinib-targeted SFKs to facilitate the membrane destabilization of phagosomes and/or phagolysosomes that engulf particulates. Furthermore, dasatinib-targeted SFKs may act on lysosomal ASM, thereby enhancing destabilization of the lysosomal membrane induced by non-particulate agents, such as LLoMe.

In the present study, p-SFKs accumulated around SPs surrounded by RAB5A. However, LAMP-1 levels around SPs surrounded by p-SFKs were negligible. Therefore, it is presumed that dasatinib-targeted SFKs act on the membranes of particulate-containing phagosomes only at the early stage of maturation; however, whether p-SFKs are dispersed, dephosphorylated, or degraded after the maturation of phagosomes into phagolysosomes remains unclear. Alternatively, p-SFK-accumulated phagosomes are vulnerable and immediately degrade after fusion with lysosomes. In our study, p-SFK-accumulated phagolysosomes were not detected under the experimental conditions. Therefore, further studies are warranted on p-SFK recruitment after engulfing particulates and their subsequent fate. These studies will help explain why p-SFKs are selectively recruited to certain phagosomes.

Microbial components adhere to the surfaces of externally invading particulates (Reed and Milton, 2001; Ichinose et al., 2008; He et al., 2013). The stimulation of pattern recognition receptors by microbial components, including toll-like receptor 4, can induce an increase in and activate dasatinib-targeted SFKs. In addition, pattern recognition receptor activation induces the expression of inflammatory mediators, including IL-1α. These effects may synergistically elevate the inflammatory responses triggered by pyroptosis on exposure to exogenously generated particulates. We also demonstrated that LPS priming enhanced SP-induced cell death and IL-1α release. Importantly, SFK inhibition by dasatinib strongly suppressed SP-induced

pyroptosis, including enhancement by LPS priming. Our study results suggest that dasatinib-targeted SFKs mediate particulate-induced phagolysosomal dysfunction, an early upstream event resulting in cell death; therefore, they are critical in determining the intensity of inflammation associated with particulate-induced pyroptosis. As a result, SFK inhibition could be an effective and rational approach to prevent excessive inflammation caused by particulates. This approach could be applicable for treating various particulate-induced diseases since dasatinib suppresses pyroptosis induced by particulates of various sizes and materials.

Moreover, we demonstrated that dasatinib treatment effectively ameliorated inflammatory manifestations in SP-induced acute lung injury in mice, characterized by the increased levels of IL-1α, IL-1β, CXCL1, neutrophils, and M1 macrophages. Importantly, the clinically relevant intragastric administration of dasatinib remarkably suppressed the SP-induced pulmonary inflammation and was as effective as its pulmonary administration. Neutrophils play an important role in acute lung injury after the inhalation of particulate irritants (Ikoma et al., 2022). Therefore, the oral administration of dasatinib can be used as an emergency measure to alleviate acute lung injury induced by the inhalation of particulate irritants. In general, SFKs are multifunctional enzymes; therefore, the use of SFK inhibitors, such as dasatinib, in clinical settings is currently limited to treating cancers, such as chronic myeloid leukemia (Aguilera and Tsimberidou, 2009). The inhalation of particulate irritants in humans causes pneumoconiosis, characterized by persistent inflammation often accompanied by lung cancer (Tsuda et al., 1997; Rayens et al., 2022). However, only palliative treatment exists for pneumoconiosis. IL-1α may promote the development of lung cancer (Chiu et al., 2021). Furthermore, neutrophilic inflammation is involved in silica-induced lung cancer progression (Satpathy et al., 2015). To expand the range of treatments with SFK inhibitors, including dasatinib, their application for treating pneumoconiosis-
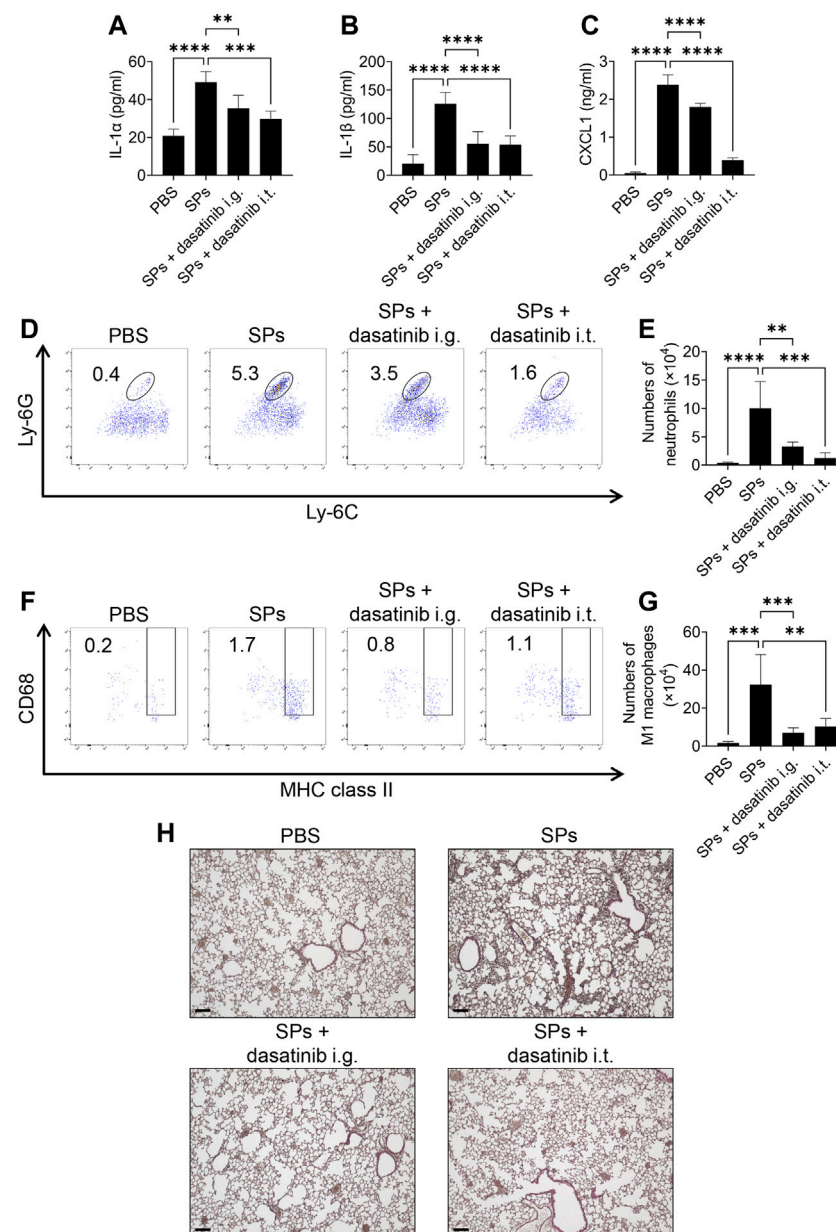
FIGURE 8

Dasatinib treatment attenuates SP-induced acute pneumonia. **(A–C)** Bronchoalveolar lavage (BAL) fluid was collected from mice 12 h after intratracheal SP administration (i.t.; 100 mg/kg) with or without the intragastric (i.g.; 30 mg/kg) and intratracheal (10 mg/kg) administration of dasatinib. Interleukin-1 alpha (IL-1α), IL-1 beta (β), and chemokine (C-X-C motif) ligand 1 (CXCL1) levels in the BAL fluid were measured using enzyme-linked immunosorbent assay (ELISA). **(D)** Neutrophils in mouse lungs 12 h after intratracheal SP administration were counted using flow cytometry. The numbers in the plots indicate the percentage of neutrophils in total leukocytes. **(E)** The total number of neutrophils. **(F)** M1 macrophages in mouse lungs 12 h after intratracheal SP administration were counted using flow cytometry. The numbers in the plots indicate the percentage of M1 macrophages in total leukocytes. **(G)** The total number of M1 macrophages. **(H)** Representative images of hematoxylin and eosin staining of mouse lungs collected 12 h after intratracheal SP administration. Scale bar; 100 μm. The results are presented as mean ± SD ($n = 5$, each group). **, $p < 0.01$; ***, $p < 0.001$; and ****, $p < 0.0001$.

associated lung cancer may be promising, particularly in the context of this study. In addition, chronic inflammation associated with pneumoconiosis often causes fibrosis. Dasatinib treatment is known to be effective in suppressing SP-induced pulmonary fibrosis (Cruz et al., 2016). Considering that IL-1 is involved in the development of SP-induced pulmonary fibrosis (Piguet et al., 1993), the suppression of pyroptosis by dasatinib may contribute to its anti-fibrotic efficacy.

The continuous intake of SFK inhibitors would be required to suppress chronic inflammation associated with pneumoconiosis and prevent lung carcinogenesis and fibrosis. In future, identifying SFKs that destabilize phagolysosomal membranes and their target molecules will aid in the development of more efficient, specific, and safe drugs for particulate-induced inflammatory disease.

Data availability statement

The original contributions presented in the study are included in the article/Supplementary Material, further inquiries can be directed to the corresponding authors.

Ethics statement

The animal study was approved by the Animal Care and Use Committee of the Graduate School of Pharmaceutical Sciences, Osaka University. The study was conducted in accordance with the local legislation and institutional requirements.

Author contributions

YP performed most of the experiments and analyzed the data. KI and RM provided assistance with the experiments. AN contributed to the material support. NT and TS designed the experiments. YP, NT, and TS wrote the manuscript. TS directed the research. All authors contributed to the article and approved the submitted version.

Funding

Acknowledgments

Conflict of interest

The authors declare that the research was conducted in the absence of any commercial or financial relationships that could be construed as a potential conflict of interest.

Publisher's note

Supplementary material

The Supplementary Material for this article can be found online at: https://www.frontiersin.org/articles/10.3389/fphar.2023.1250383/full#supplementary-material

References

Aguilera, D. G., and Tsimberidou, A. M. (2009). Dasatinib in chronic myeloid leukemia: a review. *Ther. Clin. Risk Manag.* 5, 281–289. doi:10.2147/tcrm.s3425

Amaral, E. P., Riteau, N., Moayeri, M., Maier, N., Mayer-Barber, K. D., Pereira, R. M., et al. (2018). Lysosomal cathepsin release is required for NLRP3-inflammasome activation by *Mycobacterium tuberculosis* in infected macrophages. *Front. Immunol.* 9, 1427. doi:10.3389/fimmu.2018.01427

Araujo, J., and Logothetis, C. (2010). Dasatinib: a potent SRC inhibitor in clinical development for the treatment of solid tumors. *Cancer Treat. Rev.* 36, 492–500. doi:10.1016/j.ctrv.2010.02.015

Barquera, S., Pedroza-Tobías, A., Medina, C., Hernández-Barrera, L., Bibbins-Domingo, K., Lozano, R., et al. (2015). Global overview of the epidemiology of atherosclerotic cardiovascular disease. *Arch. Med. Res.* 46, 328–338. doi:10.1016/j.arcmed.2015.06.006

Biswas, R., Trout, K. L., Jessop, F., Harkema, J. R., and Holian, A. (2017). Imipramine blocks acute silicosis in a mouse model. *Part. Fibre. Toxicol.* 14, 36. doi:10.1186/s12989-017-0217-1

Boggon, T. J., and Eck, M. J. (2004). Structure and regulation of Src family kinases. *Oncogene* 23, 7918–7927. doi:10.1038/sj.onc.1208081

Boya, P., and Kroemer, G. (2008). Lysosomal membrane permeabilization in cell death. *Oncogene* 27, 6434–6451. doi:10.1038/onc.2008.310

Byeon, S. E., Yi, Y.-S., Oh, J., Yoo, B. C., Hong, S., and Cho, J. Y. (2012). The role of Src kinase in macrophage-mediated inflammatory responses. *Mediat. Inflamm.* 2012, 512926. doi:10.1155/2012/512926

Chen, C., Wang, J., Liang, Z., Li, M., Fu, D., Zhang, L., et al. (2022). Monosodium urate crystals with controlled shape and aspect ratio for elucidating the pathological progress of acute gout. *Biomater. Adv.* 139, 213005. doi:10.1016/j.bioadv.2022.213005

Chiu, J. W., Binte Hanafi, Z., Chew, L. C. Y., Mei, Y., and Liu, H. (2021). IL-1α processing, signaling and its role in cancer progression. *Cells* 10, 92. doi:10.3390/cells10010092

Cho, W.-S., Choi, M., Han, B. S., Cho, M., Oh, J., Park, K., et al. (2007). Inflammatory mediators induced by intratracheal instillation of ultrafine amorphous silica particles. *Toxicol. Lett.* 175, 24–33. doi:10.1016/j.toxlet.2007.09.008

Cruz, F. F., Horta, L. F., Maia Lde, A., Lopes-Pacheco, M., da Silva, A. B., Morales, M. M., et al. (2016). Dasatinib reduces lung inflammation and fibrosis in acute experimental silicosis. *PLoS One* 11, e0147005. doi:10.1371/journal.pone.0147005

Dorsey, J., Cunnick, J., Lanehart, R., Huang, M., Kraker, A., Bhalla, K., et al. (2002). Interleukin-3 protects Bcr-Abl-transformed hematopoietic progenitor cells from apoptosis induced by Bcr-Abl tyrosine kinase inhibitors. *Leukemia* 16, 1589–1595. doi:10.1038/sj.leu.2402678

Dostert, C., Pétrilli, V., Van Bruggen, R., Steele, C., Mossman, B. T., and Tschopp, J. r. (2008). Innate immune activation through Nalp3 inflammasome sensing of asbestos and silica. *Science* 320, 674–677. doi:10.1126/science.1156995

Duewell, P., Kono, H., Rayner, K. J., Sirois, C. M., Vladimer, G., Bauernfeind, F. G., et al. (2010). NLRP3 inflammasomes are required for atherogenesis and activated by cholesterol crystals. *Nature* 464, 1357–1361. doi:10.1038/nature08938

Fehrenbacher, N., Bastholm, L., Kirkegaard-Sørensen, T., Rafn, B., Bøttzauw, T., Nielsen, C., et al. (2008). Sensitization to the lysosomal cell death pathway by oncogene-induced down-regulation of lysosome-associated membrane proteins 1 and 2. *Cancer Res.* 68, 6623–6633. doi:10.1158/0008-5472.CAN-08-0463

Gault, C. R., Obeid, L. M., and Hannun, Y. A. (2010). An overview of sphingolipid metabolism: from synthesis to breakdown. *Adv. Exp. Med. Biol.* 688, 1–23. doi:10.1007/978-1-4419-6741-1_1

Golas, J. M., Arndt, K., Etienne, C., Lucas, J., Nardin, D., Gibbons, J., et al. (2003). SKI-606, a 4-anilino-3-quinolinecarbonitrile dual inhibitor of Src and Abl kinases, is a potent antiproliferative agent against chronic myelogenous leukemia cells in culture and causes regression of K562 xenografts in nude mice. *Cancer Res.* 63, 375–381.

Groß, O., Yazdi, A. S., Thomas, C. J., Masin, M., Heinz, L. X., Guarda, G., et al. (2012). Inflammasome activators induce interleukin-1α secretion via distinct pathways with differential requirement for the protease function of caspase-1. *Immunity* 36, 388–400. doi:10.1016/j.immuni.2012.01.018

Halle, A., Hornung, V., Petzold, G. C., Stewart, C. R., Monks, B. G., Reinheckel, T., et al. (2008). The NALP3 inflammasome is involved in the innate immune response to amyloid-beta. *Nat. Immunol.* 9, 857–865. doi:10.1038/ni.1636

Haloul, M., Oliveira, E. R. A., Kader, M., Wells, J. Z., Tominello, T. R., El Andaloussi, A., et al. (2019). mTORC1-mediated polarization of M1 macrophages and their accumulation in the liver correlate with immunopathology in fatal ehrlichiosis. *Sci. Rep.* 9, 14050. doi:10.1038/s41598-019-50320-y

Hamby, J. M., Connolly, C. J., Schroeder, M. C., Winters, R. T., Showalter, H. D., Panek, R. L., et al. (1997). Structure-activity relationships for a novel series of pyrido[2,3-d]pyrimidine tyrosine kinase inhibitors. *J. Med. Chem.* 40, 2296–2303. doi:10.1021/jm970367n

He, M., Ichinose, T., Song, Y., Yoshida, Y., Arashidani, K., Yoshida, S., et al. (2013). Effects of two Asian sand dusts transported from the dust source regions of Inner Mongolia and northeast China on murine lung eosinophilia. *Toxicol. Appl. Pharmacol.* 272, 647–655. doi:10.1016/j.taap.2013.07.010

Hornung, V., Bauernfeind, F., Halle, A., Samstad, E. O., Kono, H., Rock, K. L., et al. (2008). Silica crystals and aluminum salts activate the NALP3 inflammasome through phagosomal destabilization. *Nat. Immunol.* 9, 847–856. doi:10.1038/ni.1631

Ichinose, T., Yoshida, S., Hiyoshi, K., Sadakane, K., Takano, H., Nishikawa, M., et al. (2008). The effects of microbial materials adhered to Asian sand dust on allergic lung inflammation. *Arch. Environ. Contam. Toxicol.* 55, 348–357. doi:10.1007/s00244-007-9128-8

Ikoma, K., Takahama, M., Kimishima, A., Pan, Y., Taura, M., Nakayama, A., et al. (2022). Oridonin suppresses particulate-induced NLRP3-independent IL-1α release to prevent crystallopathy in the lung. *Int. Immunol.* 34, 493–504. doi:10.1093/intimm/dxac018

Kayagaki, N., Kornfeld, O. S., Lee, B. L., Stowe, I. B., O'Rourke, K., Li, Q., et al. (2021). NINJ1 mediates plasma membrane rupture during lytic cell death. *Nature* 591, 131–136. doi:10.1038/s41586-021-03218-7

Kimura, Y., Tsukui, D., and Kono, H. (2021). Uric acid in inflammation and the pathogenesis of atherosclerosis. *Int. J. Mol. Sci.* 22, 12394. doi:10.3390/ijms222212394

Kinchen, J. M., and Ravichandran, K. S. (2008). Phagosome maturation: going through the acid test. *Nat. Rev. Mol. Cell Biol.* 9, 781–795. doi:10.1038/nrm2515

Kumazoe, M., Kadomatsu, M., Bae, J., Otsuka, Y., Fujimura, Y., and Tachibana, H. (2020). Src mediates epigallocatechin-3-O-Gallate-Elicited acid sphingomyelinase activation. *Molecules* 25, 5481. doi:10.3390/molecules25225481

Kuroda, E., Ozasa, K., Temizoz, B., Ohata, K., Koo, C. X., Kanuma, T., et al. (2016). Inhaled fine particles induce alveolar macrophage death and interleukin-1α release to promote inducible bronchus-associated lymphoid tissue formation. *Immunity* 45, 1299–1310. doi:10.1016/j.immuni.2016.11.010

Kusaka, T., Nakayama, M., Nakamura, K., Ishimiya, M., Furusawa, E., and Ogasawara, K. (2014). Effect of silica particle size on macrophage inflammatory responses. *PloS one* 9, e92634. doi:10.1371/journal.pone.0092634

Lombardo, L. J., Lee, F. Y., Chen, P., Norris, D., Barrish, J. C., Behnia, K., et al. (2004). Discovery of N-(2-chloro-6-methyl- phenyl)-2-(6-(4-(2-hydroxyethyl)- piperazin-1-yl)-2-methylpyrimidin-4- ylamino)thiazole-5-carboxamide (BMS-354825), a dual Src/Abl kinase inhibitor with potent antitumor activity in preclinical assays. *J. Med. Chem.* 47, 6658–6661. doi:10.1021/jm049486a

Lopez, O. L., and Kuller, L. H. (2019). Epidemiology of aging and associated cognitive disorders: prevalence and incidence of Alzheimer's disease and other dementias. *Handb. Clin. Neurol.* 167, 139–148. doi:10.1016/b978-0-12-804766-8.00009-1

Maa, M. C., and Leu, T. H. (2016). Src is required for migration, phagocytosis, and interferon beta production in Toll-like receptor-engaged macrophages. *Biomed. (Taipei)* 6, 14. doi:10.7603/s40681-016-0014-4

Majeed, M., Caveggion, E., Lowell, C. A., and Berton, G. (2001). Role of Src kinases and Syk in Fcγ receptor-mediated phagocytosis and phagosome-lysosome fusion. *J. Leukoc. Biol.* 70, 801–811. doi:10.1189/jlb.70.5.801

Martinon, F., Pétrilli, V., Mayor, A., Tardivel, A., and Tschopp, J. (2006). Gout-associated uric acid crystals activate the NALP3 inflammasome. *Nature* 440, 237–241. doi:10.1038/nature04516

Matsui, Y., Takemura, N., Shirasaki, Y., Takahama, M., Noguchi, Y., Ikoma, K., et al. (2022). Nanaomycin E inhibits NLRP3 inflammasome activation by preventing mitochondrial dysfunction. *Int. Immunol.* 34, 505–518. doi:10.1093/intimm/dxac028

Mu, Y., Sun, J., Li, Z., Zhang, W., Liu, Z., Li, C., et al. (2022). Activation of pyroptosis and ferroptosis is involved in the hepatotoxicity induced by polystyrene microplastics in mice. *Chemosphere* 291, 132944. doi:10.1016/j.chemosphere.2021.132944

Mulay, S. R., Kulkarni, O. P., Rupanagudi, K. V., Migliorini, A., Darisipudi, M. N., Vilaysane, A., et al. (2012). Calcium oxalate crystals induce renal inflammation by NLRP3-mediated IL-1β secretion. *J. Clin. Invest.* 123, 236–246. doi:10.1172/JCI63679

Nascimento Da Conceicao, V., Sun, Y., Ramachandran, K., Chauhan, A., Raveendran, A., Venkatesan, M., et al. (2021). Resolving macrophage polarization through distinct Ca(2+) entry channel that maintains intracellular signaling and mitochondrial bioenergetics. *iScience* 24, 103339. doi:10.1016/j.isci.2021.103339

Nishijima, N., Hirai, T., Misato, K., Aoyama, M., Kuroda, E., Ishii, K. J., et al. (2017). Human scavenger receptor A1-mediated inflammatory response to silica particle exposure is size specific. *Front. Immunol.* 8, 379. doi:10.3389/fimmu.2017.00379

Palmer, B. D., Thompson, A. M., Booth, R. J., Dobrusin, E. M., Kraker, A. J., Lee, H. H., et al. (2006). 4-Phenylpyrrolo[3,4-c]carbazole-1,3(2H,6H)-dione inhibitors of the checkpoint kinase Wee1. Structure-activity relationships for chromophore modification and phenyl ring substitution. *J. Med. Chem.* 49, 4896–4911. doi:10.1021/jm0512591

Palomaki, J., Valimaki, E., Sund, J., Vippola, M., Clausen, P. A., Jensen, K. A., et al. (2011). Long, needle-like carbon nanotubes and asbestos activate the NLRP3 inflammasome through a similar mechanism. *ACS Nano* 5, 6861–6870. doi:10.1021/nn200595c

Panek, R. L., Lu, G. H., Klutchko, S. R., Batley, B. L., Dahring, T. K., Hamby, J. M., et al. (1997). *In vitro* pharmacological characterization of PD 166285, a new nanomolar potent and broadly active protein tyrosine kinase inhibitor. *J. Pharmacol. Exp. Ther.* 283, 1433–1444.

Parsons, S. J., and Parsons, J. T. (2004). Src family kinases, key regulators of signal transduction. *Oncogene* 23, 7906–7909. doi:10.1038/sj.onc.1208160

Pelegrin, P., Barroso-Gutierrez, C., and Surprenant, A. (2008). P2X7 receptor differentially couples to distinct release pathways for IL-1beta in mouse macrophage. *J. Immunol.* 180, 7147–7157. doi:10.4049/jimmunol.180.11.7147

Piguet, P. F., Vesin, C., Grau, G. E., and Thompson, R. C. (1993). Interleukin 1 receptor antagonist (IL-1ra) prevents or cures pulmonary fibrosis elicited in mice by bleomycin or silica. *Cytokine* 5, 57–61. doi:10.1016/1043-4666(93)90024-y

Rabolli, V., Badissi, A. A., Devosse, R., Uwambayinema, F., Yakoub, Y., Palmai-Pallag, M., et al. (2014). The alarmin IL-1α is a master cytokine in acute lung inflammation induced by silica micro- and nanoparticles. *Part. Fibre Toxicol.* 11, 69. doi:10.1186/s12989-014-0069-x

Rashidi, M., Simpson, D. S., Hempel, A., Frank, D., Petrie, E., Vince, A., et al. (2019). The pyroptotic cell death effector gasdermin D is activated by gout-associated uric acid crystals but is dispensable for cell death and IL-1β release. *J. Immunol.* 203, 736–748. doi:10.4049/jimmunol.1900228

Rayens, N. T., Rayens, E. A., and Tighe, R. M. (2022). Co-occurrence of pneumoconiosis with COPD, pneumonia and lung cancer. *Occup. Med. (Lond.)* 72, 527–533. doi:10.1093/occmed/kqac079

Reed, C. E., and Milton, D. K. (2001). Endotoxin-stimulated innate immunity: a contributing factor for asthma. *J. Allergy Clin. Immunol.* 108, 157–166. doi:10.1067/mai.2001.116862

Satpathy, S. R., Jala, V. R., Bodduluri, S. R., Krishnan, E., Hegde, B., Hoyle, G. W., et al. (2015). Crystalline silica-induced leukotriene B4-dependent inflammation promotes lung tumour growth. *Nat. Commun.* 6, 7064. doi:10.1038/ncomms8064

Scott, C. C., Dobson, W., Botelho, R. J., Coady-Osberg, N., Chavrier, P., Knecht, D. A., et al. (2005). Phosphatidylinositol-4, 5-bis phosphate hydrolysis directs actin remodeling during phagocytosis. *J. Cell Biol.* 169, 139–149. doi:10.1083/jcb.200412162

Suzuki, T., Kono, H., Hirose, N., Okada, M., Yamamoto, T., Yamamoto, K., et al. (2000). Differential involvement of Src family kinases in Fcγ receptor-mediated phagocytosis. *J. Immunol.* 165, 473–482. doi:10.4049/jimmunol.165.1.473

Takeuchi, O., and Akira, S. (2010). Pattern recognition receptors and inflammation. *Cell* 140, 805–820. doi:10.1016/j.cell.2010.01.022

Thibodeau, M. S., Giardina, C., Knecht, D. A., Helble, J., and Hubbard, A. K. (2004). Silica-induced apoptosis in mouse alveolar macrophages is initiated by lysosomal enzyme activity. *Toxicol. Sci.* 80, 34–48. doi:10.1093/toxsci/kfh121

Tsuda, T., Babazono, A., Yamamoto, E., Mino, Y., and Matsuoka, H. (1997). A meta-analysis on the relationship between pneumoconiosis and lung cancer. *J. Occup. Health.* 39, 285–294. doi:10.1539/joh.39.285

Uchimoto, T., Nohara, H., Kamehara, R., Iwamura, M., Watanabe, N., and Kobayashi, Y. (1999). Mechanism of apoptosis induced by a lysosomotropic agent, L-Leucyl-L-Leucine methyl ester. *Apoptosis* 4, 357–362. doi:10.1023/a:1009695221038

von Schneidemesser, E., Driscoll, C., Rieder, H. E., and Schiferl, L. D. (2020). How will air quality effects on human health, crops and ecosystems change in the future? *Philos. Trans. A Math. Phys. Eng. Sci.* 378, 20190330. doi:10.1098/rsta.2019.0330

Wähe, A., Kasmapour, B., Schmaderer, C., Liebl, D., Sandhoff, K., Nykjaer, A., et al. (2010). Golgi-to-phagosome transport of acid sphingomyelinase and prosaposin is mediated by sortilin. *J. Cell Sci.* 123, 2502–2511. doi:10.1242/jcs.067686

Yang, Y., Wang, H., Kouadir, M., Song, H., and Shi, F. (2019). Recent advances in the mechanisms of NLRP3 inflammasome activation and its inhibitors. *Cell Death Dis.* 10, 128. doi:10.1038/s41419-019-1413-8

Yazdi, A. S., Guarda, G., Riteau, N., Drexler, S. K., Tardivel, A., Couillin, I., et al. (2010). Nanoparticles activate the NLR pyrin domain containing 3 (Nlrp3) inflammasome and cause pulmonary inflammation through release of IL-1α and IL-1β. *Proc. Natl. Acad. Sci. U. S. A.* 107, 19449–19454. doi:10.1073/pnas.1008155107

Suppression of inflammation-induced lung cancer cells proliferation and metastasis by exiguaflavanone A and exiguaflavanone B from *Sophora exigua* root extract through NLRP3 inflammasome pathway inhibition

Punnida Arjsri[1,2], Kamonwan Srisawad[1,2], Warathit Semmarath[1,3], Sonthaya Umsumarng[4,5], Lapamas Rueankham[6], Aroonchai Saiai[7], Methee Rungrojsakul[8], Trinnakorn Katekunlaphan[9], Songyot Anuchapreeda[6] and Pornngarm Dejkriengkraikul[1,2,4]*

[1]Department of Biochemistry, Faculty Medicine, Chiang Mai University, Chiang Mai, Thailand, [2]Anticarcinogenesis and Apoptosis Research Cluster, Faculty of Medicine, Chiang Mai University, Chiang Mai, Thailand, [3]Akkhraratchakumari Veterinary College, Walailak University, Nakhon Si Thammarat, Thailand, [4]Center for Research and Development of Natural Products for Health, Chiang Mai University, Chiang Mai, Thailand, [5]Division of Veterinary Preclinical Sciences, Department of Veterinary Biosciences and Veterinary Public Health, Faculty of Veterinary Medicine, Chiang Mai University, Chiang Mai, Thailand, [6]Department of Medical Technology, Faculty of Associated Medical Sciences, Chiang Mai University, Chiang Mai, Thailand, [7]Department of Chemistry, Faculty of Science, Chiang Mai University, Chiang Mai, Thailand, [8]Department of Traditional Chinese Medicine, Faculty of Science, Chandrakasem Rajabhat University, Bangkok, Thailand, [9]Department of Chemistry, Faculty of Science, Chandrakasem Rajabhat University, Bangkok, Thailand

Objective: Non-small cell lung cancer (NSCLC) is recognized for its aggressive nature and propensity for high rates of metastasis. The NLRP3 inflammasome pathway plays a vital role in the progression of NSCLC. This study aimed to investigate the effects of *S. exigua* extract and its active compounds on NLRP3 regulation in NSCLC using an *in vitro* model.

Methods: *S. exigua* was extracted using hexane, ethyl acetate and ethanol to obtain *S. exigua* hexane fraction (SE-Hex), *S. exigua* ethyl acetate fraction (SE-EA), and *S. exigua* ethanol fraction (SE-EtOH) respectively. The active compounds were identified using column chromatography and NMR analysis. A549 cells were primed with lipopolysaccharide (LPS) and adenosine triphosphate (ATP) for activated NLRP3 inflammasome. The anti-inflammatory properties were determined using ELISA assay. The anti-proliferation and anti-metastasis properties against LPS-ATP-induced A549 cells were determined by colony formation, cell cycle, wound healing, and trans-well migration and invasion assays. The inflammatory gene expressions and molecular mechanism were determined using RT-qPCR and Western blot analysis, respectively.

Results: SE-EA exhibited the greatest anti-inflammation properties compared with other two fractions as evidenced by the significant inhibition of IL-1β, IL-18,

and IL-6, cytokine productions from LPS-ATP-induced A549 cells in a dose-dependent manner ($p < 0.05$). The analysis of active compounds revealed exiguaflavanone A (EGF-A) and exiguaflavanone B (EGF-B) as the major compounds present in SE-EA. Then, SE-EA and its major compound were investigated for the anti-proliferation and anti-metastasis properties. It was found that SE-EA, EGF-A, and EGF-B could inhibit the proliferation of LPS-ATP-induced A549 cells through cell cycle arrest induction at the G0/G1 phase and reducing the expression of cell cycle regulator proteins. Furthermore, SE-EA and its major compounds dose-dependently suppressed migration and invasion of LPS-ATP-induced A549 cells. At the molecular level, SE-EA, EGF-A, and EGF-B significantly downregulated the mRNA expression of IL-1β, IL-18, IL-6, and NLRP3 in LPS-ATP-induced A549 cells. Regarding the mechanistic study, SE-EA, EGF-A, and EGF-B inhibited NLRP3 inflammasome activation through suppressing NLRP3, ASC, pro-caspase-1(p50 form), and cleaved-caspase-1(p20 form) expressions.

Conclusion: Targeting NLRP3 inflammasome pathway holds promise as a therapeutic approach to counteract pro-tumorigenic inflammation and develop novel treatments for NSCLC.

Introduction

Lung cancer is a major global health concern, being the second most prevalent form of cancer and the primary contributor to cancer-related fatalities on a global scale (Huang et al., 2022). It includes different subcategories, wherein non-small cell lung cancer (NSCLC) makes up the majority, representing approximately 85% of all cases (Alduais et al., 2023). Within NSCLC, there are several subtypes such as adenocarcinoma, squamous cell carcinoma, and large cell carcinoma, among others. However, the existing therapies for NSCLC, which include surgery, chemotherapy, and radiotherapy, are inadequate in effectively reducing the elevated mortality rates associated with the disease (Wu and Lin, 2022). Despite advancements in early detection and treatment of NSCLC, the prognosis for patients with this condition remains unfavorable, as evidenced by a less than 20% 5-year overall survival rate (Zappa and Mousa, 2016). The recurrence of tumors and the spread of metastases play a significant role in the unfavorable outcomes and serve as the primary factors contributing to mortality in NSCLC cases (Ko et al., 2021). Hence, acquiring a thorough comprehension of the cellular and molecular mechanisms that trigger and advance NSCLC is of utmost significance.

In recent times, alongside surgery, chemotherapy, and radiotherapy, there has been increasing attention on adjuvant therapies that focus on targeting the tumor microenvironment. A growing body of evidence suggests that chronic inflammation plays a pivotal role in the progression of cancer (Gomes et al., 2014; Stares et al., 2022). While acute inflammation serves as a protective mechanism against infectious pathogens, chronic inflammation is linked to DNA damage and tissue dysfunction, encompassing genetic and epigenetic alterations that contribute to the initiation and advancement of various types of cancer (Lee et al., 2009). The inflammasome is an intracellular complex composed of multiple proteins that activates the inflammatory response in tissues when exposed to various stimuli. Over 20 inflammasomes have been identified, among which the NLRP3 inflammasome has been extensively studied and widely recognized for its crucial involvement in inflammation (Moossavi et al., 2018). The NLRP3 inflammasome comprises three main components: the NOD-like receptor NLRP3, the adaptor protein apoptosis-associated speck-like protein containing a caspase recruitment domain (ASC), and pro-caspase-1. The activation of the NLRP3 inflammasome involves a two-step process. In the first step, pathogen-associated molecular patterns (PAMPs) or danger-associated molecular patterns (DAMPs) such as viruses, bacteria, or lipopolysaccharide (LPS) stimulate the expression of NLRP3, pro-IL-1β, and pro-IL-18. In the second step, a secondary stimulus like adenosine 5′-triphosphate (ATP), silica, or monosodium urate (MSU) triggers the activation of the NLRP3 inflammasome. This leads to the assembly of the NLRP3, ASC, and

TABLE 1 Phytochemical study of *S. exigua* extracts.

Sophora exigua extracts	Total phenolic content (mg GAE/g extract)	Total flavonoid content (mg CE/g extract)
SE-Hex	18.57 ± 3.27	10.59 ± 1.58
SE-EA	152.12 ± 8.73***	99.29 ± 11.17***
SE-EtOH	39.78 ± 1.40	7.92 ± 1.94

***$p < 0.001$ vs. others *S. exigua* extracts using independent *t*-test. Data are presented as mean ± S.D., values of three independent experiments.
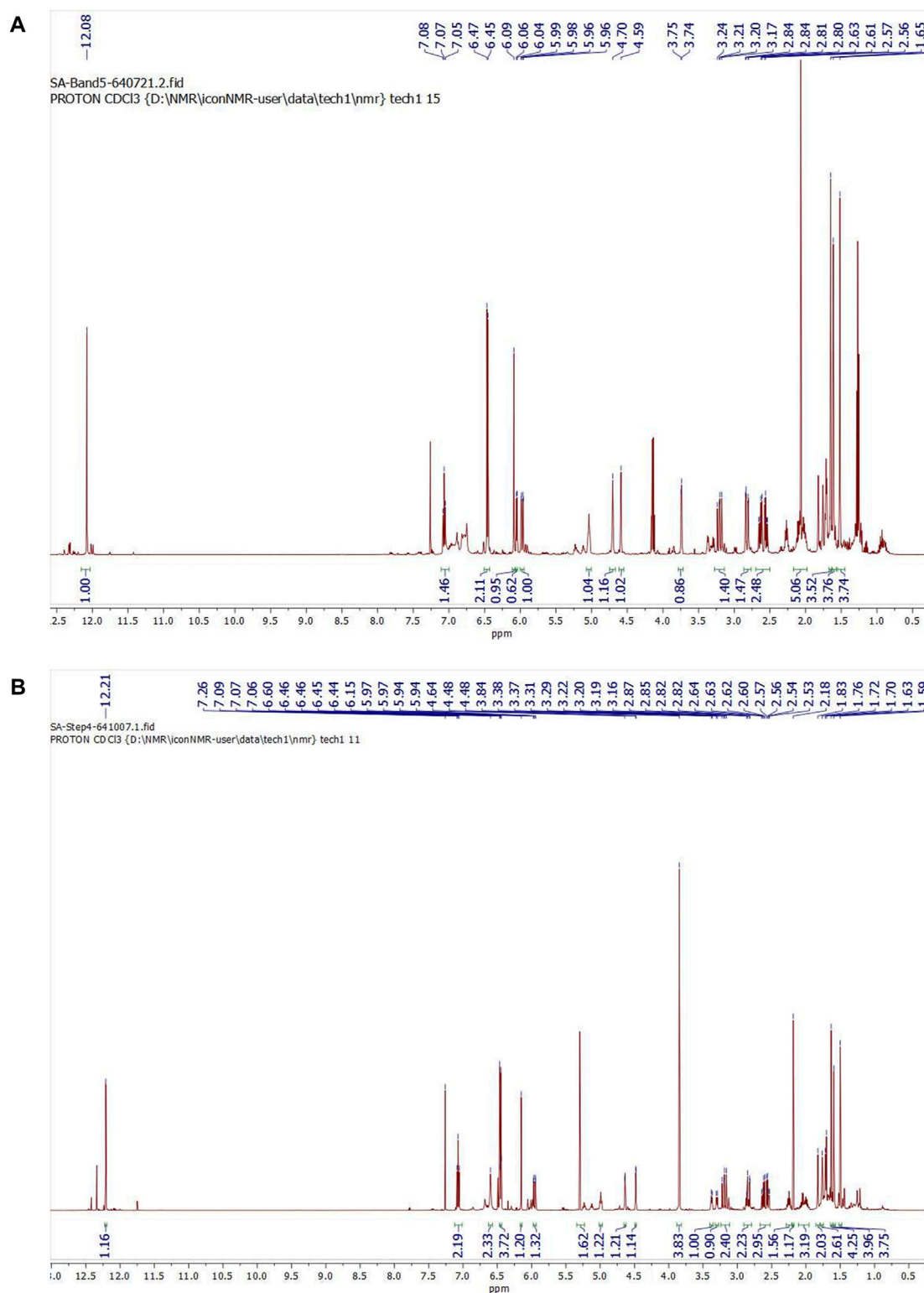
FIGURE 1
^{1}H NMR spectrums of purified compound spot **(A)** No. 1 and **(B)** No. 2 which were identified to be as exiguaflavanone A and exiguaflavanone B, respectively.

pro-caspase-1 components, resulting in the cleavage of pro-IL-1β and pro-IL-18 into their active forms, and the subsequent release of these pro-inflammatory cytokines (He et al., 2016). An increasing body of evidence indicates that the NLRP3 inflammasome plays a pivotal role in the development and progression of various types of cancer, including gastrointestinal cancer, skin cancer, breast cancer, hepatocellular carcinoma, and lung cancer (Huang et al., 2019; Gouravani et al., 2020; Lin et al., 2021; Xu et al., 2021).

TABLE 2 ¹H-NMR spectral data of Exiguaflavanone A in comparison to those previously reported by Ruangrungsi et al. (Ruangrungsi et al., 1992).

Position	Exiguaflavanone A in CDCl₃ (our results, 500 MHz)	Exiguaflavanone A in acetone-d₆ (Ruangrungsi's results)
	δ_H (*multi.*, *J* (Hz), integral)	δ_H (*multi.*, *J* (Hz), integral)
2	5.97 (*dd*, 13.8, 2.8, 1H)	6.02 (*dd*, 14, 3, 1H)
3	3.21 (*dd*, 17.6, 13.8, 1H)	3.87 (*dd*, 17, 14, 1H)
	2.82 (*dd*, 17.6, 2.8, 1H)	2.54 (*dd*, 17, 3, 1H)
5-OH	12.08 (*s*, 1H)	12.27 (*s*, 1H)
6	6.09 (*s*, 1H)	6.01(*s*, 1H)
7-OH	—	9.45 (*br s*, 1H)
2′, 6′-OH	—	8.50 (*br s*, 2H)
3′,5′	6.46 (*d*, 8.2, 2H)	6.47 (*d*, 8, 2H)
4′	7.07 (*t*, 8.1, 1H)	7.05 (*t*, 8, 1H)
1″	2.63 (*dd*, 13.9, 8.2, 1H)	2.56-2.60 (*m*, 3H)
	2.55 (*dd*, 14.0, 5.8, 1H)	
2″	2.27 (*m*, 1H)	
3″	2.01 (*m*, 2H)	2.08 (*m*, 2H)
4″	5.04 (*t*, 6.3, 1H)	4.98 (*t like*, 1H)
6″	1.61 (*s*, 3H)	1.54 (*br s*, 3H)
7″	1.52 (*s*, 3H)	1.48 (*br s*, 3H)
9″	4.70 (*br s*, 1H)	4.55 (*br s*, 2H)
	4.59 (*br s*, 1H)	
10″	1.65 (*s*, 3H)	1.61(*br s*, 3H)

Activation of the NLRP3 inflammasome leads to the release of inflammatory cytokines including IL-1β and IL-18 to promote tumorigenesis (Gouravani et al., 2020). The activation of the inflammasome has also been implicated in promoting the migration and metastasis of various types of tumor cells (Dupaul-Chicoine et al., 2015; Yao et al., 2019). Given these findings, targeting the NLRP3 inflammasome holds potential as a therapeutic strategy for the treatment of NSCLC.

Sophora exigua Craib, commonly referred to as "Phit sa nat" in Thai, is a plant belonging to the Fabaceae family and is found in different regions of Thailand. This Thai traditional medicinal plant, *S. exigua*, is known for its antipyretic and anti-inflammatory properties (Krishna et al., 2012; Wang et al., 2016a). *S. exigua* is commonly incorporated into various multi-herb medicinal preparations, including the traditional Thai formula known as "Kheaw-Hom" remedy. This traditional remedy, Kheaw-Hom, is recognized and listed in the National List of Essential Medicines 2011 in Thailand. This remedy consists of eighteen Thai medicinal plants (Sukkasem, 2015). For an extended period, *S. exigua* has been utilized in folk medicine as a treatment for fever, skin ailments, measles, and chickenpox (Sukkasem et al., 2016). Several species within the Sophora genus have been studies for their pharmacological activities and potential therapeutic applications. Some of the most notable species include *Sophora flavescens*, *Sophora japonica* and *Sophora alopecuroides* (Krishna et al., 2012). These species have a long history of use in traditional medicine, particularly in East Asian countries (Aly et al., 2019; Abd-Alla et al., 2021). It is worth noting that specific medical research for *Sophira exigua* may be limited. *S. exigua* root extract exhibited antioxidant and antimalarial properties in plasmodium berghei-infected mice (Kaewdana et al., 2021). The root extract of *S. exigua* has demonstrated antibacterial activity against methicillin-resistant *Staphylococcus aureus* (MRSA), indicating its potential in combating this antibiotic-resistant bacterial strain (Tsuchiya et al., 1996; Fakhimi et al., 2006). In Folk medicine, it is used in the treatment of fever and inflammation (Sukkasem et al., 2016). However, the effect of *S. exigua* root extract and its chemical constituents on NLRP3 inflammasome pathway in NSCLC remains largely unknown. Therefore, the underlying mechanisms and potential therapeutic applications of *S. exigua* and its active compounds on the anti-inflammation-related cancer properties should be explored.

In this study, the *in vitro* anti-inflammation-related cancer properties of *S. exigua* root extract and its bioactive compounds on NSCLC cell lines were investigated. The A549 cells were primed with lipopolysaccharide (LPS) and adenosine triphosphate (ATP) for activated NLRP3 inflammasome and treatment with *S. exigua* root extract or its bioactive compounds. The study examined the

TABLE 3 ¹H-NMR spectral data of Exiguaflavanone B in comparison to those previously reported by Ruangrungsi et al. (1992).

Position	Exiguaflavanone B in CDCl$_3$ (our results, 500 MHz)	Exiguaflavanone B in acetone-d$_6$ (Ruangrungsi's results)
	δ_H (multi., J (Hz), integral)	δ_H (multi., J (Hz), integral)
2	5.96 (dd, 13.7, 2.8, 1H)	6.02 (dd, 14, 3, 1H)
3	3.19 (dd, 17.6, 13.7, 1H)	3.89 (dd, 16, 14, 1H)
	2.84 (dd, 17.6, 2.8, 1H)	2.56 (dd,16, 3, 1H)
5-OH	12.20 (s, 1H)	12.38 (s, 1H)
6	6.15 (s, 1H)	6.13 (s, 1H)
7-OCH$_3$	3.84 (s, 3H)	3.87 (s, 3H)
2′, 6′-OH	6.78 (s, 2H)	8.55 (br s, 2H)
3′,5′	6.46 (d, 8.2, 2H)	6.48 (d, 8, 2H)
4′	7.07 (t, 8.1, 1H)	7.03 (t, 8, 1H)
1″	2.62 (dd, 13.4, 8.2, 1H)	2.00-2.55 (m, 5H)
	2.55 (dd, 13.4, 6.0, 1H)	
2″	2.29-2.22 (m, 1H)	
3″	2.09-1.95 (m, 2H)	
4″	4.99 (t, 6.7, 1H)	4.94 (t like, 1H)
6″	1.59 (s, 3H)	1.53 (br s, 3H)
7″	1.50 (s, 3H)	1.47 (br s, 3H)
9″	4.64 (m, 1H)	4.45 (br s, 1H)
	4.48 (d, 2.1, 1H)	4.49 (br s, 1H)
10″	1.63 (s, 3H)	1.60 (br s, 3H)

anti-inflammatory, anti-proliferative, and anti-metastatic properties of *S. exigua*. The findings revealed that *S. exigua* root extract and its bioactive compounds were able to suppress the proliferation and metastasis of NSCLC cells by inhibiting the activation of the NLRP3 inflammasome. These results provide scientific evidence supporting the potential use of *S. exigua* root extract or its bioactive compounds as therapeutic strategies for NSCLC, specifically by targeting the NLRP3 inflammasome pathway.

Materials and methods

Chemical and reagents

Dulbecco's Modified Eagle Medium (DMEM) medium, penicillin-streptomycin, and Fetal bovine serum (FBS) were obtained from Gibco BRL Company (Grand Island, NY, United States). Protease inhibitor cocktail, Commasie Plus™ Protein Assay Reagent, Modified Radioimmunoprecipitation assay (RIPA) lysis buffer, and chemiluminescent immunoblotting reagent were purchased from Thermo Fisher Scientific (Rockford, IL, United States). Primary antibodies for cyclin D1, cyclin E, CDK-2, CDK-4, anti-caspase-1 (p50 and p20), anti-NLRP3, anti-ASC, and horseradish peroxidase-conjugated anti-mouse or rabbit-IgG were purchased from Cell Signaling Technology (Beverly, MA,

United States). Primary antibodies for β-actin and propidium iodide (PI) dye were obtained from Sigma-Aldrich (St. Louis, MO, United States). ReverTra Ace® qPCR Master Mix was purchased from Toyobo Co., Ltd. (Osaka, Japan). SensiFAST SYBR Lo-ROX Kit was obtained from Meridian Bioscience® (Cincinnati, OH, United States).

Herb materials and preparation of *Sophora exigua* extracts

Sophora exigua was collected from natural source in 2022 from Chaiyaphum province, Thailand. Plant materials were identified and validated by Angkhana Inta, Chiang Mai University, Sukanda Chaiyong, Trinnakorn Katekulaphan, and Methee Rungrojsakul, Chandrakasem Rajabhat University, Bangkok, Thailand. The voucher specimen numbers of *S. exigua* (No. WP6605, WP6606, and WP7184) were certified by the herbarium at the Queen Sirikit Botanical Garden, Chiang Mai province, Thailand which was kept for future reference. The air-dried roots of *S. exigua* plants (100 g) were collected from 12 different sources and subjected to extraction using hexane (500 mL × 3 times), ethyl acetate (500 mL × 3 times), and ethanol (500 mL × 3 times). The resulting hexane, ethyl acetate, and ethanol extracts were filtered and concentrated under reduced pressure, yielding three crude fractional extracts.
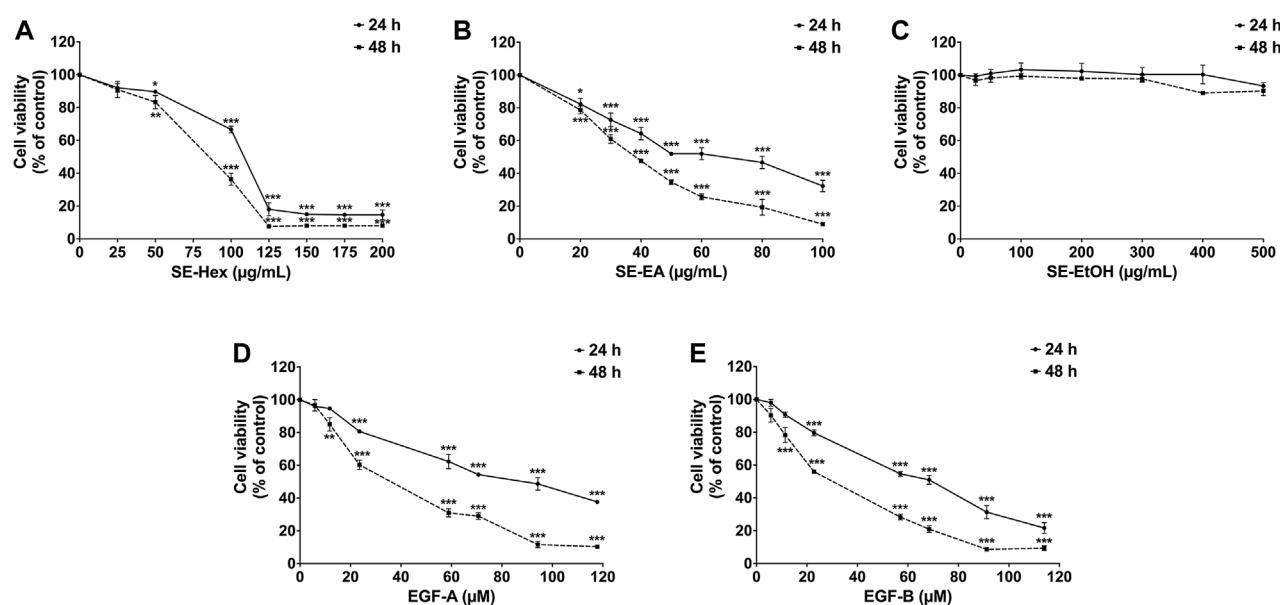
FIGURE 2
The effects of *S. exigua* extracts and its active compounds (EGF-A and EGF-B) on A549 cells viability were determined by SRB assay. The A549 cells were treated with 0–200 μg/mL of SE-Hex **(A)**, 0–100 μg/mL of SE-EA **(B)**, and 0–500 μg/mL of SE-EtOH **(C)** for 24, and 48 h. A549 cells were treated with 0–118 μM of EGF-A **(D)** and 0–114 μM of EGF-B **(E)** for 24 and 48 h. Data are presented as mean ± S.D. values of three independent experiments. *$p <$ 0.05, **$p <$ 0.01 and ***$p <$ 0.001 compared to the control (0 μg/mL or 0 μM).

Column chromatography

In the experimental procedure, silica gel grade 60 was employed as the stationary phase, packed into a 3 cm × 60 cm column. The initial crude fractional extract, weighing 5.0 g, was carefully applied to the upper portion of the silica gel within the column. To achieve effective separation of compounds, we employed varying ratios of hexane and ethyl acetate as mobile phase components. This strategic adjustment of the hexane and ethyl acetate ratios, which enhances polarity, played a crucial role in facilitating the separation of compounds of interest. Upon elution, fractions were systematically collected in individual test tubes, with each fraction comprising 8 mL of the eluted material. For the analysis of compound separation and identification, thin layer chromatography (TLC) was employed. A small aliquot from each fraction was spotted onto a TLC plate. The TLC plate was then introduced into a chamber containing a hexane and ethyl acetate mixture in a 2:1 ratio. Concurrently, a reference standard, specifically the crude fractional extract's ethyl acetate fraction, was also subjected to TLC analysis alongside the fractions. Once the solvent front had progressed approximately 0.5 cm from the top of the TLC plate, the plate was removed from the chamber and subjected to molybdate staining. In order to identify and isolate the desired sub-fraction containing active compounds, fractions exhibiting similar TLC patterns were meticulously combined. The verification of purity for the consolidated fractions was carried out using TLC. Subsequently, the prominent compounds present in the consolidated fractions underwent further analysis to elucidate their chemical structures. This was achieved through the utilization of nuclear magnetic resonance (NMR) spectroscopy, specifically employing a Bruker instrument (Bruker, Fällanden, Switzerland).

Total phenolic content

The total phenolic content of the *S. exigua* extracts used in this study was determined using a Folin-Ciocalteu assay. The Folin-Ciocalteu assay was used as a gold standard protocol for determination of total phenolic content that was descripted in the previous studies (Box, 1983; Noreen et al., 2017; Aryal et al., 2019). In summary, 0.4 mL of each concentration of the *S. exigua* extracts was mixed with 0.3 mL of 10% Folin-Ciocalteau reagent and kept in the dark at room temperature for 3 min. Subsequently, 0.3 mL of carbonated sodium (Na_2CO_3) was added to the mixture and was further incubated in the dark at room temperature for an additional 30 min. The absorbance of the resulting mixture was measured at 765 nm using a UV-visible spectrophotometer (UV-1800, SHIMADZU CO., LTD). The absorbance values were then compared to a standard curve of gallic acid (GA). The total phenolic content of the *S. exigua* extracts was expressed as milligrams of gallic acid equivalents per Gram of the herbal extracts (mg GAE/g extract).

Total flavonoid content

The total flavonoid content of the *S. exigua* extracts was determined using the aluminum chloride ($AlCl_3$) colorimetric assay with minor modifications from a previous study (Pękal and Pyrzynska, 2014). Catechin was used as the gold standard for comparison. In this assay, each concentration of the *S. exigua* extracts (250 μL) was mixed with 5% $NaNO_2$ (125 μL) and incubated for 5 min. Subsequently, 10% $AlCl_3$ (125 μL) was
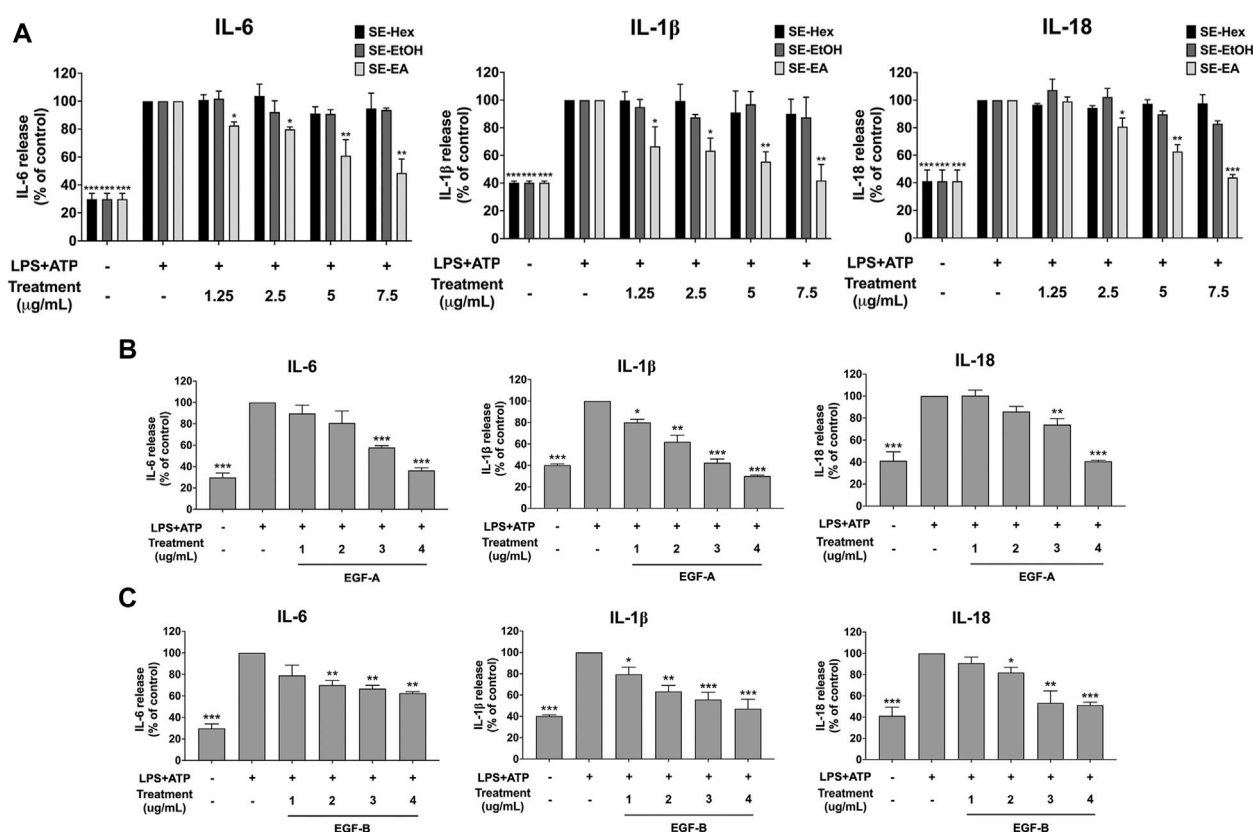
FIGURE 3
Inhibitory effects of *S. exigua* extracts and its active compounds (EGF-A and EGF-B) on the pro-inflammatory cytokine release in LPS-ATP-induced A549 cells. A549 cells were treated with *S. exigua* extracts **(A)**, SE-Hex, SE-EtOH, and SE-EA at a concentration of 0−7.5 µg/mL or active compounds, EGF-A **(B)** at a concentration of 0−4 µg/mL (0−9.42 µM) or EGF-B **(C)** at a concentration of 0−4 µg/mL (0−9.12 µM), for 4 h. Then, the cells were induced by lipopolysaccharide (LPS) at concentration 1,000 ng/mL for 18 h following with (ATP) adenosine triphosphate 5 nM for further 6 h. The IL-6, IL-1β and IL-18 releases into the culture supernatant were examined by ELISA. The LPS-ATP-induced A549 as 100%. Data are presented as mean ± S.D. values of three independent experiments, $*p < 0.05$, $**p < 0.01$ and $***p < 0.001$ compared to the LPS-ATP-induced control group.

added to the mixture, followed by an additional 5 min of incubation. Afterward, 1.0 mL of NaOH was added, and the mixture was incubated for 15 min at room temperature. The absorbance of the resulting mixture was measured at 510 nm using a spectrophotometer and compared to a standard catechin. The total flavonoid content was expressed as milligrams of catechin equivalents (CE) per Gram of extract (mg CE/g extract).

Cell culture

The human lung adenocarcinoma cell line (A549) (CCL-185™) was obtained from American Type Culture Collection (ATCC) (Manassas, VA, United States). The cells were cultured in Dulbecco's Modified Eagle Medium (DMEM) medium supplemented with 10% FBS, 50 IU/mL penicillin, and 50 µg/mL streptomycin. The cells were maintained in a humidified incubator at 37°C with an atmosphere consisting of 95% air and 5% CO_2. When the cells reached 70%–80% confluency, they were harvested and seeded for subsequent experiments.

The cell viability assay

The cytotoxicity of *S. exigua* extracts and its active compounds, exiguaflavanone A (EGF-A) and exiguaflavanone B (EGF-B), against A549 cells was determined by a sulforhodamine B (SRB) assay as was previously described (Vichai and Kirtikara, 2006; Sodde et al., 2015; Kabała-Dzik et al., 2017). In this study, we aimed to assess the cytotoxicity of *S. exigua* extracts and its active compounds over the course of our experiment, spanning 24 and 48 h. Thus, we made slight modifications to the protocols to tailor them to our specific experimental conditions. These modifications allow us to capture the dynamic effects of the test compounds within our desired timeframe, enhancing the precision of our investigation. Briefly, A549 cells (3×10^3 cells/well) were seeded in a 96-well plate and incubated at 37°C, 5% CO_2 overnight. After that, the cells were treated with or without various concentrations of *S. exigua* extracts (0–500 µg/mL) and EGF-A (0–118 µM; MW = 424.5 g/mol) and EGF-B (0–114 µM; MW = 438.5 g/mol) for 24, and 48 h to observe the dose-response curve. Following incubation, the cells were treated with 10% (w/v) trichloroacetic acid (TCA) and incubated at 4°C for 1 h. Subsequently, the medium was aspirated, and the cells were rinsed with gently running tap water. Next, 100 µL of a 0.054% (w/v)
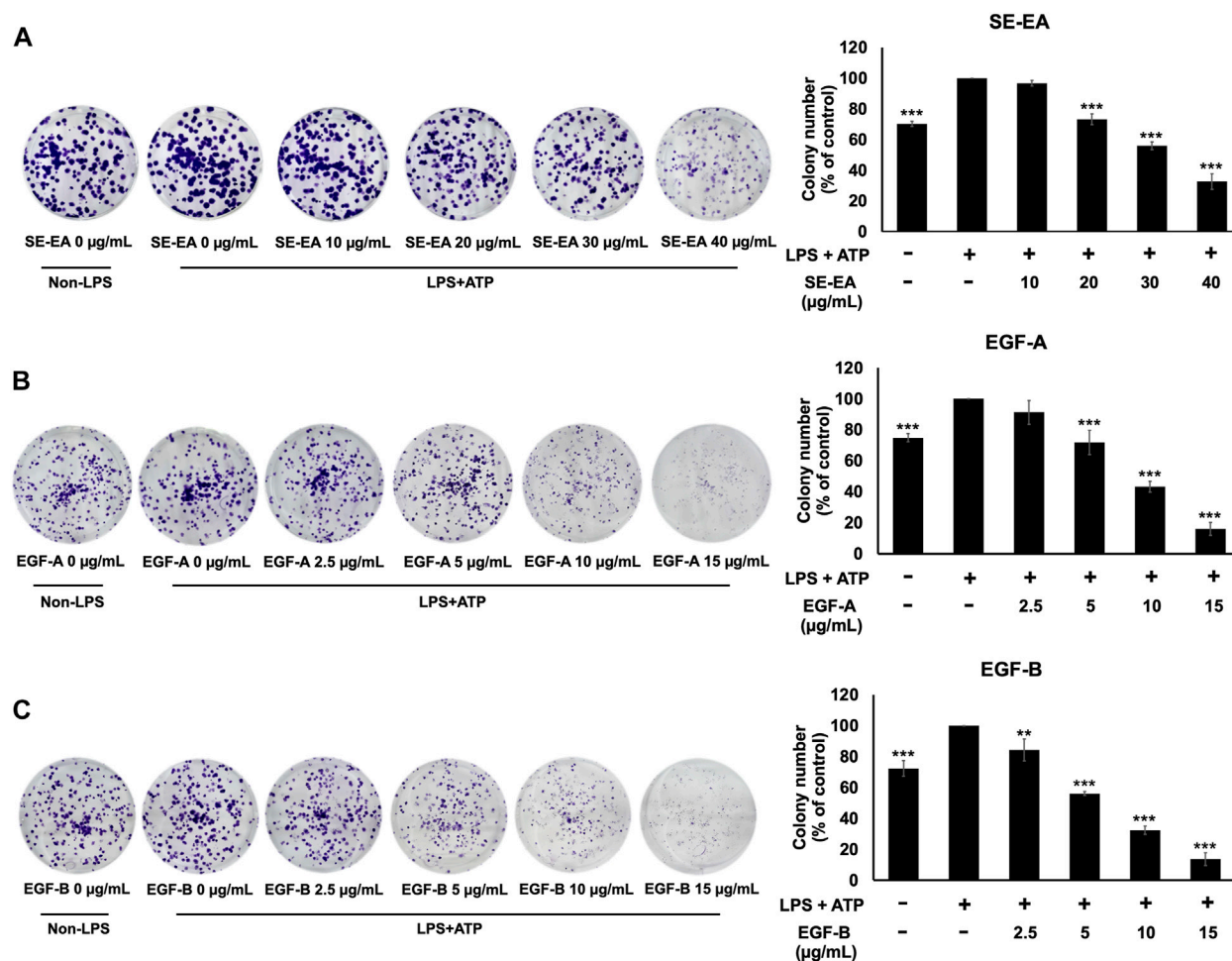
FIGURE 4
The effects of SE-EA and its active compounds (EGF-A and EGF-B) on LPS-ATP-induced A549 cells proliferation using a colony formation assay. A549 cells were treated with SE-EA **(A)** at 0−40 μg/mL, EGF-A **(B)** at 0−15 μg/mL (0−35.33 μM), and EGF-B **(C)** at 0−15 μg/mL (0−34.20 μM) for 7 days. The resulting colonies were photographed and quantified using ImageJ software. Data are presented as the mean ± S.D. of three independent experiments. *$p < 0.05$, **$p < 0.01$ and ***$p < 0.001$ compared to the LPS-ATP-induced control group.

solution of sulforhodamine B (SRB) was added to each well, and the cells were incubated at room temperature for 30 min. After the incubation period, the SRB solution was removed, and the cells were washed four times with 1% (v/v) acetic acid. The cells were then allowed to dry at room temperature. To dissolve the dye, 150 μL of a 10 mM tris-based solution (pH 10.5) was added to each well, and the absorbance was measured at 510 nm using a microplate reader. The cell viability was calculated by comparing the absorbance of the treated cells to that of the control cells.

Determination of cytokine production

The levels of pro-inflammatory cytokines, specifically IL-1β, IL-18, and IL-6, in the cell culture supernatants were measured using an ELISA kit sourced from Biolegend (San Diego, CA, United States), following the manufacturer's protocol as previously outlined (Arjsri et al., 2022). A549 cells were seeded in a 6-well plate at a density of 2×10^5 cells per well. After overnight incubation, the cells were treated with various concentrations (0–7.5 μg/mL) of *S. exigua* extracts or its active

compounds, exiguaflavanone A (EGF-A) and exiguaflavanone B (EGF-B) (0–4 μg/mL), for 4 h. Lipopolysaccharide (LPS) and adenosine triphosphate (ATP) could stimulate the inflammatory responds, one of them was NLRP3 inflammasome pathway (Wang et al., 2016b; Huang et al., 2017). Therefore, the cells were induced by LPS at a concentration of 1,000 ng/mL for 18 h, followed by the ATP at a concentration of 5 nM for an additional 6 h. The culture supernatant was collected for ELISA analysis to measure cytokine release. Calibration standards for IL-6, IL-1β, and IL-18 (ranging from 0 to 500 pg/mL) were utilized to establish a standard curve for the ELISA assay as an internal quality control during the quantitative ELISA. The amount of cytokine released into the supernatant was calculated and compared to the standard curves provided by the ELISA kit.

Colony formation assay

The inhibitory effect of *S. exigua* extract and its active compounds, exiguaflavanone A (EGF-A) and exiguaflavanone B (EGF-B), on A549 cells proliferation were determined using a colony formation
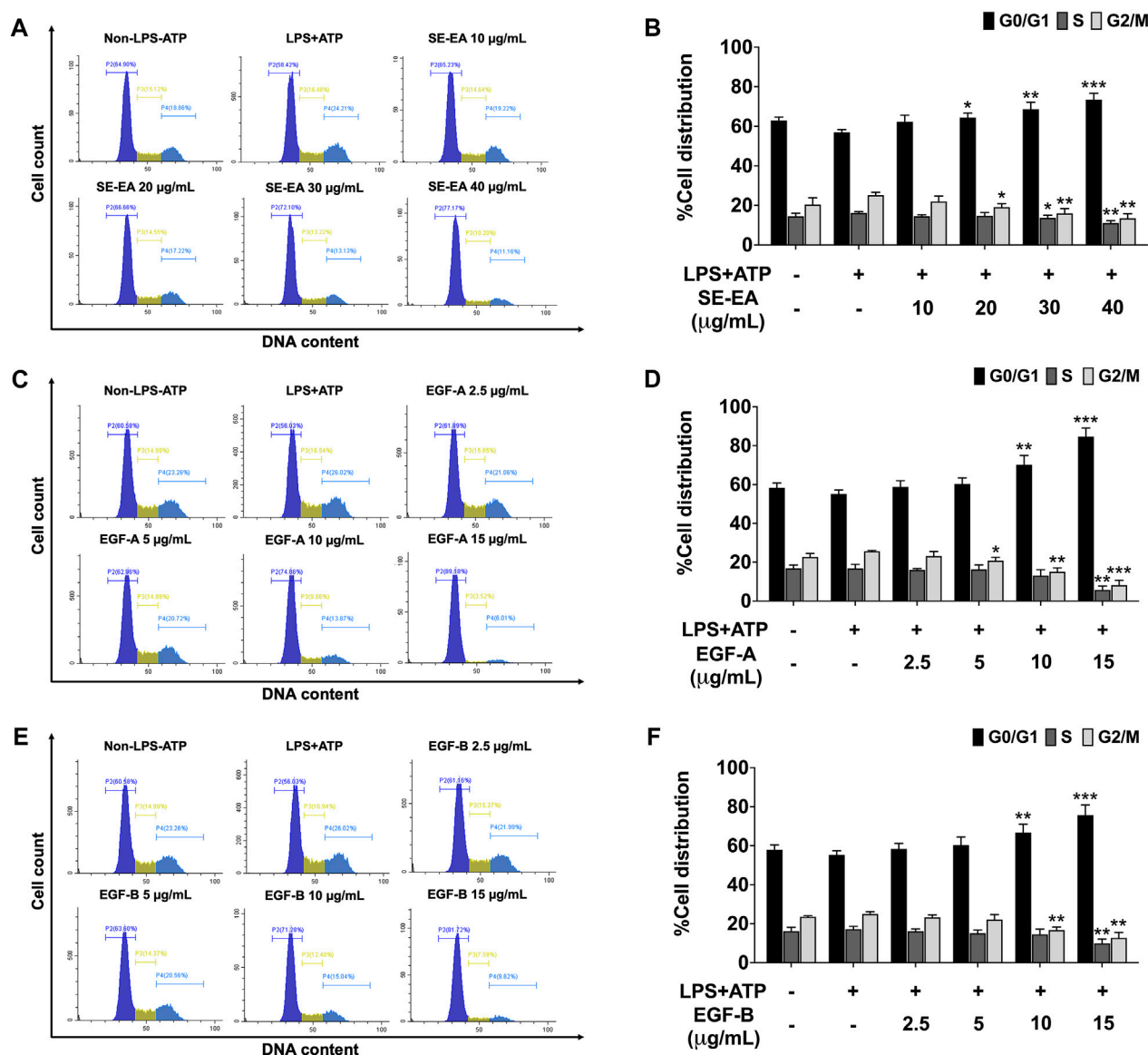
FIGURE 5
The effect of SE-EA and its active compounds (EGF-A and EGF-B) on cell cycle distribution in LPS-ATP-induced A549 cells. The cells were treated with SE-EA **(A, B)** at a concentration range of 0−40 μg/mL or active compounds, EGF-A **(C, D)** or EGF-B **(E, F)**, at a concentration range of 0−15 μg/mL (0−35.33 μM) and 0−15 μg/mL (0−34.20 μM), respectively, for 4 h. The cells were then induced by lipopolysaccharide (LPS) at a concentration 1,000 ng/mL for 18 h, followed by adenosine triphosphate (ATP) at 5 nM for a further 6 h. After staining the cells with PI dye, cell cycle distribution was analyzed by flow cytometry **(A, C, E)** and the percentages of cells in the G0, S and G2/M phase were quantified **(B, D, F)**. The data were obtained from three independent experiments and are presented as mean ± S.D. values. Statistical significance was determined with respect to the LPS-ATP-induced control group, and indicated as *$p < 0.05$, **$p < 0.01$ and ***$p < 0.001$.

assay, as per the established methodology outlined in the previous protocol (Franken et al., 2006). The A549 cells were seeded at 500 cells/well in a 6-well plate and incubated for 24 h. The cells were pre-treated with 0–40 μg/mL of SE-EA and 0–15 μg/mL of EGF-A and EGF-B for 24 h. Then, the cells were induced by lipopolysaccharide (LPS) at concentration 1,000 ng/mL for 18 h following with adenosine triphosphate (ATP) 5 nM for further 7 days before harvest. The cells were fixed with 6% glutaraldehyde for 30 min and stained with Toluidine dye for 15 min. The dye was removed by water. The stained cells were visualized, and the images were captured using the iBright™ CL-1500 imaging system (Thermo Fisher Scientific). The

colony numbers were calculated using the "Analyze Particles." function in ImageJ 1.410 software (https://imagej.nih.gov/ij/). The parameters were set to include colonies of provide specific parameters used, e.g., size range, circularity, etc., ensuring accurate quantification. In each experiment, determinations were carried out in triplicate.

Cell cycle assay

To investigate the distribution of the cell cycle, we followed a previously established method (Crowley et al., 2016). A549 cells
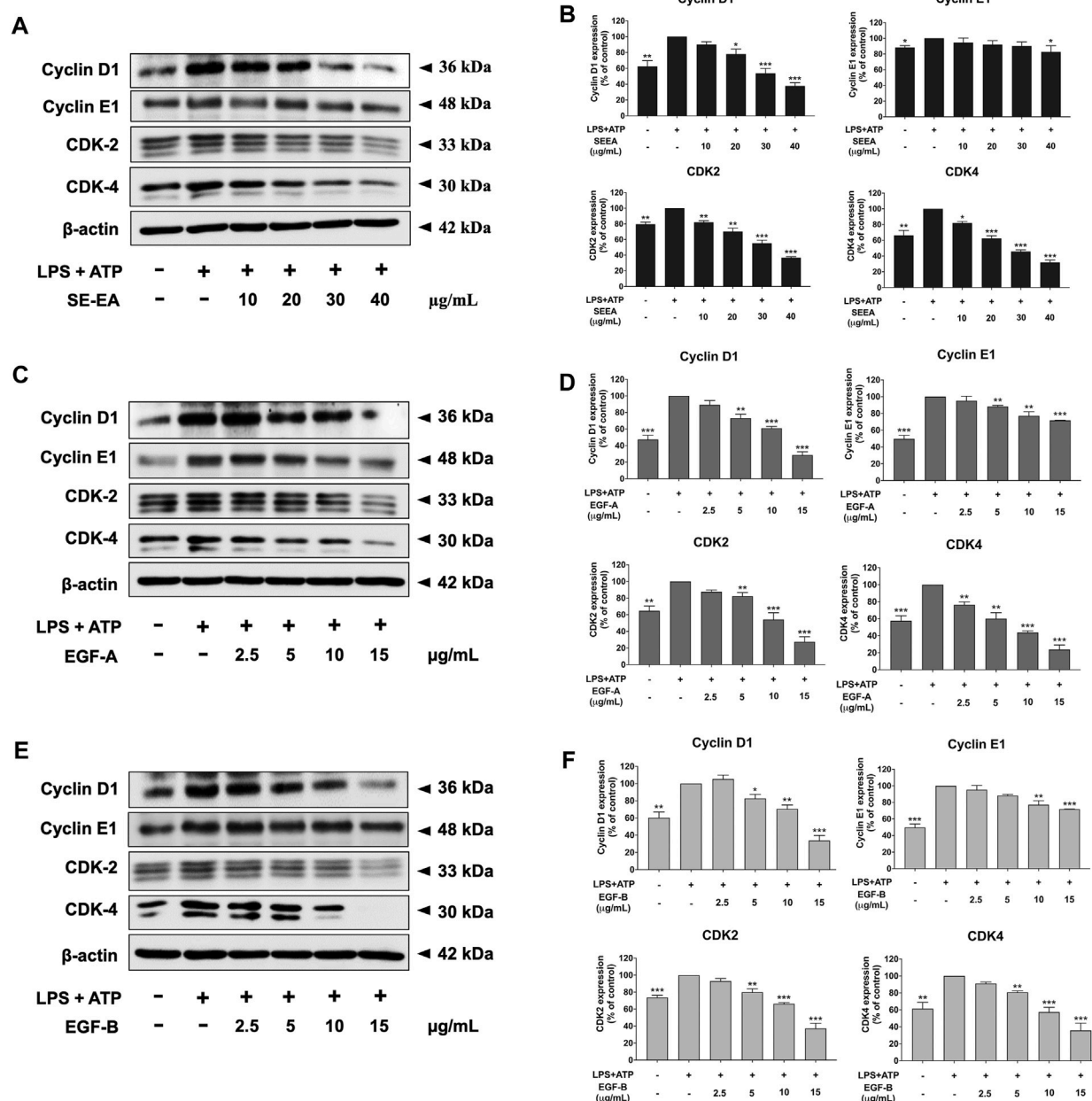
FIGURE 6
The effects of SE-EA and its active compounds (EGF-A and EGF-B) on cell cycle regulator proteins (Cyclin D1, Cyclin E1, CDK-2, and CDK-4) expression in LPS-ATP-induced A549 cells. The cells were treated with SE-EA **(A, B)** at concentrations of 0−40 µg/mL or active compounds, EGF-A **(C, D)** or EGF-B **(E, F)**, at a concentration range of 0−15 µg/mL (0−35.33 µM) and 0−15 µg/mL (0−34.20 µM), respectively, for 4 h. Following treatment, the cells were induced by lipopolysaccharide (LPS) at a concentration of 1,000 ng/mL for 18 h, followed by adenosine triphosphate (ATP) at a concentration of 5 nM for an additional 6 h before being harvested. The protein expression of Cyclin D1, Cyclin E1, CDK-2, and CDK-4 was determined by Western blot analysis, and the band density was measured using ImageJ 1.410 software. The LPS-ATP-induced A549 cells are presented as 100% of the control. Data are presented as mean ± S.D. values of three independent experiments. $*p < 0.05$, $**p < 0.01$ and $***p < 0.001$ compared to the LPS-ATP-induced control group.

were seeded at a density of 1×10^5 cells per well in a 6-well plate and cultured with 0.5% fetal bovine serum (FBS) in DMEM for 18 h. After the starvation period, the cells were treated with various doses of SE-EA or its active compounds, exiguaflavanone A (EGF-A), and exiguaflavanone B (EGF-B). The cells were incubated with SE-EA or EGF-A or EGF-B for 4 h. Then, the cells were induced by lipopolysaccharide (LPS) at concentration 1,000 ng/mL for 18 h

following with adenosine triphosphate (ATP) 5 nM for further 6 h before harvest. Following the treatment, the cells were harvested and processed for cell cycle analysis. This typically involves trypsinizing the cells to detach them from the culture plate, fixing them in ice-cold 70% ethanol in −20°C overnight. After washing the cell pellets with PBS, 12.5 µL of ribonuclease A (RNase A) was added to the pellets and incubated at 37°C in a CO_2

FIGURE 7
The effects of SE-EA and its active compounds (EGF-A and EGF-B) on the migration of LPS-ATP-induced A549 cells. A scratch assay was used to assess the anti-migration effects of SE-EA **(A)** at concentrations of 0–7.5 µg/mL, EGF-A **(B)** at concentrations of 0–4 µg/mL (0–9.42 µM), and EGF-B **(C)** at concentrations of 0–4 µg/mL (0–9.12 µM). Photographs were taken at 0 and 24 h following the initial scratch assay. The trans-well migration assay was used to confirm the anti-metastasis properties of SE-EA **(D)**, EGF-A **(E)**, and EGF-B **(F)** against LPS-ATP-induced A549 cells. The migrated cells were photographed under phase-contrast microscopy at 0 and 24 h and quantified using ImageJ software. Data are presented as mean ± S.D. of three independent experiments. **$p < 0.01$ and ***$p < 0.001$ indicating statistical significance compared to the LPS-ATP-induced control group.

incubator for 15 min. Following the RNase A treatment, 200 µL of propidium iodide (PI) dye was added to the cell pellets and incubated at 37 °C in a CO2 incubator for 45 min. After the incubation period, the cells were centrifuged to remove the PI dye and the cell pellets were then re-suspended with 500 µL of PBS. The stained cells would then be subjected to flow cytometry analysis (Beckman Coulter Inc., Indiana, United States) to determine the distribution of cells in different phases of the cell cycle (G0/G1, S, and G2/M).

Wound-scratch assay

The wound-scratch assay was conducted to examine the migratory capacity of A549 cells as per the established protocol (Liang et al., 2007). Briefly, A549 cells were seeded at 2.5×10^5 cells in a 6-well plate and incubated for 24 h and then were cultured with 0.5% FBS in DMEM for overnight. A549 cells were cultured to 90%–100% confluence, a 200 µL pipette tip was used to generate a wound in the surface of the cells in a 6-well plate, and then the cells were treated with 0–7.5 µg/mL of SE-EA or (0–4 µg/mL) of its active compounds, exiguaflavanone A (EGF-A) and exiguaflavanone B (EGF-B) for 4 h. Then, the cells were induced by lipopolysaccharide (LPS) at concentration 1,000 ng/mL for 18 h following with (ATP) adenosine triphosphate 5 nM for further 6 h. Images of the same fields at the indicated time-points (0 and 24 h) were captured under a light microscope at a magnification of ×100. The images were captured under a phase-contrast microscope (Nikon Eclipse TS100, NIKON INSTRUMENT INC). The wound area was calculated using the " Wound healing size" plugin in ImageJ 1.410 software
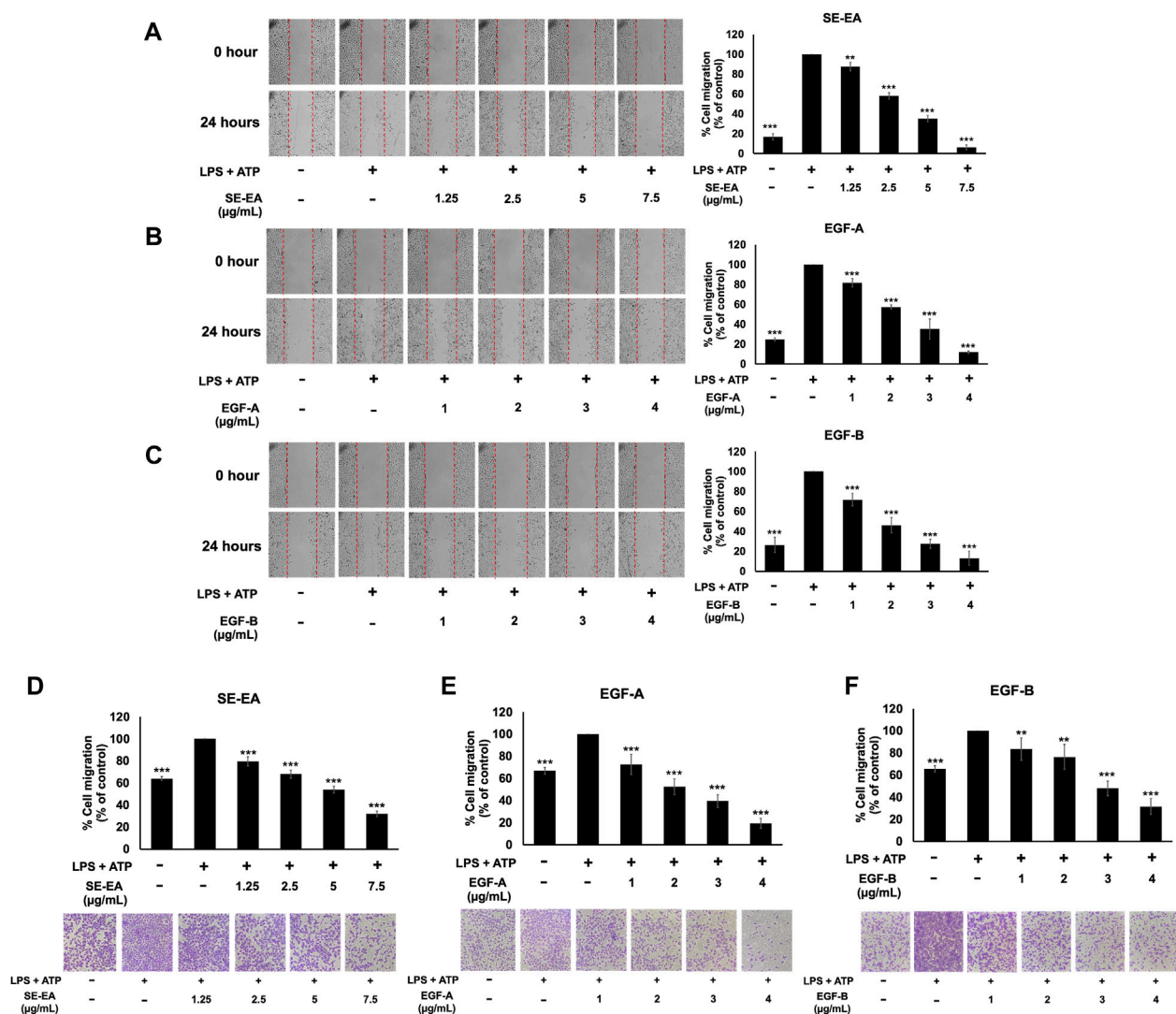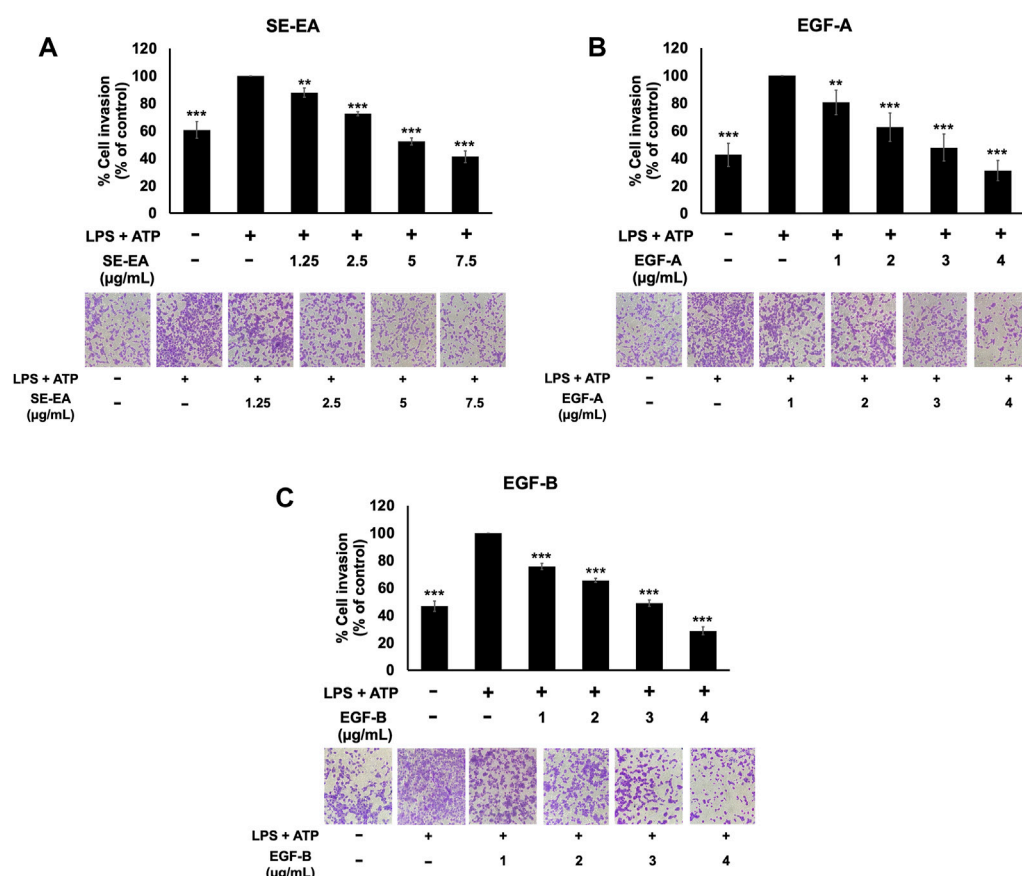
FIGURE 8
The effects of SE-EA and its active compounds (EGF-A and EGF-B) on the invasion of LPS-ATP-induced A549 cells. The anti-invasion effects of SE-EA **(A)** at concentrations ranging from 0–7.5 µg/mL, EGF-A **(B)** at concentrations of 0–4 µg/mL (0–9.42 µM), and EGF-B **(C)** at concentrations of 0–4 µg/mL (0–9.12 µM) on LPS-ATP-induced A549 cells were determined using a trans-well invasion assay. The migrated cells were imaged under phase-contrast microscopy at 0 and 24 h and quantified using ImageJ software. The data from three independent experiments are presented as mean $\pm$ S.D. The statistical significance was indicated as **$p < 0.01$ and ***$p < 0.001$, compared to the LPS-ATP-induced control group.

(Suarez-Arnedo et al., 2020). The plugin parameters were adjusted to accurately delineate the wound area for each experimental condition.

Trans-well migration and invasion assay

To evaluate the impact of SE-EA (*S. exigua* extract), exiguaflavanone A (EGF-A), and exiguaflavanone B (EGF-B) on the invasion and migration of A549 cells, trans-well migration and invasion assays were performed following the previously outlined protocol (Pitchakarn et al., 2012). Polyvinylpyrrolidone-free polycarbonate filters with 8 µm pore size (BD Biosciences, Franklin Lakes, NJ, United States) were used. For the invasion assay, the filters were coated with 15 µg of Matrigel per filter, while for the migration assay, the filters were coated with 10 µg/mL fibronectin. A549 cells were seeded into the upper chamber of the trans-well inserts at a density of 5×10^4 cells per well. The cells were cultured in 0.1% FBS DMEM containing different concentrations of SE-EA, EGF-A, or EGF-B (0–7.5 µg/mL for SE-EA and 0–4 µg/mL for EGF-A and EGF-B). The lower chamber of the trans-well was filled with 10% FBS DMEM, which acts as a chemoattractant. After 4 h of incubation, the cells were induced by lipopolysaccharide (LPS) at a concentration of 1,000 ng/mL for 18 h, followed by the addition of adenosine triphosphate (ATP) at a concentration of 5 nM for an additional 6 h. The invading or migrating cells on the lower surface of the trans-well filter were fixed with 95% ethanol for 5 min and then stained with 0.5% crystal violet in 20% methanol for 30 min. The stained cells were visualized under a phase-contrast microscope (Nikon Eclipse TS100, NIKON INSTRUMENT INC.), and images were captured. To quantify the extent of invasion or migration, the percentages of the areas occupied by cells were determined using the "Threshold" function in ImageJ 1.410 software (https://imagej.nih.gov/ij/). The threshold parameters were fine-tuned to distinguish cells and background, ensuring reliable assessment.

Determination of IL-6, IL-1β, IL-18 and NLRP3 gene expressions by RT-qPCR analysis

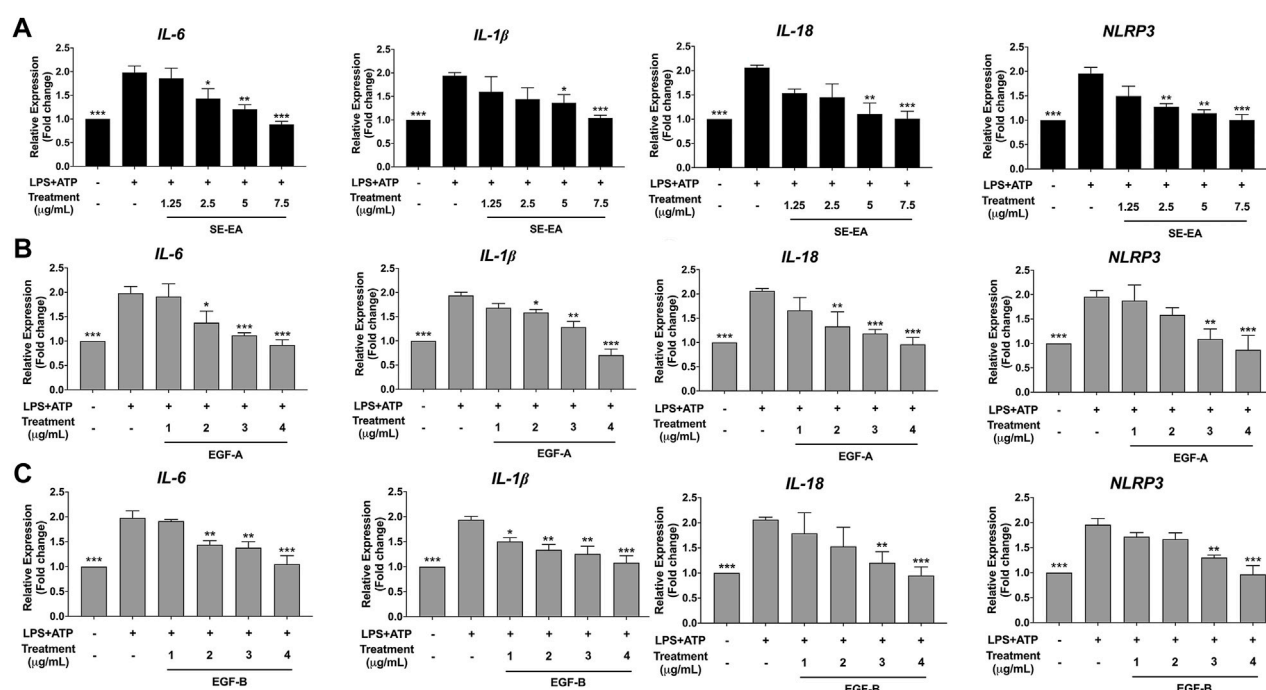To quantify the gene expressions of IL-6, IL-1β, IL-18 and NLRP3 at 24 h after LPS + ATP induction, we adopted the

FIGURE 9
Inhibitory effects of SE-EA extract and its active compounds (EGF-A and EGF-B) on the NLRP3, IL-1β and IL-18 gene expression in LPS-ATP-induced A549 cells. A549 cells were treated with SE-EA extract **(A)** at concentrations of 0−7.5 μg/mL or active compounds, EGF-A **(B)** at concentrations of 0−4 μg/mL (0−9.42 μM) or EGF-B **(C)**, at concentrations of 0−4 μg/mL (0−9.12 μM) for 4 h. After treatment, the cells were induced by lipopolysaccharide (LPS) at a concentration of 1,000 ng/mL for 18 h, followed by adenosine triphosphate (ATP) at 5 nM for a further 6 h. The mRNA expressions of NLRP3, IL-6, IL-1β and IL-18 were determined using RT-qPCR. The LPS-ATP-induced A549 cells were used as a control group, and their expression levels were considered as 100%. The data are presented as mean ± S.D. values of three independent experiments. Statistical analysis was performed, *$p < 0.05$, **$p < 0.01$ and ***$p < 0.001$ were considered statistically significant compared to the LPS-ATP -induced control group.

RT-qPCR analysis method described by (Olcum et al., 2021; Semmarath et al., 2023). A549 cells were pre-treated with 0–7.5 μg/mL of *S. exigua* extracts or (0–4 μg/mL) of its active compounds, exiguaflavanone A (EGF-A) and exiguaflavanone B (EGF-B) for 4 h. Then, the cells were induced by lipopolysaccharide (LPS) at concentration 1,000 ng/mL for 18 h following with (ATP) adenosine triphosphate 5 nM for further 6 h. After incubation, total mRNA was isolated from the cells using TRI reagent®, a commonly used reagent for RNA extraction. The concentration and purity of the isolated RNA were determined using NanoDrop™ 2000/2000c Spectrophotometers (Thermo Fisher Scientific, Waltham, MA, United States of America), which measure the absorbance of the RNA sample at specific wavelengths. The A260/A280 ratio (>1.8) indicates pure RNA without contamination. To obtain cDNA (complementary DNA), reverse transcription was performed using a Mastercycler® nexus gradient machine (Eppendorf, GA, Germany). For quantitative real-time PCR (qRT-PCR), the cDNA samples were amplified and quantified using a qRT-PCR ABITM 7500 Fast and 7500 real-time PCR machine (Thermo Fisher Scientific, Waltham, MA, United States). This technique allows for the detection and quantification of specific target genes in the samples. According to the internal quality control during the qPCR, deionized water was use as a no-template control in every experiment. To assess the precision of our assays and ensure the reliability of the data, the duplicate runs have been performed for each sample and control. The gene expressions were analyzed using the software provided with the QuantStudio6 Flex real-time PCR system (Applied Biosystems). The $2^{-\Delta\Delta CT}$ method with normalization to GAPDH and controls was used for calculation of results. All primer sequences used in this study were as follows: IL-6 forward, 5′-ATG AAC TCC TTC ACA AGC-3′, reverse, 5′-GTT TTC TGC CAG TGC CTC TTT G-3′; IL-1β forward, 5′- ATG ATG GCT TAT TAC AGT GGC AA-3′, reverse, 5′- GTC GGA GAT TCG TAG CTG GA -3′; IL-18 forward, 5′- AAA CTA TTT GTC GCA GGA ATA AAG AT -3′ reverse, 5′- GCT TGC CAA AGT AAT CTG ATT CC -3′; NLRP3 forward, 5′- AAG GGC CAT GGA CTA TTT CC -3′ reverse, 5′- GAC TCC ACC CGA TGA CAG TT -3′and GAPDH forward, 5′- TCA ACA GCG ACA CCC AC -3′ reverse, 5′- GGG TCT CTC TCT TCC TCT TGT G -3′ (Humanizing Genomics Macrogen, Geumcheon-gu, Seoul, South Korea).

Western blot analysis

To determine the expression of cell cycle regulator proteins (CDK-2, CDK-4, cyclin D1 and cyclin E), The cells (5×10^5 cells per well) were plated in 6-well plate and cultured with 0.5% FBS in DMEM for 18 h before they were treated with 0–7.5 μg/mL of SE-EA or 0–4 μg/mL of its active compounds, exiguaflavanone A (EGF-A) and exiguaflavanone B (EGF-B) for 4 h. Then, the cells were induced inflammation by LPS at concentration 1,000 ng/mL for 18 h
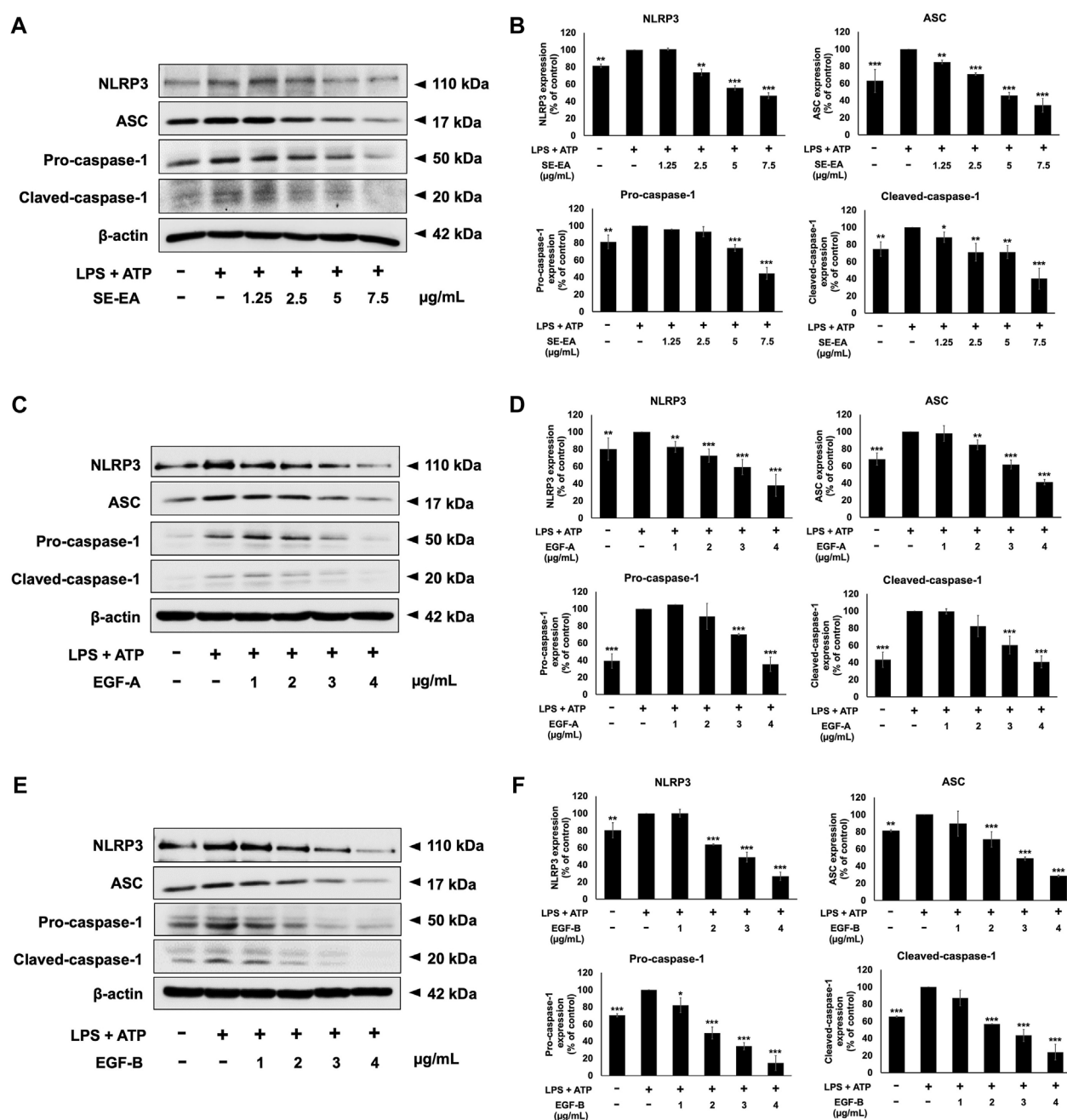
FIGURE 10
Inhibitory effects of *S. exigua* extracts and its active compounds (EGF-A and EGF-B) on the NLRP3 inflammasome pathway in LPS-ATP-induced A549 cells. A549 cells were treated with SE-EA **(A)** at concentrations ranging from 0–7.5 μg/mL or active compounds, EGF-A **(C)** at concentrations of 0–4 μg/mL (0–9.42 μM) or EGF-B **(E)**, at concentrations of 0–4 μg/mL (0–9.12 μM) for 4 h. The cells were induced by lipopolysaccharide (LPS) at a concentration of 1,000 ng/mL for 18 h, followed by adenosine triphosphate (ATP) at a concentration of 5 nM for a further 6 h. The inhibitory effects of SE-EA **(A, B)**, EGF-A **(C, D)**, and EGF-B **(E, F)** on the expression of NLRP3, ASC, and pro-caspase-1 and cleaved-caspase-1 proteins in A549 cells were measured using Western blot and band density measurements. The results were presented as a percentage of the LPS-ATP-induced A549 cells, where the control group was set to 100%. The data are presented as mean $\pm$ S.D. values of three independent experiments, with *$p < 0.05$, **$p < 0.01$ and ***$p < 0.001$ indicating statistical significance compared to the LPS-ATP-induced control group.

followed by ATP adenosine triphosphate 5 nM for further 6 h before harvested. In order to determine the effects of SE-EA or its active compounds, exiguaflavanone A (EGF-A) and exiguaflavanone B (EGF-B) on NLRP3 inflammasome pathway, the A549 cells were pre-treated with 0–7.5 μg/mL of SE-EA or 0–4 μg/mL of its active compounds, exiguaflavanone A (EGF-A) and exiguaflavanone B

(EGF-B) for 4 h. After inducing inflammation by lipopolysaccharide (LPS) and adenosine triphosphate (ATP) for 6 h, the cells were harvested, and the resulting cell pellets were lysed using RIPA buffer, adhering to the methodology outlined in the previous study (Chittasupho et al., 2023). RIPA buffer contains detergents and salts that help to solubilize and extract proteins from the cells. The

protein concentration in the lysate was determined using the Bradford assay, which is a commonly used method for protein quantification. The Bradford assay relies on the binding of Coomassie Brilliant Blue dye to proteins, resulting in a color change that can be measured spectrophotometrically. For protein analysis, the whole-cell lysate was subjected to 10% SDS-PAGE (sodium dodecyl sulfate-polyacrylamide gel electrophoresis). To prevent non-specific binding, the membranes were blocked with 5% bovine serum albumin (BSA) in 0.5% TBS-Tween. After blocking, the membranes were washed with 0.5% TBS-Tween to remove excess BSA and unbound proteins. Following the cyclin D1, cyclin E1, CDK-2, CDK-4, NLRP3, ASC, or caspase-1 primary antibody incubation, the membranes were washed multiple times with 0.5% TBS-Tween to remove any unbound primary antibody. Subsequently, the membranes were incubated with a horseradish peroxidase (HRP)-conjugated secondary antibody, either anti-mouse or anti-rabbit IgG, depending on the primary antibody used. Finally, the membranes were exposed to an imaging system such as the iBright™ CL-1500 imaging system (Thermo Fisher Scientific) to capture the chemiluminescent signal. The resulting images were used for the analysis of band density levels using the "Measure" function in ImageJ 1.410 software (https://imagej.nih.gov/ij/).

Statistical analysis

The experiments were performed in triplicate independent experiments to ensure reproducibility. The data obtained from each experiment were presented as the mean ± standard deviation (mean ± SD), which provides an indication of the variability within the data set. Statistical analysis was performed using Prism version 8.0 software, which is a commonly used statistical analysis tool. The independent t-test and one-way ANOVA with Dunnett's test were used for data analysis in various experiments. The significance level for determining statistical significance was set at $*p < 0.05$, $**p < 0.01$, and $***p < 0.001$. These values indicate the probability of obtaining the observed results by chance. A smaller p-value indicates a higher level of statistical significance.

Results

Extraction of Sophora exigua and phytochemicals study

After subjecting S. exigua to solvent partition extraction, three fractions were obtained: S. exigua hexane extract (SE-Hex), S. exigua ethyl acetate extract (SE-EA), S. exigua ethanolic extract (SE-EtOH). Table 1 displays the total phenolic and total flavonoid contents of each fraction. The results indicate that SE-EA has the highest total phenolic content (152.12 ± 8.73 mg of GAE/g extract) and the total flavonoid content (112.75 ± 4.32 mg of CE/g extract), followed by SE-EtOH and SE-Hex respectively. Thus, the solvent partition extraction technique can increase the phenolic content in the extracts, as observed in SE-EA, this fraction can be used further to identify the bioactive phytochemical compounds present. Among

the three fractional extracts tested, the ethyl acetate extract had the highest yield, with a value of 15.8 ± 0.05, followed by the ethanolic and hexane extracts with values of 4.53 ± 0.06, and 3.88% ± 0.09%, respectively. The ethyl acetate extract (5 g) was further purified using silica gel column chromatography, yielding two dominant compounds with yields of 3.94% and 5.96%, respectively. The compounds were identified as exiguaflavanone A and exiguaflavanone B through comparison of their ^{1}H-NMR spectra (Figure 1; Tables 2, 3) with previously published data (Ruangrungsi et al., 1992). Exiguaflavanone A was obtained as a brown gum-like material (purity degree is >90%), while exiguaflavanone B was obtained as a yellow viscous oil (purity degree is >90%).

Effects of S. exigua extracts and its active compounds on A549 cells viability

Prior to investigating the anti-inflammatory properties of S. exigua extracts and its bioactive compounds, the cytotoxic effects of SE-EA and its bioactive compounds on A549 cells were evaluated. The viability of A549 lung cells was measured using SRB assay after treatment with different concentrations of SE-Hex, SE-EA, and SE-EtOH, as well as exiguaflavanone A and exiguaflavanone B, for 24 and 48 h. The results revealed that SE-EA exhibited a cytotoxic effect on A549 cells, with an IC_{50} of 64.00 ± 6.46 and 37.00 ± 1.53 μg/mL after 24 and 48 h of incubation, respectively. On the other hand, SE-Hex had a higher IC_{50} value of 111.67 ± 7.64 and 85.00 ± 5.00 μg/mL after 24 and 48 h of incubation, respectively (Figure 2), indicating less cytotoxicity than SE-EA. SE-EtOH did not exhibit any cytotoxic effects on A549 cells at any concentration or time point tested. Exiguaflavanone A and exiguaflavanone B also showed cytotoxicity on A549 cells, with an IC_{50} of 88.74 ± 11.14 and 68.42 ± 7.48 μM, respectively after 24 h of incubation, and with an IC_{50} of 34.94 ± 6.05 and 30.03 ± 2.37 μM, respectively, after 48 h of incubation. Non-toxic concentrations of SE-Hex, SE-EtOH, SE-EA (0–7.5 μg/mL), and the active compounds exiguaflavanone A (0–9.42 μM or 0–4 μg/mL) and exiguaflavanone B (0–9.12 μM or 0–4 μg/mL) were selected for further experiments to investigate their anti-inflammatory properties on A549 cells.

Anti-inflammatory effects of S. exigua extracts and its active compounds on LPS-ATP-induced A549 cells

To assess the anti-inflammatory effects of S. exigua extracts (SE-Hex, SE-EtOH and SE-EA) and their bioactive compounds (exiguaflavanone A and exiguaflavanone B) on LPS-ATP-induced inflammation, we measured the release of pro-inflammatory cytokines (IL-6, IL-1β, and IL-18) in the supernatant of A549 cells using ELISA. The levels of these cytokines were significantly increased in LPS-ATP-induced A549 cells compared to non-induced cells ($p < 0.001$), as shown in Figure 3. Treatment with SE-EA resulted in a dose dependent decrease in the release of IL-6, IL-1β, and IL-18 from LPS-ATP-induced A549 cells ($p < 0.001$). However, SE-Hex and SE-EtOH did not exhibit any inhibitory effects on cytokine releases (IL-6, IL-1β, and IL-18), as shown in Figure 3A. Moreover, the bioactive compounds

exiguaflavanone A and exiguaflavanone B also demonstrated significant inhibition of IL-6, IL-1β, and IL-18 release from LPS-ATP-induced A549 cells in a dose-dependent manner ($p < 0.001$), as shown in Figures 3B, C. These results indicate that SE-EA and its bioactive compounds, exiguaflavanone A and exiguaflavanone B, possess anti-inflammatory properties against LPS-ATP induced inflammation by reducing the release of IL-6, IL-1β, and IL-18 cytokines in A549 cell culture supernatant.

Effects of SE-EA and its active compounds (EGF-A and EGF-B) on LPS-ATP-induced A549 cells proliferation

Based on previous research, it is known that the activation of NLRP3 inflammasome can promote cancer progression by releasing inflammatory cytokines such as IL-1β. In this study, A 549 lung cancer cells were induced with inflammation through the NLRP3 inflammasome pathways using LPS bacterial inflammation-inducing agents in combination with adenosine triphosphate (ATP), and measured cell proliferation using colony formation assay. The result indicated that lung cancer cells induced by LPS and ATP showed a greater ability to proliferate than lung cancer cells that were not induced with inflammation in A549 cells, as shown in Figure 4. Next, the effectiveness of SE-EA extract and its active compounds, EGF-A and EGF-B, in inhibiting the growth of A549 lung cancer cells were investigated, it was found that the SE-EA extract (Figure 4A) as well as EGF-A (Figure 4B) and EGF-B (Figure 4C) had significant inhibitory effects on the proliferation of A549 lung cancer cells induced by LPS and ATP. To further understand the mechanism by which SE-EA extract and its active compounds, EGF-A and EGF-B, inhibit cell growth, we conducted a cell cycle analysis assay. As shown in Figure 5, the results showed that the SE-EA (Figures 5A, B) and its active compounds EGF-A (Figures 5C, D) and EGF-B (Figures 5E, F) were able to arrest the growth of A 549 lung cancer cells induced by LPS and ATP at the G1 phase of the cell cycle. To gain insight into the underlying mechanism of SE-EA and its bioactive compounds, Western blotting analysis was conducted to assess the expression of cell cycle regulator proteins. The results showed that SE-EA, EGF-A, and EGF-B markedly reduced the expression of cyclin D1, cyclin E1, CDK-2, and CDK-4 in LPS-ATP-induced A549 cells in a dose-dependent manner, as shown in Figure 6.

Effects of SE-EA and its active compounds (EGF-A and EGF-B) on LPS-ATP-induced A549 cells migration

Inflammatory response of lung cancer cells through the NLRP3 inflammasome pathway not only promotes cancer cell growth but also enhances cancer cell invasion and metastasis. Therefore, the effects of the SE-EA extract and its two active compounds, EGF-A and EGF-B, on the inhibition of lung cancer cell migration were investigated using would healing and trans-well assays in LPS-ATP-induced A549 lung cancer cells. The study found that LPS-ATP-induced A549 lung cancer cells had a higher migration capability than non-induced A549 cells, as shown in

Figure 7. However, when treated with SE-EA extract, significant inhibition of cancer cell migration was observed in LPS-ATP-induced A549 lung cancer cells, as shown in Figures 7A, D. Moreover, the two active compounds, EGF-A and EGF-B, derived from SE-EA extract, also exhibited a significant inhibition of cancer cell migration in LPS-ATP-induced A549 lung cancer cells, as indicated in Figures 7B, C; Figures 7E, F.

Effects of SE-EA and its active compounds (EGF-A and EGF-B) on LPS-ATP-induced A549 cells invasion

The effect of SE-EA and its two major compounds, EGF-A and EGF-B, on the invasion of A549 lung cancer cells were investigated using trans-well assay. The results showed that A549 lung cancer cells stimulated by LPS and ATP exhibited a higher invasion capability than non-stimulated A549 lung cancer cells, as shown in Figure 8. However, treatment with SE-EA extract and its active compounds, EGF-A and EGF-B, significantly inhibited the invasion of A549 lung cancer cells via the trans-well assay. Therefore, it can be concluded that the inflammatory response triggered by LPS-ATP via the NLRP3 inflammasome pathway enhances the invasive capability of A549 lung cancer cells. SE-EA extract and its active compounds, EGF-A and EGF-B can effectively suppress the invasion of A549 lung cancer cells stimulated by LPS-ATP via the NLRP3 inflammasome pathway.

Effects of SE-EA and its active compounds (EGF-A and EGF-B) on inhibition of pro-inflammatory cytokines (IL-6, IL-1β, and IL-18) and NLRP3 gene expressions in LPS-ATP-induced A549 cells

The study aimed to investigate the mechanism of action of SE-EA extract, specifically EGE-A and EGF-B, in inhibiting the expression of pro-inflammatory cytokines IL-6 and inflammasome related cytokines IL-1β and IL-18, as well as the NLRP3 protein at the mRNA level using RT-qPCR. The results demonstrated that treatment of lung cancer A549 cells with LPS and ATP induced the expression of IL-6 and inflammasome-related cytokines IL-1β and IL-18, as well as increased NLRP3 gene expression. Conversely, treatment with SE-EA extract (Figure 9A), EGF-A (Figure 9B), and EGF-B (Figure 9C) significantly inhibited the expression of IL-6, IL-1β, IL-18, and NLRP3 genes in A549 cells stimulated with LPS and ATP in a concentration-dependent manner (*$p < 0.05$, **$p < 0.01$ and ***$p < 0.001$), compared to the LPS and ATP only group.

Effects of SE-EA and its active compounds (EGF-A and EGF-B) on the NLRP3 inflammasome pathway in LPS-ATP-induced A549 cells

To induce inflammation, we treated A549 cells with LPS and ATP and compared these cells to a control group A549 cells that

were not induced. It was found that, in A549 lung epithelial cells, the induction of inflammation using LPS and ATP resulted in elevated expression levels of NLRP3, ASC, pro-caspase-1 (p50), and cleaved-caspase-1 (p20) proteins when compared to non-induced control cells. Next, we performed Western blot analysis to evaluate the effects of SE-EA extract, EGF-A and EGF-B on the expression of these proteins in the LPS and ATP-induced A549 cells. Our results revealed that the SE-EA extract (Figures 10A, B), as well as EGF-A (Figures 10C, D) and EGF-B (Figures 10 E, F), significantly reduced the expression of NLRP3, ASC, pro-caspase-1 (p50), and cleaved-caspase-1 (p20) proteins in the LPS and ATP-induced A549 cells.

Discussion

Research on the anticancer potential of *Sophora* species, including *Sophora flavescens* and *Sophora japonica*, has yielded promising results in inhibiting the growth of cancer cells (Krishna et al., 2012; Chen et al., 2013; He et al., 2015). For example, *Sophora flavescens*, commonly used in traditional Chinese medicine, has shown potential as an anticancer agent against lung cancer cells. Extracts from *Sophora flavescens* have demonstrated anti-proliferative effects and induced apoptosis in A549 and NCI-H226 cell lines (Chen et al., 2019). Similarly, extracts from *Sophora flavescens* and *Sophora japonica* have been investigated for their potential anticancer effects in MCF-7 breast cancer (Cao and He, 2020). Studies have isolated certain compounds from *Sophora* species that exhibit promising anticancer effects against liver cancer cells. These compounds, including flavonoids and alkaloids, have demonstrated inhibitory effects on cell proliferation, migration, and invasion in HepG2 cell lines (Lin et al., 2023). *Sophora japonica* and *Sophora subprostrata* have been studied for their potential anticancer effects on colorectal cancer cells. Extracts from these plants have shown cytotoxic activity against HT29 colorectal cancer cells and induced apoptosis in these cells (Fang et al., 2018; Chen et al., 2021). However, information specifically related to *Sophora exigua* and its anticancer potential is scarce. Hence, it is essential to study the anticancer properties of *S. exigua* plant extract and its bioactive compounds on the A549 non-small cell lung cancer cell line. Furthermore, investigating the underlying mechanisms involved in cancer progression is of utmost importance.

Exiguaflavanones, specifically flavanones, which are a subclass of flavonoids, are known for their diverse chemical structures and various biological activities (Ruangrungsi et al., 1992; Boozari et al., 2019; Abd-Alla et al., 2021). Flavanones have been studied for their potential health benefits and medicinal properties, including antioxidant, anti-inflammatory, antimicrobial, and anticancer activities (Tsuchiya et al., 1996; Fakhimi et al., 2006; Kaewdana et al., 2021). In the root of *Sophora exigua*, a plant known for its medicinal properties, two important flavanone compounds called Exiguaflavanone A (EGF-A) and exiguaflavanone (EGF-B) can be found. These compounds are obtained from the ethyl acetate fraction of the plant extract (SE-EA) and have yields of 3.94% and 5.96%, respectively. In the context of the NLRP3 inflammasome pathway, which plays a crucial role in the inflammatory response of lung cancer cells, we have expanded upon the mechanisms discussed in the references. Specifically, we have detailed the role of the

NLRP3 inflammasome pathway in promoting cancer cell growth, invasion, and metastasis. This is achieved partly through the activation of the NLRP3 inflammasome pathway and the subsequent release of the IL-1β cytokine, as highlighted in previous studies (Fan et al., 2014; Wang et al., 2016b). Therefore, this study aimed to investigate the potential of the SE-EA extract and its active compounds, EGF-A and EGF-B, in inhibiting lung cancer cell proliferation, migration, and invasion. To induce inflammation in A549 non-small cell lung cancer cells, a combination of LPS, a bacterial inflammation-inducing agent, and ATP was used. The findings of our investigation revealed that SE-EA extract and its active compounds, EGF-A and EGF-B, effectively inhibited LPS- and ATP-induced proliferation of A549 cells. These compounds caused cell cycle arrest at the G1 phase and significantly downregulated the expression of cell cycle regulator proteins. Moreover, the SE-EA extract and its active compounds demonstrated a significant inhibitory effect on LPs-ATP-induced cell migration and invasion.

Inflammation is a complex process that involves the release of various cytokines and mediators. Notably, IL-6, Il-1β, and IL-18 are well-known pro-inflammatory cytokines that play a crucial role in the pathogenesis of many inflammatory diseases (Fenini et al., 2017). Previous studies have indicated that the activation of NLRP3 inflammasome can contribute to cancer progression by releasing inflammatory cytokines such as IL-1β and IL-18 (Vidal-Vanaclocha et al., 2000; Fabbi et al., 2015; Fenini et al., 2017). Our findings confirm the anti-inflammatory effects of SE-EA and its active compounds, EGF-A and EGF-B, by modulating the NLRP3 inflammasome pathway. These compounds effectively reduce cytokine release and downregulate key proteins involved in the NLRP3 inflammasome pathway, including NLRP3, ASC, pro-caspase-1 and cleaved-caspase-1. Furthermore, in our molecular investigations, we observed significant downregulation of mRNA expression of IL-1β, IL-18, and NLRP3 in LPS-ATP-induced A549 cells treated with SE-EA, EGF-A, and EGF-B, ultimately leading to a decrease in the release of inflammatory cytokines. The downregulation suggested that these compounds have the ability to suppress the transcriptional activity of these pro-inflammatory molecules. One potential mechanism through which this downregulation may occur is by inhibiting the activation of NF-kB. Several studies have reported that natural compounds can exert their anti-inflammatory effects by modulating NF-kB activity (Song et al., 2018; Semmarath et al., 2022; Lan et al., 2023). These compounds can interfere with the suppression of NF-kB nuclear translocation. By disrupting these steps, the compounds prevent the transactivation of NF-kB target genes involved in the inflammatory response. While the precise mechanism through which SE-EA, EGF-A, and EGF-B inhibit NF-kB activation and subsequently suppress transcriptional activity is not specified in this study, it is reasonable to propose NF-kB as a potential target. Further investigations, such as assessing NF-kB activation status would be necessary to confirm this hypothesis and provide more mechanistic insights into the transcriptional regulation.

Our study also contributes to the understanding of the role of inflammation in cancer progression. This observation aligns with previous research that has established a link between inflammation and cancer. For instance, the overexpression of

NLRP3 inflammasome stimulated proliferation, migration, and invasion of esophageal squamous cell carcinoma (ESCC) *in vitro*. As evidence by the knocking down using NLRP3-siRNAs could result in the attenuation of ESCC metastatic potential. Hence, NLRP3 could be a promising new candidate of cancer targeted therapy (Yu et al., 2020). In the context of non-small cell lung cancer, the activation of the NLRP3 inflammasome pathway in response to LPS and ATP enhanced the cell proliferation and invasive capability of A549 cells. Furthermore, the caspase-1 inhibitor, Z-YVAD-FMK, suppressed LPS-ATP-induced cell migration and invasion by abolishing Akt phosphorylation and inhibiting ERK1/2 and CREB phosphorylation (Wang et al., 2016b). Our findings coincide with these previous reports, highlighting the potential influence of LPS and ATP-induced NLRP3 inflammasome pathway, consequently impacting cancer cell behavior.

Moreover, the previous reports emphasize the crucial role of NLRP3 inflammasome in regulating the proliferation, invasion, and migration of A549 cells. These studies underline the significance of chronic inflammation as a recognized risk factor for cancer development (Moossavi et al., 2018; Gouravani et al., 2020; Xu et al., 2021). Inflammasomes can contribute to tumor development by influencing host tumor immunity, promoting tumor cell proliferation and differentiation, and regulating the tumor microenvironment. Notably, the activation of the NLRP3 inflammasome in cancer-associated fibroblast (CAF) or CAF-derived IL-1β could facilitate lung cancer metastasis, as demonstrated by Moossavi et al., 2018; Gouravani et al., 2020. Nevertheless, it is essential to acknowledge the context-dependent and sometimes contrasting effects of the NLRP3 inflammasome and its product, IL-1β, on tumorigenesis depending on various cancer cell types. Evidence from documented studies and *in vivo* experiments suggests the activation of inflammasomes and related cytokines, such as IL-1β, in many human cancers. IL-1β plays a pivotal role in connecting innate and adaptive immune responses (Ghiringhelli et al., 2009), inducing the polarization of IFN-γ-secreting $CD8^+$ T cells and triggering the formation of IL-17-producing γδT cells, which γδT cells have the ability to recognize tumor-associated antigens and perform anti-cancer activities (Ma et al., 2011). However, recent studies have identified IL-1β as a pro-cancer factor due to its immunosuppressive and chemo-resistant properties (Voronov et al., 2003). In the context of our study, we align with these recent findings, as we have observed that NLRP3 activation contributes to the progression of cancer cells in A549 lung cancer cells. Given the complex role of NLRP 3 inflammasome in the initiation and progression of neoplasia, the NLRP3 inflammasome and its associated pathways represent promising therapeutic targets for the prevention and treatment of lung cancer.

Our findings suggest that SE-EA extract and its active compounds, EGF-A and EGF-B, possess potential anti-cancer properties as they inhibit the invasion of A549 lung cancer cells stimulated by LPS and ATP via the NLRP3 inflammasome pathway. This discovery is significant since invasion is a crucial feature of cancer progression and inhibiting this process could potentially slow down or even halt cancer growth. However, before considering the clinical application of SE-EA extract and its active compounds, EGF-A and EGF-B, further studies are necessary to elucidate the underlying mechanisms of their metabolic pathways and to evaluate potential side effects in animal models. Understanding the precise mechanisms by which these compounds exert their anti-inflammatory and anti-cancer effects is essential for their

therapeutic potential. Additionally, a comprehensive assessment of any possible adverse effects is crucial to ensure the safety and efficacy of these compounds. Animal models provide a valuable platform for investigating the pharmacokinetics, metabolic pathways, and toxicity profiles of SE-EA extract and its active compounds, thus aiding in determining their suitability for clinical use.

In conclusion, this study investigated the effects of *Sophora exigua* extract and its active compounds on the NLRP3 inflammasome pathway in non-small cell lung cancer (NSCLC). The results demonstrated that the extract, particularly the ethyl acetate fraction (SE-EA), exhibited significant anti-inflammatory properties and inhibited the production of pro-inflammatory cytokines in NSCLC cells. The active compounds, exiguaflavanone (EGF-A) and exiguaflavanone (EGF-B), were found to contribute to these effects. Moreover, SE-EA, EGF-A, and EGF-B showed anti-proliferative and anti-metastatic properties by affecting cell cycle progression, migration, and invasion in NSCLC cells. These findings suggest that targeting the NLRP3 inflammasome pathway could be a promising therapeutic approach for NSCLC treatment, providing insights into the development of novel anti-cancer therapeutics.

Data availability statement

The original contributions presented in the study are included in the article/Supplementary material, further inquiries can be directed to the corresponding author.

Author contributions

PA, SA, and PD: primary draft of manuscript, performed the experiment, data collection and analysis. KS and WS: experimental design, performed the experiments, data analysis, and revised the manuscript. SU, LR, AS, MR, and TK: performed the experiments. PD: review and critical appraisal of manuscript, obtained grant funding, and made the final decisions on the manuscript preparation. All authors contributed to the article and approved the submitted version.

Funding

Conflict of interest

The authors declare that the research was conducted in the absence of any commercial or financial relationships that could be construed as a potential conflict of interest.

Publisher's note

All claims expressed in this article are solely those of the authors and do not necessarily represent those of their affiliated organizations, or those of the publisher, the editors and the reviewers. Any product that may be evaluated in this article, or claim that may be made by its manufacturer, is not guaranteed or endorsed by the publisher.

References

Abd-Alla, H. I., Souguir, D., and Radwan, M. O. (2021). Genus Sophora: a comprehensive review on secondary chemical metabolites and their biological aspects from past achievements to future perspectives. *Archives pharmacal Res.* 44, 903–986. doi:10.1007/s12272-021-01354-2

Alduais, Y., Zhang, H., Fan, F., Chen, J., and Chen, B. (2023). Non-small cell lung cancer (NSCLC): a review of risk factors, diagnosis, and treatment. *Medicine* 102, e32899. doi:10.1097/MD.0000000000032899

Aly, S. H., Elissawy, A. M., Eldahshan, O. A., Elshanawany, M. A., Efferth, T., and Singab, A. N. B. (2019). The pharmacology of the genus Sophora (Fabaceae): an updated review. *Phytomedicine* 64, 153070. doi:10.1016/j.phymed.2019.153070

Arjsri, P., Srisawad, K., Mapoung, S., Semmarath, W., Thippraphan, P., Umsumarng, S., et al. (2022). Hesperetin from root extract of clerodendrum petasites s. Moore inhibits sars-Cov-2 spike protein S1 subunit-induced Nlrp3 inflammasome in A549 lung cells via modulation of the Akt/Mapk/Ap-1 pathway. *Int. J. Mol. Sci.* 23, 10346. doi:10.3390/ijms231810346

Aryal, S., Baniya, M. K., Danekhu, K., Kunwar, P., Gurung, R., and Koirala, N. (2019). Total phenolic content, flavonoid content and antioxidant potential of wild vegetables from Western Nepal. *Plants* 8, 96. doi:10.3390/plants8040096

Boozari, M., Soltani, S., and Iranshahi, M. (2019). Biologically active prenylated flavonoids from the genus Sophora and their structure–activity relationship—a review. *Phytotherapy Res.* 33, 546–560. doi:10.1002/ptr.6265

Box, J. (1983). Investigation of the Folin-Ciocalteau phenol reagent for the determination of polyphenolic substances in natural waters. *Water Res.* 17, 511–525. doi:10.1016/0043-1354(83)90111-2

Cao, X., and He, Q. (2020). Anti-tumor activities of bioactive phytochemicals in Sophora flavescens for breast cancer. *Cancer Manag. Res.* 12, 1457–1467. doi:10.2147/CMAR.S243127

Chen, H., Yang, J., Hao, J., Lv, Y., Chen, L., Lin, Q., et al. (2019). A novel flavonoid kushenol Z from Sophora flavescens mediates mTOR pathway by inhibiting phosphodiesterase and Akt activity to induce apoptosis in non-small-cell lung cancer cells. *Molecules* 24, 4425. doi:10.3390/molecules24244425

Chen, H., Zhang, J., Luo, J., Lai, F., Wang, Z., Tong, H., et al. (2013). Antiangiogenic effects of oxymatrine on pancreatic cancer by inhibition of the NF-κB-mediated VEGF signaling pathway. *Oncol. Rep.* 30, 589–595. doi:10.3892/or.2013.2529

Chen, M.-H., Gu, Y.-Y., Zhang, A. L., Sze, D.M.-Y., Mo, S.-L., and May, B. H. (2021). Biological effects and mechanisms of matrine and other constituents of Sophora flavescens in colorectal cancer. *Pharmacol. Res.* 171, 105778. doi:10.1016/j.phrs.2021.105778

Chittasupho, C., Srisawad, K., Arjsri, P., Phongpradist, R., Tingya, W., Ampasavate, C., et al. (2023). Targeting spike glycoprotein S1 mediated by NLRP3 inflammasome machinery and the cytokine releases in A549 lung epithelial cells by nanocurcumin. *Pharmaceuticals* 16, 862. doi:10.3390/ph16060862

Crowley, L. C., Chojnowski, G., and Waterhouse, N. J. (2016). Measuring the DNA content of cells in apoptosis and at different cell-cycle stages by propidium iodide staining and flow cytometry. *Cold Spring Harb. Protoc.* 2016, prot087247. doi:10.1101/pdb.prot087247

Dupaul-Chicoine, J., Arbazadeh, A., Dagenais, M., Douglas, T., Champagne, C., Morizot, A., et al. (2015). The Nlrp3 inflammasome suppresses colorectal cancer metastatic growth in the liver by promoting natural killer cell tumoricidal activity. *Immunity* 43, 751–763. doi:10.1016/j.immuni.2015.08.013

Fabbi, M., Carbotti, G., and Ferrini, S. (2015). Context-dependent role of IL-18 in cancer biology and counter-regulation by IL-18BP. *J. Leukoc. Biol.* 97, 665–675. doi:10.1189/jlb.5RU0714-360RR

Fakhimi, A., Iranshahi, M., Emami, S. A., Amin-Ar-Ramimeh, E., Zarrini, G., and Shahverdi, A. R. (2006). Sophoraflavanone G from Sophora pachycarpa enhanced the antibacterial activity of gentamycin against *Staphylococcus aureus*. *Z. für Naturforsch. C* 61, 769–772. doi:10.1515/znc-2006-9-1026

Fan, S.-H., Wang, Y.-Y., Lu, J., Zheng, Y.-L., Wu, D.-M., Li, M.-Q., et al. (2014). Luteoloside suppresses proliferation and metastasis of hepatocellular carcinoma cells by inhibition of NLRP3 inflammasome. *PloS one* 9, e89961. doi:10.1371/journal.pone.0089961

Fang, R., Wu, R., Zuo, Q., Yin, R., Zhang, C., Wang, C., et al. (2018). Sophora flavescens containing-QYJD formula activates Nrf2 anti-oxidant response, blocks cellular transformation and protects against DSS-induced colitis in mouse model. *Am. J. Chin. Med.* 46, 1609–1623. doi:10.1142/S0192415X18500829

Fenini, G., Contassot, E., and French, L. E. (2017). Potential of IL-1, IL-18 and inflammasome inhibition for the treatment of inflammatory skin diseases. *Front. Pharmacol.* 8, 278. doi:10.3389/fphar.2017.00278

Franken, N. A., Rodermond, H. M., Stap, J., Haveman, J., and Van Bree, C. (2006). Clonogenic assay of cells *in vitro*. *Nat. Protoc.* 1, 2315–2319. doi:10.1038/nprot.2006.339

Ghiringhelli, F., Apetoh, L., Tesniere, A., Aymeric, L., Ma, Y., Ortiz, C., et al. (2009). Activation of the NLRP3 inflammasome in dendritic cells induces IL-1beta-dependent adaptive immunity against tumors. *Nat. Med.* 15, 1170–1178. doi:10.1038/nm.2028

Gomes, M., Teixeira, A. L., Coelho, A., Araujo, A., and Medeiros, R. (2014). The role of inflammation in lung cancer. *Inflamm. cancer* 816, 1–23. doi:10.1007/978-3-0348-0837-8_1

Gouravani, M., Khalili, N., Razi, S., Keshavarz-Fathi, M., Khalili, N., and Rezaei, N. (2020). The NLRP3 inflammasome: a therapeutic target for inflammation-associated cancers. *Expert Rev. Clin. Immunol.* 16, 175–187. doi:10.1080/1744666X.2020.1713755

He, X., Fang, J., Huang, L., Wang, J., and Huang, X. (2015). Sophora flavescens Ait.: traditional usage, phytochemistry and pharmacology of an important traditional Chinese medicine. *J. Ethnopharmacol.* 172, 10–29. doi:10.1016/j.jep.2015.06.010

He, Y., Hara, H., and Núñez, G. (2016). Mechanism and regulation of NLRP3 inflammasome activation. *Trends Biochem. Sci.* 41, 1012–1021. doi:10.1016/j.tibs.2016.09.002

Huang, C.-F., Chen, L., Li, Y.-C., Wu, L., Yu, G.-T., Zhang, W.-F., et al. (2017). NLRP3 inflammasome activation promotes inflammation-induced carcinogenesis in head and neck squamous cell carcinoma. *J. Exp. Clin. Cancer Res.* 36, 116–213. doi:10.1186/s13046-017-0589-y

Huang, J., Deng, Y., Tin, M. S., Lok, V., Ngai, C. H., Zhang, L., et al. (2022). Distribution, risk factors, and temporal trends for lung cancer incidence and mortality: a global analysis. *Chest* 161, 1101–1111. doi:10.1016/j.chest.2021.12.655

Huang, L., Duan, S., Shao, H., Zhang, A., Chen, S., Zhang, P., et al. (2019). NLRP3 deletion inhibits inflammation-driven mouse lung tumorigenesis induced by benzo (a) pyrene and lipopolysaccharide. *Respir. Res.* 20, 20–29. doi:10.1186/s12931-019-0983-4

Kabała-Dzik, A., Rzepecka-Stojko, A., Kubina, R., Jastrzębska-Stojko, Ż., Stojko, R., Wojtyczka, R. D., et al. (2017). Migration rate inhibition of breast cancer cells treated by caffeic acid and caffeic acid phenethyl ester: an *in vitro* comparison study. *Nutrients* 9, 1144. doi:10.3390/nu9101144

Kaewdana, K., Chaniad, P., Jariyapong, P., Phuwajaroanpong, A., and Punsawad, C. (2021). Antioxidant and antimalarial properties of Sophora exigua Craib. root extract in Plasmodium berghei-infected mice. *Trop. Med. Health* 49, 24–11. doi:10.1186/s41182-021-00314-2

Ko, J., Winslow, M. M., and Sage, J. (2021). Mechanisms of small cell lung cancer metastasis. *EMBO Mol. Med.* 13, e13122. doi:10.15252/emmm.202013122

Krishna, P. M., Knv, R., and Banji, D. (2012). A review on phytochemical, ethnomedical and pharmacological studies on genus Sophora, Fabaceae. *Rev. Bras. Farmacogn.* 22, 1145–1154. doi:10.1590/s0102-695x2012005000043

Lan, C., Qian, Y., Wang, Y., Chen, Y., Lin, C., Zhang, Y., et al. (2023). The protective role of curcumin in human dental pulp stem cells stimulated by lipopolysaccharide via inhibiting NF-κB p65 phosphorylation to suppress NLRP3 inflammasome activation. *Clin. Oral Investig.* 27, 2875–2885. doi:10.1007/s00784-023-04885-8

Lee, G., Walser, T. C., and Dubinett, S. M. (2009). Chronic inflammation, chronic obstructive pulmonary disease, and lung cancer. *Curr. Opin. Pulm. Med.* 15, 303–307. doi:10.1097/MCP.0b013e32832c975a

Liang, C.-C., Park, A. Y., and Guan, J.-L. (2007). *In vitro* scratch assay: a convenient and inexpensive method for analysis of cell migration *in vitro*. *Nat. Protoc.* 2, 329–333. doi:10.1038/nprot.2007.30

Lin, T.-Y., Tsai, M.-C., Tu, W., Yeh, H.-C., Wang, S.-C., Huang, S.-P., et al. (2021). Role of the NLRP3 inflammasome: insights into cancer hallmarks. *Front. Immunol.* 11, 610492. doi:10.3389/fimmu.2020.610492

Lin, Y., Chen, X.-J., Li, J.-J., He, L., Yang, Y.-R., Zhong, F., et al. (2023). A novel type lavandulyl flavonoid from Sophora flavescens as potential anti-hepatic injury agent that inhibit TLR2/NF-κB signaling pathway. *J. Ethnopharmacol.* 307, 116163. doi:10.1016/j.jep.2023.116163

Ma, Y., Aymeric, L., Locher, C., Mattarollo, S. R., Delahaye, N. F., Pereira, P., et al. (2011). Contribution of IL-17-producing gamma delta T cells to the efficacy of anticancer chemotherapy. *J. Exp. Med.* 208, 491–503. doi:10.1084/jem.20100269

Moossavi, M., Parsamanesh, N., Bahrami, A., Atkin, S. L., and Sahebkar, A. (2018). Role of the NLRP3 inflammasome in cancer. *Mol. cancer* 17, 158–213. doi:10.1186/s12943-018-0900-3

Noreen, H., Semmar, N., Farman, M., and Mccullagh, J. S. (2017). Measurement of total phenolic content and antioxidant activity of aerial parts of medicinal plant Coronopus didymus. *Asian Pac. J. Trop. Med.* 10, 792–801. doi:10.1016/j.apjtm.2017.07.024

Olcum, M., Tufekci, K. U., Durur, D. Y., Tastan, B., Gokbayrak, I. N., Genc, K., et al. (2021). Ethyl pyruvate attenuates microglial NLRP3 inflammasome activation via inhibition of HMGB1/NF-κB/miR-223 signaling. *Antioxidants* 10, 745. doi:10.3390/antiox10050745

Pękal, A., and Pyrzynska, K. (2014). Evaluation of aluminium complexation reaction for flavonoid content assay. *Food Anal. Methods* 7, 1776–1782. doi:10.1007/s12161-014-9814-x

Pitchakarn, P., Suzuki, S., Ogawa, K., Pompimon, W., Takahashi, S., Asamoto, M., et al. (2012). Kuguacin J, a triterpeniod from Momordica charantia leaf, modulates the progression of androgen-independent human prostate cancer cell line, PC3. *Food Chem. Toxicol.* 50, 840–847. doi:10.1016/j.fct.2012.01.009

Ruangrungsi, N., Iinuma, M., Tanaka, T., Ohyama, M., Yokoyama, J., and Mizuno, M. (1992). Three flavanones with a lavandulyl group in the roots of Sophora exigua. *Phytochemistry* 31, 999–1001. doi:10.1016/0031-9422(92)80202-p

Semmarath, W., Mapoung, S., Umsumarng, S., Arjsri, P., Srisawad, K., Thippraphan, P., et al. (2022). Cyanidin-3-O-glucoside and peonidin-3-O-glucoside-rich fraction of black rice germ and bran suppresses inflammatory responses from SARS-CoV-2 spike glycoprotein S1-induction *in vitro* in A549 lung cells and THP-1 macrophages via inhibition of the NLRP3 inflammasome pathway. *Nutrients* 14, 2738. doi:10.3390/nu14132738

Semmarath, W., Srisawad, K., Arjsri, P., Umsumarng, S., Yodkeeree, S., Jamjod, S., et al. (2023). Protective effects of proanthocyanidin-rich fraction from red rice germ and bran on lung cell inflammation via inhibition of NF-κB/NLRP3 inflammasome pathway. *Nutrients* 15, 3793. doi:10.3390/nu15173793

Sodde, V. K., Lobo, R., Kumar, N., Maheshwari, R., and Shreedhara, C. (2015). Cytotoxic activity of Macrosolen parasiticus (L.) Danser on the growth of breast cancer cell line (MCF-7). *Pharmacogn. Mag.* 11, S156–S160. doi:10.4103/0973-1296.157719

Song, D., Zhao, J., Deng, W., Liao, Y., Hong, X., and Hou, J. (2018). Tannic acid inhibits NLRP3 inflammasome-mediated IL-1β production via blocking NF-κB signaling in macrophages. *Biochem. biophysical Res. Commun.* 503, 3078–3085. doi:10.1016/j.bbrc.2018.08.096

Stares, M., Ding, T.-E., Stratton, C., Thomson, F., Baxter, M., Cagney, H., et al. (2022). Biomarkers of systemic inflammation predict survival with first-line immune checkpoint inhibitors in non-small-cell lung cancer. *ESMO open* 7, 100445. doi:10.1016/j.esmoop.2022.100445

Suarez-Arnedo, A., Figueroa, F. T., Clavijo, C., Arbeláez, P., Cruz, J. C., and Muñoz-Camargo, C. (2020). An image J plugin for the high throughput image analysis of *in vitro* scratch wound healing assays. *PloS one* 15, e0232565. doi:10.1371/journal.pone.0232565

Sukkasem, K. (2015). *Biological activities of Thai traditional remedy called Kheaw-Hom and its plant ingredients*. Bangkok, Thailand: Thammasat University.

Sukkasem, K., Panthong, S., and Itharat, A. (2016). Antimicrobial activities of Thai traditional remedy "kheaw-hom" and its plant ingredients for skin infection treatment in chickenpox. *J. Med. Assoc. Thail. Chotmaihet Thangphaet* 99, 116–123.

Tsuchiya, H., Sato, M., Miyazaki, T., Fujiwara, S., Tanigaki, S., Ohyama, M., et al. (1996). Comparative study on the antibacterial activity of phytochemical flavanones against methicillin-resistant *Staphylococcus aureus*. *J. Ethnopharmacol.* 50, 27–34. doi:10.1016/0378-8741(96)85514-0

Vichai, V., and Kirtikara, K. (2006). Sulforhodamine B colorimetric assay for cytotoxicity screening. *Nat. Protoc.* 1, 1112–1116. doi:10.1038/nprot.2006.179

Vidal-Vanaclocha, F., Fantuzzi, G., Mendoza, L., Fuentes, A. M., Anasagasti, M. J., Martín, J., et al. (2000). IL-18 regulates IL-1beta-dependent hepatic melanoma metastasis via vascular cell adhesion molecule-1. *Proc. Natl. Acad. Sci.* 97, 734–739. doi:10.1073/pnas.97.2.734

Voronov, E., Shouval, D. S., Krelin, Y., Cagnano, E., Benharroch, D., Iwakura, Y., et al. (2003). IL-1 is required for tumor invasiveness and angiogenesis. *Proc. Natl. Acad. Sci.* 100, 2645–2650. doi:10.1073/pnas.0437939100

Wang, H., Chen, L., Zhang, L., Gao, X., Wang, Y., and Weiwei, T. (2016a). Protective effect of sophoraflavanone G on streptozotocin (STZ)-induced inflammation in diabetic rats. *Biomed. Pharmacother.* 84, 1617–1622. doi:10.1016/j.biopha.2016.10.113

Wang, H., Kong, H., Zeng, X., Liu, W., Wang, Z., Yan, X., et al. (2016b). Activation of NLRP3 inflammasome enhances the proliferation and migration of A549 lung cancer cells. *Oncol. Rep.* 35, 2053–2064. doi:10.3892/or.2016.4569

Wu, J., and Lin, Z. (2022). Non-small cell lung cancer targeted therapy: drugs and mechanisms of drug resistance. *Int. J. Mol. Sci.* 23, 15056. doi:10.3390/ijms232315056

Xu, Z., Wang, H., Qin, Z., Zhao, F., Zhou, L., Xu, L., et al. (2021). NLRP3 inflammasome promoted the malignant progression of prostate cancer via the activation of caspase-1. *Cell death Discov.* 7, 399. doi:10.1038/s41420-021-00766-9

Yao, M., Fan, X., Yuan, B., Takagi, N., Liu, S., Han, X., et al. (2019). Berberine inhibits NLRP3 Inflammasome pathway in human triple-negative breast cancer MDA-MB-231 cell. *BMC Complementary Altern. Med.* 19, 216–311. doi:10.1186/s12906-019-2615-4

Yu, S., Yin, J. J., Miao, J. X., Li, S. G., Huang, C. Z., Huang, N., et al. (2020). Activation of NLRP3 inflammasome promotes the proliferation and migration of esophageal squamous cell carcinoma. *Oncol. Rep.* 43, 1113–1124. doi:10.3892/or.2020.7493

Zappa, C., and Mousa, S. A. (2016). Non-small cell lung cancer: current treatment and future advances. *Transl. Lung Cancer Res.* 5, 288–300. doi:10.21037/tlcr.2016.06.07

Check for updates

A real-world disproportionality analysis of mepolizumab based on the FDA adverse event reporting system

Huqun Li[1], Chongshu Wang[2], Aiping Deng[1] and Cuilian Guo[2]*

[1]Department of Pharmacy, The Central Hospital of Wuhan, Tongji Medical College, Huazhong University of Science and Technology, Wuhan, China, [2]Department of Otolaryngology-Head and Neck Surgery, Tongji Hospital, Tongji Medical College, Huazhong University of Science and Technology, Wuhan, China

Background: Mepolizumab has been approved by the FDA for add-on maintenance treatment of severe asthma with an eosinophilic phenotype. Real-world studies on mepolizumab-associated adverse events are limited. The present study aimed to explore mepolizumab-related adverse events based on the US Food and Drug Administration Adverse Event Reporting System (FAERS) database.

Methods: A disproportionality analysis was performed to assess the safety profile of mepolizumab based on the reports from the FAERS database between October 2015 and December 2022. Demographic information, the time to onset, the safety of long-term mepolizumab exposure as well as safety in pediatric patients were also investigated.

Results: A total of 736 significant preferred terms (PTs) were identified among the 13,497 mepolizumab-associated adverse events (AEs) reports collected from the FAERS database. The frequently reported AEs including dyspnea, fatigue, and headache were in line with drug instruction and previous studies. Unexpected significant AEs such as cough, malaise, and chest discomfort were also identified. Most AEs occurred within the first month after mepolizumab initiation. Pneumonia and wheezing were frequently reported in patients with long-term mepolizumab exposure as well as in the pediatric population.

Conclusion: Our results were consistent with the observations in previous clinical and real-world studies. New and unexpected AE signals of mepolizumab were also identified. Close attention should be paid to the long-term safety of mepolizumab as well as safety in the pediatric population. Prospective studies are required for optimal use of mepolizumab.

KEYWORDS

mepolizumab, asthma, pharmacovigilance, disproportionality, pediatric, long term

Introduction

Asthma is a chronic and heterogeneous inflammatory disease that affects an estimated 358 million people all over the world (Khurana et al., 2019). Patients with severe asthma including severe eosinophilic asthma comprise 5%–10% of the total asthma population and have uncontrolled or partially controlled asthma despite historically inhaled corticosteroids and beta-agonists treatment (Pertzov et al., 2021). Recently, several biologics targeting

various interleukin signaling pathways have been developed as an add-on treatment to standard-of-care asthma therapy with improved asthma control for patients with severe asthma (Charles et al., 2022; Hashimoto et al., 2022; Liu et al., 2023).

Interleukin 5 (IL-5) is a key regulator of eosinophil biology that has been implicated in the pathophysiology of severe eosinophilic asthma (Passalacqua, 2017). Mepolizumab, an anti-IL-5 monoclonal antibody, was approved by FDA in 2015 for add-on maintenance treatment of adult and pediatric patients aged 12 years and older with severe asthma and with an eosinophilic phenotype. Mepolizumab has also been approved for patients with eosinophilic diseases including chronic rhinosinusitis with nasal polyps (CRSwNP), eosinophilic granulomatosis with polyangiitis (EGPA), and hypereosinophilic syndrome (HES) (Roufosse et al., 2013; Wechsler et al., 2017). Although mepolizumab has demonstrated promising efficacy and good tolerance in clinical and real-world studies (Chupp et al., 2017; Khatri et al., 2019; Khurana et al., 2019; Pertzov et al., 2021), adverse events (AEs) such as headache and back pain were frequently reported in placebo-controlled trials. In addition, although mepolizumab has exhibited favorable long-term safety in clinical studies (Gleich et al., 2021; Maspero et al., 2022), long-term safety data beyond 1 year in real-world settings are lacking. Moreover, mepolizumab has been approved recently for severe eosinophilic asthma in patients aged 6 years and older in many countries (Drick et al., 2022). However, there is limited data available to evaluate the safety of mepolizumab in the pediatric population. As randomized clinical trials are sometimes very far from real-world conditions, comprehensive real-world pharmacovigilance to explore the adverse event profile of mepolizumab is urgently required.

The US Food and Drug Administration Adverse Event Report System (FAERS) database is a publicly accessible and the world's largest pharmacovigilance database that receives drug-related AEs all over the world, including the United States and other countries (Shu et al., 2023). Therefore, it was particularly suitable for identifying potential associations between drugs and AEs due to the large size and global coverage. In addition, previous reports have shown notable accuracy of well-designed pharmacovigilance analysis based on the FAERS database (Harpaz et al., 2013; Raschi et al., 2021). Therefore, in the present study, we aim to conduct a comprehensive pharmacovigilance analysis of mepolizumab based on the FAERS database. Moreover, the long-term safety of mepolizumab, together with safety concerns in the pediatric population were also investigated for the first time. Our study indicated that mepolizumab should be prescribed with caution, and further studies are required to identify optimal treatment regimens, duration of treatment, and target patients. Our findings may serve as a valuable clinical reference.

Materials and methods

Data sources

The present study was designed to evaluate whether a possible association exists between mepolizumab and an interest AE via a disproportionality analysis based on the FAERS database. Reports from the fourth quarter of 2015 (FDA marketing approval of mepolizumab) to the last quarter of 2022 (the most recent update of the FAERS database at the time this study was performed) were extracted to perform the disproportionality analysis. FAERS data were published quarterly by FDA and consisted of the following eight datasets: demographic and administrative information (DEMO), drug information (DRUG), adverse events (REAC), patient outcomes (OUTC), report sources (RPSR), start and end dates for reported drugs (THER), indications for use (INDI), and an additional deleted file (DELETED). As the FAERS inevitably contains duplicate reports, according to the FDA's recommendations, we took the higher PRIMARYID when the CASEIDs were the same and the latest FDA_DT when the CASEIDs were the same to remove duplicates. In addition, the deleted cases were also removed. Both the generic name (mepolizumab) and brand names (nucala) were used to extract mepolizumab-associated reports in the DRUG file. In consideration of credibility, reports in which mepolizumab was deemed to cause adverse events with a role_cod of PS (Primary Suspect) were extracted for the disproportional analysis. AEs in the REAC file were recorded as the preferred term (PT) and subsequently system organ class (SOC) coded by the Medical Dictionary for Regulatory Activities (MedDRA) (version 26.0). The clinical characteristics of reports including gender, age, reporting countries, reporting year, reporter, outcomes, indications, therapy start time, and end time were collected and analyzed based on the available data. The time to onset of mepolizumab-associated AEs was calculated as the event onset date minus the therapy start date. Reports were excluded when an inaccurate date entry or an input error (EVENT_DT earlier than START_DT) occurred. The medication time of mepolizumab was calculated as the therapy end date minus the therapy start date. The flowchart of our study is shown in Figure 1.

Statistical analysis

As the actual denominators were unclear, the incidence of AEs cannot be calculated by the FAERS database (Kinoshita et al., 2020). Therefore, as an effective and widely used method in pharmacovigilance studies, a disproportionality analysis was applied to identify potential signals of AEs related to mepolizumab in our study. The comparator group in disproportionality analysis is the background frequency of the same AE across all other drugs in FAERS compared with mepolizumab. The disproportionality analysis was performed using the reporting odds ratio (ROR) calculated by the case/non-case method (Lin et al., 2023). A higher ROR represented a stronger association between mepolizumab and AEs. ROR and 95% CI were calculated based on the 2 × 2 contingency tables with the formulas in Table 1.

A significant signal was identified when the lower-bound 95% CI of the ROR was above 1.0 and the number of the cases was above 3. Data processing and analyses were performed by MYSQL 8.0, Microsoft Excel 2019, and GraphPad Prism 8. $p < 0.05$ was considered statistically significant.

Result

General characteristics

A total of 11,846,436 adverse events reports were submitted to the FAERS during the study period. After deduplication,

TABLE 1 Calculation of reporting odds ratio (ROR) and 95% confidence interval (CI).

Drug category	Event of interest	All other events
Mepolizumab	a	b
All other drugs	c	d

ROR, ad/bc.

95% CI, $e^{\ln(ROR)\pm1.96(1/a+1/b+1/c+1/d)0.5}$.

13,497 mepolizumab-associated reports were included in the study, and the general descriptions were presented in Table 2. The reports showed a generally increasing tendency year by year possibly due to the widespread use of mepolizumab. The mepolizumab-associated reports were more common in female than male patients (43.71% vs. 21.19%). Patients aged 18–60 years (13.92%) and elderly patients aged above 60 years (15.42%) accounted for most reports. A small proportion of reports were in children patients aged below 12 years

TABLE 2 Clinical characteristics of mepolizumab associated reports from the FAERS database (October 2015 to December 2022).

Characteristics	Case Number, n	Proportion, %
Number of events	13497	
Gender		
Female	5900	43.71
Male	2860	21.19
Unknown	4737	35.10
Age (years)		
<12	105	0.78
12≤ and <18	65	0.48
18≤ and <60	1879	13.92
≥60	2081	15.42
Unknown	9367	69.40
Indications (top five)		
Asthma	11132	82.48
Eosinophilic granulomatosis with polyangiitis	478	3.54
Hypereosinophilic syndrome	75	0.56
Chronic obstructive pulmonary disease	43	0.32
Nasal polyps	38	0.28
Serious outcome		
Death (DE)	273	2.02
Life-threatening (LT)	69	0.51
Hospitalization-initial or prolonged (HO)	3318	24.58
Disability (DS)	58	0.43
Congenital anomaly (CA)	4	0.03
Other important medical events (OT)	6595	48.86
Required intervention (RI)	8	0.06
Reported countries (top five)		
Canada (CA)	5505	40.79
America (US)	4008	29.70
Japan (JP)	401	2.97
Brazil (BR)	371	2.75
Australia (AU)	336	2.49
Reporting year		
2022	4070	30.15
2021	2328	17.25
2020	2851	21.12
2019	2461	18.23
2018	601	4.45
2017	826	6.12
2016	356	2.64
2015Q4[a]	4	0.03

[a]the fourth quarter of 2015.

TABLE 3 Signal strength of mepolizumab associated reports at the preferred terms level ($n \geq 100$).

SOC	Preferred terms (PTs)	Cases (n)	ROR (95% two-sided CI)
Cardiac disorders	Cardiac disorder	124	2.11 (1.77–2.52)
	Myocardial infarction	107	1.44 (1.19–1.75)
Eye disorders	Cataract	181	4.04 (3.49–4.68)
General disorders and administration site conditions	Asthenia	348	1.29 (1.16–1.43)
	Chest discomfort	395	5.68 (5.14–6.28)
	Chest pain	255	2.22 (1.96–2.51)
	Chills	131	1.61 (1.35–1.91)
	Condition aggravated	551	2.24 (2.06–2.44)
	Fatigue	1026	1.69 (1.58–1.80)
	Ill-defined disorder	148	4.30 (3.65–5.06)
	Illness	146	2.44 (2.07–2.87)
	Influenza like illness	115	2.08 (1.73–2.50)
	Injection site pain	263	1.49 (1.32–1.68)
	Malaise	890	2.58 (2.41–2.76)
	Pain	598	1.15 (1.06–1.25)
	Peripheral swelling	190	1.23 (1.06–1.42)
	Pyrexia	520	2.09 (1.92–2.29)
	Secretion discharge	133	12.04 (10.14–14.31)
	Therapeutic product effect incomplete	670	9.83 (9.09–10.63)
Immune system disorders	Hypersensitivity	210	1.52 (1.33–1.74)
Infections and infestations	Bronchitis	242	3.88 (3.42–4.41)
	Cellulitis	111	2.84 (2.36–3.43)
	COVID-19	310	2.16 (1.93–2.42)
	Herpes zoster	172	3.55 (3.05–4.13)
	Infection	248	2.26 (2.00–2.57)
	Influenza	347	3.72 (3.35–4.14)
	Lower respiratory tract infection	184	4.40 (3.80–5.09)
	Nasopharyngitis	437	2.82 (2.56–3.10)
	Pneumonia	1807	7.92 (7.54–8.33)
	Respiratory tract infection	143	6.83 (5.78–8.05)
	Sinusitis	291	3.47 (3.09–3.90)
	Urinary tract infection	179	1.32 (1.14–1.53)
Injury, poisoning and procedural complications	Accidental exposure to product	228	3.57 (3.13–4.07)
	Contusion	104	1.39 (1.15–1.69)
	Exposure via skin contact	255	84.00 (73.77–95.65)
	Fall	385	1.55 (1.40–1.71)
	Inappropriate schedule of product administration	804	5.82 (5.42–6.25)
	Product dose omission issue	1265	4.85 (4.58–5.14)

TABLE 3 (*Continued*) Signal strength of mepolizumab associated reports at the preferred terms level (*n* ≥ 100).

SOC	Preferred terms (PTs)	Cases (n)	ROR (95% two-sided CI)
	Underdose	173	2.75 (2.36–3.19)
	Wrong technique in device usage process	248	7.05 (6.22–8.00)
Investigations	Full blood count abnormal	169	8.04 (6.90–9.37)
	Blood pressure increased	271	2.09 (1.85–2.36)
	Heart rate increased	140	1.95 (1.65–2.30)
	Oxygen saturation decreased	182	4.13 (3.57–4.79)
Metabolism and nutrition disorders	Diabetes mellitus	126	2.51 (2.11–3.00)
Musculoskeletal and connective tissue disorders	Arthralgia	407	1.25 (1.13–1.38)
	Back pain	464	2.64 (2.41–2.90)
	Muscular weakness	103	1.30 (1.07–1.57)
	Myalgia	211	1.83 (1.59–2.09)
	Pain in extremity	339	1.46 (1.31–1.63)
Nervous system disorders	Cerebrovascular accident	118	1.29 (1.08–1.55)
	Headache	839	1.83 (1.71–1.97)
	Loss of consciousness	107	1.33 (1.10–1.61)
	Syncope	118	1.75 (1.46–2.09)
Product issues	Product availability issue	140	10.14 (8.58–11.99)
	Product complaint	274	14.08 (12.48–15.88)
Psychiatric disorders	Sleep disorder due to a general medical condition	591	59.67 (54.80–64.97)
Respiratory, thoracic and mediastinal disorders	Asthma	2804	41.37 (39.66–43.16)
	Asthmatic crisis	714	238.84 (219.45–259.93)
	Bronchospasm	101	11.33 (9.30–13.80)
	Chronic obstructive pulmonary disease	212	5.84 (5.10–6.69)
	Cough	1348	6.56 (6.20–6.94)
	Dysphonia	150	3.40 (2.89–3.99)
	Dyspnoea	2879	8.74 (8.38–9.10)
	Dyspnoea exertional	246	7.48 (6.59–8.49)
	Lung disorder	193	5.29 (4.59–6.10)
	Nasal congestion	247	5.30 (4.68–6.02)
	Obstructive airways disorder	178	14.57 (12.55–16.91)
	Oropharyngeal pain	182	2.38 (2.06–2.76)
	Productive cough	467	10.90 (9.93–11.96)
	Respiratory disorder	128	6.01 (5.05–7.16)
	Rhinorrhoea	163	2.94 (2.52–3.43)
	Sputum discoloured	214	20.18 (17.60–23.14)
	Wheezing	1445	33.99 (32.15–35.92)
Skin and subcutaneous tissue disorders	Pruritus	318	1.29 (1.15–1.44)
	Urticaria	167	1.52 (1.31–1.77)

TABLE 3 (*Continued*) Signal strength of mepolizumab associated reports at the preferred terms level (*n* ≥ 100).

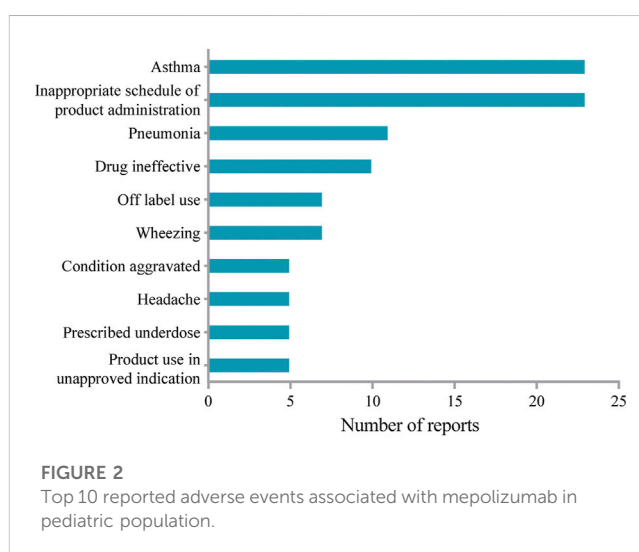| SOC	Preferred terms (PTs)	Cases (n)	ROR (95% two-sided CI)
Social circumstances	Loss of personal independence in daily activities	928	19.19 (17.94–20.52)
	Social problem	164	61.13 (52.12–71.70)
Surgical and medical procedures	Hospitalization	677	5.94 (5.49–6.41)
	Therapy interrupted	149	4.42 (3.76–5.19)
Vascular disorders	Hypertension	178	1.18 (1.02–1.37)

SOC, system organ class; ROR, reporting odds ratio; CI, confidence interval.

FIGURE 1
The flowchart of identifying mepolizumab related AEs in FAERS database. FAERS: Food and drug administration adverse event report system.

FIGURE 2
Top 10 reported adverse events associated with mepolizumab in pediatric population.
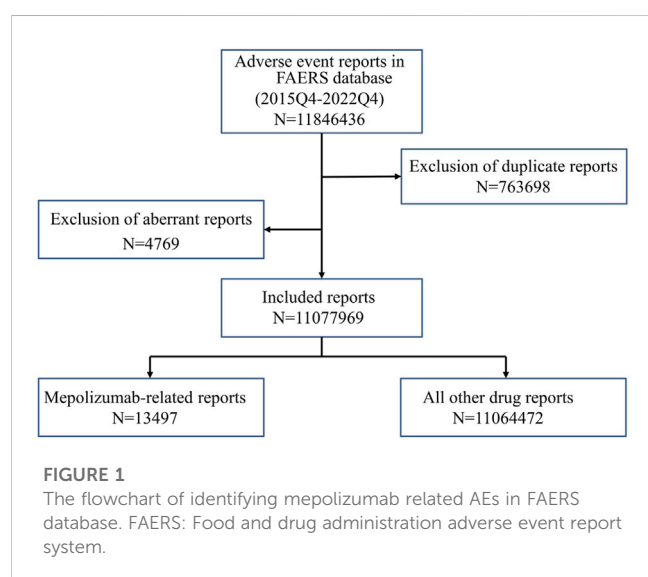
(0.78%) and a smaller proportion in patients aged 12–18 years (0.48%). The most reported indication was asthma (82.48%), followed by EGPA (3.54%), HES (0.56%), Chronic obstructive pulmonary disease (COPD) (0.32%), and NP (0.28%). Regarding the report country, Canada (40.79%) submitted most reports, followed by America (29.70%), Japan (2.97%), Brazil (2.75%), and Australia (2.49%), respectively. The most frequently reported severe outcomes were OT (48.86%) and HO (24.58%).

Signal detection

Table 3 lists the identified 83 significant PTs of interest. In the current study, AEs including dyspnoea (PT: 10013968), fatigue (PT: 10016256), headache (PT: 10019211), pyrexia (PT: 10037660), back pain (PT: 10003988), nasopharyngitis (PT: 10028810), arthralgia (PT: 10003239), asthenia (PT: 10003549), influenza (PT: 10022000), pruritus (PT: 10037087) were detected in data mining, which was consistent with the label for mepolizumab. Of note, unexpected AEs that were not listed in the FDA drug prescription were uncovered including pneumonia (PT: 10035664), wheezing (PT: 10047924), cough (PT: 10011224), malaise (PT: 10025482), chest discomfort (PT: 10008469), peripheral swelling (PT: 10048959), cataract (PT: 10007739), obstructive airways disorder (PT: 10061877) and so on. However, AEs such as abdominal pain, angioedema, diarrhea, dizziness, erythema, and flushing, which were listed in the drug label, did not meet the criteria for significant RORs in the present study.
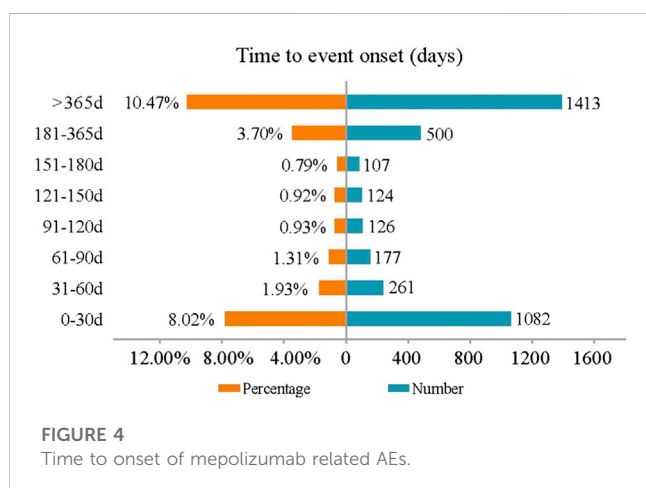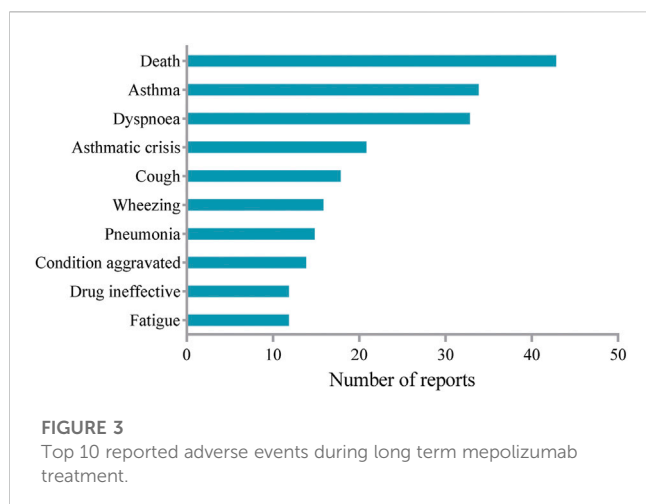
AEs reported in pediatric patients aged less than 12 years were extracted to study the safety profile in the pediatric population. The top 10 most frequently reported AEs were shown in Figure 2. Headache in the instructions was present among the top 10 most frequently reported AEs in the study. Of note, unexpected AEs such as wheezing and pneumonia were not included in the label. However, AEs including diarrhea, ear infection, and gastroenteritis as indicated in the label of mepolizumab were not recognized in the pediatric population.

AEs with a period above 52 weeks of mepolizumab medication were extracted to evaluate the long-term safety profile of mepolizumab. The top 10 most frequently reported AEs were summarized in Figure 3. Fatigue in the instructions was identified among the top 10 most frequently reported AEs. It is noteworthy that unexpected AEs including wheezing and pneumonia were uncovered in the label. However, AEs such as gastroenteritis and pharyngitis in the instruction were not observed after long-term mepolizumab treatment.

Onset time of events

Figure 4 displays the onset times of mepolizumab-associated AEs. The median onset time was 685 days [interquartile range (IQR)

FIGURE 3
Top 10 reported adverse events during long term mepolizumab treatment.

FIGURE 4
Time to onset of mepolizumab related AEs.

299–1176 days]. Most AEs occurred within the first 1 month (n = 1082, 8.02%) after mepolizumab initiation with almost half of the reports (n = 522, 3.88%) on the day of mepolizumab dosing. However, it should be noted that a considerable proportion of AEs (n = 1413, 10.47%) occurred after long-term (more than 1 year) mepolizumab treatment.

Discussion

In the present study, we characterized the safety profile of mepolizumab based on the FAERS database. We identified new unexpected AEs associated with mepolizumab such as pneumonia and wheezing, and AEs listed in the drug label. Moreover, the long-term safety of mepolizumab as well as safety in pediatric patients was also evaluated in the current study. To our knowledge, the present study was the first pharmacovigilance analysis to explore the post-marketing safety of mepolizumab, providing a valuable reference for further optimal clinical use of mepolizumab.

In the present study, adult patients aged 18 years and older accounted for most AEs. Although mepolizumab has been approved for severe asthma in patients aged 6 years and older, and HES in patients aged 12 years and older, patients aged younger than

18 years accounted for a small proportion. Consistent with the instructions, mepolizumab has been prescribed mainly for asthma. However, a minor proportion of mepolizumab was used for COPD which was not included in the label. Despite the frequent coexistence and common pathophysiology of asthma and COPD (Maspero et al., 2022), previous studies have reported inconsistent results regarding the efficacy of mepolizumab for COPD (Drick et al., 2022; Ohnishi et al., 2022). Concerning the reporter countries, Canada and America accounted for most reports. Interestingly, China contributed to a minor proportion. Chronic rhinosinusitis with nasal polyposis (CRSwNP) is frequently associated with severe eosinophilic asthma and contributes to poor control of asthma (Detoraki et al., 2021). In white patients, 80%–90% of nasal polyps (NPs) are characterized by prominent eosinophilia with high amounts of IL-5. However, NPs of Chinese patients usually lack IL-5 and eotaxin expression which leads to lower numbers of tissue eosinophils (Gevaert et al., 2011). Furthermore, mepolizumab was approved recently in November 2021 in China for EGPA. Therefore, different races and ethnic backgrounds might be important underlying factors.

In line with the drug instructions, AEs such as nasopharyngitis, lower respiratory tract infection, and bronchitis were identified in the present study, which demonstrated the reliability of our research. However, new unexpected AEs including pneumonia, wheezing, lung disorder, and lung infection were also recognized as significant signals with high frequency. Moreover, in the sub-group analysis, pneumonia and wheezing were still frequently reported in patients after long-term mepolizumab treatment as well as in pediatric patients. Of note, pneumonia was also identified after long-term mepolizumab treatment while at a low rate in previous studies (Lugogo et al., 2016; Khatri et al., 2019).

Asthma affected approximately 11% of children aged 6–12 years (Nordlund et al., 2014). Moreover, mepolizumab was approved as an add-on treatment for severe eosinophilic asthma by the European Medicines Agency for patients 18 years and older in 2015, and later for patients 6 years and older in 2018 (Gupta et al., 2019). Therefore, we examined the mepolizumab-associated AEs in pediatric patients (aged less than 12 years old). Consistent with previous studies (Gupta et al., 2019), we identified mepolizumab-associated AEs such as bronchitis, headache, pyrexia, and so on, which were listed in the drug label. However, unexpected AEs including pneumonia and wheezing were also found in more than 7 reports in our study. Local injection-site reactions, which occurred with an incidence of 12% in adults in the COLUMBA study (Khatri et al., 2019), was not observed in our study as well as in Atul Gupta's report (Gupta et al., 2019). Interestingly, local injection-site reaction was included in the drug label with an occurrence rate of 8% in severe asthma patients receiving mepolizumab. Moreover, we also identified mepolizumab-related anaphylaxis in children, which was not reported in adults (Lugogo et al., 2016; Khatri et al., 2019). Of note, inappropriate schedule of product administration, drug ineffective, and prescribed underdose were present among the frequently reported AEs, which suggested that inappropriate dose regimens might be common in pediatric patients due to the special physiology. Therefore, there exists an obvious difference in mepolizumab-associated AEs between adults and children. Mepolizumab should be prescribed for pediatric patients with more caution.

In the present study, asthma (exacerbation) and asthmatic crisis were identified among the most frequently reported AEs after long-term mepolizumab treatment, which were also most commonly reported in the COLUMBA study (Khatri et al., 2019). Consistently, no anaphylaxis was reported after long-term treatment of mepolizumab. However, pneumonia, which was frequently reported in the present study, was reported at a low rate in previous studies (Lugogo et al., 2016; Khatri et al., 2019). In addition, the most commonly reported AEs such as nasopharyngitis and upper respiratory tract infection in previous studies were present in limited reports in our study. It is noteworthy that death was present among the most frequently reported AEs during the long-term mepolizumab treatment. Given that these reports were voluntary, the relationship between mepolizumab and death requires further research and validation. Interestingly, herpes zoster infection, an opportunistic infection, was present in several reports in our study, which was also identified in previous studies (Khatri et al., 2019; Khurana et al., 2019). As mepolizumab significantly decreased eosinophils which might result in a loss of immune function regulation after long-term exposure, AEs occurred more likely compared with the shorter-term study. Therefore, further studies are needed to fully address the long-term safety profile of mepolizumab.

Concerning the onset time, most AEs occurred on the day of mepolizumab initiation, which was consistent with a previous multicenter and retrospective study (Montero-Pérez et al., 2019). Of note, AEs that occurred more than 365 days after mepolizumab initiation account for a considerable proportion. Therefore, a longer follow-up study is required to comprehensively address the mepolizumab-related AEs in clinical practice.

Severe eosinophilic asthma is characterized by chronic eosinophilic inflammation, mostly type 2 (T2) inflammation, in which IL-5 plays a central pathogenic role (Han et al., 2021). Moreover, Th2 response played a key role in most CRSwNP, especially in Western countries (Vinciguerra et al., 2022). Mepolizumab inhibited IL-5 signaling, reduced the Th2 response, and therefore alleviated the hypereosinophilia-related syndrome such as severe eosinophilic asthma. However, as a necessary part for viral immunity, the Th2 response inhibition raised the concern of an increased risk for viral infection among patients receiving mepolizumab. Indeed, we identified herpes zoster as a significant AE signal in our study, which is consistent with the warnings in the drug label of mepolizumab. Consistently, Sumita et al. identified opportunistic infections including herpes zoster infection after long-term mepolizumab treatment in patients with severe eosinophilic asthma (Khatri et al., 2019). Therefore, attention should be paid to the opportunistic infections associated with the mepolizumab treatment in clinical studies and real-world settings.

In the present study, we identified both allergic systemic reactions (rash and urticaria) and non-allergic systemic reactions (fatigue and paresthesia), which were consistent with the drug label. Of note, anaphylaxis identified in our study was reported to be mepolizumab unrelated in previous studies. It has been reported that humanized biologics such as mepolizumab have 90% of human component with a higher potential of immunogenicity compared with dupilumab that has 99% of human component (Bian et al., 2021). Therefore, the risk of anaphylaxis might be high for mepolizumab. Indeed, the post-marketing experience suggests a possible link between mepolizumab and hypersensitivity reactions including anaphylaxis in the drug label. Interestingly, mepolizumab-related anaphylaxis was identified in the pediatric population in our study as well as in previous studies, which suggested a predisposition to anaphylaxis for children. Therefore, further studies are needed to evaluate the systemic reactions during mepolizumab treatment, especially in pediatric patients.

We noted a recently published FAERS study of post-marketing safety of anti-IL-5 monoclonal antibodies including mepolizumab (Zou et al., 2023). Data mining methods mainly include frequency analysis and Bayesian analysis, and the sensitivity of Bayesian analysis is relatively lower than that of frequency analysis (Liu et al., 2022). In the recent study, both methods were used. Additionally, the AE of asthma and AE reports submitted by consumers were also excluded. In our study, only frequency analysis with higher sensitivity was applied to identify potential new and overlooked significant AEs. Therefore, AEs in the drug instructions such as arthralgia and AEs not included in the drug instructions such as peripheral swelling identified in our study were not observed in Shu-Peng Zou's study. To some extent, our study provided a more comprehensive characterization of the AE signals for mepolizumab.

There are several limitations in our study. First, the voluntary reports in FAERS might be influenced by various factors such as FDA warnings which might lead to underreporting or overreporting of adverse events. Second, disproportionality analysis only provides a statistical evaluation of the signal strength but not real risk. A causal relationship between drug and AE does not require confirmation in the FAERS database, and some AE reports may have incomplete clinical and medical information such as age in the present study. Therefore, the causal relationship could not be established and requires further validation. Nevertheless, this real-world pharmacovigilance analysis provided wide monitoring and suspected AE signals of mepolizumab in an unselected population which might contribute to the rational use of mepolizumab in clinical practice. Moreover, prospective clinical studies and basic research are required to validate and confirm the AEs identified in the current study.

Conclusion

The present study extends our knowledge of the safety concerns of mepolizumab in real-world clinical settings. Close attention should be paid to the AEs with strong real-world signals such as pneumonia and wheezing that are not listed in the label. Moreover, clinicians should take care of the long-term safety of mepolizumab for both children and adults, together with safety concerns in the pediatric population. In conclusion, it seems that mepolizumab should be prescribed with caution, and further clinical and real-world studies are required to identify optimal treatment regimens, duration of treatment, and target patients.

Data availability statement

The original contributions presented in the study are included in the article/Supplementary Material, further inquiries can be directed to the corresponding author.

Ethics statement

Ethical approval was not required for the study involving humans in accordance with the local legislation and institutional requirements. Written informed consent to participate in this study was not required from the participants or the participants' legal guardians/next of kin in accordance with the national legislation and the institutional requirements.

Author contributions

HL: Conceptualization, Writing–original draft. CW: Formal Analysis, Writing–original draft. AD: Writing–review and editing. CG: Supervision, Writing–review and editing.

Funding

The authors declare that no financial support was received for the research, authorship, and/or publication of this article.

Conflict of interest

The authors declare that the research was conducted in the absence of any commercial or financial relationships that could be construed as a potential conflict of interest.

Publisher's note

All claims expressed in this article are solely those of the authors and do not necessarily represent those of their affiliated organizations, or those of the publisher, the editors and the reviewers. Any product that may be evaluated in this article, or claim that may be made by its manufacturer, is not guaranteed or endorsed by the publisher.

Supplementary material

The Supplementary Material for this article can be found online at: https://www.frontiersin.org/articles/10.3389/fphar.2023.1280490/full#supplementary-material

References

Bian, S., Zhang, P., Li, L., Wang, Z., Cui, L., Xu, Y., et al. (2021). Anaphylaxis associated with allergen specific immunotherapy, omalizumab, and dupilumab: a real world study based on the US Food and drug administration adverse event reporting system. *Front. Pharmacol.* 12, 767999. doi:10.3389/fphar.2021.767999

Charles, D., Shanley, J., Temple, S. N., Rattu, A., Khaleva, E., and Roberts, G. (2022). Real-world efficacy of treatment with benralizumab, dupilumab, mepolizumab and reslizumab for severe asthma: a systematic review and meta-analysis. *Clin. Exp. Allergy* 52 (5), 616–627. doi:10.1111/cea.14112

Chupp, G. L., Bradford, E. S., Albers, F. C., Bratton, D. J., Wang-Jairaj, J., Nelsen, L. M., et al. (2017). Efficacy of mepolizumab add-on therapy on health-related quality of life and markers of asthma control in severe eosinophilic asthma (MUSCA): a randomised, double-blind, placebo-controlled, parallel-group, multicentre, phase 3b trial. *Lancet Respir. Med.* 5 (5), 390–400. doi:10.1016/s2213-2600(17)30125-x

Detoraki, A., Tremante, E., D'Amato, M., Calabrese, C., Casella, C., Maniscalco, M., et al. (2021). Mepolizumab improves sino-nasal symptoms and asthma control in severe eosinophilic asthma patients with chronic rhinosinusitis and nasal polyps: a 12-month real-life study. *Ther. Adv. Respir. Dis.* 15, 17534666211009398. doi:10.1177/17534666211009398

Drick, N., Fuge, J., Seeliger, B., Speth, M., Vogel-Claussen, J., Welte, T., et al. (2022). Treatment with interleukin (IL)-5/IL-5 receptor antibodies in patients with severe eosinophilic asthma and COPD. *ERJ Open Res.* 8 (4), 00207-2022. doi:10.1183/23120541.00207-2022

Gevaert, P., Van Bruaene, N., Cattaert, T., Van Steen, K., Van Zele, T., Acke, F., et al. (2011). Mepolizumab, a humanized anti-IL-5 mAb, as a treatment option for severe nasal polyposis. *J. Allergy Clin. Immunol.* 128 (5), 989–995. doi:10.1016/j.jaci.2011.07.056

Gleich, G. J., Roufosse, F., Chupp, G., Faguer, S., Walz, B., Reiter, A., et al. (2021). Safety and efficacy of mepolizumab in hypereosinophilic syndrome: an open-label extension study. *J. Allergy Clin. Immunol. Pract.* 9 (12), 4431–4440.e1. doi:10.1016/j.jaip.2021.07.050

Gupta, A., Ikeda, M., Geng, B., Azmi, J., Price, R. G., Bradford, E. S., et al. (2019). Long-term safety and pharmacodynamics of mepolizumab in children with severe asthma with an eosinophilic phenotype. *J. Allergy Clin. Immunol.* 144 (5), 1336–1342. doi:10.1016/j.jaci.2019.08.005

Han, J. K., Bachert, C., Fokkens, W., Desrosiers, M., Wagenmann, M., Lee, S. E., et al. (2021). Mepolizumab for chronic rhinosinusitis with nasal polyps (SYNAPSE): a randomised, double-blind, placebo-controlled, phase 3 trial. *Lancet Respir. Med.* 9 (10), 1141–1153. doi:10.1016/s2213-2600(21)00097-7

Harpaz, R., DuMouchel, W., LePendu, P., Bauer-Mehren, A., Ryan, P., and Shah, N. H. (2013). Performance of pharmacovigilance signal-detection algorithms for the FDA adverse event reporting system. *Clin. Pharmacol. Ther.* 93 (6), 539–546. doi:10.1038/clpt.2013.24

Hashimoto, S., Kroes, J. A., Eger, K. A., Mau Asam, P. F., Hofstee, H. B., Bendien, S. A., et al. (2022). Real-world effectiveness of reslizumab in patients with severe eosinophilic

asthma - first initiators and switchers. *J. Allergy Clin. Immunol. Pract.* 10 (8), 2099–2108.e6. doi:10.1016/j.jaip.2022.04.014

Khatri, S., Moore, W., Gibson, P. G., Leigh, R., Bourdin, A., Maspero, J., et al. (2019). Assessment of the long-term safety of mepolizumab and durability of clinical response in patients with severe eosinophilic asthma. *J. Allergy Clin. Immunol.* 143 (5), 1742–1751. doi:10.1016/j.jaci.2018.09.033

Khurana, S., Brusselle, G. G., Bel, E. H., FitzGerald, J. M., Masoli, M., Korn, S., et al. (2019). Long-term safety and clinical benefit of mepolizumab in patients with the most severe eosinophilic asthma: the COSMEX study. *Clin. Ther.* 41 (10), 2041–2056. doi:10.1016/j.clinthera.2019.07.007

Kinoshita, S., Hosomi, K., Yokoyama, S., and Takada, M. (2020). Time-to-onset analysis of amiodarone-associated thyroid dysfunction. *J. Clin. Pharm. Ther.* 45 (1), 65–71. doi:10.1111/jcpt.13024

Lin, X., Yang, J., Weng, L., and Lin, W. (2023). Differences in hypersensitivity reactions to iodinated contrast media: analysis of the US Food and drug administration adverse event reporting system database. *J. Allergy Clin. Immunol. Pract.* 11 (5), 1494–1502.e6. doi:10.1016/j.jaip.2023.01.027

Liu, M. C., Bagnasco, D., Matucci, A., Pilette, C., Price, R. G., Maxwell, A. C., et al. (2023). Mepolizumab in patients with severe asthma and comorbidities: 1-year REALITI-A analysis. *J. Allergy Clin. Immunol. Pract.* doi:10.1016/j.jaip.2023.07.024

Liu, Y., Chen, C., Rong, C., He, X., and Chen, L. (2022). Anaplastic lymphoma kinase tyrosine kinase inhibitor-associated cardiotoxicity: a recent five-year pharmacovigilance study. *Front. Pharmacol.* 13, 858279. doi:10.3389/fphar.2022.858279

Lugogo, N., Domingo, C., Chanez, P., Leigh, R., Gilson, M. J., Price, R. G., et al. (2016). Long-term efficacy and safety of mepolizumab in patients with severe eosinophilic asthma: a multi-center, open-label, phase IIIb study. *Clin. Ther.* 38 (9), 2058–2070. doi:10.1016/j.clinthera.2016.07.010

Maspero, J., Adir, Y., Al-Ahmad, M., Celis-Preciado, C. A., Colodenco, F. D., Giavina-Bianchi, P., et al. (2022). Type 2 inflammation in asthma and other airway diseases. *ERJ Open Res.* 8 (3), 00576-2021. doi:10.1183/23120541.00576-2021

Montero-Pérez, O., Contreras-Rey, M. B., and Sánchez-Gómez, E. (2019). Effectiveness and safety of mepolizumab in severe refractory eosinophilic asthma: results in clinical practice. *Drugs Context* 8, 212584. doi:10.7573/dic.212584

Nordlund, B., Melén, E., Schultz, E. S., Grönlund, H., Hedlin, G., and Kull, I. (2014). Prevalence of severe childhood asthma according to the WHO. *Respir. Med.* 108 (8), 1234–1237. doi:10.1016/j.rmed.2014.05.015

Ohnishi, H., Eitoku, M., and Yokoyama, A. (2022). A systematic review and integrated analysis of biologics that target Type 2 inflammation to treat COPD with increased peripheral blood eosinophils. *Heliyon* 8 (6), e09736. doi:10.1016/j.heliyon.2022.e09736

Passalacqua, G. (2017). Anti-interleukin 5 therapies in severe asthma. *Lancet Respir. Med.* 5 (7), 537–538. doi:10.1016/s2213-2600(17)30206-0

Pertzov, B., Unterman, A., Shtraichman, O., Shitenberg, D., Rosengarten, D., and Kramer, M. R. (2021). Efficacy and safety of mepolizumab in a real-world cohort of

patients with severe eosinophilic asthma. *J. Asthma* 58 (1), 79–84. doi:10.1080/02770903.2019.1658208

Raschi, E., Fusaroli, M., Ardizzoni, A., Poluzzi, E., and De Ponti, F. (2021). Thromboembolic events with cyclin-dependent kinase 4/6 inhibitors in the FDA adverse event reporting system. *Cancers (Basel)* 13 (8), 1758. doi:10.3390/cancers13081758

Roufosse, F. E., Kahn, J. E., Gleich, G. J., Schwartz, L. B., Singh, A. D., Rosenwasser, L. J., et al. (2013). Long-term safety of mepolizumab for the treatment of hypereosinophilic syndromes. *J. Allergy Clin. Immunol.* 131 (2), 461–467. doi:10.1016/j.jaci.2012.07.055

Shu, Y., Chen, J., Ding, Y., and Zhang, Q. (2023). Adverse events with risankizumab in the real world: postmarketing pharmacovigilance assessment

of the FDA adverse event reporting system. *Front. Immunol.* 14, 1169735. doi:10.3389/fimmu.2023.1169735

Vinciguerra, A., Rampi, A., Yacoub, M. R., Tresoldi, M., Tanzini, U., Bussi, M., et al. (2022). Hypereosinophilia management in patients with type 2 chronic rhinosinusitis treated with dupilumab: preliminary results. *Eur. Arch. Otorhinolaryngol.* 279 (11), 5231–5238. doi:10.1007/s00405-022-07389-5

Wechsler, M. E., Akuthota, P., Jayne, D., Khoury, P., Klion, A., Langford, C. A., et al. (2017). Mepolizumab or placebo for eosinophilic granulomatosis with polyangiitis. *N. Engl. J. Med.* 376 (20), 1921–1932. doi:10.1056/NEJMoa1702079

Zou, S. P., Yang, H. Y., Ouyang, M., Cheng, Q., Shi, X., and Sun, M. H. (2023). Post-marketing safety of anti-IL-5 monoclonal antibodies (mAbs): an analysis of the FDA Adverse Event Reporting System (FAERS). *Expert Opin. Drug Saf.*, 1–10. doi:10.1080/14740338.2023.2251382

Frontiers in
Pharmacology

Explores the interactions between chemicals and living beings

The most cited journal in its field, which advances access to pharmacological discoveries to prevent and treat human disease.

Discover the latest Research Topics

See more →

frontiers | Research Topics